The Covalent Modification of Proteins: New Therapeutics and Probing Function and Mechanism

by

Mark Howard Dornan

Thesis submitted to the
Faculty of Graduate & Postdoctoral Studies
In partial fulfillment of the requirements for the
Ph.D. degree in Chemistry

Ottawa-Carleton Chemistry Institute

Department of Chemistry and Biomolecular Sciences, Faculty of Science
University of Ottawa

Candidate

_____

Mark Howard Dornan

Supervisor

_____

Prof. Christopher N. Boddy

Abstract

Covalent bond-forming reactions between small molecules and proteins are ubiquitous. These reactions play a central role in the diversification and functionalization of proteins, enabling normal cell growth and life. Scientists routinely employ electrophilic compounds to modify proteins by exploiting the intrinsic nucleophilicity found on amino acid side-chains. These modifications permit a wide variety of experiments and allow for new insights and a deeper understanding of the chemistry and biology of living systems. The three research projects described in this thesis employ electrophilic, protein-modifying agents to meet unique goals.

The first study (Chapter 2) details the development of a novel class of compounds that enhance the efficacy of therapeutic oncolytic viruses specifically in cancer cells. A medicinal chemistry-based approach was used to understand, measure and improve physicochemical and pharmacological properties of these small molecules.

Inspired by the unique scaffold identified in Chapter 2, the second study of this thesis (Chapter 3) explores the bioactivity of the structurally related armeniaspirole natural products. Chemical synthesis enabled the uncovering of structure-activity relationships and ultimately allowed for the design of an activity-based probe.

The final study (Chapter 4) details investigations of the terminal thioesterase involved in the biosynthesis of valinomycin. Small molecules substrates for the enzyme were synthesized and used to reveal details of the enzymatic mechanisms.

Acknowledgements

It is an absolute pleasure to express my gratitude to the many people who made the completion of this thesis possible. First, I must acknowledge my Ph.D. supervisor, Professor Christopher Boddy. Thank you for your constant guidance. Your passion, enthusiasm and fearless approach to science is inspiring and was paramount to my training as a scientist.

I must also acknowledge all of my colleagues in the Boddy Lab, past and present. Thank you for your support. I was very fortunate to work in an environment where there were always people willing and eager to help each other. Thank you for your help with experiments, studying for classes, preparing for presentations and all the coffee runs we took together. Most importantly, thank you for your friendship.

Most of the projects in this thesis were made possible by the many scientists and students who collaborated with our group over the years. Especially, Dr. Jean-Simon Diallo, Professor Jeffrey Smith, Professor Martin Schmeing, Ramya Krishnan, Andrew Macklin and Diego Alonzo.

Thank you to Roxana, for your patience and love. And finally, none of this would have been possible without my family: Patrick, Carolyn, Katie and Stephen. I am grateful for your endless love and encouragement.

Table of Contents

List of Figures

List of Schemes

List of Tables

List of Abbreviations

°C	-	degrees Celsius
A	-	adenylation
AAV2	-	adeno-associated virus serotype 2
ABPP	-	activity-based protein profiling
Ac	-	acetyl
Ad5	-	adenovirus serotype 5
Arg	-	arginine
Asp	-	aspartic acid
ATP	-	adenosine triphosphate
Bn	-	benzyl
Boc	-	*tert*-butyloxycarbonyl
C	-	condensation
C_{max}	-	maximum serum concentration
CYP	-	cytochrome P450
Cys	-	cysteine
Da	-	dalton
DCE	-	1,2-dichloroethane
DMAP	-	4-(dimethylamino)pyridine
DMF	-	*N*,*N*-dimethylformamide
DMSO	-	dimethyl sulfoxide
DNA	-	deoxyribonucleic acid
EDC	-	*N*-(3-dimethylaminopropyl)-*N′*-ethylcarbodiimidehydrochloride
Et	-	ethyl
FDA	-	Food and Drug Administration
Fluc	-	firefly luciferase
g	-	gram
GFP	-	green fluorescent protein
Glu	-	glutamic acid
GSH	-	glutathione
h	-	hours
HDAC	-	histone deacetylase
His	-	histidine
HIV	-	α-hydroxyisovaleric acid
HPLC	-	high-performance liquid chromatography
HSV	-	herpes simplex virus
IADR	-	idiosyncratic adverse drug reactions
IFN	-	interferon
IVIS	-	*in vivo* imaging system
J	-	coupling constant

JAK - Janus kinase
L - liter
LAC - lactic acid
LC - liquid chromatography
LD - lethal dose
Lys - lysine
MALDI - matrix assisted laser desorption/ionization
Me - methyl
MHC - major histocompatibility complex
MIC - minimum inhibition concentration
MOI - multiplicity of infection
MRM - multiple reaction monitoring
MRSA - methicillin-resistant *Staphylococcus aureus*
MS - mass spectrometry
Ms - methanesulfonyl
mTOR - mammalian target of rapamycin
N - nitrogen
NCS - *N*-chlorosuccinimide
NK - natural killer
NMR - nuclear magnetic resonance
NRP - nonribosomal peptide
NRPS - nonribosomal peptide synthetase
O - oxygen
PAGE - polyacrylamide gel electrophoresis
PBS - phosphate-buffered saline
PCP - peptidyl carrier protein
PFE - peak fold enhancement
PFU - plaque forming units
Ph - phenyl
ppm - parts per million
PRSP - penicillin resistant *Streptococcus pneumoniae*
PTM - posttranslational modification
RLU - relative light units
RNA - ribonucleic acid
SAR - structure-activity relationship
SDS - sodium dodecyl sulfate
Ser - serine
SNAC - *N*-acetylcysteamine
SPhos - 2-Dicyclohexylphosphino-2′,6′-dimethoxybiphenyl
$t_{1/2}$ - half-life

TBS	-	*tert*-butyldimethylsilyl
TBTA	-	tris[(1-benzyl-*1H*-1,2,3-triazol-4-yl)methyl]amine
TCEP	-	tris(2-carboxyethyl)phosphine hydrochloride
TE	-	thioester
TFA	-	trifluoroacetic acid
THF	-	tetrahydrofuran
Thr	-	threonine
TLC	-	thin layer chromatography
Tyr	-	tyrosine
UPLC	-	ultra performance liquid chromatography
UV	-	ultraviolet
Val	-	valine
VEU	-	viral expression unit
Vis	-	visible
Vlm	-	valinomycin
VRE	-	vancomycin-resistant *Enterococci*
VSF	-	viral sensitization factor
V_{ss}	-	apparent volume of distribution at steady state
VSV	-	vesicular stomatitis virus
δ	-	chemical shift in parts per million

Statement of contribution

The original research described in this thesis was completed in collaboration with researchers at a number of different institutions. Descriptions of the contributions to each project are detailed below.

Chapter 2: Small Molecule Potentiation of Oncolytic Viral Therapy

This project was a highly collaborative effort by members of Prof. Christopher Boddy's (University of Ottawa), Dr. Jean-Simon Diallo's (Ottawa Hospital Research Institute), and Prof. Jeffrey Smith's (Carleton University) research groups. The synthesis and design of all compounds was completed by members of Professor Christopher Boddy's research group. This includes Mark Dornan, Christina Moi, Christophe Pardin, and Penny Le. The LC-MS glutathione stability assay was developed and carried out by Mark Dornan. The plasma stability assay was conducted at Carleton University in Prof. Jeffrey Smith's laboratory by Andrew Macklin and Mark Dornan. All *in vitro*, *ex vivo* and *in vivo* experiments were completed at the Ottawa Hospital Research Institute in Dr. Jean-Simon's laboratory by Ramya Krishnan, Mohammed Selman, Nader El Sayes, Colin Davis, Andrew Chen, Paula Ou, and Fabrice Le Boeuf.

Chapter 3: Development of an Armeniaspirole-based Chemical Biology Probe

The chemical synthesis and ABPP experiments described in this chapter were conducted by Mark Dornan. The *in vitro* evaluation of the compounds with the MIC assay was carried out by Mark Dornan and Melanie Cyr.

Chapter 4: Insights into the Valinomycin Thioesterase Mechanism

The SNAC thioester tetradepsipeptide substrates were synthesized and characterized by Mark Dornan. Diego Alonzo and Janice Reimer of Prof. Martin Schmeing's research group at McGill University prepared the purified VlmTE, carried out all *in vitro* experiments, acquired the mass spectrometry data, and generated the chromatogram figures.

Chapter 1: Introduction

1.1 Covalent modification of proteins

Chemical reactions involving the generation of a covalent bond between a protein and a small molecule are prevalent in nature, the laboratory, and the clinic. Proteins are intrinsically nucleophilic given the presence of heteroatom-containing side chains on proteinogenic amino acids. This includes thiol (Cys), alcohol (Ser, Thr), phenol (Tyr), amino (Lys, His, Arg) and carboxylic acid (Asp, Glu) containing groups (Figure 1.1).[1] Reactions between these nucleophilic residues with small molecules allows nature, scientists, and physicians to exert a wide variety of biological effects.

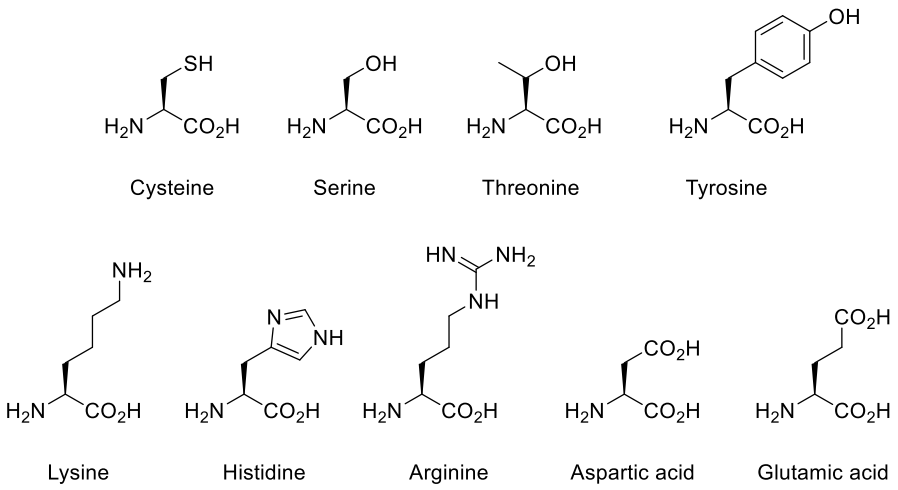

Figure 1.1. Proteinogenic amino acids with nucleophilic side chains.

The covalent modification of proteins is important for the maintenance of cell regulation.[2] To become functional, many proteins must undergo posttranslational modification. The term posttranslational modification (PTM) refers to enzyme-catalyzed processes that lead to the formation or cleavage of covalent bonds in fully translated proteins. This process drastically increases the amount of different proteins in the human proteome (>10 to 100-fold higher than the

number of protein-encoding genes).[3] This diversification is important as proteins are responsible for the implementation of most genetically instructed programmes and tasks involved in cell growth and life. Examples of PTMs that involve the generation of a new covalent bond include phosphorylation, methylation, *N*-acetylation, lipidation, glycosylation, hydroxylation and amidation.

Covalent bond formation and cleavage also plays an important role in controlling transcription activity.[4] External or environmental factors can induce modifications of histone proteins in a chromatin complex. These modifications can activate or deactivate the transcription of genes. This process is often referred to as epigenetic control. Acetylation of Lys, methylation of Lys and Arg, and phosphorylation of Ser and Thr are examples of reversible covalent modifications to histone protein amino acid side chains that leads to epigenetic effects on transcriptional activity.

In addition to maintaining regulation and homeostasis, many organisms produce metabolites that can change the biological state of other species through the modification of proteins. For example, unicellular organisms like bacteria and yeast have evolved enzymatic machinery that allows for the production of complex and potent secondary metabolites. These molecules are often purposed to give the producing organism an advantage when growing in competitive environments with other species.[5]

Humans also employ reactive, electrophilic compounds to exert changes in biological states through covalent protein modification. The mechanism of action of many modern pharmaceuticals relies on the formation of a covalent bond between an electrophilic small molecule and a protein or enzyme. In past decades, pharmaceutical companies have focused on

developing drugs that function through non-covalent mechanisms. Recently, there has been a revival of interest in industry towards developing electrophilic pharmaceuticals.[6,7]

In addition to therapeutic purposes, scientists design and use covalent molecules to interrogate and learn about biological processes. In particular, the development of covalent affinity capture experiments has facilitated the determination biological targets and mechanisms of action for many molecules. Activity-based protein profiling (ABPP) experiments also often rely on the generation of a covalent bond to identify and characterize small molecule / protein interactions. Furthermore, covalent substrates can also be used to study enzymatic function *in vitro*.[8] This is a common technique used to study enzymes involved in polyketide synthases and nonribosomal peptide synthetases.

Both X-ray crystallography and mass spectrometry have facilitated the analysis and characterization of covalently modified proteins. Obtaining an X-ray can allow for extensive 3D characterization of the site of covalent modification and identification of other characteristics that give rise to reactivity and selectivity. One major limitation of this technique is low throughput. It can take extensive time to both develop crystallization conditions for a protein and solve the crystal structure.[9] In addition to protein crystallography, various mass spectrometry techniques are used to identify and characterize sites of covalent modification. Electrospray-ionization mass spectrometry (ESI-MS) is often used after extensive proteolysis which generates a distinct set of shorter peptides from the protein of interest.[10] Comparing the generated peptides to a database or predicted structures can allow for the identification of the protein and/or identification of the sites of modification. Another technique that can be used is matrix assisted laser desorption/ionization (MALDI). MALDI is another soft ionization technique that allows for the generation and detection of large molecular ions, and has been used to map the sites of labile PTM bonds.[11]

1.2 Prevalence of covalent pharmaceuticals

Healthcare has benefited tremendously from the use of pharmaceuticals that covalently modify their targets. There are examples of FDA approved covalent drugs for about one third of all enzyme targets with approved inhibitors.[12] In 2009, three of the ten best-selling drugs (United States) functioned through covalent inhibition.[7]

There are many potential advantages cited by proponents of covalent drug development. These include the potential for increased potency and selectivity by achieving a reaction at a specific amino acid.[6] It is also said that the desired effect can be achieved with lower doses as competition with endogenous ligands is removed after modification. Another benefit is said to be reduced susceptibility to resistance caused by weak or transient binding to mutant forms of the biological target. This could have important implications in anti-infective drug development, where resistance often develops quickly.

The prevalence of covalent pharmaceuticals on the market today is somewhat surprising given the fact that many major industry drug discovery programs generally sought to avoid advancing small molecules with electrophilic functionality through the pipeline.[13,14] This philosophy was built on important research uncovered in the 1970s and 1980s which attributed reactive drug metabolites to organ toxicity. Promiscuous electrophiles have the ability to label a wide range of large and small biomolecules, specifically and non-specifically. This has the potential to induce idiosyncratic adverse drug reactions (IADRs).[15] Often, the underlying mechanisms leading to IADRs are unknown. It is also common for IADRs of a drug to only affect a subset of the population. It is believed that many IADRs are instigated when the electrophilic molecule binds to a biological macromolecule resulting in the formation of a hapten, which can induce an immune response, or directly disrupt cell function.[16]

1.3 Covalent natural products

Many natural products contain reactive moieties that allow them to form covalent bonds with proteins, leading to inhibition of activity. The electrophilic structural features and mechanisms utilized for this type of reactivity is diverse, including and not limited to the use of epoxides, maleimides, carbamates, α,β-unsaturated lactones, vinyl sulfones, furans and β-lactones (Figure 1.2).[17]

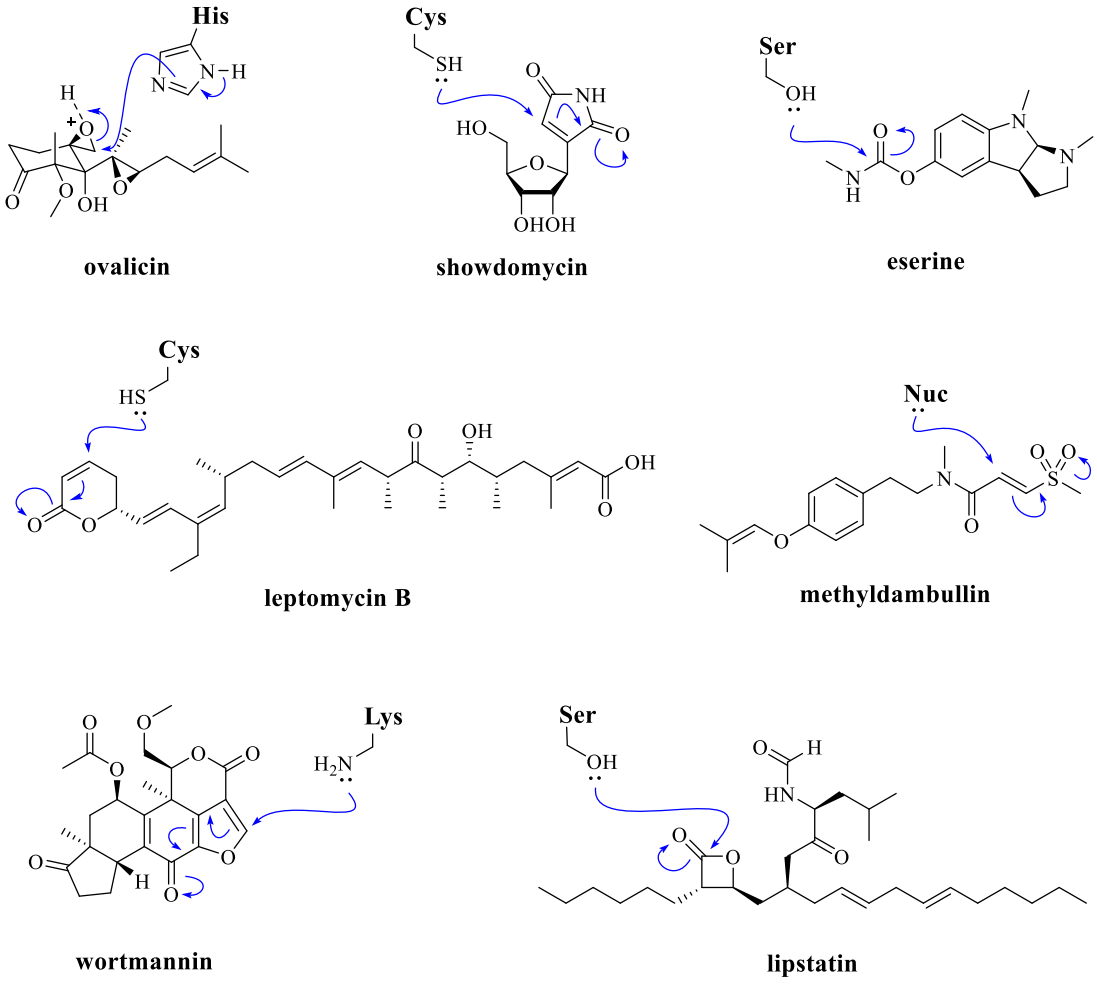

Figure 1.2. Examples of electrophilic natural products.

These protein reactive natural products often modify specific nucleophilic residues at specific protein targets. This reactivity has enabled or facilitated many different types of pharmacology and chemical biology based studies. This includes the identification of biological targets and mechanisms of action using affinity capture assays, the study of enzyme chemistry, proteomic profiling, and even providing the basis for the design of new pharmaceuticals.

Epoxomicin is an example of natural product with electrophilic features that facilitated a diverse set of studies. The uncovering of the underlying biology leading to the observed bioactivity ultimately enabled the development and FDA approval of a new natural product-inspired pharmaceutical. Epoxomicin was isolated from an *Actinomycetes* strain in 1992 and shown to be a potent antitumor agent (Figure 1.3).[18] This potent activity and the unusual α-β-epoxyketone moiety prompted Professor Craig Crews and coworkers at Yale University to synthesize a biotinylated conjugate of the natural product and attempt to identify the biological targets using affinity capture experiments with streptavidin beads.[19] Interestingly, this assay indicated that epoxomicin was a powerful proteasome inhibitor, impeding chymotrypsin-like activity through irreversible inhibition.

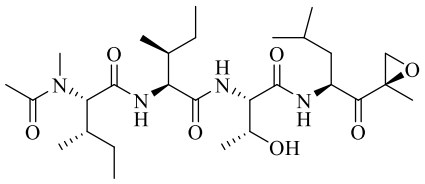

epoxomicin

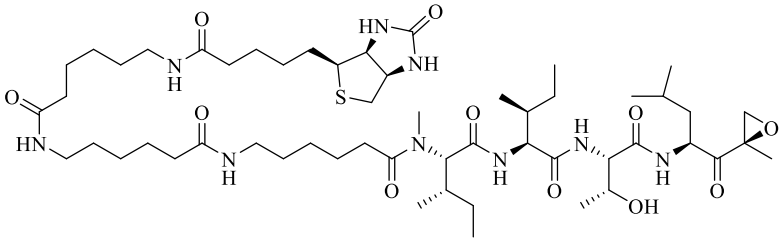

epoxomicin-biotin conjugate

Figure 1.3. Structures of epoxomicin and the epoxomicin-biotin conjugate.

In a follow up study published just months later, Crews and coworkers reported a co-crystal structure of epoxomicin bound to the 20S proteasome.[20] The X-ray showed that the covalent modification of the proteasome results in the formation of a morpholino-ring, formed with a terminal Thr residue (Figure 1.4).

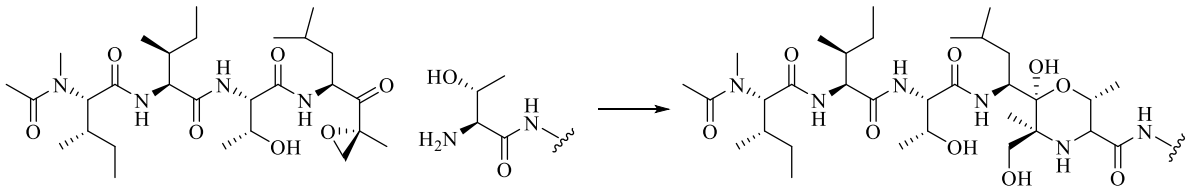

Figure 1.4. Adduct formation between epoxomicin and a terminal threonine residue.

Crews and coworkers then worked on refining the structure to optimize activity and drug-like properties and eventually licencing the technology to Proteolix, which was acquired by

Onyx Pharmaceuticals.[21] Carfilzomib (Figure 1.5) was granted fast-track status in 2011 and approved by the FDA in 2012 for the treatment of multiple myeloma.

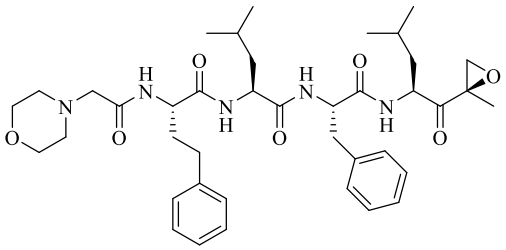

Figure 1.5. Structure of carfilzomib.

1.4 Activity-based protein profiling

Activity-based protein profiling (ABPP) probes are small molecules that are designed to allow investigators to ask questions about protein function and mechanism. These probes typically contain an electrophile or a photoreactive group, allowing for the covalent modification of target proteins. In addition, a reporter tag should be integrated into the probe structure (often a fluorophore or affinity tag).[22] The reporter tag allows for target protein purification and/or identification using gel analysis or mass spectrometry. Often the reporter tag is integrated into the structure through a click chemistry reaction after the proteome is labelled with the probe. One of the benefits of ABPP evaluation of protein expression over other techniques, is the ability to study and compare the proteomic states of living cells and tissues.

ABPP has been used by investigators in many different applications. For example, ABPP has facilitated the study of biological mechanisms implicated in pathology and the identification of druggable targets. Differences in labelling between the two states can be characterized through

comparison of the extent of protein labelling in a disease state with the healthy state.[23] ABPP can also be used for inhibitor identification. Using a similar comparative method, compounds that compete with the probe for active sites can be screened using ABPP.

Kinases are a large class of enzymes that catalyze the transfer of phosphate groups, and have attracted major attention from the pharmaceutical industry as therapeutic targets to address disease. Approximately 50 % to 70 % of all cancer drug programs are focused on kinases.[24] Recently, ABPP was shown to be useful in vetting the proteome-wide selectivity of covalent kinase inhibitors.[25] Benjamin Cravatt and coworkers successfully used this technique to identify specific and nonspecific targets of the inhibitors. One of the major benefits of ABPP in this application is the ability to assess target inhibition and the extent of off-target labelling, simultaneously.

It is often more difficult and complicated to understand the mechanism of action of reactive covalent drugs that may impart activity through multiple biological targets. Artemisinin, a natural product, is an effective antimalarial drug that functions through the generation of radicals following endoperoxide cleavage. The antimalarial activity is a result of target covalent modification with these reactive intermediates. Recently, an artemisinin-based activity probe was developed (Figure 1.6) and used to identify 124 binding targets, many of which have been implicated in biological processes essential for parasitic life. This allowed for the characterization of this drug as functioning through a haem-activated promiscuous targeting mechanism, rather than functioning through the inhibition of a single biological target as other groups have proposed.[26]

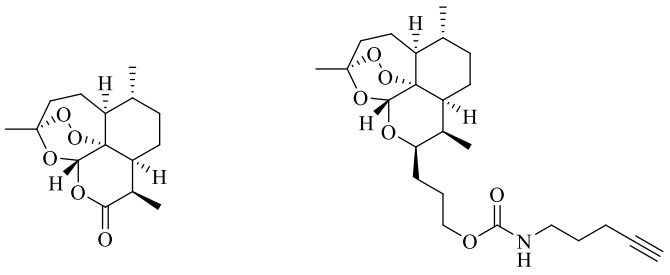

artemisinin **artemisinin ABPP probe**

Figure 1.6. Structures of artemisinin and the artemisinin ABPP probe.

1.5 Summary and outlook

In summary, reactions between electrophilic molecules and proteins are prevalent and astonishingly useful. There is a revival of interest in developing covalent pharmaceuticals, which may offer strategic advantages over non-covalent targeting of proteins. This may help address some of the most urgent needs in healthcare today. Reactive activity-based probes are indispensable to the chemical biology community and can be used for many different purposes. Examples include the identification of biological targets, the annotation of protein function, and the identification and assessment of inhibitors. Electrophilic compounds can also be used to study enzymatic function and mechanisms *in vitro*.

The three chapters in this thesis rely on use of electrophilic compounds to explore different biological questions. In Chapter 2, a new class of electrophilic compounds are developed for the use of potentiating oncolytic virus replication. Chapter 3 describes the study of armeniaspirole A, a natural product and the development of an activity-based probe. Chapter 4 details investigations of a NRPS thioesterase domain involved in the biosynthesis of valinomycin. Substrates that covalently load onto the enzyme are synthesized to explore the catalytic mechanisms.

1.6 References

(1) Roger, L. *Chemical reagents for protein modification*; 4th ed.; Taylor & Francis Group: Chapel Hill, 2014.

(2) Wang, Y.-C.; Peterson, S. E.; Loring, J. F. *Cell Res.* **2014**, *24*, 143–160.

(3) Walsh, C. T. *Posttranslational Modification of Proteins*; Ben Roberts: Englewood, Colorado, 2006.

(4) Li, E. *Nat. Rev. Genet.* **2002**, *3*, 662–673.

(5) Ridley, C. P.; Lee, H. Y.; Khosla, C. *Proc. Natl. Acad. Sci. U. S. A.* **2008**, *105*, 4595–4600.

(6) Kalgutkar, A. S.; Dalvie, D. K. *Expert Opin. Drug Discov.* **2012**, *7*, 561–581.

(7) Singh, J.; Petter, R. C.; Baillie, T. A.; Whitty, A. *Nat. Rev. Drug Discov.* **2011**, *10*, 307–317.

(8) Pieper, R.; Luo, G.; Crane, D. E.; Khosla, C. *Nature* **1995**, *378*, 287–292.

(9) Acharya, K. R.; Lloyd, M. D. *Trends Pharmacol. Sci.* **2005**, *26*, 10–14.

(10) Kelleher, N. L.; Lin, H. Y.; Valaskovic, G. a; Aaserud, D. J.; Fridriksson, E. K.; McLafferty, F. W. *J. Am. Chem. Soc.* **1999**, *121*, 806–812.

(11) Qin, J.; Chait, B. T. *Anal. Chem.* **1997**, *69*, 4002–4009.

(12) Robertson, J. G. *Biochemistry* **2005**, *44*.

(13) Lipinski, C.; Hopkins, A. *Nature* **2004**, *432*, 855–861.

(14) Rishton, G. M. *Drug Discov. Today* **2003**, *8*, 86–96.

(15) Knowles, S. R.; Uetrecht, J.; Shear, N. H. *Lancet* **2000**, *356*, 1587–1591.

(16) Uetrecht, J.; Naisbitt, D. J. *Pharmacol. Rev.* **2013**, *65*, 779–808.

(17) Gersch, M.; Kreuzer, J.; Sieber, S. *Nat. Prod. Rep.* **2012**, *29*, 659–682.

(18) Hanada, M.; Sugawara, K.; Kaneta, K.; Toda, S.; Nishiyama, Y.; Tomita, K.; Yamamoto, H.; Masataka, K.; Oki, T. *J. Antibiot. (Tokyo).* **1992**, *45*, 1746–1752.

(19) Meng, L.; Mohan, R.; Kwok, B. H.; Elofsson, M.; Sin, N.; Crews, C. M. *Proc. Natl. Acad. Sci. U. S. A.* **1999**, *96*, 10403–10408.

(20) Groll, M.; Kim, K. B.; Kairies, N.; Huber, R.; Crews, C. M. *J. Am. Chem. Soc.* **2000**, *122*, 1237–1238.

(21) Myung, J.; Kim, K. B.; Lindsten, K.; Dantuma, N. P.; Crews, C. M. *Mol. Cell* **2001**, *7*, 411–420.

(22) Berger, A. B.; Vitorino, P. M.; Bogyo, M. *Am. J. Pharmacogenetics* **2004**, *4*, 371–381.

(23) Cravatt, B. F.; Wright, A. T.; Kozarich, J. W. *Annu. Rev. Biochem.* **2008**, *77*, 383–414.

(24) Cohen, P.; Alessi, D. R. *ACS Chem. Biol.* **2013**, *8*, 96–104.

(25) Lanning, B. R.; Whitby, L. R.; Dix, M. M.; Douhan, J.; Gilbert, A. M.; Hett, E. C.; Johnson, T. O.; Joslyn, C.; Kath, J. C.; Niessen, S.; Roberts, L. R.; Schnute, M. E.; Wang, C.; Hulce, J. J.; Wei, B.; Whiteley, L. O.; Hayward, M. M.; Cravatt, B. F. *Nat. Chem. Biol.* **2014**, *10*, 760–767.

(26) Eckstein-Ludwig, U.; Webb, R. J.; Van Goethem, I. D. a; East, J. M.; Lee, A. G.; Kimura, M.; O'Neill, P. M.; Bray, P. G.; Ward, S. A.; Krishna, S. *Nature* **2003**, *424*, 957–961.

Chapter 2: Small Molecule Potentiation of Oncolytic Viral Therapy

2.1 Introduction

Cancer is a diverse and widespread disease that is broadly defined as uncontrolled growth of abnormal cells in the body. It is estimated that 2 in 5 Canadians will develop cancer in their lifetime, and 1 in 4 Canadians will die from cancer. Currently, there is a 63 % likelihood of surviving 5 years after cancer diagnosis.[1] Goals of modern cancer treatment strive toward prevention, cure, control or palliation of disease. Available treatment methods and strategies are diverse and most commonly include surgical removal, radiation therapy, and/or pharmacological intervention.

Investigations into the ability of viruses to preferentially infect and destroy cancer cells has yielded a new class of anti-cancer agents referred to as oncolytic viruses. Oncolytic viral therapy has proven to be promising strategy for the effective and safe treatment of cancer. While there has been interest in the use of viruses to treat cancer since the early 20th century, the first oncolytic virus to be approved by a government regulatory body was the modified adenovirus Oncorine (H101) in 2005 by China's State Food and Drug Administration. More recently, herpes simplex virus-1 talimogene laherparepvec was approved for use in October 2015 by the United States Food and Drug Administration. A growing number of oncolytic viruses are currently undergoing clinical trials including adenovirus, herpes simplex virus, poliovirus, reovirus, vaccinia virus, and vesicular stomatitis virus-based platforms, signalling the growing importance of this mode of therapy.[2]

This introduction will provide an overview of the use of oncolytic viruses as agents in cancer therapy. Also discussed is current understanding of the interplay between oncolytic viral therapy and the immune system, hurdles in the development of effective oncolytic viruses, and a review of the use of small molecule agents to enhance the replication and spread of oncolytic viruses.

2.1.1 Viral agents and tools in biotechnology

Viruses are small, prevalent and remarkably efficient infectious agents that function by replicating inside the cells of other organisms. It is estimated that viruses kill up to 40 % of all bacteria in the ocean every day.[3] The viral genome is diverse in size and can contain more than 1,000 protein-coding genes or as few as one. Genetically modified viruses that are created through selection or genetic recombinant technology have been employed in a growing number of pharmaceutical and biotechnology platforms as agents or tools.

Live attenuated viral vaccines are vaccines that are derived from disease-causing viral pathogens. These vaccines stimulate an immune response and allow for the development of adaptive immunity. The use of live attenuated viral vaccines has had a major impact on global health.[4] Attenuation of the viral strains is achieved through either selection or the use of genetic recombinant technology to modify the genome leading to a reduction in the degree of pathogenicity while remaining viable. The effect is that virulence is diminished and the host immune system can swiftly eliminate the virus while taking the opportunity to develop adaptive immunological memory. Many viral-based infectious diseases have been eradicated or are prevented with these live attenuated viral vaccines including polio, smallpox, mumps, measles, and yellow fever.[5]

Genetically modified viruses have also found use in gene therapy.[6] A normal viral life cycle involves binding and delivery of viral genetic material into host cells. Gene therapy strategies often employ a viral vector to deliver desired genetic information to host cells. Viral vectors created from pathogenic strains are attenuated to improve therapeutic safety. While viral-based vaccines have a strong historical record of use in humans, gene therapy still resides in the developmental stage and has not yet been realised for clinical use.

A third use for genetically engineered viruses, oncolytic viral therapy, is poised to make a major impact in the clinic. Oncolytic viruses are viruses that are selected or engineered to be effective, cancer cell selective antineoplastic agents.

2.1.2 Early investigation of oncolytic viruses

Early documentation of the viral propensity for replication in malignant cells was published in 1904 after a patient was vaccinated for rabies and regression of cervical cancer was observed.[7] In another example it was noted that a patient who had been infected with measles entered remission for Burkitt's and Hodgkin's lymphoma. These, and further examples prompted interest into the use of viruses to treat cancer in animal models in the 1940s. In 1949 at the Sloan-Kettering Institute for Cancer Research, Dr. Chester M. Southam and colleagues became the first to experiment with using viruses as antineoplastic agents in humans.[8] Over the course of four years they inoculated and followed 129 patients with various viral strains isolated from human blood, mice or mosquitos. This study included the use of the West Nile virus, Ilheus virus, Bunyamwera virus, Semliki Forest virus, Newcastle-disease virus, Dengue virus, Mumps virus and Vaccinia. Limited response across patients and incomplete therapeutic efficacy led to temporary abandonment of this strategy.

Following advances in virology and the development of tissue and cell culture techniques, virotherapy research re-emerged in the 1960s in a less crude form using purified and selected viruses.[9] Eclipsed by promising results in emerging chemotherapy treatment regimes, oncolytic viral therapy research eventually declined again after results demonstrated that appropriate therapeutic efficacy was not reached.

Since the 1960s major leaps in science including in the understanding of virology, cancer biology, immunology and genetics has prompted a revived interest in oncolytic viral therapy.[9] The uncovering and understanding of the nature of viral life cycles and tumor cell genetic and epigenetic alterations leading to cell immortality have helped to explain viral tendency for replication within cancer cells. Described hallmarks of cancer biology include sustained proliferative signalling, resistance to cell death, the evasion of growth suppressors and enabling replicative immortality.[10] These hallmarks have been shown to provide a favourable environment for viral infection and replication. Characterization of the mechanisms by which the human immune system protects the body from both foreign pathogens and malignant cell growth has also been crucial to the development of oncolytic viruses. Finally, the advent of genetic recombinant technology has allowed for manipulation of the viral genome yielding oncolytic viruses with favourable pharmacological agent characteristics in terms of efficacy and selectivity.

2.1.3 Oncolytic viruses and the immune system

A thorough understanding of the dynamics between both viruses and the immune system and tumors and the immune system has been needed to develop effective oncolytic virus treatment strategies. Upon viral infection, the innate immune response works to limit the success of virus replication and clear it from the body. Infected cells release a class of cell-to-cell signalling proteins called interferons. Importantly, type 1 interferon (α and β) signalling promotes the production of molecules that interfere with viral DNA and RNA production in uninfected cells, leading to cell protection.[11] In contrast, type 2 interferon (γ) acts directly on the immune system, altering the transcription of up to 30 different genes. This leads to a variety of effects important for protection against viruses including stimulation of natural killer (NK) cells, activation of

macrophages, and enhancement of antigen presentation on infected cells by increasing MHC class II expression.[12]

Many of the immune mechanisms important for eradication of cells compromised by viral infection are also used for the surveillance and clearance of cancer cells. Because of this, tumor growth and survival is largely dependent on the tumor's ability to manipulate the host environment and evade both innate and adaptive immune responses. This can be done through limiting the display of tumor cell neo-antigens, the suppression of tumor response to immune effectors, or neutralization of penetrating immune cells.[13] These factors that lead to successful tumor growth through immune evasion give rise to viral propensity for replication in malignant cells over normal cells.

Interestingly, oncolytic viruses can also mediate tumor cell death by triggering an anti-tumor immune response. Initial viral infection of tumor cells causes the release of pro-inflammatory cytokines. After lysis, virus and tumor antigens are exposed to the immune system and the tumors ability to evade immune surveillance is disrupted. This has been shown to induce both innate and adaptive rejection of the cancer cells.[14] These findings have prompted many researchers to focus on investigating and developing oncolytic viruses as immunotherapy agents.[15]

2.1.4 Oncolytic virus engineering strategies impacting efficacy

Treatment with oncolytic viruses can lead to desired cancer cell death through a number of different mechanisms. Many oncolytic viruses directly kill the cancer cells as part of a replicating lytic life cycle, releasing virus progeny that subsequently infect and lyse adjacent cancer cells. This is referred to as oncolysis. Viruses can also cause cell death through induction of apoptosis through the production of cytotoxic proteins. For example, the late-stage expression of the adenovirus death

protein E3-11.6K has been shown to accelerate cell death and lysis.[16] Oncolytic viruses have also been shown to impart cell death by disrupting the tumor's natural ability to evade innate immune system surveillance and response. For example, adenovirus E1A expression potentiates apoptosis by inducing response from natural killer cells, activated macrophages and cytotoxic T cells.[17] In addition to sensitizing tumors to immune response-mediated destruction, adenovirus expressing E1A has been shown to enhance chemosensitivity, representing another mechanism by which oncolytic viruses can induce cell death. Published results also indicate that some oncolytic viruses can effect acute vascular-disruption in tumors, contributing to demise.[18] Lastly, recombinant technology allows for the insertion of transgenes into the viral genome that can cause or enhance oncolysis. For instance, herpes simplex virus expressing immunomodulatory interleukin-12 (IL-12), have been used to treat brain tumors in mouse models.[19]

2.1.5 Oncolytic virus engineering strategies impacting selectivity

Genetic modifications to the viral genome impacting cell selectivity have been made in development of effective oncolytic viruses. These genetic modifications take advantage of the distinct environment in a tumor cell compared with normal healthy cells. One strategy is the disruption of genes responsible for the generation of products critical for infection in normal cells, but without impacting on the ability of the virus to replicate in distinct tumor cells. For example, oncolytic vesicular stomatitis virus VSVΔ51 contains a mutation in the gene responsible for the production of the viral M protein, a virulence protein responsible for disruption of the host interferon (IFN) response to infection.[20] Since a common genetic defect of tumor cells results in diminished IFN responsiveness, this mutation improves tumor cell selectivity over normal cells. Another engineering strategy for imparting selectivity is the introduction of a replication-

restricting promotor specifically induced in the tumor environment. For instance, a strain of adenovirus was developed that had the E1A gene expression controlled by an α-fetoprotein gene promotor, a tumor specific protein.[21] Both of these strategies can result in the development of agents with a high therapeutic index.

2.1.6 Challenges in developing effective oncolytic viruses

In 2014, oncolytic viruses from nine different families were under investigation in human clinical trials including Adenoviridae, Herpesviridae, Paramyxoviridae, Parvoviridae, Picornaviridae, Poxviridae, Reoviridae, Retroviridae and Rhabdoviridae. Yet, only two oncolytic viruses have received approval from a government regulatory agency. This includes H101, an engineered adenovirus strain approved for use in China for the treatment of head and neck cancer and HSV-1-based talimogene laherparepvec, approved in the United States in 2015 for the treatment of advanced melanoma. In most instances, oncolytic viruses studied in clinical trials have failed to reach therapeutic efficacy targets due to limited replication efficiency of the virus in the tumor.[22]

While the treatment of cancer with oncolytic viruses has shown to be tremendously effective in some patients, minimal response has been noted in others. This heterogeneity of clinical response has proven to be a major hurdle for the development of successful oncolytic viruses, as shown in numerous models and human clinical trials.[23,2,24] An estimated 30 – 35% of tumors retain the ability to mount an effective antiviral defense. This resistance of tumors to oncolytic viral therapy has been attributed to a number of factors including variability of the immunosuppressive microenvironment within the tumor, pre-existing immunity and the presence of partially or fully intact antiviral mechanisms that are often mutated or defective in tumors. [20,25,26]

A number of strategies have been used to overcome this resistance to oncolytic virus treatment. The repair or restoration of the virulence genes leading to attenuation can lead to a more effective virus, but also compromises the selectivity of the virus for malignant cells, which presents safety concerns. In one example of this, researchers armed an engineered oncolytic measles virus with the P gene found in the wild-type measles virus and known to be responsible for the production of IFN antagonizing proteins.[27] Alternatively, the virulence genes from different viral strains can be incorporated into an oncolytic virus genome. The oncolytic potency of a vesicular stomatitis virus was substantially increased through the genetic incorporation of equine herpes virus-1 glycoprotein G, which resulted in a reduction of NK and NK-T cells in the tumors and led to increased tumor necrosis.[28] A third strategy to improve efficacy is to co-treat the tumors with a second oncolytic virus designed to be complementary. For example, administration of an interferon-sensitive vesicular stomatitis virus strain was enhanced when co-administered with an oncolytic poxvirus encoded to secrete an interferon antagonist.[29]

2.1.7 Pharmacological enhancement of oncolytic viral therapy

In an effort to advance therapeutic efficiency, studies have been completed investigating the use of various classes of small molecules in conjunction with oncolytic viruses (Figure 2.1). Noteworthy, the pharmacological modulation of oncolytic virus induced anti-tumor immunity has been recently reviewed by Forbes *et al.*[30] The combination of several oncolytic viruses with various classic chemotherapeutic agents has been extensively investigated. The immunosuppressive nature of these agents was found to be the reason for enhancement of oncolytic virus replication and spread. For example cyclophosphamide was found to enhance oncolytic HSV replication and oncolysis in animal models.[31] Towards a mechanistic understanding

of this response, treatment with cyclophosphamide was shown to decrease intratumoral levels of NK cells and $CD68^+$ macrophages and inhibit IFN-γ production.[32]

Another pharmacological approach to enhancing oncolytic viral therapy is with the use of compounds that have the ability to effect changes in gene transcription activity, known as epigenetic modulating compounds. Histone deacetylase (HDAC) are a class of enzymes that deacetylate lysine amino acids on histones, leading to a reduction in transcription. HDAC activity has been shown to have impact on the transcriptional activation of interferon-stimulated genes.[33] Thus, HDAC inhibitory compounds including suberoylanilide hydroxamic acid, trichostatin A, entinostat and valproic acid have been used to mute viral inhibiting IFN signalling pathways leading to enhancement of viral replication.[34,35,36]

Rapamycin has also been shown to augment oncolytic viruses through inhibition of the kinase mammalian target of rapamycin (mTOR). This kinase was found to be deregulated in many types of cancer. Inhibition of this mTOR with rapamycin has been reported to impact the translation of IFN and other mediators known to be crucial for an effective anti-viral response.[37]

Janus kinase (JAK) has also proven to be an interesting target for cancer sensitization to viral infection. JAK1 activity is known to be necessary for type I IFN signalling. Pre-treatment of cells with a compound called JAK Inhibitor I led to enhancement of a vesicular stomatitis virus *in vitro*.[38]

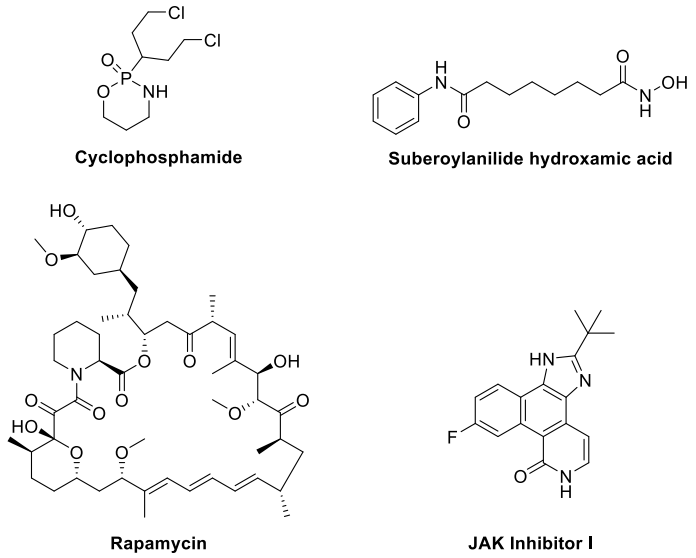

Figure 2.1. Representative example of small molecules used to enhance oncolytic viral therapy.

2.1.8 Identification of new oncolytic virus potentiating agents

In an effort to identify new oncolytic virus enhancing small molecules, the Bell lab designed a phenotypic high-throughput screening experiment of a library of 12,280 compounds. They screened the compound library for the ability to enhance the replication of VSVΔ51 in a partially-resistant mouse breast cancer cell line (4T1). The cytotoxicity of each compound alone and in combination with VSVΔ51-RFP was compared to identify compounds that enhance viral-mediated cell death. This ratio of these two measurements is referred to as the relative viral sensitization factor (VSF). Analysis of the high-throughput screening data yielded 30 compounds that outperformed the positive control HDAC inhibitor suberoylanilide hydroxamic acid. In total, 15 of these 30 compounds exhibited validated activity.

The compound 3,4-dichloro-5-phenyl-2,5-dihydrofuran-2-one (**2.1**, Figure 2.2) was found to have the highest activity of all compounds screened. It was shown that **2.1** was able to potentiate VSVΔ51 activity in a dose-dependent manner in three additional cell lines partially or highly resistant to viral infection. This included mice colon cancer cells (CT26), human glioblastoma

cells (U-251) and human renal cell carcinoma cells (786-O). In the cell line most resistant to VSVΔ51 infection, 786-O cells, viral titers were increased by over 1,000 fold when pre-treated with **2.1**.

Oncolytic virus VSVΔ51 is attenuated through the deletion of the 51st amino acid which leads to the disruption of the gene encoding for the virulence M protein. Bell and coworkers hypothesized that **2.1** enhances activity by complementing this genetic defect. To support this idea, it was found that **2.1** did not enhance the replication of a VSV strain with the wild type, functional M-protein. Further, it was found that **2.1** disrupts IFN-induced antiviral effects. This was demonstrated through measuring the output of virus production in glioblastoma U-251 cells with and without IFN-α treatment to induce a strong antiviral response. It was found that **2.1** had the ability to rescue virus activity in the presence of IFN-α.

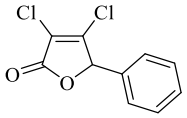

3,4-dichloro-5-phenyl-2,5-dihydrofuran-2-one

Figure 2.2 Structure of **2.1**.

2.2 Results and discussion

As discussed above, **2.1** (3,4-dichloro-5-phenyl-2,5-dihydrofuran-2-one) was reported to have a remarkable ability to potentiate VSVΔ51 replication in highly resistant 786-O cells. Given the potential of this strategy to improve the therapeutic efficiency of oncolytic viral therapeutics, medicinal chemistry based studies were launched. The goal of these studies were to gain better understanding of physicochemical properties and elucidate structure-activity relationships leading to the optimization of this novel class of pharmacoviral compounds.

2.2.1 Physicochemical properties and nature of activity of 2.1

To gain appreciation of the physicochemical nature of **2.1**, a LC/MRM assay was developed to monitor degradation in buffered mouse plasma (Figure 2.3). This assay was based on a published method.[39] **2.1** was found to degrade quickly, with a $t_{1/2}$ of 2.1 minutes.

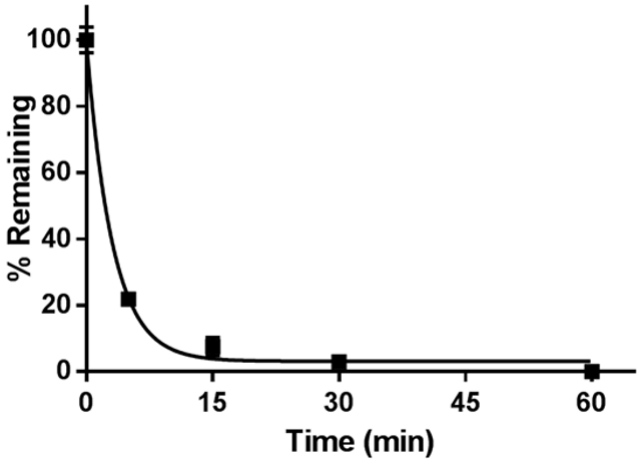

Figure 2.3. Stability of **2.1** in mouse plasma over time measured by LC-MRM.

The short half-life suggests that parent compound **2.1** may not be responsible for the observed enhancement of viral titers. Rather, impartment of activity may be from a degradation

product. To test this hypothesis, **2.1** was incubated in aqueous media for 0 h, 1.5 h, 3 h, or 24 h prior to addition to the cells (Figure 2.4). At 4 h post-treatment the cells were inoculated with a firefly luciferase encoded VSVΔ51 (VSVΔ51-FLuc) and viral output was measured by viral expression units (VEUs) using a luciferase reporter-based titration assay developed by the Diallo lab.[40] It was found that this pre-incubation eliminated the observed enhancement of viral titers, suggesting that the biological activity is likely dependent on the presence of short-lived **2.1**.

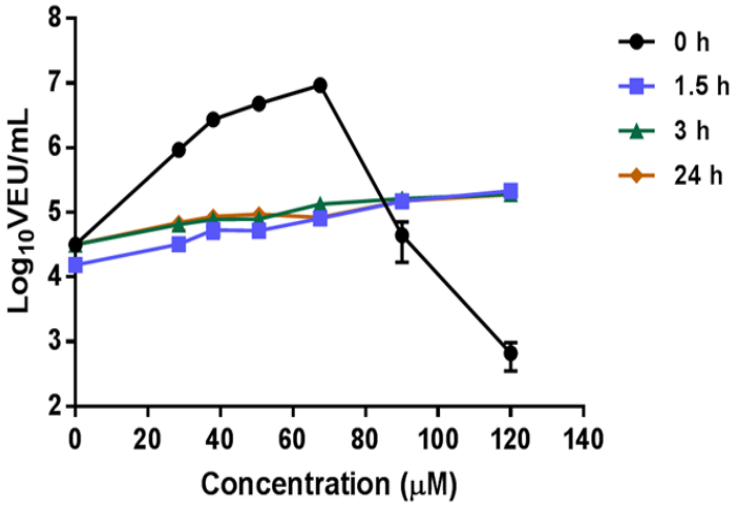

Figure 2.4. Effects of the pre-incubation of **2.1** in sterile water on the ability to enhance viral replication. **2.1** was at different concentrations for 0 h, 1.5 h, 4 h or 24 h before being used to treat 786-O. At 4 h post treatment, cells were infected with VSVΔ51-Fluc at MOI 0.005. 40 h later, VEUs were measured with the luciferase reporter assay.

The inactivity of **2.1** following incubation in simple aqueous media implies that sensitization of the cells to viral infection occurs quickly. To gain appreciation for the speed by which **2.1** functions and to investigate of the importance of sustained chemical pressure, 786-O cells were treated with **2.1** at various concentrations with removal at different time-points (Figure 2.5). The media containing **2.1** was removed and replaced with fresh media at 1 h, 1.5 h, 2 h, 2.5 h and 6 h. **2.1** was not removed in the control experiment. The cells were infected with VSVΔ51-

FLuc at 4 h post-treatment with **2.1**, with exception of the 6 h experiment where the cells were infected immediately following media replacement. VEUs were determined with the luciferase reporter-based titration assay.

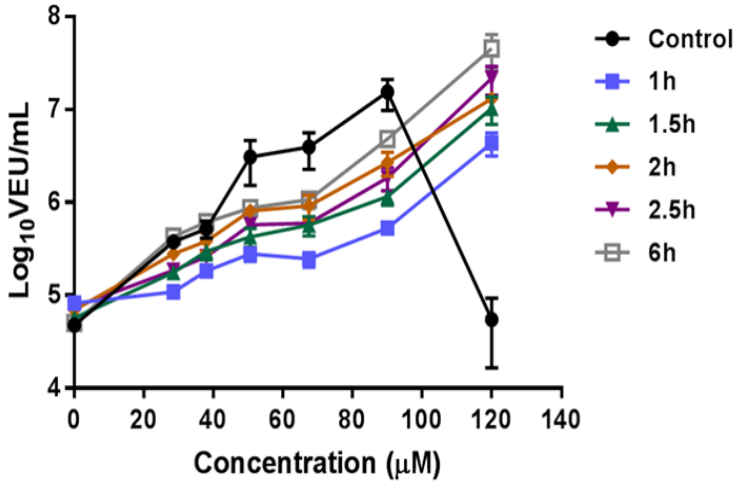

Figure 2.5. Effects of removing **2.1** at various times across various concentrations. 786-O cells were treated with **2.1** at various doses. **2.1** was removed and replaced with fresh media after 1 h, 1.5 h, 2 h, 2.5 h and 6 h. **2.1** was not removed in the control condition. 4 hours post-treatment, cells were infected with VSVΔ51-FLuc at an MOI of 0.005. For the condition where **2.1** was replaced with fresh media 6 h after treatment, infection was performed immediately following media replacement. 40 hours later, VEUs were measured with the luciferase reporter assay.

Sustained activity of **2.1** following removal of the compound suggests the compound functions with an irreversible nature. Interestingly, enhancement of VEUs at higher concentrations outperformed the control experiment where **2.1** was not removed. This suggests that toxicity of **2.1** at high concentration may impede the enhancement of viral replication.

2.2.2 Synthesis of analogs and initial SAR elucidation

The stability and toxicity issues with **2.1** provoked studies with the goal of further developing this class of compounds and identifying analogs with improved stability and toxicity

parameters. A small, diverse library of analogs was synthesized with the goal of revealing structure-activity relationships (SAR) (Scheme 2.1). Exploration of SAR was facilitated by using mucochloric acid, a well described and versatile synthetic building block.[41] Mucochloric acid is an inexpensive and multifunctional compound that has been used to generate a wide range of biologically active compounds including substituted butenolides, butenolactams and 4,5-dichloropyridazin-3(2H)-ones.[42] Under normal conditions mucochloric acid exists in both a cyclized and open-chain form, favouring the cyclized state. Reactivity can be achieved from either isomer, providing access to compounds with diverse scaffolds. For example, **2.1** is synthesized using a Friedel–Crafts acylation reaction from benzene, $AlCl_3$ and mucochloric acid, which reacts in the cyclized form to generate an electrophilic oxonium ion intermediate. Alternatively, the aldehyde of the linear isomer can be reduced with $NaBH_4$, which is then cyclized to yield butenolide **2.5** (Scheme 2.1).

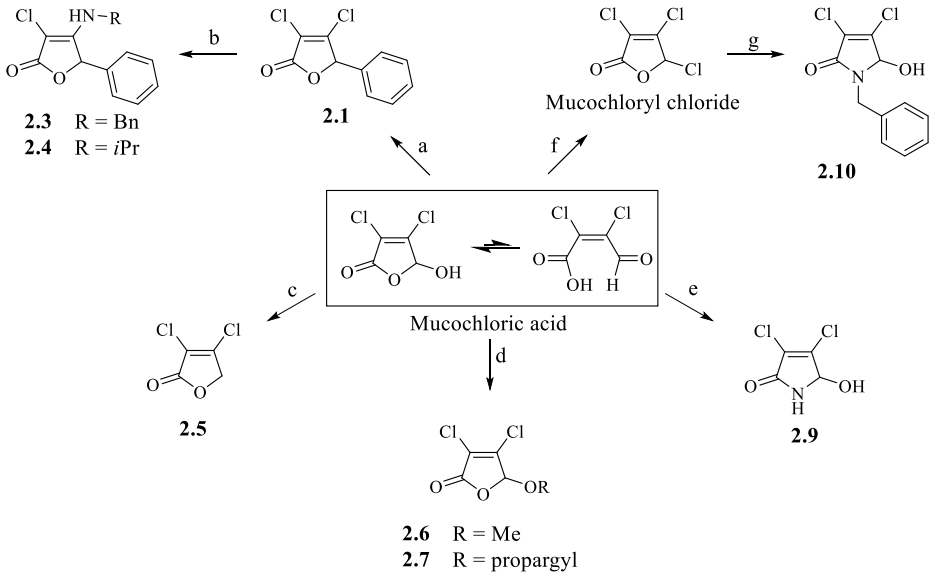

Scheme 2.1. Synthesis of diverse set of analogs of **2.1** starting from mucochloric acid. Conditions: a) $AlCl_3$, benzene, 24 h, rt, 71 %. b) amine, DMF, 16 h, rt, 90 % c) 1. $NaBH_4$, CH_3OH, 0.5 h, 0 °C 2. H_2SO_4, rt, 0.5 h, 85 % d) H_2SO_4 cat., alcohol, reflux, 16 h. e) NH_4OH, Na_2CO_3, H_2O, 0 °C, 84 % f) $SOCl_2$, DMF cat. g) benzylamine, dioxane, rt, 16 h, 58 %.

Evaluation of analog activity was conducted using the luciferase reporter-based titration assay. To control for generational variations of the 786-O cells and the VSVΔ51 virus, the maximal viral enhancing activity was controlled to **2.1**. Assessment of analog cytotoxicity was completed using resazurin to assess the metabolic activity of the cells both in the presence and absence of virus, and is reported as an LD_{50}. The physicochemical stability of the analogs was assessed with two methods. A mouse plasma stability assay was used and is reported as percent remaining after 3 h, as measured by LC-MRM. Further, a glutathione (GSH) challenge assay was adapted from the literature and used to indicate analog susceptibility to nucleophilic attack from a thiol, and is reported as a $t_{1/2}$ in minutes.[43] This data is summarized in Table 2.1.

Brominated analog **2.2** was synthesized from mucobromic acid and displayed a similar stability profile to **2.1** with reduced activity. A substitution/elimination reaction between **2.1** and benzylamine or *iso*-butylamine generated **2.3** and **2.4**, respectively. These compounds had low activity with improved activity in the GSH challenge assay, where no reaction was observed. Reduction of mucochloric acid with $NaBH_4$ generated **2.5**, which allowed for an assessment of the importance of the aromatic group. **2.5** exhibited some activity, with no apparent improvement in stability. Ether-containing analogs **2.6** and **2.7** were synthesized and assessed for tolerability to replacement of the aromatic ring. Commercially available compound **2.8** showed no enhancement of viral titer. Analogs **2.9** and **2.10** were synthesized with the intention that the replacement of the lactone with a lactam would confer a less electrophilic compound. The lactam switch also offers the benefit of introducing a new site of variation on the nitrogen. **2.10** displayed low to moderate activity with a clear improvement in stability in the plasma stability assay.

Table 2.1. Initial structure-activity relationship study.

Compound	Structure	PFE[a]	PFE dose (μM)	LD_{50} (μM)	LD_{50} with virus (μM)	GSH $t_{1/2}$ (min.)	Plasma stability (% remaining)
2.1	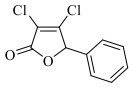	1910	60	79	16	<5	0
2.2	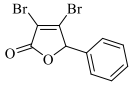	705	72	87	50	<5	0
2.3	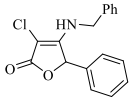	365	96	140	140	NR[c]	65.6 ± 6.5
2.4	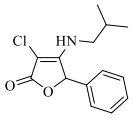	345	80	90	90	NR	0
2.5		515	36	41	27	<5	0
2.6	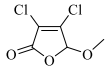	400	60	73	51	<5	0
2.7	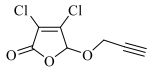	575	60	52	17	<5	0
2.8	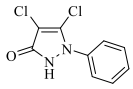	NE[a]	-	>180	>180	NR	88.3 ± 9.3
2.9	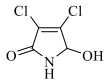	1280	120	148	87	117	0
2.10	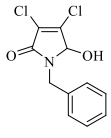	555	48	67	51	32	19.8 ± 0.4

[a] Peak fold enhancement. [b] No enhancement. [c] No reaction.

2.2.3 Investigation of butenolactam derivative activity, stability, and SAR

From early SAR conclusions it was determined that a more detailed characterization of the apparent stability of butenolactam **2.10** was needed. When assessed using the HPLC GSH assay, **2.10** offers another clear stability benefit over **2.1**. While **2.1** degrades into a complex mixture of compounds, **2.10** cleanly reacts to produce the glutathione adduct with loss of a chlorine as the sole product identified by LC-MS (Figure 2.6). Further, **2.10** behaved in a similar fashion to **2.1** with regards to fast sensitization of the cells to a viral susceptible state in an irreversible manner. This was shown in a study of the effects of removing **2.10** at various time points across various concentrations (Figure 2.7).

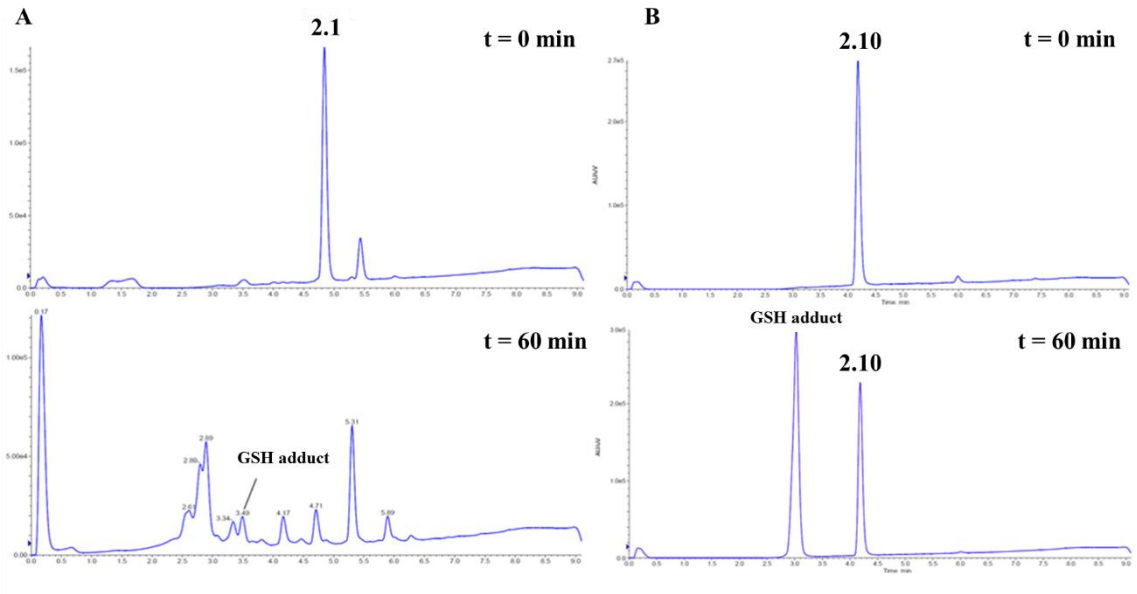

Figure 2.6. GSH stability assay HPLC chromatographs. (A) **2.1** at t = 0 min (top) and t = 60 min (bottom) **a**nd (B) **2.10** at t = 0 min (top) and t = 60 min (bottom).

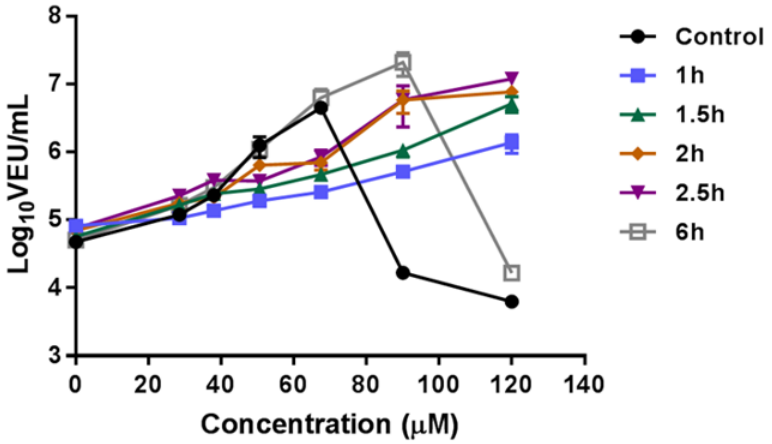

Figure 2.7. Effects of removing **2.10** at various times across various concentrations. 786-O cells were treated with **2.10** at various doses. **2.10** was removed and replaced with fresh media after 1 h, 1.5 h, 2 h, 2.5 h and 6 h. **2.10** was not removed in the control condition. 4 hours post-treatment, cells were infected with VSVΔ51-FLuc at an MOI of 0.005. For the condition where **2.10** was replaced with fresh media 6 h after treatment, infection was performed immediately following media replacement. 40 hours later, VEUs were measured with the luciferase reporter assay.

Encouraged by the discovery of **2.10** as an active analog of **2.1** with improved chemical stability, analogs of **2.10** were synthesized to draw a more detailed picture of SAR around the butenolactam scaffold. The aim was to understand the importance of the different fragments of **2.10** in activity and stability, specifically the dichloro-α,β-unsaturated carbonyl, the hydroxyl group in the 5-position, and alkyl substitution on the amide nitrogen atom.

Table 2.2. Structure-activity relationships of butenolactam derivatives.

Compound	Structure	PFE[a]	PFE dose (μM)	LD_{50} (μM)	LD_{50} with virus (μM)	GSH $t_{1/2}$ (min.)	Plasma stability (% remaining)
2.11	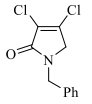	55	240	332	332	64	42.5 ± 9.6
2.12	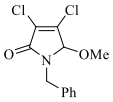	535	180	206	203	118	47.6 ± 1.4
2.13	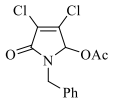	305	60	61	45	21	0
2.14	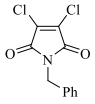	75	96	91	85	<5	70.2 ± 8.4
2.15	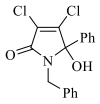	NE[b]	-	66	66	340	14.9 ± 7.1
2.16	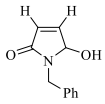	NE	-	>360	>360	NR[c]	98.2 ± 3.7
2.17	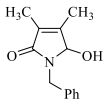	NE	-	>360	>360	NR	82.0 ± 10.2
2.18	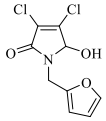	475	60	67	28	45	54.1 ± 5.1
2.19	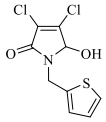	975	60	64	27	40	50.1 ± 10.5
2.20	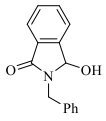	NE	-	>360	>360	NR	102.9 ± 1.6
2.21	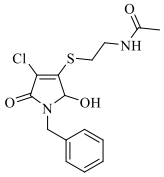	55	504	630	567	NR	102.7 ± 10.8

[a] Peak fold enhancement. [b] No enhancement. [c] No reaction.

From the tabulated data it was concluded that establishment of an ether-linkage through the hydroxyl group in the 5- position was tolerated, as shown with **2.12**. Other variations at the 5-position such as removal of the hydroxyl completely (**2.11**), the introduction of a second carbonyl group to afford a dichloromaleimide derivative (**2.14**), or the introduction of quaternary substituted carbon (**2.15**) were not tolerated. Examples **2.16**, **2.17**, **2.20** and **2.21** support the conclusion that the disruption of the dichloro-α,β-unsaturated carbonyl moiety is not tolerated. This implies that the ability of these compounds to act as a Michael-acceptor is important for exerting biological activity. Replacement of the *N*-benzyl group with alternate aromatic rings such as a furan **2.18** or a thiophene **2.19** was tolerated and suggests that variation at this position could be used to tune physicochemical properties without disruption of the moiety necessary for compound activity.

2.2.4 *N*-substitution on the 3,4-dichloro-5-hydroxy-*1H*-pyrrole-2-(*5H*)-one core

A thorough investigation of the SAR of **2.10** suggested that the presence of the dichloronated α,β-unsaturated carbonyl was imperative for activity. The use of a lactam was also preferred as this offered significant benefits to chemical stability over the lactone. Removal of the 5-hydroxyl group or alternate substitution did not lead to improvement of compound parameters of interest. Moving forward with the goals of structure optimization and exploration of SAR, focus was shifted to the *N*-substitution group of the amide. This site of variation is physically removed from the electrophilic dichloro-α,β-unsaturated carbonyl fragment believed to be necessary for activity. Thus, it was hypothesized that variation at this site could be used to tune physicochemical parameters with minimal risk of disrupting biological target engagement. Phenotypic activity cell-based assays, such as the luciferase titration assay, provide a holistic assessment of parameters important for activity including cell permeability, target binding, compound toxicity, biological

stability, and off-target reactivity. Compounds containing the 3,4-dichloro-5-hydroxy-*1H*-pyrrole-2-(*5H*)-one scaffold can be synthesized from mucochloric acid in a two-step procedure (Scheme 2.2).[44] Mucochloryl chloride is generated from mucochloric acid, thionyl chloride and catalytic DMF. The introduction of a primary amine to the pseudo-acid chloride in dioxane affords the desired corresponding *N*-substituted derivative. Employing this route, a large library of analogs were synthesized (Table 2.3).

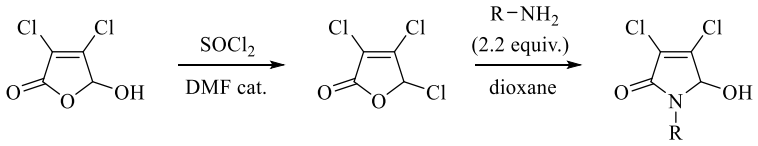

Scheme 2.2. General route for synthesis of compounds with the 3,4-dichloro-5-hydroxy-1H-pyrrole-2-(5H)-one scaffold.

Compounds **2.22** – **2.28** had complete replacement of the benzyl fragment. This included simple saturated and unsaturated alkyl substitutions (**2.22** – **2.27**), and incorporation of a solubilizing morpholine moiety **2.28**. Further, a set of compounds (**2.29** – **2.33**) were synthesized to explore the effects of alkyl spacing between the electrophilic lactam core and the benzene ring. Secondary amines were used to generate **2.34** and **2.35** to probe the effects of alkyl substitution at the benzyl position. Compounds **2.36** – **2.48** were synthesized and tested to explore the effects of various substitution on the aromatic group. Pyridine containing compounds **2.49** – **2.51** were also prepared.

Noteworthy, cyclopropyl derivative **2.25** and morpholine containing **2.28** displayed retained activity with improved *in vitro* toxicity and stability profiles. Two or three carbon spacing between the electrophilic core and the benzyl group was noted to be favourable, as in **2.29** and **2.30**. 4-trifluoromethyl substituted **2.40** displayed the highest activity of all analogs tested (2005

fold enhancement of PFE, 105 % of **2.1**) and had desired stability properties. These results allowed us to conclude that a variety of *N*-substitution is tolerated on the amide, and can be used to tune compound activity, toxicity, stability, and physicochemical properties.

Table 2.3. Structure-activity relationships of *N*-substituted butenolactam derivatives.

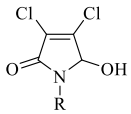

Compound	R	PFE[a]	PFE dose (μM)	LD_{50} (μM)	LD_{50} with virus (μM)	GSH $t_{1/2}$ (min.)	Plasma stability (% remaining)
2.22		895	96	119	76	68	72.0 ± 3.0
2.23		1105	120	171	89	ND[b]	ND
2.24		915	120	174	96	61	91.6 ± 5.2
2.25		1415	80	127	51	53	54.8 ± 3.6
2.26		995	96	110	66	46	64.8 ± 7.7
2.27		40	48	100	87	21	9.0 ± 1.4
2.28	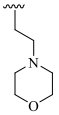	1910	80	153	55	96	38.9 ± 5.2
2.29		975	72	74	27	74	57.6 ± 6.6
2.30		1090	32	36	20	50	42.9 ± 7.2
2.31	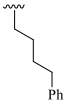	495	40	40	34	72	40.1 ± 9.8

[a] Peak fold enhancement. [b] No data

Table 2.3 continued. Structure-activity relationships of *N*-substituted butenolactam derivatives.

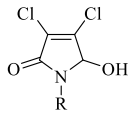

Compound	R	PFE[a]	PFE dose (μM)	LD_{50} (μM)	LD_{50} with virus (μM)	GSH $t_{1/2}$ (min.)	Plasma stability (% remaining)
2.32	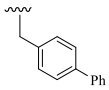	210	27	28	5	24	ND[b]
2.33		575	18	18	12	24	0
2.34		630	72	74	6	31	48.0 ± 16.5
2.35	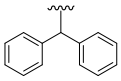	265	27	36	23	43	63.8 ± 3.2
2.36	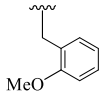	55	72	56	56	34	28.2 ± 2.6
2.37		1070	48	58	38	41	0.7 ± 0.1
2.38		670	216	215	107	32	25.7 ± 2.9
2.39	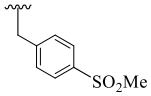	975	60	90	25	34	41.4 ± 5.4
2.40	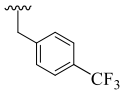	2005	27	36	13	32	15.3 ± 2.5
2.41	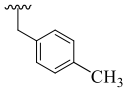	365	40	39	30	35	51.4 ± 8.2

[a] Peak fold enhancement. [b] No data

Table 2.3 continued. Structure-activity relationships of *N*-substituted butenolactam derivatives.

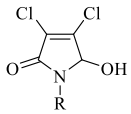

Compound	R	PFE[a]	PFE dose (μM)	LD_{50} (μM)	LD_{50} with virus (μM)	GSH $t_{1/2}$ (min.)	Plasma stability (% remaining)
2.42	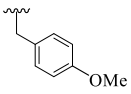	190	40	55	17	40	49.1 ± 12.4
2.43	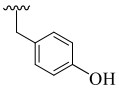	285	60	90	45	69	58.3 ± 0.6
2.44		155	60	63	39	31	45.9 ± 8.1
2.45	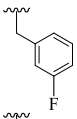	115	48	43	37	31	54.2 ± 4.2
2.46	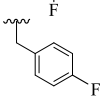	170	40	42	36	32	23.1 ± 0.8
2.47	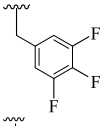	190	40	36	35	35	22.7 ± 8.4
2.48	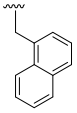	1240	32	38	24	14	36.5 ± 7.6
2.49		590	96	131	67	64	44.6 ± 1.2
2.50		800	60	85	29	54	39.6 ± 2.6
2.51		590	72	89	28	53	44.0 ± 1.0

[a] Peak fold enhancement.

2.2.5 Selectivity of viral enhancement in ex vivo tissue specimens

Therapeutic safety is one of the most appreciated advantages that oncolytic viral therapy holds over traditional cytotoxic cancer treatment strategies. Oncolytic viruses are generally selective for cancer cells, causing mild side effects in humans. As the goal of this project was to develop compounds that enhance attenuated viral replication, it was important to ensure that co-treatment with these small molecules does not lead to viral enhancement in healthy cells, and that a large therapeutic index is maintained.

A subset of analogs (**2.1**, **2.10**, **2.28** – **2.30** and **2.40**) were chosen to be tested for their capability of enhancing VSVΔ51 oncolytic activity in different *ex vivo* tissue samples. This assay is an established method developed and published by the Diallo lab.[45] CT26 murine colon cancer tumors, known to be resistant to VSVΔ51 infection, along with normal mouse brain, lung and spleen tissues were excised and cored from Balb/c mice. Viable cores were treated with each compound in triplicate at an optimized concentration determined through the titer assay. At 4 h following compound administration, the tissues were infected with 1×10^4 plaque-forming units of VSVΔ51 expressing green fluorescent protein (VSVΔ51-GFP). Virus replication was assessed by fluorescence microscopy 24 h post-infection. Representative images are shown in Figure 2.8 A. At 36 h post infection, the infected cores and supernatants were collected, homogenized and titered by plaque assay (Figure 2.8 B-G). Both microscopy images and viral titers indicate that these compounds do not enhance oncolytic viral propagation in the normal tissues.

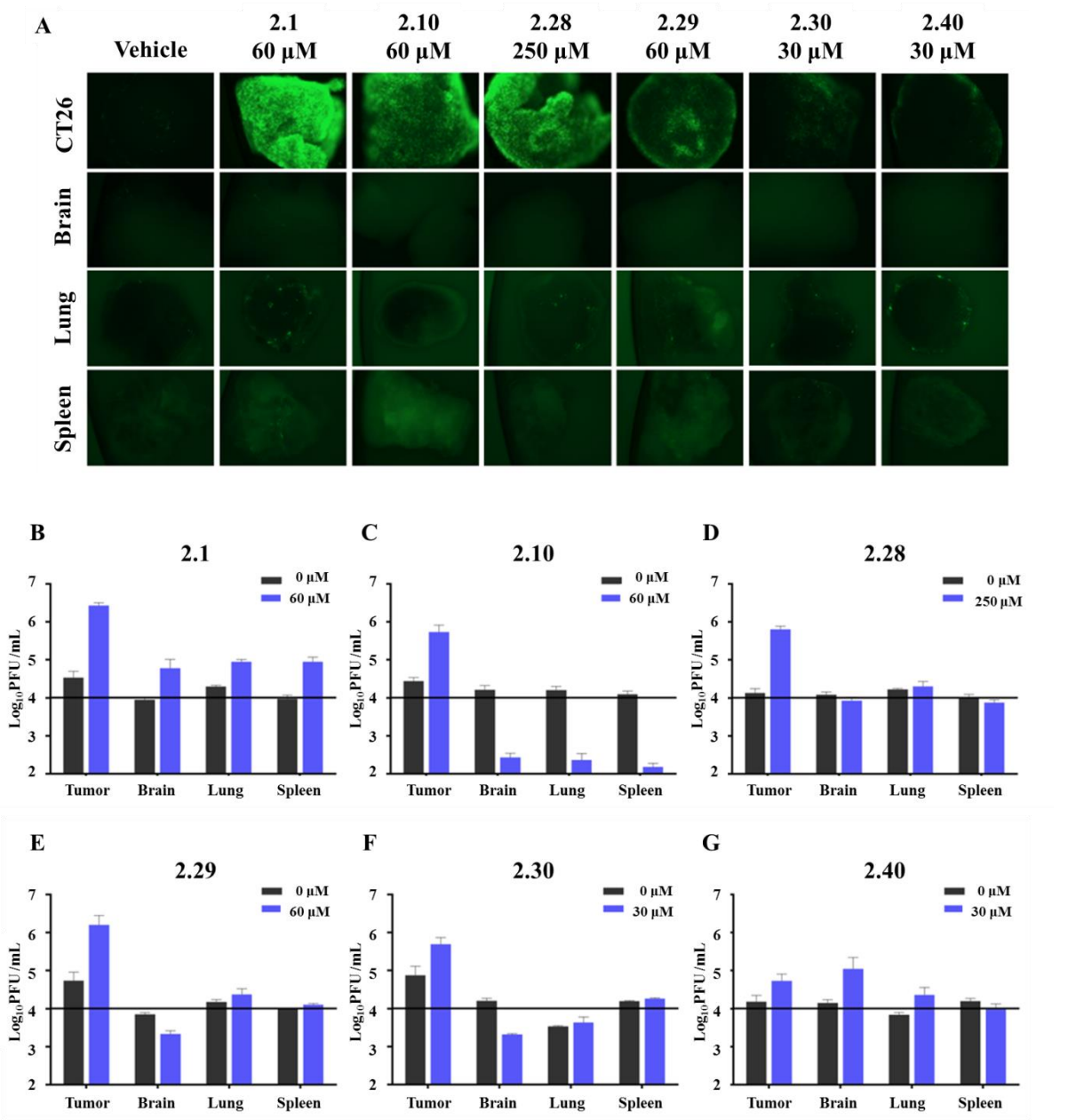

Figure 2.8. Compound **2.1** and analogs selectively enhance the replication of oncolytic VSV in ex vivo tumor tissues. (A) Representative images of VSVΔ51-GFP expression in CT26 tumor, brain, lung and spleen tissues assessed by fluorescence microscopy 24 h post-infection. (B-G) Quantification of VSVΔ51-GFP plaque forming units (PFU) by standard plaque assay. Graphs show the sum of infectious titer from core and supernatant for each compound in each tissue type. Doses shown are those that are depicted in panel A. The horizontal black line on each graph at $1x10^4$ PFU /mL represents the amount of VSVΔ51-GFP used to initially infect each core.

2.2.6 Dose escalation of analogs in vivo

After establishing analog efficacy *in vitro* and tissue selectivity *ex vivo*, it was desirable to determine the *in vivo* tolerability of the compounds in mice. Tolerability can be assessed using dose escalation studies, where groups of mice are administered a compound at various doses to identify the maximum dose of a compound that does not cause unacceptable side effects. **2.1**, **2.10**, **2.24** and **2.28** were selected for this study (Figure 2.9). Each compound was administered intraperitoneally to normal Balb/c mice and mouse body weight was monitored over time. As an endpoint, the mice were sacrificed if they reached a 20 % decrease of body weight or if they exhibited significant signs of toxicity. Interestingly, **2.1** was toxic at the lowest dose tested, 10 mg/kg, and none of the mice survived past three days. **2.10** was well tolerated up to 50 mg/kg, with toxicity exhibited at 100 mg/kg. Compounds **2.24** and **2.28** were well tolerated, with no toxic effects apparent at a dose as high as 100 mg/kg, the highest tested in this experiment. As demonstrated previously with the HPLC assay, the optimized analogs form a predictable addition/elimination product in the presence of a nucleophile. In contrast, **2.1** degrades into a complex mixture of products. This difference suggests that it is possible that **2.1** degrades into or is metabolized into toxic compounds that are not formed from the butenolactam-based analogs. This result further supports the use of the optimized analogs for further studies *in vivo*.

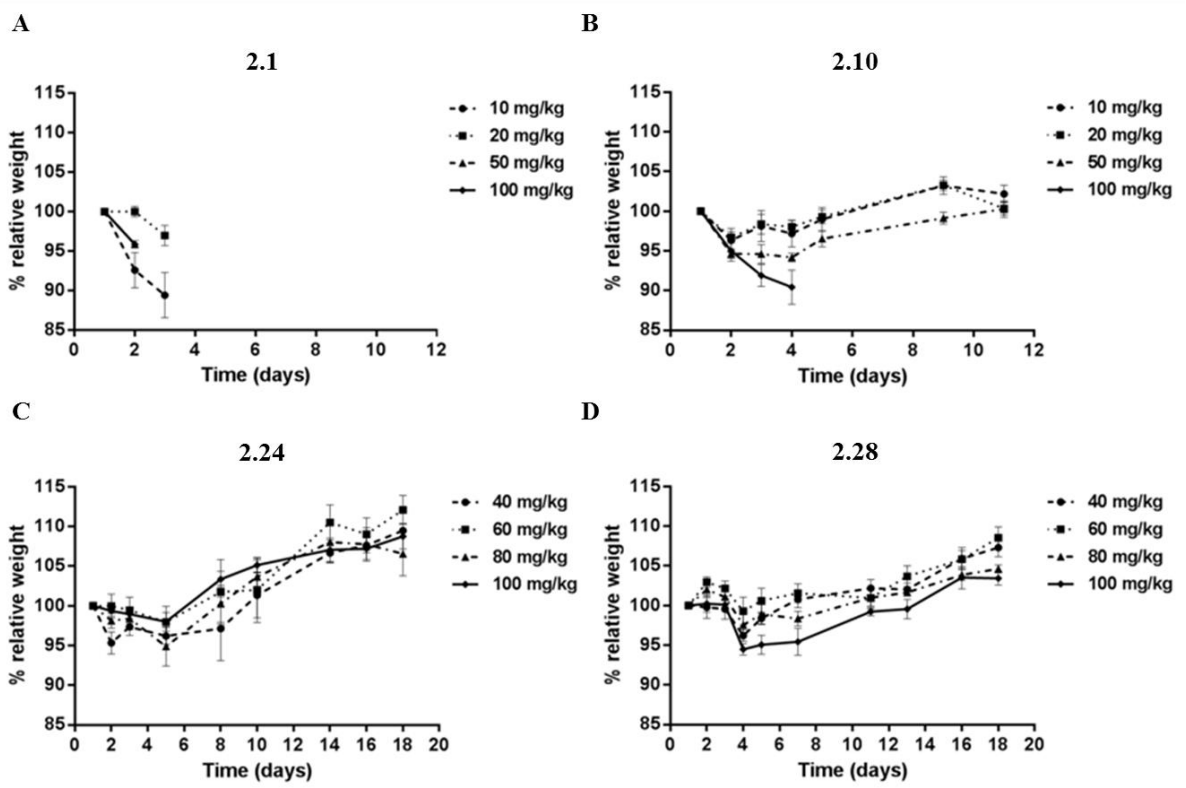

Figure 2.9. Dose escalation of **2.1**, **2.10**, **2.24** and **2.28** in mice. Balb/c mice were given (A) **2.1**, (B) **2.10**, (C) **2.24**, or (D) **2.28** dissolved in DMSO via intraperitoneal administration. Five mice were assigned to each dose group for each compound. The dose was adjusted for individual mice based on weight. Graphs stop when the first mouse in the group was euthanized. (A-B) Mice were injected on Day 1 and weights were recorded over a 10 day period. (C-D) Mice were injected on Day 1, 3 and 5. Weights were recorded over an 18 day period. For all groups, weights are reported relative to initial weight on Day 1.

2.2.7 Enhancement of VSVΔ51 in vivo

Due to its high *in vitro* and *ex vivo* activity and as it was shown to be highly tolerated in mice, **2.28** was selected for *in vivo* efficacy studies. The goal of this experiment was to evaluate **2.28** for the ability to enhance oncolytic viral expression in tumors in mice. Balb/c mice were subcutaneously engrafted with CT26 cells and treated intra-tumorally with VSVΔ51-FLuc alone or in combination with **2.28**. To assess viral replication, an *in vivo* imaging system (IVIS) was used to detect luciferase expression. Gratifyingly, treatment with **2.28** led to a significant enhancement of VSVΔ51-FLuc replication-associated luciferase expression specifically in the

tumor (Figure 2.10). The use of **2.28** resulted in a 14-fold increase the detected luminescence. This validates the proposed pharmacological strategy toward enhancement of oncolytic viruses *in vivo*.

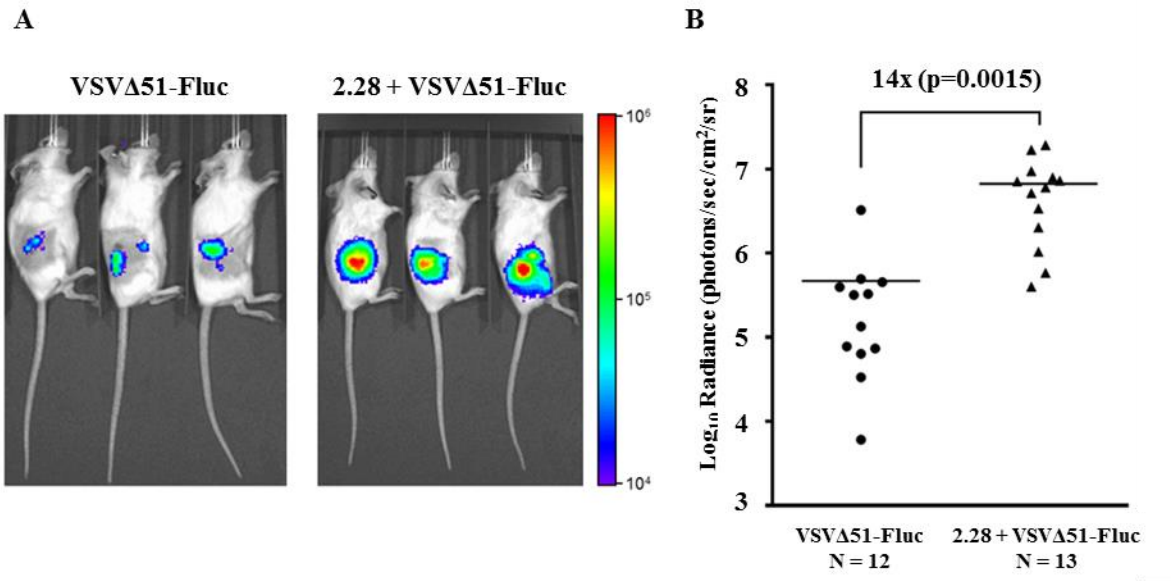

Figure 2.10. In vivo assessment of **2.28** for enhancement of VSVΔ51 in a resistant tumor model. (A) VSVΔ51-resistant CT26 cells were subcutaneously engrafted into female Balb/c mice. After 11 days, mice were given 30 μL of vehicle (DMSO), or 40 mg/kg of **2.28** by intratumoral injection. Four hours later, mice were treated with $1x10^8$ plaque-forming units of VSVΔ51-FLuc. Virus replication was monitored Twenty-four hours later by measuring luminescence using an IVIS (representative images are shown, color scale bar represents photons) and (B) tumor radiance was quantified.

2.2.8 Potentiation of other oncolytic viruses and viral-platforms

With the goal of uncovering further applications and the limitations of this novel class of compounds, it was desirable to test for the capability of enhancing viral activity with different virus platforms. While all compound optimization was completed with oncolytic VSVΔ51 virus, these compounds may prove useful for other viral systems if they inhibit broad and general antiviral mechanisms. Compounds **2.1**, **2.10**, **2.27** and **2.26** were tested for their ability to enhance a green fluorescent protein encoded herpes simplex-1 virus (HSV-N212eGFP) (Figure 2.11 A).

HSV titers were then determined 48 h following infection (Figure 2.11 B). A dose dependent response was observed with **2.10** leading to the greatest enhancement at over 3 log units greater plaque forming units.

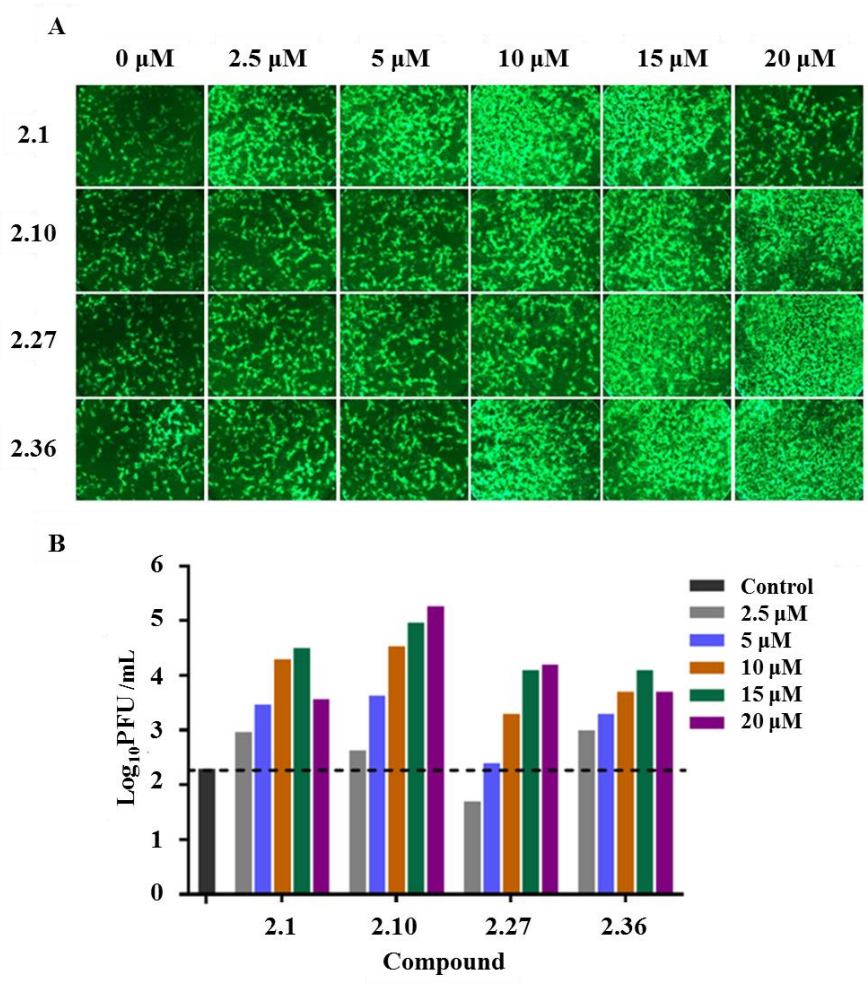

Figure 2.11. Enhancement of oncolytic HSV-1 in mouse mammory carcinoma 4T1 cells. (A) Cells were left untreated or treated with **2.1**, **2.10**, **2.27**, or **2.36** at various concentrations: 2.5 µM, 5 µM, 10 µM, 15 µM or 20 µM. HSV-N212eGFP was then added at MOI 0.005. eGFP fluorescence was detected 48h after HSV infection. (B) HSV titers were determined 48h after infection.

Further, it was shown that these compounds had the ability to enhance a Maraba MG-1 virus in 4T1 cells (Figure 2.12). The cells were exposed to **2.1**, **2.10** or **2.38** at various

concentrations. After 4 h, cells were infected with Maraba MG1 or VSVΔ51. Viral efficacy was assessed by measuring the cytotoxicity with resazurin.

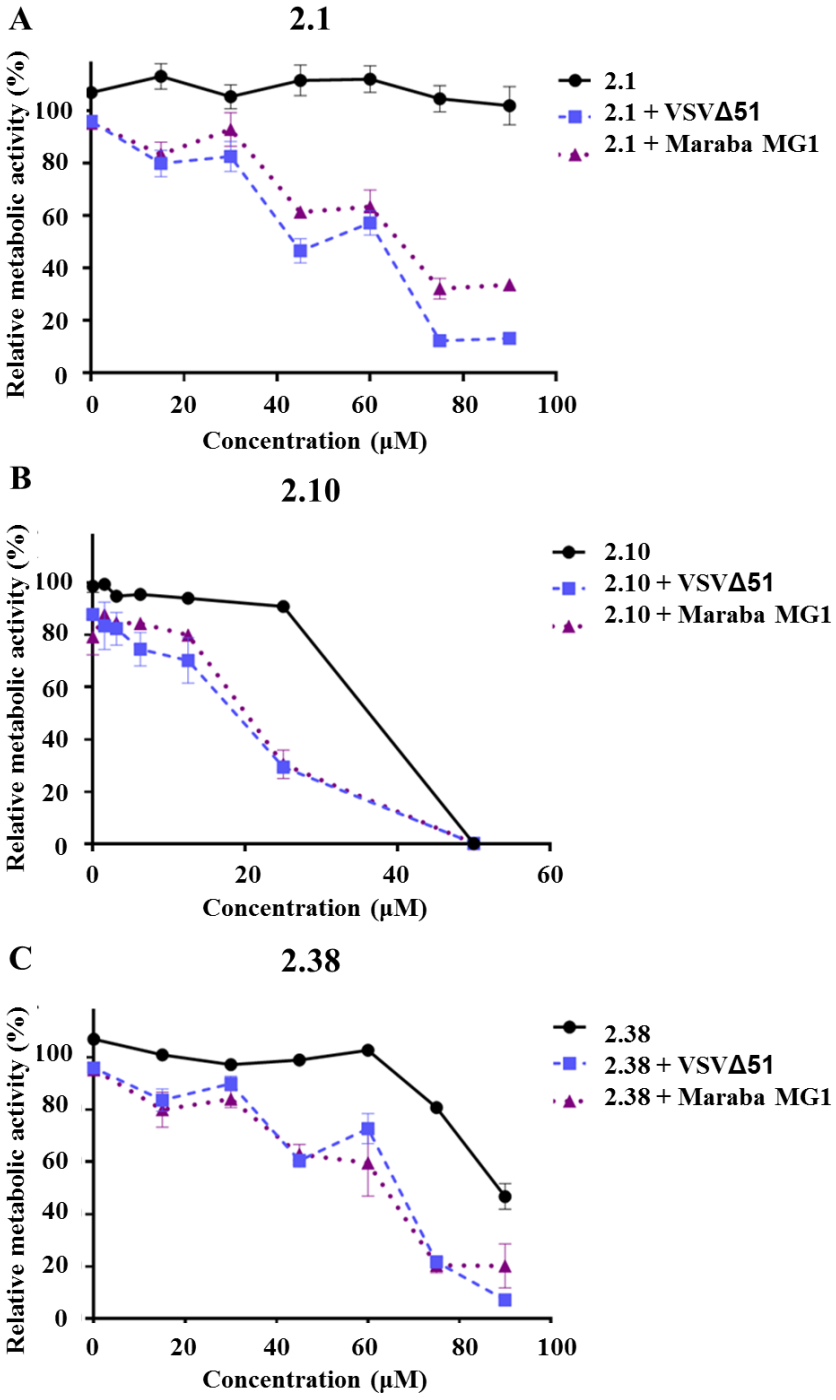

Figure 2.12. Analogs of **1.1** enhance oncolytic VSV activity in murine breast cancer cells (4T1). Murine mammary carcinoma (4T1) cells were treated with vehicle, (A) **2.1**, (B) **2.10**, or (C) **2.38** for 4h at the specified concentrations. 4 hours later, cells were infected with VSVΔ51 or Maraba

MG1 at MOI 0.005. 40 hours post-infection, cytotoxicity was assessed by incubating samples with alamarBlue® for 2 h at 37 °C before measuring fluoresence (530nm excitation, 590 nm emission). Values were normalized to that of untreated controls.

Moving forward, the use of these compounds for the ability to enhance the activity and therapeutic efficiency of gene therapy vectors was investigated. Currently, there are numerous clinical trials employing replication-defective gene therapy vectors which express therapeutic transgenes. It was hypothesized that the inhibition of general immune systems responsible for the disruption of viral activity may lead to enhanced transgene expression of adeno-associated virus serotype 2 expressing luciferase (AAV2-luc) and adenovirus serotype 5 expressing luciferase (Ad5-luc).

It was demonstrated that **2.10** had superior activity to **2.1** in the ability to enhance both replication-deficient viruses in A549 cells as measured by RLU (Figure 2.13). AAV2-luc expression of firefly luciferase was increased more than 25-fold with **2.10** at 50 μM. Ad5-luc expression of firefly luciferase was increased by more than 15-fold with 80 μM treatment of **2.10**. These results extend the use of these compounds to gene therapy applications and support the hypothesis that these compounds target important, broad antiviral cell defense mechanisms.

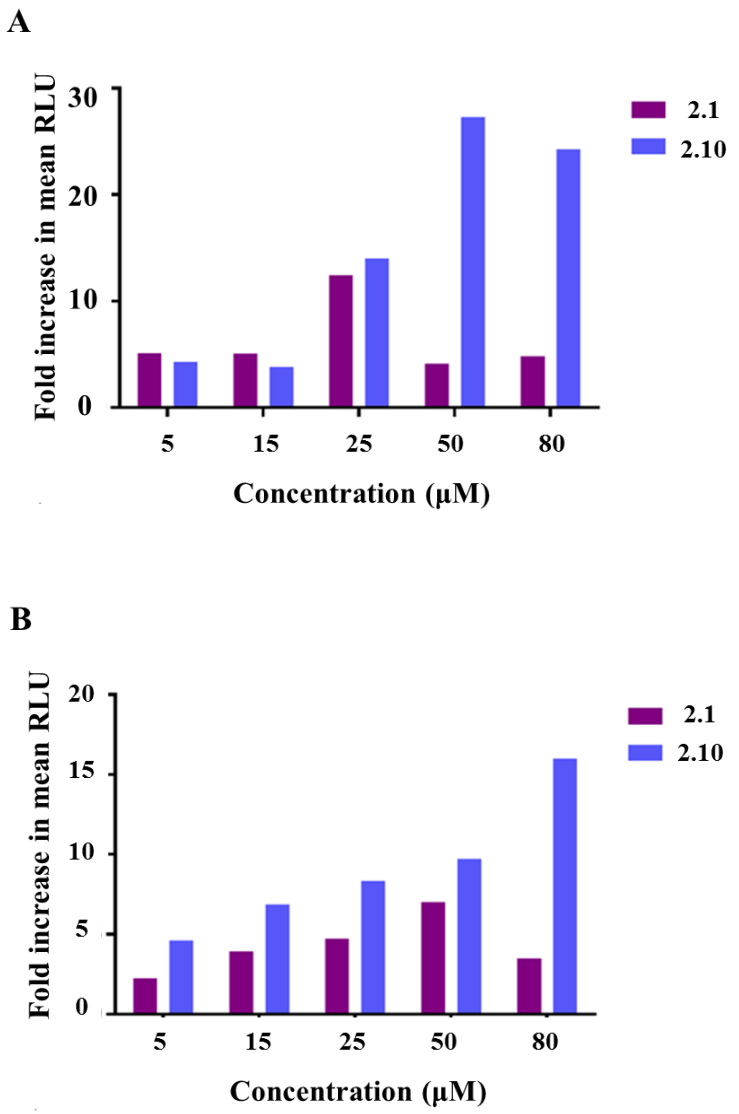

Figure 2.13. 2.1 and **2.10** enhance the transduction of non-replicating gene therapy vectors in human lung carcinoma cells. Human lung carcinoma (A549) cells were treated with **2.1** or **2.10** at various concentrations. 4 hours later, cells were infected with (A) replication defective adeno-associated virus expressing firefly luciferase (AAV2-luc) or (B) replication defective adenovirus expressing firefly luciferase (Ad5-luc) at an MOI of 1. 24 hours later, luciferase activity was measured. Data is represented as the fold increase in mean relative light units of treated samples versus untreated controls.

2.2.9 Analogs of 2.1 disrupt interferon induced antiviral effects

The activity of initial hit compound **2.1** was discovered through a high-throughput phenotypic cell based assay and the exact biological target(s) are unknown. The results of this

paper discussed in section 2.1.8 points toward the disruption of interferon-induced antiviral response mechanisms. Because the advanced analogs contain distinct structural motifs and stability properties from **2.1**, it was desirable to confirm that an association with the interferon response system persists. 786-O cells were left untreated or treated with **2.1**, **2.2**, **2.10** or **2.28** and the innate cellular antiviral response was activated with the addition of IFN-β (Figure 2.14). After 4 h, the cells were challenged with VSVΔ51-GFP. The virus was titered to determine plaque forming units at 48 h post infection. All compounds tested were shown to have the ability to rescue viral replication in cells with activated interferon response systems.

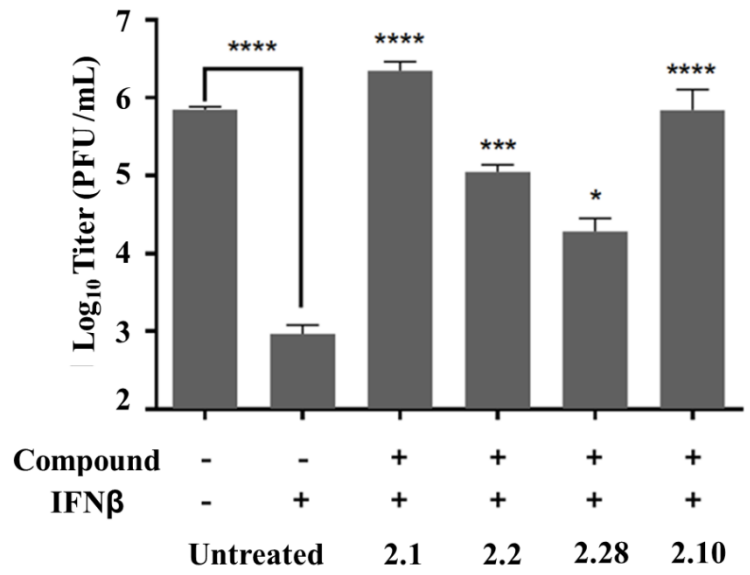

Figure 2.14. Interferon-induced antiviral response is overcome by **2.1** and analogs. Human renal carcinoma (786-O) cells were co-treated with compound and IFN-β for 4 hours and then challenged with VSVΔ51-GFP at MOI 0.01. Samples were titered 48 post-infection. *p = 0.0109, ***p = 0.001, ****p = <0.0001 (one-way ANOVA with Dunnett's multiple comparisons test), Error bars represent standard error.

2.2.10 LC-MRM detection of analogs in tumors

One of the most important improvements to the physicochemical parameters of this class of oncolytic virus potentiating compounds is the vastly improved chemical stability. Although it has been shown that these compounds rapidly sensitize cells to viral infection with a sustained effect, **2.1** rapidly degrades in aqueous physiological conditions. This makes it difficult to study the pharmacokinetic properties of compound, and limits administration to direct injection (ie. intratumoral). It was hypothesized that the advanced analogs identified from the SAR studies would have more favourable stability properties allowing for temporal detection of the compound in the tumor tissue.

Mice with CT26 tumors were injected intratumorally with either 50 mg/kg of **2.1**, **2.10** or **2.24**. Tumors were excised at various time points and analyzed for the presence of each compound by LC-MRM. Not surprisingly, **2.1** was not detected (Data not shown). **2.10** and **2.24** had a persistent presence in the tumors and can be detected for up to at least 3 h (Figure 2.15).

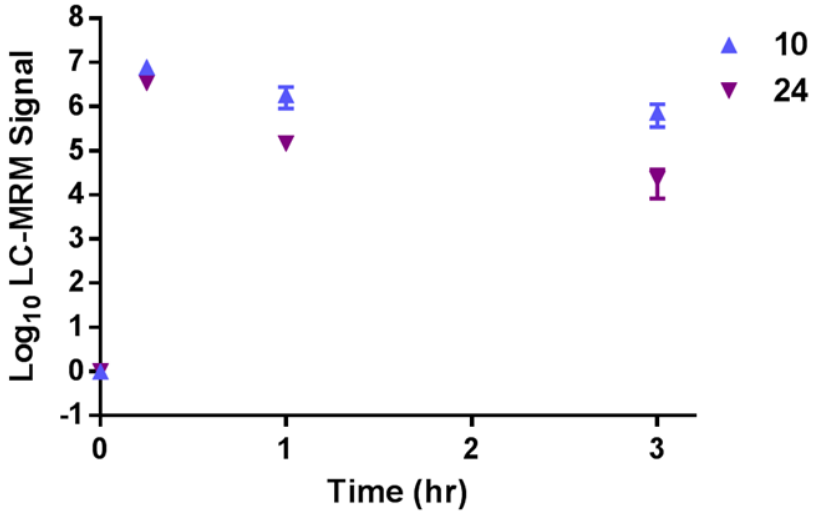

Figure 2.15. Compounds **2.10** and **2.24** can be detected in the tumor following intratumoral injection. Mice (N = 1 per timepoint) bearing subcutaneous CT26 tumors were injected intratumorally with 50 mg/kg of **2.10** or **2.24**. Tumors were excised at various times post-injection and analysed for the presence of compound by LC-MRM.

2.3 Summary and outlook

In summary, important medicinal chemistry-based studies have been completed to develop a novel class of compounds that potentiate oncolytic virus efficacy. *In vitro*, *ex vivo* and *in vivo* assays were employed to understand and characterize biological activity.

Following the identification of **2.1**, a library of compounds (**2.2** – **2.51**) was synthesized to elucidate SAR and identify the optimized 3,4-dichloro-5-hydroxy-*1H*-pyrrole-2-(*5H*)-one core. It has been shown that active analogs can be generated with drastically improved physicochemical properties, including improved temporal mouse plasma stability and minimized nucleophilic susceptibility. Optimized analogs were also shown to have a more predictable degradation profile when compared to **2.1**. The biological activity of these compounds was probed, showing that they rapidly sensitize the cells to viral infection, and do so with a sustained and irreversible nature. *Ex vivo* tissue studies then showed that these compounds preferentially enhance viral activity in tumor tissue over normal tissues, highlighting the therapeutic safety of this system. Further safety studies included dose escalation experiments in mice. This demonstrated that the optimized analogs were much more tolerated *in vivo* compared to **2.1**. It was then showed that an intratumoral injection of **2.28** preceding infection enhanced VSVΔ51 replication efficacy in CT26 tumors in mice, validating this approach to improving oncolytic viral therapy.

In addition to modulating VSVΔ51, this class of compounds was shown to enhance the activity of other oncolytic virus systems including HSV-1 and Maraba MG-1. Broadening the use of these compounds to other viral-platforms, the efficiency of replication-deficient gene therapy vector transgene expression was also enhanced when cells were pre-treated with these compounds. Towards understanding the mechanisms by which the compounds impart activity, optimized compounds were shown to disrupt the interferon-associated antiviral defense systems.

Looking forward, these experiments lay the foundation for additional investigations of using this class of compounds to enhance oncolytic viral therapy. The improved stability and elucidated SAR should facilitate important chemical biology studies into the mechanism of action of these compounds. The identification of the biological targets and pathways affected by inhibition should promote future use of small molecules in synergy with oncolytic viruses.

2.4 Experimental Section

2.4.1 Cell lines

786-O (human renal carcinoma), A549 (human lung adenocarcinoma), Vero (monkey kidney), CT26 (murine colon carcinoma), 4T1 cells (murine mammary carcinoma), and B16F10-LacZ (murine melanoma) cells were obtained from the American Type Culture Collection (Manassas, VA) and maintained in Dulbecco's Modified Eagle's medium (Corning, Manassas, VA) supplemented with 10% fetal bovine serum (Sigma-Aldrich, St Louis, MO) and buffered with 30 mM Hepes (Thermo Fisher Scientific, Waltham, MA). All cell lines were incubated at 37 °C with 5% CO_2 in a humidified incubator.

2.4.2 Viruses

Oncolytic Rhabdoviruses

VSVΔ51 is a recombinant variant of the Indiana serotype of VSV harbouring a deletion of the 51st methionine in the M protein. VSVΔ51 expressing green fluorescent protein (GFP) or firefly luciferase (FLuc) are recombinant derivatives of VSVΔ51 that have been previously described.[20] Maraba MG-1 as described was obtained from Dr David F. Stojdl.[46] All virus stocks were propagated in Vero cells, purified on Optiprep gradient and titered on Vero cells as previously described.[47]

Oncolytic Herpes simplex-1

HSV-1 N212 (an ICPO-deleted oncolytic strain) expressing GFP was obtained from Dr. Karen Mossman and has been described previously.[48] HSV-1 samples were titered on Vero cells. Vero cells (2.5×10^5 cells) were infected with serial dilutions of virus containing samples in 12-

well dishes. Cell were incubated at 37 °C for 1 h, after which the inoculum was removed and replaced with fresh culture media. After a 48 h incubation at 37 °C, GFP positive plaques were visualized and counted.

Non-replicating vectors

AAV2-luciferase (adeno-associated virus serotype 2 expressing luciferase) was obtained from Dr. Sarah Wootton (University of Guelph) and Ad5-luciferase (adenovirus serotype 5 expressing luciferase) was obtained from Dr. Jack Gauldie (McMaster University).

2.4.3 Luciferase reporter-based viral titration assay

This assay has previously been described in detail.[40] Briefly, 786-O cells were seeded in 96-well plates at a density of $3x10^4$ cells/100 μL/ well and allowed to adhere over a 24 h period. Cells were then pre-treated for 4 h with control vehicle (DMSO) or compound at various concentrations and subsequently infected with VSVΔ51-FLuc at a multiplicity of infection (MOI) of 0.005. Forty hours later, 25 μL of 786-O supernatant from each well was transferred into corresponding wells containing a confluent monolayer of Vero cells. At the same time, known amounts of virus (starting at $1x10^8$ plaque forming units (pfu) and decreasing by 1 log unit to 10 pfu) were added to Vero cells to generate a standard curve. Plates were centrifuged at 1400 rpm for 5 minutes and then incubated for 5 h at 37 °C. Luciferase expression was then measured and bioluminescence was expressed in mean relative light units (mRLU; SynergyMx Microplate Reader, BioTek). To generate the standard curve, mRLU was plotted against known input pfu. Four-parameter non-linear regression analysis generated a Hill plot from which unknown input pfu (estimate of viral titer) was interpolated. Data transformation was conducted in R. These

estimated titers are termed “viral expression units” (VEU). After supernatant transfer as described, cytotoxicity of compounds was assessed by incubating 786-O cells with alamarBlue® (AbD Serotec) as per the manufacturer’s instructions. After 2.5 h, fluorescence was measured (530 nm excitation and 590 nm emission) on a Fluoroskan Ascent Microplate Fluorometer (Thermo Scientific, Hudson, NH). Emission values were normalized to that of untreated controls.

2.4.4 Glutathione stability experiment

Glutathione stability was assessed using an assay adapted from a recently reported method.[43] 250 μL of a 40 mM DMSO stock solution of each compound was added to L-glutathione (15.4 mg, 5 mol equiv.) suspended in 250 μL of DMSO. The resulting mixture was placed in a 37 °C shaker. 10 μL aliquots were removed and quenched in 990 μL of water (containing 0.5% formic acid) at various time points, including at t = 0 min, for analysis by ESI-LC-MS. All ESI-LC-MS analyses were collected on an API2000 LC/MS/MS System (Applied Biosystems) equipped with a turbo-ion spray ESI probe interfaced with a Prominence UFLC (Shimadzu) equipped with a reverse phase BDS Hypersil C18 50 × 2.1 mm column, particle size 3 μm (Thermo Scientific). HPLC/LCMS UV absorption was monitored at 254 nm and 210 nm. Both the compound and the glutathione adduct were identified by MS. Area of the UV peak was recorded for each time point.

2.4.5 Plasma stability assay

10 mM methanol stock solutions of each analog were prepared and diluted to 1 μM with aqueous 0.1% formic acid. 5 μL of the diluted solution was inserted into a Proxeon nanoelectrospray emitter (Thermo Scientific, Odense, Denmark) and analyzed in positive ion mode via nanoESI MS on a QStarXL hybrid quadrupole time-of-flight mass spectrometer (AB

Sciex, Framingham, MA, USA). Product ion spectra were collected for each compound at varying CID collision energies using an ESI voltage of 1000 V, a declustering potential of 30 V and a focusing potential of 120 V. Two fragments were chosen as multiple reaction monitoring (MRM) transitions for each compound with optimized collision energies. The quantitative transition was used to determine the relative quantities of each compound and the confirmatory transition was used to validate the ion signal observed for the first transition.

1 mM methanol stock solutions of each analog were prepared and mixed in experimental triplicate with Balb/c mouse plasma (Innovative Research, Novi, MI, USA) that was buffered 1:1 with phosphate buffered saline (PBS, pH=7.4). The compounds were multiplexed into sets of three and added to a final concentration of 10 µM in a total volume of 400 µL. Immediately after mixing, 200 µL of the sample mixture was quenched with 300 µL of aqueous formic acid (5%) to prevent further analog degradation. The remaining 200 µL of sample was incubated at 37 °C for 3 h and quenched in an identical fashion. The quenched samples were passed through 3 kDa Amicon molecular weight cut off filters (Millipore, Billerica, MA, USA) by centrifugation at 14,000 rpm for 15 minutes. 20 µL samples of the filtrates were subjected to LC-MRM analysis using a Qtrap 4000 (AB Sciex, Framingham, MA, USA) hybrid triple quadrupole linear ion trap mass spectrometer with an ion spray voltage of 5000 V and a declustering potential of 25V. The MS was equipped with a Turbo V ion spray source coupled to a Dionex Ultimate3000 HPLC (Thermo Fisher Scientific, Waltham, MA, USA). Fritted fused silica columns (200 µm ID) (Molex, Lisle, IL, USA) were packed with 5 µm Magic C18 (MICHROM Bioresources Inc., Auburn, CA, USA) reversed-phase beads to a length of 5 cm using an in-house high-pressure vessel. Chromatographic separation employed a linear gradient using reversed phase solvents (water and acetonitrile both containing 0.1% formic acid) over 10 minutes. Automatic quantitation was achieved using

MultiQuant software (AB Sciex, Framingham, MA, USA) by integrating the peak areas of the quantitative MRM transition extracted ion chromatogram. The plasma stability of each compound was calculated as a percentage of the compound ion signal detected after 3 h of plasma incubation relative to the original amount.

2.4.6 *Ex vivo* studies

Balb/c mice were implanted with CT26-WT (murine colon carcinoma) cells. Mice were sacrificed 24 days later, after tumors had reached at least 10mm x 10mm in size. Tumor, lung, spleen, brain, and abdominal muscle tissue were extracted from the mice, cut into 2 mm thick slices and cored into 2mm x 2mm pieces via punch biopsy. Each tissue core was incubated in 1 mL of Dulbecco's Modified Eagle's Medium (DMEM) supplemented with 10% fetal bovine serum, 30 mM HEPES and 2.5 mg/L amphotericin B, in a 37 ℃, 5% CO_2 humidified incubator. In order to assess the viability of each core, alamarBlue® was added to each well for a 4-hour incubation period. Viable cores were selected and treated with various concentrations of VSe1 and analogs. The cores were then infected with VSVΔ51 expressing a GFP transgene (VSVΔ51-GFP) four hours post treatment. GFP pictures were taken for each core 24 h post infection. Cores and supernatants were collected 30 hours post infection and titered by plaque assay.

2.4.7 *In vivo* dose escalation studies

Nine-week-old Balb/c mice were intraperitoneally administered various doses of compounds 1, 10, 24, or 28 dissolved in DMSO (approximately 50 μL). Weight loss and other outward signs of toxicity (piloerection, malaise, quiet behaviour) were recorded over a 10 (compounds **2.1**, **2.10**) or 18-day (compounds **2.24**, **2.28**) period.

2.4.8 *In vivo* enhancement of virus replication

Nine-week-old female Balb/c mice were given subcutaneous tumors by injecting ~ 3×10^5 syngeneic CT26 cells suspended in 100 µL serum-free DMEM. Eleven days post-implantation (average tumor size = 90 mm^3), mice were treated with 40 mg/kg of compound 28 dissolved in DMSO or vehicle control administered intratumorally (approximately 30 µL). Four hours later, mice were treated with an intratumoral injection of VSVΔ51-FLuc (1×10^8 plaque-forming units). For in vivo imaging, an IVIS (Perkin Elmer, Waltham, MA) was used as described previously.[29] Briefly, 200 µL of a 10 mg/mL D-Luciferin (Biotium Hayward, CA) solution in PBS (Corning, Manassas, VA) was administered to mice intraperitoneally. Five minutes later, mice were anaesthetized using 3% isoflurane and imaged according to the manufacturer's instructions. For quantification of luminescence described in Fig 5c, bioluminescent signal intensities were measured using Living Image® v2.50.1 software. Background intensities were measured using the software and subtracted from user-defined regions of interest (ROIs) that were manually delineated around the tumor for each mouse.

2.4.9 Pharmacokinetics

Nine-week-old female Balb/c mice were given subcutaneous tumors by injecting ~ 3×10^5 syngeneic CT26 cells suspended in 100 µL serum-free DMEM. Nineteen days post-implantation (average tumor size = 90 mm^3), mice were intratumorally administered 50 mg/kg of compound 10 or 28 dissolved in DMSO (approximately 50 µL). Tumors were excised after 0 h, 15 minutes, 1 h and 3 h and homogenized immediately at 30 Hz for 5 minutes with a TissueLyser II (Qiagen). Samples were the centrifuged (20,000 rpm, 30 s, 4 °C) and homogenized again in 500 µL PBS.

After another round of centrifugation, the supernatant was passed through Amicon Ultra-0.5 mL 3 kDa molecular weight cut off filters (EMD Millipore) by centrifugation, and the filtrate was quantified by LC-MRM.

2.4.10 Synthetic methods and characterization

General information

All reactions were performed in oven-dried glass round-bottom flasks equipped with magnetic stir bars. Purification of reaction products was carried out by flash column chromatography using silica gel. Analytical thin-layer chromatography (TLC) was performed using silica gel 60 F_{254} plates from EMD. ^{1}H and ^{13}C NMR spectra were recorded on a Bruker 400 MHz and 100 MHz, respectively, at ambient temperature. Spectra are recorded in parts per million using residual solvent as the internal standard ($(CD_3)_2SO$ at 2.50 ppm, $CDCl_3$ at 7.26 ppm and CD_3OD at 3.31 ppm for ^{1}H NMR and $(CD_3)_2SO$ at 39.52 ppm, $CDCl_3$ at 77.16 ppm and CD_3OD at 49.00 ppm for ^{13}C NMR.) ^{1}H NMR data was reported as: multiplicity (br = broad, s = singlet, d = doublet, t = triplet, q = quartet, quin. = quintet, sext. = sextuplet, sept = septuplet, m = multiplet), integration and coupling constant(s) in Hz. High-resolution mass spectrometry was performed in positive ion mode via nanoESI MS using a QStarXL hybrid quadrupole time-of-flight mass spectrometer.

Materials

Unless otherwise noted, all commercially available materials were purchased from commercial sources and used without further purification.

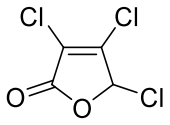

Mucochloryl chloride

Mucochloric acid (5 g, 26.7 mmol) was added to 17.8 mL of thionyl chloride. A catalytic amount of dimethylformamide (3 drops) was added and the mixture was heated at 70 °C for 5 h. The mixture was cooled and excess thionyl chloride was evaporated under vacuum. Toluene (100 mL) was added to the flask and evaporated under vacuum 3 times to azeotrope any residual thionyl chloride. The crude product was isolated as a yellow oil was used in subsequent reactions without further purification.

General procedure A

An amine (2.2 equiv.) was added to dioxane (0.3 M). Mucochloryl chloride (1.0 equiv.) was added dropwise and the mixture was allowed to stir at room temperature for 16 h. The reaction mixture was quenched with $NH_4Cl_{(aq)}$ and extracted 3 × with EtOAc. The organic fractions were washed with brine, dried over Na_2SO_4 and concentrated. The desired compound was purified by silica column chromatography.

General procedure B

3,4-dichloro-5-phenyl-2,5-dihydrofuran-2-one (1 equiv.) was added to DMF (0.05 M) and an amine (3 equiv.) was added. The reaction was allowed to stir at room temperature for 16 h. $NH_4Cl_{(aq)}$ was added to quench the reaction and the mixture was extracted 3x with EtOAc. The organic fractions were combined and washed with brine, dried over Na_2SO_4 and concentrated. The desired compound was purified with silica column chromatography.

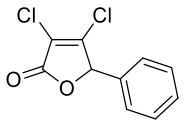

3,4-dichloro-5-phenyl-2,5-dihydrofuran-2-one, Compound 2.1

Mucochloric acid (2.00 g, 1 equiv.) was dissolved in benzene (10 mL) in a round-bottom flask equipped with a stir bar. $AlCl_3$ (2.37 g, 1.5 equiv.) was added and the solution was allowed to stir for 3 days. The mixture was poured over an HCl / ice mixture (5.7 mL conc. HCl). The mixture was extracted 3 × with Et_2O and the combined organic fractions were washed with brine, dried over Na_2SO_4 and concentrated. The desired compound was recrystallized from ethanol. ^{1}H NMR (400 MHz, DMSO) δ 7.51 – 7.41 (m, 5H), 6.40 (s, 1H). ^{13}C NMR (100 MHz, DMSO) δ 165.25, 152.50, 132.05, 130.34, 129.21, 127.83, 119.91, 83.10. HRMS (ESI): Exact mass calculated for $C_{10}H_6Cl_2O_2$ $[M + H]^+$: 228.9823. Found: 228.9944

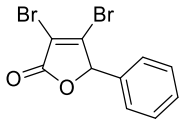

3,4-dibromo-5-phenyl-2,5-dihydrofuran-2-one, Compound 2.2

Mucobromic acid (2.00 g, 1 equiv.) was dissolved in benzene (10 mL) in a round-bottom flask equipped with a stir bar. $AlCl_3$ (1.56 g, 1.5 equiv.) was added and the solution was allowed to stir for 3 days. The mixture was poured over a HCl / ice mixture (5.7 mL conc. HCl). The mixture was extracted 3 × with Et_2O and the combined organic fractions were washed with brine, dried over Na_2SO_4 and concentrated. The desired compound was purified with silica column chromatography. ^{1}H NMR (400 MHz, DMSO) δ 7.50 – 7.43 (m, 3H), 7.42 – 7.34 (m, 2H), 6.37

(s, 1H). ^{13}C NMR (100 MHz, DMSO) δ 166.54, 149.41, 132.64, 130.18, 129.15, 127.73, 113.95, 85.91. HRMS (ESI): Exact mass calculated for $C_{10}H_6Br_2O_2$ [M + H]$^+$: 316.8812. Found: 316.8970

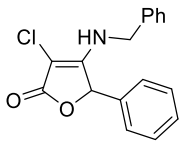

4-(benzylamino)-3-chloro-5-phenyl-2,5-dihydrofuran-2-one, Compound 2.3

General procedure B. ^{1}H NMR (400 MHz, DMSO) δ 7.35 (s, 1H), 7.33 – 7.29 (m, *J* = 7.4 Hz, 5H), 7.18 – 7.05 (m, 5H), 6.57 (s, 1H), 4.32 (d, *J* = 15.7 Hz, 1H), 4.04 (d, *J* = 15.6 Hz, 1H). ^{13}C NMR (100 MHz, DMSO) δ 167.11, 154.95, 137.85, 136.03, 128.66, 128.40, 127.77, 127.74, 126.53, 126.12, 121.95, 92.07, 42.65. HRMS (ESI): Exact mass calculated for $C_{17}H_{14}ClNO_2$ [M + H]$^+$: 300.0791. Found: 300.0780

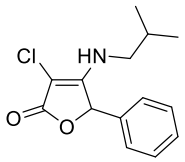

3-chloro-4-[(2-methylpropyl)amino]-5-phenyl-2,5-dihydrofuran-2-one, Compound 2.4

General procedure B. ^{1}H NMR (400 MHz, DMSO) δ 7.43 – 7.32 (m, 5H), 7.23 (s, 1H), 6.51 (s, 1H), 3.04 (dd, *J* = 13.9, 7.4 Hz, 1H), 2.55 (dd, *J* = 13.9, 7.6 Hz, 1H), 1.65 – 1.50 (m, 1H), 0.69 (dd, *J* = 6.6, 4.0 Hz, 6H). ^{13}C NMR (100 MHz, DMSO) δ 167.31, 154.53, 136.51, 128.73, 128.53, 125.92, 122.03, 91.95, 46.64, 27.08, 20.27, 20.22.

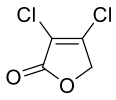

3,4-dichloro-2,5-dihydrofuran-2-one, Compound 2.5

Compound 5 was synthesized as described by Bellina *et al*.[49] ^{1}H NMR (400 MHz, $CDCl_3$) δ 4.87 (s, 2H). ^{13}C NMR (100 MHz, $CDCl_3$) δ 165.93, 149.05, 121.26, 71.09. HRMS (ESI): Exact mass calculated for $C_4H_2Cl_2O_2$ $[M + H]^+$: 152.9510. Found: 152.9637

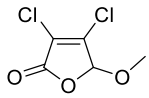

3,4-dichloro-5-methoxy-2,5-dihydrofuran-2-one, Compound 2.6

Mucochloric acid (250 mg, 1.47 mmol) was dissolved in 15 mL of methanol. A catalytic amount of H_2SO_4 was added and the mixture was allowed to stir overnight. The solution was quenched with a saturated solution of $NaHCO_3$ and extracted 3 × with EtOAc. The organic fractions were combined and washed with brine, dried over Na_2SO_4 and concentrated. The desired compound (119 mg, 45%) was purified by silica column chromatography (10 % EtOAc in hexanes). ^{1}H NMR (400 MHz, $CDCl_3$) δ 5.77 (s, 1H), 3.59 (s, 3H). ^{13}C NMR (100 MHz, $CDCl_3$) δ 163.22, 147.36, 124.73, 101.58, 56.53.

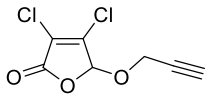

3,4-dichloro-5-(prop-2-yn-1-yloxy)-2,5-dihydrofuran-2-one, Compound 2.7

Mucochloric acid (200 mg, 1.47 mmol) was dissolved in 2 mL of toluene. Propargyl alcohol (119 mg, 1.5 equiv.) and a catalytic amount of H_2SO_4 was added. The flask was equipped with a Dean-stark trap and the solution was refluxed overnight. The solution was quenched with a saturated solution of $NaHCO_3$ and extracted 3 × with EtOAc. The organic fractions were combined and washed with brine, dried over Na_2SO_4 and concentrated. The desired compound (232 mg, 76 %)

was purified from the crude mixture by silica column chromatography (10 % EtOAc in hexanes). ^{1}H NMR (400 MHz, CDCl3) δ 6.05 (s, 1H), 4.50 (dd, *J* = 4.0, 2.4 Hz, 2H), 2.64 (t, *J* = 2.4 Hz, 1H). ^{13}C NMR (100 MHz, $CDCl_3$) δ 163.11, 147.51, 124.61, 98.59, 77.74, 76.75, 57.41. HRMS (ESI): Exact mass calculated for $C_7H_4Cl_2O_3$ $[M + H]^+$: 206.9615. Found: 206.9595

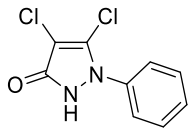

4,5-dichloro-1-phenyl-*1H*-pyrazol-3(2H)-one, Compound 2.8

Commercial compound used without further purification. HRMS (ESI): Exact mass calculated for $C_9H_6Cl_2N_2O$ $[M + H]^+$: 228.9935. Found: 228.9950

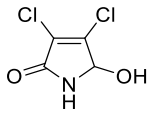

3,4-dichloro-5-hydroxy-2,5-dihydro-*1H*-pyrrol-2-one, Compound 2.9

Compound 9 (238 mg, 18 %) was synthesized as described by Ratts *et al.*[44] ^{1}H NMR (400 MHz, DMSO) δ 9.18 (s, 1H), 6.79 (d, *J* = 9.6 Hz, 1H), 5.46 (dd, *J* = 9.6, 1.6 Hz, 1H). ^{13}C NMR (100 MHz, DMSO) δ 163.41, 145.70, 124.94, 79.05. HRMS (ESI): Exact mass calculated for $C_4H_3Cl_2NO_2$ $[M + H]^+$: 167.9619. Found: 167.9630

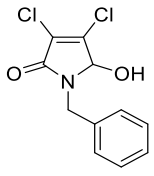

1-benzyl-3,4-dichloro-5-hydroxy-2,5-dihydro-*1H*-pyrrol-2-one, Compound 2.10

General procedure A. ^{1}H NMR (400 MHz, DMSO) δ 7.41 – 7.17 (m, 6H), 5.34 (d, *J* = 9.3 Hz, 1H), 4.72 (d, *J* = 15.6 Hz, 1H), 4.33 (d, *J* = 15.6 Hz, 1H). ^{13}C NMR (100 MHz, DMSO) δ 161.65, 144.47, 136.93, 128.51, 127.69, 127.29, 124.67, 81.46, 43.26.

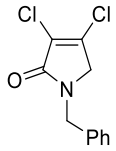

1-benzyl-3,4-dichloro-*1H*-pyrrol-2(*5H*)-one, Compound 2.11

Compound 11 (249 mg, 35 %) was synthesized as described by Zhang *et al*.[50] ^{1}H NMR (400 MHz, $CDCl_3$) δ 7.38 – 7.22 (m, 5H), 4.65 (s, 2H), 3.90 (s, 2H). ^{13}C NMR (100 MHz, $CDCl_3$) δ 164.37, 139.96, 136.00, 129.16, 128.37, 128.29, 125.69, 52.93, 47.10. HRMS (ESI): Exact mass calculated for $C_{11}H_9Cl_2NO$ $[M + H]^+$: 242.0139. Found: 242.0674

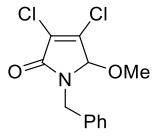

1-benzyl-3,4-dichloro-5-methoxy-*1H*-pyrrol-2(*5H*)-one, Compound 2.12

1-benzyl-3,4-dichloro-5-hydroxy-2,5-dihydro-1H-pyrrol-2-one (150 mg, 0.58 mmol) was dissolved in 5 mL of methanol. A catalytic amount of H_2SO_4 was added and the mixture was allowed to stir overnight. The solution was quenched with a saturated solution of $NaHCO_3$ and extracted 3 × with EtOAc. The organic fractions were combined and washed with brine, dried over Na_2SO_4 and concentrated. The desired compound (104 mg, 66 %) was purified from the crude mixture by silica column chromatography (10 to 15 % EtOAc in hexanes).^{1}H NMR (400 MHz, DMSO) δ 7.38 – 7.25 (m, 5H), 5.55 (s, 1H), 4.67 (d, *J* = 15.4 Hz, 1H), 4.35 (d, *J* = 15.4 Hz, 1H), 2.98 (s, 3H). ^{13}C NMR (100 MHz, DMSO) δ 162.07, 141.34, 136.42, 128.57, 128.01, 127.53,

126.51, 86.84, 50.49, 44.14. HRMS (ESI): Exact mass calculated for $C_{12}H_{11}Cl_2NO_2$ $[M + H]^+$: 272.0245. Found: 272.0350

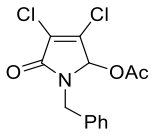

1-benzyl-3,4-dichloro-5-oxo-2,5-dihydro-*1H*-pyrrol-2-yl acetate, Compound 2.13

1-benzyl-3,4-dichloro-5-hydroxy-2,5-dihydro-1H-pyrrol-2-one (150 mg, 0.58 mmol) was dissolved in 3 mL of acetic anhydride. Pyridine (1.16 mol, 2.0 equiv.) was added and the mixture was allowed to stir for 6 hours at room temperature. The reaction was quenched with 10% $HCl_{(aq)}$ and extracted 3 × with EtOAc. The organic fractions were combined and washed with brine, dried over Na_2SO_4 and concentrated. The desired compound (159 mg, 91 %) was purified from the crude mixture by silica column chromatography (5 to 15 % EtOAc in hexanes). ^{1}H NMR (400 MHz, DMSO) δ 7.41 – 7.18 (m, 5H), 6.71 (s, 1H), 4.61 (d, *J* = 15.7 Hz, 1H), 4.48 (d, *J* = 15.7 Hz, 1H), 1.88 (s, 3H). ^{13}C NMR (100 MHz, DMSO) δ 169.51, 162.47, 140.89, 136.22, 128.51, 127.68, 127.49, 126.48, 80.42, 44.95, 20.04. HRMS (ESI): Exact mass calculated for $C_{13}H_{11}Cl_2NO_3$ $[M + H]^+$: 300.0194. Found: 300.0236

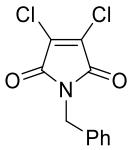

1-benzyl-3,4-dichloro-*1H*-pyrrole-2,5-dione, Compound 2.14

Compound 14 was synthesized as described by Holz *et al*.[51] ^{1}H NMR (400 MHz, DMSO) δ 7.44 – 7.17 (m, 5H), 4.67 (s, 2H). ^{13}C NMR (100 MHz, DMSO) δ 163.04, 135.76, 132.56, 128.49,

127.54, 127.42, 42.02. HRMS (ESI): Exact mass calculated for $C_{11}H_7Cl_2NO_2$ $[M + H]^+$: 255.9932. Found: 256.0033

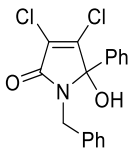

1-benzyl-3,4-dichloro-5-hydroxy-5-phenyl-*1H*-pyrrol-2(*5H*)-one, Compound 2.15

1-benzyl-3,4-dichloro-1H-pyrrole-2,5-dione (100 mg, 0.39 mmol) was dissolved in 1.95 mL of THF and the solution was cooled to -78 ° C. Phenyllithium (0.39 mmol, 1.0 equivalent, 1.9 M in dibutyl ether) was added dropwise and the solution was allowed to stir for 1 h before warming to room temperature. The reaction was quenched with a saturated $NH_4Cl_{(aq)}$ solution and extracted 3 × with EtOAc. The organic fractions were combined and washed with brine, dried over Na_2SO_4 and concentrated. The desired compound (64 mg, 49 %) was purified from the crude mixture by silica column chromatography (5 to 15 % EtOAc in hexanes). ^{1}H NMR (400 MHz, DMSO) δ 7.62 (s, 1H), 7.34 (s, 5H), 7.19 – 7.06 (m, 5H), 4.37 (d, *J* = 15.6 Hz, 1H), 4.12 (d, *J* = 15.6 Hz, 1H). ^{13}C NMR (100 MHz, DMSO) δ 162.22, 147.86, 137.09, 135.26, 129.04, 128.61, 127.89, 127.88, 126.81, 126.18, 124.16, 90.83, 43.32. HRMS (ESI): Exact mass calculated for $C_{17}H_{13}Cl_2NO_2$ $[M + H]^+$: 334.0401. Found: 334.0520

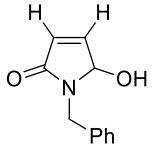

1-benzyl-5-hydroxy-*1H*-pyrrol-2(*5H*)-one, Compound 2.16

Compound 16 (104 mg, 55 %) was synthesized as described by Yamashita *et al*.[52] ^{1}H NMR (400 MHz, DMSO) δ 7.37 – 7.19 (m, 5H), 7.09 (dd, *J* = 6.0, 1.5 Hz, 1H), 6.42 (d, *J* = 8.7 Hz, 1H), 6.18 (d, *J* = 6.0 Hz, 1H), 5.26 (d, *J* = 8.7 Hz, 1H), 4.71 (d, *J* = 15.4 Hz, 1H), 4.20 (d, *J* = 15.4 Hz, 1H). ^{13}C NMR (100 MHz, DMSO) δ 168.80, 147.76, 138.10, 128.43, 127.49, 127.06, 126.99, 81.87, 41.73. HRMS (ESI): Exact mass calculated for $C_{11}H_{11}NO_2$ $[M + H]^+$: 190.0868. Found: 190.0870

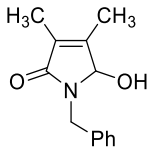

1-benzyl-5-hydroxy-3,4-dimethyl-*1H*-pyrrol-2(*5H*)-one, Compound 2.17

2,3-Dimethylmaleic anhydride (630 mg, 5 mmol) was dissolved in acetic acid (7.5 mL). Benzylamine (535 mg, 5 mmol) was added drop wise and the mixture was refluxed for 2 h. The solution was concentrated and *1-benzyl-3,4-dimethyl-1H-pyrrole-2,5-dione* (956 mg, 89 %) was isolated by silica column chromatography (10 % EtOAc in hexanes). 1-benzyl-3,4-dimethyl-1H-pyrrole-2,5-dione (215 mg, 1 mmol) was dissolved in THF (3 mL). The solution was cooled to -15 °C and a solution of $LiAlH(O^tBu)_3$ (305 mg, 1.2 equiv.) in THF (2 mL) was added dropwise and the resulting mixture was allowed to react for 1 hour. The solution was warmed to room temperature and stirred for another hour. The reaction was subsequently quenched with 10 % $HCl_{(aq)}$ and extracted 3 × with EtOAc. The organic fractions were combined and washed with brine, dried over Na_2SO_4 and concentrated. The desired compound (147 mg, 68 %) was purified from the crude mixture by silica column chromatography (50 % EtOAc in hexanes). ^{1}H NMR (400 MHz, DMSO) δ 7.38 – 7.17 (m, 5H), 6.25 (d, *J* = 8.7 Hz, 1H), 4.92 (d, *J* = 8.6 Hz, 1H), 4.71 (d, *J* = 15.4 Hz, 1H), 4.19 (d, *J* = 15.4 Hz, 1H), 1.86 (s, *J* = 0.5 Hz, 3H), 1.70 (s, *J* = 1.1 Hz, 3H). ^{13}C NMR (100 MHz, DMSO) δ 169.94, 149.58, 138.33, 128.39, 127.56, 127.27, 126.91, 82.19, 42.04,

11.18, 8.25. HRMS (ESI): Exact mass calculated for $C_{13}H_{15}NO_2$ $[M + H]^+$: 218.1181. Found: 218.1077

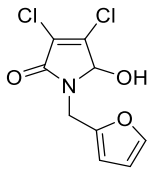

3,4-dichloro-1-(furan-2-ylmethyl)-5-hydroxy-*1H*-pyrrol-2(*5H*)-one, Compound 2.18

General procedure A. ^{1}H NMR (400 MHz, DMSO) δ 7.59 (d, *J* = 1.1 Hz, 1H), 7.21 (d, *J* = 9.3 Hz, 1H), 6.40 (dd, *J* = 3.1, 1.9 Hz, 1H), 6.36 (d, *J* = 3.1 Hz, 1H), 5.34 (d, *J* = 8.9 Hz, 1H), 4.71 (d, *J* = 16.0 Hz, 1H), 4.32 (d, *J* = 16.0 Hz, 1H). ^{13}C NMR (100 MHz, DMSO) δ 161.29, 149.86, 144.73, 142.77, 124.56, 110.55, 108.22, 81.37, 36.17. HRMS (ESI): Exact mass calculated for $C_9H_7Cl_2NO_3$ $[M + H]^+$: 247.9881. Found: 247.9958

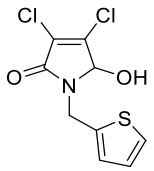

3,4-dichloro-5-hydroxy-1-(thiophen-2-ylmethyl)-*1H*-pyrrol-2(*5H*)-one, Compound 2.19

General procedure A. ^{1}H NMR (400 MHz, DMSO) δ 7.45 (dd, *J* = 5.1, 1.1 Hz, 1H), 7.28 (d, *J* = 9.3 Hz, 1H), 7.05 (d, *J* = 2.8 Hz, 1H), 6.98 (dd, *J* = 5.0, 3.5 Hz, 1H), 5.36 (d, *J* = 9.3 Hz, 1H), 4.84 (d, *J* = 15.8 Hz, 1H), 4.52 (d, *J* = 15.8 Hz, 1H). ^{13}C NMR (101 MHz, DMSO) δ 155.26, 138.69, 132.99, 120.95, 120.94, 120.05, 118.54, 75.12, 31.88. HRMS (ESI): Exact mass calculated for $C_9H_7Cl_2NO_2S$ $[M + H]^+$: 263.9652. Found: 263.9713

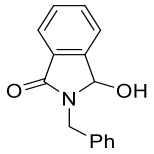

2-benzyl-3-hydroxyisoindolin-1-one, Compound 2.20

Phthalic anhydride (1.48 g, 10 mmol) was dissolved in acetic acid (15 mL). Benzylamine (1.70 g, 10 mmol) was added dropwise and the mixture was refluxed for 2 h. The solution was concentrated and *2-benzylisoindoline-1,3-dione* (2.07 g, 96 %) was isolated by silica column chromatography (10% EtOAc in hexanes). 2-benzylisoindoline-1,3-dione (237 mg, 1 mmol) was dissolved in THF (3 mL). The solution was cooled to -15 °C and a solution of $LiAlH(O^tBu)_3$ (305 mg, 1.2 equiv.) in THF (2 mL) was added dropwise and the resulting mixture was allowed to react for 1 h. The solution was warmed to room temperature and stirred for another hour. The reaction was subsequently quenched with 10 % $HCl_{(aq)}$ and extracted 3 × with EtOAc. The organic fractions were combined and washed with brine, dried over Na_2SO_4 and concentrated. The desired compound (161 mg, 67 %) was purified from the crude mixture by silica column chromatography (40 % EtOAc in hexanes)^{1}H NMR (400 MHz, DMSO) δ 7.75 – 7.50 (m, 4H), 7.39 – 7.21 (m, 5H), 6.75 (d, *J* = 8.8 Hz, 1H), 5.67 (d, *J* = 8.8 Hz, 1H), 4.92 (d, *J* = 15.3 Hz, 1H), 4.37 (d, *J* = 15.3 Hz, 1H). ^{13}C NMR (100 MHz, DMSO) δ 166.14, 144.88, 137.73, 132.07, 131.41, 129.40, 128.48, 127.67, 127.09, 123.74, 122.45, 80.28, 42.11. HRMS (ESI): Exact mass calculated for $C_{15}H_{13}NO_2$ $[M + H]^+$: 240.1024. Found: 240.1022

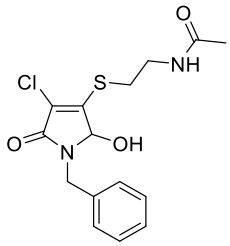

***N*-(2-(1-benzyl-4-chloro-2-hydroxy-5-oxo-2,5-dihydro-*1H*-pyrrol-3-ylthio)ethyl)acetamide, Compound 2.21**

1-benzyl-3,4-dichloro-5-hydroxy-2,5-dihydro-1H-pyrrol-2-one (100 mg, 0.39 mmol) and N-acetylcysteamine (52 mg, 0.43 mmol) were added to 1 mL of DMSO. The mixture was allowed to stir overnight at room temperature. The desired compound (73 mg, 55 %) was purified from the mixture by silica column chromatography (70 % EtOAc in hexanes). ^{1}H NMR (400 MHz, DMSO) δ 8.11 (s, 1H), 7.38 – 7.20 (m, 5H), 7.04 (d, *J* = 9.9 Hz, 1H), 5.48 (d, *J* = 9.9 Hz, 1H), 4.69 (d, *J* = 15.6 Hz, 1H), 4.29 (d, *J* = 15.6 Hz, 1H), 3.32 – 3.14 (m, 4H), 1.75 (s, 3H). ^{13}C NMR (100 MHz, DMSO) δ 169.46, 162.55, 151.04, 137.36, 128.48, 127.62, 127.18, 119.59, 81.14, 43.07, 38.77, 29.61, 22.42. HRMS (ESI): Exact mass calculated for $C_{15}H_{17}ClN_2O_3S$ $[M + H]^+$: 341.0726. Found: 341.0738

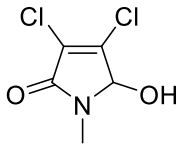

3,4-dichloro-5-hydroxy-1-methyl-*1H*-pyrrol-2(*5H*)-one, Compound 2.22

General procedure A. ^{1}H NMR (400 MHz, MeOD) δ 5.28 (s, 1H), 2.97 (s, 3H). ^{13}C NMR (100 MHz, MeOD) δ 164.28, 145.42, 126.72, 84.67, 26.90. HRMS (ESI): Exact mass calculated for $C_5H_5Cl_2NO_2$ $[M + H]^+$: 181.9775. Found: 181.9820

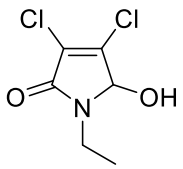

3,4-dichloro-1-ethyl-5-hydroxy-1H-pyrrol-2(*5H*)-one, Compound 2.23

General procedure A. ^{1}H NMR (400 MHz, $CDCl_3$) δ 5.29 (s, 1H), 4.67 (s, 1H), 3.61 (dq, *J* = 14.5, 7.3 Hz, 1H), 3.35 (dq, *J* = 14.2, 7.1 Hz, 1H), 1.18 (t, *J* = 7.2 Hz, 3H). ^{13}C NMR (100 MHz, $CDCl_3$) δ 162.97, 143.68, 126.38, 81.98, 35.43, 13.63.

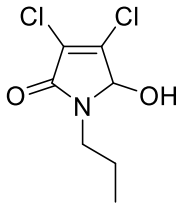

3,4-dichloro-5-hydroxy-1-propyl-*1H*-pyrrol-2(*5H*)-one, Compound 2.24

General procedure A. ^{1}H NMR (400 MHz, $CDCl_3$) δ 5.26 (s, 1H), 3.89 (s, 1H), 3.52 (ddd, *J* = 14.0, 8.5, 7.2 Hz, 1H), 3.28 (ddd, *J* = 14.0, 8.5, 5.6 Hz, 1H), 1.72 – 1.51 (m, 2H), 0.92 (t, *J* = 7.4 Hz, 3H). ^{13}C NMR (100 MHz, $CDCl_3$) δ 163.06, 143.44, 126.71, 82.35, 42.18, 21.71, 11.42. HRMS (ESI): Exact mass calculated for $C_7H_9Cl_2NO_2$ $[M + H]^+$: 210.0088. Found: 210.0150

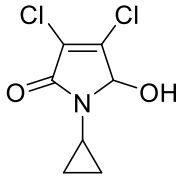

3,4-dichloro-1-cyclopropyl-5-hydroxy-*1H*-pyrrol-2(*5H*)-one, Compound 2.25

General procedure A. ^{1}H NMR (400 MHz, MeOD) δ 5.32 (s, 1H), 2.65 – 2.58 (m, 1H), 1.04 – 0.96 (m, 1H), 0.89 – 0.71 (m, 4H). ^{13}C NMR (100 MHz, MeOD) δ 165.39, 145.51, 126.40, 84.48, 24.26, 5.85, 5.34. HRMS (ESI): Exact mass calculated for $C_7H_7Cl_2NO_2$ $[M + H]^+$: 207.9932. Found: 207.9984

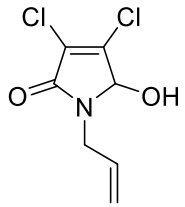

1-allyl-3,4-dichloro-5-hydroxy-*1H*-pyrrol-2(*5H*)-one, Compound 2.26

General procedure A. ^{1}H NMR (400 MHz, DMSO) δ 7.07 (d, *J* = 9.3 Hz, 1H), 5.79 (dddd, *J* = 16.6, 10.3, 6.3, 4.9 Hz, 1H), 5.39 (d, *J* = 9.1 Hz, 1H), 5.16 (ddq, *J* = 14.6, 10.2, 1.5 Hz, 2H), 4.11 (ddt, *J* = 16.1, 4.7, 1.6 Hz, 1H), 3.78 (ddt, *J* = 16.1, 6.3, 1.3 Hz, 1H). ^{13}C NMR (100 MHz, DMSO) δ 161.29, 144.36, 133.01, 124.65, 117.21, 81.34, 42.01. HRMS (ESI): Exact mass calculated for $C_7H_7Cl_2NO_2$ $[M + H]^+$: 207.9932. Found: 207.9976

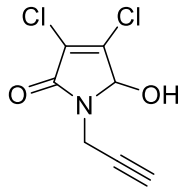

3,4-dichloro-5-hydroxy-1-(prop-2-ynyl)-*1H*-pyrrol-2(*5H*)-one, Compound 2.27

General procedure A. ^{1}H NMR (400 MHz, DMSO) δ 7.24 (d, *J* = 9.3 Hz, 1H), 5.47 (d, *J* = 9.0 Hz, 1H), 4.33 (dd, *J* = 17.9, 2.5 Hz, 1H), 3.95 (dd, *J* = 17.9, 2.5 Hz, 1H), 3.27 (t, *J* = 2.5 Hz, 1H). ^{13}C NMR (100 MHz, DMSO) δ 161.10, 145.01, 124.42, 81.19, 78.48, 74.51, 29.11. HRMS (ESI): Exact mass calculated for $C_7H_5Cl_2NO_2$ $[M + H]^+$: 205.9775. Found: 205.9814

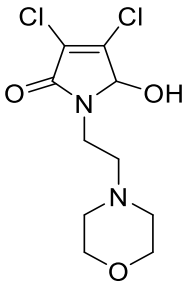

3,4-dichloro-5-hydroxy-1-(2-morpholinoethyl)-*1H*-pyrrol-2(*5H*)-one, Compound 2.28

General procedure A. ^{1}H NMR (400 MHz, $CDCl_3$) δ 9.10 (s, 1H), 5.22 (s, 1H), 4.14 (dt, *J* = 15.3, 3.0 Hz, 1H), 3.77 (t, *J* = 4.6 Hz, 4H), 3.22 (ddd, *J* = 15.3, 11.6, 2.1 Hz, 1H), 2.80 – 2.71 (m, 2H), 2.67 (ddd, *J* = 14.2, 11.6, 2.7 Hz, 1H), 2.53 – 2.44 (m, 3H). ^{13}C NMR (100 MHz, $CDCl_3$) δ 163.02, 144.37, 125.84, 82.91, 66.27, 58.20, 53.36, 39.37. HRMS (ESI): Exact mass calculated for $C_{10}H_{14}Cl_2N_2O_3$ $[M + H]^+$: 281.0459. Found: 281.0402

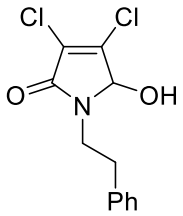

3,4-dichloro-5-hydroxy-1-phenethyl-*1H*-pyrrol-2(*5H*)-one, Compound 2.29

General procedure A. ^{1}H NMR (400 MHz, MeOD) δ 7.38 – 7.17 (m, 5H), 5.13 (s, 1H), 3.85 – 3.73 (m, 1H), 3.61 – 3.44 (m, 1H), 3.04 – 2.81 (m, 2H). ^{13}C NMR (100 MHz, MeOD) δ 164.13, 145.56, 139.92, 129.78, 129.67, 127.64, 83.66, 42.95, 35.43. HRMS (ESI): Exact mass calculated for $C_{12}H_{11}Cl_2NO_2$ $[M + H]^+$: 272.0245. Found: 272.0350

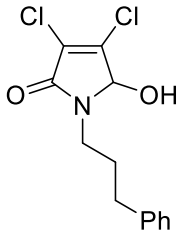

3,4-dichloro-5-hydroxy-1-(3-phenylpropyl)-*1H*-pyrrol-2(*5H*)-one, Compound 2.30

General procedure A. ^{1}H NMR (400 MHz, DMSO) δ 7.21 (qdd, *J* = 8.5, 5.1, 1.5 Hz, 5H), 7.03 (d, *J* = 9.6 Hz, 1H), 5.45 (d, *J* = 9.5 Hz, 1H), 3.46 (dt, *J* = 14.9, 7.5 Hz, 1H), 3.25 (ddd, *J* = 13.8, 7.9,

5.8 Hz, 1H), 2.58 (t, *J* = 7.8 Hz, 2H), 1.93 – 1.74 (m, 2H). ^{13}C NMR (100 MHz, DMSO) δ 161.49, 144.02, 141.43, 128.27, 128.25, 125.77, 124.67, 81.55, 39.65, 32.47, 29.53. HRMS (ESI): Exact mass calculated for $C_{13}H_{13}Cl_2NO_2$ $[M + H]^+$: 286.0401. Found: 286.0529

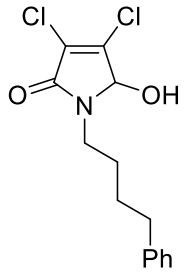

3,4-dichloro-5-hydroxy-1-(4-phenylbutyl)-*1H*-pyrrol-2(*5H*)-one, Compound 2.31

General procedure A. ^{1}H NMR (400 MHz, DMSO) δ 7.32 – 7.23 (m, 2H), 7.22 – 7.13 (m, 3H), 7.03 (d, *J* = 9.4 Hz, 1H), 5.41 (d, *J* = 9.3 Hz, 1H), 3.44 (dd, *J* = 13.8, 7.2 Hz, 1H), 3.30 – 3.19 (m, 1H), 2.64 – 2.53 (m, 2H), 1.63 – 1.48 (m, 4H). ^{13}C NMR (100 MHz, DMSO) δ 161.45, 143.98, 142.01, 128.28, 128.22, 125.66, 124.67, 81.50, 39.60, 34.70, 28.25, 27.44. HRMS (ESI): Exact mass calculated for $C_{14}H_{15}Cl_2NO_2$ $[M + H]^+$: 300.0558. Found: 300.0699

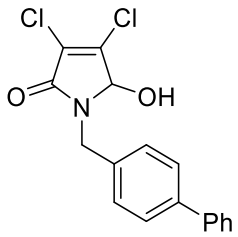

1-(biphenyl-4-ylmethyl)-3,4-dichloro-5-hydroxy-*1H*-pyrrol-2(*5H*)-one, Compound 2.32

General procedure A. ^{1}H NMR (400 MHz, DMSO) δ 7.68 – 7.60 (m, 4H), 7.50 – 7.32 (m, 5H), 7.27 (d, *J* = 9.2 Hz, 1H), 5.40 (d, *J* = 9.2 Hz, 1H), 4.75 (d, *J* = 15.6 Hz, 1H), 4.39 (d, *J* = 15.6 Hz,

1H). ^{13}C NMR (100 MHz, DMSO) δ 161.68, 144.50, 139.82, 139.24, 136.18, 128.92, 128.36, 127.42, 126.82, 126.61, 124.68, 81.53, 43.03.

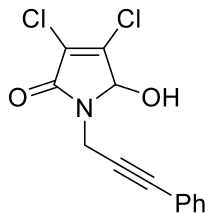

3,4-dichloro-5-hydroxy-1-(3-phenylprop-2-ynyl)-*1H*-pyrrol-2(*5H*)-one, Compound 2.33

General procedure A. ^{1}H NMR (400 MHz, DMSO) δ 7.45 (dt, *J* = 8.6, 3.7 Hz, 2H), 7.41 – 7.35 (m, 3H), 7.28 (d, *J* = 9.3 Hz, 1H), 5.60 (d, *J* = 9.0 Hz, 1H), 4.60 (d, *J* = 18.0 Hz, 1H), 4.22 (d, *J* = 18.0 Hz, 1H). ^{13}C NMR (100 MHz, DMSO) δ 161.12, 145.11, 131.53, 128.78, 128.61, 124.43, 121.83, 84.26, 82.88, 81.24, 29.81. HRMS (ESI): Exact mass calculated for $C_{13}H_9Cl_2NO_2$ $[M + H]^+$: 282.0088. Found: 282.0056

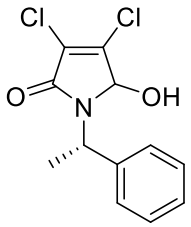

3,4-dichloro-5-hydroxy-1-(1-phenylethyl)-*1H*-pyrrol-2(*5H*)-one, Compound 2.34

General procedure A. Compound isolated as a 1:1 mixture of diastereoisomers. ^{1}H NMR (400 MHz, DMSO) δ 7.44 – 7.22 (m, 5H+5H), 7.19 (d, *J* = 9.4 Hz, 1H), 7.11 (d, *J* = 9.8 Hz, 1H), 5.62 (d, *J* = 9.4 Hz, 1H), 5.29 (d, *J* = 9.7 Hz, 1H), 5.12 (q, *J* = 7.2 Hz, 1H), 4.97 (q, *J* = 7.3 Hz, 1H), 1.68 (d, *J* = 7.4 Hz, 3H), 1.65 (d, *J* = 7.3 Hz, 3H). ^{13}C NMR (100 MHz, DMSO) δ 161.46, 161.21, 144.22, 144.14, 142.59, 140.49, 128.38, 128.13, 127.32, 127.09, 126.86, 126.69, 124.46, 124.41,

81.49, 81.31, 52.00, 51.30, 18.72, 18.14. HRMS (ESI): Exact mass calculated for $C_{12}H_{11}Cl_2NO_2$ $[M + H]^+$: 272.0245. Found: 272.0298

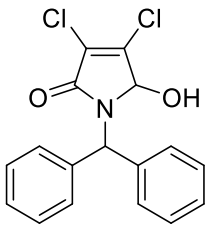

1-benzhydryl-3,4-dichloro-5-hydroxy-*1H*-pyrrol-2(*5H*)-one, Compound 2.35

General procedure A. ^{1}H NMR (400 MHz, DMSO) δ 7.43 – 7.19 (m, 11H), 6.12 (s, 1H), 5.26 (s, 1H). ^{13}C NMR (100 MHz, DMSO) δ 161.42, 144.45, 139.63, 138.62, 129.12, 128.18, 128.10, 127.49, 127.21, 124.40, 81.91, 60.56. HRMS (ESI): Exact mass calculated for $C_{17}H_{13}Cl_2NO_2$ $[M + H]^+$: 334.0401. Found: 334.0435

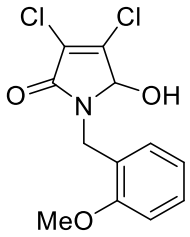

3,4-dichloro-5-hydroxy-1-(2-methoxybenzyl)-*1H*-pyrrol-2(*5H*)-one, Compound 2.36

General procedure A. ^{1}H NMR (400 MHz, DMSO) δ 7.26 (td, *J* = 8.2, 1.6 Hz, 1H), 7.14 (dd, *J* = 7.5, 1.4 Hz, 1H), 6.99 (d, *J* = 7.8 Hz, 1H), 6.90 (td, *J* = 7.4, 0.8 Hz, 1H), 5.35 (s, 1H), 4.58 (d, *J* = 16.1 Hz, 1H), 4.40 (d, *J* = 16.1 Hz, 1H), 3.80 (s, 3H). ^{13}C NMR (100 MHz, DMSO) δ 161.71, 156.65, 144.48, 128.59, 128.30, 124.68, 124.38, 120.21, 110.64, 81.75, 55.38, 38.51. HRMS (ESI): Exact mass calculated for $C_{12}H_{11}Cl_2NO_3$ $[M + Na]^+$: 310.0276. Found: 310.0014

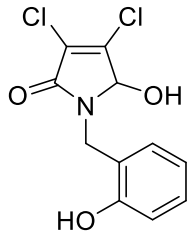

3,4-dichloro-5-hydroxy-1-(2-hydroxybenzyl)-*1H*-pyrrol-2(*5H*)-one, Compound 2.37

General procedure A. ^{1}H NMR (400 MHz, DMSO) δ 9.61 (s, 1H), 7.15 – 7.03 (m, 3H), 6.81 (dd, *J* = 7.9, 0.7 Hz, 1H), 6.74 (td, *J* = 7.5, 1.0 Hz, 1H), 5.34 (d, *J* = 8.8 Hz, 1H), 4.57 (d, *J* = 15.9 Hz, 1H), 4.36 (d, *J* = 15.9 Hz, 1H). ^{13}C NMR (100 MHz, DMSO) δ 161.68, 154.85, 144.38, 128.70, 128.29, 124.70, 122.78, 118.88, 114.96, 81.67, 38.66. HRMS (ESI): Exact mass calculated for $C_{11}H_9Cl_2NO_3$ $[M + H]^+$: 274.0037. Found: 274.0120

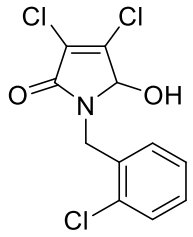

3,4-dichloro-1-(2-chlorobenzyl)-5-hydroxy-*1H*-pyrrol-2(*5H*)-one, Compound 2.38

General procedure A. ^{1}H NMR (400 MHz, DMSO) δ 7.51 – 7.42 (m, 1H), 7.37 – 7.26 (m, 3H), 7.21 (d, *J* = 9.3 Hz, 1H), 5.41 (d, *J* = 9.3 Hz, 1H), 4.70 (d, *J* = 16.4 Hz, 1H), 4.52 (d, *J* = 16.4 Hz, 1H). ^{13}C NMR (100 MHz, DMSO) δ 161.88, 144.77, 133.98, 131.85, 129.27, 129.19, 129.07, 127.33, 124.60, 81.93, 41.29. HRMS (ESI): Exact mass calculated for $C_{11}H_8Cl_3NO_2$ $[M + H]^+$: 291.9698. Found: 291.9922

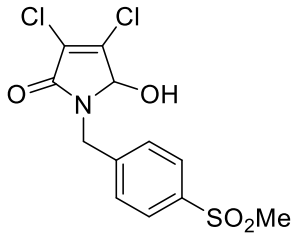

3,4-dichloro-5-hydroxy-1-(4-(methylsulfonyl)benzyl)-*1H*-pyrrol-2(*5H*)-one, Compound 2.39

General procedure A. ^{1}H NMR (400 MHz, DMSO) δ 7.89 (d, *J* = 8.3 Hz, 2H), 7.56 (d, *J* = 8.3 Hz, 2H), 7.25 (d, *J* = 9.3 Hz, 1H), 5.44 (d, *J* = 9.2 Hz, 1H), 4.74 (d, *J* = 16.2 Hz, 1H), 4.52 (d, *J* = 16.3 Hz, 1H), 3.20 (s, 3H). ^{13}C NMR (100 MHz, DMSO) δ 161.87, 144.69, 143.09, 139.72, 128.36, 127.15, 124.59, 81.92, 43.52, 43.17. HRMS (ESI): Exact mass calculated for $C_{12}H_{11}Cl_2NO_4S$ [M + H]$^{+}$: 335.9864. Found: 335.9834

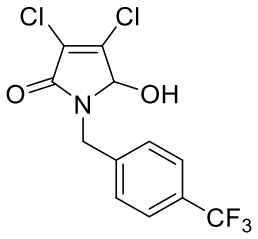

3,4-dichloro-5-hydroxy-1-(4-(trifluoromethyl)benzyl)-*1H*-pyrrol-2(*5H*)-one,

Compound 2.40

General procedure A. ^{1}H NMR (400 MHz, DMSO) δ 7.70 (d, *J* = 8.2 Hz, 2H), 7.52 (d, *J* = 8.1 Hz, 2H), 7.24 (d, *J* = 9.3 Hz, 1H), 5.43 (d, *J* = 9.3 Hz, 1H), 4.74 (d, *J* = 16.1 Hz, 1H), 4.49 (d, *J* = 16.1 Hz, 1H). ^{13}C NMR (100 MHz, DMSO) δ 161.85, 144.67, 141.91 (d, $J_{(C,F)}$ = 1.1 Hz), 128.38, 127.40 (q, $J_{(C,F)}$ = 31.7 Hz), 125.32 (q, $J_{(C,F)}$ = 3.8 Hz), 124.60, 124.27 (q, $J_{(C,F)}$ = 272.0 Hz), 81.84, 43.13. HRMS (ESI): Exact mass calculated for $C_{12}H_8Cl_2F_3NO_2$ [M + H]$^{+}$: 325.9962. Found: 325.9960

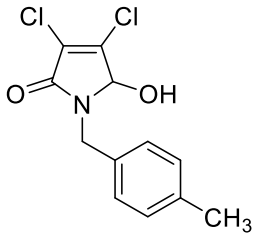

3,4-dichloro-5-hydroxy-1-(4-methylbenzyl)-*1H*-pyrrol-2(*5H*)-one, Compound 2.41

General procedure A. ^{1}H NMR (400 MHz, DMSO) δ 7.23 – 7.11 (m, 5H), 5.30 (d, *J* = 9.3 Hz, 1H), 4.68 (d, *J* = 15.4 Hz, 1H), 4.26 (d, *J* = 15.4 Hz, 1H), 2.27 (s, 3H). ^{13}C NMR (100 MHz, DMSO) δ 161.54, 144.40, 136.46, 133.86, 129.05, 127.73, 124.66, 81.30, 42.95, 20.66. HRMS (ESI): Exact mass calculated for $C_{12}H_{11}Cl_2NO_2$ $[M + H]^+$: 272.0245. Found: 272.0455

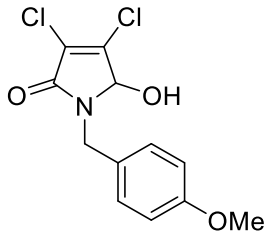

3,4-dichloro-5-hydroxy-1-(4-methoxybenzyl)-*1H*-pyrrol-2(*5H*)-one, Compound 2.42

General procedure A. ^{1}H NMR (400 MHz, DMSO) δ 7.30 – 7.10 (m, 3H), 6.90 (t, *J* = 5.7 Hz, 2H), 5.29 (d, *J* = 9.3 Hz, 1H), 4.66 (d, *J* = 15.2 Hz, 1H), 4.23 (d, *J* = 15.2 Hz, 1H), 3.73 (s, 3H). ^{13}C NMR (100 MHz, DMSO) δ 155.48, 152.58, 138.37, 123.23, 122.82, 118.65, 107.91, 75.21, 49.08, 36.67. HRMS (ESI): Exact mass calculated for $C_{12}H_{11}Cl_2NO_3$ $[M + H]^+$: 288.0194. Found: 288.0409

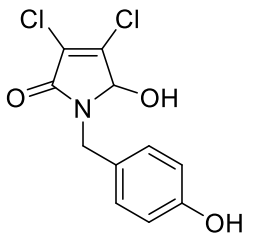

3,4-dichloro-5-hydroxy-1-(4-hydroxybenzyl)-*1H*-pyrrol-2(*5H*)-one, Compound 2.43

General procedure A. ^{1}H NMR (400 MHz, DMSO) δ 9.37 (s, 1H), 7.18 (d, *J* = 9.1 Hz, 1H), 7.08 (d, *J* = 8.5 Hz, 2H), 6.71 (d, *J* = 8.5 Hz, 2H), 5.26 (d, *J* = 8.3 Hz, 1H), 4.63 (d, *J* = 15.1 Hz, 1H), 4.15 (d, *J* = 15.2 Hz, 1H). ^{13}C NMR (100 MHz, DMSO) δ 161.41, 156.71, 144.33, 129.24, 127.00, 124.66, 115.25, 81.07, 42.68. HRMS (ESI): Exact mass calculated for $C_{11}H_9Cl_2NO_3$ $[M + H]^+$: 274.0037. Found: 274.0144

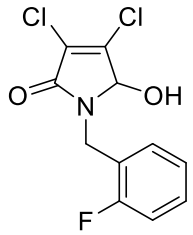

3,4-dichloro-1-(2-fluorobenzyl)-5-hydroxy-*1H*-pyrrol-2(*5H*)-one, Compound 2.44

General procedure A. ^{1}H NMR (400 MHz, DMSO) δ 7.43 – 7.27 (m, 2H), 7.25 – 7.11 (m, 3H), 5.36 (d, *J* = 9.4 Hz, 1H), 4.70 (d, *J* = 15.8 Hz, 1H), 4.46 (d, *J* = 15.8 Hz, 1H). ^{13}C NMR (100 MHz, DMSO) δ 161.66, 160.04 (d, $J_{(C,F)}$ = 245.1 Hz), 144.68, 130.13 (d, $J_{(C,F)}$ = 4.0 Hz), 129.51 (d, $J_{(C,F)}$ = 8.1 Hz), 124.55, 124.47 (d, $J_{(C,F)}$ = 3.5 Hz), 123.63 (d, $J_{(C,F)}$ = 14.7 Hz), 115.26 (d, $J_{(C,F)}$ = 21.1 Hz), 81.71, 37.18, 37.16 (d, $J_{(C,F)}$ = 4.5 Hz). HRMS (ESI): Exact mass calculated for $C_{11}H_8Cl_2FNO_2$ $[M + H]^+$: 275.9994. Found: 276.0044

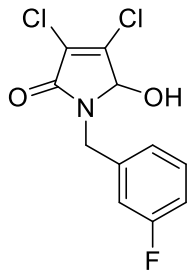

3,4-dichloro-1-(3-fluorobenzyl)-5-hydroxy-*1H*-pyrrol-2(*5H*)-one, Compound 2.45

General procedure A. ^{1}H NMR (400 MHz, DMSO) δ 7.43 – 7.33 (m, 1H), 7.23 (d, *J* = 9.3 Hz, 1H), 7.11 (ddd, *J* = 16.9, 8.8, 2.7 Hz, 3H), 5.41 (d, *J* = 9.2 Hz, 1H), 4.68 (d, *J* = 15.9 Hz, 1H), 4.40 (d, *J* = 15.9 Hz, 1H). ^{13}C NMR (100 MHz, DMSO) δ 162.24 (d, $J_{(C,F)}$ = 243.6 Hz), 161.79, 144.60, 139.98 (d, $J_{(C,F)}$ = 7.2 Hz), 130.42 (d, $J_{(C,F)}$ = 8.3 Hz), 124.62, 123.62 (d, $J_{(C,F)}$ = 2.7 Hz), 114.36 (d, $J_{(C,F)}$ = 21.8 Hz), 114.05 (d, $J_{(C,F)}$ = 20.9 Hz), 81.73, 42.94. HRMS (ESI): Exact mass calculated for $C_{11}H_8Cl_2FNO_2$ $[M + H]^+$: 275.9994. Found: 275.9965

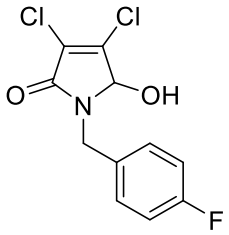

3,4-dichloro-1-(4-fluorobenzyl)-5-hydroxy-*1H*-pyrrol-2(*5H*)-one, Compound 2.46

General procedure A. ^{1}H NMR (400 MHz, DMSO) δ 7.38 – 7.29 (m, 2H), 7.22 (d, *J* = 9.3 Hz, 1H), 7.19 – 7.12 (m, 2H), 5.35 (d, *J* = 9.2 Hz, 1H), 4.67 (d, *J* = 15.5 Hz, 1H), 4.34 (d, *J* = 15.6 Hz, 1H). ^{13}C NMR (100 MHz, DMSO) δ 162.65, 161.46 (d, $J_{(C,F)}$ = 243.0 Hz), 144.49, 133.18 (d, $J_{(C,F)}$ = 3.0 Hz), 129.83 (d, $J_{(C,F)}$ = 8.2 Hz), 124.64, 115.22 (d, $J_{(C,F)}$ = 23.4 Hz), 81.51, 42.66. HRMS (ESI): Exact mass calculated for $C_{11}H_8Cl_2FNO_2$ $[M + H]^+$: 275.9994. Found: 276.0105

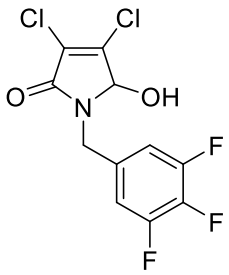

3,4-dichloro-5-hydroxy-1-(3,4,5-trifluorobenzyl)-*1H*-pyrrol-2(*5H*)-one, Compound 2.47

General procedure A. ^{1}H NMR (400 MHz, DMSO) δ 7.31 – 7.23 (m, 2H), 7.19 (d, *J* = 9.5 Hz, 1H), 5.47 – 5.42 (m, 1H), 4.62 (d, *J* = 16.2 Hz, 1H), 4.41 (d, *J* = 16.2 Hz, 1H). ^{13}C NMR (100 MHz, DMSO) δ 161.94, 151.37 (m), 148.91 (m), 144.72, 134.60 (m), 124.56, 112.09 (dd, $J_{(C,F)}$ = 15.8 Hz, 5.4 Hz), 81.89, 42.47. HRMS (ESI): Exact mass calculated for $C_{11}H_6Cl_2F_3NO_2$ $[M + H]^+$: 311.9805. Found: 311.9908

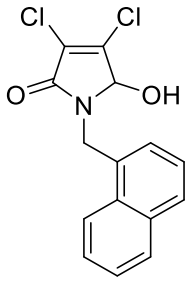

3,4-dichloro-5-hydroxy-1-(naphthalen-1-ylmethyl)-*1H*-pyrrol-2(*5H*)-one, Compound 2.48

General procedure A. ^{1}H NMR (400 MHz, DMSO) δ 8.17 (d, *J* = 8.2 Hz, 1H), 7.95 (dd, *J* = 9.6, 8.4 Hz, 1H), 7.89 (d, *J* = 7.7 Hz, 1H), 7.64 – 7.40 (m, 4H), 7.25 (d, *J* = 9.4 Hz, 1H), 5.27 (d, *J* = 10.6 Hz, 1H), 5.23 (d, *J* = 4.1 Hz, 1H), 4.75 (d, *J* = 15.7 Hz, 1H). ^{13}C NMR (100 MHz, DMSO) δ 161.51, 144.71, 133.35, 131.90, 130.71, 128.61, 128.15, 126.53, 126.31, 125.96, 125.45, 124.55, 123.14, 81.39, 40.88. HRMS (ESI): Exact mass calculated for $C_{15}H_{11}Cl_2NO_2$ $[M + H]^+$: 308.0245. Found: 308.0365

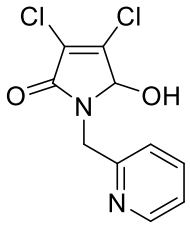

3,4-dichloro-5-hydroxy-1-(pyridin-2-ylmethyl)-*1H*-pyrrol-2(*5H*)-one, Compound 2.49

General procedure A. ^{1}H NMR (400 MHz, $CDCl_3$) δ 8.46 (d, *J* = 5.0 Hz, 1H), 7.80 (td, *J* = 7.7, 1.7 Hz, 1H), 7.47 (d, *J* = 7.8 Hz, 1H), 7.32 (dd, *J* = 7.4, 5.1 Hz, 1H), 5.50 (s, 1H), 5.04 (d, *J* = 16.0 Hz, 1H), 4.64 (d, *J* = 16.0 Hz, 1H). ^{13}C NMR (100 MHz, $CDCl_3$) δ 163.17, 155.25, 147.93, 145.39, 138.88, 125.81, 123.57, 123.47, 83.45, 46.46. HRMS (ESI): Exact mass calculated for $C_{10}H_8Cl_2N_2O_2$ $[M + H]^+$: 259.0041. Found: 259.0025

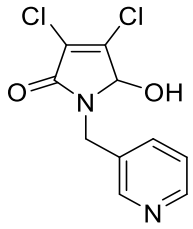

3,4-dichloro-5-hydroxy-1-(pyridin-3-ylmethyl)-*1H*-pyrrol-2(*5H*)-one, Compound 2.50

General procedure A. ^{1}H NMR (400 MHz, DMSO) δ 8.54 (s, 1H), 8.48 (d, *J* = 3.9 Hz, 1H), 7.71 (d, *J* = 7.9 Hz, 1H), 7.36 (dd, *J* = 7.8, 4.8 Hz, 1H), 7.25 (d, *J* = 9.2 Hz, 1H), 5.43 (d, *J* = 8.8 Hz, 1H), 4.67 (d, *J* = 15.8 Hz, 1H), 4.44 (d, *J* = 15.8 Hz, 1H). ^{13}C NMR (100 MHz, DMSO) δ 161.80, 149.03, 148.46, 144.61, 135.68, 132.71, 124.58, 123.57, 81.84, 41.28. HRMS (ESI): Exact mass calculated for $C_{10}H_8Cl_2N_2O_2$ $[M + H]^+$: 259.0041. Found: 259.0009

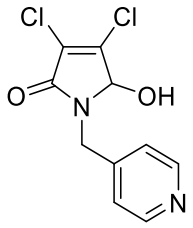

3,4-dichloro-5-hydroxy-1-(pyridin-4-ylmethyl)-*1H*-pyrrol-2(*5H*)-one, Compound 2.51

General procedure A. ^{1}H NMR (400 MHz, DMSO) δ 8.53 (d, *J* = 6.0 Hz, 2H), 7.34 (d, *J* = 5.7 Hz, 2H), 7.29 (s, 1H), 5.47 (s, 1H), 4.67 (d, *J* = 16.7 Hz, 1H), 4.48 (d, *J* = 16.7 Hz, 1H). ^{13}C NMR (100 MHz, DMSO) δ 161.99, 149.17, 146.80, 144.77, 124.60, 122.58, 82.05, 42.67. HRMS (ESI): Exact mass calculated for $C_{10}H_8Cl_2N_2O_2$ $[M + H]^+$: 259.0041. Found: 259.0214

2.4.11 MRM Transition Data

Compound ID	Quantitative Transition		Confirmatory Transition		Collision Energy (eV)	Chromatography Scheme
	Parent Ion (*m/z*)	Fragment Ion (*m/z*)	Parent Ion (*m/z*)	Fragment Ion (*m/z*)		
2.1	229.0	163.0	231.0	165.0	25	A
2.2	318.9	209.0	318.9	237.0	18	A
2.3	300.1	193.0	302.1	195.0	20	A
2.5	237.0	209.0	239.0	211.0	15	A
2.7	152.9	61.0	152.9	117.0	22	B

2.8	183.0	150.9	185.0	152.9	15	A
2.9	207.0	150.9	209.0	152.9	20	B
2.10	229.0	165.0	229.0	158.1	22	A
2.11	168.0	132.0	170.0	134.0	20	A
2.12	258.0	91.1	260.0	91.1	20	A
2.13	242.1	91.1	244.1	91.1	22	A
2.14	272.0	91.1	274.0	91.1	20	B
2.15	300.0	91.1	300.0	258.0	20	A
2.16	256.0	91.1	256.0	178.0	17	B
2.17	334.1	227.0	336.1	229.0	20	B
2.18	190.1	91.1	190.1	112.0	18	B
2.19	218.1	91.1	218.1	140.1	22	A
2.20	248.0	180.0	250.0	182.0	18	A
2.21	264.0	180.0	266.0	182.0	17	B
2.22	240.1	91.1	240.1	133.0	27	A
2.24	210.0	132.0	212.0	134.0	20	B
2.25	208.0	150.9	210.0	152.9	23	A
2.26	208.0	150.9	210.0	152.9	23	A
2.27	206.0	134.0	208.0	134.0	23	A
2.28	281.1	178.0	283.0	180.0	25	A
2.29	272.1	105.1	274.1	105.1	25	A
2.30	286.1	164.0	286.1	117.1	20	A
2.31	300.1	131.1	302.1	131.1	23	A
2.33	282.0	133.1	284.0	133.1	20	A
2.34	272.0	105.1	272.0	168.0	25	A
2.35	334.0	167.1	336.0	167.1	25	A
2.36	288.0	121.1	290.0	121.1	18	A
2.37	274.0	107.1	276.0	107.1	30	B
2.38	292.0	125.0	294.0	125.0	22	A
2.39	336.0	169.0	338.0	169.0	22	A
2.40	326.0	159.0	328.0	159.0	25	A
2.41	272.0	105.1	274.0	105.1	20	A
2.42	288.0	121.1	290.0	121.1	17	A
2.43	274.0	107.1	276.0	107.1	20	A
2.44	276.0	109.1	278.0	109.1	22	A
2.45	276.0	109.1	276.0	258.0	20	A
2.46	276.0	109.1	278.0	109.1	22	A
2.47	312.0	145.0	312.0	294.0	18	B
2.48	308.0	180.0	310.0	182.0	17	A
2.49	259.0	241.0	261.0	243.0	20	B
2.50	259.0	92.1	261.0	92.1	35	A
2.51	259.0	107.1	261.0	107.1	32	B

* - compound not analyzed

LC-MRM Gradient A:

Retention Time (min)	Flow Rate (µL/min)	Water (0.1 % formic acid) (%)	Acetonitrile (0.1 % formic acid) (%)
0	250	98	2
5	250	50	50
5.5	275	20	80
10	350	0	100

LC-MRM Gradient B:

Retention Time (min)	Flow Rate (µL/min)	Water (0.1 % formic acid) (%)	Acetonitrile (0.1 % formic acid) (%)
0	250	98	2
2	250	50	50
5.5	275	20	80
10	350	0	100

2.5 References

(1) *Canadian Cancer Society Statistics*; Toronto, ON, 2015.

(2) Russell, S. J.; Peng, K.-W.; Bell, J. C. *Nat. Biotechnol.* **2012**, *30*, 658–670.

(3) Fuhrman, J.; Noble, R. T. *Limnol. Oceanogr.* **1995**, *40*, 1236–1242.

(4) Minor, P. D. *Virology* **2015**, *479-480*, 379–392.

(5) Lauring, A. S.; Jones, J. O.; Andino, R. *Nat. Biotechnol.* **2010**, *28*, 573–579.

(6) Waehler, R.; Russell, S. J.; Curiel, D. T. *Nat. Rev. Genet.* **2007**, *8*, 573–587.

(7) Dock, G. *Am. J. Med. Sci.* **1904**, *127*, 563.

(8) Newman, W.; Southam, C. M. *Cancer* **1954**, *7*, 106–118.

(9) Kelly, E.; Russell, S. J. *Mol. Ther.* **2007**, *15*, 651–659.

(10) Hanahan, D.; Weinberg, R. A. *Cell* **2011**, *144*, 646–674.

(11) Parkin, J.; Cohen, B. *Lancet* **2001**, *357*, 1777–1789.

(12) Schroder, K.; Hertzog, P. J.; Ravasi, T.; Hume, D. A. *J. Leukozyte Biol.* **2004**, *75*.

(13) Pardoll, D. M. *Nat. Rev. Cancer* **2012**, *12*, 252–264.

(14) Steele, L.; Errington, F.; Prestwich, R.; Ilett, E.; Harrington, K.; Pandha, H.; Coffey, M.; Selby, P.; Vile, R.; Melcher, A. *Mol. Cancer* **2011**, *10*, 20.

(15) Lichty, B. D.; Breitbach, C. J.; Stojdl, D. F.; Bell, J. C. *Nat. Rev. Cancer* **2014**, *14*, 559–567.

(16) Murali, V. K.; Ornelles, D. A.; Gooding, L. R.; Wilms, H. T.; Huang, W.; Tollefson, A. E.; Wold, W. S. M.; Garnett-Benson, C. *J. Virol.* **2014**, *88*, 903–912.

(17) Cook, J.; Routes, J. *Front. Biosci.* **2005**, *10*, 1396–1414.

(18) Liu, T.-C.; Hwang, T.; Park, B.-H.; Bell, J.; Kirn, D. H. *Mol. Ther.* **2008**, *16*, 1637–1642.

(19) Parker, J. N.; Gillespie, G. Y.; Love, C. E.; Randall, S.; Whitley, R. J.; Markert, J. M. *Proc. Natl. Acad. Sci. U. S. A.* **2000**, *97*, 2208–2213.

(20) Stojdl, D. F.; Lichty, B. D.; Benjamin, R.; Paterson, J. M.; Power, A. T.; Knowles, S.; Marius, R.; Reynard, J.; Poliquin, L.; Atkins, H.; Brown, E. G.; Durbin, R. K.; Durbin, J. E.; Hiscott, J.; Bell, J. C. *Cancer Cell* **2003**, *4*, 263–275.

(21) Liebert, M. A.; Hallenbeck, P. L.; Chang, Y.; Hay, C.; Golightly, D.; Art, D. S.; Lin, J.; Phipps, S.; Chiang, Y. L. **1999**, *1733*, 1721–1733.

(22) Miest, T. S.; Cattaneo, R. *Nat. Rev. Microbiol.* **2014**, *12*, 23–34.

(23) Breitbach, C. J.; Burke, J.; Jonker, D.; Stephenson, J.; Haas, A. R.; Chow, L. Q. M.; Nieva, J.; Hwang, T.-H.; Moon, A.; Patt, R.; Pelusio, A.; Le Boeuf, F.; Burns, J.; Evgin, L.; De Silva, N.; Cvancic, S.; Robertson, T.; Je, J.-E.; Lee, Y.-S.; Parato, K.; Diallo, J.-S.; Fenster, A.; Daneshmand, M.; Bell, J. C.; Kirn, D. H. *Nature* **2011**, *477*, 99–102.

(24) Heo, J.; Reid, T.; Ruo, L.; Breitbach, C. J.; Rose, S.; Bloomston, M.; Cho, M.; Lim, H. Y.; Chung, H. C.; Kim, C. W.; Burke, J.; Lencioni, R.; Hickman, T.; Moon, A.; Lee, Y. S.; Kim, M. K.; Daneshmand, M.; Dubois, K.; Longpre, L.; Ngo, M.; Rooney, C.; Bell, J. C.; Rhee, B.-G.; Patt, R.; Hwang, T.-H.; Kirn, D. H. *Nat. Med.* **2013**, *19*, 329–336.

(25) Ilkow, C. S.; Swift, S. L.; Bell, J. C.; Diallo, J.-S. *PLoS Pathog.* **2014**, *10*, e1003836.

(26) Stojdl, D. F.; Lichty, B.; Knowles, S.; Marius, R.; Atkins, H.; Sonenberg, N.; Bell, J. C. *Nat. Med.* **2000**, *116*, 821–825.

(27) Haralambieva, I.; Iankov, I.; Hasegawa, K.; Harvey, M.; Russell, S. J.; Peng, K.-W. *Mol. Ther.* **2007**, *15*, 588–597.

(28) Altomonte, J.; Wu, L.; Chen, L.; Meseck, M.; Ebert, O.; García-Sastre, A.; Fallon, J.; Woo, S. L. *Mol. Ther.* **2008**, *16*, 146–153.

(29) Le Boeuf, F.; Diallo, J.-S.; McCart, J. A.; Thorne, S.; Falls, T.; Stanford, M.; Kanji, F.; Auer, R.; Brown, C. W.; Lichty, B. D.; Parato, K.; Atkins, H.; Kirn, D.; Bell, J. C. *Mol. Ther.* **2010**, *18*, 888–895.

(30) Forbes, N. E.; Krishnan, R.; Diallo, J.-S. *Front. Oncol.* **2014**, *4*, 191.

(31) Ikeda, K.; Ichikawa, T.; Wakimoto, H.; Silver, J. S.; Deisboeck, T. S.; Finkelstein, D.; Harsh, G. R.; Louis, D. N.; Bartus, R. T.; Hochberg, F. H.; Chiocca, E. A. *Nat. Med.* **1999**, *5*, 881–887.

(32) Fulci, G.; Breymann, L.; Gianni, D.; Kurozomi, K.; Rhee, S. S.; Yu, J.; Kaur, B.; Louis, D. N.; Weissleder, R.; Caligiuri, M. A.; Chiocca, E. A. *Proc. Natl. Acad. Sci. U. S. A.* **2006**, *103*, 12873–12878.

(33) Chang, H.-M.; Paulson, M.; Holko, M.; Rice, C. M.; Williams, B. R. G.; Marié, I.; Levy, D. E. *Proc. Natl. Acad. Sci. U. S. A.* **2004**, *101*, 9578–9583.

(34) Nguyên, T. L.-A.; Abdelbary, H.; Arguello, M.; Breitbach, C.; Leveille, S.; Diallo, J.-S.; Yasmeen, A.; Bismar, T. A.; Kirn, D.; Falls, T.; Snoulten, V. E.; Vanderhyden, B. C.; Werier, J.; Atkins, H.; Vähä-Koskela, M. J. V; Stojdl, D. F.; Bell, J. C.; Hiscott, J. *Proc. Natl. Acad. Sci. U. S. A.* **2008**, *105*, 14981–14986.

(35) Alvarez-Breckenridge, C. A.; Yu, J.; Price, R.; Wei, M.; Wang, Y.; Nowicki, M. O.; Ha, Y. P.; Bergin, S.; Hwang, C.; Fernandez, S. A.; Kaur, B.; Caligiuri, M. A.; Chiocca, E. A. *J. Virol.* **2012**, *86*, 4566–4577.

(36) Liu, T.-C.; Castelo-Branco, P.; Rabkin, S. D.; Martuza, R. L. *Mol. Ther.* **2008**, *16*, 1041–1047.

(37) Kaur, S.; Lal, L.; Sassano, A.; Majchrzak-Kita, B.; Srikanth, M.; Baker, D. P.; Petroulakis, E.; Hay, N.; Sonenberg, N.; Fish, E. N.; Platanias, L. C. *J. Biol. Chem.* **2007**, *282*, 1757–1768.

(38) Paglino, J. C.; van den Pol, A. N. *J. Virol.* **2011**, *85*, 9346–9358.

(39) Di, L.; Kerns, E. H.; Hong, Y.; Chen, H. *Int. J. Pharm.* **2005**, *297*, 110–119.

(40) Garcia, V.; Krishnan, R.; Davis, C.; Batenchuk, C.; Le Boeuf, F.; Abdelbary, H.; Diallo, J.-S. *J. Vis. Exp.* **2014**, 1–8.

(41) Zhang, J.; Blazecka, P. G.; Belmont, D.; Davidson, J. G. *Org. Lett.* **2002**, *4*, 4559–4561.

(42) Zhang, J.; Sarma, K.; Curran, T. *Synlett* **2013**, *24*, 550–569.

(43) Budke, B.; Kalin, J. H.; Pawlowski, M.; Zelivianskaia, A. S.; Wu, M.; Kozikowski, A. P.; Connell, P. P. *J. Med. Chem.* **2013**, *56*, 254–263.

(44) Ratts, K. W.; Phillips, W. G. *J. Org. Chem.* **1974**, *39*, 3300–3301.

(45) Diallo, J.-S.; Roy, D.; Abdelbary, H.; De Silva, N.; Bell, J. C. *J. Vis. Exp.* **2011**, 2–6.

(46) Brun, J.; McManus, D.; Lefebvre, C.; Hu, K.; Falls, T.; Atkins, H.; Bell, J. C.; McCart, J. A.; Mahoney, D.; Stojdl, D. F. *Mol. Ther.* **2010**, *18*, 1440–1449.

(47) Le Bœuf, F.; Batenchuk, C.; Vähä-Koskela, M.; Breton, S.; Roy, D.; Lemay, C.; Cox, J.; Abdelbary, H.; Falls, T.; Waghray, G.; Atkins, H.; Stojdl, D.; Diallo, J.-S.; Kærn, M.; Bell, J. C. *Nat. Commun.* **2013**, *4*, 1974.

(48) Jordan, R.; Schaffer, P. *J. Virol.* **1997**, *71*, 6850–6862.

(49) Bellina, F.; Anselmi, C.; Martina, F.; Rossi, R. *Eur. J. Org. Chem.* **2003**, *2003*, 2290–2302.

(50) Zhang, J.; Blazecka, P. G.; Davidson, J. G. *Org. Lett.* **2003**, *5*, 553–556.

(51) Holz, J.; Zayas, O.; Jiao, H.; Baumann, W.; Spannenberg, A.; Monsees, A.; Riermeier, T. H.; Almena, J.; Kadyrov, R.; Börner, A. *Chem. - A Eur. J.* **2006**, *12*, 5001–5013.

(52) Yamashita, S.; Mase, N.; Takabe, K. *Tetrahedron Asymmetry* **2008**, *19*, 2115–2118.

Chapter 3: Development of an Armeniaspirole-based Chemical Biology Probe

3.1 Introduction

3.1.1 A brief history of antibacterial agents

The use of antibacterial agents has had a colossal impact on controlling infectious diseases, known to be leading causes of morbidity and mortality in humans worldwide. While evidence suggests the protective use of antibacterial agents in humans could date as far back as 350 – 550 AD,[1] the use of rigours science and a systemic approach to drug discovery and development began in the early 1900s. The beginning of the modern antibacterial era is often associated with Paul Ehrlich's efforts to develop a drug for the treatment of syphilis. Towards this, Ehrlich and his team synthesized hundreds of organoarsenic derivatives of arsanilic acid and tested them in an infected rabbit model. These pioneering efforts yielded arsphenamine, which was marketed by the German company Hoechst AG under the tradename Salvarsan in 1911.[2] Hoechst AG shipped 65,000 free samples of Salvarsan to doctors around the world, receiving international acclaim.[3] These organoarsenic agents were prescribed for human use until they were replaced by less toxic penicillin compounds.

Penicillin was discovered at St. Mary's Hospital in London in 1928 when Alexander Fleming, a bacteriology professor, noted that the presence of the fungal strain *Penicillium chrysogenum* on his petri dishes inhibited staphylococcal colony growth. Fleming and coworkers then set forward to isolate the agent responsible for antibacterial activity, later identified as the small molecule penicillin.[4] In the late 1930s, Oxford University scientists Howard Florey and Ernst Chain began investigations into the production and use of penicillin as a therapeutic agent to treat bacterial infections. In 1940, crucial animal experiments demonstrated efficacy and in 1942 human treatments began. Remarkable efficacy spurred innovations in the commercial production of

penicillin by a number of companies including Merck, Pfizer, Squibb, and Abbot to support the allies World War II effort.

Another revolutionary discovery in antibacterial drug development was the development of sulfonamide drugs. Sulfonamides were shown to have broad activity against streptococcal infections and are credited with saving the lives of millions of people with systemic bacterial infections. Prontosil, the first sulfonamide drug, was developed by Bayer chemists Josef Klarer and Fritz Mietzsch in the 1930s. Prontosil was later discovered to be a prodrug, metabolized in the body to liberate the active agent, sulfanilamide. This drug remained on the market until the 1960s while derivatives are still investigated and used today.

The early success of penicillins and sulfonamides in controlling infectious diseases paved the way to the 'golden era' of antibiotic development. The mid-20th century saw the emergence of many more important classes of antibiotics including aminoglycosides (1944), cephalosporins (1945), tetracyclines (1950), macrolides (1952), glycopeptides (1956), rifamycins (1957), nitroimadazoles (1959), and quinolones (1962).[5] By the late 1960s, experts believed that infectious disease would eventually be conquered. This optimism did not last. By the early 1990s it became evident that the emergence and surge of new antibiotic resistant bacterial strains would continue to pose a serious threat to the ability to effectively treat bacterial infections.

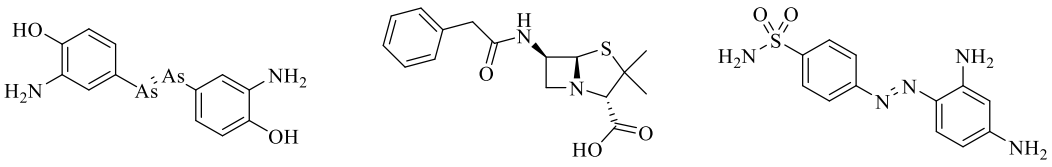

arsphenamine penicillin G Prontosil

Figure 3.1 Examples of early 20th century antibacterial agents.

3.1.2 The rise of antibacterial resistance

The term antibacterial resistance refers to the emergence of new bacterial strains that resist or continue to grow in the presence of drugs that are purposed to kill them. The basis of this problem stems from the ability of bacteria to gain resistance through genetic mutation under drug pressure, or by the acquisition of resistance genes through horizontal gene transfer. Recently, this problem has been amplified as the rate by which novel antibiotics are discovered and developed for clinical use has been decreased while the use of antibiotics has increased.

Bacterial strains that exhibit the most concerning resistance levels today include *Klebsiella pneumonia*, *Escherichia coli*, and *Staphylococcus aureus*. A study aiming to characterize the prevalence and rise of *K. pneumonia* drug resistance was completed by reviewing more than 3 million *K. pneumonia* antimicrobial susceptibility tests from US inpatients taken between 1998 and 2010.[6] An increase in resistance was found for all agents. The most dramatic increases over this timeline were for aztreonam (7.7 % to 22.2 %), ceftazidime (5.5 % to 17.2 %), and ciprofloxacin (5.5 % to 16.8 %). In a similar retrospective study of drug resistance in *E. coli*, 1,729 strains collected between 1950 and 2002 showed significant increases in resistance for ampicillin, sulfonamide, and tetracycline, and a 7.2 % increase in strains resistant to more than three classes of antibacterial agents. Methicillin-resistant *S. aureus* (MRSA), has emerged as a significant pathogen associated with high levels of morbidity and mortality.[7] Recently it has been reported that there is an emergence of MRSA strains that are less-susceptible or resistant to Vancomycin, the gold standard of MRSA infection treatment.[8] The conclusion shared by these studies is that the bacterial infections easily treated today will require new control strategies in the future.

Antibacterial resistance poses a serious threat to global human health. A recent UK government sponsored review completed by KPMG and RAND reported that antimicrobial

resistant infections were responsible for at least 700,000 deaths worldwide in 2015, and a continued rise in resistance could lead to 10 million deaths annually by 2050.[9] A concerted international effort is needed to make changes in the way antibiotics are used and to bolster the development of new antibacterial agents to attenuate the rise and impact of antibacterial resistance.

3.1.3 Natural products as leads to new antibiotic scaffolds

While it is clear that there is a dire need to develop new therapeutics for infectious disease, a successful undertaking against antibacterial resistance will require the discovery of antibiotics that function with new mechanisms of action. Currently, the global pipeline of antibiotics is filled with derivatives of established chemical classes which target previously known mechanisms of action. A 2011 study showed that out of the 90 antibacterial agents in clinical development, only two acted on new biological targets and none of them acted by a new mechanism of action.[10] The problem with this approach is that resistance mechanisms already exist for all established chemical classes.

Despite the advent of combinatorial chemistry in the 1980s, natural product chemistry has maintained a staggering role in drug discovery.[11] It has been recognized that superior screening libraries can be built using natural products and compounds resembling natural products in terms of the amount of stereo centers, heterocyclic substituents and polycyclic structures. These compounds have been described as “privileged structures” as leads to identifying compounds with therapeutic potential. Fortunately, genomic studies have hinted that microorganisms will continue to be a productive source for the discovery of new natural products.[12] This will rely on the development of new techniques allowing for exploitation of producers with greater biodiversity (Currently, more than 99 % of bacteria in external environments are unculturable[13]), and the ability

to find and maximize the genomic potential of producers through genomic mining, variation of culture conditions and the induction of silent genes.[14]

In a recent development striving toward the abovementioned goal of exploiting biodiversity to facilitate the identification of new bioactive natural products, the growth of soil bacteria using a channeled device called the iChip was shown to both isolate bacteria and facilitate the diffusion of nutrients and growth factors enabling colony growth under natural-like conditions.[15] This *in situ* method was shown to improve growth recovery of these environmental species under laboratory conditions, from approximately 1 % to nearly 50 %. The colonies that formed on the iChip were then grown *in vitro* and the isolates were screened for antimicrobial activity. This approach led to the discovery of teixobactin (Figure 3.2), a novel antibiotic with potent activity against many drug resistant pathogens including *S. aureus* (MRSA), *E. faecalis* (VRE) and *S. pneumoniae* (PRSP) .[16] Remarkably, this compound was produced from a previously unknown species of β-proteobacteria named *Eleftheria terrae*.

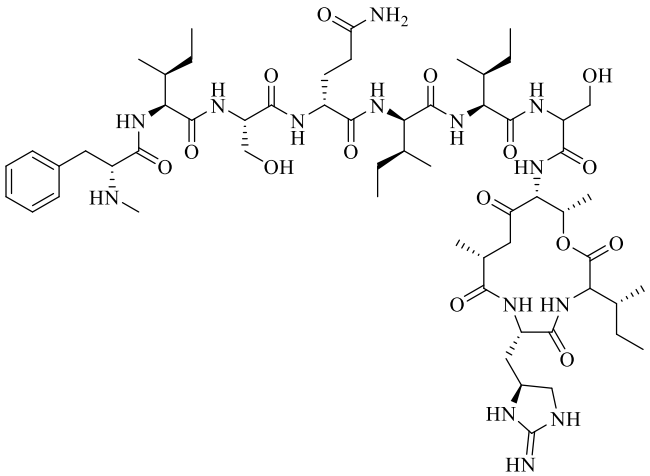

Figure 3.2 Structure of the novel antibiotic teixobactin.

3.1.4 Discovery and evaluation of armeniaspiroles

In 2012, the isolation and structural elucidation of armeniaspiroles A-C was published by an antibiotic lead discovery team at Sanofi.[17] In this study, the authors describe the emergence of three new peaks on the HPLC chromatogram of methanolic extracts when a *Streptomyces armeniacus* (DSM19369) strain was grown on ISP-2 medium. Variations in the media used for bacterial growth has been shown to strongly influence the secondary metabolite profiles of producing microorganisms.[14] Following the isolation of these three new compounds by prep-HPLC, the structures were elucidated using mass spectrometry, NMR studies and X-ray crystallography (Figure 3.3). They were named armeinaspiroles to pay homage to the Armenian origin of the *Streptomyces* strain and the unprecedented spiro-[4.4]non-8-ene structural skeleton contained by all three compounds.

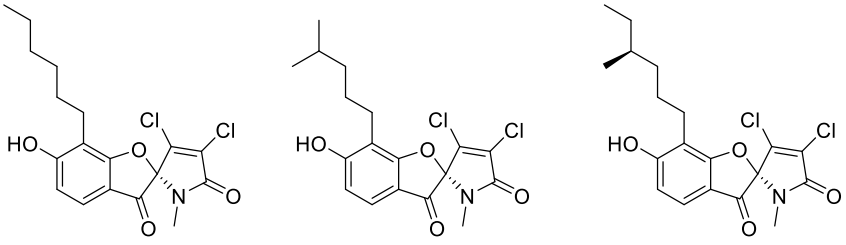

Figure 3.3 Structure of Armeniaspiroles A-C.

The armeniaspirole compounds exhibited moderate to high activity against a number of drug resistant Gram-positive strains including *S. aureus* (MRSA), *S. pneumoniae* (PRSP), and *E. faecium* (VRE) (Table 3.1). No activity was observed in examples of Gram-negative strains that were tested (*E. coli* and *P. aeruginosa*) or the fungus *C. albicans*. Additionally, no cytotoxicity was observed in human hepatocyte HepG2 cells. Studies on time-kill kinetics showed that **3.1** is

bacteriostatic with time-dependent effects. Importantly, a serial passaging experiment showed that the development of drug resistance was not observed after 30 passages with *S. aureus*. Despite the presence of the electrophilic core, **3.1** exhibits acceptable physicochemical properties including full stability in PBS buffer over 24 hours. In the presence of 10 mM glutathione or 10 mM iso-butylamine in PBS, **3.1** decreased by only 30 % and < 10 % respectively. In addition, **3.1** has no strong interaction with cytochromes CYP3A4 and CYP2D6 and displays no activity on the hERG cardiac channel.

Table 3.1 In vitro activities of **3.1** – **3.3**.

Strain	**3.1**		**3.2**		**3.3**	
	IC_{80} (μg/mL)	MIC (μg/mL)	IC_{80} (μg/mL)	MIC (μg/mL)	IC_{80} (μg/mL)	MIC (μg/mL)
S. aureus (ATCC13709)	0.3	1	0.7	1	0.5	1
S. aureus (ATCC29213)	0.35	1	0.85	2	0.75	2
S. aureus (ATCC33592)	<0.125	0.25	<0.125	0.25	<0.125	0.125
S. pneumonia (DSM11865)	2.30	4	1.80	4	1.80	4
S. pyogenes (ATCC12344)	6.20	16	5.80	32	4.30	64
E. faecium (DSM17050)	8.20	16	5.80	8	5.90	8
E. faecalis (ATCC29212)	25.20	32	17.80	32	24.70	64
M. smegmatis (ATCC607)	0.30	2	0.60	8	0.50	4
P. aeruginosa (ATCC27853)	>64	>64	>64	>64	>64	>64
E. coli (ATCC25922)	>64	>64	>64	>64	>64	>64
C. albicans (FH2173)	>64	>64	>64	>64	>64	>64

In a second publication, the Sanofi group published a study describing initial SAR findings following the generation of a small set of semi-synthetic derivatives.[18] This set included aromatic halogenated derivatives **3.4** and **3.5**, the aromatic methyl ether **3.6**, derivatives where the β-chlorine was substituted with various nucleophiles including amines (**3.7** and **3.8**), an alcohol (**3.9**)

and a thiol (**3.10**). Both diastereoisomers (**3.11** and **3.12**) of a secondary alcohol containing compound generated though reduction of the ketone in **3.1** were also prepared. While the full activity results of this library was not published, it is stated in the paper that these compounds "did not show any improved antibacterial activities except with the incorporation of halogen into the phenol group."[18] Further experiments described in this paper include efforts toward the chemical synthesis of armeniaspirole A. One hurdle towards this goal was the unintended and unavoidable chlorination of the phenol ring during the construction of the di-chlorinated *spiro*-cycle. Thus, the authors report the synthesis of the previously tested semi-synthetic derivative (**3.4**) 5-chloro-armeniaspirole A. Interestingly, both enantiomers of **3.4** were found to be active with similar potency across a panel of Gram-positive strains.

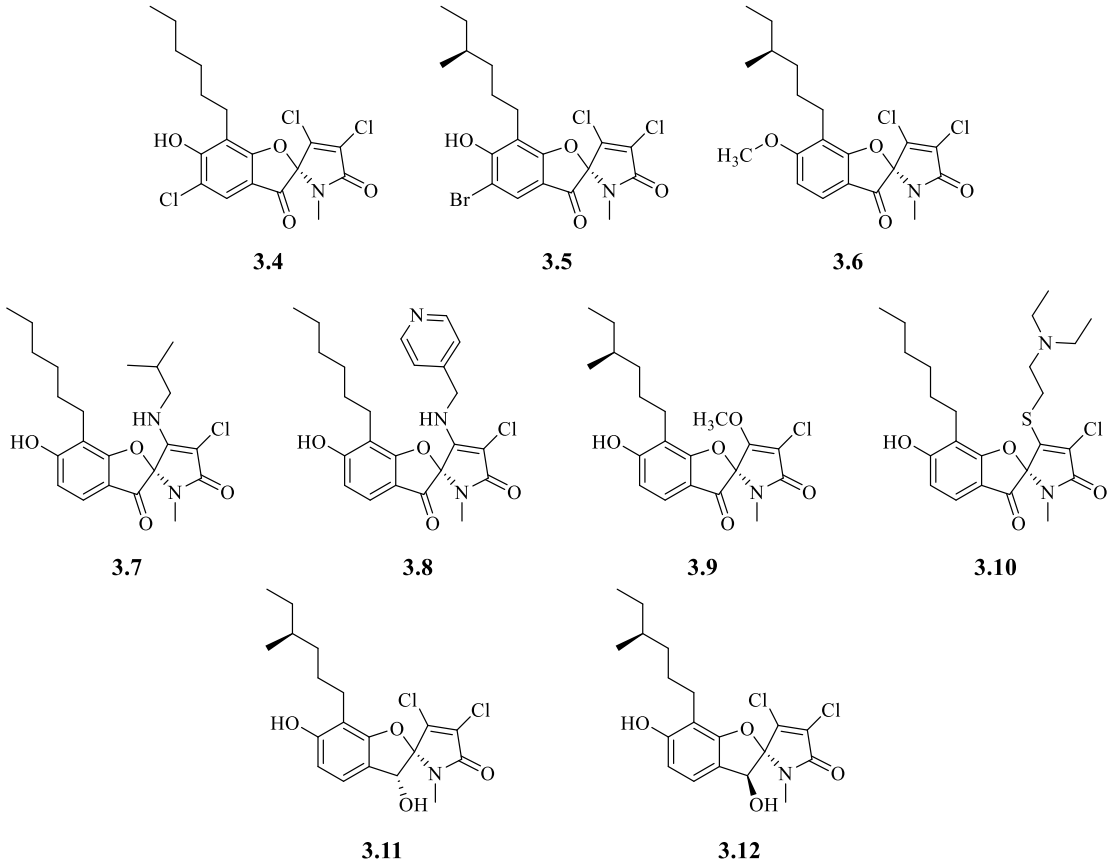

Figure 3.4. Semi-synthetic analogs of armeniaspiroles A and C.

The study also detailed investigations involving the use of **3.1** *in vivo* in pharmacokinetic studies and efficacy studies. Pharmacokinetic studies in healthy mice showed that **3.1** had a moderate plasma half-life ($t_{1/2}$ = 3 h), moderate clearance (1.2 L/h/kg), a large volume of distribution (V_{ss} = 2.4 L /kg), a C_{max} of 27.4 μg /mL. The efficacy of **3.1** was tested in a mouse model for MRSA-induced septicemia. **3.1** was administered by subcutaneous injection at doses of 20, 40 and 80 mg /kg. The % survival of the group (n = 6) was increased from 0 % to 50 % at both 40 and 80 mg /kg. Notably, the group administered with 80 mg /kg exhibited a 1.7 log reduction in bacteremia. In summary, due to their unprecedented scaffold and *in vitro* and *in vivo* activities, armeniaspirole natural products invite further investigations exploring activity, SAR and mechanism of action.

3.2. Results and discussion

Interestingly, armeniaspiroles and the 3,4-dichloro-5-hydroxy-*1H*-pyrrole-2-(*5H*)-one lead core, identified with the medicinal chemistry studies described in Chapter 2, are strikingly similar with regards to both structural features and SAR. Particularly, the steep SAR around the dichloronated Michael-acceptor suggests that the activity of both of these classes of compounds relies on the ability to covalently react with a biological target. It is well known that in terms of drug development, natural products and natural product mimics are privileged structures and are not subject to the same design criteria used to develop synthetic drug entities.[19] Thus, it was hypothesized that armeniaspiroles may exhibit potent and improved oncolytic virus potentiating activity. Notably, it was also hypothesized that if these two classes of compounds share a common biological target leading to enhancement of virus efficacy, the presence of the spiro-cycle in the armeniaspirole scaffold could reduce off-target reactivity.

3.2.1 Synthesis and evaluation of 5-chloro-armeniaspirole

To test the hypothesis that the armeniaspirole class of compounds could be used to potentiate oncolytic viral therapy, the active analog 5-chloro-armeniaspirole A (**3.4**) was synthesized employing the route published by the Sanofi group.[18] A synthetic route for the production of armeniaspirole A has not been published, but antimicrobial activity data suggests that the unnatural chlorinated analog would serve as an appropriate surrogate to draw conclusions about the ability of this class of natural products to enhance attenuated viral efficiency.

The synthesis of **3.4** began with the preparation of the tri-substituted benzene **3.15** (Scheme 3.1). Commercially available 1,3-dimethoxybenzene was treated with n-butyllithium resulting in directed ortho-lithiation of the aromatic ring. The solution was cooled to -50 °C before the introduction of bromine which resulted in halogenation of the aromatic ring to yield **3.14**. To install

the n-hexyl alkyl chain in the 2-position, a Suzuki reaction between aryl bromide and n-hexylboronic acid was used to afford the desired trisubstituted aromatic compound **3.15** in good yield (91 %).

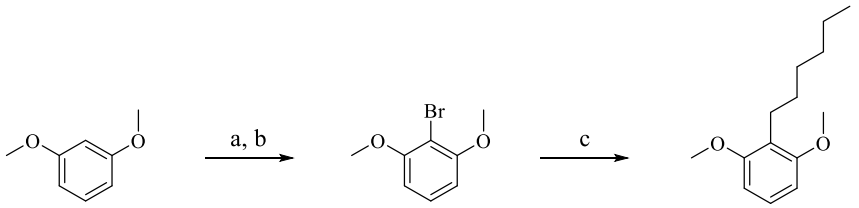

3.13 **3.14** **3.15**

Scheme 3.1. Conditions for the synthesis of 1,3-dimethoxy-2-hexylbenzene (**3.15**). a) n-BuLi, Et_2O, rt; b) Br_2, Et_2O, -50 °C to -20 °C, 42 % over 2 steps; c) n-Hexylboronic acid, $Pd(OAc)_2$, SPhos, K_3PO_4, toluene, 100 °C, 91 %.

A Friedel-Crafts acylation reaction between **3.15** and pyrrole-2-carbonyl chloride (generated from the corresponding carboxylic acid) allowed for the formation of the ketone **3.16** (Scheme 3.2). Next, the selective mono-demethylation of **3.16** was achieved with the Lewis acid BBr_3 at cold temperature (-20 °C to -10 °C) in excellent yield (>99 %). Chlorination of the pyrrole ring in **3.17** was completed using NCS in acetic acid. Consistent with previously published results, the benzene ring was also chlorinated at the 5-position. Subsequently, treatment with triethylamine in chloroform at reflux induced cyclization to give spirocyclic **3.18** in 56 % yield over two steps.

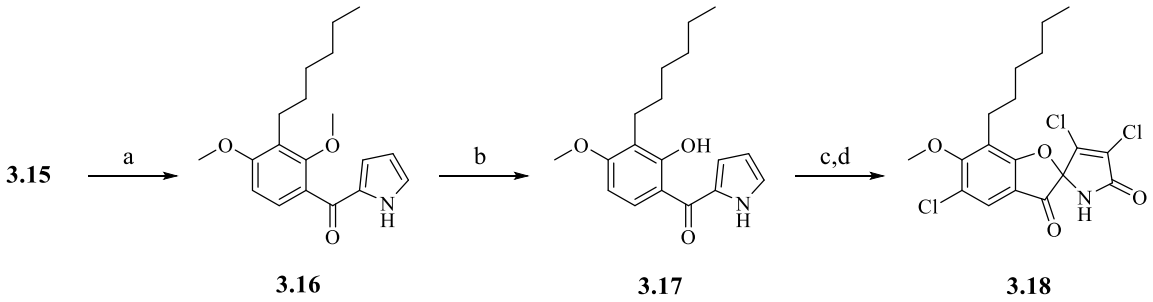

Scheme 3.2. Conditions for the synthesis of **3.18.** a) pyrrole-2-carbonyl chloride, $SnCl_4$, CH_2Cl_2, 0 °C to rt, 96 %; b) BBr_3, DCE, 96 %; c) NCS, AcOH, 70 °C; d) Et_3N, $CHCl_3$, reflux, 56 % over 2 steps.

Following the formation of the spiro-cycle, the lactam in **3.18** was deprotonated using NaH and CH_3I was introduced to afford alkylated **3.19** in excellent yield (> 99 %) (Scheme 3.3). Finally, deprotection of the aromatic methyl ether with BBr_3 in DCE at ambient temperature produced the active analog 5-chloro-armeniasprirole A (**3.4**). Of note, **3.4** was produced and used for activity evaluation as a racemate at the *spiro*-stereocentre, whereas naturally occurring armeniaspirole A is isolated as the enantiopure (*R*)-isomer.

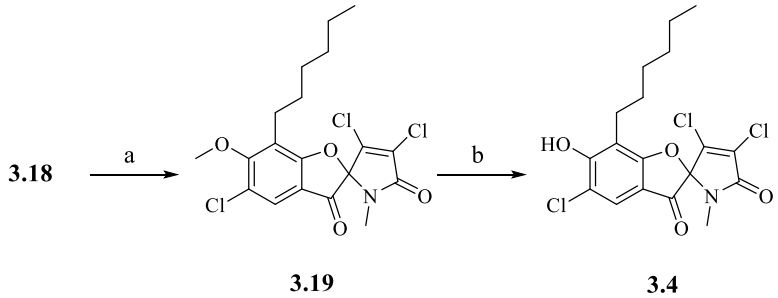

Scheme 3.3. Conditions for the synthesis of 5-chloro-armeniaspirole A (**3.4).** a) NaH, CH_3I, DMF, 0 °C to rt, > 99 %; b) BBr_3, DCE, rt, 93 %.

The evaluation of 5-chloro-armeniaspirole A for its ability to enhance oncolytic viral replication was completed using the luciferase reporter-based viral titration assay described in

Chapter 2. Compared to the optimized lead compounds identified in Chapter 2, 5-chloro-armeniaspirole A (**3.4**) did not enhance VSVΔ51-FLuc replication by an appreciable amount in resistant renal cell carcinoma cells (786-O) (Figure 3.5).

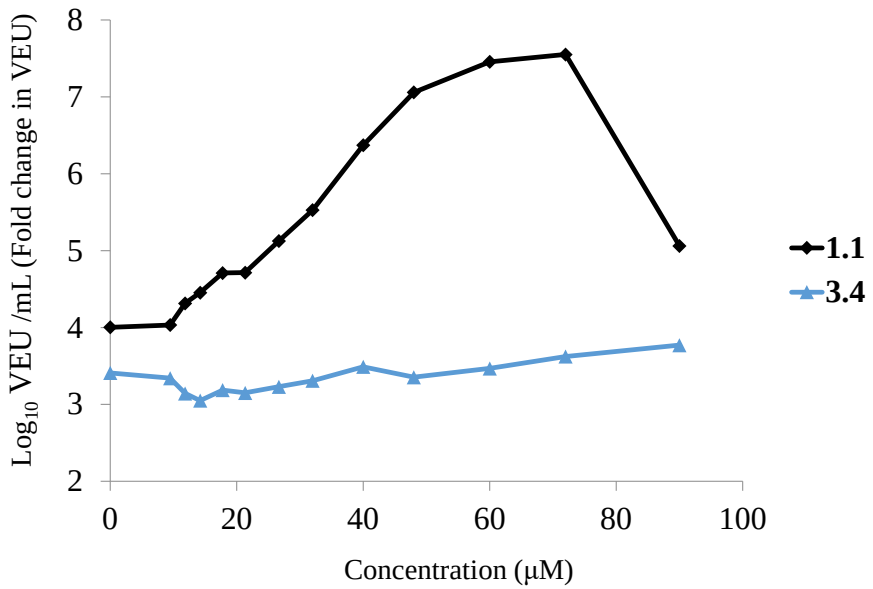

Figure 3.5 Fold change of VSVΔ51-Fluc viral expression units (VEU) in 786-O cells at 40 h post-infection. Cells were pretreated with **1.1** or **3.4** at various concentrations for 4 h prior to infection (MOI 0.05).

To further uncover the similarities and differences between the bioactivity profiles of armeniaspiroles and lead oncolytic virus potentiating compounds, a select set of compounds were screened for antimicrobial activity using a minimum inhibition concentration (MIC) assay (Table 3.2). While 5-chloro-armeniaspirole A (**3.4**) exhibited potent antibiotic activity (1.0 μg /mL) in *B. subtilis*, none of the tested lead oncolytic virus potentiating compounds (**2.10**, **2.24**, **2.25**, **2.28**, **2.29**, **2.40**) demonstrated cytotoxic behaviour.

The previously published SAR studies of armeniaspiroles and derivatives strongly suggest that the antimicrobial activity of this class of compounds was dependent on the presence of the electrophilic α,β-dichloro-γ-lactam. This implies that the biological mechanism may be reliant on

a Michael-addition and elimination process leading to the covalent modification of a biological target. The same trend in SAR and suggestion of a Michael-addition and elimination covalent biological mechanism was echoed with the oncolytic virus potentiating agents developed in Chapter 2. Upon analysis of the luciferase reporter-based viral titration assay data, it is clear that the unique spirocyclic skeleton of the armeniaspirole class of compounds does not offer improvement in oncolytic viral potentiating activity over the lead compounds identified in Chapter 2. It can be concluded that the armeniaspirole class of compounds may interact with the biological target(s) necessary for enhancement of virus efficiency, though there is no benefit to the more sophisticated natural product structure for this application. In contrast, the MIC data suggests that like the α,β-dichloro-γ-lactam, the spirocyclic skeleton and features unique to the armeniaspirole compounds are vital for arresting bacterial cell growth.

The differences in the bioactivity profiles of these two classes of compounds does not incentivize further exploration of armeniaspiroles as enhancers of oncolytic viral therapy. Instead, the focus of studies was pivoted towards chemical biology studies aimed at identifying the biological target(s) of armeniaspiroles. As the lead oncolytic virus enhancing agents share the same electrophilic fragment necessary for the exertion of biological activity, discovery of the mechanism of action of armeniaspiroles could provide information on the types of biological nucleophiles and biomolecules likely to react with this unique core.

Table 3.2. *In vitro* activities of lead virus potentiating compounds.

Compound	Structure	*Bacillus subtilis* MIC (μg / mL)[a]
2.10	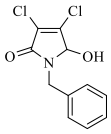	**>32**
2.24	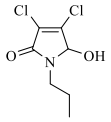	**>32**
2.25	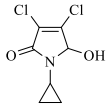	**>32**
2.28	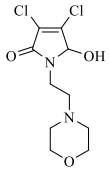	**>32**
2.29	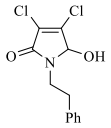	**>32**
2.40	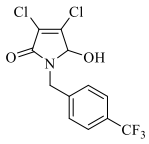	**>32**
3.4	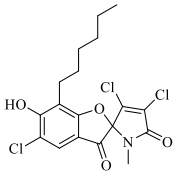	**1.0**
(standard)	Tetracycline	**4.0**

[a] Concentrations tested: 32, 16, 8.0, 4.0, 2.0, 1.0, 0.50, 0.25, 0.125, 0.0625 μg / mL

3.2.2 Development of an armeniaspirole-based chemical biology probe

This section details efforts towards the synthesis and development of an armeniaspirole-based probe that would be useful for chemical biology investigations. A functional probe would allow for the identification of biological targets that are covalently modified by this class of natural

products using a well-established method such as affinity-chromatography or activity based-protein profiling coupled with SDS-Page analysis and mass spectrometry. It was determined that an armeniaspirole A derivative with an alkyne reactive group incorporated into the structure would be synthesized. Since the introduction of chemical alterations to the native natural product structure has the potential to disrupt biological target engagement, the suitability of the probe would be confirmed with an MIC assay to ensure antimicrobial activity is maintained. This problem also provides the opportunity to draw new SAR conclusions for this relatively uninvestigated class of natural products.

With the active analog **3.4** in hand from experiments discussed in section 3.2.1, the incorporation of an alkyne at the end of an alkyl linking chain was achieved at the phenolic position (Equation 3.1). In the presence of the base K_2CO_3 and 6-iodo-1-hexyne in acetone at reflux, ether-containing **3.20** was isolated in low yield (28 %).

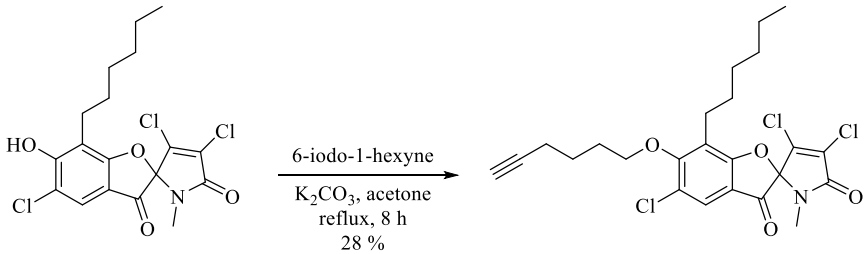

3.4 **3.20** (3.1)

A second alkyne-containing probe **3.21** was synthesized in one step from the advanced 5-chloro-armeniaspirole A intermediate **3.18** (Equation 3.2). Deprotection of the aromatic methyl ether was not possible due to the requirement for a harsh Lewis acid such as BBr_3, which would likely react with the alkyne to give the haloboration product.

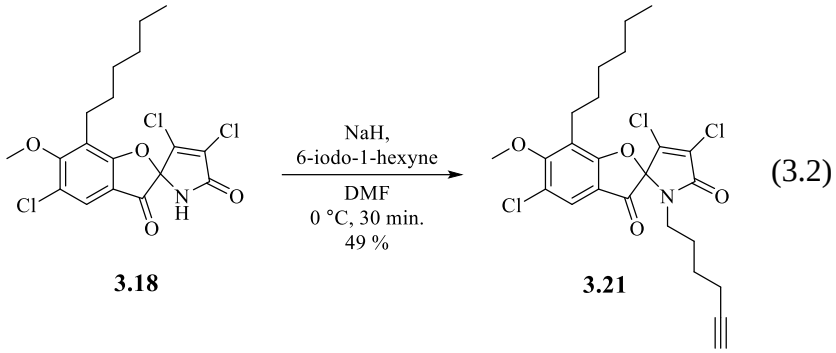

3.18 **3.21** (3.2)

With two potential armeniaspirole-derived probes synthesized, the *B. subtilis* antibacterial activities of **3.20** and **3.21** and analogs **3.4** and **3.19** were tested using the MIC assay (Table 3.3). Unfortunately, **3.20** failed to inhibit the bacterial cell growth at all concentrations tested. The inactivity of the related analog **3.19** to also inhibit growth suggested that the presence of the aromatic alcohol is important for the maintenance of compound bioactivity. Therefore, it was decided that future probe synthesis should focus on alkylation at a different portion of the scaffold, while preserving the aromatic alcohol. The second probe **3.22**, synthesized though incorporation of the linker and reactive group through *N*-alkylation of the lactam, was also shown to be inactive in arresting bacterial growth. The inactivity of **3.19** and **3.20** suggest that the failure of **3.21** to inhibit cell growth may be due to disruption of the aromatic alcohol. Further investigations were needed to understand if the incorporation of a long alkyl chain on the amide would be tolerated.

Table 3.3. *In vitro* activities of armeniaspirole-derived probes.

Compound	Structure	*Bacillus subtilis* MIC (μg / mL)[a]
3.4	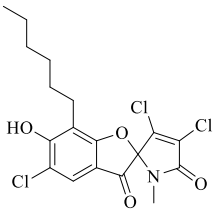	**1.0**
3.19	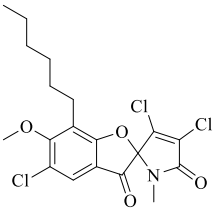	**>32**
3.20	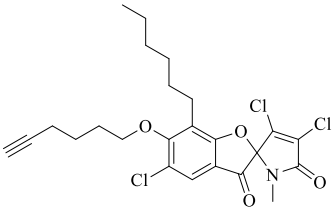	**>32**
3.21	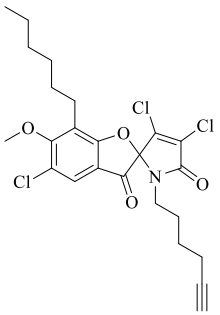	**>32**
(standard)	Tetracycline	**4.0**

[a] Concentrations tested: 32, 16, 8.0, 4.0, 2.0, 1.0, 0.50, 0.25, 0.125, 0.0625 μg / mL

To test the hypothesis that *N*-alkyl substitution on the lactam would be tolerated when the aromatic alcohol is preserved, the analog **3.23** was synthesized which incorporated a simple hexyl alkyl chain (Scheme 3.4). The absence of an alkyne allowed for the deprotection of the aromatic methyl ether using BBr_3.

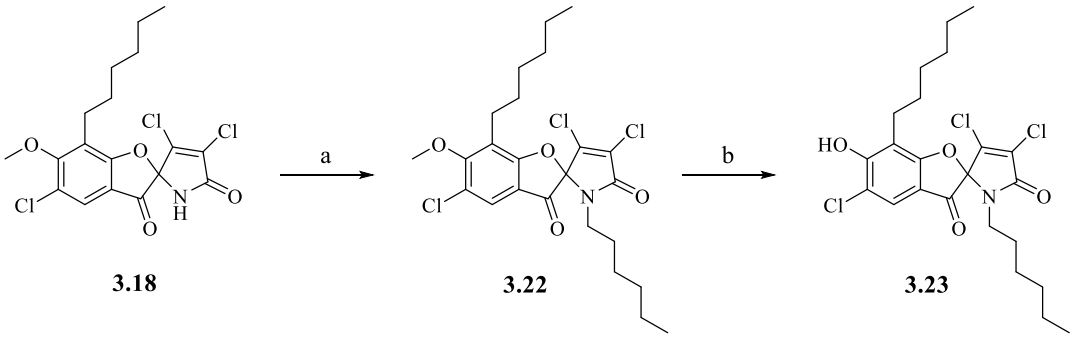

Scheme 3.4. Conditions for the synthesis of **3.24**. a) NaH, 1-iodohexane, DMF, 57 %; b) BBr_3, DCE, rt, 60 %.

With **3.23** and precursor **3.22** in hand, growth inhibition activity was tested with the MIC assay (Table 3.4). Satisfyingly, **3.23** was active in *B. subtilis* (MIC = 0.5 μg / mL). Additionally, the inability of **3.22** to halt bacterial growth supports the original hypothesis that the aromatic alcohol is indeed imperative for the exertion of biological activity. Moving forward, a synthetic route was developed to access a probe with the reactive group incorporated at the amide while conserving the aromatic alcohol found in naturally occurring armeniaspiroles.

Table 3.4. *In vitro* activities of amide substituted armeniaspirole-derived probes.

Compound	Structure	*Bacillus subtilis* MIC (μg / mL)[a]
3.22	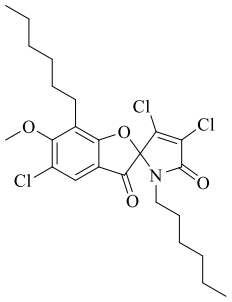	**>32**
3.23	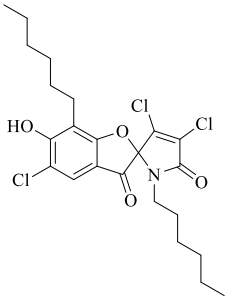	**0.5**
(standard)	tetracycline	**4.0**

[a] Concentrations tested: 32, 16, 8.0, 4.0, 2.0, 1.0, 0.50, 0.25, 0.125, 0.0625 μg / mL

A synthetic strategy involving a late-stage incorporation of an alkyne was envisioned. This would allow for facile deprotection of the aromatic methyl ether. Towards this, a Boc-protected amine **3.26** was synthesized from amino-alcohol **3.24** (Scheme 3.5).

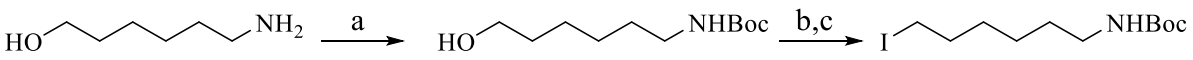

3.24 **3.25** **3.26**

Scheme 3.5. Conditions for the synthesis of **3.26.** a) Boc_2O, CH_3OH, rt, >99%; b) MsCl, Et_3N, CH_2Cl_2; c) NaI, CH_3CN, 70 % (over 2 steps).

Treatment of **3.18** with NaH followed by the introduction of the alkyl iodide **3.26** yielded the desired adduct **3.27**. BBr_3 was then used to deprotect both the aromatic methyl ether and the Boc-protected amine simultaneously, yielding the primary amine **3.28** (Scheme 3.6).

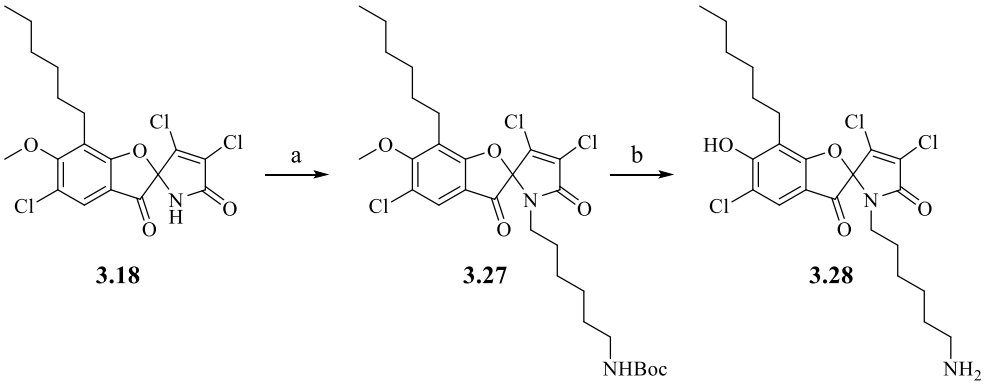

Scheme 3.6. Conditions for the synthesis of **3.28.** a) NaH, **3.26**, DMF, 27 %; b) BBr_3, DCE, rt, 63 %.

The generation of compound **3.28** allows for the incorporation of additional chemical fragments through the modification of the primary amine. To incorporate a terminal alkyne-containing fragment, *N*-hydroxysuccinimide ester **3.29** was used to transform **3.28** (Equation 3.3). This provided the arminiaspirole A derived chemical biology probe **3.30**, with the alkyl-spaced alkyne integrated through the generation of a new amide bond. Gratifyingly, probe **3.30** was found to be active in the inhibition of *B. subtilis* growth in the MIC assay (MIC = 8.0 μg /mL).

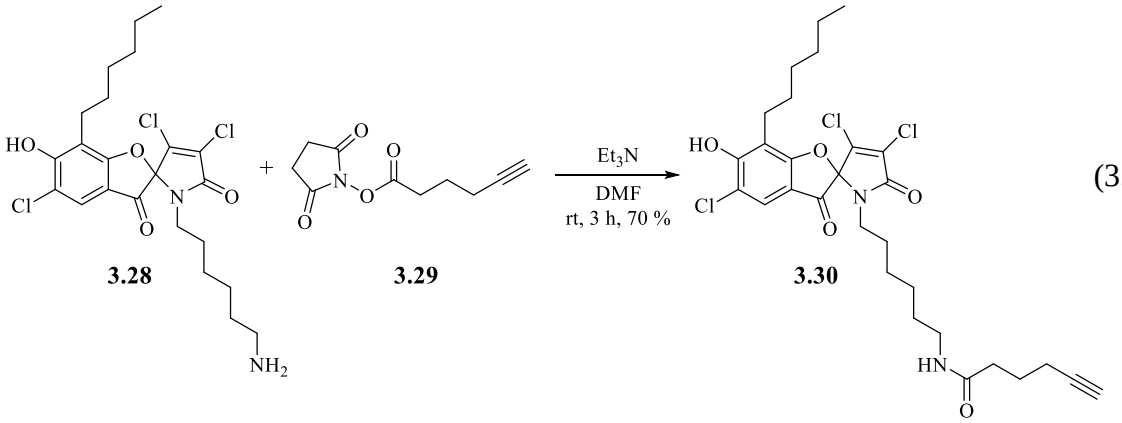

(3.3)

In conclusion, the chemical synthesis and MIC evaluation of various armeniaspirole analogs facilitated the uncovering of important SAR, allowing for the development of an active chemical biology probe. Important findings include the conclusion that modification of the armeniaspirole aromatic alcohol, specifically though the generation of an ether, are not tolerated and lead to inactive compounds. Further, it has been shown that the integration of long carbon chains through alkylation of the lactam nitrogen is tolerated and can lead to the generation of compounds that are more potent than 5-chloro-armeniaspirole A as evaluated by MIC. Finally, these findings were used to generate an active terminal alkyne containing probe (**3.30**).

3.2.3 Activity-based protein profiling

The proteome-wide selectivity of armeniaspirole-based probe **3.30** was investigated using activity-based protein profiling. The Gram-positive *B. subtilis* 168 strain has been extensively studied. Less than 300 of its ≈ 4,100 genes were found to be essential.[20] Since it is susceptible to growth inhibition by **3.30**, it was chosen for this investigation. In addition to assessing general labelling, 5-chloro-armeniaspirole (**3.4**) was used as a probe inhibitor to attempt to differentiate proteins that are specifically and non-specifically modified by the probe.

B. subtilis was grown in LB at 37 °C and the cells harvested by centrifugation. After washing, the cells were aliquoted into 5 different samples and the cells were labelled. Samples 3, 4 and 5 were incubated with probe inhibitor **3.4** at 100 μM, 500 μM and 1 mM, respectively, for two hours at ambient temperature. Following this, the probe **3.30** was added to all samples (1 – 5) to reach a final concentration of 10 μM, and they were incubated for two hours at room temperature. The cells were then washed to remove excess **3.4** and **3.30** and lysed by sonication to obtain the soluble proteome. The protein concentration was determined using a Bradford assay and the concentrations were adjusted to 1.2 mg / mL. Click chemistry was performed on samples 2 – 5 using the rhodamine azide Azide Fluor 488 (100 μM), TCEP (1 mM), TBTA (100 μM), and $CuSO_4$ (100 mM). The click chemistry control sample 1 was treated with all reagents except $CuSO_4$ and TCEP. All samples were incubated for 2 hours at ambient temperature and the reaction was quenched by acetone precipitation. The precipitated protein was washed with cold methanol and resuspended in PBS plus 0.2% SDS. The samples were loaded and resolved on a 11 % SDS-PAGE gel (Figure 3.5).

Upon analysis of the SDS-PAGE gel, it is clear that the proteome is labelled extensively by the probe. The click-chemistry control (Sample 1) shows that the observed labelling is dependent on conjugation of the probe to the fluorophore. At high concentrations of inhibitor, labelling of all major bands is still present. This indicates that specific modification of biological molecules cannot be detected using this method.

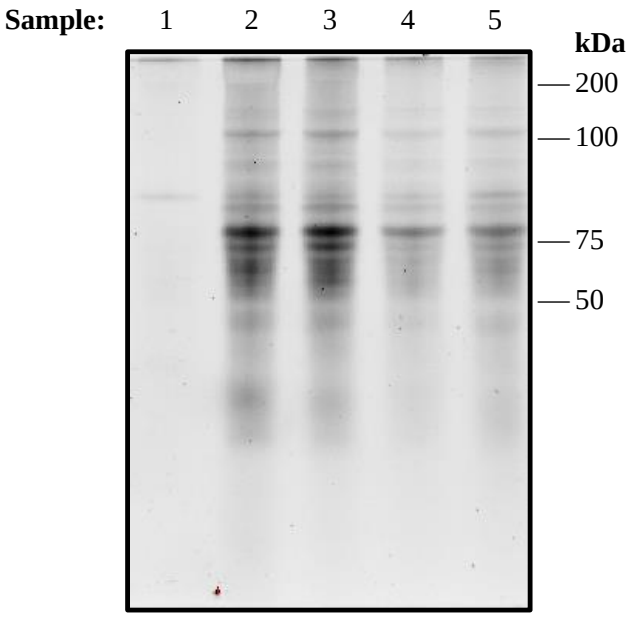

Figure 3.6. Fluorescent SDS-PAGE gel showing the labelling of armeniaspirole probe **3.30** in B. subtilis 168. Sample 1 (control sample, no $CuSO_4$ or TCEP) and sample 2 were treated with probe (10 μM) for 2 h. Samples 3 – 5 were pretreated with probe inhibitor (100 μM, 500 μM and 1 mM, respectively) for 2 h, and followed by probe (10 μM) for 2 h.

3.3 Summary and outlook

In summary, analogs of the armeniaspirole class of natural products have been synthesized and evaluated for both antimicrobial and oncolytic virus potentiating activity to identify similarities and differences in bioactivity profiles. Further, an armeniaspirole-based chemical biology probe was developed. Initial activity-based protein profiling experiments were then launched to begin to investigate the extent and identity of protein labelling by this probe.

It was found that despite the structural similarities at the electrophilic core, armeniaspirole compounds do not enhance oncolytic virus efficacy. In addition, lead oncolytic virus potentiating agents do not exhibit antimicrobial activity. This strongly suggests that these two classes of compounds impart their activities using distinct and specific interactions, a conclusion not obvious before, due to the electrophilic nature.

Towards the goal of developing a new armeniaspirole-derived chemical biology probe, important SAR conclusions were made to determine the site of incorporation of a reactive group. Surprisingly, the SAR studies indicated that the aromatic alcohol of armeniaspirole compounds was essential for antimicrobial activity. After further SAR studies indicated that long chain alkyl-substitution on the nitrogen of the lactam was tolerated, an analog was synthesized that included the incorporation of a terminal alkyne. The analog was then shown to be active in arresting bacterial cell growth using the MIC assay. Early investigations into using this probe in activity-based protein profiling experiments showed extensive labelling of the bacterial proteome. This may complicate the identification of specific labelling using an SDS-PAGE gel-based method.

Looking forward, studies into using the developed probe to identify labelling targets using affinity protein purification and mass spectrometry will be completed. The use of this compound

as a general chemical biology probe is also being investigated by characterizing differential labelling in various mammalian cell lines.

Electrophilic natural products with antibacterial activity provide unique opportunities to study and discover new mechanisms of action. These types of studies will be important to maintain the ability to treat serious bacterial infections in the face of a global rise of strains resistant to current treatments. This work has contributed to the foundation of knowledge with regards to armeniaspiroles, and should assist in the discovery of its biological target and mechanism of action.

3.4 Experimental section

3.4.1 Minimum inhibition assay

Compound-mediated growth inhibition of *Bacillus subtilis* in Mueller Hinton broth was obtained using a 96-well plate assay. In triplicate, various concentrations of the analogs were prepared through multiple 1 in 2 serial dilutions. The plates were incubated at 37 °C for 16 hours. The MIC was determined though visual inspection and represents the lowest concentration of compounds that prevents any observed bacterial growth.

3.4.2 Synthetic methods and characterization

General information

All reactions were performed in oven-dried or flame-dried glass round-bottom flasks equipped with magnetic stir bars. Purification of reaction products was carried out by flash column chromatography using silica gel. ^{1}H NMR spectra were recorded on either a Bruker 400 MHz or Bruker 300 MHz at ambient temperature. ^{13}C NMR spectra were recorded on either a Bruker 100 MHz or Bruker 75 MHz at ambient temperature. Spectra are recorded in parts per million using residual solvent as the internal standard ($(CD_3)_2SO$ at 2.50 ppm, $CDCl_3$ at 7.26 ppm and CD_3OD at 3.31 ppm for ^{1}H NMR and $(CD_3)_2SO$ at 39.52 ppm, $CDCl_3$ at 77.16 ppm and CD_3OD at 49.00 ppm for ^{13}C NMR.) ^{1}H NMR data was reported as: multiplicity (br = broad, s = singlet, d = doublet, t = triplet, q = quartet, quin. = quintet, sext. = sextuplet, sept = septuplet, m = multiplet), integration and coupling constant(s) in Hz. High-resolution mass spectrometry was performed by electrospray ionization (ESI) in positive ion or negative ion mode using a Micromass Q-TOF 1 mass spectrometer.

Materials

Unless otherwise noted, all commercially available materials were purchased from commercial sources and used without further purification.

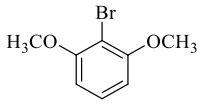

1-Bromo-2,6-dimethoxybenzene, Compound 3.14

1,3-dimethoxybenzene (14.40 g, 0.104 mol, 1.0 equiv.) was dissolved in Et_2O (375 mL) in a round-bottom flask. n-BuLi (50 mL of a 2.5 M solution, 1.2 equiv.) was added and the solution was allowed to stir at ambient temperature for 4 hours. The reaction mixture was then cooled to – 50 °C using a dry ice/acetone bath. Bromine (18.65 g, 0.117 mol, 1.1 equiv.) was added dropwise. The solution was then heated to room temperature and allowed to react for another two hours. To the resulting mixture, 250 mL of a 10 % sodium thiosulfate solution was added and the resulting mixture was allowed to stir for 1 hour. The solution was extracted 2 × with Et_2O. The resulting organic fractions were combined and washed with brine. The organic phase was then dried with Na_2SO_4 and concentrated to yield the desired compound (9.45 g, 43.5 mmol, 42 % yield) which was used without further purification. The NMR data were consistent with literature values.[21] ^{1}H NMR (400 MHz, $CDCl_3$) δ 7.23 (t, *J* = 8.3 Hz, 1H), 6.58 (d, *J* = 8.4 Hz, 1H), 3.90 (s, 3H). ^{13}C NMR (100 MHz, $CDCl_3$) δ 157.34, 128.38, 104.82, 101.08, 56.58.

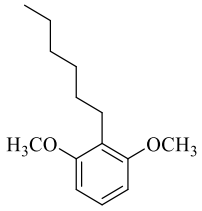

2-Hexyl-1,3-dimethoxy-benzene, Compound 3.15

In a round-bottom flask, **3.14** (5.0 g, 23.0 mmol, 1.0 equiv.) was dissolved in toluene (230 mL). To the resulting solution, *n*-hexylboronic acid (5.98 g, 46 mmol, 2.0 equiv.), $K_3PO_4 \cdot H_2O$ (10.6 g, 46 mmol, 2.0 equiv.), $Pd(OAc)_2$ (516 mg, 2.3 mmol, 0.1 equiv.), and SPhos (1.89 g, 4.6 mmol, 0.2 equiv.) were added at ambiant temperature. The mixture was stirred at 100 °C for 15 hours. After cooling, the reaction mixture was quenched with $NH_4Cl_{(aq)}$ and extracted 3 × with EtOAc. The organic fractions were combined, washed with brine, dried over Na_2SO_4 and concentrated. The desired compound (4.65 g, 20.9 mmol, 91 % yield) was purified from the crude mixture by silica column chromatography (100 % hexanes). The NMR data were consistent with literature values.[18] ^{1}H NMR (300 MHz, DMSO) δ 7.10 (t, *J* = 8.3 Hz, 1H), 6.59 (d, *J* = 8.3 Hz, 2H), 3.74 (s, 6H), 2.56 – 2.51 (m, 2H), 1.43 – 1.31 (m, 2H), 1.29 – 1.19 (m, 6H), 0.85 (d, *J* = 6.9 Hz, 3H). ^{13}C NMR (75 MHz, DMSO) δ 157.75, 126.78, 117.98, 103.85, 55.59, 31.17, 28.82, 28.81, 22.38, 22.11, 13.98.

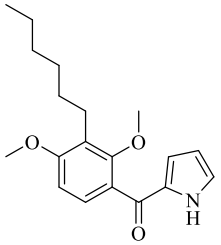

(3-Hexyl-2,4-dimethoxy-phenyl)-(1*H*-pyrrol-2-yl)-methanone, Compound 3.16

In a round-bottom flask, **3.15** (4.09 g, 18.4 mmol, 1.0 equiv.) was dissolved in CH_2Cl_2 (92 mL) and cooled to 0 °C with an ice bath. 1H-Pyrrole-2-carbonyl chloride (46 mmol, 2.5 equiv.) was

added, followed by $SnCl_4$ (92 mL of a 1.0 M solution, 5 equiv.). The mixture was stirred for 1 hour at 0 °C, then warmed to ambient temperature. The reaction mixture was quenched with a saturated $NaHCO_{3(aq)}$ and extracted 3 × with EtOAc. The organic fractions were combined, washed with brine, dried over Na_2SO_4 and concentrated. The desired compound (5.59 g, 17.7 mmol, 96 % yield) was purified from the crude mixture by silica column chromatography (10 to 25 % EtOAc in hexanes). The NMR data were consistent with literature values.[18] ^{1}H NMR (400 MHz, DMSO) δ 11.98 (s, 1H), 7.25 (d, *J* = 8.5 Hz, 1H), 7.18 – 7.13 (m, 1H), 6.80 (d, *J* = 8.6 Hz, 1H), 6.51 – 6.48 (m, 1H), 6.18 (dt, *J* = 4.2, 2.3 Hz, 1H), 3.83 (s, 3H), 3.59 (s, 3H), 2.61 – 2.54 (m, 2H), 1.51 – 1.40 (m, 2H), 1.35 – 1.22 (m, 6H), 0.86 (t, *J* = 6.8 Hz, 3H). ^{13}C NMR (100 MHz, DMSO) δ 183.86, 159.98, 157.39, 132.47, 128.49, 126.58, 125.90, 124.13, 119.54, 110.44, 105.88, 62.55, 56.26, 31.54, 29.64, 29.43, 23.61, 22.52, 14.41.

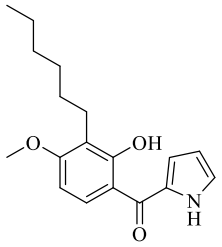

(3-Hexyl-2-hydroxy-4-methoxy-phenyl)-(1*H*-pyrrol-2-yl)-methanone, Compound 3.17

In a round-bottom flask, **3.16** (5.585 g, 17.7 mmol, 1.0 equiv.) was dissolved in 1,2-dichloroethane (21 mL). The solution was cooled to -20 °C using a dry ice/acetone bath. BBr_3 (21.2 mL of a 1 M solution, 1.2 equiv.) was added dropwise and the reaction mixture was stirred at -20 to – 10 °C for 2 hours. Subsequently, Et_3N / water was added and the solution was extracted 3 × with EtOAc. The organic fractions were combined, washed with brine, dried over Na_2SO_4, and concentrated. The desired compound (5.15 g, 17.1 mmol, 97 % yield) was purified from the crude mixture by silica column chromatography (15 % EtOAc in hexanes). The NMR data were consistent with

literature values.[18] ^{1}H NMR (400 MHz, DMSO) δ 12.08 (s, 1H), 7.95 (d, *J* = 9.0 Hz, 1H), 7.25 – 7.22 (m, 1H), 6.99 (ddd, *J* = 3.8, 2.4, 1.3 Hz, 1H), 6.66 (d, *J* = 9.1 Hz, 1H), 6.31 (dt, *J* = 4.0, 2.3 Hz, 1H), 3.86 (s, 3H), 3.35 (s, 3H), 2.62 – 2.54 (m, 2H), 1.49 – 1.38 (m, 2H), 1.33 – 1.21 (m, 6H), 0.84 (t, *J* = 6.9 Hz, 3H). ^{13}C NMR (100 MHz, DMSO) δ 185.75, 162.24, 160.99, 130.71, 129.36, 126.34, 119.05, 117.12, 113.09, 110.73, 102.60, 55.85, 31.17, 28.86, 28.30, 22.10, 22.08, 13.96.

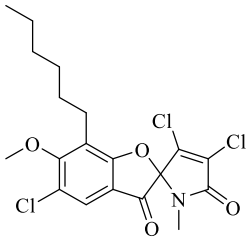

3',4',5-Trichloro-7-hexyl-6-methoxy-1'-methyl-1'*H*-spiro[1-benzofuran-2,2'-pyrrole]-3,5'-dione, Compound 3.19

In a round-bottom flask, **3.17** (1.50 g, 5.0 mmol, 1.0 equiv.) was dissolved in acetic acid (50 mL). *N*-chlorosuccinimide (1.33 g, 10.0 mmol, 2.0 equiv.) was added and the mixture was stirred at ambient temperature for 2 hours. Following this, *N*-chlorosuccinimide (2.67 g, 20 mmol, 4.0 equiv.) was added and the resulting mixture was heated to 70 °C for 16 hours. The reaction mixture was then quenched with a 10 % $K_2CO_{3(aq)}$ and extracted 3 × with EtOAc. The organic fractions were combined, washed with brine, dried over Na_2SO_4 and concentrated. The resulting oil was dissolved in $CHCl_3$ (33 mL) and Et_3N (1.4 mL) was added. The mixture was heated at 60 °C for 5 hours. The solution was cooled to ambient temperature, concentrated, and the spiro- intermediate 5,3',4'-trichloro-6-methoxy-7-hexyl-spiro[benzofuran-2(3H),2'-[2H]pyrrole]-3,5'(1'H)-dione (**3.18**) (1.133 g, 2.8 mmol, 56 % yield over two steps) was isolated by from the crude mixture by silica column chromatography (2 % to 20 % EtOAc in hexanes). The *spiro*- intermediate (40 mg, 0.096 mmol, 1.0 equiv.) was dissolved in DMF (2 mL). The solution was cooled to 0 °C using an

ice bath and NaH (3.4 mg, 0.143 mmol, 1.5 equiv.) was added and allowed to stir for 15 min. Subsequently, MeI (17.6 mg, 0.124 mmol, 1.3 equiv.) was added dropwise and stirring was continued at 0 °C to ambient temperature for 5 hours. The mixture was quenched with $NH_4Cl_{(aq)}$, extracted 3 × with EtOAc, washed with brine, dried over Na_2SO_4, and concentrated. The desired compound (40.0 mg, 0.095 mmol, >99% yield) was purified from the crude mixture by silica column chromatography (15 % EtOAc in hexanes). The NMR data were consistent with literature values.[18] ^{1}H NMR (400 MHz, $CDCl_3$) δ 7.63 (s, 1H), 4.00 (s, 3H), 2.79 (s, 3H), 2.76 – 2.70 (m, 2H), 1.64 – 1.55 (m, 3H), 1.41 – 1.24 (m, 6H), 0.88 (t, *J* = 7.0 Hz, 3H). ^{13}C NMR (100 MHz, $CDCl_3$) δ 189.88, 170.33, 163.79, 163.16, 138.24, 129.38, 124.84, 124.33, 123.73, 115.65, 97.05, 61.92, 31.73, 29.46, 29.38, 25.96, 24.00, 22.71, 14.19. HRMS (ESI): Exact mass calculated for $C_{19}H_{20}Cl_3NNaO_4$ $[M + Na]^+$: 454.0350. Found: 454.0356

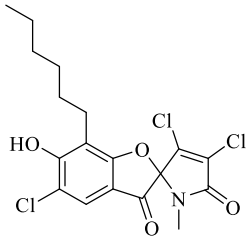

3',4',5-Trichloro-7-hexyl-6-hydroxy-1'-methyl-1'*H*-spiro[1-benzofuran-2,2'-pyrrole]-3,5'-dione, Compound 3.4

In a round-bottom flask, **3.18** (54.2 mg, 0.125 mmol, 1.0 equiv.) was dissolved in 1,2-dichloroethane (1 mL). The mixture was cooled to 0 °C using an ice bath and BBr_3 (380 μL of a 1 M solution, 3.0 equiv.) was added dropwise. The reaction was allowed to proceed for 4 hours from 0 °C to ambient temperature. Et_3N / water was added and the solution was extracted 3 × with EtOAc. The organic fractions were combined, washed with brine, dried over Na_2SO_4, and concentrated. The desired compound (48.7 mg, 0.116 mmol, 93 %) was purified from the crude

mixture by silica column chromatography (5 to 20 % EtOAc in hexanes). The NMR data were consistent with literature values.[18] ^{1}H NMR (400 MHz, $CDCl_3$) δ 7.63 (s, 1H), 6.62 (s, 1H), 2.79 (s, 3H), 2.76 (t, *J* = 7.6 Hz, 2H), 1.66 – 1.56 (m, 2H), 1.39 – 1.24 (m, 6H), 0.87 (t, *J* = 7.0 Hz, 3H). ^{13}C NMR (100 MHz, $CDCl_3$) δ 188.93, 170.34, 163.21, 158.77, 138.43, 129.27, 122.56, 117.67, 115.79, 112.66, 97.16, 31.77, 29.22, 28.47, 25.91, 23.37, 22.74, 14.21. HRMS (ESI): Exact mass calculated for $C_{18}H_{17}Cl_3NO_4$ [M - H]$^-$: 416.0229. Found: 416.0223

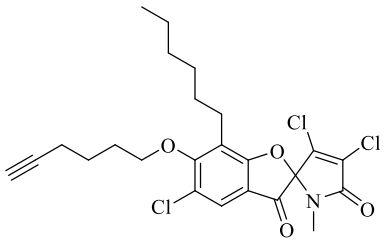

3',4',5-Trichloro-7-hexyl-6-(5-hexynyloxy)-1'-methyl-1'*H*-spiro[1-benzofuran-2,2'-pyrrole]-3,5'-dione, Compound 3.20

In a round-bottom flask, **3.4** (28 mg, 0.067 mmol, 1.0 equiv.) was dissolved in 2 mL of acetone. K_2CO_3 (27.7 mg, 0.201, 3.0 equiv.) was added, followed by the dropwise addition of 6-iodo-1-hexyne (18 μL, 0.134 mmol, 2.0 equiv.). The mixture was heated at reflux for 8 hours. The mixture was cooled to ambient temperature and $NH_4Cl_{(aq)}$ was added. The solution was extracted 3 × with EtOAc, washed with brine, dried over Na_2SO_4 and concentrated. The desired compound (9.4 mg, 0.0188 mmol, 28 % yield) was purified from the reaction mixture by silica column chromatography (5 to 20 % EtOAc in hexanes). ^{1}H NMR (400 MHz, DMSO) δ 7.95 (s, 1H), 4.11 (t, *J* = 6.3 Hz, 2H), 2.80 (t, *J* = 2.6 Hz, 1H), 2.75 – 2.68 (m, 5H), 2.27 (td, *J* = 7.1, 2.6 Hz, 2H), 1.95 – 1.86 (m, 2H), 1.74 – 1.65 (m, 2H), 1.56 (dd, *J* = 14.9, 7.6 Hz, 2H), 1.37 – 1.22 (m, 6H), 0.84 (t, *J* = 7.0 Hz, 3H). ^{13}C NMR (100 MHz, DMSO) δ 189.41, 169.91, 162.46, 162.07, 137.89, 128.32, 124.15, 123.88, 123.62, 114.89, 96.36, 84.12, 74.13, 71.46, 30.90, 28.77, 28.48,

28.44, 25.71, 24.51, 23.32, 21.94, 17.47, 13.88. HRMS (ESI): Exact mass calculated for $C_{24}H_{26}Cl_3NNaO_4$ $[M + Na]^+$: 520.0820. Found: 520.0825

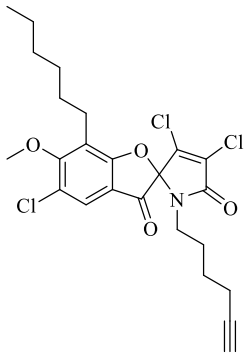

3',4',5-Trichloro-7-hexyl-1'-(5-hexynyl)-6-methoxy-1'*H*-spiro[1-benzofuran-2,2'-pyrrole]-3,5'-dione, Compound 3.21

The *spiro*- intermediate **3.18** (250 mg, 0.60 mmol, 1.0 equiv.) was dissolved in DMF (6 mL). The solution was cooled to 0 °C using an ice bath and NaH (14.4 mg, 0.60 mmol, 1.0 equiv.) was added and allowed to stir for 15 min. Subsequently, 6-iodo-1-hexyne (150 mg, 0.72 mmol, 1.2 equiv.) was added dropwise and stirring was continued at 0 °C to ambient temperature for 5 hours. The mixture was quenched with $NH_4Cl_{(aq)}$, extracted 3 × with EtOAc, washed with brine, dried over Na_2SO_4, and concentrated. The desired compound (146.4 mg, 0.294 mmol, 49 % yield) was purified from the crude mixture by silica column chromatography (5 to 20 % EtOAc in hexanes). ^{1}H NMR (400 MHz, $CDCl_3$) δ 7.63 (s, 1H), 4.00 (s, 3H), 3.53 – 3.37 (m, 1H), 3.14 – 2.97 (m, 1H), 2.78 – 2.65 (m, 2H), 2.14 (td, *J* = 6.8, 2.6 Hz, 2H), 1.84 (t, *J* = 2.6 Hz, 1H), 1.62 – 1.26 (m, 12H), 0.88 (t, *J* = 7.1 Hz, 3H). ^{13}C NMR (100 MHz, $CDCl_3$) δ 190.16, 169.99, 163.76, 163.54, 138.42, 129.21, 124.81, 124.37, 123.76, 115.77, 97.28, 83.64, 68.85, 61.93, 40.97, 31.73, 29.53, 29.45, 27.73, 25.42, 24.01, 22.70, 17.94, 14.20. HRMS (ESI): Exact mass calculated for $C_{24}H_{26}Cl_3NNaO_4$ $[M + Na]^+$: 520.0820. Found: 520.0825

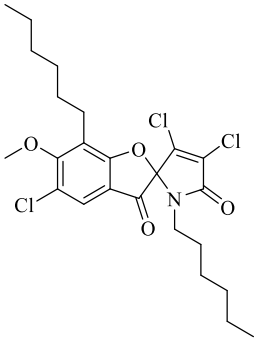

3',4',5-Trichloro-7-hexyl-1'-hexyl-6-methoxy-1'*H*-spiro[1-benzofuran-2,2'-pyrrole]-3,5'-dione, Compound 3.22

The *spiro*- intermediate **3.18** (360 mg, 0.936 mmol, 1.0 equiv.) was dissolved in DMF (5 mL). The solution was cooled to 0 °C using an ice bath and NaH (48.8 mg, 1.22 mmol, 1.3 equiv.) was added and allowed to stir for 15 min. Subsequently, 1-iodohexane (238 mg, 1.123 mmol, 1.2 equiv.) was added dropwise and stirring was continued at 0 °C to ambient temperature for 5 hours. The mixture was quenched with $NH_4Cl_{(aq)}$, extracted 3 × with EtOAc, washed with brine, dried over Na_2SO_4, and concentrated. The desired compound (269 mg, 0.535 mmol, 57 % yield) was purified from the crude mixture by silica column chromatography (15 % EtOAc in hexanes). ^{1}H NMR (400 MHz, $CDCl_3$) δ 7.63 (s, 1H), 4.00 (s, 3H), 3.42 (dt, *J* = 14.5, 7.3 Hz, 1H), 3.00 (dt, *J* = 14.5, 7.3 Hz, 1H), 2.78 – 2.64 (m, 2H), 1.65 – 1.53 (m, 2H), 1.48 – 1.12 (m, 14H), 0.88 (t, *J* = 6.9 Hz, 3H), 0.83 (t, *J* = 6.8 Hz, 3H). ^{13}C NMR (100 MHz, $CDCl_3$) δ 190.25, 170.00, 163.71, 163.46, 138.25, 129.29, 124.75, 124.33, 123.72, 115.84, 97.38, 61.93, 41.67, 31.74, 31.36, 29.54, 29.47, 28.76, 26.47, 24.00, 22.71, 22.56, 14.20, 14.10. HRMS (ESI): Exact mass calculated for $C_{24}H_{30}Cl_3NNaO_4$ $[M + Na]^+$: 524.1133. Found: 524.1133

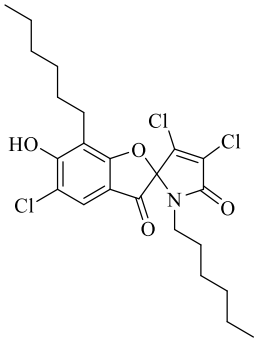

3',4',5-Trichloro-7-hexyl-1'-hexyl-6-hydroxy-1'*H*-spiro[1-benzofuran-2,2'-pyrrole]-3,5'-dione, Compound 3.23

In a round-bottom flask, **3.22** (100 mg, 0.198 mmol, 1.0 equiv.) was dissolved in 1,2-dichloroethane (1.4 mL). The mixture was cooled to 0 °C using an ice bath and BBr_3 (596 µL of a 1 M solution, 3.0 equiv.) was added dropwise. The reaction was allowed to proceed for 4 hours from 0 °C to ambient temperature. Et_3N / water was added and the solution was extracted 3 × with EtOAc. The organic fractions were combined, washed with brine, dried over Na_2SO_4, and concentrated. The desired compound (58.3 mg, 0.119 mmol, 60 %) was purified from the crude mixture by silica column chromatography (5 to 20 % EtOAc in hexanes). ^{1}H NMR (400 MHz, $CDCl_3$) δ 7.62 (s, 1H), 6.51 (s, 1H), 3.46 – 3.36 (m, 1H), 3.04 – 2.91 (m, 1H), 2.80 – 2.63 (m, 2H), 1.65 – 1.11 (m, 16H), 0.86 (t, *J* = 7.1 Hz, 3H), 0.81 (t, *J* = 6.9 Hz, 3H). ^{13}C NMR (100 MHz, $CDCl_3$) δ 189.33, 170.01, 163.50, 158.65, 138.42, 129.20, 122.54, 117.57, 115.82, 112.88, 97.50, 41.65, 31.79, 31.39, 29.31, 28.76, 28.56, 26.50, 23.38, 22.74, 22.58, 14.22, 14.10. HRMS (ESI): Exact mass calculated for $C_{23}H_{27}Cl_3NO_4$ $[M - H]^-$: 486.1011. Found: 486.1006

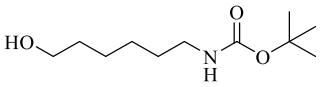

6-(*tert*-Butoxycarbonylamino)-1-hexanol, Compound 3.25

In a round-bottom flask, 6-amino-1-hexanol (2.0 g, 17.1 mmol, 1.0 equiv.) was dissolved in methanol (40 mL). Di-tert-butyl dicarbonate (4.1 g, 18.8 mmol, 1.1 equiv.) was added and the reaction was stirred for 1.5 hours at ambient temperature. The reaction mixture was concentrated and the desired product (3.72 g, 17.1 mmol, >99 % yield) was purified from the crude residue by silica column chromatography (2 % methanol in CH_2Cl_2). The NMR data were consistent with literature values.[22] ^{1}H NMR (300 MHz, $CDCl_3$) δ 3.63 (t, *J* = 6.5 Hz, 2H), 3.11 (t, *J* = 6.9 Hz, 2H), 1.62 – 1.29 (m, 17H). ^{13}C NMR (75 MHz, $CDCl_3$) δ 156.21, 79.21, 62.71, 40.50, 32.68, 30.16, 28.52, 26.50, 25.39.

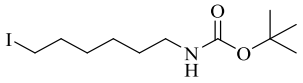

(6-Iodo-hexyl)-carbamic acid tert-butyl ester, Compound 3.26

3.25 (2.25 g, 10.35 mmol, 1.0 equiv.) was dissolved in CH_2Cl_2 (30 mL) in a round-bottom flask. Et_3N (2.2 mL, 15.53 mmol, 1.5 equiv.) was added and the solution was cooled to 0 °C using an ice bath. Methanesulfonyl chloride (881 μL, 11.39 mmol, 1.1 equiv.) was added dropwise and the mixture was stirred for 2 hours, while warming to ambient temperatre. The resulting solution was washed with H_2O, washed with brine, dried over Na_2SO_4 and concentrated. The crude oil was dissolved in acetonitrile (45 mL) in a round-bottom flask and NaI (7.73 g, 51.6 mmol, 5 equiv.) was added. The mixture was stirred at room temperature for 16 hours. The reaction mixture was concentrated, and the residue was partitioned between EtOAc and H_2O. The organic phase was separated, washed with brine, dried over Na_2SO_4 and concentrated. The desired

compound (2.37 g, 7.24 mmol, 70 % yield) was purified from the crude mixture by silica column chromatography (10 % EtOAc in hexanes). The NMR data were consistent with literature values.[22] ^{1}H NMR (400 MHz, $CDCl_3$) δ 4.52 (br, 1H), 3.17 (t, *J* = 7.0 Hz, 2H), 3.13 – 3.05 (m, 2H), 1.86 – 1.75 (m, 2H), 1.53 – 1.27 (m, 14H). ^{13}C NMR (100 MHz, $CDCl_3$) δ 156.10, 79.20, 40.60, 33.49, 30.26, 30.04, 28.55, 25.84, 7.05.

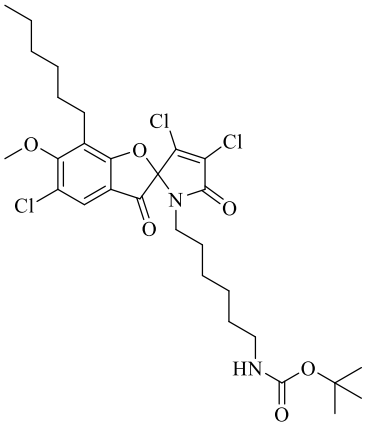

3',4',5-Trichloro-7-hexyl-6-methoxy-1'-[6-(*tert*-butoxycarbonylamino)hexyl]-1'*H*-spiro[1-benzofuran-2,2'-pyrrole]-3,5'-dione, Compound 3.27

The *spiro*- intermediate **3.18** (80 mg, 0.191 mmol, 1.0 equiv.) was dissolved in DMF (2 mL). The solution was cooled to 0 °C using an ice bath and NaH (5.95 mg, 0.248 mmol, 1.3 equiv.) was added and allowed to stir for 15 min. Subsequently, (6-iodo-hexyl)-carbamic acid tert-butyl ester (75 mg, 0.229 mmol, 1.2 equiv.) was added and stirring was continued at 0 °C to ambient temperature for 5 hours. The mixture was quenched with $NH_4Cl_{(aq)}$, extracted 3 × with EtOAc, washed with brine, dried over Na_2SO_4, and concentrated. The desired compound (32.4 mg, 0.053 mmol, 27 % yield) was purified from the crude mixture by silica column chromatography (0 to 15 % EtOAc in hexanes). ^{1}H NMR (400 MHz, $CDCl_3$) δ 7.63 (s, 1H), 4.50 (br, 1H), 4.00 (s, *J* = 9.0 Hz, 3H), 3.37 (dt, *J* = 14.6, 7.3 Hz, 1H), 3.13 – 2.97 (m, 3H), 2.79 – 2.63 (m, 2H), 1.65 –

1.17 (m, 28H), 0.88 (s, 3H). ^{13}C NMR (100 MHz, $CDCl_3$) δ 190.21, 169.97, 163.75, 163.50, 156.09, 138.31, 129.24, 124.80, 124.30, 123.75, 115.77, 97.28, 61.94, 41.40, 40.53, 31.73, 29.98, 29.83, 29.51, 29.42, 28.71, 28.55, 26.41, 26.31, 23.98, 22.69, 14.20. HRMS (ESI): Exact mass calculated for $C_{29}H_{39}Cl_3N_2NaO_6$ $[M + H]^+$: 639.1766. Found: 639.1771

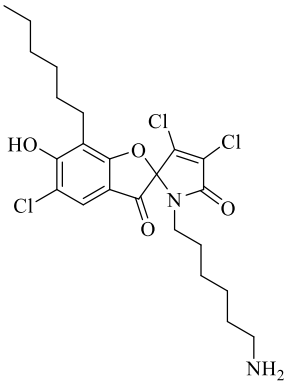

1'-(6-Aminohexyl)-3',4',5-trichloro-7-hexyl-6-hydroxy-1'*H*-spiro[1-benzofuran-2,2'-pyrrole]-3,5'-dione, Compound 3.28

In a round-bottom flask, **3.27** (30 mg, 0.0485 mmol, 1.0 equiv.) was dissolved in 1,2-dichloroethane (1 mL). The mixture was cooled to 0 °C using an ice bath and BBr_3 (243 μL of a 1 M solution, 5.0 equiv.) was added dropwise. The reaction was allowed to proceed for 4 hours from 0 °C to ambient temperature. Et_3N / water was added and the solution was extracted 3 × with EtOAc. The organic fractions were combined, washed with brine, dried over Na_2SO_4, and concentrated. The desired compound (15.4 mg, 0.0305 mmol, 63 %) was purified from the crude mixture by silica column chromatography (5 to 20 % methanol in CH_2Cl_2). ^{1}H NMR (400 MHz, MeOD) δ 7.44 (s, 1H), 3.41 (dt, *J* = 14.3, 7.1 Hz, 1H), 3.35 (s, 1H), 3.09 (dt, *J* = 14.4, 7.1 Hz, 1H), 2.85 (t, *J* = 7.5 Hz, 2H), 2.65 – 2.49 (m, 2H), 1.62 – 1.46 (m, 6H), 1.40 – 1.23 (m, 10H), 0.88 (t, *J* = 6.6 Hz, 3H). ^{13}C NMR (100 MHz, MeOD) δ 185.04, 176.36, 171.68, 165.19, 142.00,

128.54, 126.71, 122.87, 115.03, 104.80, 99.00, 41.68, 40.60, 33.07, 30.43, 29.85, 29.25, 28.33, 27.09, 26.71, 24.16, 23.75, 14.50.

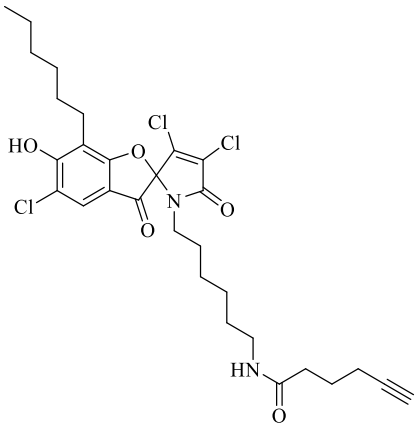

3',4',5-Trichloro-7-hexyl-1'-[6-(5-hexynoylamino)hexyl]-6-hydroxy-1'*H*-spiro[1-benzofuran-2,2'-pyrrole]-3,5'-dione, Compound 3.30

In a round-bottom flask, **3.28** (87.8 mg, 0.175 mmol, 1.0 equiv.) was dissolved in DMF (1.75 mL). 2,5-Dioxo-1-pyrrolidinyl 5-hexynoate (37 mg, 0.175, 1.0 equiv.) and Et_3N (12 μl, 0.0875 mmol, 0.5 equiv.) were added to the mixture and the solution was stirred at room temperature for 6 hours. The reaction mixture was quenched with $NH_4Cl_{(aq)}$, extracted with EtOAc, washed with brine, dried over Na_2SO_4 and concentrated. The desired product (72.8 mg, 0.122 mmol, 70 % yield) was purified by silica column chromatography (5 to 25 % EtOAc in hexanes). ^{1}H NMR (400 MHz, MeOD) δ 7.67 (s, 1H), 3.44 (dt, *J* = 14.5, 7.2 Hz, 1H), 3.11 (t, *J* = 7.0 Hz, 2H), 3.08 – 3.01 (m, 1H), 2.81 – 2.68 (m, 2H), 2.28 (d, *J* = 7.3 Hz, 2H), 2.25 – 2.17 (m, 3H), 1.78 (p, *J* = 7.1 Hz, 2H), 1.67 – 1.56 (m, 2H), 1.51 – 1.22 (m, 14H), 0.89 (t, *J* = 6.7 Hz, 3H). ^{13}C NMR (101 MHz, MeOD) δ 189.88, 175.24, 171.17, 164.73, 163.07, 140.26, 129.59, 124.10, 120.14, 117.01, 112.69, 98.52, 84.12, 70.20, 49.85, 42.19, 40.19, 35.81, 32.81, 30.14, 29.59, 29.52, 27.36, 27.33,

25.97, 23.98, 23.64, 18.64, 14.44. HRMS (ESI): Exact mass calculated for $C_{29}H_{35}Cl_3N_2NaO_5$ [M + Na]$^+$: 619.1504. Found: 619.1509.

3.4.3 Activity-based protein profiling

In situ treatment

Bacterial strain *Bacillus subtilis* 168 (ATCC 23857) was grown in 100 mL of lysogeny broth (14 h, 37 °C, 200 rpm), harvested by centrifugation at 6,500 × g, washed once with PBS and resuspended in 10 mL of PBS. The cell suspension was pipetted into 5 x 1 mL aliquots. Probe inhibitor **3.4** was added (5 μL of a 200x DMSO stock) to samples 3, 4 and 5 so that the final concentration was 100, 500 and 1000 μM, respectively. DMSO (5 μL) was added to samples 1 and 2 and all samples were gently mixed at ambient temperature for 2 h. Probe **3.30** (5 μL of a 200x DMSO stock) was then added to all samples to achieve a final concentration of 10 μM followed by gently mixing at ambient temperature for 2 h. The cells were harvested by centrifugation at 6,500 × g, washed three times with PBS and stored in a -20 °C freezer overnight.

Preparation of proteome

The labelled cells were resuspended in 1 mL of PBS plus protease inhibitor cocktail (Roche). The cells were lysed by sonication (3 × 20s) pulsed at 70 % power. The samples were then centrifuged at 20,000 × g for 90 minutes and the supernatant containing the soluble proteome was collected and stored on ice. The protein concentration was determined by Bradford assay and adjusted with PBS to 1.2 mg /mL.

Click chemistry

Click chemistry was performed on each sample using a final concentration of 100 μM Azide-fluor 488 (5 μL from a 20 mM DMSO stock), 1 mM tris(2-carboxyethyl)phosphine hydrochloride (5 μL from a freshly prepared 200 mM H_2O stock), 100 μM tris[(1-benzyl-1H-1,2,3-triazol-4-yl)methyl]amine (5 μL from a 20 mM 8:2 ^{t}BuOH/DMSO stock) and 1 mM of $CuSO_4$ (5 μL from a freshly prepared 200 mM stock in H_2O). The reagents were added in sequential order as written and were then incubated at room temperature for 2 h. To quench the reaction, 1 mL of cold acetone was added to precipitate the proteome and the samples were stored in the freezer at -20 °C overnight to ensure complete precipitation.

SDS-gel analysis

The samples were centrifuged at 13,000 × g for 15 minutes to pellet the precipitated protein. The precipitated protein was washed with cold methanol and resuspended by sonication (30 % power) 3 times to remove excess click chemistry reagents. The precipitated protein was then resuspended in PBS plus 0.2 % SDS. 2x SDS loading buffer was added and the samples were loaded (20 μL) and resolved on an 11 % SDS-PAGE gel and then scanned using a Bio-Rad Fluor-S MultiImager.

3.5 References

(1) Bassett, E. J.; Keith, M. S.; Armelagos, G. J.; Martin, D. L.; Villanueva, A. R. *Science.* **1980**, *209*, 1532–1534.

(2) Ehrlich, P.; Hata, S. *Die experimentelle Chemotherapie der Sprillosen.*; Julius Springer: Berlin, 1910.

(3) Jolliffe, D. M. *J. R. Soc. Med.* **1993**, *86*, 287–289.

(4) American Chemical Society International Historic Chemical Landmarks. Discovery and Development of Penicillin. http://www.acs.org/content/acs/en/education/whatischemistry/landmarks/flemingpenicillin.html (accessed Jan 1, 2016).

(5) Conly, J.; Johnston, B. *Can. J. Infect. Dis. Med. Microbiol.* **2005**, *16*, 159–160.

(6) Sanchez, G. V.; Master, R. N.; Clark, R. B.; Fyyaz, M.; Duvvuri, P.; Ekta, G.; Bordon, J. *Emerg. Infect. Dis.* **2013**, *19*, 133–136.

(7) Rodvold, K. A.; McConeghy, K. W. *Clin. Infect. Dis.* **2014**, *58*, S20–S27.

(8) Stryjewski, M. E.; Corey, G. R. *Clin. Infect. Dis.* **2014**, *58*, 10–20.

(9) O'Neill, J. *Antimicrobial Resistance : Tackling a crisis for the health and wealth of nations*; 2014.

(10) Freire-Moran, L.; Aronsson, B.; Manz, C.; Gyssens, I. C.; So, A. D.; Monnet, D. L.; Cars, O. *Drug Resist. Updat.* **2011**, *14*, 118–124.

(11) Newman, D. J.; Cragg, G. M. *J. Nat. Prod.* **2012**, *75*, 311–335.

(12) Bode, H. B.; Müller, R. *Angew. Chemie - Int. Ed.* **2005**, *44*, 6828–6846.

(13) Pham, V. H. T.; Kim, J. *Trends Biotechnol.* **2012**, *30*, 475–484.

(14) Müller, R.; Wink, J. *Int. J. Med. Microbiol.* **2014**, *304*, 3–13.

(15) Nichols, D.; Cahoon, N.; Trakhtenberg, E. M.; Pham, L.; Mehta, A.; Belanger, A.; Kanigan, T.; Lewis, K.; Epstein, S. S. *Appl. Environ. Microbiol.* **2010**, *76*, 2445–2450.

(16) Ling, L. L.; Schneider, T.; Peoples, A. J.; Spoering, A. L.; Engels, I.; Conlon, B. P.; Mueller, A.; Hughes, D. E.; Epstein, S.; Jones, M.; Lazarides, L.; Steadman, V. a; Cohen, D. R.; Felix, C. R.; Fetterman, K. A.; Millett, W. P.; Nitti, A. G.; Zullo, A. M.; Chen, C.; Lewis, K. *Nature* **2015**, *517*, 455–459.

(17) Dufour, C.; Wink, J.; Kurz, M.; Kogler, H.; Olivan, H.; Sablé, S.; Heyse, W.; Gerlitz, M.; Toti, L.; Nußer, A.; Rey, A.; Couturier, C.; Bauer, A.; Brönstrup, M. *Chemistry* **2012**, *18*, 16123–16128.

(18) Couturier, C.; Bauer, A.; Rey, A.; Schroif-Dufour, C.; Broenstrup, M. *Bioorg. Med. Chem. Lett.* **2012**, *22*, 6292–6296.

(19) Welsch, M. E.; Snyder, S. a; Stockwell, B. R. *Curr. Opin. Chem. Biol.* **2010**, *14*, 347–361.

(20) Kobayashi, K.; Ehrlich, S. D.; Albertini, A.; Amati, G.; Andersen, K. K.; Arnaud, M.; Asai, K.; Ashikaga, S.; Aymerich, S.; Bessieres, P.; Boland, F.; Brignell, S. C.; Bron, S.; Bunai, K.; Chapuis, J.; Christiansen, L. C.; Danchin, a; Débarbouille, M.; Dervyn, E.; Deuerling, E.; Devine, K.; Devine, S. K.; Dreesen, O.; Errington, J.; Fillinger, S.; Foster, S. J.; Fujita, Y.; Galizzi, a; Gardan, R.; Eschevins, C.; Fukushima, T.; Haga, K.; Harwood, C. R.; Hecker, M.; Hosoya, D.; Hullo, M. F.; Kakeshita, H.; Karamata, D.; Kasahara, Y.; Kawamura, F.; Koga, K.; Koski, P.; Kuwana, R.; Imamura, D.; Ishimaru, M.; Ishikawa, S.; Ishio, I.; Le Coq, D.; Masson, A.; Mauël, C.; Meima, R.; Mellado, R. P.; Moir, A.; Moriya, S.; Nagakawa, E.; Nanamiya, H.; Nakai, S.; Nygaard, P.; Ogura, M.; Ohanan, T.; O'Reilly, M.; O'Rourke, M.; Pragai, Z.; Pooley, H. M.; Rapoport, G.; Rawlins, J. P.; Rivas, L. A.; Rivolta, C.; Sadaie, A.; Sadaie, Y.; Sarvas, M.; Sato, T.; Saxild, H. H.; Scanlan, E.; Schumann, W.; Seegers, J. F. M. L.; Sekiguchi, J.; Sekowska, A.; Séror, S. J.; Simon, M.; Stragier, P.; Studer, R.; Takamatsu, H.; Tanaka, T.; Takeuchi, M.; Thomaides, H. B.; Vagner, V.; van Dijl, J. M.; Watabe, K.; Wipat, A.; Yamamoto, H.; Yamamoto, M.; Yamamoto, Y.; Yamane, K.; Yata, K.; Yoshida, K.; Yoshikawa, H.; Zuber, U.; Ogasawara, N. *Proc. Natl. Acad. Sci. U. S. A.* **2003**, *100*, 4678–4683.

(21) Kamikawa, T.; Hayashi, T. *Tetrahedron* **1999**, *55*, 3455–3466.

(22) Isomura, S.; Wirsching, P.; Janda, K. D. *J. Org. Chem.* **2001**, *66*, 4115–4121.

Chapter 4: Insights into the Valinomycin Thioesterase Mechanism

4.1 Introduction

4.1.1 Brief introduction to nonribosomal peptide synthetases and depsipeptides

Secondary metabolite nonribosomal peptides (NRPs) are a class of natural products that are synthesized by nonribosomal peptide synthetases (NRPSs).[1] NRPSs are multifunctional enzyme complexes that are organized in a modular fashion. These complexes provide the template and machinery to synthesize a specific type of peptidyl natural product. NRPs typically consist of 3-22 residues. This can include non-proteinogenic amino acids and amino acid derivatives. *N*-methylated, hydroxylated, glycosylated and epimerized amino acid derivatives are some examples of the non-proteinogenic residues that can be incorporated into NRP products. [2]

The four most common NRPS catalytic domains are adenylation domains (A), peptidyl carrier protein domains (PCP), condensation domains (C), and thioester domains (TE).[3] A domains are responsible for selecting the amino acid residues that are to be incorporated into the NRP, and activating them by using ATP to convert them into aminoacyl-adenosine monophosphate products. PCP domains are modified with a phosphopantetheinyl cofactor that contains a terminal thiol. This free thiol forms a thioester bond with the activated residue, and serves to carry the growing peptide chain while the long pantetheinyl arm serves to allow access to the different enzymatic domains. C domains catalyze the addition of amino groups from PCP linked residues onto neighboring thioester carbonyls. This results in the formation of new peptide bonds between different residues. Offloading of the NRP from the NRPS complex is often catalyzed by terminal TE domains. These TE domain can mediate the release of a linear peptide chain, or by mediating the formation of a macrocycle. Together, these different NRPS catalytic domains allow for the generation of highly diverse natural product structures with biological activity.

Depsipeptides are NRP products that contain residues condensed through ester bonds in addition to traditional amide bonds. The ester bonds typically arise through the integration of amino acid derived α–hydroxy carboxylic acid residues into the peptide chain.[4] Depsipeptides are a relatively common class of natural products and can be very diverse in structure and function (Figure 4.1).

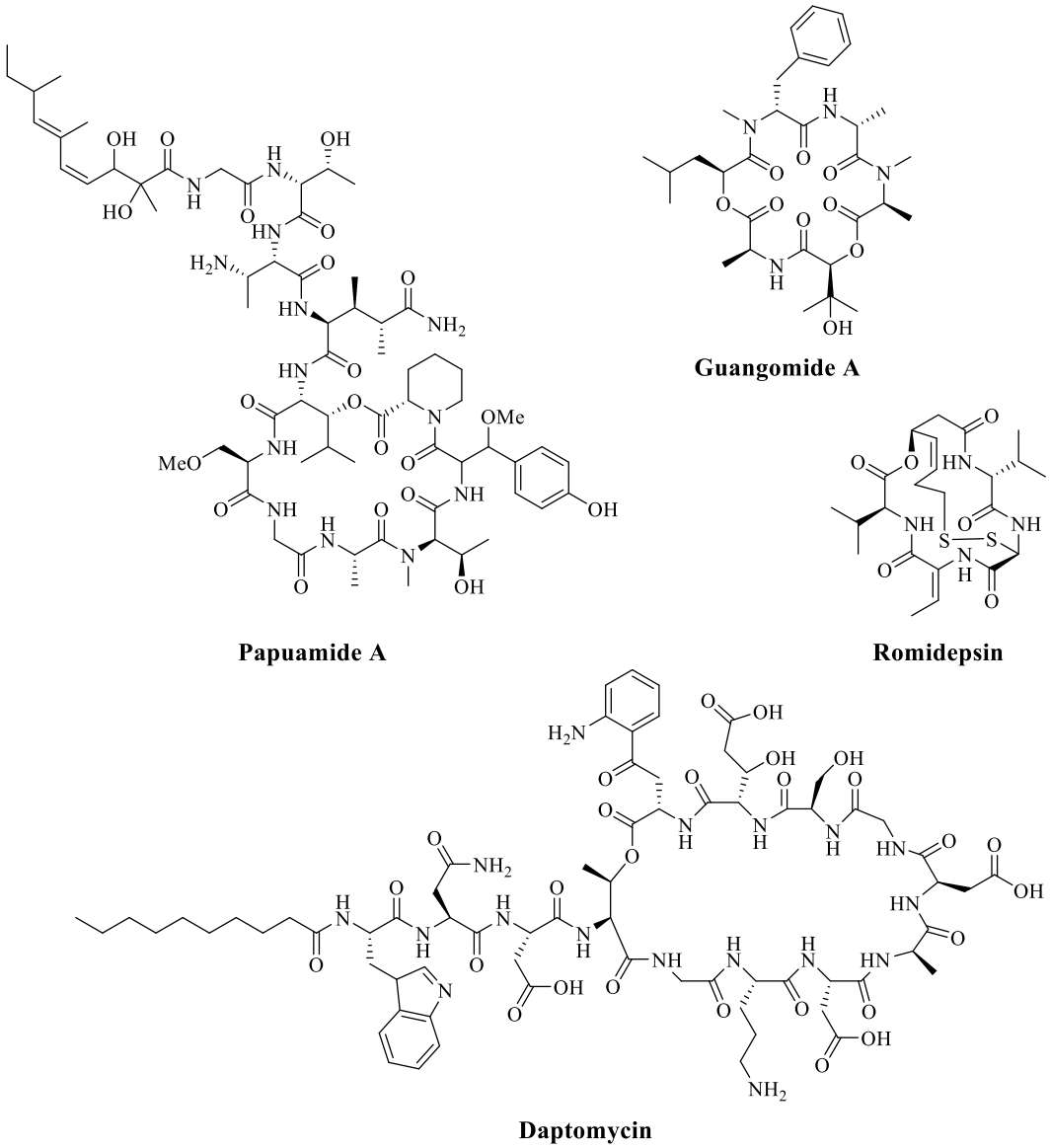

Figure 4.1. Examples of depsipeptide natural products.

4.1.2 Dodecadepsipeptide ionophores cereulide and valinomycin

Depsipeptide ionophores are NRP products that exert their biological activity by disrupting the cellular electrical potential maintained between two sides of a membrane.[5] Valinomycin and cereulide are both potent depsipeptide ionophores with similar and interesting structures (Figure 4.2). These compounds contain three repeats of a tetradepsipeptide fragment containing two α-amino acids and two α-hydroxy acids, linked in alternating ester and amide bonds. The trimer of this tetradepsipeptide is cyclized to form a 36-membered ring.[5] The hydrophobic side-chains of the residues in cereulide and valinomycin allows the compounds to insert into lipophilic membranes where they form a hydrophilic pore. This allows these natural products to facilitate the selective transport of potassium ions across the membrane and down the potential gradient.

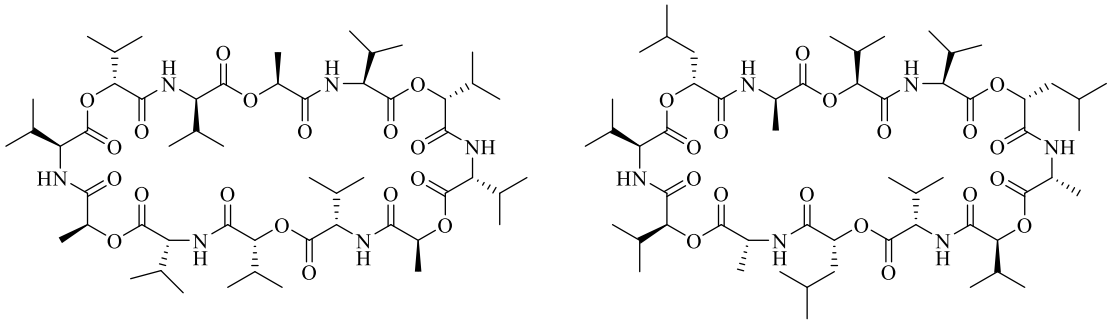

Valinomycin **Cereulide**

Figure 4.2. Structures of valinomycin and cereulide.

In addition to remarkable selectivity for K^+ ions over Na^+ and other ions,[6] valinomycin and cereulide were found to exhibit pH-dependent activity against several Gram-positive bacterial strains, including *Staphylococcus aureus*, *Listeria innocua*, *Listeria monocytogenes*, and *Bacillus subtilis*. Antimicrobial activity was not observed when tested in Gram-negative strains.[7]

4.1.3 Elucidating cereulide and valinomycin biosynthesis

Valinomycin and cereulide have attracted considerable attention from natural product biosynthesis research groups. While cereulide is synthesized by *Bacillus* and valinomycin from *Streptomyces*, generalizations are often drawn between both in terms of the details of biosynthesis. This is due to the similarities in both structure and function between these two compounds.

In 2006, the Walsh group reported that cereulide NRPS machinery likely incorporates the α-hydroxy acids through A domain selection of α-keto acids.[8] After recognition by the A domain, the α-keto acids are then tethered to the PCP as thioesters. The carbonyl is then stereospecifically reduced to α-hydroxyacyl moieties by a ketoreductase domain embedded in the A domain.

More recently, the Hofmann group published further evidence detailing the biosynthesis of the tetradepsipeptide monomeric unit.[9] In this study, UPLC-MS metabolite analysis was used to support a proposed biosynthetic mechanism of the tetradepsipeptide substrate involving the formation of two dipeptides on independent modules. This is suggested to be followed by a C domain catalyzed esterification to form the tetramer. It is also hypothesized that trimerization of the tetradepsipeptide substrate is catalyzed by a C-terminal C domain. Another interesting result in Hofmann's study was the characterization of the high chemical stability of cereulide. This finding helped conclude that the observance of di-, hexa- and decadepsipeptide metabolites is likely due to the hydrolytic release of NRPS enzyme bound thioesters or esters. While the presence of trace levels of hexa-depsipeptide fragements does not corroborate the tetradepsipeptide forming mechanism, this is explained with incorrect transfer of a dipeptide onto a tetrapeptide.

Towards developing a process for the production of valinomycin and related analogs, the Neubauer group heterologously expressed the 654 kDa valinomycin NRPS in *E. coli*.[10] Through

condition optimization, production was increased from 0.3 mg / L to 10 mg / L. This system should facilitate the study of the involved NRPS machinery.

While detailed descriptions of the tetradepsipeptide biosynthesis are emerging in the literature from different research groups, relatively little is known about the TE-mediated tetradepsipeptide trimerization and oligomerization process necessary for both valinomycin and cereulide formation.

4.1.4 Thioesterase macrocyclization of iterativly built NRPSs

Thioester domains belong to the α/β-hydrolase superfamily, which includes proteases, lipases and esterases. TEs mediate the offloading of NRPs covalently bound through an acyl-*O*-TE bond. Intermolecular attack from an endogenous nucleophile can result in hydrolysis or transesterification of the acyl-*O*-TE intermediate, leading to the release of a linear product. The TE can also mediate an intramolecular macrocycle forming reaction, resulting in the generation of a lactam or lactone.

Macrocyclization as a strategy for natural product biosynthesis serves to improve compound potency and stability. Cyclization of the long peptide chains rigidifies the compound structure, and can confer proper orientation for specific interaction with a biological target. A cyclic structure can also protect against the peptidase degradation.

Cereulide and valinomycin have been classified by some as iterative NRPSs.[11] The iterative descriptor is used because their NRPS modules are used more than once to assemble a single NRP. This results in a compound that contains smaller, repeated sequences. Iterative NRPSs are known to oligomerize and macrocyclize through different mechanistic processes.

Enterobactin, an iron-chelating siderophore, contains a cyclic trimer of dihydroxybenzoyl-serine units.[12] After the first unit is loaded from the PCP to the terminal TE, a second unit is synthesized and loaded onto the PCP. Dimerization occurs when the free hydroxyl group on the TE-loaded fragment attacks the PCP loaded thioester, forming a new ester bond (Figure 4.3). Once the process repeats and the trimer is formed, the TE catalyzes the offloading macrolactonization.

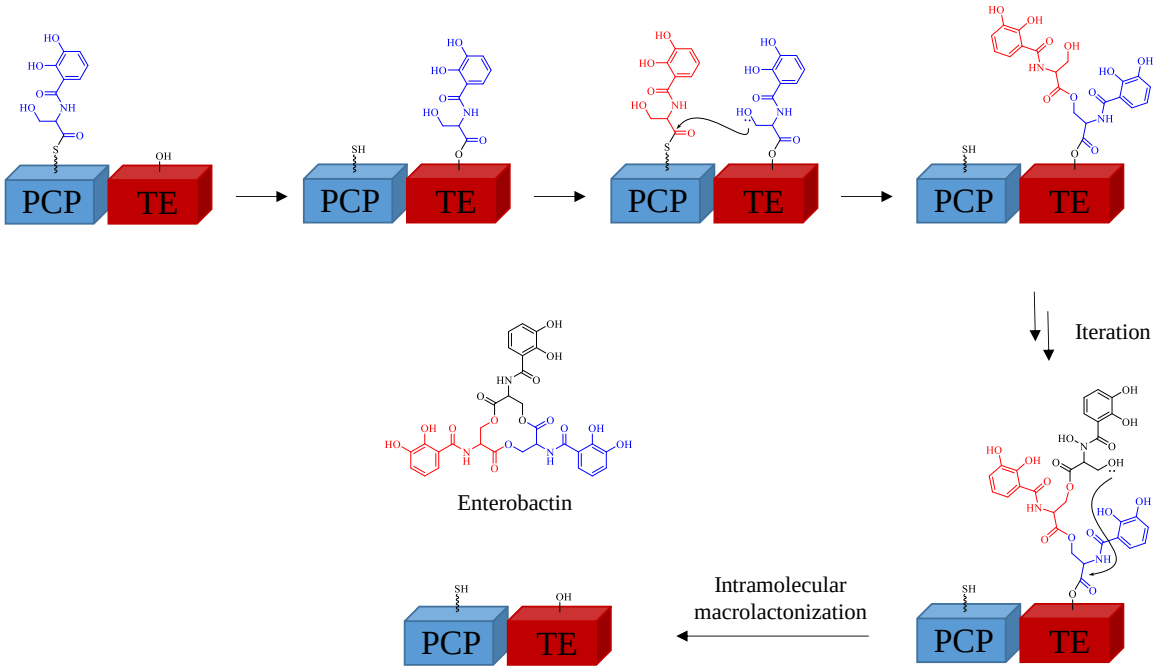

Figure 4.3. Biosynthetic trimerization and macrocyclization of iteratively built enterobactin.

Gramacidin is another iteratively built macrocyclic NRPS. It contains a dimer of five amino acid residues. *In vitro* assays with the purified TE helped to elucidate the mechanism of dimerization and cyclization (Figure 4.4).[13] The first substrate is loaded onto the TE. Then, the second pentapeptide is built and loaded onto the PCP. The terminal amine on the PCP linked fragment attacks the acyl-*O*-TE intermediate ester, effectively removing the pentapeptide from the

TE and forming a new amide bond. The PCP loaded dimer is then transferred to the TE from the PCP and offloading occurs through TE catalyzed macrolactamization.

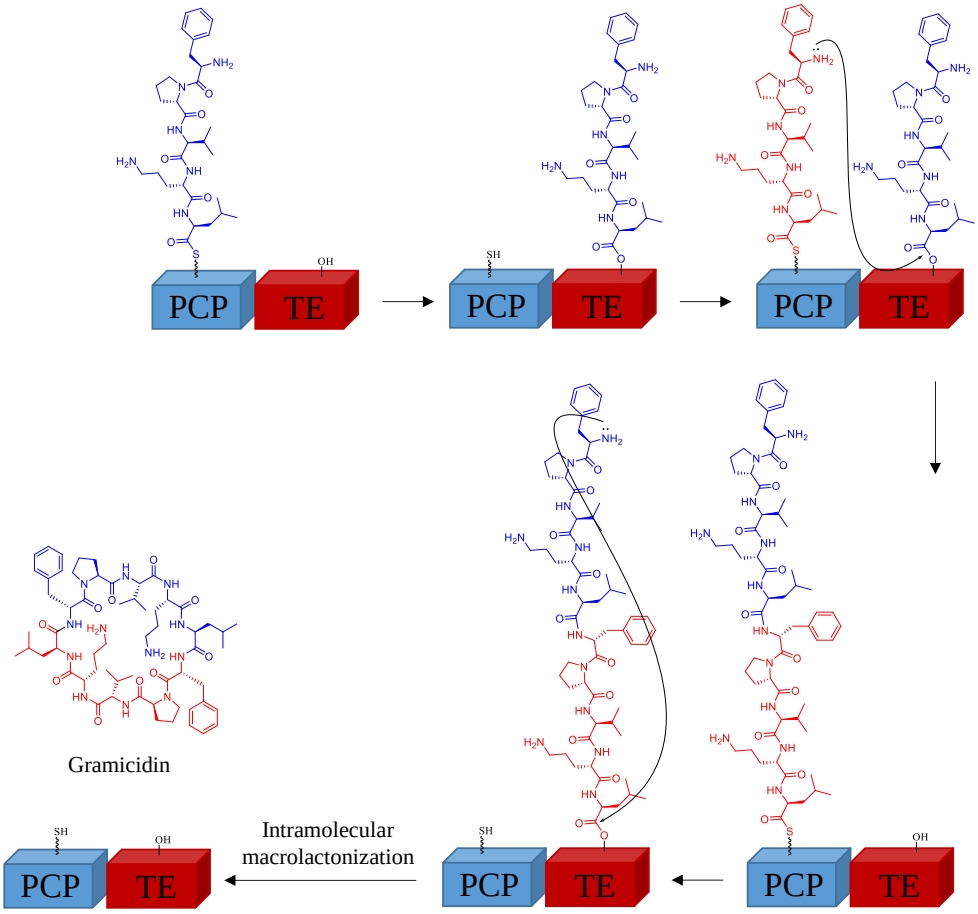

Figure 4.4. Biosynthetic dimerization and macrocyclization of iteratively built gramicidin.

4.1.5 Valinomycin thioesterase

The terminal valinomycin thioesterase domain (VlmTE) catalyzes the trimerization of a precursor tetradepsipeptide followed by an off-loading macrolactonization to produce valinomycin. To characterize this interesting enzymatic process, purified VlmTE was prepared and crystallized by the Schmeing group at McGill University.

To verify the activity of the purified VlmTE and enable further mass spectrometry and structural biology studies, an *N*-acetylcysteamine (SNAC) thioester tetradepsipeptide unit (**Figure 4.5**) was envisioned. It was hypothesized that this substrate would be capable of covalently loading onto the TE active site serine, followed by undergoing enzyme-mediated trimerization and macrolactonization to form the natural product valinomycin. It was also hypothesized that use of this substrate and similar ones would allow for both the characterization of the reaction mechanism steps using mass spectrometry, and help to identify key enzyme-substrate interactions important for the formation of the natural product using X-ray crystallography. This chapter begins by detailing the synthetic work carried out in the Boddy laboratory to prepare SNAC thioester substrates. Also included is early results of *in vitro* evaluation of the SNAC thioester substrates, completed in Professor Martin Schmeing's laboratory by Diego Alonzo and Janice Reimer at McGill University.

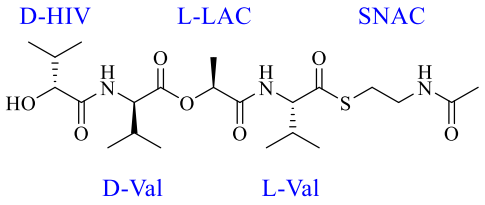

Figure 4.5. Structure of the SNAC thioester tetradepsipeptide unit

4.2. Results and discussion

The retrosynthetic analysis in Figure 4.6 details the general synthetic strategy used to access the desired SNAC tetradepsipeptide substrate. The tetrapeptide backbone would be synthesized through the generation of the ester bond from a TBS-protected carboxylic acid dipeptide and a thioester containing secondary alcohol. Both of these dipeptide fragments would be prepared from simple and commercially available amino acids or amino acid derivatives.

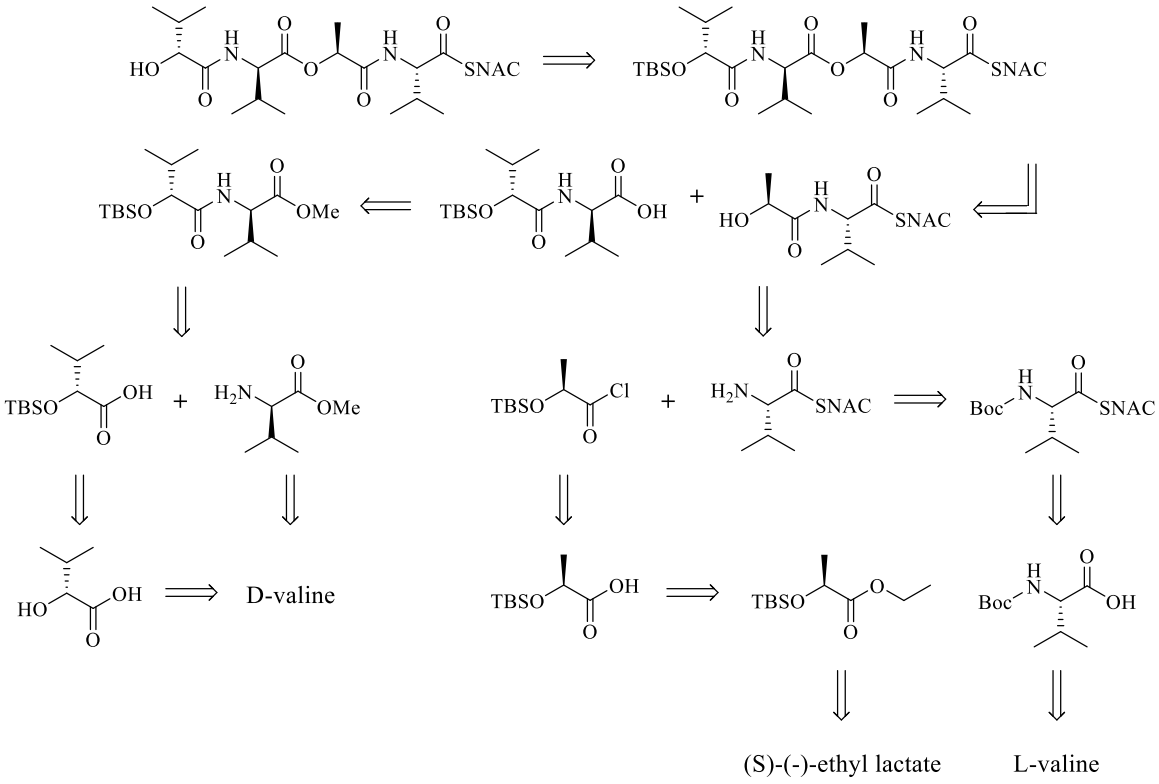

Figure 4.6. Retrosynthetic analysis for VlmTE SNAC substrates

4.2.1 Synthesis of an SNAC tetradepsipeptide substrate

The SNAC L-valine derivative **4.3** was synthesized in two steps from the commercially available Boc-L-valine (**4.1**) (Scheme 4.1). EDC-mediated coupling of this carboxylic acid and *N*-

acetylcysteamine afforded the thioester **4.2** in good yield (72 %). TFA was then used to deprotect the amine, producing **4.3** quantitatively.

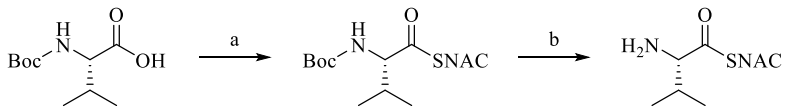

4.1 **4.2** **4.3**

Scheme 4.1. Conditions for the synthesis of **4.3**. a) *N*-acetylcysteamine, EDC, DMAP, 16 h, 72 %; b) TFA, 0 °C to rt, 45 min., > 99 %.

To prepare the silyl ether protected lactic acid fragment (**4.5**), (-)-ethyl L-lactate was treated with TBS-Cl to protect the secondary alcohol (Scheme 4.2). Following this, hydrolysis of the ethyl ester liberated the carboxylic acid **4.5**. Oxalyl chloride was then used to generate the acid chloride (**4.6**) which was used directly in subsequent steps.

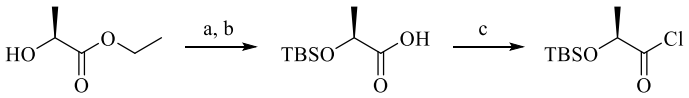

4.4 **4.5** **4.6**

Scheme 4.2. Conditions for the synthesis of **4.6**. a) TBS-Cl, imidazole, 0 °C to rt, 2 h; b) LiOH, 0 °C to rt, 4 h, 78 % over two steps; c) $(COCl)_2$, DMF, 0 °C to rt, 2 h.

Synthesis of the TBS-protected SNAC dipeptide **4.8** was completed upon introduction of the acid chloride (**4.6**) to the thioester-containing amine (**4.3**) in the presence of Et_3N (Scheme 4.3). Deprotection of the silyl ether was then completed with HF to yield **4.8**.

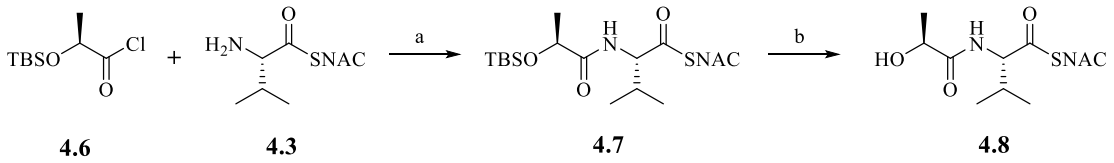

4.6 **4.3** **4.7** **4.8**

Scheme 4.3. Conditions for the synthesis of **4.8**. a) Et_3N, 4 h, 53 %; b) HF, pyridine, 16 h, 84 %.

Both residues of the second dipeptide were derived from D-valine. First, the methyl ester of D-valine (**4.9**) was prepared by treatment with thionyl chloride in the presence of methanol (Equation 4.1).

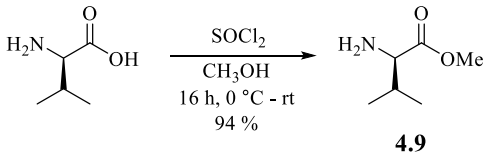

4.9 (4.1)

Diazotisation of D-valine in aqueous H_2SO_4 afforded the corresponding β–hydroxy-amino acid intermediate. The secondary alcohol was then protected with TBS-Cl to give **4.10** (Scheme 4.4). Treatment of this compound with thionyl chloride produced the acid chloride **4.11**, which was used in subsequent reactions immediately.

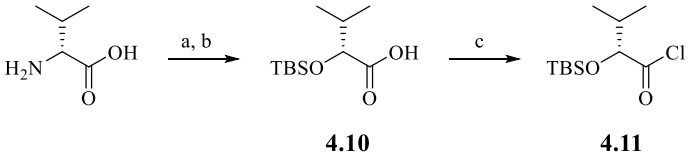

4.10 **4.11**

Scheme 4.4. Conditions for the synthesis of **4.11**. a) $NaNO_2$, H_2SO_4, 0 °C to rt, 3 h, 50 %; b) TBS-Cl, imidazole, rt, 24 h, 51 %; c) $SOCl_2$, DMF, 2 h.

The amide bond in **4.12** was formed in good yield (79 %) by treating the acid chloride **4.11** with the amine **4.9** in the presence of a base (Scheme 4.5). Hydrolysis of the methyl ester was then completed using LiOH which produced the desired carboxylic acid **4.13**.

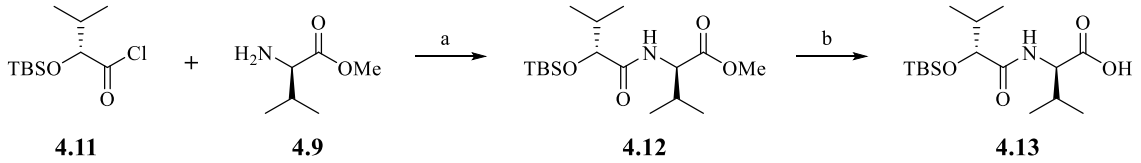

4.11 **4.9** **4.12** **4.13**

Scheme 4.5. Conditions for the synthesis of **4.13**. a) Et_3N, rt, 16 h, 79 %; b) LiOH, 0 °C to rt, 3 h, 77 %.

Coupling of the carboxylic acid (**4.13**) and alcohol (**4.8**) was achieved using EDC and DMAP (Scheme 4.6). Upon analysis of the ^{1}H and ^{13}C NMR spectra, it was noted that partial racemization of the valine residue originating from **4.13** occurred, likely through azlactone formation. This gave a 7:3 mixture of diastereomers **4.14A** and **4.14B** (determined by ^{1}H NMR). These compounds were not separable and the mixture of the two diastereomers was used in the subsequent reaction. Deprotection of the TBS group of the diastereomeric mixture was completed using HF to give the desired SNAC tetradepsipeptide substrate. Fortunately, the diastereomers **4.15A** and **4.15B** were separable using prep-TLC.

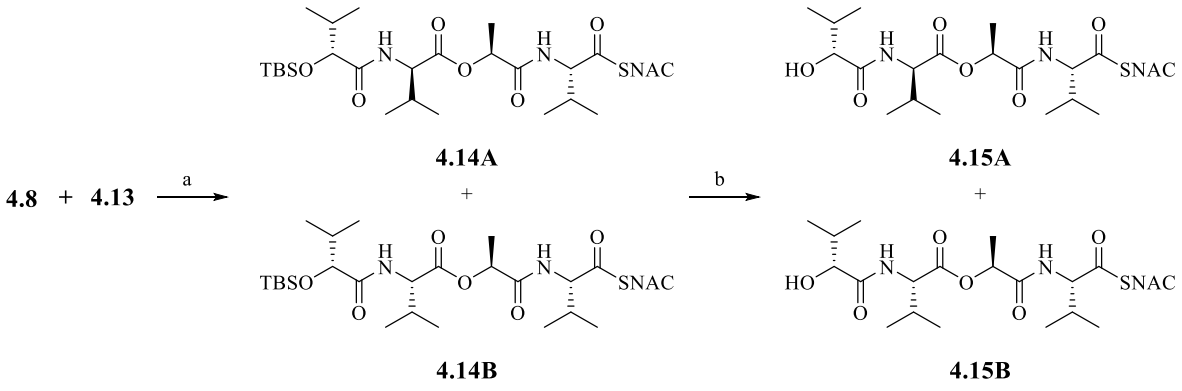

4.14A **4.15A** **4.14B** **4.15B**

Scheme 4.6. Conditions for the synthesis of **4.15A** and **4.14B**. a) EDC, DMAP, rt, 16 h, 62 %; b) HF, pyridine, >99 %.

4.2.2 Synthesis of an SNAC deoxy-tetradepsipeptide substrate

In addition to **4.15A**, it was desirable to synthesize an analog that would bind to VlmTE, but would not undergo the oligomerization process. This was hypothesized to allow for X-Ray crystallography studies that could help describe the precise enzyme / small molecule interactions important for initial tetradepsipeptide substrate binding, and how this binding might facilitate oligomerization. Towards this, the synthesis of a deoxy-SNAC thioester tetradepsipeptide substrate (Figure 4.7) was envisioned. The removal of the terminal hydroxyl group is a minimal structural change which should not impact the overall ability of the substrate to load and bind the VlmTE.

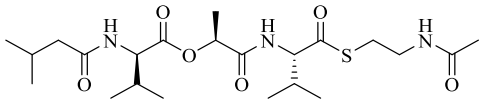

Figure 4.7. Structure of the SNAC deoxy-tetradepsipeptide substrate.

A deoxy-analog of the dipeptide **4.13** was synthesized in two steps. The amide bond in **4.16** was built from the amine **4.9** and isovaleric acid using EDC (Scheme 4.7). Subsequent hydrolysis of the methyl ester afforded the carboxylic acid **4.17**.

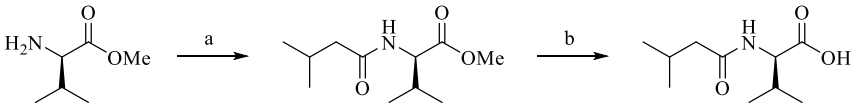

4.9 **4.16** **4.17**

Scheme 4.7. Conditions for the synthesis of **4.17**. a) Isovaleric acid, EDC, DMAP, Et_3N, rt, 16 h, 60 %; b) LiOH, 0 °C to rt, 4 h, 60 %.

The previously synthesized alcohol **4.8** and the carboxylic acid **4.17** were coupled with EDC and DMAP to form the desired deoxy-tetradepsipeptide substrate in good yield (92 %) (Scheme 4.8). Analysis of the ^{1}H NMR spectrum indicated partial racemization of the valine reside in **4.17** occurred to give a 5:4 ratio of **4.18A** and **4.18B**. The two diastereomers were separated by prep-TLC.

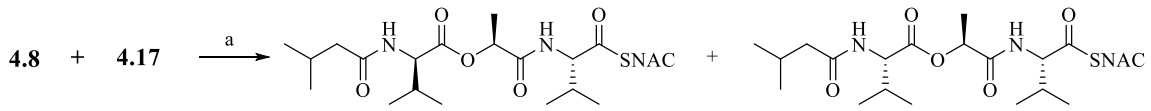

4.18A **4.18B**

Scheme 4.8. Conditions for the synthesis of **4.18A** and **4.18B**. a) EDC, DMAP, - 20 °C to rt, 16 h, 92 %.

4.2.3 *In vitro* evaluation of SNAC substrates

The SNAC depsitetrapeptide substrate **4.15A** was evaluated for the ability to act as a substrate for the purified VlmTE by Diego Alonzo and Janice Reimer in Prof. Martin Schmeing's laboratory at McGill University. The enzymatic reaction mixture was separated by HPLC and seven different analytes were identified using mass spectrometry (Figure 4.8). Compounds identified included the substrate (**4.15A**), the SNAC thioester dimer (**4.19**), the SNAC thioester trimer (**4.20**) and valinomycin (**4.21**). The other three analytes were the hydrolyzed products of the intermediate SNAC thioesters (**4.22**, **4.23**, and **4.24**).

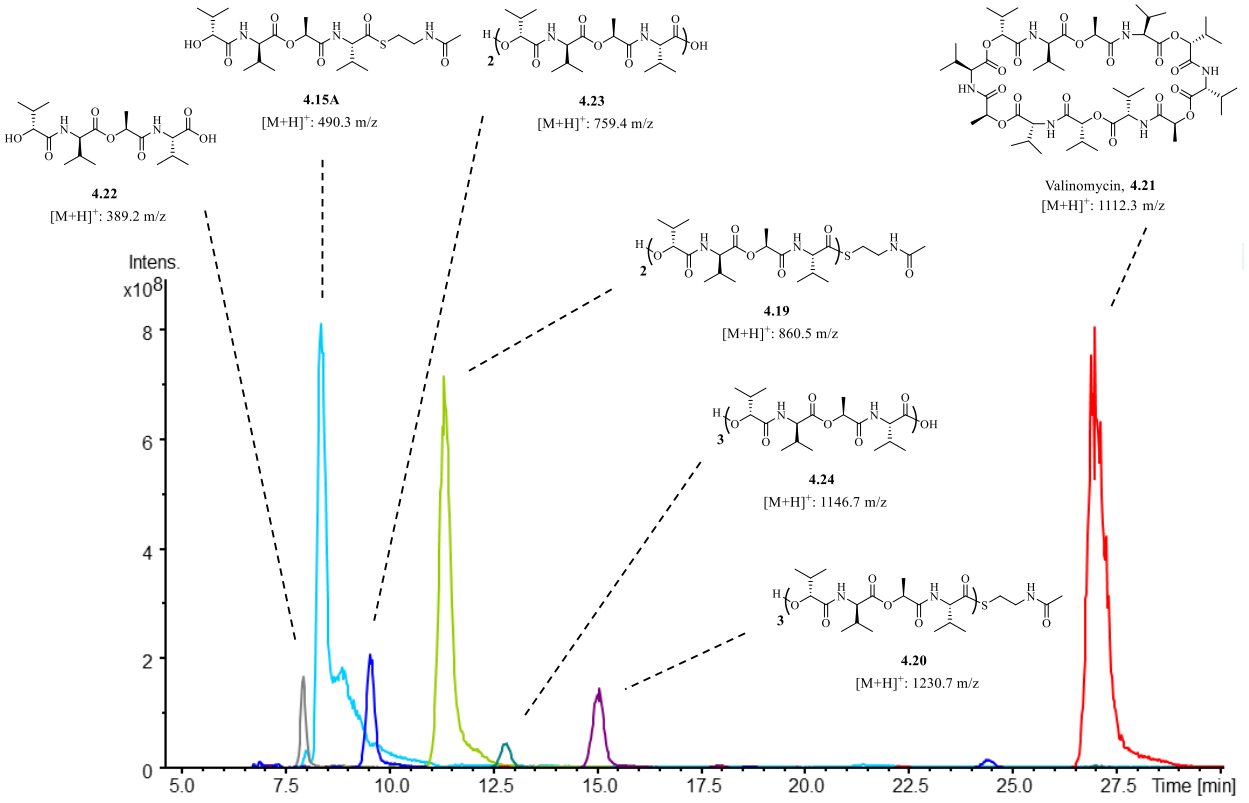

Figure 4.8. The depsitetrapeptide substrate **4.15A** loads onto the VlmTE undergoes oligomerization and cyclization. Shown are the overlayed selected ion traces with the structure of the analytes.

Unfortunately, attempts to soak the SNAC deoxy-depsipeptide substrate **4.18A** into VlmTE crystals and obtain an X-ray were unsuccessful. It was found that **4.18A** is hydrolyzed off of the active site too quickly. Moving forward, **4.18A** was also evaluated for activity using purified VlmTE. In this experiment, only the substrate and its hydrolysis product were observed by LC-MS (data not shown). **4.18A** was then reacted with VlmTE in the presence of the active SNAC depsipeptide substrate **4.15A**. In the reaction mixture, thirteen analytes were identified. All seven analytes from Figure 4.8 were present, indicating fragments that formed without the integration of the deoxy substrate (data not shown). The six substrates identified that contained the deoxy-depsipeptide fragment were the deoxy-substrate itself **4.18A**, the SNAC thioester heterodimer

4.25, and the SNAC trimer **4.26** (Figure 4.9). The hydrolyzed deoxy-substrate **4.27**, hydrolyzed heterodimer **4.28**, and hydrolyzed trimer **4.29** were also observed.

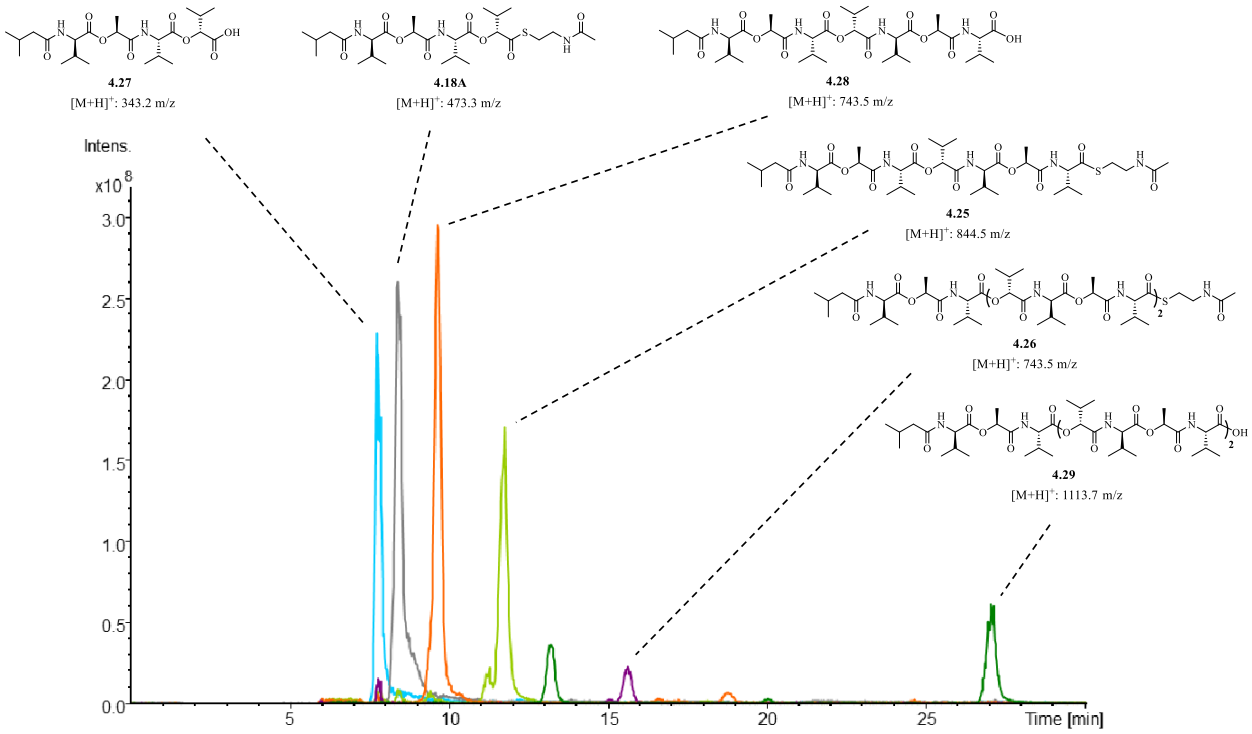

Figure 4.9. The deoxy-tetradepsitetrapeptide substrate **4.18A** is integrated into the elongating depsipeptide by VlmTE. Shown are the overlayed selected ion traces of deoxy-depsipeptide substrate containing intermediates with the structures of the analytes.

The presence of the seven compounds shown in Figure 4.8 and the additional six compounds identified in Figure 4.9 can be used to propose a mechanism that results in the formation of valinomycin (Figure 4.10). The data suggests that elongation of the initial VlmTE loaded substrate occurs though the formation of a new ester bond between the terminal secondary alcohol of the second equivalent of tetradepsipeptide and the carboxyl group of the first equivalent, which is initially bound directly to the TE active site serine. This results in the release of the newly formed SNAC thioester-containing dimer (**4.19**) from the TE. At this point **4.19** can reload onto the active site of VlmTE and undergo another intermolecular elongation reaction to produce the

SNAC thioester-containing trimer (**4.20**). This growing chain once again loads onto the TE before undergoing macrolactonization, forming valinomycin (**4.21**). Compounds **4.19** and **4.20** would likely not be observed as major products if elongation occurred at the terminal hydroxyl group of the first TE loaded substrate.

The hydrolysis products for all enzyme loaded intermediates in both experiments were also identified (**4.22**, **4.23**, and **4.24**). It is likely that the hydrolysis reaction competes with the TE-mediated oligomerization/macrocyclization process. The formation of these products may also occur spontaneously after substrate is release from the enzyme.

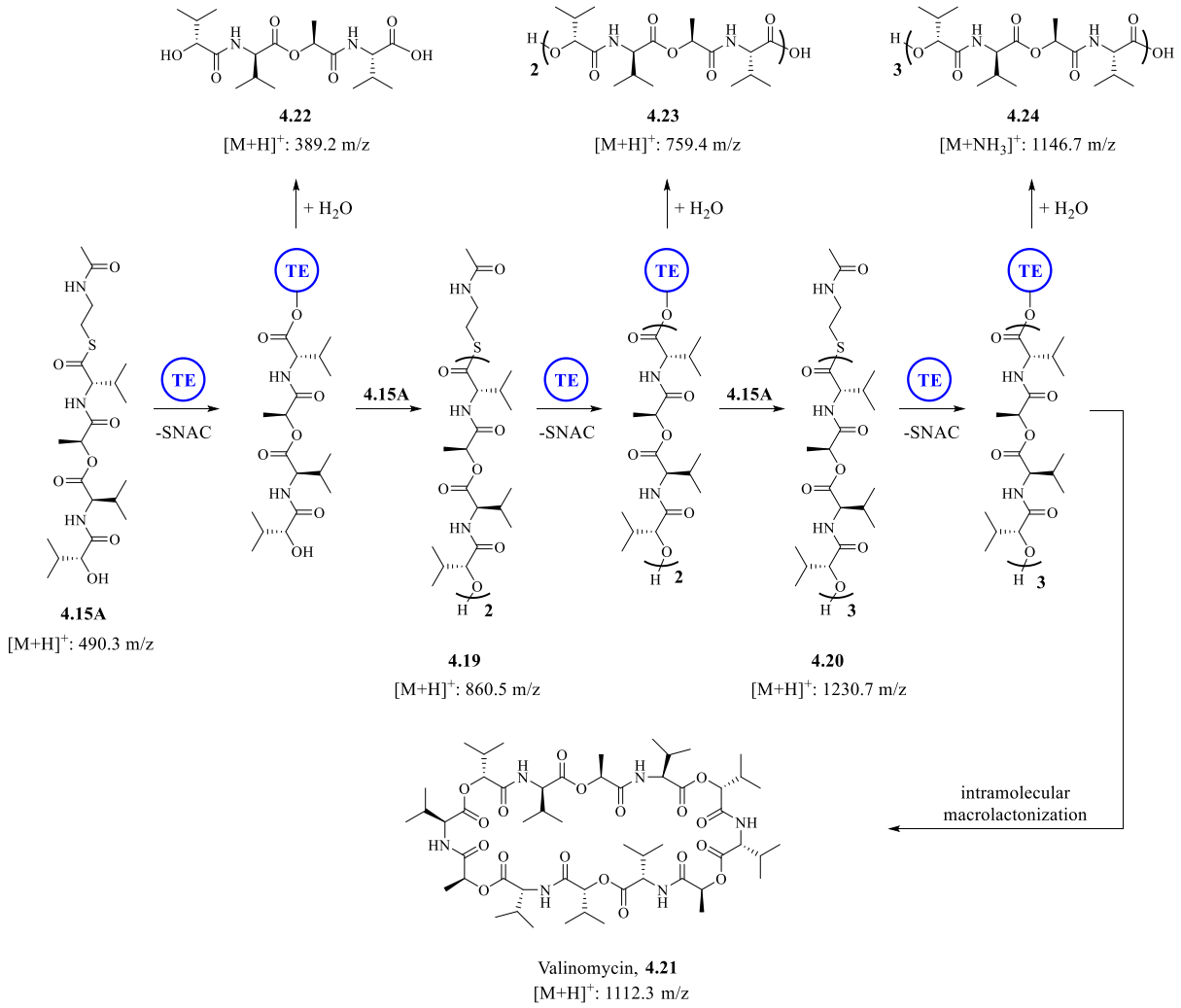

Figure 4.10. Proposed steps for purified VlmTE mediated oligomerization and macrolactonization to product valinomycin, intermediates and hydrolyzed products.

4.2.4 Proposal of an oligomerization mechanism for the biosynthesis of valinomycin

The proposed method for purified VlmTE-mediated oligomerization of the SNAC tetradepsipeptide substrates can be translated to describe an iterative and cooperative dynamic between the PCP and VlmTE during the oligomerization process of valinomycin biosynthesis (Figure 4.11). This is similar to the mechanism described for the biosynthesis of gramicidin.[13] In this model, the PCP loads the first substrate onto the vacant VlmTE. After the PCP receives the second equivalent of the tetradepsipeptide substrate, the PCP and TE mediate dimerization between the first tetradepsipeptide equivalent at the TE active site and the terminal hydroxyl group of the second equivalent which remains bound to the PCP. During this transesterification process, the dimer is effectively transferred back to the PCP from the TE. The PCP then transfers the newly formed dimer to VlmTE and this process repeats to add the third tetradepsipeptidyl equivalent. Once the third equivalent is added to the growing chain and the substrate is transferred to the TE, the macrolactonization step occurs.

This model differs from previously postulated biosynthetic cyclo-trimerization mechanisms that show elongation and oligomerization either occurring at the terminal end of the growing chain, or mediation of elongation solely completed by the TE.[12] In this proposed model, the PCP has two important functions. The first function is to transfer monomer, dimer and trimer valinomycin intermediates to the TE. The second function is to facilitate the addition of each monomeric unit onto the TE loaded substrate though transesterification, which results in simultaneous chain growth and substrate release from the TE.

Another important feature of this model is that the PCP and TE mediate two transesterifications that follow the same molecular geometry during the oligomerization steps. The electrophilic activated ester is always located at the active site serine and the nucleophile is always at the terminal hydroxyl-group of the PCP loaded tetradepsipeptide equivalent. This suggests that there may be important substrate/enzyme (TE and/or PCP) structural features that mediate the transesterifications. If chain growth occurred at the terminal end of the TE loaded tetradepsipeptide, a tightly controlled pathway for enzyme-mediated nucleophilic attack would not be as likely, as the additions would have to occur at the changing, elongating end of the substrate.

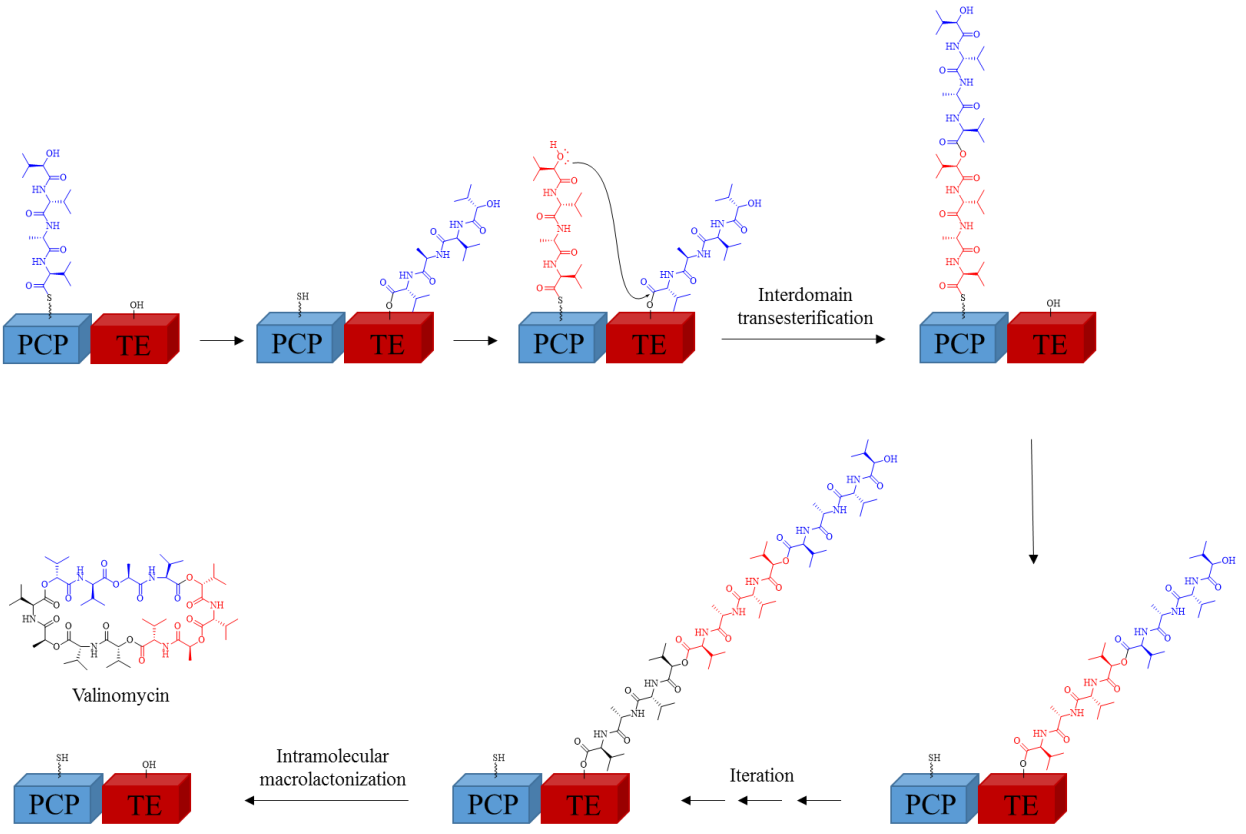

Figure 4.11. Proposed mechanism for oligomerization during valinomycin biosynthesis.

4.3 Summary and outlook

In summary, the synthesis and *in vitro* evaluation of the SNAC thioester substrates **4.15A** and **4.18A** have allowed for the determination of the basic biosynthetic mechanistic steps that the valinomycin NRPS employs to trimerize and cyclize a tetradepsipeptide building block. Oligomerization occurs in a fashion similar to the mechanism employed in the biosynthesis of the NRPS product gramicidin.

Future efforts will be directed towards obtaining an X-ray of a tetradepsipeptide substrate bound to the purified VlmTE active site. This will allow for characterization of the important substrate / VlmTE interactions necessary for binding, facilitation of the polymerizing transesterification process and induction of macrolactonization. As initial efforts towards this goal showed that the rate of hydrolysis of the deoxy- SNAC thioester substrate **4.18A** off of the enzyme prevented the acquisition of an X-ray structure, future analog design should aim to minimize this background reaction.

4.4 Experimental section

4.4.1 Synthetic methods and characterization

General information

All reactions were performed in oven-dried or flame-dried glass round-bottom flasks equipped with magnetic stir bars. Purification of reaction products was carried out by flash column chromatography using silica gel. ^{1}H NMR spectra were recorded on either a Bruker 400 MHz or Bruker 300 MHz at ambient temperature. ^{13}C NMR spectra were recorded on either a Bruker 100 MHz or Bruker 75 MHz at ambient temperature. Spectra are recorded in parts per million using residual solvent as the internal standard ($(CD_3)_2SO$ at 2.50 ppm, $CDCl_3$ at 7.26 ppm and CD_3OD at 3.31 ppm for ^{1}H NMR and $(CD_3)_2SO$ at 39.52 ppm, $CDCl_3$ at 77.16 ppm and CD_3OD at 49.00 ppm for ^{13}C NMR.) ^{1}H NMR data was reported as: multiplicity (br = broad, s = singlet, d = doublet, t = triplet, q = quartet, quin. = quintet, sext. = sextuplet, sept = septuplet, m = multiplet), integration and coupling constant(s) in Hz. High-resolution mass spectrometry was performed by electrospray ionization (ESI) in positive ion or negative ion mode using a Micromass Q-TOF 1 mass spectrometer.

Materials

Unless otherwise noted, all commercially available materials were purchased from commercial sources and used without further purification.

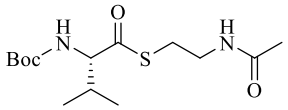

(*S*)-1-[(2-Acetylaminoethylthio)carbonyl]-2-methylpropylamino 2,2-dimethylpropionate, Compound 4.2

Boc-L-Valine (7.29 g, 33.56 mmol, 1.0 equiv.) was dissolved in CH_2Cl_2. *N*-Acetylcysteamine (4.00 g, 33.56 mmol, 1.0 equiv.), *N*-(3-dimethylaminopropyl)-*N′*-ethylcarbodiimide hydrochloride (7.72 g, 40.27 mmol, 1.2 equiv.) and 4-(dimethylamino)pyridine (410 mg, 3.36 mmol, 0.1 equiv.) were added to the mixture. The reaction was allowed to stir for 16 h at ambient temperature. The reaction mixture was quenched with $NH_4Cl_{(aq)}$ and extracted 3 × with EtOAc. The organic fractions were combined, washed with brine, dried over Na_2SO_4 and concentrated. The desired product (7.69 g, 24.16 mmol, 72 % yield) was purified with silica column chromatography (5 % MeOH in CH_2Cl_2). ^{1}H NMR (300 MHz, $CDCl_3$) δ 5.86 (s, 1H), 4.96 (d, *J* = 8.8 Hz, 1H), 4.24 (dd, *J* = 9.0, 4.8 Hz, 1H), 3.53 – 3.32 (m, 2H), 3.04 (td, *J* = 6.4, 1.6 Hz, 2H), 2.25 (td, *J* = 13.7, 7.0 Hz, 1H), 1.95 (s, 3H), 1.46 (s, 9H), 0.99 (d, *J* = 6.8 Hz, 3H), 0.88 (d, *J* = 6.9 Hz, 3H).

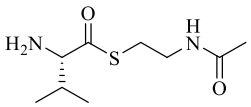

***S*-2-Acetylaminoethyl (*S*)-2-amino-3-methylbutanethioate, Compound 4.3**

In a round-bottom flask, **4.2** (0.5 g, 1.57 mmol, 1.0 equiv.) was dissolved in CH_2Cl_2 (3 mL). The solution was cooled to 0 °C using an ice bath and trifluoroacetic acid (3 mL) was added. The reaction was allowed to proceed at ambient temperature for 45 min. The reaction mixture was concentrated and the desired product (341 mg, 1.56 mmol, >99 % yield) was purified by silica column chromatography (5 % to 10 % MeOH in Ch_2Cl_2). ^{1}H NMR (300 MHz, DMSO) δ 8.45 (s,

2H), 8.10 (t, *J* = 5.5 Hz, 1H), 4.15 (d, *J* = 4.8 Hz, 1H), 3.27 – 3.17 (m, 2H), 3.13 – 2.98 (m, 2H), 2.28 – 2.09 (m, 1H), 0.99 (d, *J* = 6.9 Hz, 3H), 0.95 (d, *J* = 7.0 Hz, 3H). ^{13}C NMR (75 MHz, DMSO) δ 196.18, 169.35, 63.48, 37.78, 30.10, 28.40, 22.50, 18.03, 17.26.

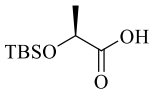

(S)-(-)-ethyl 2-(tert-butyldimethylsilyloxy)propanoate, Compound 4.5

In a round-bottom flask, (-)-ethyl L-lactate (5.08 g, 43.0 mmol, 1.0 equiv.) was dissolved in CH_2Cl_2 (55 mL) and the solution was cooled to 0 °C using an ice bath. tert-Butyldimethylsilyl chloride (6.48 g, 45.15 mmol, 1.05 equiv.) and imidazole (3.51 g, 51.6 mmol, 1.2 equiv.) was added to this mixture, after which the reaction was allowed to proceed at ambient temperature for 2 h. The reaction mixture was then diluted with H_2O and extracted 3 × with CH_2Cl_2. The organic fractions were combined, washed with ice cold 5 % $HCl_{(aq)}$, washed with brine, dried over Na_2SO_4 and concentrated. The crude intermediate (*S*)-(-)-ethyl 2-(tert-butyldimethylsilyloxy)propanoate was used in the subsequent reaction. (*S*)-(-)-ethyl 2-(tert-butyldimethylsilyloxy)propanoate (43 mmol, 1.0 equiv.) was dissolved in THF (215 mL). The mixture was cooled to 0 °C using an ice bath and a cooled solution of LiOH (0.4 M, 215 mL) was added dropwise over 20 min. The reaction mixture was stirred for 4 h at ambient temperature. The resulting reaction mixture was concentrated to half-volume, and the resulting aqueous solution was extracted 3 × with Et_2O. The organic fractions were combined and extracted 3 × with a saturated solution of $NaHCO3_{(aq)}$. The aqueous fractions were combined, acidified to pH 4 with 1 M $KHSO_{4(aq)}$ and extracted 3 × with Et_2O. The organic fraction were combined, dried over Na_2SO_4 and concentrated. The desired product (6.88 g, 33.7 mmol, 78 % yield over two steps) was obtained and used without further purification. The NMR

data were consistent with literature values.[14] ^{1}H NMR (300 MHz, $CDCl_3$) δ 4.36 (q, *J* = 6.8 Hz, 1H), 1.45 (d, *J* = 6.8 Hz, 3H), 0.92 (s, 9H), 0.13 (s, 6H).

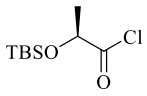

(2S)-2-((1,1-Dimethylethyl)dimethylsilyloxy)propanoyl chloride, Compound 4.6

In a round-bottom flask, **4.5** (3.7 g, 18 mmol, 1.0 equiv.) was dissolved in DMF (45 mL) and the solution was cooled to 0 °C using an ice bath. Oxalyl chloride (13.6 mL of a 2.0 M solution, 10.0 equiv.) and a catalytic amount of DMF were added. The reaction proceeded for 2 h from 0 °C to ambient temperature. The reaction mixture was concentrated and the crude oil was used in subsequent reactions without purification.

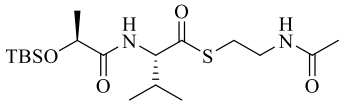

TBSO-L-LAC-L-Val-SNAC, Compound 4.7

In a round-bottom flask, **4.3** (1.95 g, 9 mmol, 1.0 equiv.) was dissolved in CH_2Cl_2 (40 mL). The crude oil **4.6** (18 mmol, 2.0 equiv.) was dissolved in CH_2Cl_2 (5 ml) and added to the mixture. Et_3N (2.5 mL, 18 mmol, 2.0 equiv.) was added and the reaction was allowed to proceed for 4 h. The reaction mixture was quenched with $NH_4Cl_{(aq)}$, extracted 3 × with EtOAc, washed with brine and concentrated. The desired product (1.93 g, 4.77 mmol, 53 % yield) was purified from the crude mixture by silica column chromatography (50 % to 90 % EtOAc in hexanes). ^{1}H NMR (300 MHz, $CDCl_3$) δ 7.22 (d, *J* = 9.3 Hz, 1H), 6.03 (s, 1H), 4.53 (dd, *J* = 9.3, 4.5 Hz, 1H), 4.25 (q, *J* = 6.7 Hz, 1H), 3.38 (q, *J* = 6.2 Hz, 2H), 3.07 – 2.98 (m, 2H), 2.40 – 2.21 (m, 1H), 1.93 (s, 3H), 1.38 (d, *J* =

6.7 Hz, 3H), 1.01 – 0.82 (m, 15H), 0.13 (s, 3H), 0.12 (s, 3H). ^{13}C NMR (75 MHz, $CDCl_3$) δ 200.34, 174.90, 170.47, 70.03, 63.48, 39.47, 31.04, 28.51, 25.82, 23.23, 22.04, 19.47, 18.00, 16.83, -4.54, -5.03.

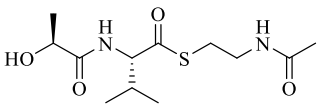

HO-L-LAC-L-Val-SNAC, Compound 4.8

Compound **4.7** (250 mg, 0.617 mmol, 1.0 equiv.) was dissolved in acetonitrile (20 mL) in a 50 mL polypropylene Falcon tube. Pyridine (249 µL, 3.09 mmol, 5 equiv.) and HF (533 µL, 30.9 mmol, 50 equiv.) were added. The reaction was stirred at ambient temperature for 16 h. The reaction mixture was quenched with $NH_4Cl_{(aq)}$, extracted 3 × with EtOAc, washed with brine, dried over Na_2SO_4 and concentrated. The desired product (150.1 mg, 0.517 mmol, 84 % yield) was purified with silica column chromatography (2 % to 8 % MeOH in CH_2Cl_2). ^{1}H NMR (400 MHz, $CDCl_3$) δ 7.21 (d, *J* = 9.2 Hz, 1H), 6.20 (s, 1H), 4.54 (dd, *J* = 9.2, 5.4 Hz, 1H), 4.30 (q, *J* = 6.8 Hz, 1H), 4.15 (s, 1H), 3.52 – 3.32 (m, 2H), 3.12 – 2.94 (m, 2H), 2.36 – 2.21 (m, 1H), 1.95 (s, 3H), 1.44 (t, *J* = 6.3 Hz, 3H), 0.97 (d, *J* = 6.8 Hz, 3H), 0.91 (d, *J* = 6.8 Hz, 3H). ^{13}C NMR (100 MHz, $CDCl_3$) δ 200.20, 175.47, 170.94, 68.66, 63.77, 39.24, 30.90, 28.71, 23.25, 21.28, 19.45, 17.27.

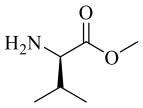

(*R*)-methyl 2-amino-3-methylbutanoate, Compound 4.9

In a round-bottom flask, D-valine (5.0g, 42.7 mmol, 1.0 equiv.) was dissolved in MeOH (50 mL). The solution was cooled to 0 °C using an ice bath and thionyl chloride (9.3 mL, 128.1 mmol, 3.0

equiv.) was added dropwise, after which the mixture was stirred for 16 h at ambient temperature. The reaction mixture was then concentrated and the resulting solid was washed with Et_2O to yield the desired product (6.69 g, 39.9 mmol, 94 % yield). The NMR data were consistent with literature values.[15] ^{1}H NMR (400 MHz, DMSO) δ 8.70 (s, 3H), 3.81 (d, *J* = 4.7 Hz, 1H), 3.73 (s, 3H), 2.27 – 2.13 (m, 1H), 0.98 (d, *J* = 6.9 Hz, 3H), 0.93 (d, *J* = 6.9 Hz, 3H).

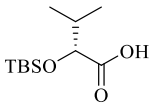

(*R*)-2-(tert-butyldimethylsilyl)oxy-3,3-dimethylbutanoic acid, Compound 4.10

D-Valine (2.00 g, 17.1 mmol, 1.0 equiv.) was dissolved in a 2.5 M aqueous solution of H_2SO_4 (25 mL). The mixture was cooled to 0 °C. $NaNO_2$ (2.36 g, 34.2 mmol, 2.0 equiv.) was dissolved in H_2O (5 mL) and added dropwise to the solution over 30 minutes, after which the reaction was allowed to proceed for 3 h from 0 °C to ambient temperature. The reaction mixture was quenched with H_2O, extracted with EtOAc, washed with brine, dried over Na_2SO_4, and concentrated to yield the crude intermediate (2R)-2-hydroxy-3-methylbutanoic acid (771 mg, 8.56 mmol, 50.1 % yield). This crude intermediate was dissolved in DMF (11.5 mL). tert-Butyldimethylsilyl chloride (3.1 g, 20.5 mmol, 2.4 equiv.) and imidazole (2.79 g, 41.1 mmol, 4.8 equiv.) was added to this mixture, after which the reaction was allowed to proceed at ambient temperature for 24 h. The reaction mixture was diluted with EtOAc, washed with a saturated aqueous citric acid solution, washed with saturated $NaHCO_3$, and washed with brine. The organic phase was then dried over Na_2SO_4 and concentrated. The resulting oil was dissolved in MeOH (80 mL) and cooled to 0 °C using an ice bath. K_2CO_3 (2.35 g, 17 mmol, 2.0 equiv.) was dissolved in H_2O (20 mL) and this was added to the solution. The resulting mixture was stirred for 2.5 h. The solution pH was adjusted to 4 with an aqueous HCl solution (1.0 M) and the aqueous phase was extracted with EtOAc. The organic

phase was dried over Na_2SO_4 and concentrated. The desired product (1.01 g, 4.34 mmol, 51 % yield) was purified by silica column chromatography (5 % to 20 % EtOAc in hexanes). ^{1}H NMR (400 MHz, $CDCl_3$) δ 4.08 (d, *J* = 3.8 Hz, 1H), 2.15 – 2.03 (m, 1H), 1.00 – 0.92 (m, 15H), 0.12 (s, 3H), 0.11 (s, 3H).

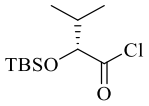

(*R*)-2-(tert-butyldimethylsilyl)oxy-3,3-dimethylbutanoyl chloride, Compound 4.11

In a round-bottom flask, **4.10** (550 mg, 2.37 mmol, 1.0 equiv.) was dissolved in CH_2Cl_2 (12 mL). Thionyl chloride (210 μL, 2.84 mmol, 1.2 equiv.) was added dropwise followed by a catalytic amount of DMF (2 drops). The solution was stirred at ambient temperature for 2 h and the reaction mixture was concentrated. The crude oil was used in subsequent reactions without purification.

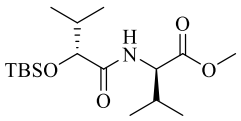

TBSO-D-HIV-D-Val-OMe, Compound 4.12

The crude oil **4.11** (2.37 mmol, 1.0 equiv.) was dissolved in CH_2Cl_2 (12 mL) in a round-bottom flask. The amine **4.9** (595 mg, 3.55 mmol, 1.5 equiv.) and Et_3N (720 mg, 7.11 mmol, 3.0 equiv.) were added to the mixture and the reaction was allowed to proceed for 16 h at ambient temperature. H_2O was added to quench the reaction, the phases were separated and the aqueous phase was extracted 3 × with CH_2Cl_2. The organic fractions were combined, washed with 10 % $HCl_{(aq)}$, washed with a saturated solution of $NaHCO_{3(aq)}$, washed with brine, dried over Na_2SO_4 and concentrated. The desired product (650 mg, 1.88 mmol, 79 %) was purified with silica column

chromatography (15 % EtOAc in hexanes). ^{1}H NMR (300 MHz, $CDCl_3$) δ 7.03 (d, *J* = 9.0 Hz, 1H), 4.54 (dd, *J* = 9.2, 4.6 Hz, 1H), 3.97 (d, *J* = 3.1 Hz, 1H), 3.71 (s, 3H), 2.23 – 2.05 (m, 2H), 0.98 – 0.85 (m, 21H), 0.08 (s, 6H). ^{13}C NMR (100 MHz, $CDCl_3$) δ 173.21, 172.00, 77.76, 56.57, 52.03, 32.76, 31.30, 25.84, 19.46, 19.16, 18.08, 17.77, 16.32, -4.88, -5.14.

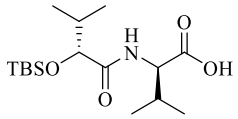

TBSO-D-HIV-D-Val-OH, Compound 4.13

In a round-bottom flask, **4.12** (590 mg, 1.71 mmol, 1 equiv.) was dissolved in THF (34 mL) and the solution was cooled to 0 °C using an ice bath. An aqueous solution of LiOH (1 M, 34 mL) was added dropwise. The mixture was allowed to react from 0 °C to ambient temperature for 3 h. The reaction mixture was concentrated to half-volume and the resulting aqueous mixture was washed 2 × with Et_2O. The organic fractions were combined and extracted 2 × with a saturated solution of $NaHCO_{3(aq)}$. All aqueous fractions were combined and the pH was adjusted to 4 using an solution of $KHSO_{4(aq)}$ (1 M). The aqueous layer was extracted 3 × with Et_2O and the organic fractions were combined, dried over Na_2SO_4 and concentrated. The desired product (434 mg, 1.31 mmol, 77 % yield) was purified with silica column chromatography (8 % MeOH in CH_2Cl_2). ^{1}H NMR (400 MHz, $CDCl_3$) δ 7.09 (d, *J* = 9.0 Hz, 1H), 4.58 (dd, *J* = 9.1, 4.3 Hz, 1H), 4.03 (d, *J* = 3.1 Hz, 1H), 2.34 – 2.21 (m, 1H), 2.19 – 2.06 (m, 1H), 1.02 – 0.93 (m, 18H), 0.88 (t, *J* = 7.2 Hz, 3H), 0.10 (s, 3H), 0.07 (s, 3H). ^{13}C NMR (100 MHz, $CDCl_3$) δ 175.98, 174.00, 77.70, 56.61, 32.84, 31.05, 25.92, 19.51, 19.33, 18.13, 17.63, 16.36, -4.78, -5.08.

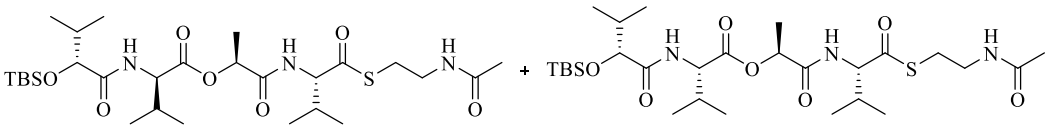

A B

TBSO-D-HIV-D-Val-L-LAC-L-Val-SNAC, Compound 4.14A and

TBSO-D-HIV-L-Val-L-LAC-L-Val-SNAC, Compound 14.B

In a round-bottom flask, the carboxylic acid **4.13** (84 mg, 0.2525 mmol, 1.0 equiv.) and the alcohol **4.8** (110 mg, 0.3788 mmol, 1.5 equiv.) were dissolved in CH_2Cl_2 (2.5 mL). To this mixture, *N*-(3-dimethylaminopropyl)-N′-ethylcarbodiimide hydrochloride (73 mg, 0.3788 mmol, 1.5 equiv.) and 4-(dimethylamino)pyridine (47 mg, 0.3788 mmol, 1.5 equiv.) were added and the reaction was stirred for 16 h at ambient temperature. The reaction mixture was quenched with a saturated solution of $NH_4Cl_{(aq)}$ and extracted 3 × with EtOAc. The organic phase was washed with brine, dried over Na_2SO_4, and concentrated. The desired product (77 mg, 0.157 mmol, 62 % yield) was purified with silica column chromatography (1 % to 4 % MeOH in CH_2Cl_2) as a mixture of diastereomers in a 7 : 3 ratio (**4.14A** : **4.14B**). **4.14A** ^{1}H NMR (300 MHz, $CDCl_3$) δ 7.27 (d, *J* = 6.4 Hz, 1H), 7.03 (d, *J* = 7.3 Hz, 1H), 6.20 (s, 1H), 5.33 (q, *J* = 6.9 Hz, 1H), 4.41 (dd, *J* = 8.3, 6.5 Hz, 1H), 4.26 (t, *J* = 6.9 Hz, 1H), 3.97 (d, *J* = 3.1 Hz, 1H), 3.49 – 3.30 (m, 2H), 3.08 – 2.96 (m, 2H), 2.42 – 2.00 (m, 3H), 1.94 (s, *J* = 1.5 Hz, 3H), 1.52 (d, *J* = 6.9 Hz, 3H), 1.07 – 0.84 (m, 27H), 0.13 – 0.05 (m, 6H). **4.14B** ^{1}H NMR (300 MHz, $CDCl_3$) δ 7.22 (d, *J* = 8.8 Hz, 1H), 6.95 (d, *J* = 6.3 Hz, 1H), 6.13 (s, 1H), 5.22 (q, *J* = 7.1 Hz, 1H), 4.49 (dd, *J* = 8.8, 6.7 Hz, 1H), 4.39 – 4.34 (m, 1H), 4.06 (d, *J* = 2.8 Hz, 1H), 3.49 – 3.30 (m, 2H), 3.10 – 2.95 (m, 2H), 2.42 – 2.00 (m, 3H), 1.95 (s, *J* = 1.5 Hz, 3H), 1.49 (d, *J* = 7.0 Hz, 3H), 1.07 – 0.85 (m, 27H), 0.13 – 0.06 (m, 6H).

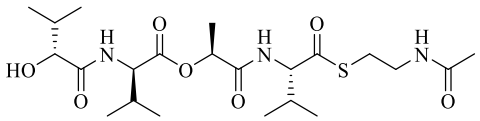

HO-D-HIV-D-Val-L-LAC-L-Val-SNAC, Compound 4.15A

In a 2 mL polypropylene microcentrifuge tube, **4.14** (75 mg, 0.124 mmol, 1.0 equiv.) was dissolved in acetonitrile (1.24 mL). HF (107 μL, 6.21 mmol, 50 equiv.) and pyridine (50 μL, 0.621 mmol, 5 equiv.) were added and the reaction was mixed overnight at ambient temperature. The reaction was quenched with a saturated solution of $NH_4Cl_{(aq)}$ and the mixture was extracted 3 × with EtOAc. The organic fractions were combined, washed with brine and dried over Na_2SO_4. The crude mixture of diastereomers was purified (61 mg, 0.124 mmol, > 99%) with silica column chromatography. The desired diastereomer (23.8 mg) was purified from the mixture using prep-TLC (3.5 % MeOH in CH_2Cl_2) **4.15A.** ^{1}H NMR (300 MHz, $CDCl_3$) δ 7.29 (s, 1H), 6.20 (t, *J* = 5.7 Hz, 1H), 5.26 (q, *J* = 7.0 Hz, 1H), 4.55 (br, 1H), 4.47 (dd, *J* = 9.0, 6.5 Hz, 1H), 4.26 (t, *J* = 7.7 Hz, 1H), 3.99 (d, *J* = 2.9 Hz, 1H), 3.52 – 3.25 (m, 2H), 2.99 (ddt, *J* = 20.4, 13.3, 6.5 Hz, 2H), 2.39 – 2.25 (m, 1H), 2.20 – 2.06 (m, 2H), 1.97 (s, 3H), 1.54 (d, *J* = 7.0 Hz, 3H), 1.06 – 0.93 (m, 15H), 0.88 (d, *J* = 6.9 Hz, 3H). ^{13}C NMR (75 MHz, $CDCl_3$) δ 200.05, 175.25, 171.69, 171.43 (2C), 76.33, 71.14, 64.55, 58.39, 38.95, 31.95, 30.25, 30.12, 28.64, 23.22, 19.49, 19.17, 19.13, 18.83, 18.18, 18.04, 16.15. HRMS (ESI): Exact mass calculated for $C_{22}H_{39}N_3NaO_7S$ $[M + Na]^+$: 512.2401. Found: 512.2406

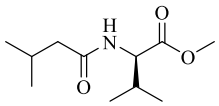

Methyl (*R*)-2-isovalerylamino-3-methylbutyrate, Compound 4.16

In a round-bottom flask, the amine **4.9** (250 mg, 1.5 mmol, 1.0 equiv.) was dissolved in CH_2Cl_2 (15 mL). Isovaleric acid (230 mg, 2.25 mmol, 1.5 equiv.), *N*-(3-dimethylaminopropyl)-N′-ethylcarbodiimide hydrochloride (430 mg, 2.25 mmol, 1.5 equiv.), 4-(dimethylamino)pyridine (276 mg, 2.25 mmol, 1.5 equiv.), and Et_3N (420 μL, 3.00 mmol, 2.0 equiv.) were added and the reaction was allowed to mix at ambient temperature for 16 h. The reaction was quenched with $NH_4Cl_{(aq)}$, extracted 3 × with CH_2Cl_2, washed with $NaHCO_{3(aq)}$, washed with brine, dried over Na_2SO_4, and concentrated. The desired compound (193.7 mg, 0.90 mmol, 60 % yield) was purified with silica column chromatography (20 to 50 % EtOAc in hexanes). ^{1}H NMR (400 MHz, $CDCl_3$) δ 5.96 (d, *J* = 8.0 Hz, 1H), 4.57 (dd, *J* = 8.8, 4.9 Hz, 1H), 3.71 (s, 3H), 2.19 – 2.04 (m, 4H), 0.97 – 0.86 (m, 12H). ^{13}C NMR (100 MHz, $CDCl_3$) δ 172.85, 172.49, 56.91, 52.19, 46.14, 31.35, 26.29, 22.56, 22.53, 19.07, 17.93.

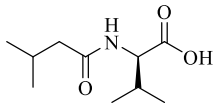

(*R*)-2-Isovalerylamino-3-methylbutyric acid, Compound 4.17

In a round-bottom flask, **4.16** (180 mg, 1.2 mmol, 1.0 equiv.) was dissolved in MeOH (24 mL) and THF (24 mL) and the solution was cooled to 0 °C using an ice bath. LiOH (1 M, 24 mL) was added dropwise and the solution was allowed to proceed from 0 °C to ambient temperature over 4 h. The solution was concentrated to one third volume and the resulting aqueous solution was acidified to pH 3 with 10 % HCl. The solution was extracted 3 × with CH_2Cl_2, dried over Na_2SO_4 and concentrated. The desired product (145 mg, 0.72 mmol, 60 % yield) was purified with silica

column chromatography (5 % MeOH in CH_2Cl_2 + 0.5 % acetic acid). ^{1}H NMR (300 MHz, MeOD) δ 4.32 (d, *J* = 5.8 Hz, 1H), 2.23 – 2.01 (m, 4H), 1.01 – 0.92 (m, 12H). ^{13}C NMR (75 MHz, MeOD) δ 175.84, 174.93, 59.00, 45.90, 31.53, 27.50, 22.76, 22.72, 19.65, 18.41.

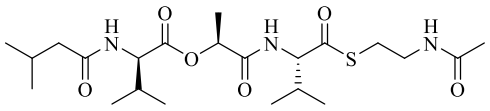

A

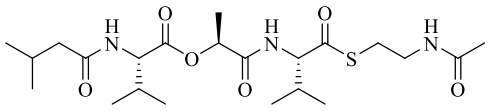

B

(*S*)-2-{(*S*)-1-[(2-Acetylaminoethylthio)carbonyl]-2-methylpropylamino}-1-methyl-2-oxoethyl (*R*)-2-isovalerylamino-3-methylbutyrate, Compounds 4.18A and **(*S*)-2-{(*S*)-1-[(2-Acetylaminoethylthio)carbonyl]-2-methylpropylamino}-1-methyl-2-oxoethyl (*S*)-2-isovalerylamino-3-methylbutyrate, Compound 4.18B**

In a round bottom flask, the alcohol **4.8** (25.2 mg, 0.087 mmol, 1.0 equiv.) and carboxylic acid **4.17** (35 mg, 0.174 mmol, 2.0 equiv.) were dissolved in DMF (1 mL). The solution was cooled to – 20 °C using a dry ice / acetone bath and *N*-(3-dimethylaminopropyl)-N′-ethylcarbodiimide hydrochloride (67 mg, 0.35 mmol, 4.0 equiv.) and 4-(dimethylamino)pyridine (21 mg, 0.174 mmol, 2.0 equiv.) were added. The mixture was allowed to warm to ambient temperature and the reaction proceeded for 16 h. The reaction was quenched with $NH_4Cl_{(aq)}$ and extracted 3 × with EtOAc. The organic fractions were combined, washed with brine, dried over Na_2SO_4 and concentrated. A mixture of diastereomers (37.9 mg, 0.08 mmol, 92 % yield) in a 5:4 ratio (**4.18A** : **4.18B**) was purified from the crude residue by silica column chromatography (1 % to 5 % MeOH in CH_2Cl_2). The diastereomers were separated with prep-TLC. **4.18A** ^{1}H NMR (400 MHz, $CDCl_3$) δ 7.21 (d, *J* = 8.2 Hz, 1H), 6.15 (s, 1H), 5.93 (d, *J* = 6.8 Hz, 1H), 5.35 (q, *J* = 7.0 Hz, 1H), 4.44

(dd, *J* = 8.3, 6.4 Hz, 1H), 4.29 (t, *J* = 7.0 Hz, 1H), 3.50 – 3.32 (m, 2H), 3.08 – 2.95 (m, 2H), 2.41 – 2.29 (m, 1H), 2.19 – 2.00 (m, 4H), 1.96 (s, 3H), 1.53 (d, *J* = 6.9 Hz, 3H), 1.05 – 0.92 (m, 18H). ^{13}C NMR (100 MHz, $CDCl_3$) δ 200.14, 173.48, 171.62, 171.04, 170.65, 71.03, 64.93, 58.71, 45.66, 39.33, 30.37, 30.35, 28.75, 26.31, 23.27, 22.63, 22.57, 19.48, 19.07, 18.79, 18.11, 17.91. **4.18B** ^{1}H NMR (400 MHz, $CDCl_3$) δ 6.95 (d, *J* = 8.7 Hz, 1H), 6.04 (s, 1H), 5.81 (d, *J* = 7.2 Hz, 1H), 5.25 (q, *J* = 6.8 Hz, 1H), 4.54 (dd, *J* = 8.8, 5.9 Hz, 1H), 4.49 (dd, *J* = 7.3, 4.7 Hz, 1H), 3.47 – 3.36 (m, 2H), 3.11 – 2.98 (m, 2H), 2.38 – 2.26 (m, 2H), 2.20 – 2.09 (m, 3H), 1.95 (s, 3H), 1.51 (d, *J* = 6.9 Hz, 3H), 1.04 (d, *J* = 6.9 Hz, 3H), 0.99 (dd, *J* = 6.7, 2.5 Hz, 12H), 0.94 (d, *J* = 6.8 Hz, 3H). ^{13}C NMR (100 MHz, $CDCl_3$) δ 199.74, 173.66, 170.84, 170.68, 170.49, 71.63, 64.29, 57.90, 46.06, 39.32, 30.72, 30.55, 28.91, 26.35, 23.30, 22.64, 22.57, 19.42 (2C), 18.16, 17.94, 17.70. HRMS (ESI): Exact mass calculated for $C_{22}H_{39}N_3NaO_6S$ $[M + Na]^+$: 496.2452. Found: 496.2457

4.5 References

(1) Schwarzer, D.; Finking, R.; Marahiel, M. A. *Nat. Prod. Rep.* **2003**, *20*, 275–287.

(2) Felnagle, E. A.; Jackson, E. E.; Chan, Y. A.; Podevels, A. M.; Berti, D.; Mcmahon, M. D.; Thomas, M. G. *Mol. Pharm.* **2011**, *5*, 191–211.

(3) Dewick, P. M. *Medicinal Natural Products: A Biosynthetic Approach*; 3rd ed.; Wiley, 2009.

(4) Ballard, C.E.; Yu, H.; Wang, B. *Curr. Med. Chem.* **2002**, *9*, 471–498.

(5) Kroteń, M. A.; Bartoszewicz, M.; Swiecicka, I. *Polish J. Microbiol.* **2010**, *59*, 3–10.

(6) Rose, M. C.; Henkens, R. W. *Biochim. Biophys. Acta - Gen. Subj.* **1974**, *372*, 426–435.

(7) Tempelaars, M. H.; Rodrigues, S.; Abee, T. *Appl. Environ. Microbiol.* **2011**, *77*, 2755–2762.

(8) Magarvey, N. A.; Ehling-Schulz, M.; Walsh, C. T. *J. Am. Chem. Soc.* **2006**, *128*, 10698–10699.

(9) Marxen, S.; Stark, T. D.; Rütschle, A.; Lücking, G.; Frenzel, E.; Scherer, S.; Ehling-Schulz, M.; Hofmann, T. *Sci. Rep.* **2015**, *5*, 10637.

(10) Li, J.; Jaitzig, J.; Theuer, L.; Legala, O. E.; Sussmuth, R. D.; Neubauer, P. *J. Biotechnol.* **2015**, *193*, 16–22.

(11) Mootz, H. D.; Schwarzer, D.; Marahiel, M. A. *ChemBioChem* **2002**, *3*, 490–504.

(12) Gehring, A. M.; Mori, I.; Walsh, C. T. *Biochemistry* **1998**, *37*, 2648–2659.

(13) Hoyer, K. M.; Mahlert, C.; Marahiel, M. A. *Chem. Biol.* **2007**, *14*, 13–22.

(14) Mayer, S. C.; Ramanjulu, J.; Vera, M. D.; Pfizenmayer, A. J.; Joullie, M. M. *J. Org. Chem.* **1994**, *59*, 5192–5205.

(15) Campbell, C. D.; Concellón, C.; Smith, A. D. *Tetrahedron: Asymmetry* **2011**, *22*, 797–811.

Chapter 5: Future perspective

Together, the three chapters in this thesis illustrate the variety of studies that can be launched based upon the reactivity of electrophilic molecules with proteins. In chapter two, electrophilic compounds were used as therapeutic agents to enhance oncolytic viral therapy, likely through the inhibition of host anti-viral mechanisms. Optimization of the compounds was completed in part by characterizing and modulating the electrophilic nature of the molecules. This was shown to lead to a reduction in toxicity and a more controlled electrophilic reaction. Given the success of *in vitro* and *in vivo* studies of activity and toxicity of these compounds, this work highlights a new strategy for researchers interested in virotherapy to enhance efficacy. Moving forward, the electrophilic nature of these compounds will be exploited to identify the biological target(s) which will be used to provide insight into the mechanism of action. The reduced electrophilicity and enhanced stability of the optimized compounds identified should be more selective for the relevant biological target(s). Additionally, this work provides detailed structure-activity relationships that hint at appropriate sites of reactive-group or biotin incorporation which will allow for these studies.

In chapter three, structure-activity relationships were defined for armeniaspiroles, a relatively unexplored class of natural products. The toleration for structure disruption was very low for two of fragments of the molecule, a fragment that is likely directly involved in covalently modifying the target, and an aryl alcohol fragment which more likely interacts with the target in a non-covalent fashion. This information has allowed for the synthesis of an active activity-based probe. Next steps will be to identify proteins that specifically interact with the probe, which was shown to extensively label the bacteria proteome. The structure-activity data suggests that it is possible that a comparative ABPP study using an inactive probe with a disrupted aryl alcohol, will

allow for the identification of specifically inhibited proteins. The chemical tools developed throughout this project provides for a very interesting opportunity to identify a novel antibacterial mechanism of action. Toward this end, affinity-capture studies using a biotin-labelled reporter molecule are being completed.

Using mass spectrometry, a mechanism for oligomerization was proposed for valinomycin thioesterase in chapter four. This research was enabled by the design and use of covalently loading substrates to react with the purified enzyme *in vitro*. Future efforts will be toward the synthesis and evaluation of a non-hydrolyzable, reversibly modifying substrate. This should enable further characterization of the enzyme using X-ray crystallography. This approach will allow for the uncovering of the structural and functional details that allow VlmTE to catalyze both the oligomerization and macrocyclization. This information can be extended to other NRPS systems that produce similar natural products.

Appendix

Chapter 2 spectra and VEU titers

2.1

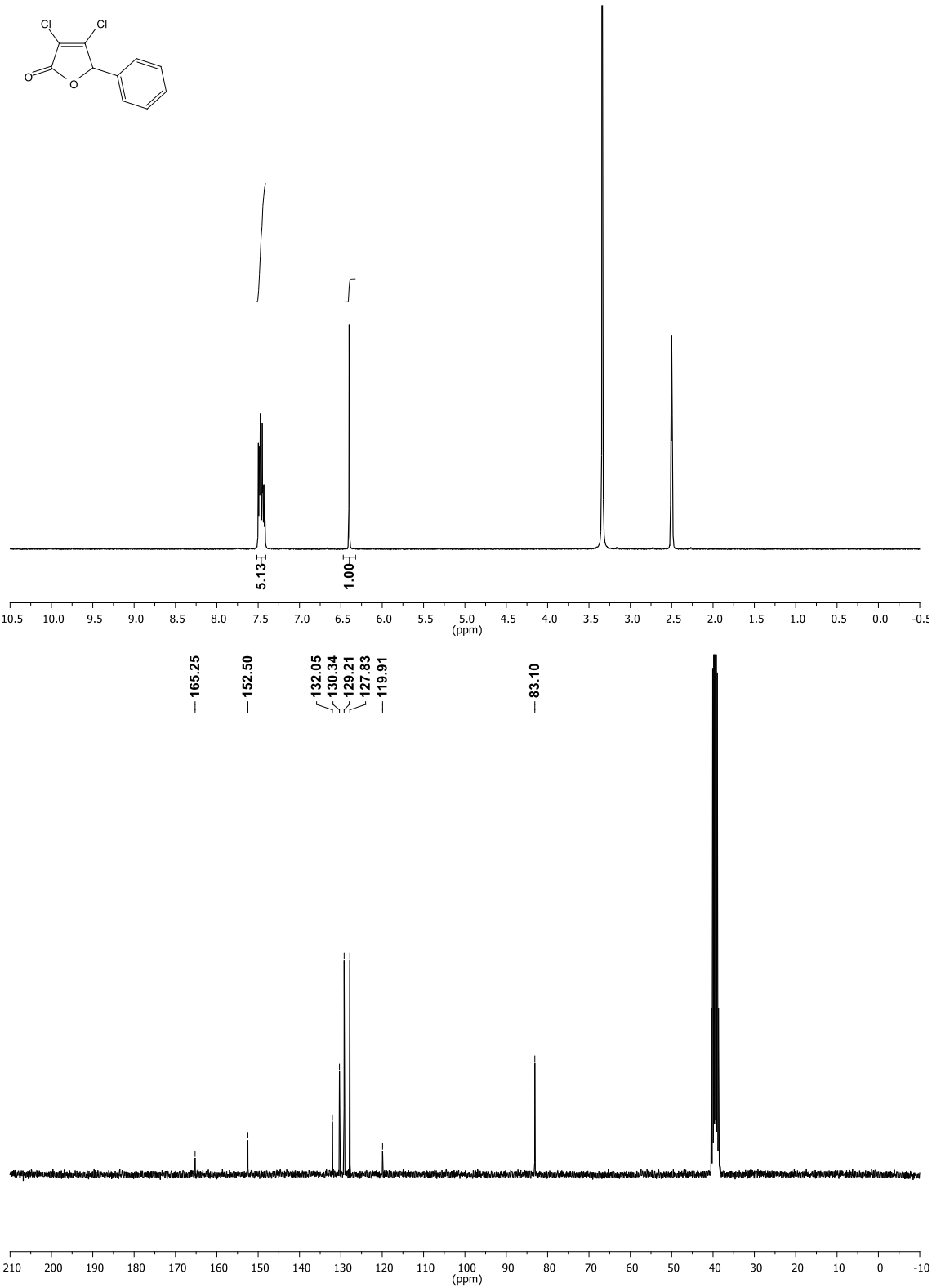
Cl
Cl
O
O
5.13
1.00
(ppm)
165.25
152.50
132.05
130.34
129.21
127.83
119.91
83.10
(ppm)

2.1

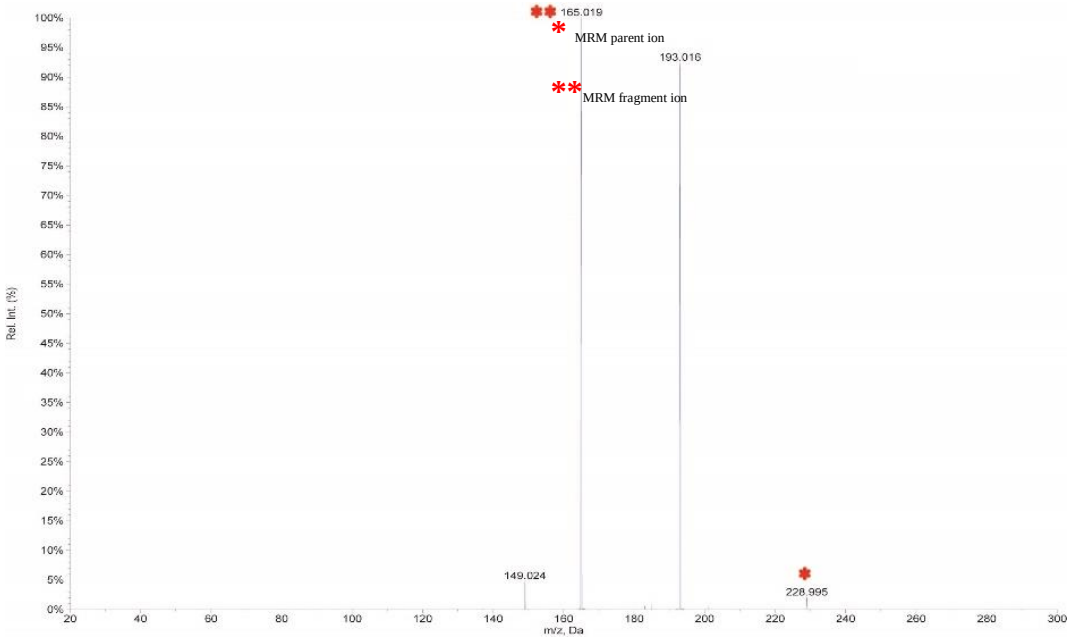
165.019
MRM parent ion
193.016
MRM fragment ion
149.024
228.995
Rel. Int. (%)
m/z, Da

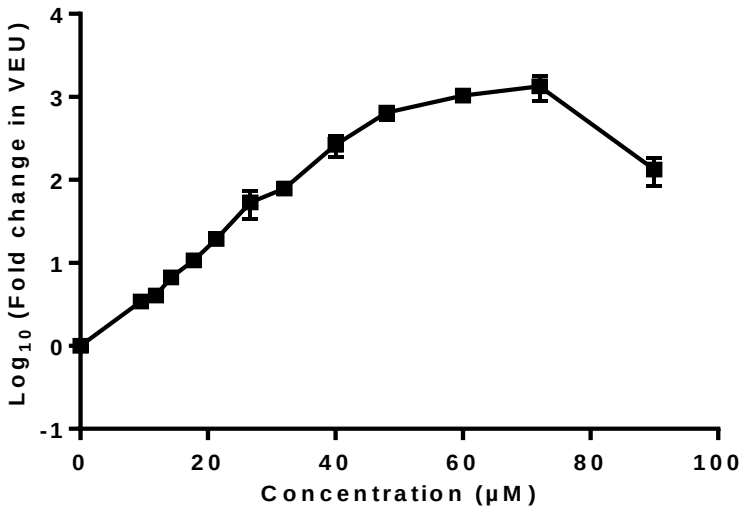
Log10 (Fold change in VEU)
Concentration (µM)

2.2

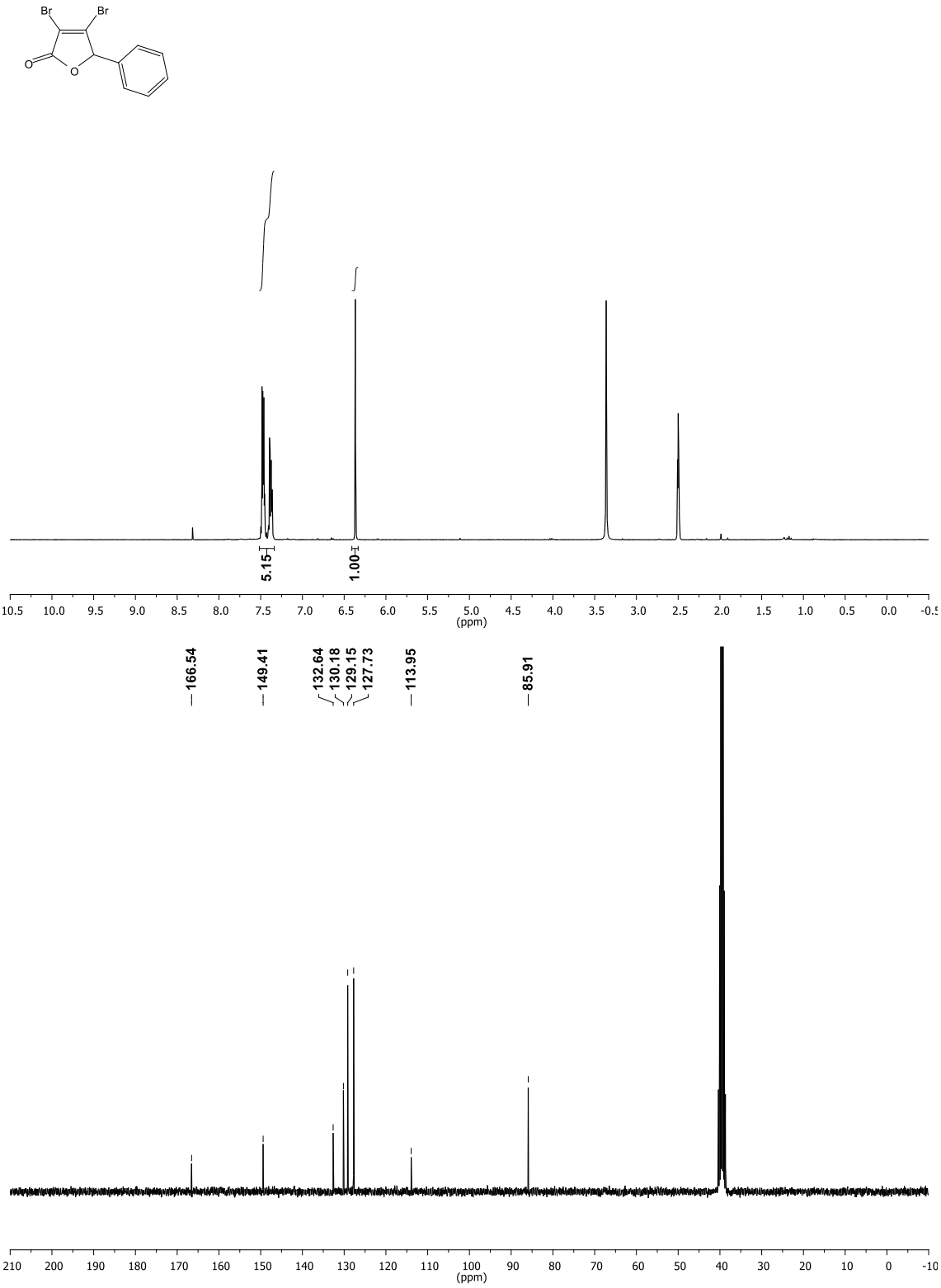
Br
Br
O
O
5.15
1.00
(ppm)
166.54
149.41
132.64
130.18
129.15
127.73
113.95
85.91
(ppm)

2.2

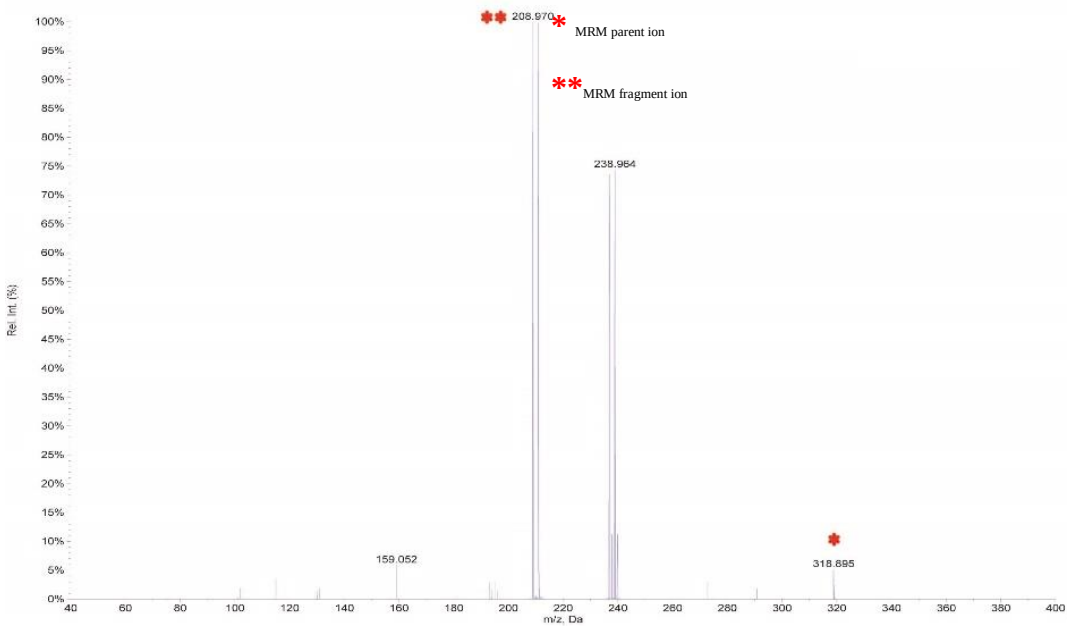
208.970
MRM parent ion
MRM fragment ion
238.954
159.052
318.895
Rel. Int. (%)
m/z, Da

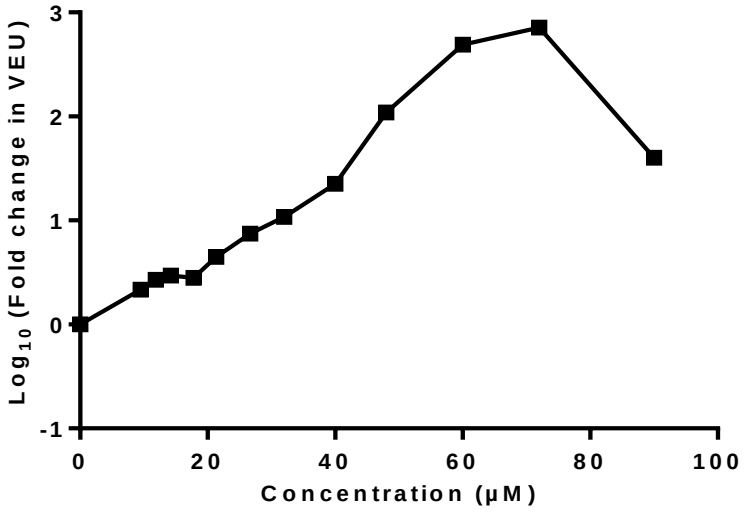
Log10 (Fold change in VEU)
Concentration (μM)

2.3

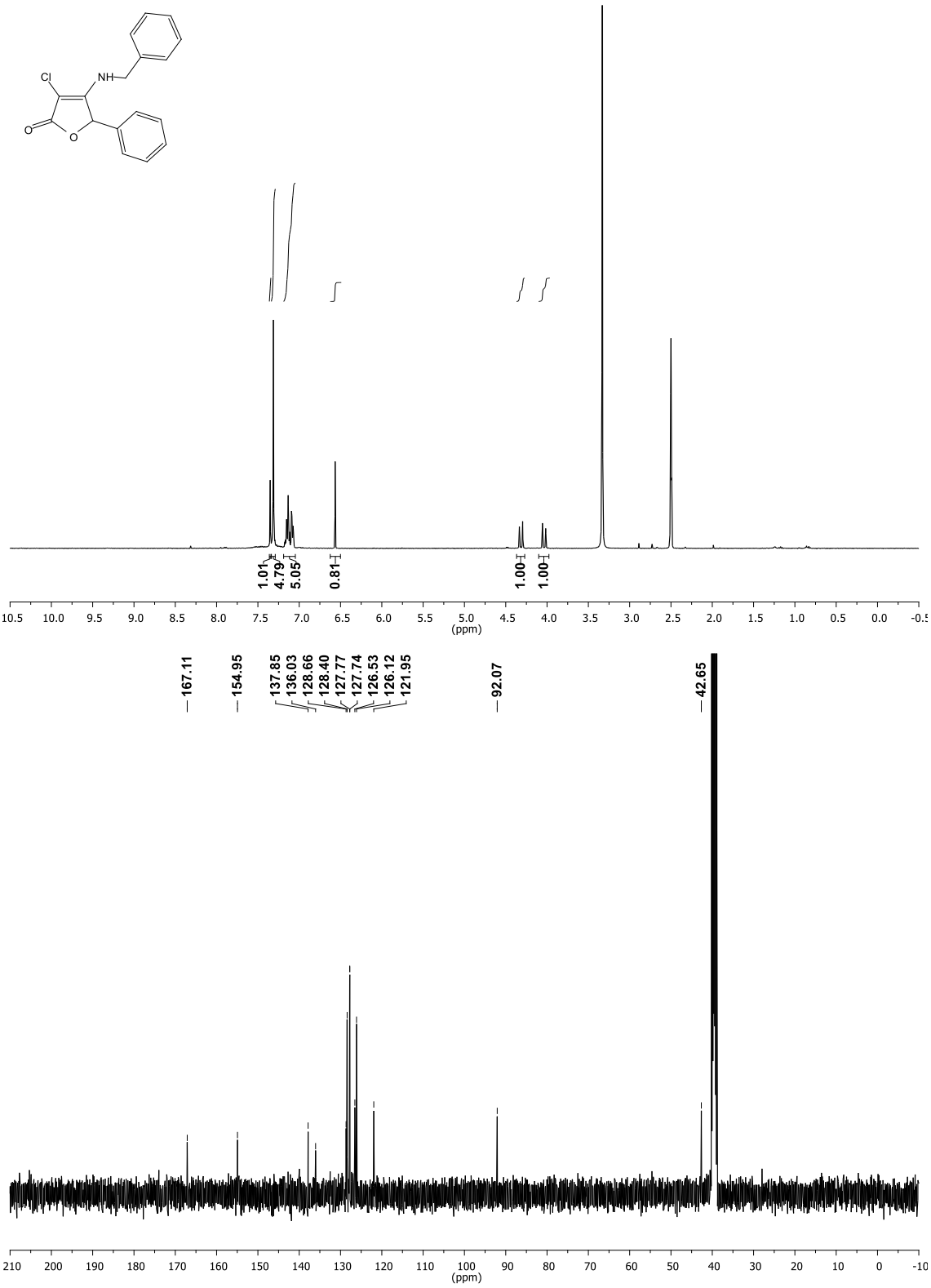
Cl
NH
O
O
1.01
4.79
5.05
0.81
1.00
1.00
(ppm)
167.11
154.95
137.85
136.03
128.66
128.40
127.77
127.74
126.53
126.12
121.95
92.07
42.65
(ppm)

2.3

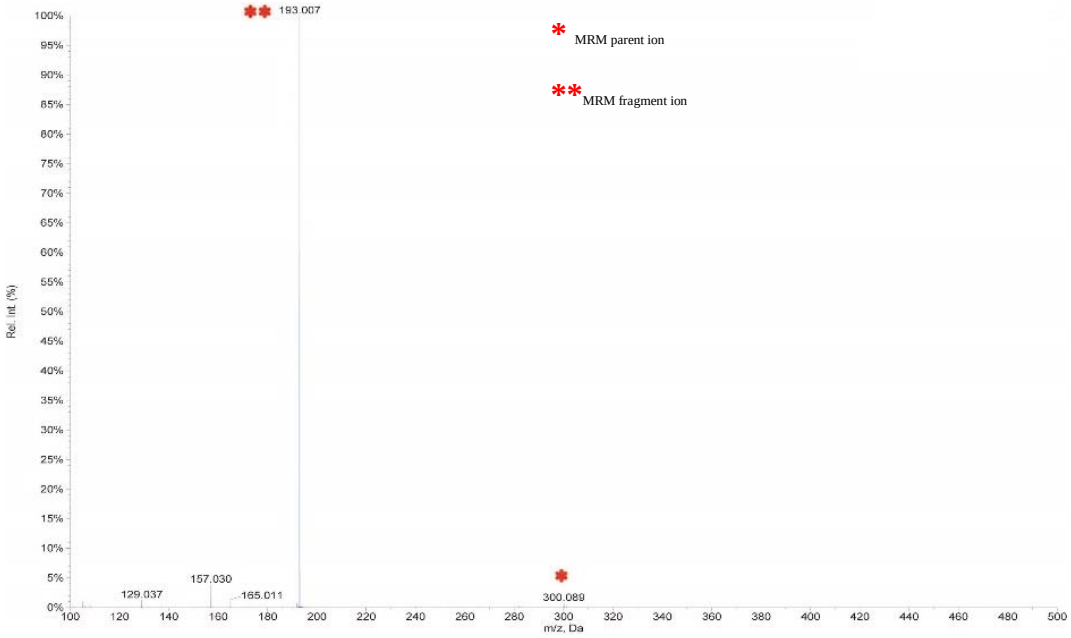
193.007
* MRM parent ion
** MRM fragment ion
Rel. int. (%)
100%
95%
90%
85%
80%
75%
70%
65%
60%
55%
50%
45%
40%
35%
30%
25%
20%
15%
10%
5%
0%
129.037
157.030
165.011
300.089
100
120
140
160
180
200
220
240
260
280
300
320
340
360
380
400
420
440
460
480
500
m/z, Da

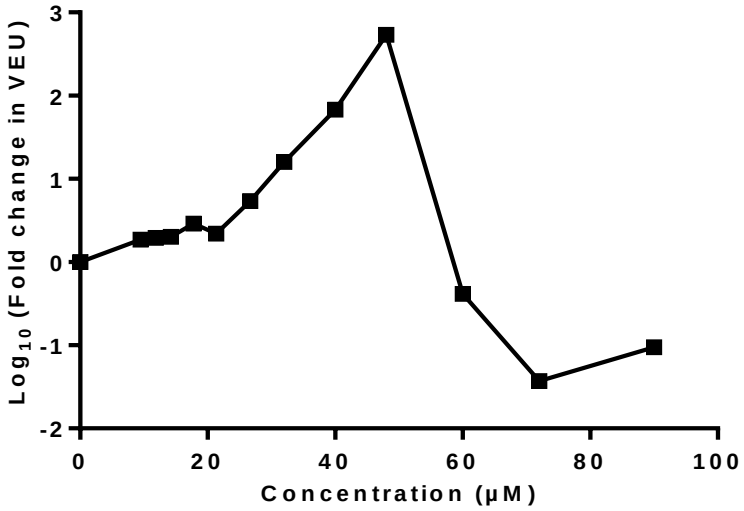
Log10 (Fold change in VEU)
3
2
1
0
-1
-2
0
20
40
60
80
100
Concentration (µM)

2.4

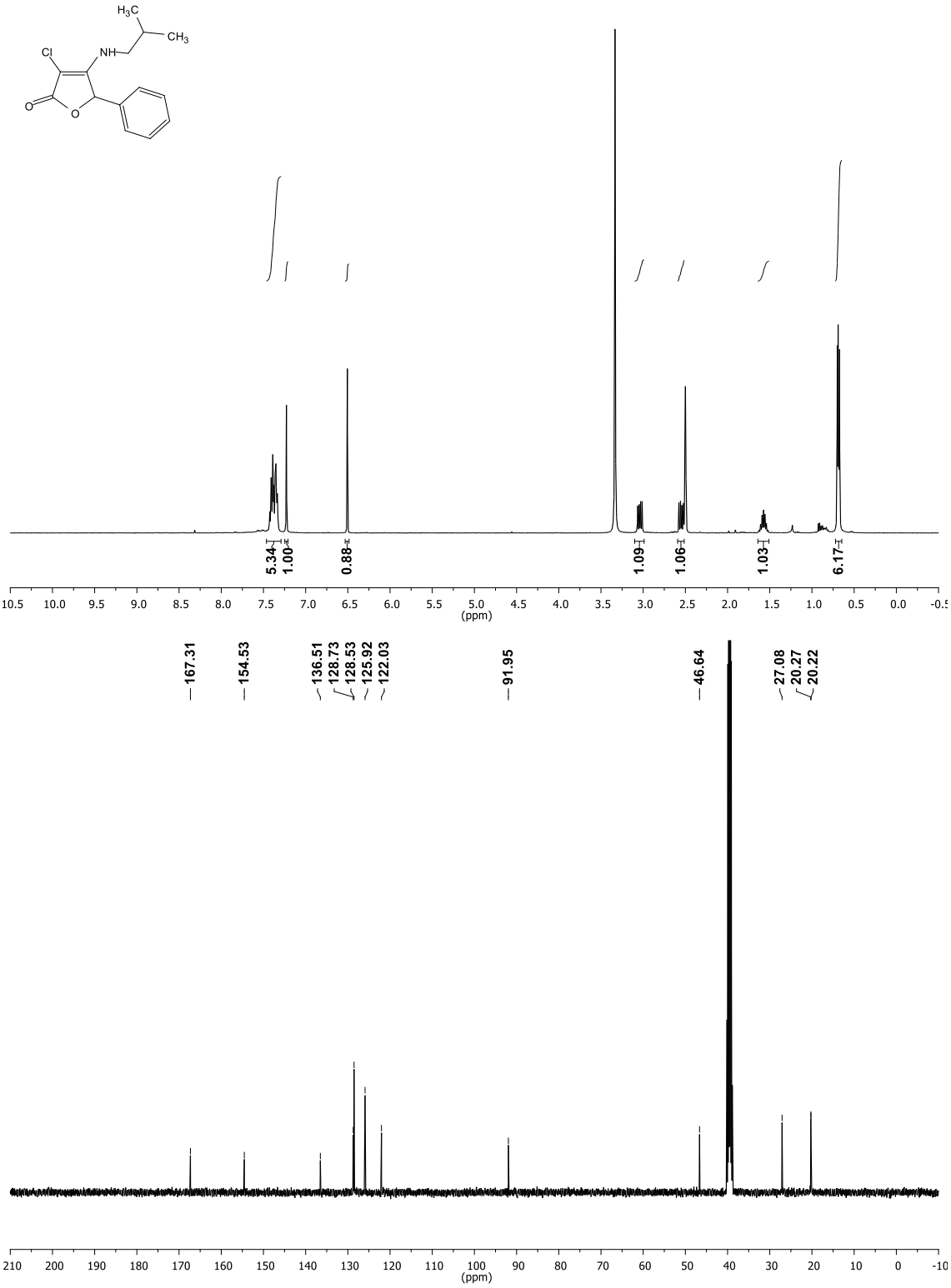
H3C
CH3
NH
Cl
O
O
5.34
1.00
0.88
1.09
1.06
1.03
6.17
(ppm)
167.31
154.53
136.51
128.73
128.53
125.92
122.03
91.95
46.64
27.08
20.27
20.22
(ppm)

2.4

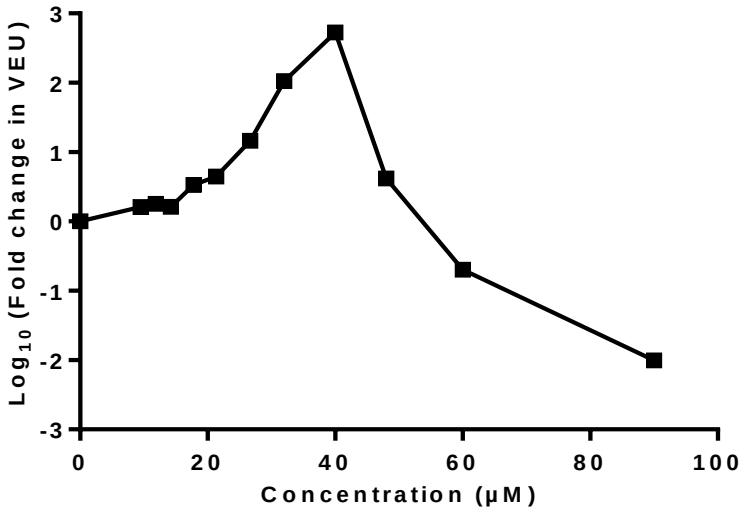
Log10 (Fold change in VEU)
3
2
1
0
-1
-2
-3
0
20
40
60
80
100
Concentration (μM)

2.5

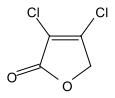
Cl
Cl
O
O

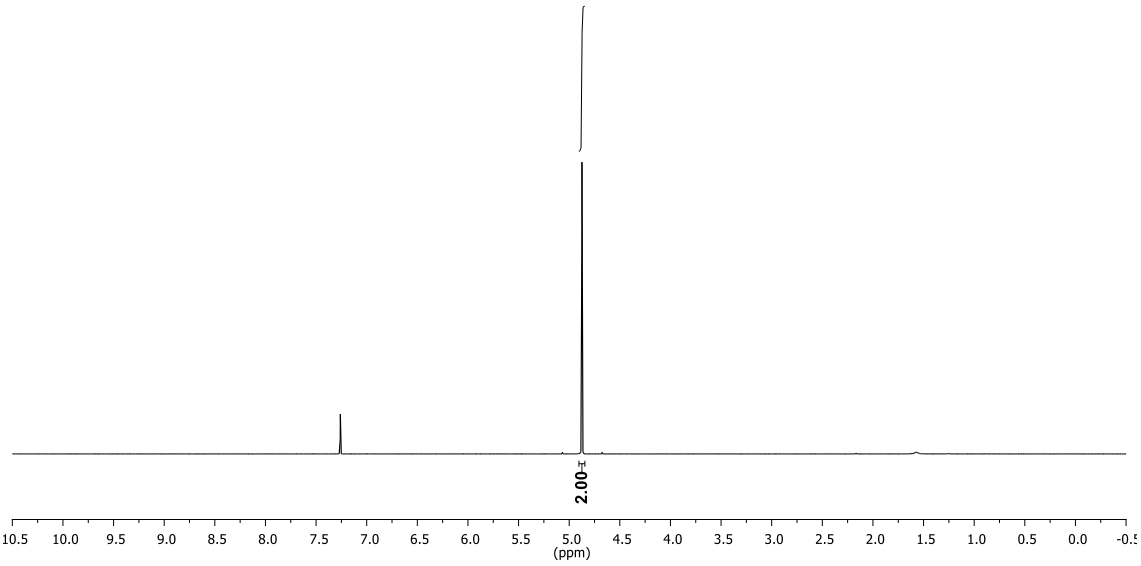
2.00
10.5 10.0 9.5 9.0 8.5 8.0 7.5 7.0 6.5 6.0 5.5 5.0 4.5 4.0 3.5 3.0 2.5 2.0 1.5 1.0 0.5 0.0
(ppm)

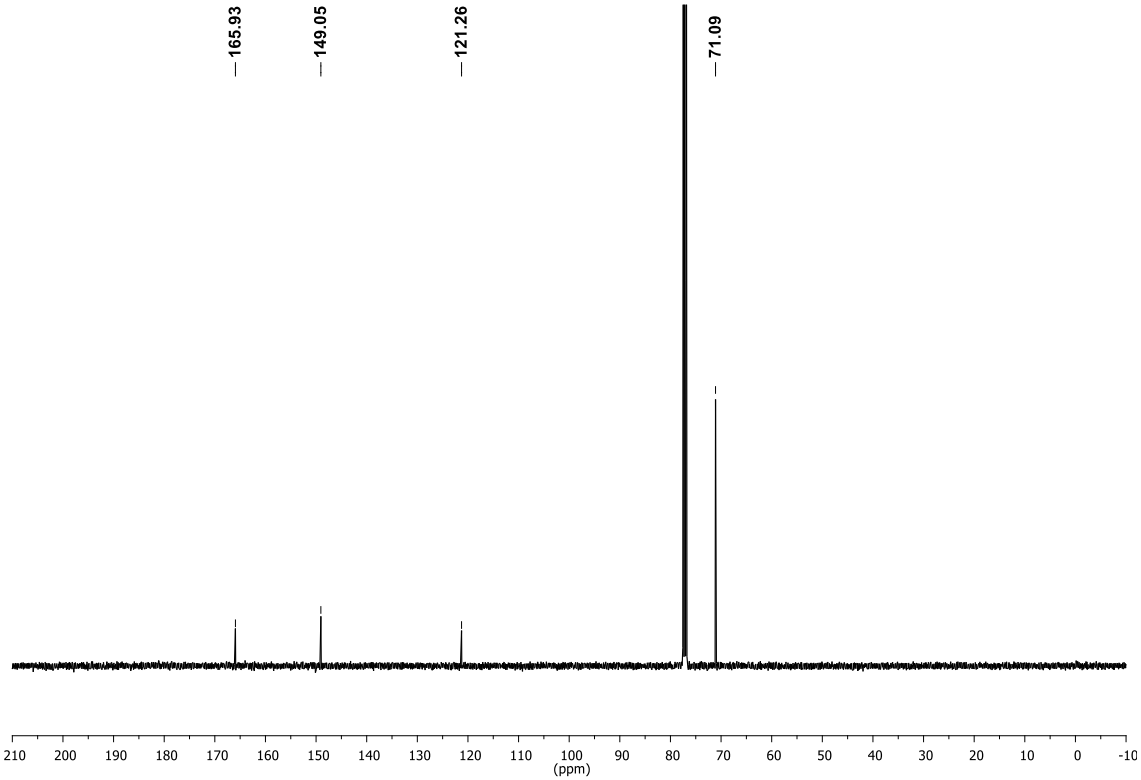
165.93
149.05
121.26
71.09
210 200 190 180 170 160 150 140 130 120 110 100 90 80 70 60 50 40 30 20 10 0
(ppm)

2.5

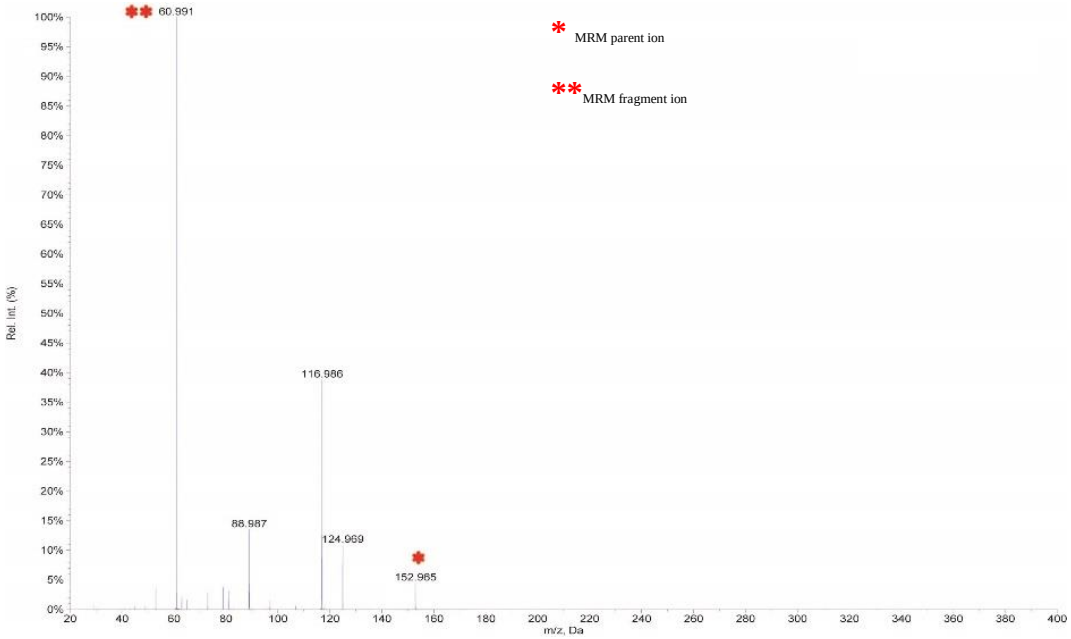
60.991
MRM parent ion
MRM fragment ion
116.986
88.987
124.969
152.985
Rel. int. (%)
m/z, Da

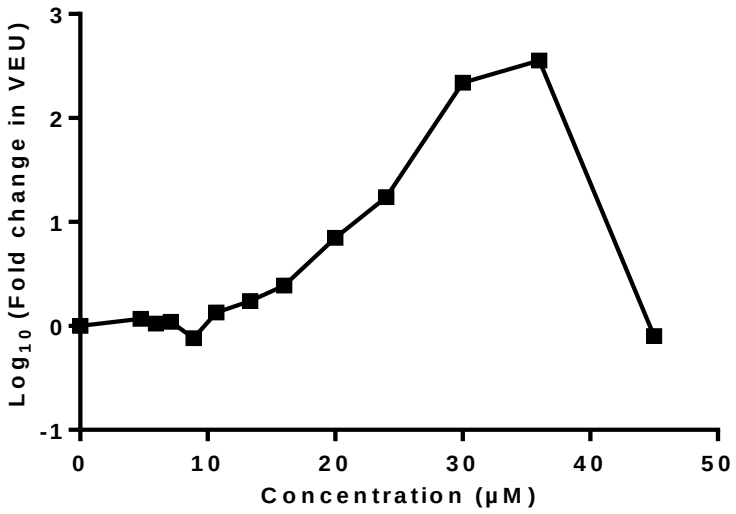
Log10 (Fold change in VEU)
Concentration (µM)

2.6

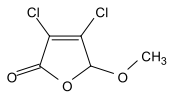
Cl
Cl
O
O
O
CH3

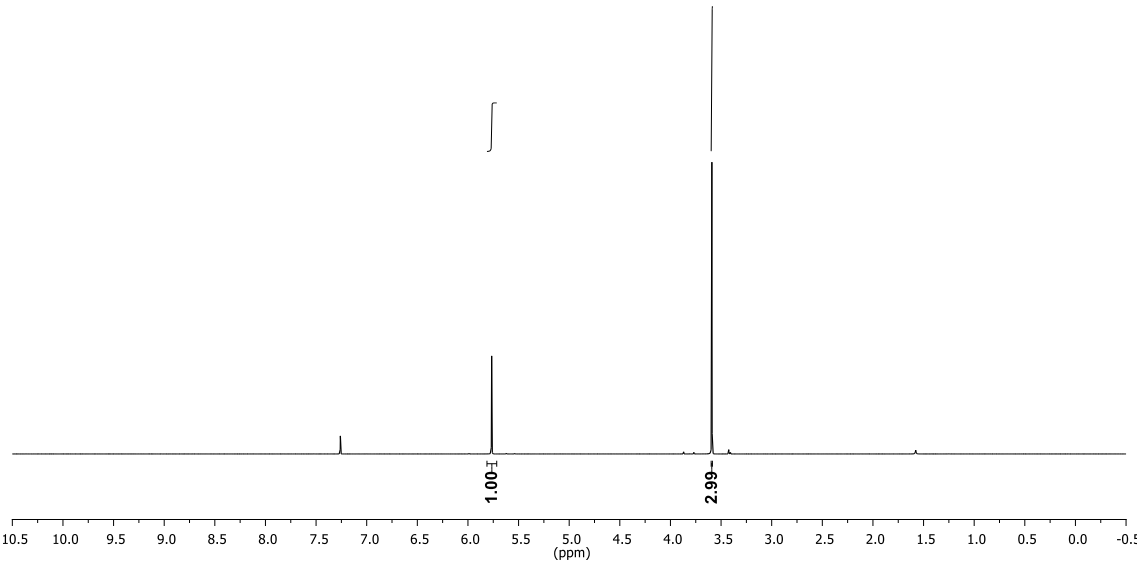
1.00
2.99
10.5 10.0 9.5 9.0 8.5 8.0 7.5 7.0 6.5 6.0 5.5 5.0 4.5 4.0 3.5 3.0 2.5 2.0 1.5 1.0 0.5 0.0
(ppm)

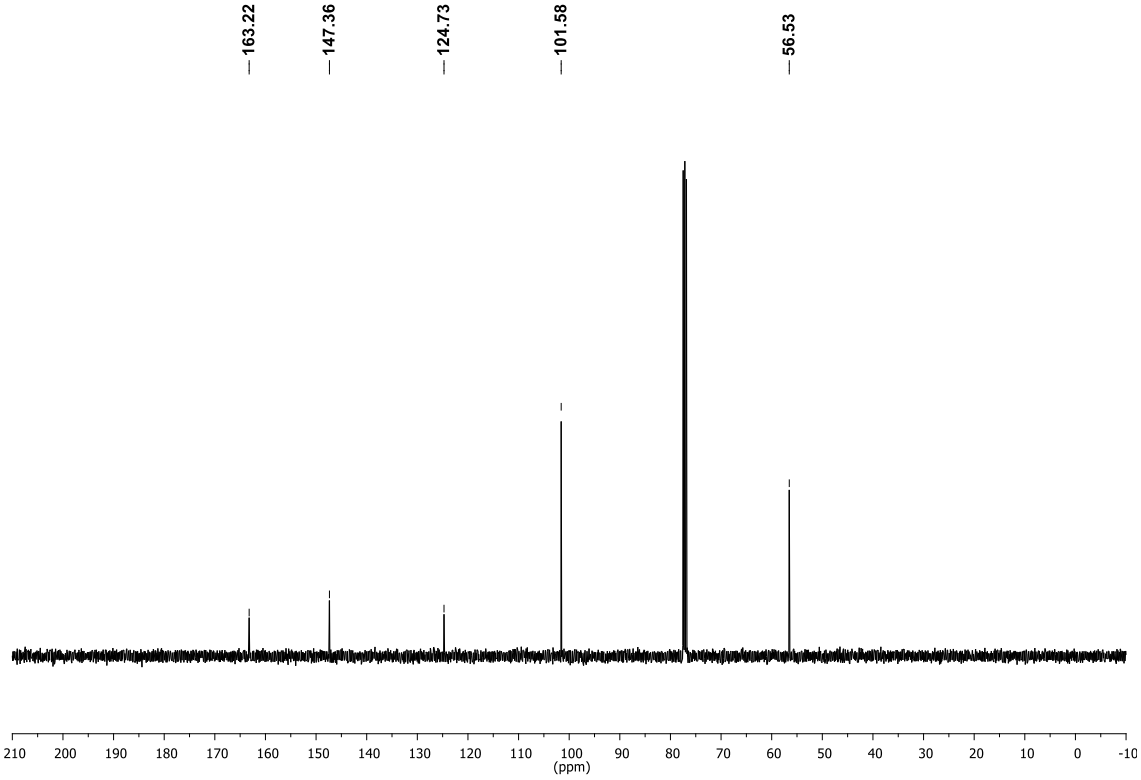
163.22
147.36
124.73
101.58
56.53
210 200 190 180 170 160 150 140 130 120 110 100 90 80 70 60 50 40 30 20 10 0
(ppm)

2.6

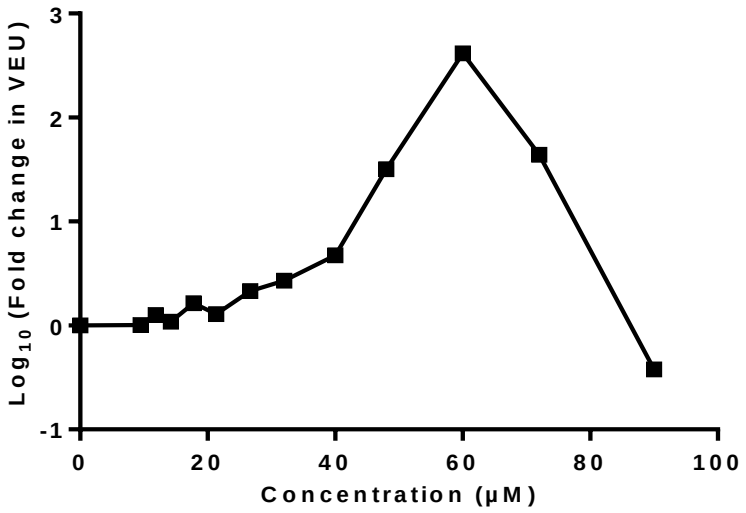
3
2
1
0
-1
Log10 (Fold change in VEU)
0
20
40
60
80
100
Concentration (µM)

2.7

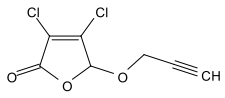
Cl
Cl
O
O
O
CH

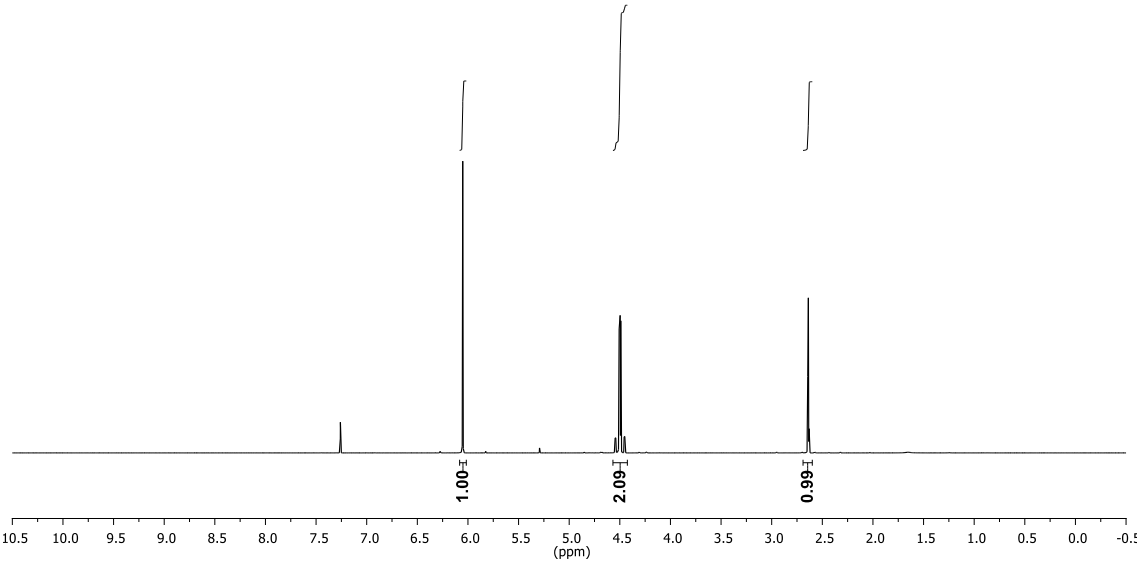
1.00
2.09
0.99
10.5 10.0 9.5 9.0 8.5 8.0 7.5 7.0 6.5 6.0 5.5 5.0 4.5 4.0 3.5 3.0 2.5 2.0 1.5 1.0 0.5 0.0
(ppm)

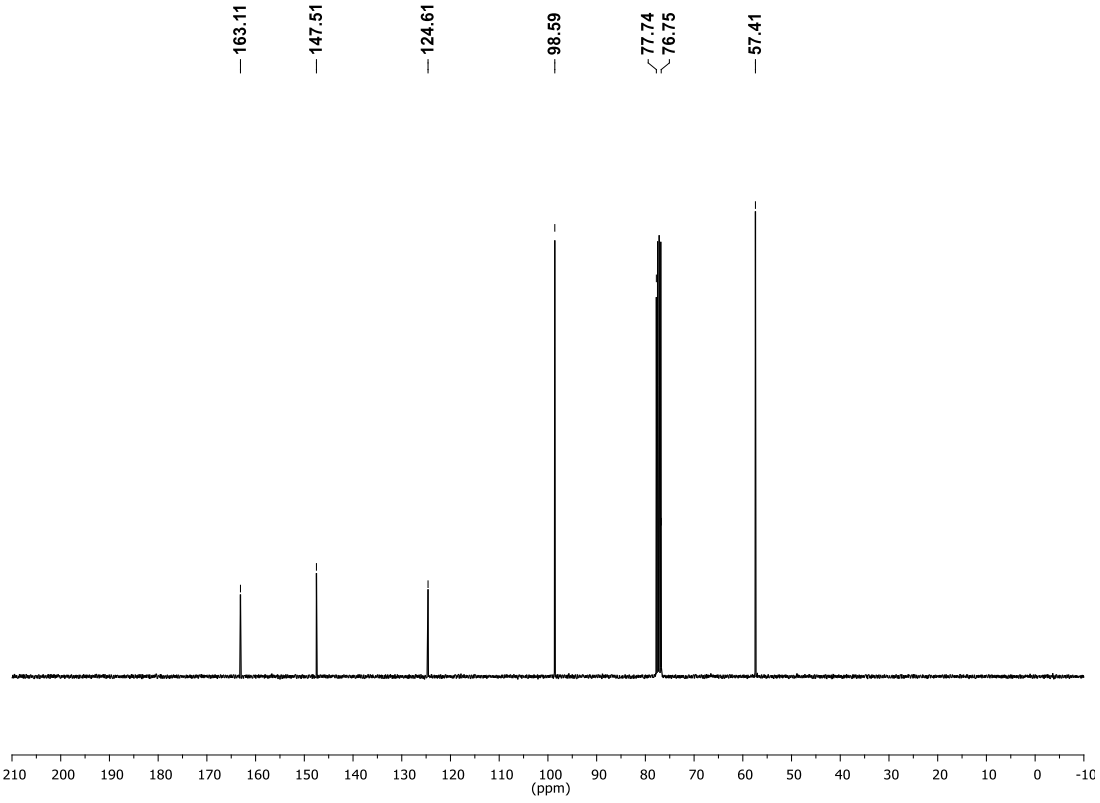
163.11
147.51
124.61
98.59
77.74
76.75
57.41
210 200 190 180 170 160 150 140 130 120 110 100 90 80 70 60 50 40 30 20 10 0
(ppm)

2.7

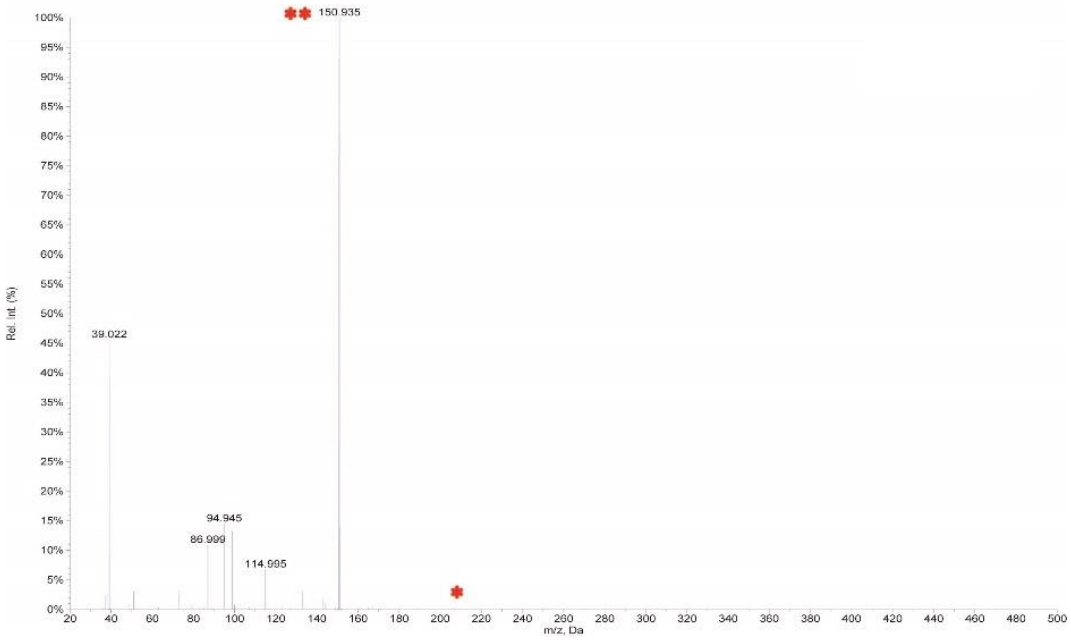
150.935
39.022
94.945
86.999
114.995
Rel. Int. (%)
m/z, Da

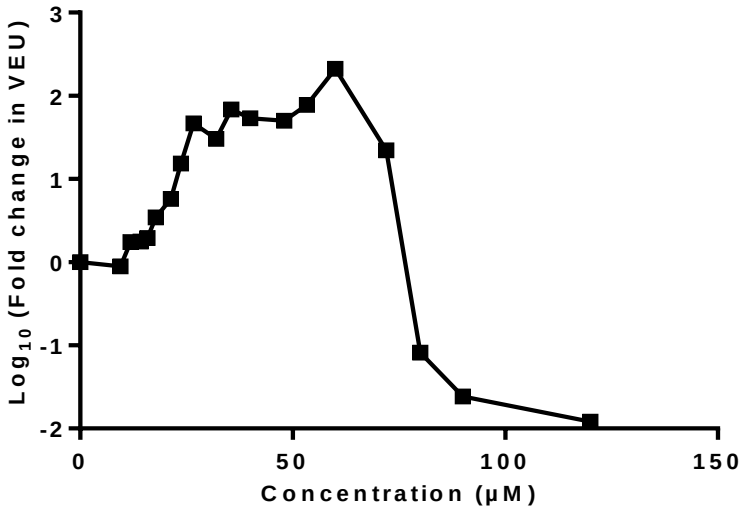
Log10 (Fold change in VEU)
Concentration (μM)

2.8

Compound purchased from a commercial supplier.

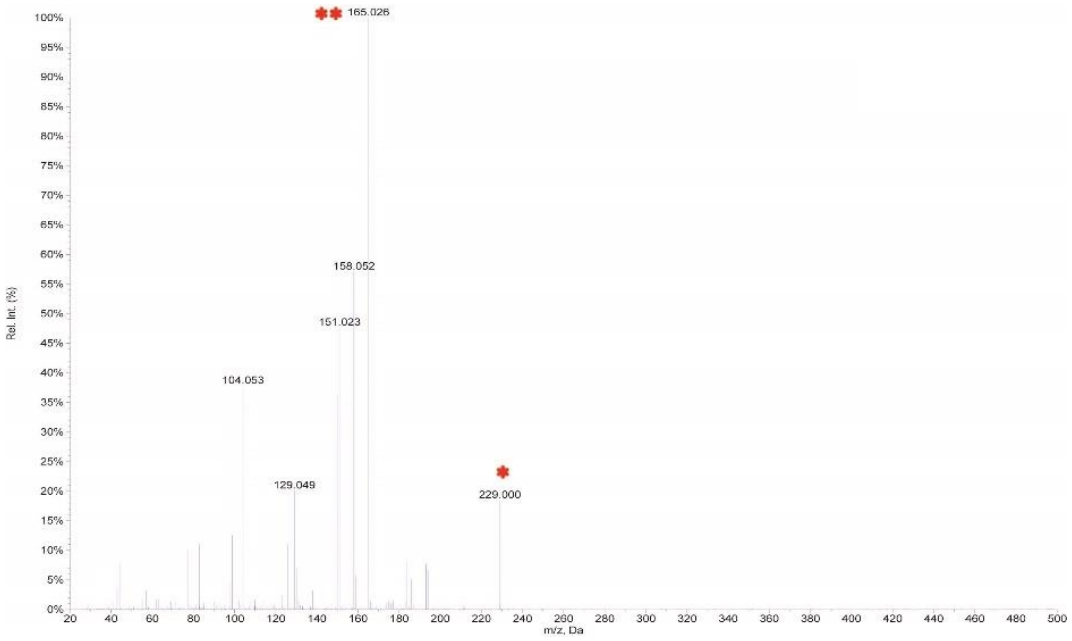

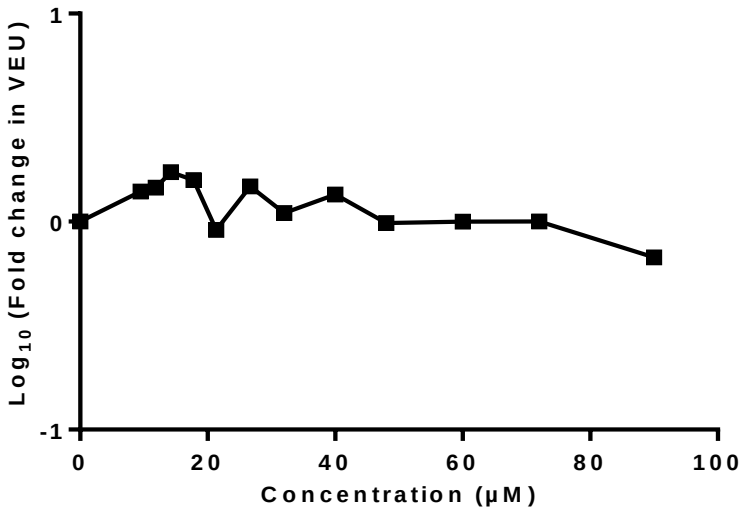

2.9

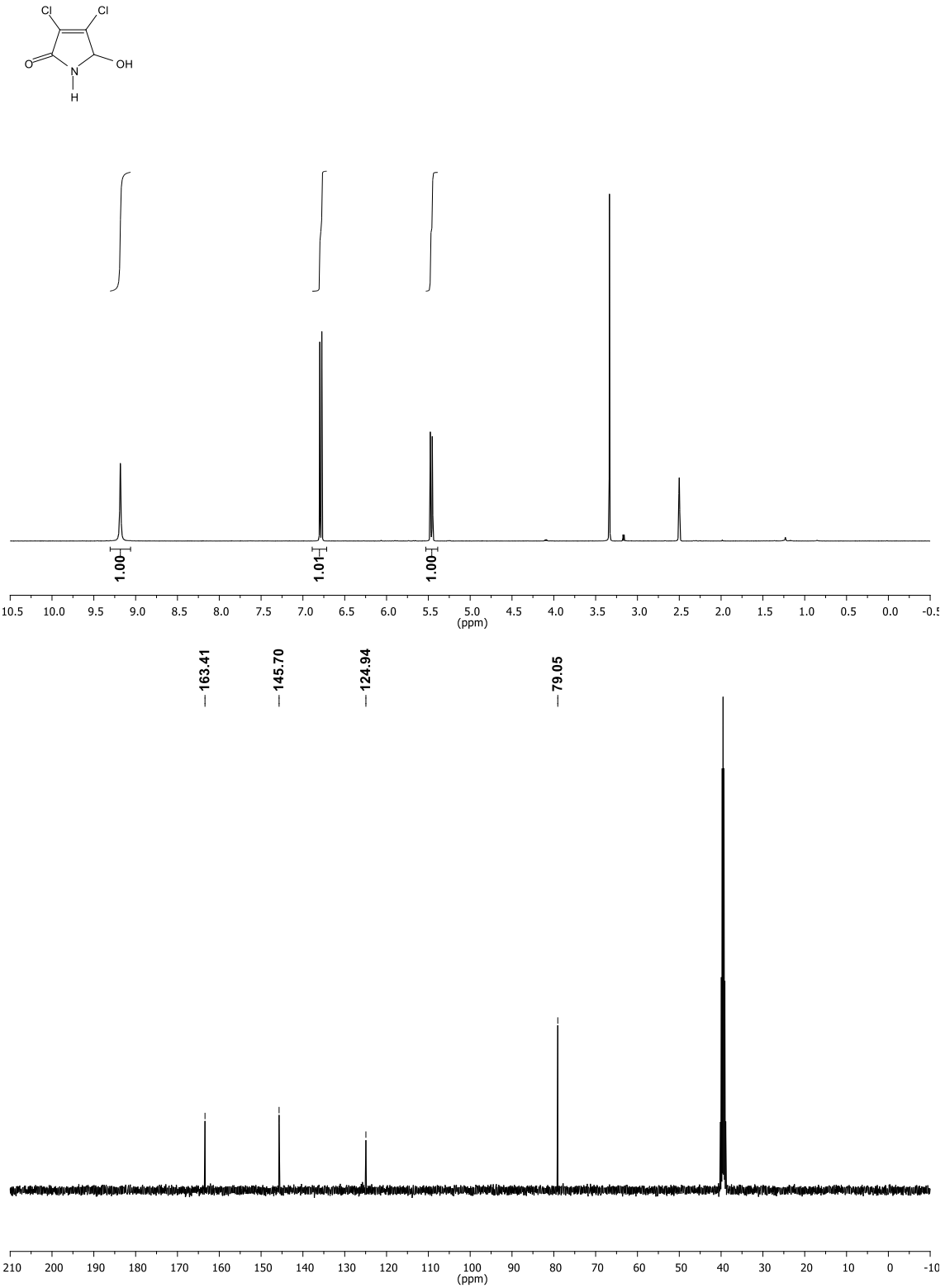
Cl
Cl
O
N
H
OH
1.00
1.01
1.00
10.5 10.0 9.5 9.0 8.5 8.0 7.5 7.0 6.5 6.0 5.5 5.0 4.5 4.0 3.5 3.0 2.5 2.0 1.5 1.0 0.5 0.0
(ppm)
163.41
145.70
124.94
79.05
210 200 190 180 170 160 150 140 130 120 110 100 90 80 70 60 50 40 30 20 10 0
(ppm)

2.9

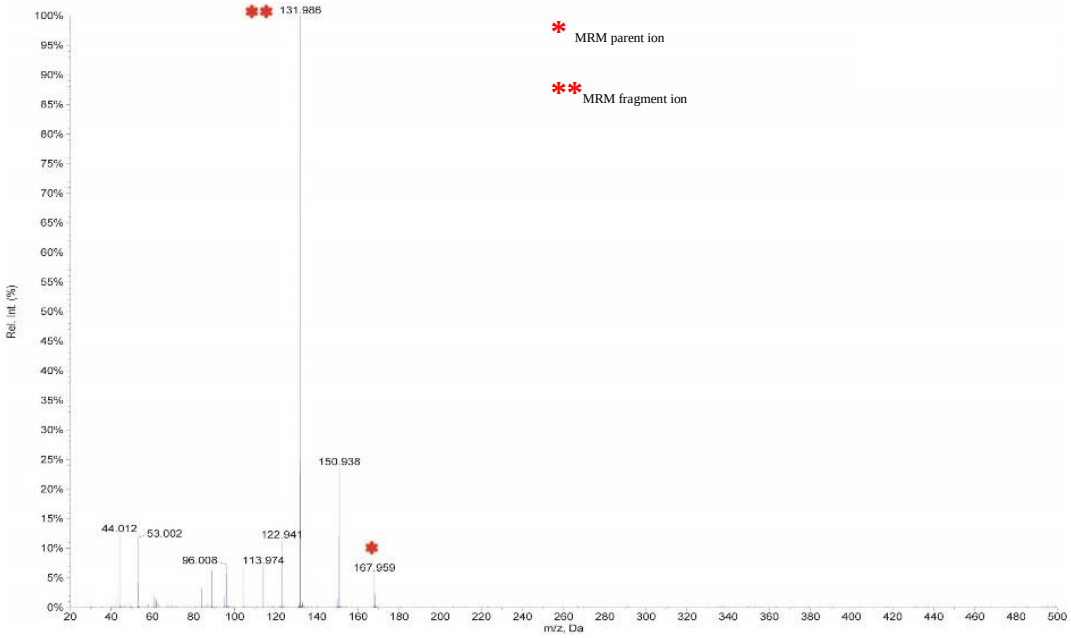
131.986
* MRM parent ion
** MRM fragment ion
150.938
44.012
53.002
122.941
96.008
113.974
167.959
Rel. int. (%)
m/z, Da

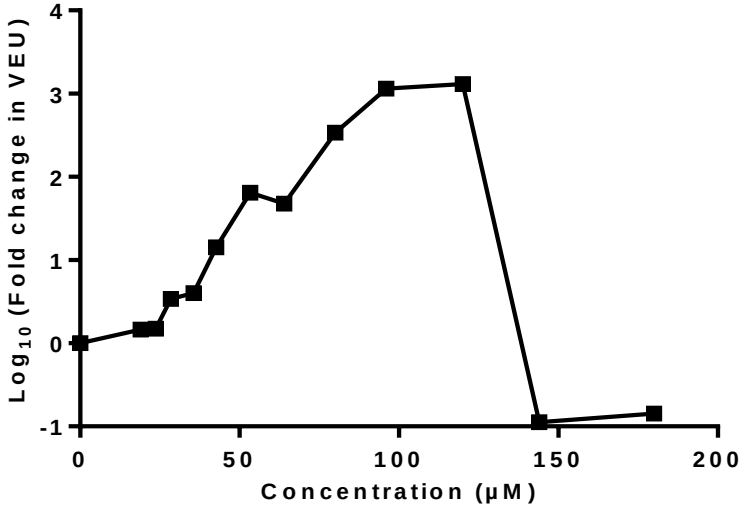
Log10 (Fold change in VEU)
Concentration (µM)

2.10

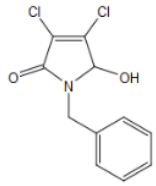
Cl
Cl
O
N
OH

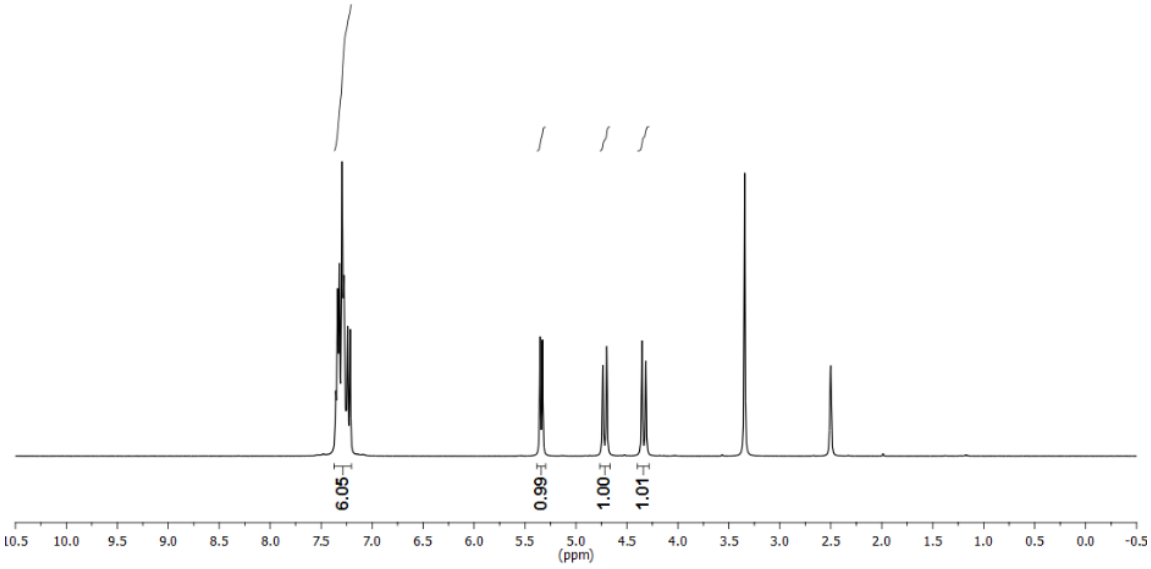
6.05
0.99
1.00
1.01
10.5 10.0 9.5 9.0 8.5 8.0 7.5 7.0 6.5 6.0 5.5 5.0 4.5 4.0 3.5 3.0 2.5 2.0 1.5 1.0 0.5 0.0 -0.5
(ppm)

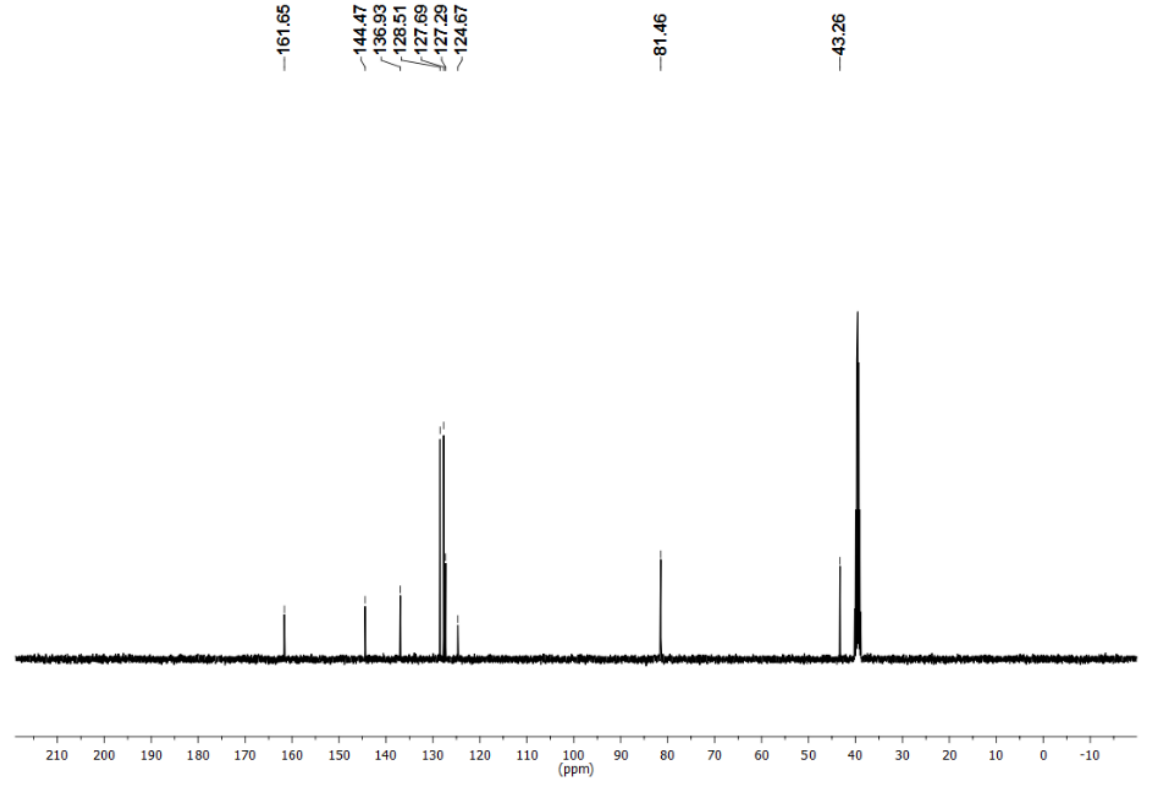
161.65
144.47
136.93
128.51
127.69
127.29
124.67
81.46
43.26
210 200 190 180 170 160 150 140 130 120 110 100 90 80 70 60 50 40 30 20 10 0 -10
(ppm)

2.10

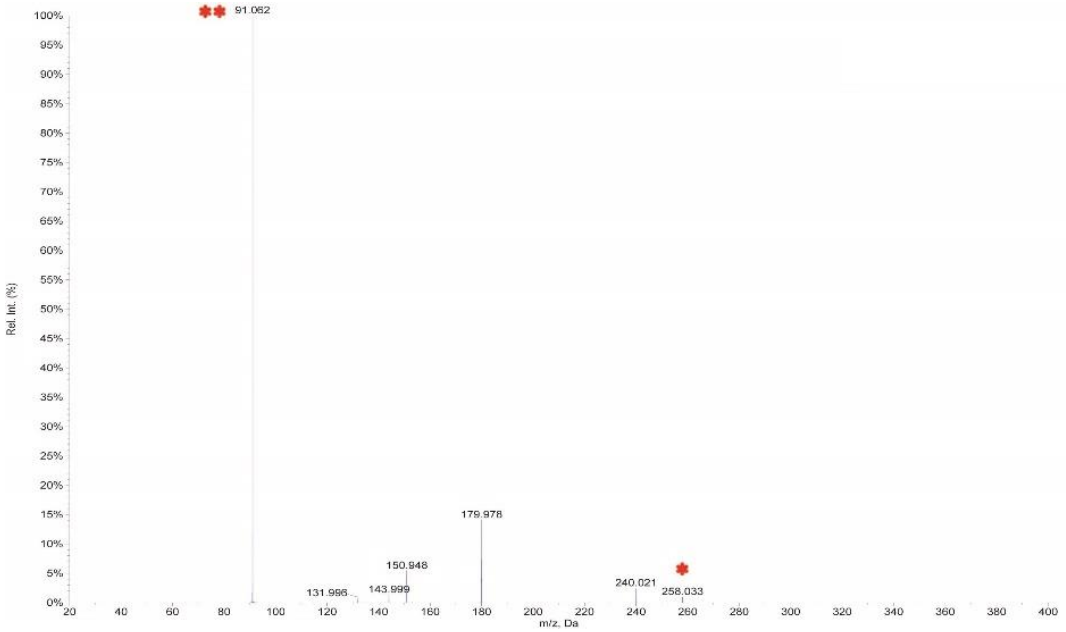
91.062
179.978
150.948
143.999
131.986
240.021
258.033
Rel. Int. (%)
m/z, Da

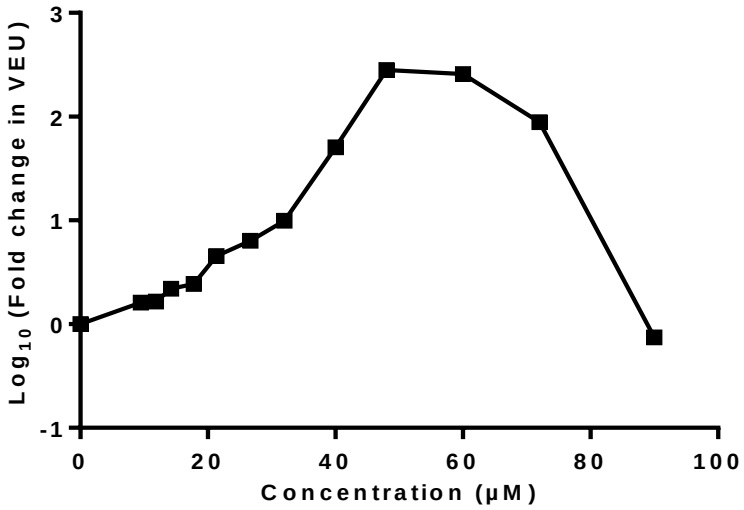
Log10 (Fold change in VEU)
Concentration (μM)

2.11

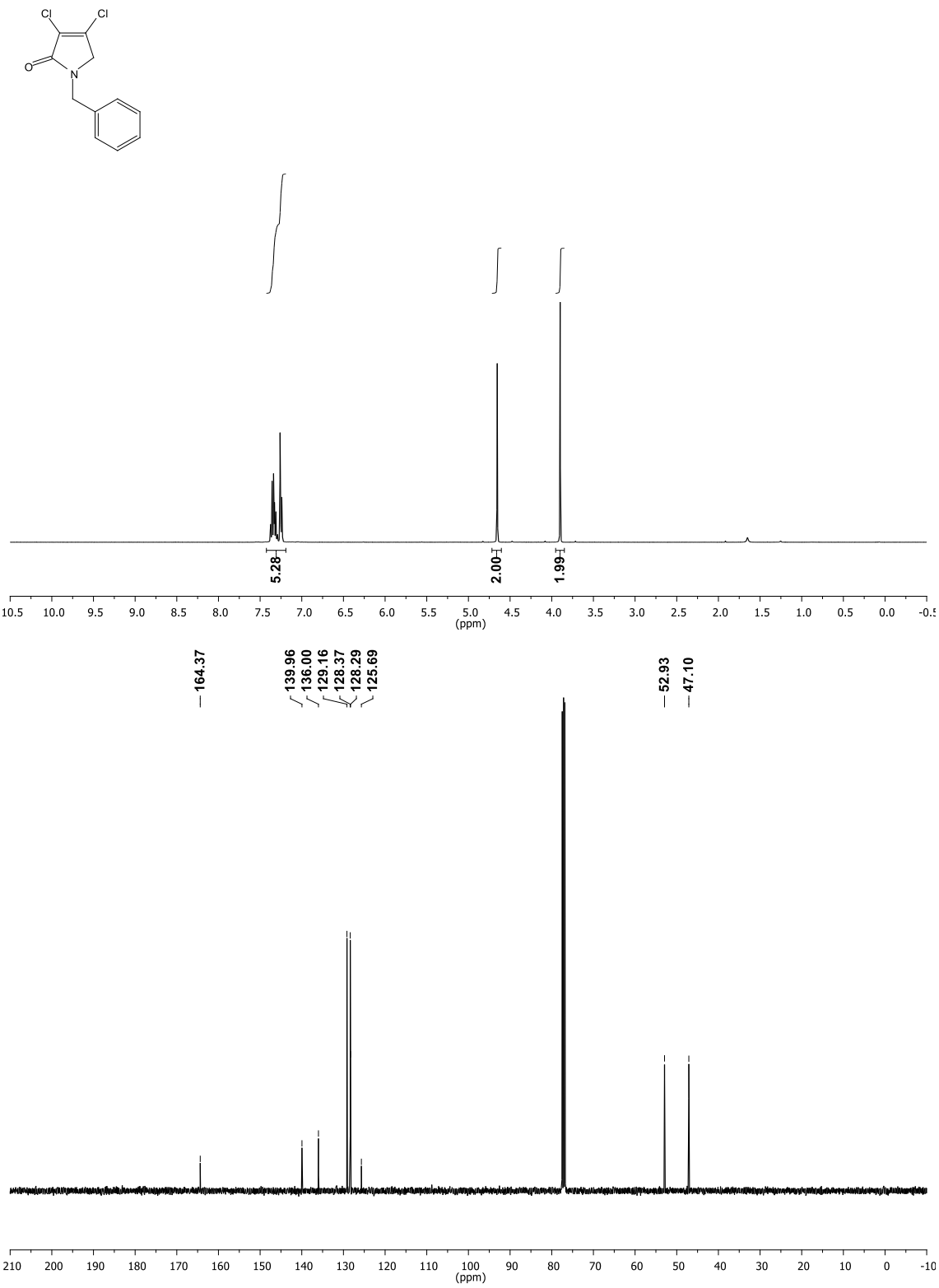
Cl
Cl
O
N
5.28
2.00
1.99
(ppm)
164.37
139.96
136.00
129.16
128.37
128.29
125.69
52.93
47.10
(ppm)

2.11

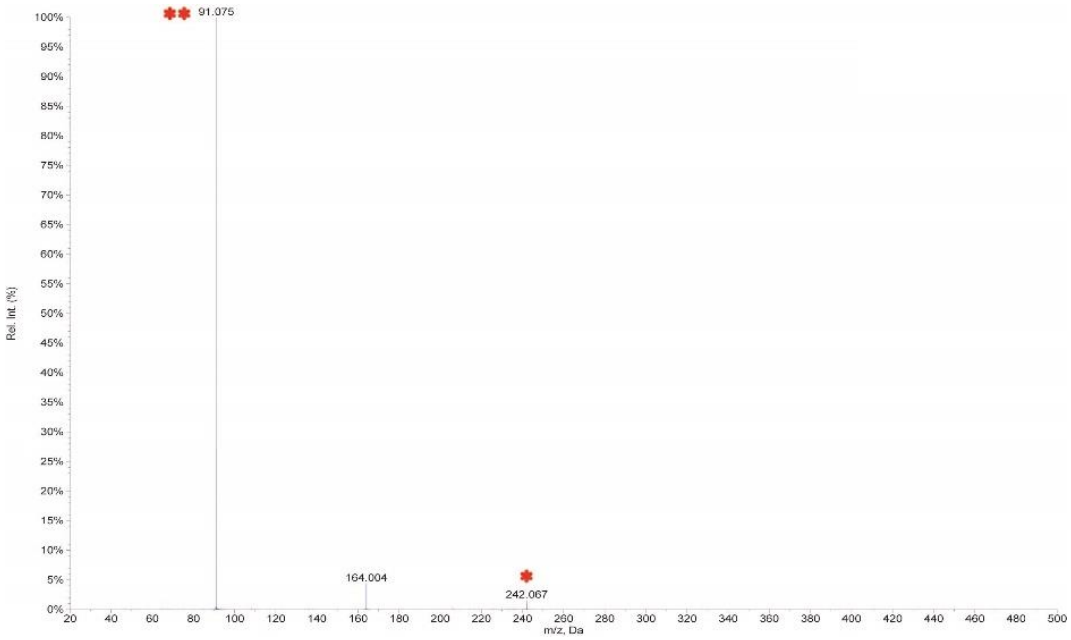
91.075
164.004
242.067
Rel. Int. (%)
m/z, Da

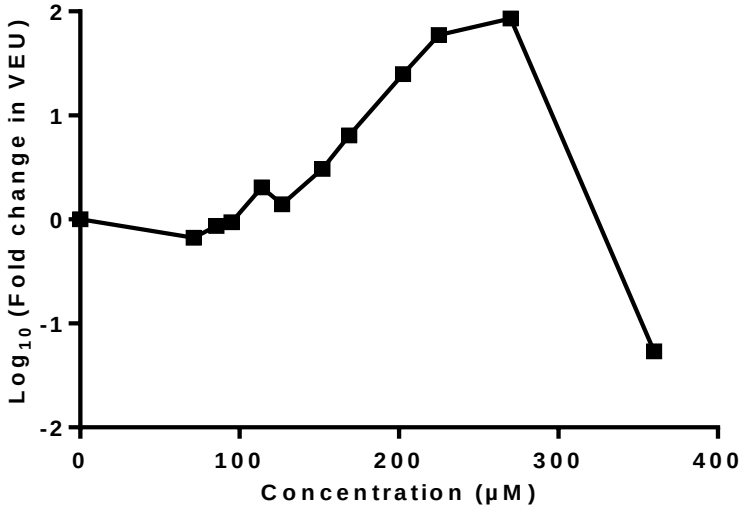
Log10 (Fold change in VEU)
Concentration (μM)

2.12

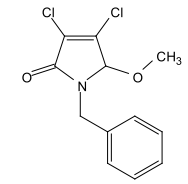
Cl
Cl
O
N
O
CH3

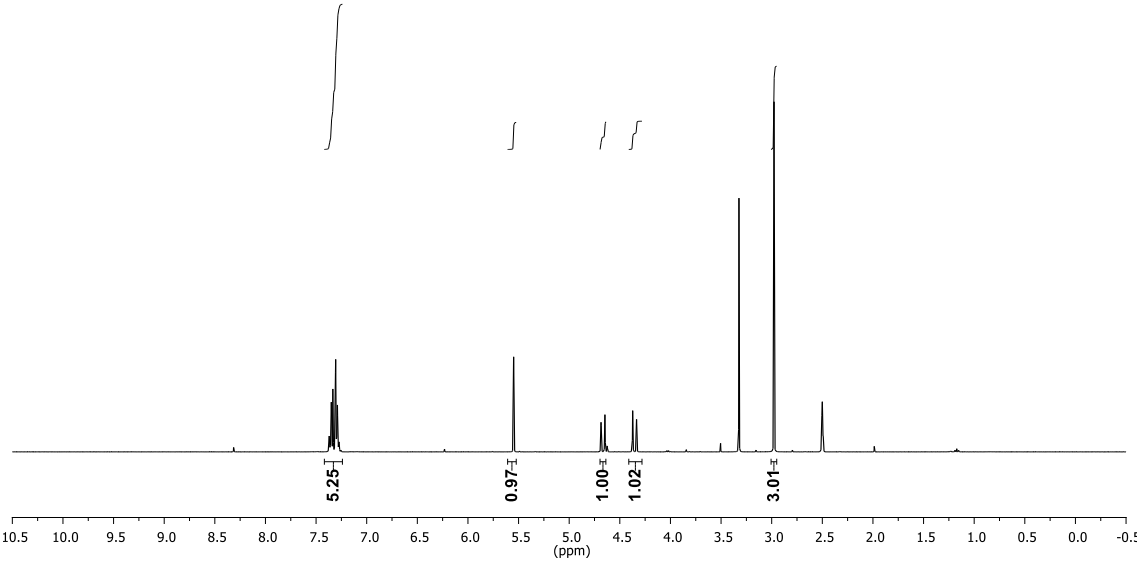
5.25
0.97
1.00
1.02
3.01
(ppm)

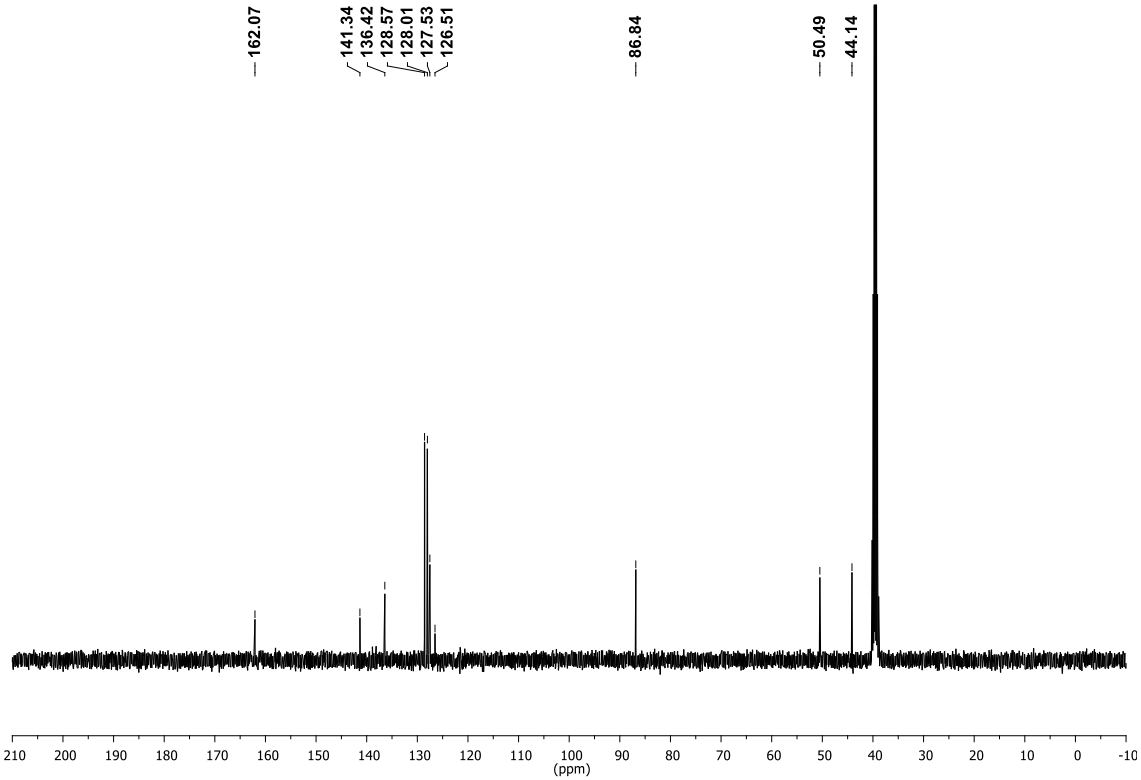
162.07
141.34
136.42
128.57
128.01
127.53
126.51
86.84
50.49
44.14
(ppm)

2.12

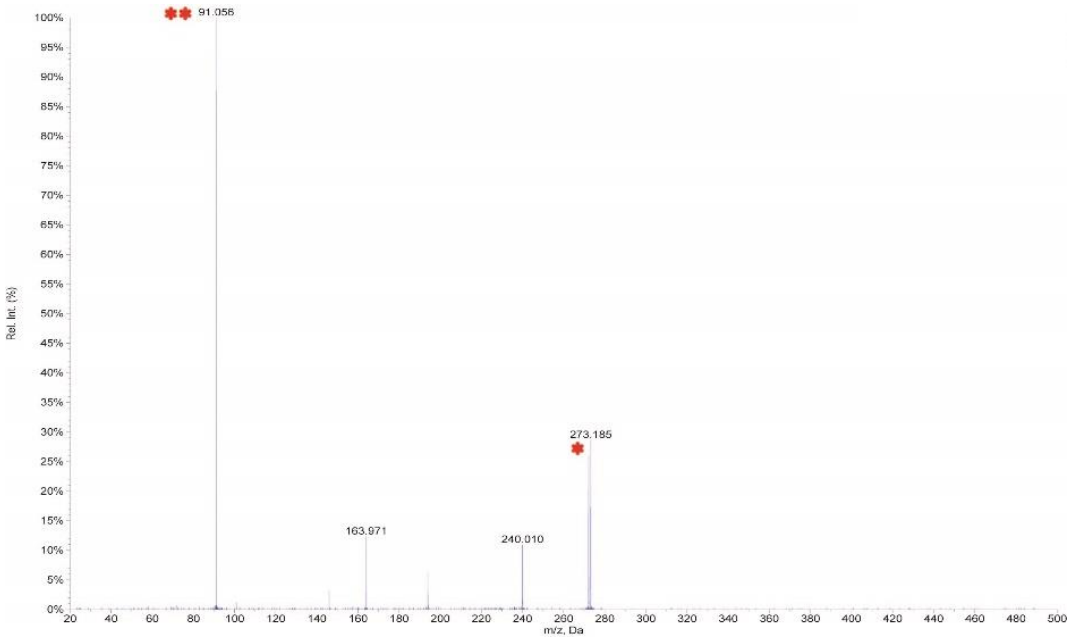
91.056
273.185
163.971
240.010
Rel. Int. (%)
m/z, Da

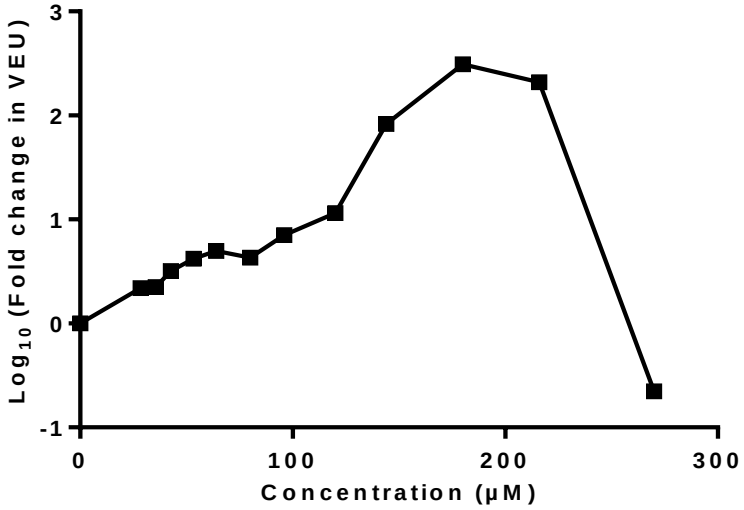
Log10 (Fold change in VEU)
Concentration (μM)

2.13

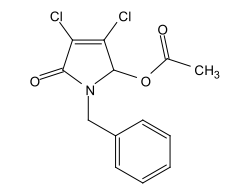
Cl
Cl
O
O
CH3
O
N

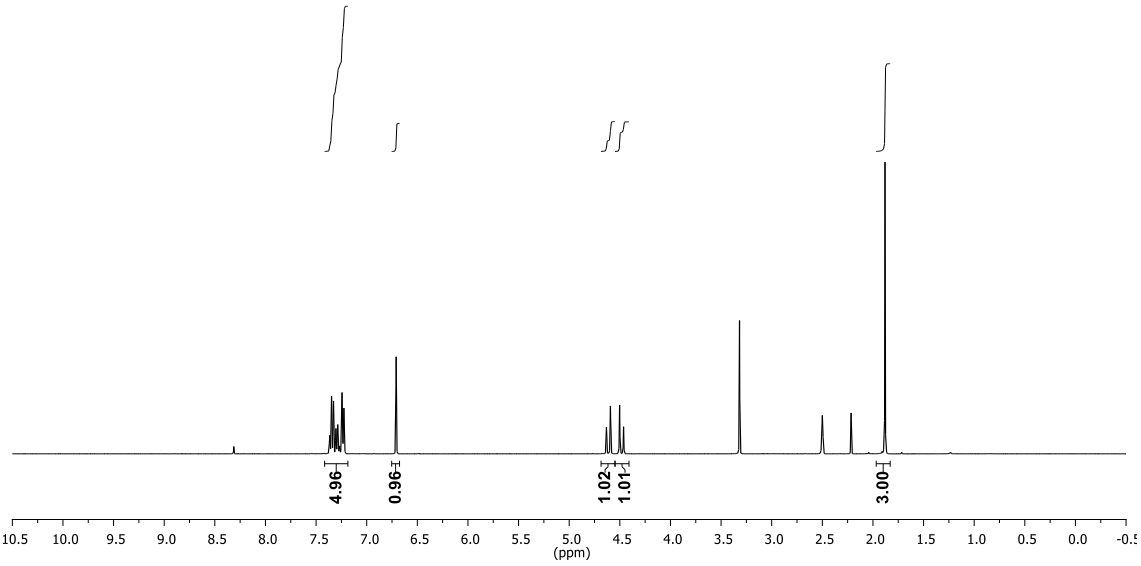
4.96
0.96
1.02
1.01
3.00
(ppm)

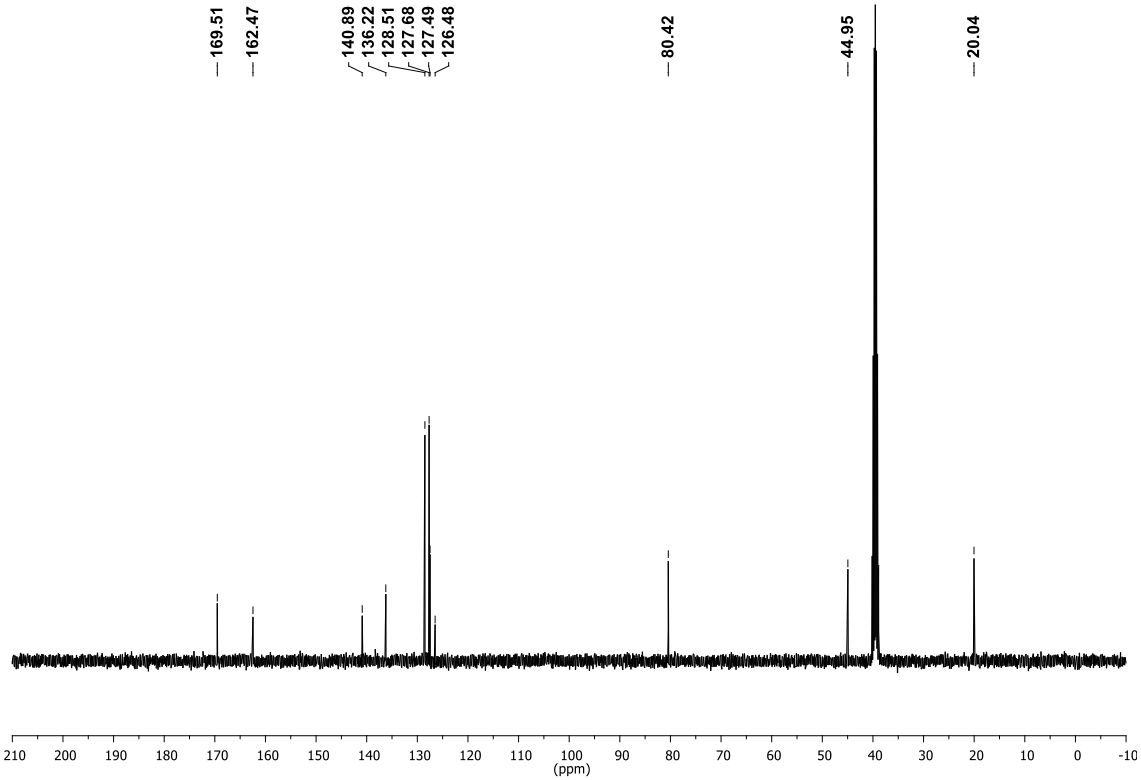
169.51
162.47
140.89
136.22
128.51
127.68
127.49
126.48
80.42
44.95
20.04
(ppm)

2.13

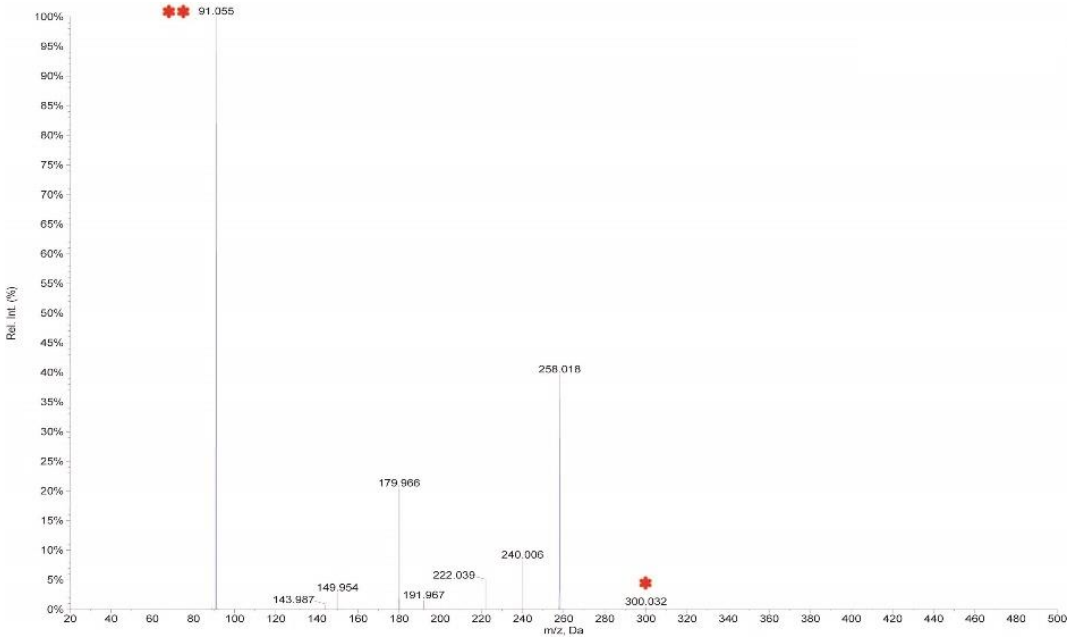
91.055
258.018
179.966
240.006
222.039
149.954
143.987
191.967
300.032
Rel. Int. (%)
m/z, Da

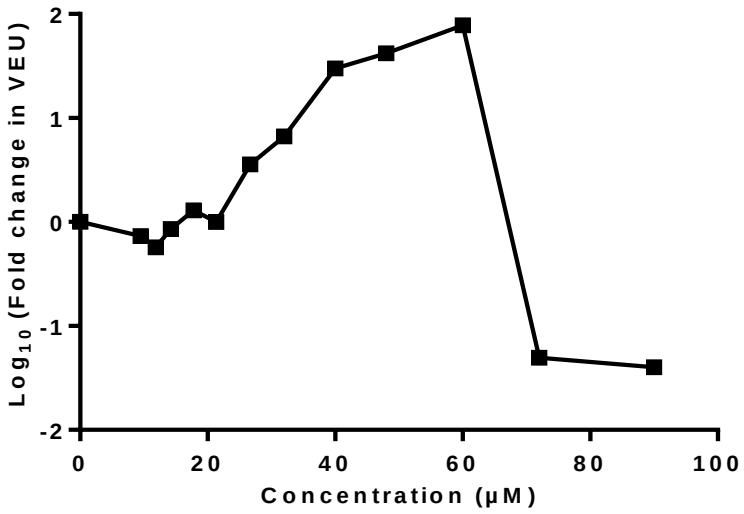
Log10 (Fold change in VEU)
Concentration (μM)

2.14

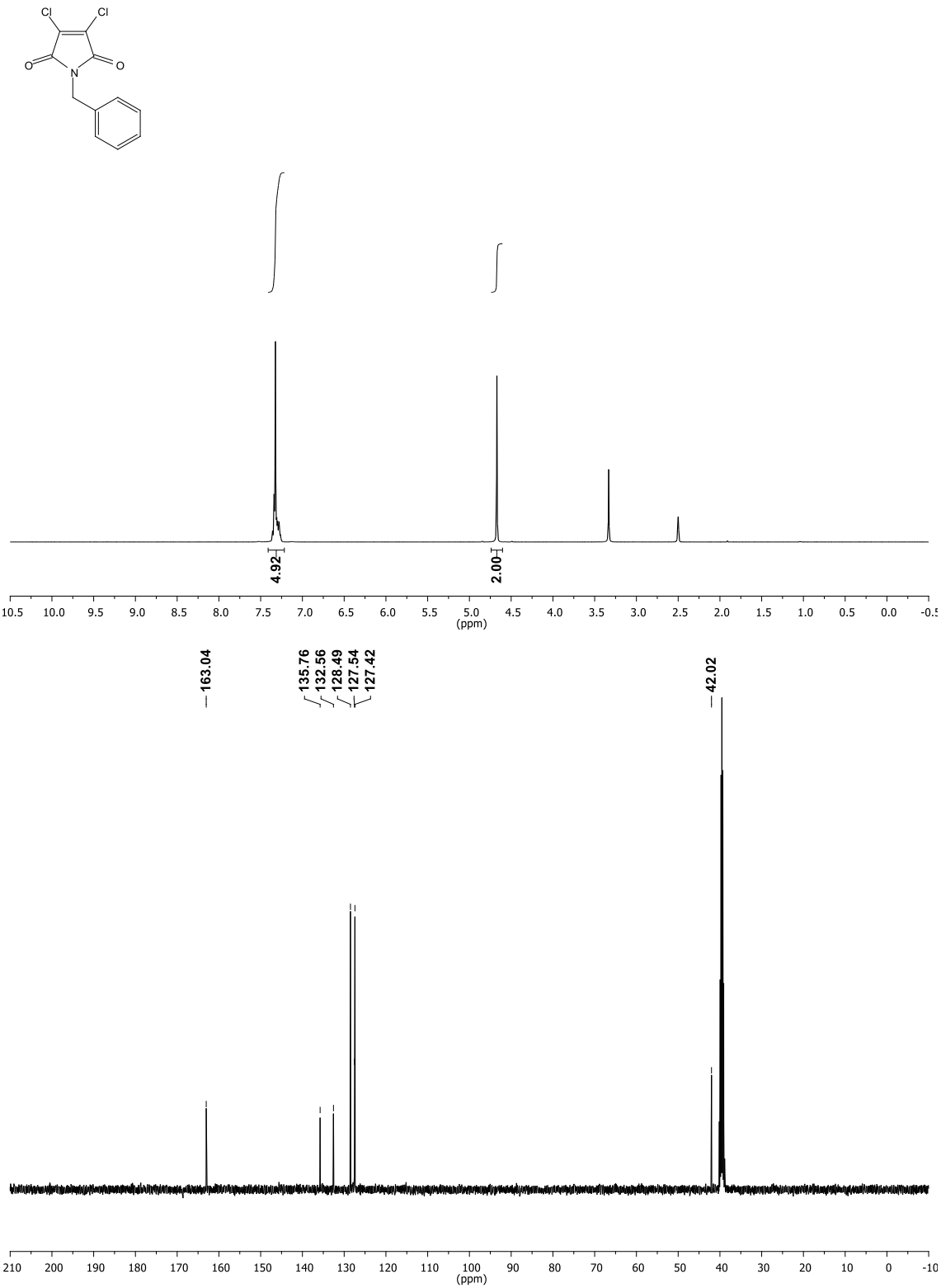
Cl
Cl
O
O
N
4.92
2.00
(ppm)
163.04
135.76
132.56
128.49
127.54
127.42
42.02
(ppm)

2.14

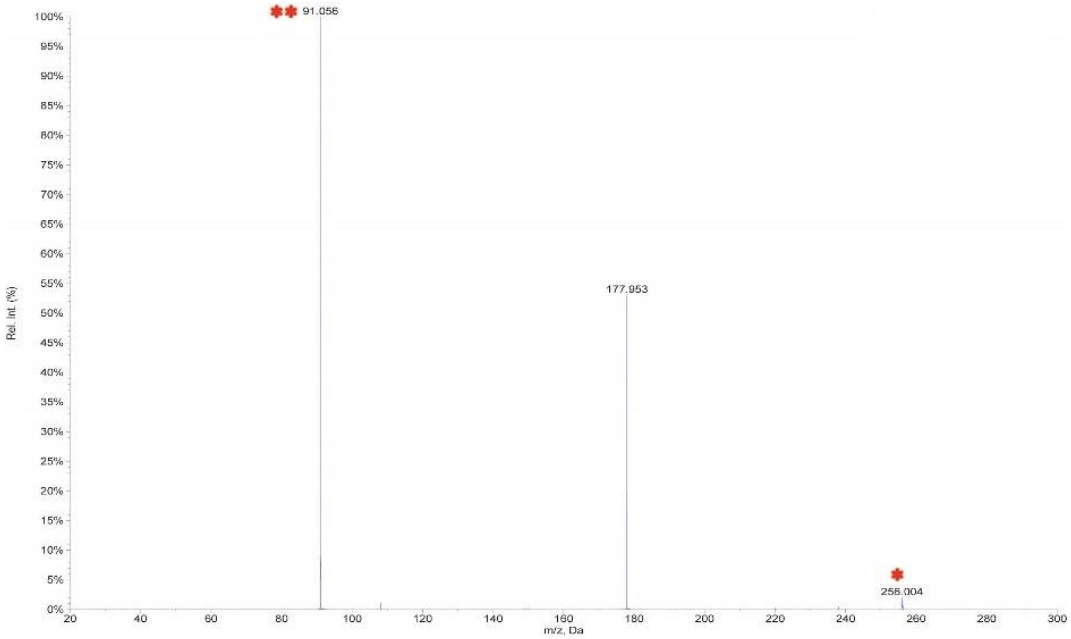
91.056
177.953
258.004
Rel. Int. (%)
m/z, Da

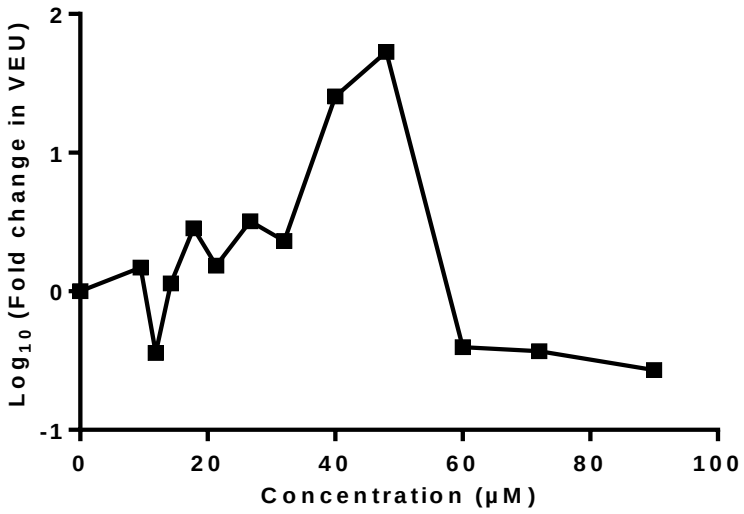
Log10 (Fold change in VEU)
Concentration (µM)

2.15

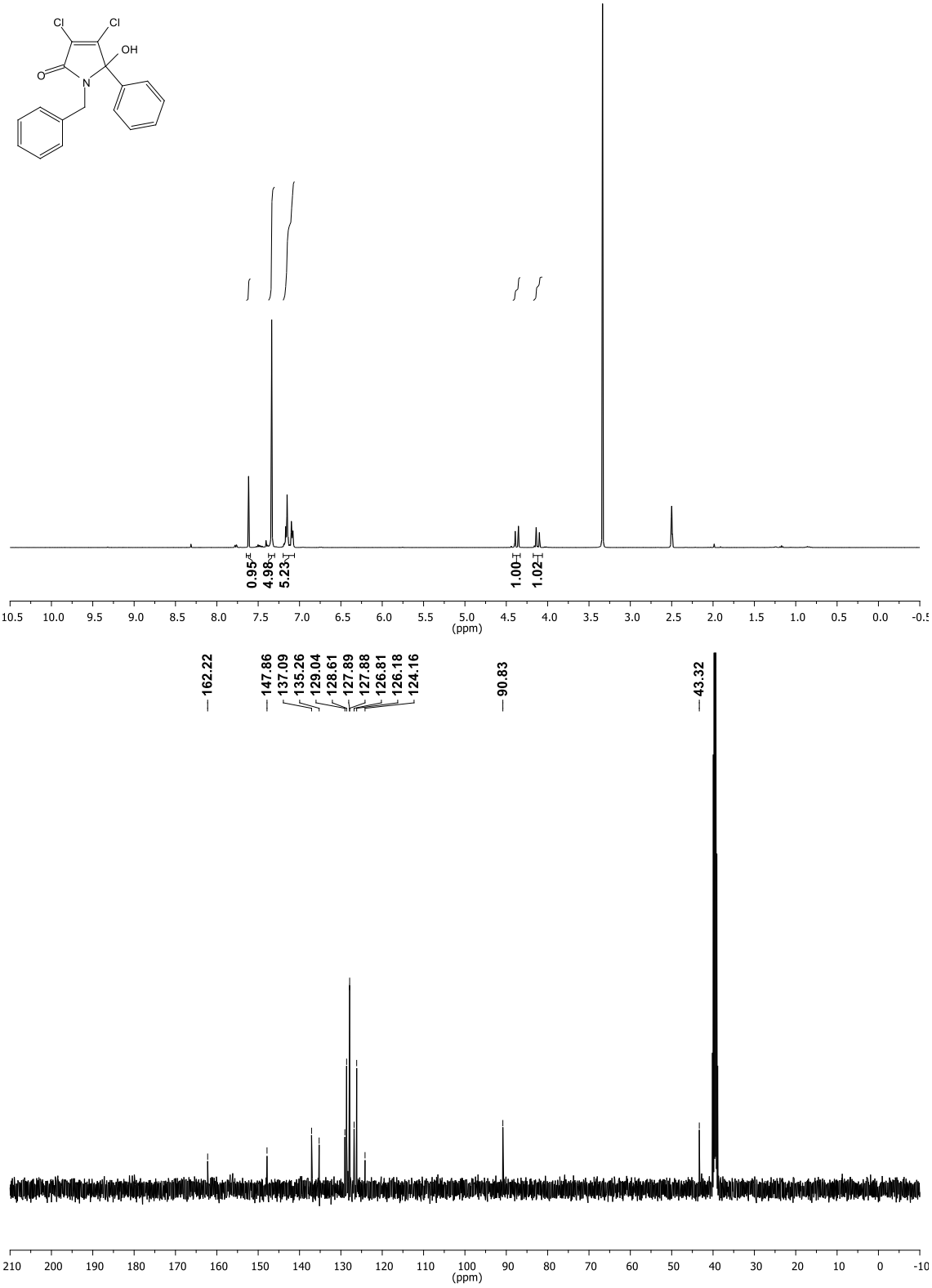
Cl
Cl
OH
O
N
0.95
4.98
5.23
1.00
1.02
(ppm)
162.22
147.86
137.09
135.26
129.04
128.61
127.89
127.88
126.81
126.18
124.16
90.83
43.32
(ppm)

2.15

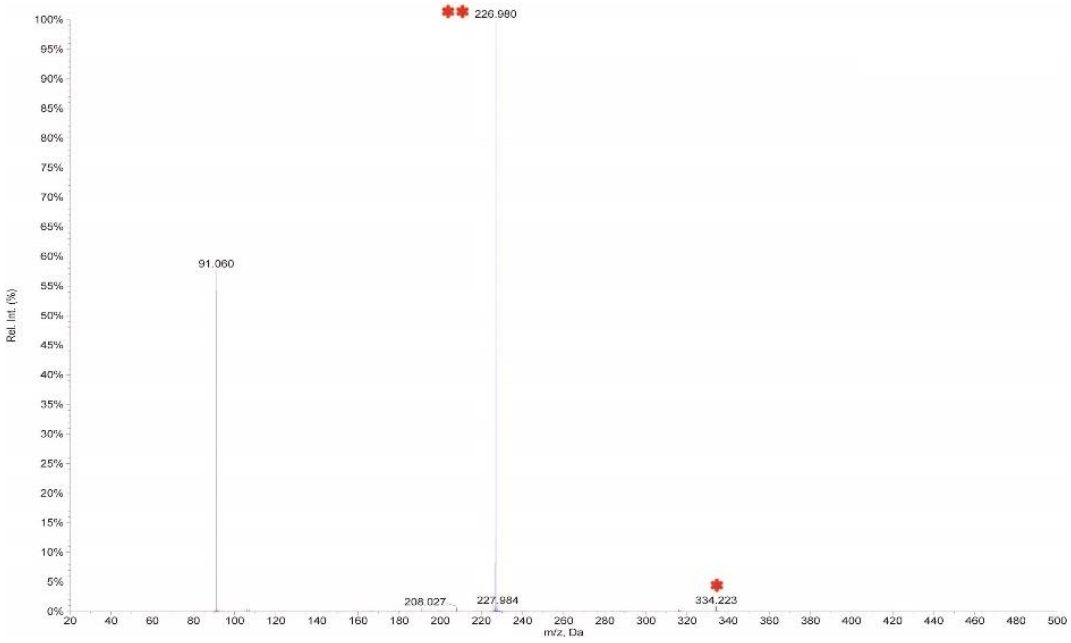
226.980
91.060
208.027
227.984
334.223
Rel. Int. (%)
m/z, Da

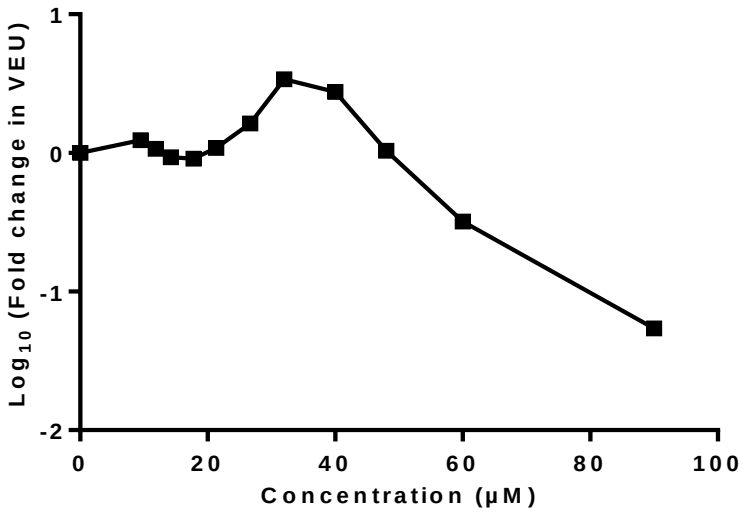
Log10 (Fold change in VEU)
Concentration (μM)

2.16

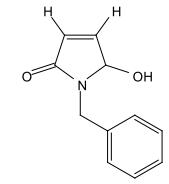
H
H
O
N
OH

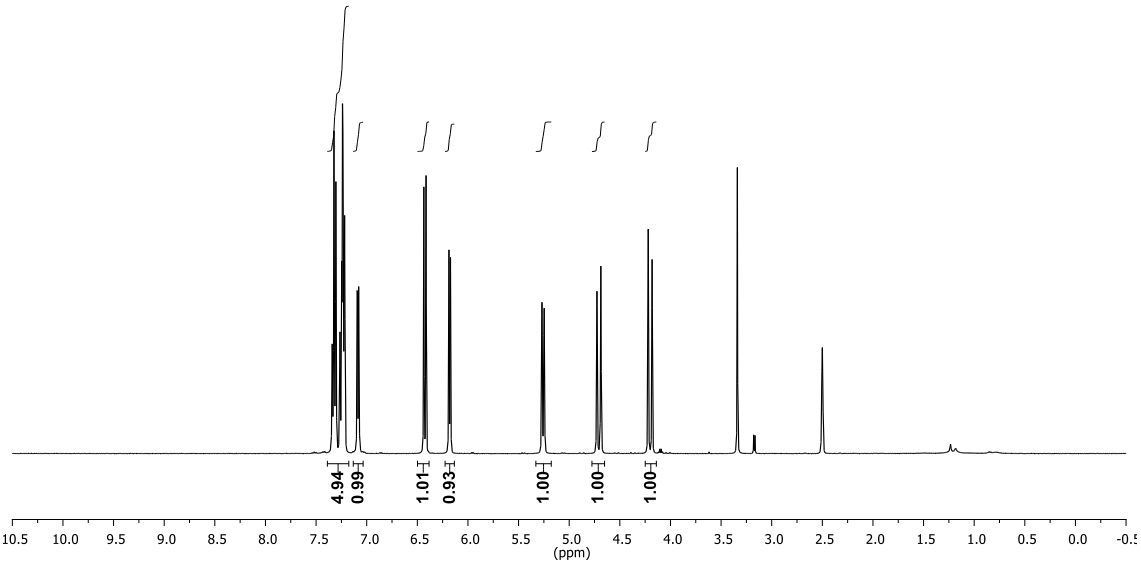
4.94
0.99
1.01
0.93
1.00
1.00
1.00
(ppm)

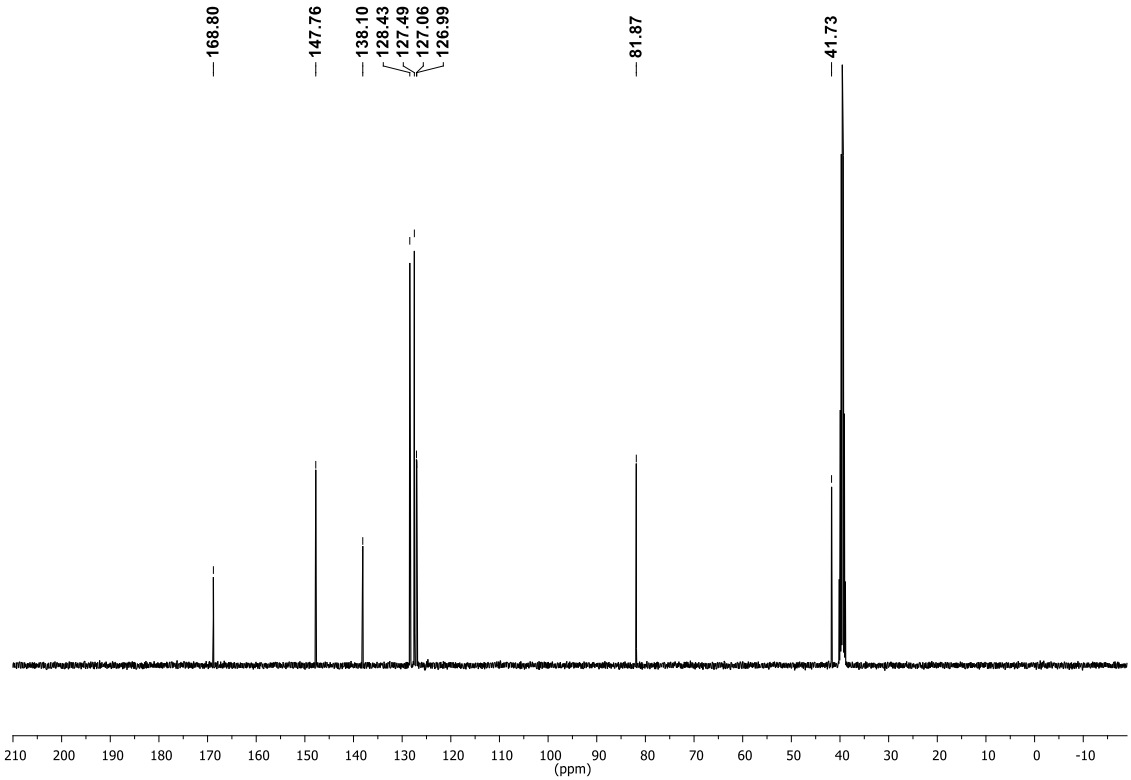
168.80
147.76
138.10
128.43
127.49
127.06
126.99
81.87
41.73
(ppm)

2.16

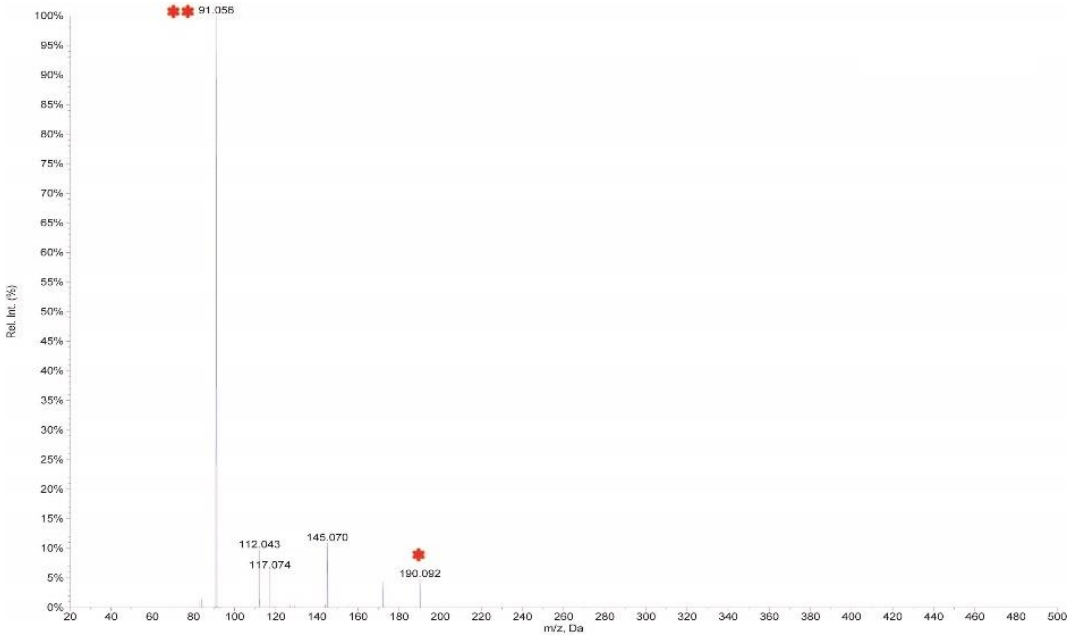
91.056
112.043
117.074
145.070
190.092
Rel. Int. (%)
m/z, Da

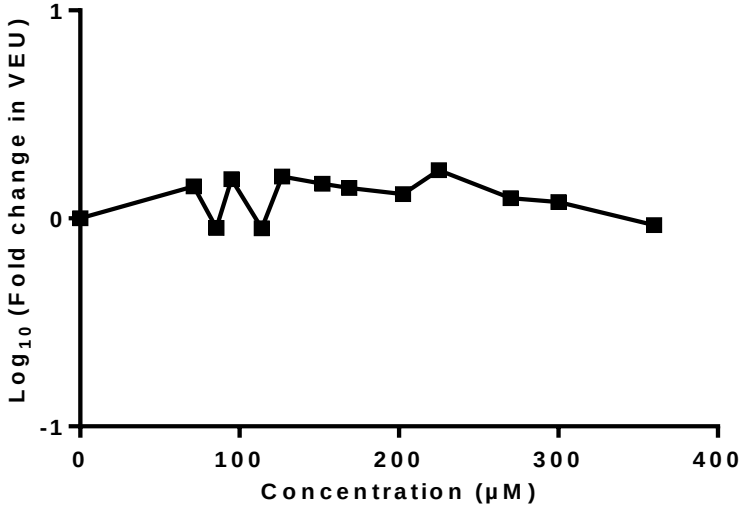
Log10 (Fold change in VEU)
Concentration (μM)
1
0
-1
0
100
200
300
400

2.17

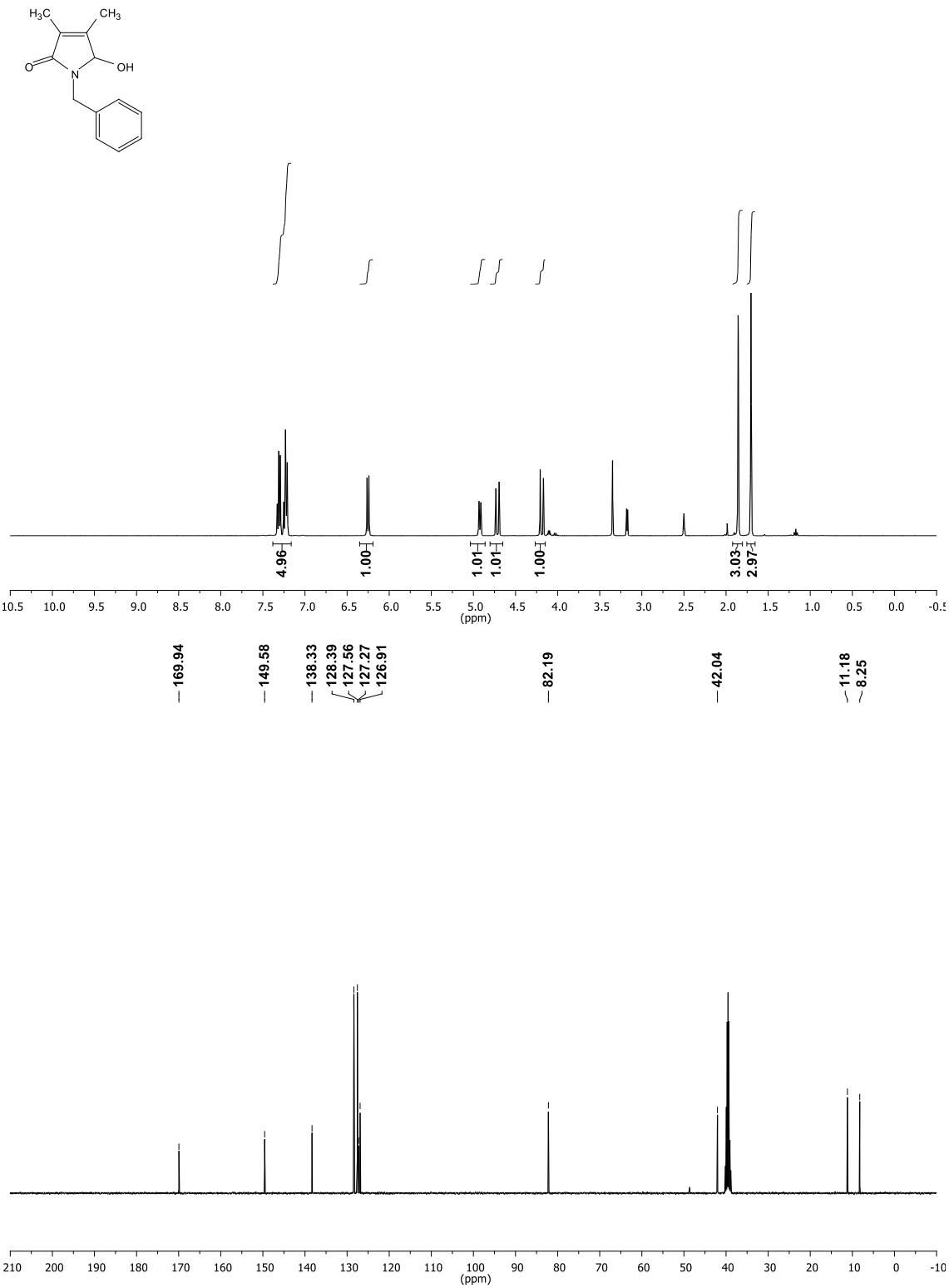
H3C
CH3
O
N
OH
4.96
1.00
1.01
1.01
1.00
3.03
2.97
(ppm)
169.94
149.58
138.33
128.39
127.56
127.27
126.91
82.19
42.04
11.18
8.25
(ppm)

2.17

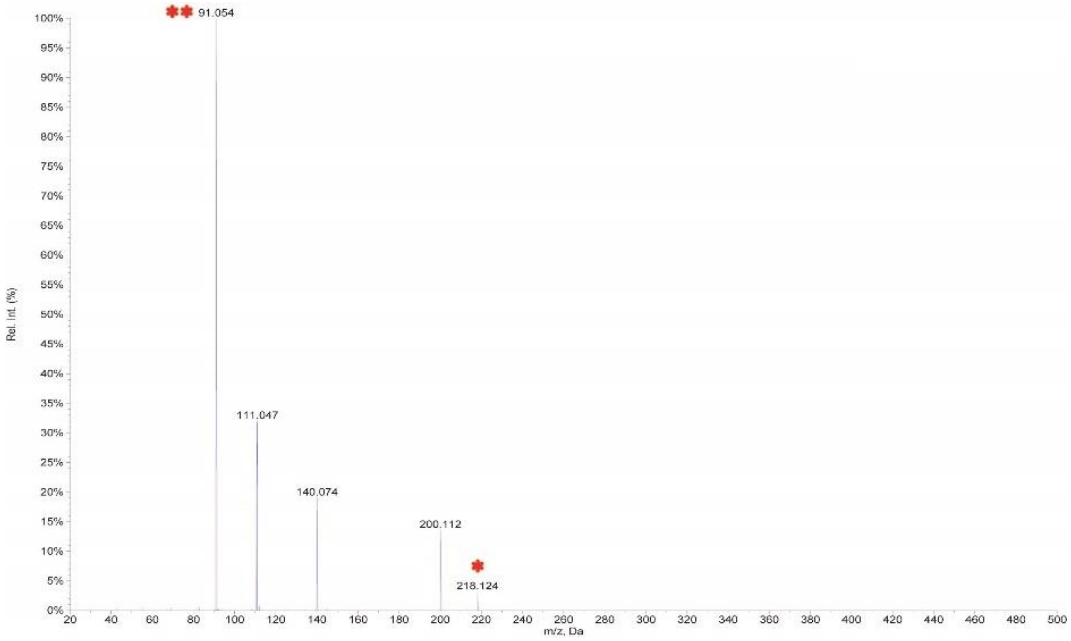
91.054
111.047
140.074
200.112
218.124
Rel. Int. (%)
m/z, Da

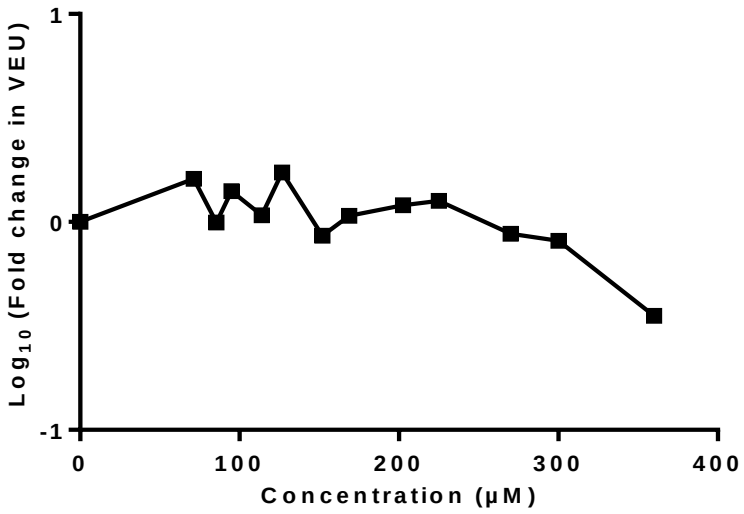
Log10 (Fold change in VEU)
Concentration (µM)
1
0
-1
0
100
200
300
400

2.18

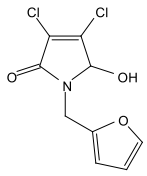
Cl
Cl
O
N
OH
O

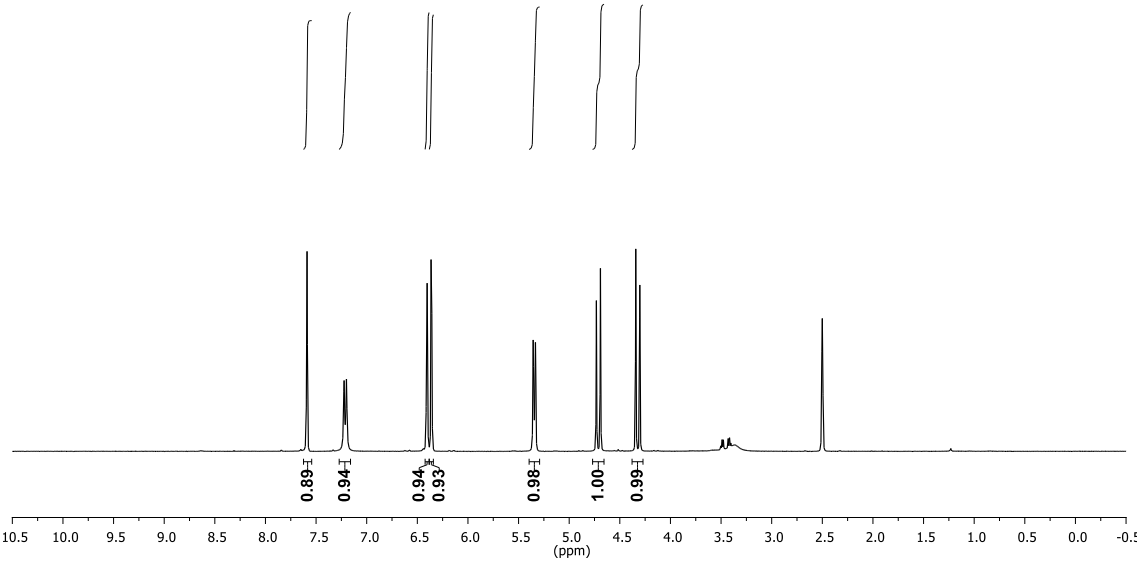
0.89
0.94
0.94
0.93
0.98
1.00
0.99
10.5 10.0 9.5 9.0 8.5 8.0 7.5 7.0 6.5 6.0 5.5 5.0 4.5 4.0 3.5 3.0 2.5 2.0 1.5 1.0 0.5 0.0
(ppm)

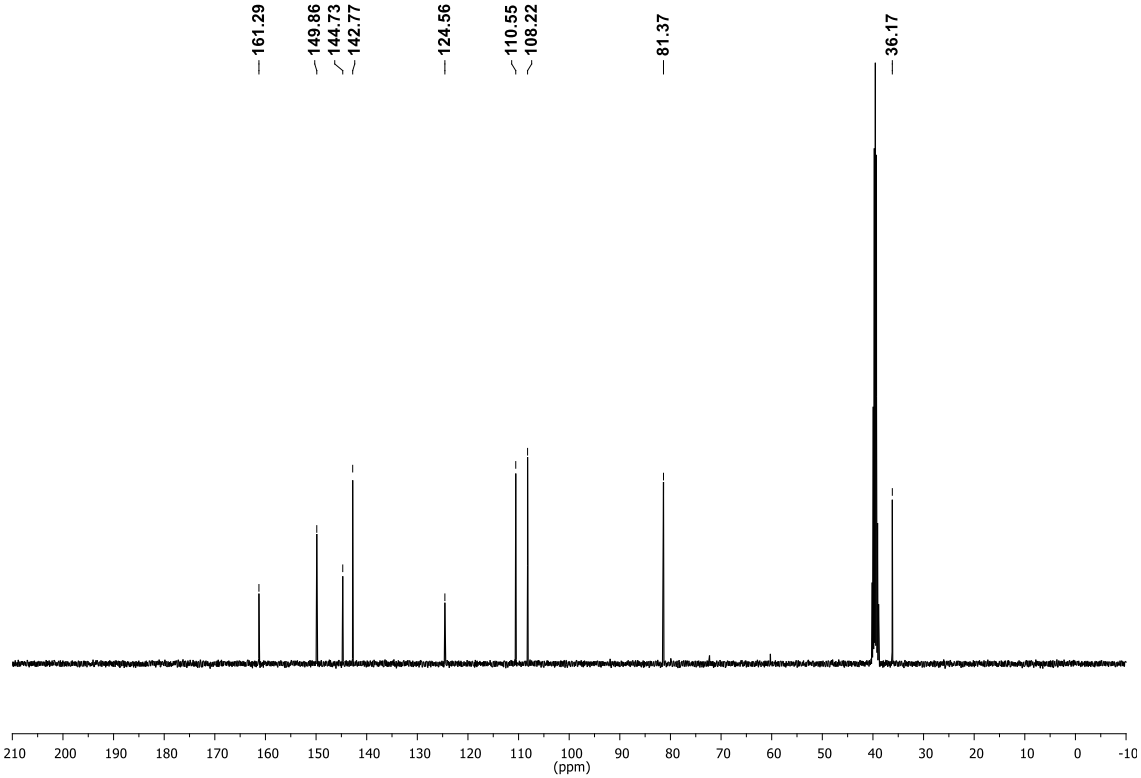
161.29
149.86
144.73
142.77
124.56
110.55
108.22
81.37
36.17
210 200 190 180 170 160 150 140 130 120 110 100 90 80 70 60 50 40 30 20 10 0
(ppm)

2.18

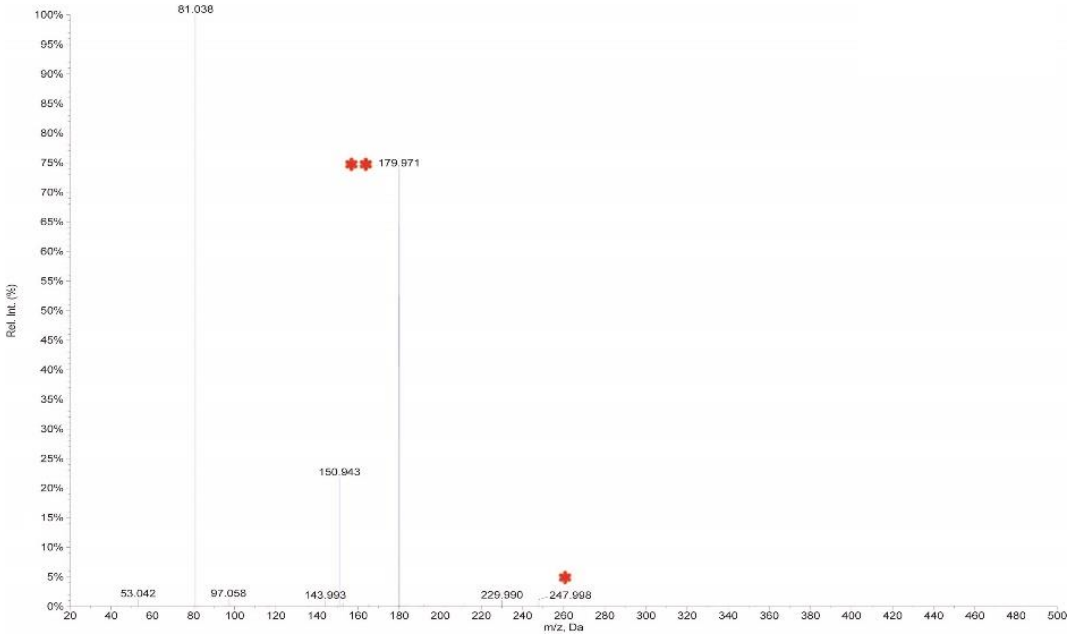
81.038
179.971
150.943
53.042
97.058
143.993
229.990
247.998
Rel. Int. (%)
m/z, Da

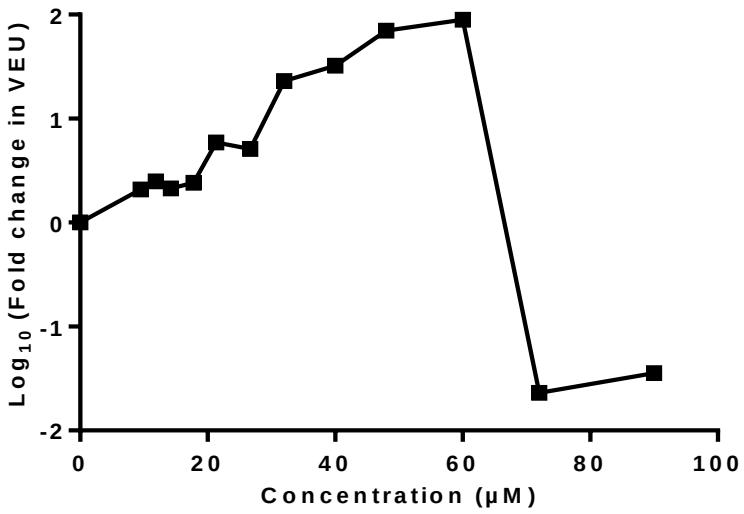
Log10 (Fold change in VEU)
Concentration (μM)

2.19

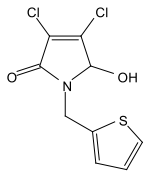
Cl
Cl
O
N
OH
S

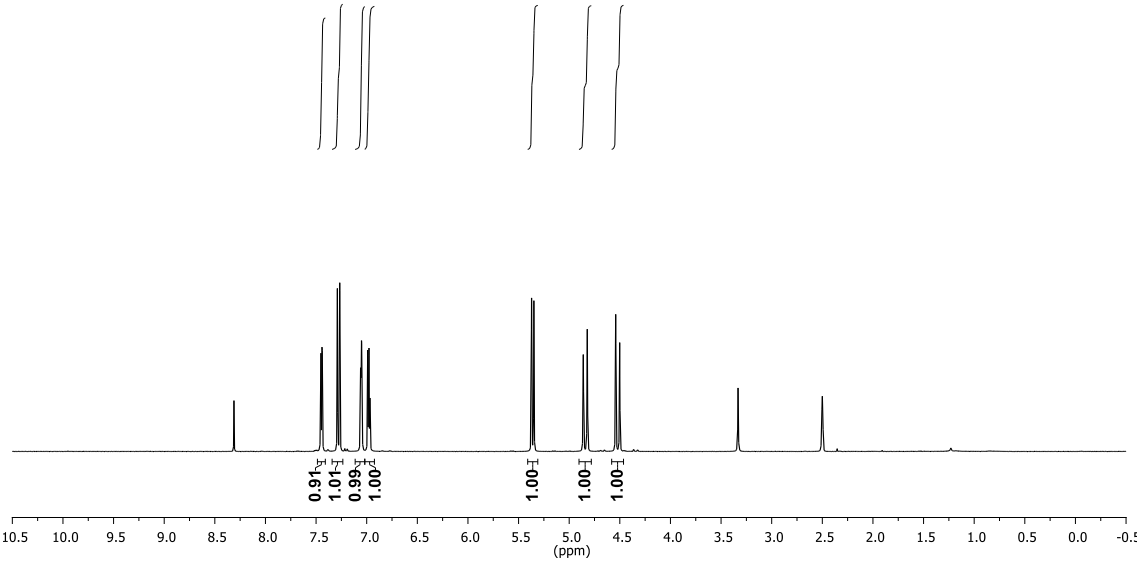
0.91
1.01
0.99
1.00
1.00
1.00
1.00
10.5 10.0 9.5 9.0 8.5 8.0 7.5 7.0 6.5 6.0 5.5 5.0 4.5 4.0 3.5 3.0 2.5 2.0 1.5 1.0 0.5 0.0
(ppm)

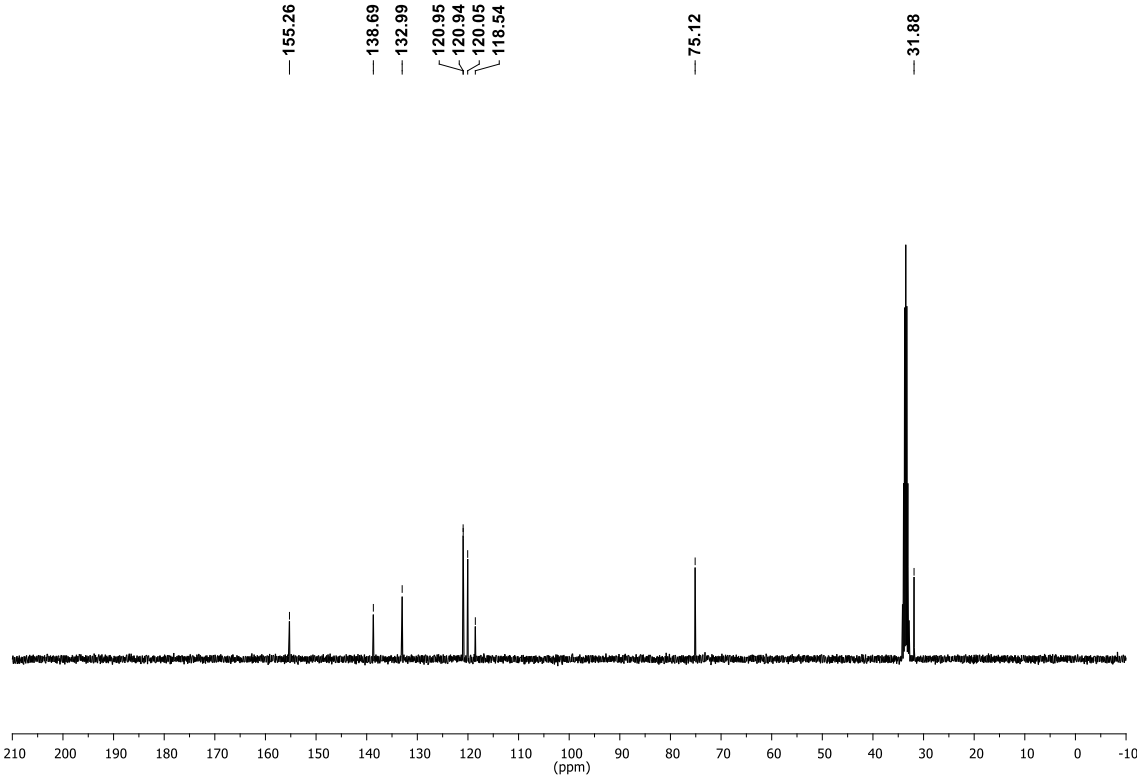
155.26
138.69
132.99
120.95
120.94
120.05
118.54
75.12
31.88
210 200 190 180 170 160 150 140 130 120 110 100 90 80 70 60 50 40 30 20 10 0
(ppm)

2.19

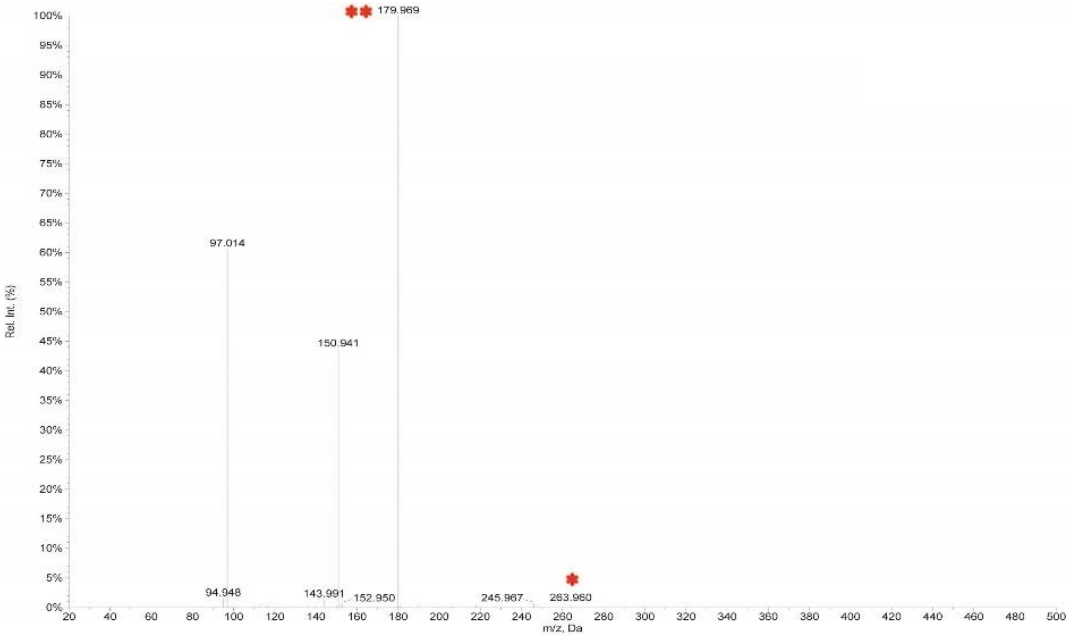
179.969
97.014
150.941
94.948
143.991
152.950
245.967
263.960
Rel. Int. (%)
m/z, Da

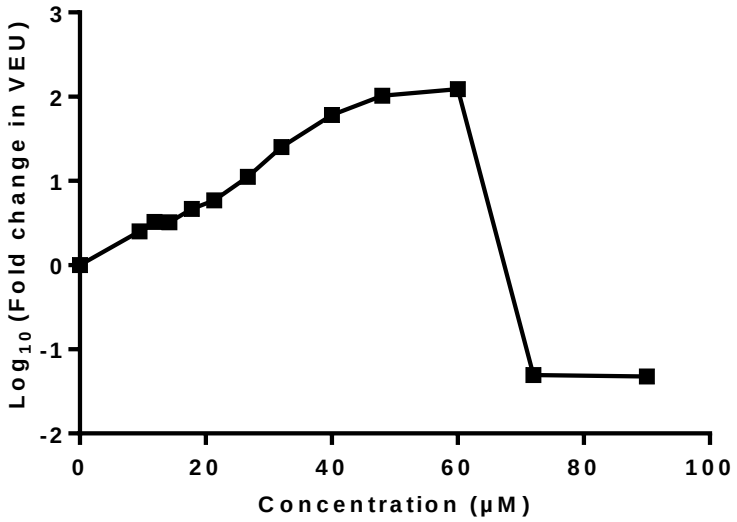
Log10 (Fold change in VEU)
Concentration (µM)

2.20

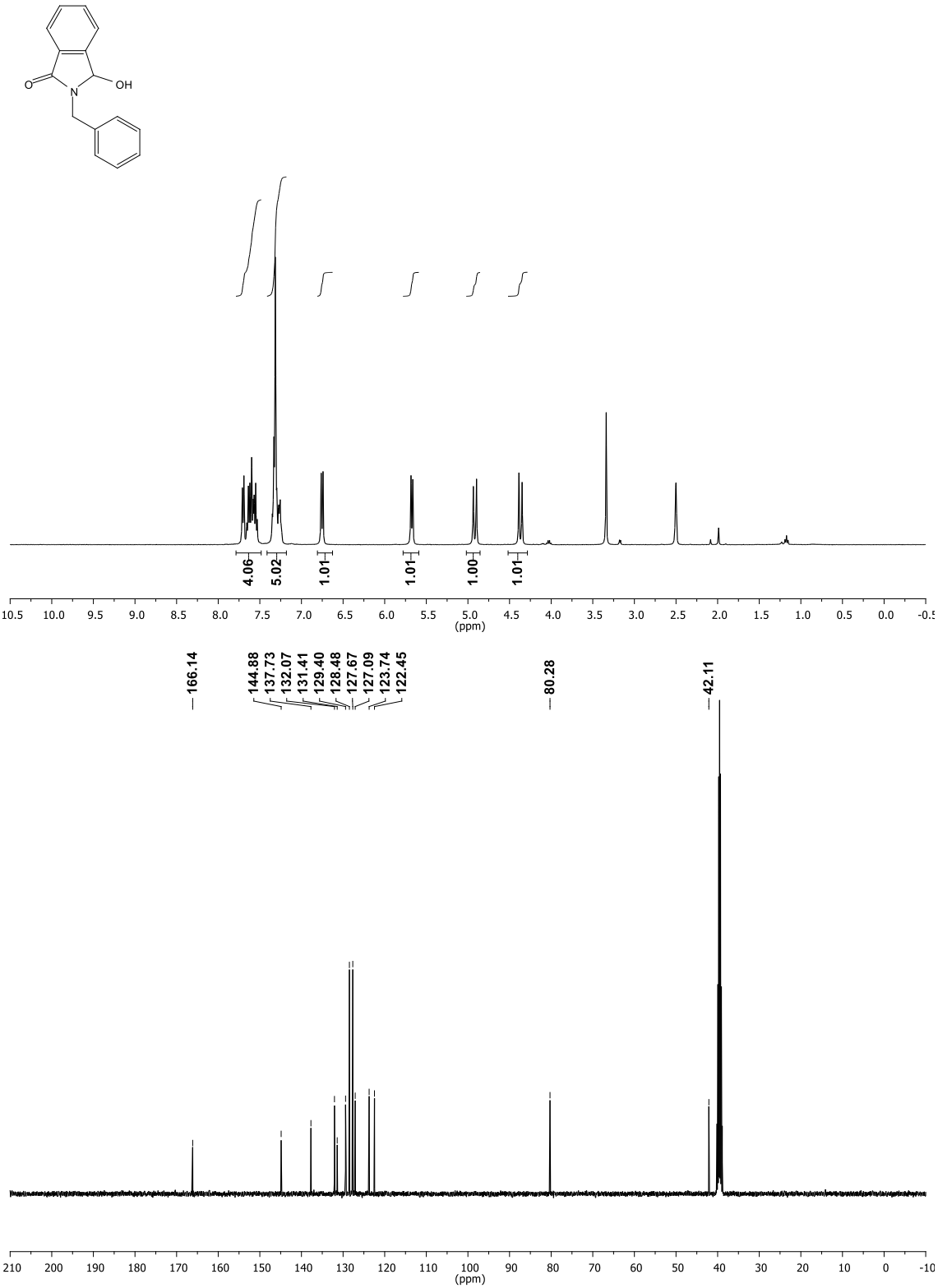
O
N
OH
4.06
5.02
1.01
1.01
1.00
1.01
(ppm)
166.14
144.88
137.73
132.07
131.41
129.40
128.48
127.67
127.09
123.74
122.45
80.28
42.11
(ppm)

2.20

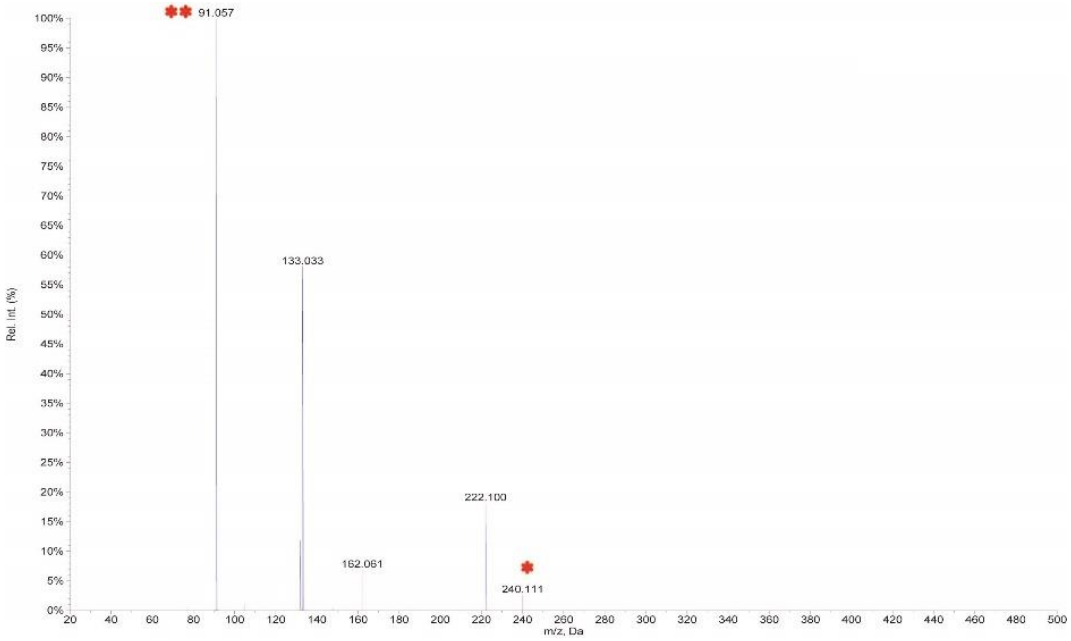
91.057
133.033
222.100
162.061
240.111
Rel. Int. (%)
m/z, Da

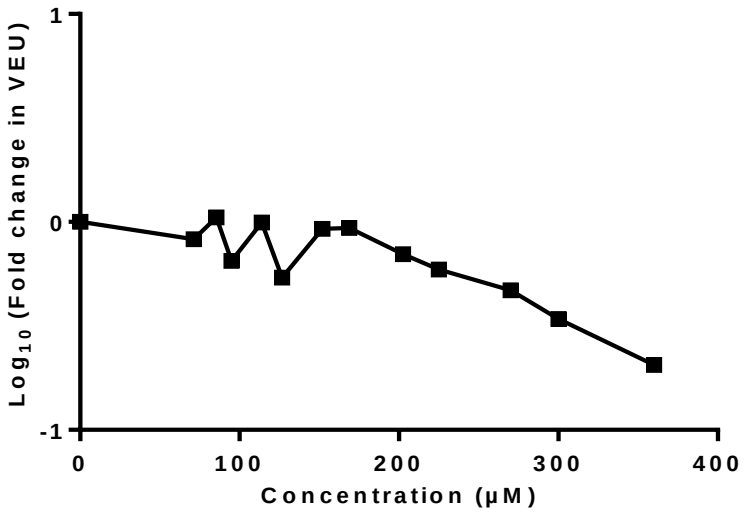
Log10 (Fold change in VEU)
Concentration (µM)
1
0
-1
0
100
200
300
400

2.21

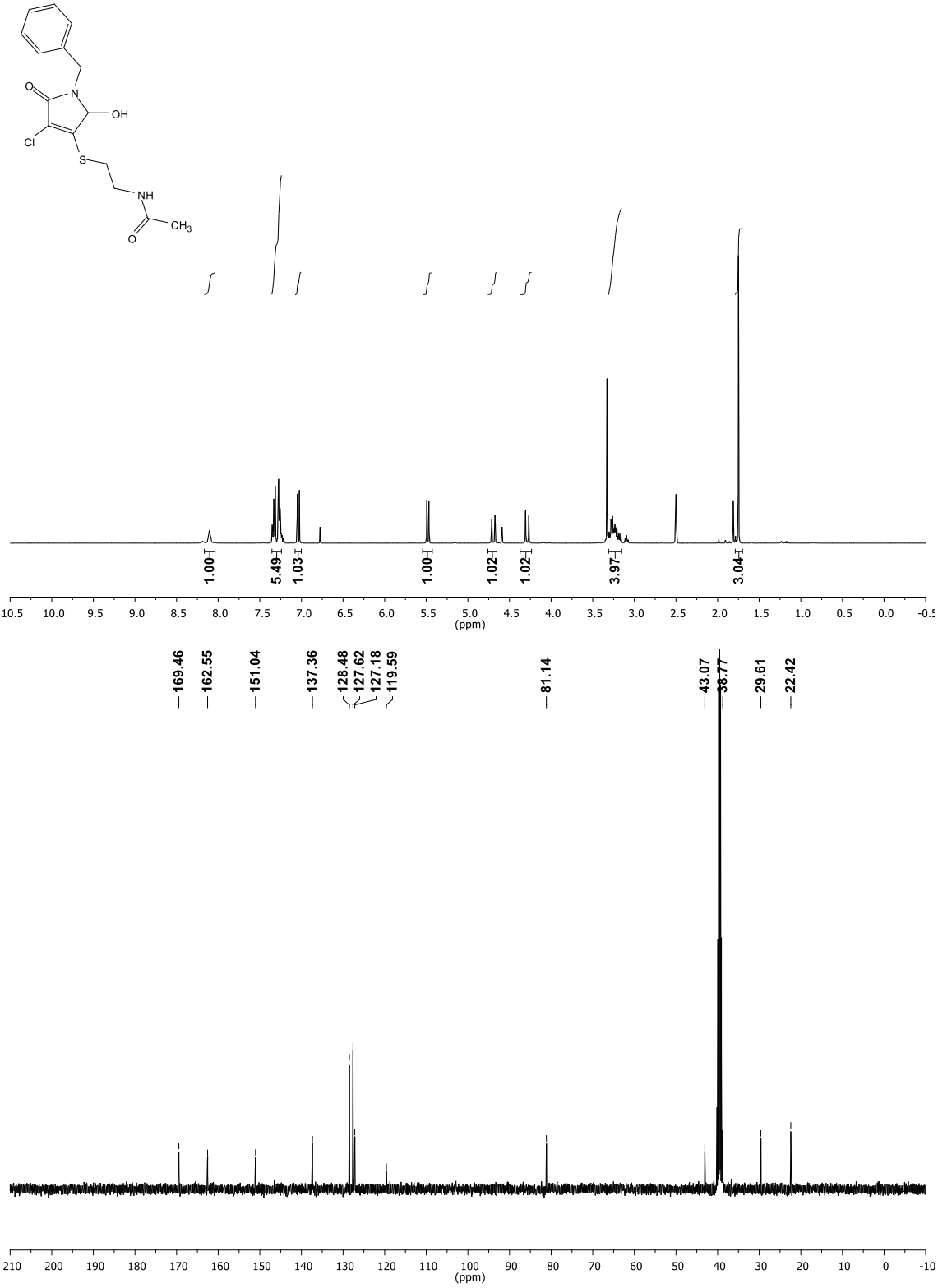
O
N
OH
Cl
S
NH
CH3
O
1.00
5.49
1.03
1.00
1.02
1.02
3.97
3.04
(ppm)
169.46
162.55
151.04
137.36
128.48
127.62
127.18
119.59
81.14
43.07
38.77
29.61
22.42
(ppm)

2.21

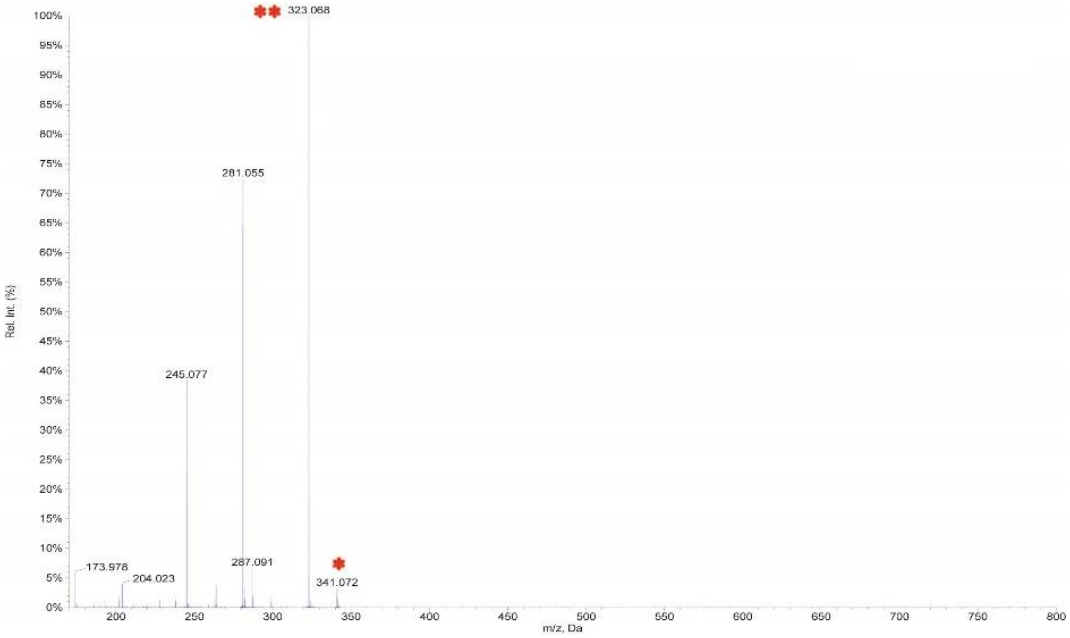
323.068
281.055
245.077
173.978
204.023
287.091
341.072
Rel. Int. (%)
m/z, Da

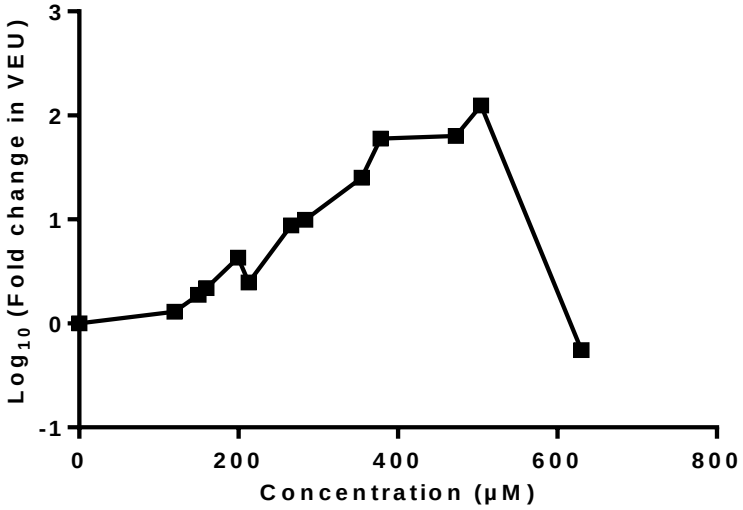
Log10 (Fold change in VEU)
Concentration (μM)

2.22

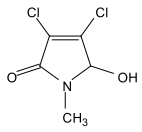
Cl
Cl
O
N
OH
CH3

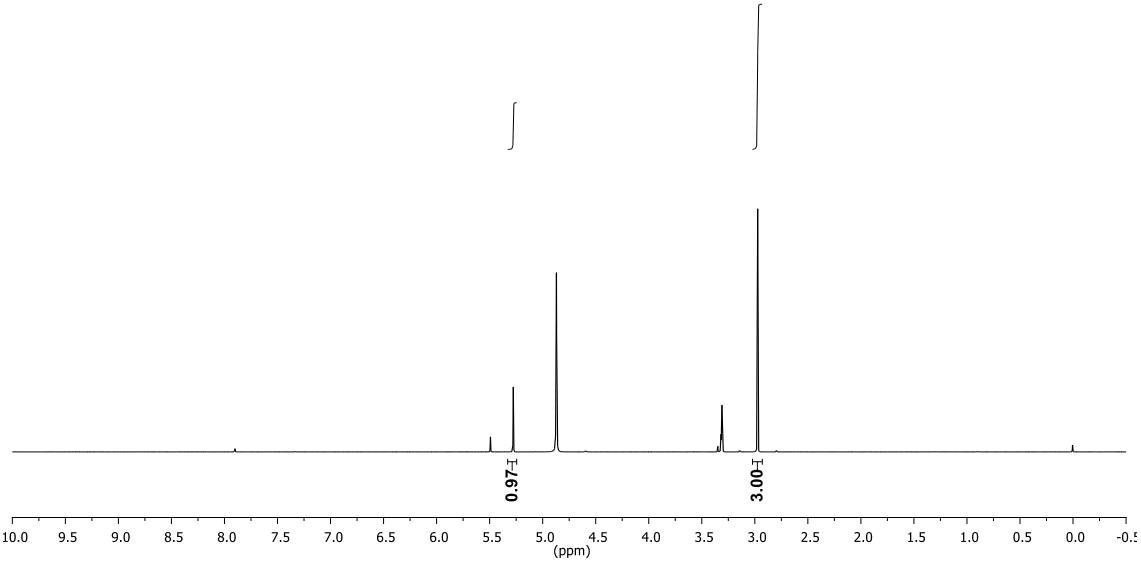
0.97
3.00
10.0 9.5 9.0 8.5 8.0 7.5 7.0 6.5 6.0 5.5 5.0 4.5 4.0 3.5 3.0 2.5 2.0 1.5 1.0 0.5 0.0
(ppm)

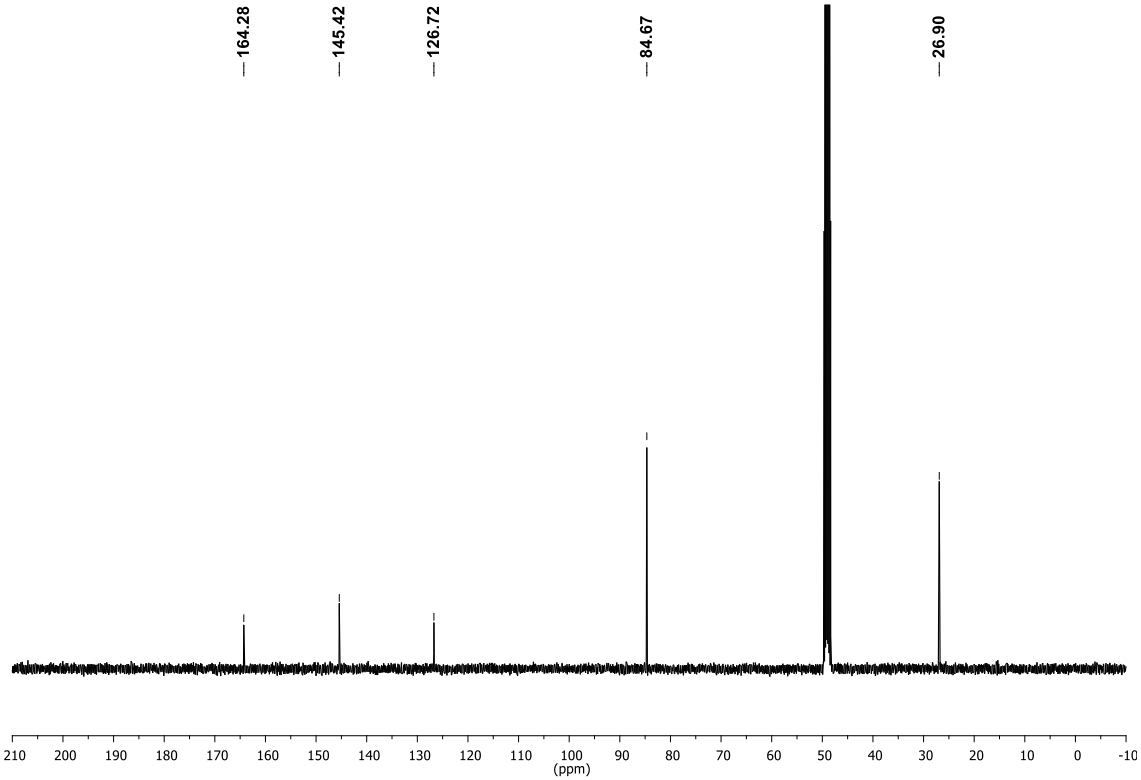
164.28
145.42
126.72
84.67
26.90
210 200 190 180 170 160 150 140 130 120 110 100 90 80 70 60 50 40 30 20 10 0
(ppm)

2.22

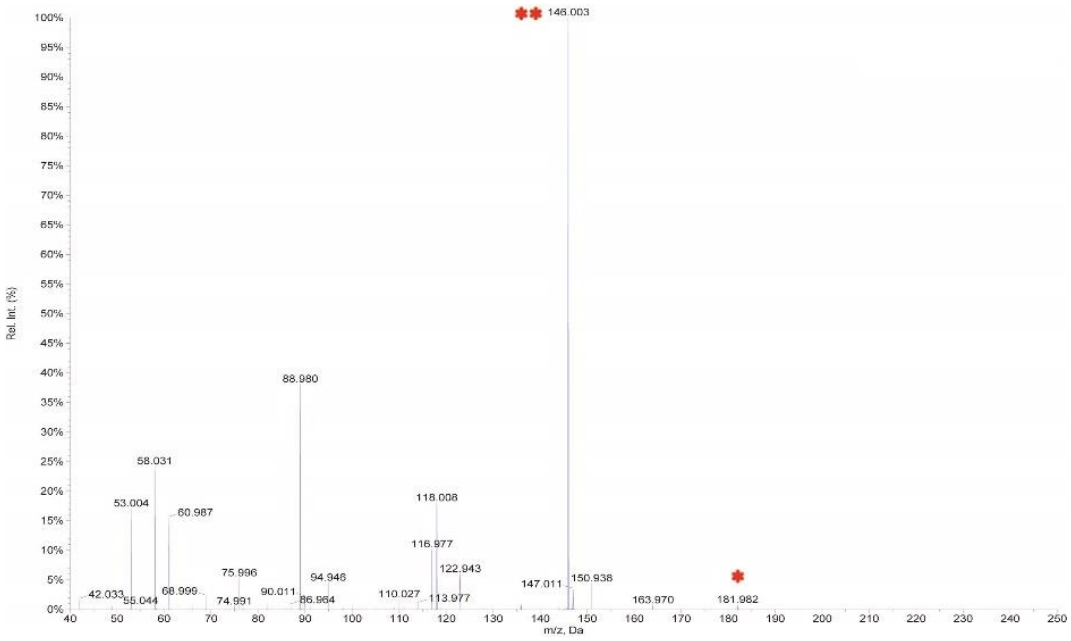
146.003
88.980
58.031
53.004
60.987
118.008
116.977
122.943
75.996
94.946
147.011
150.938
42.033
55.044
68.999
74.991
90.011
86.964
110.027
113.977
163.970
181.982
Rel. Int. (%)
m/z, Da

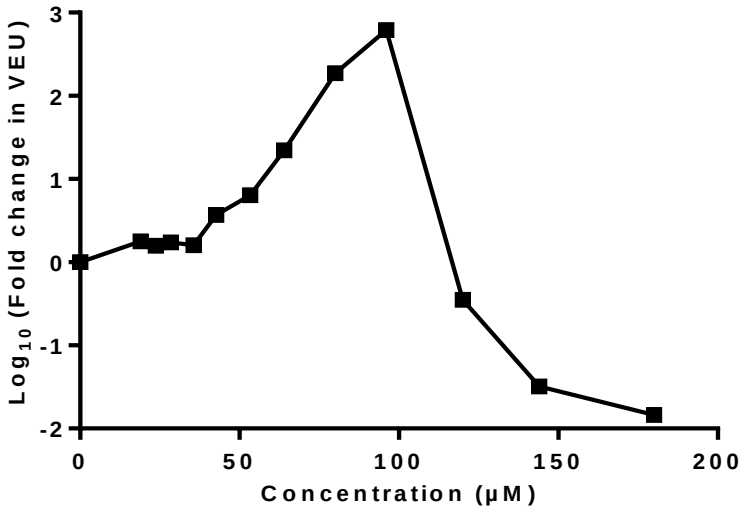
Log10 (Fold change in VEU)
Concentration (µM)

2.23

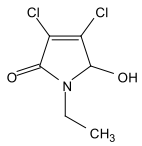
Cl
Cl
O
N
OH
CH3

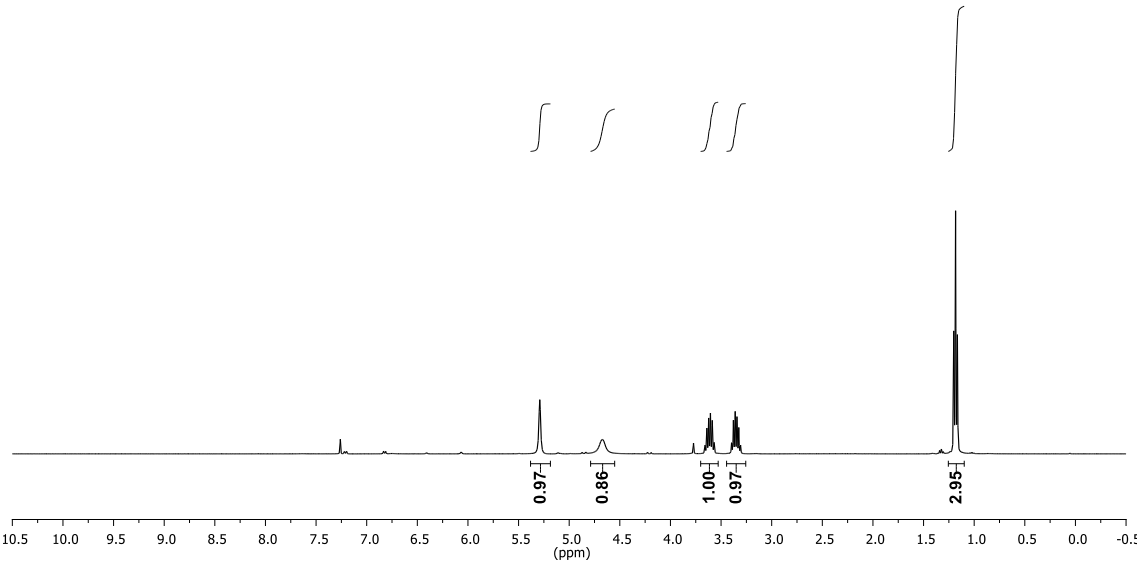
0.97
0.86
1.00
0.97
2.95
(ppm)

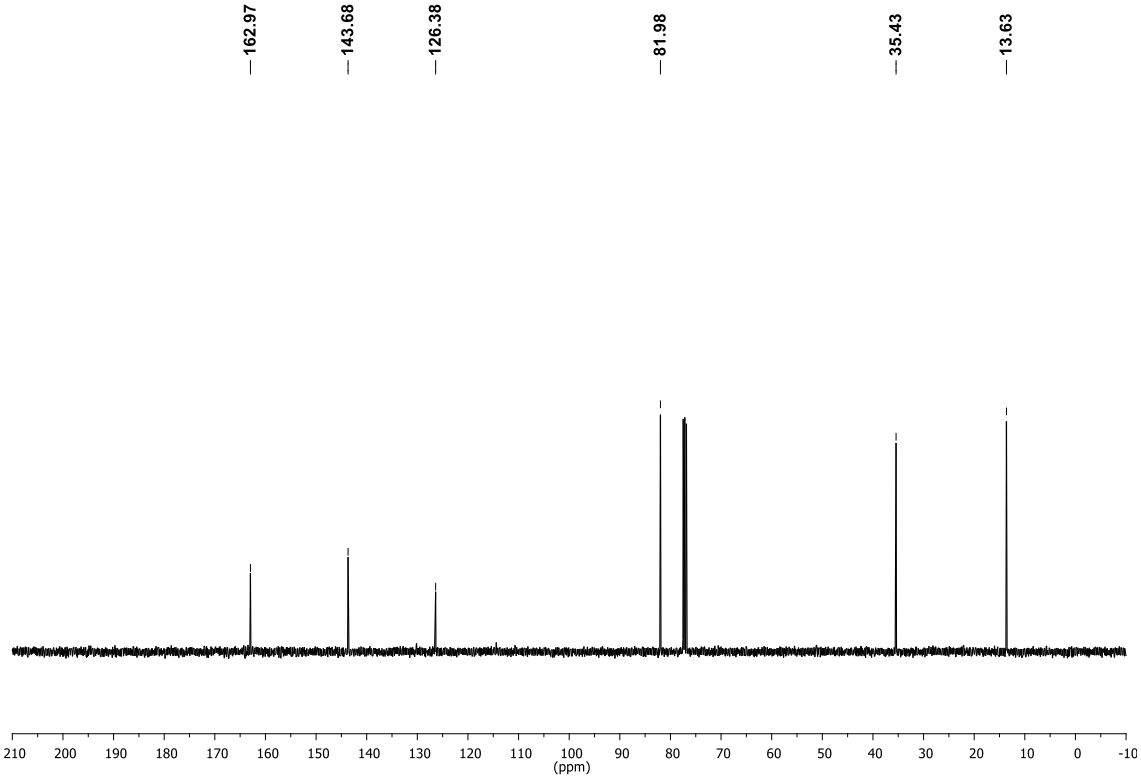
162.97
143.68
126.38
81.98
35.43
13.63
(ppm)

2.23

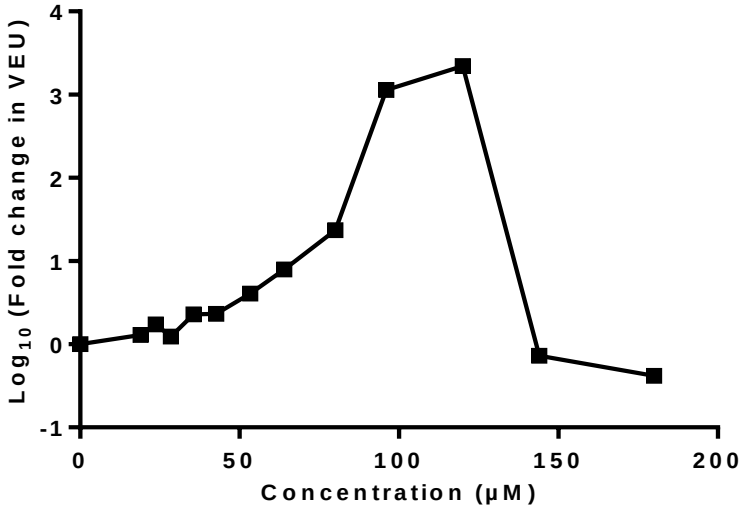
Log10 (Fold change in VEU)
4
3
2
1
0
-1
0
50
100
150
200
Concentration (µM)

2.24

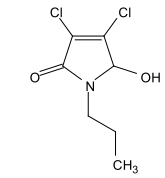
Cl
Cl
O
N
OH
CH3

0.93
0.92
1.01
1.00
2.04
3.03
(ppm)

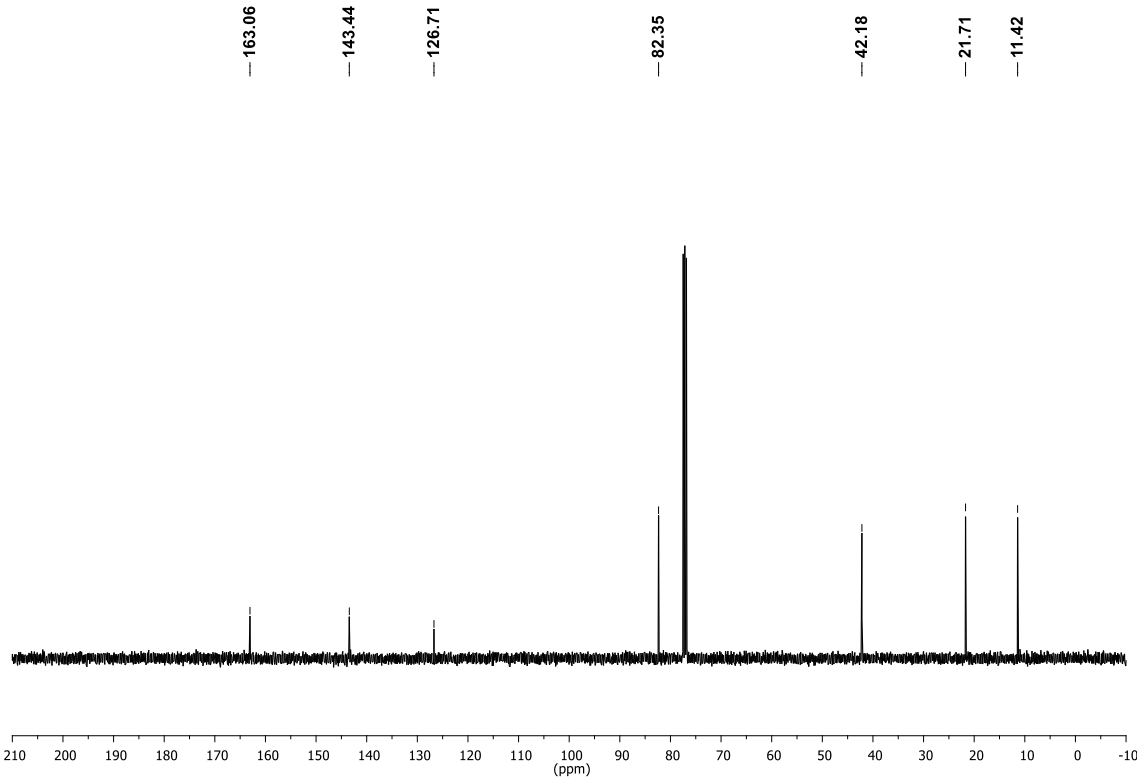
163.06
143.44
126.71
82.35
42.18
21.71
11.42
(ppm)

2.24

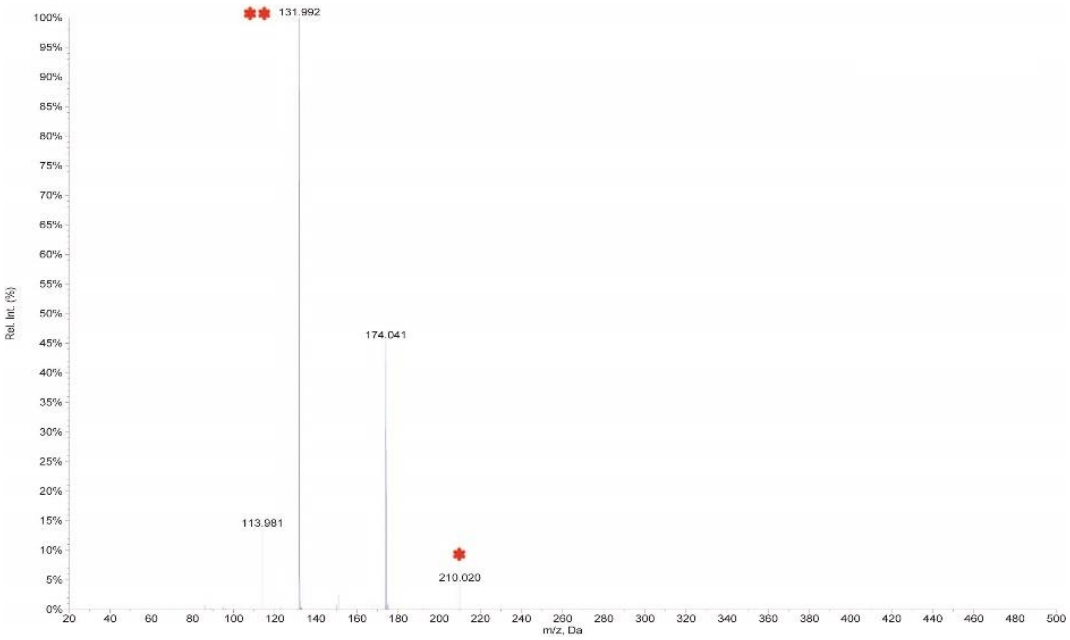
131.992
174.041
113.981
210.020
Rel. Int. (%)
m/z, Da

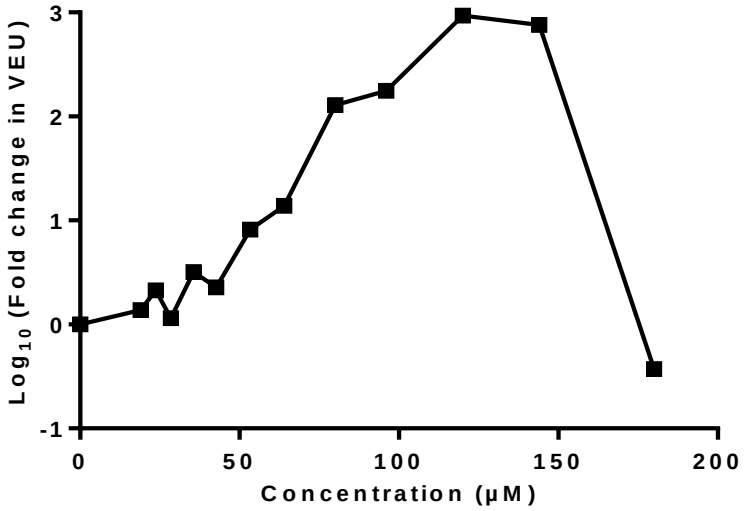
Log10 (Fold change in VEU)
Concentration (μM)

2.25

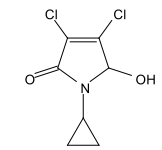
Cl
Cl
O
N
OH

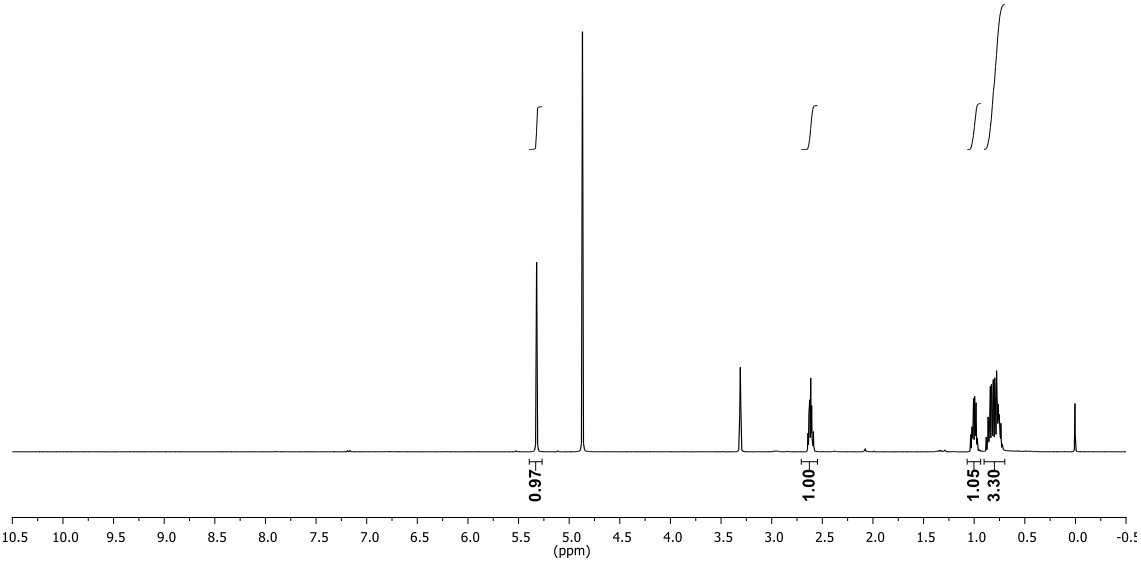
0.97
1.00
1.05
3.30
10.5 10.0 9.5 9.0 8.5 8.0 7.5 7.0 6.5 6.0 5.5 5.0 4.5 4.0 3.5 3.0 2.5 2.0 1.5 1.0 0.5 0.0
(ppm)

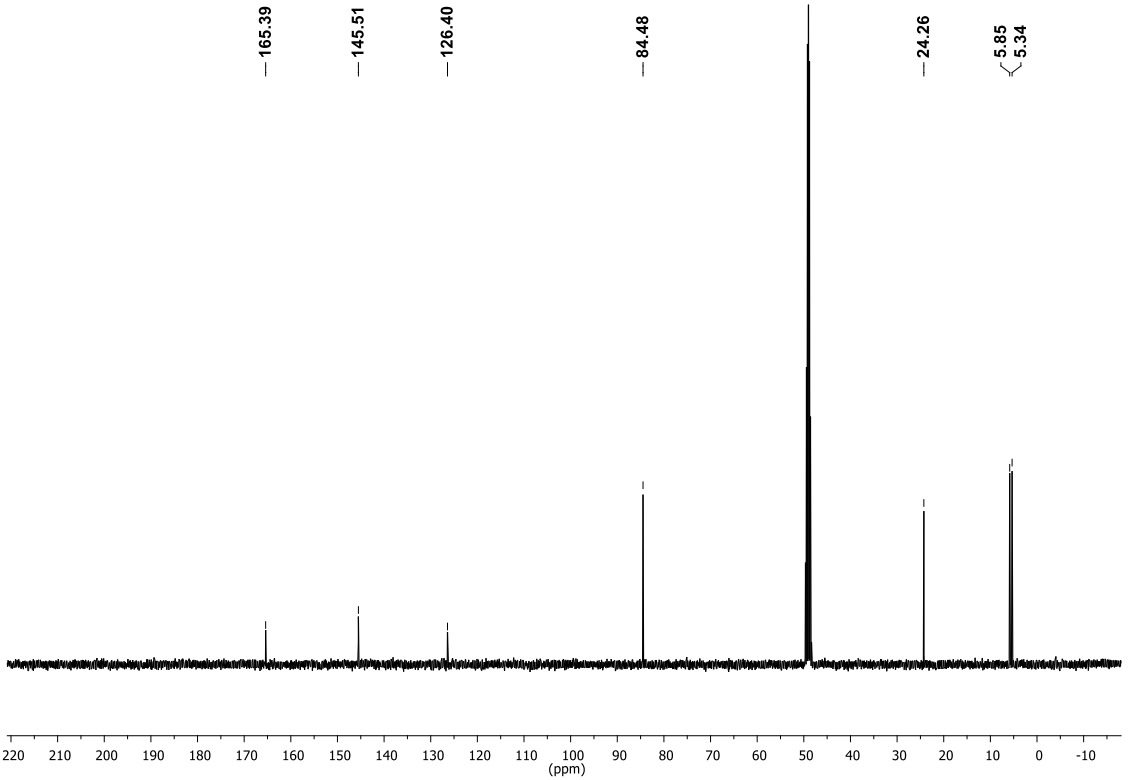
165.39
145.51
126.40
84.48
24.26
5.85
5.34
220 210 200 190 180 170 160 150 140 130 120 110 100 90 80 70 60 50 40 30 20 10 0 -10
(ppm)

2.25

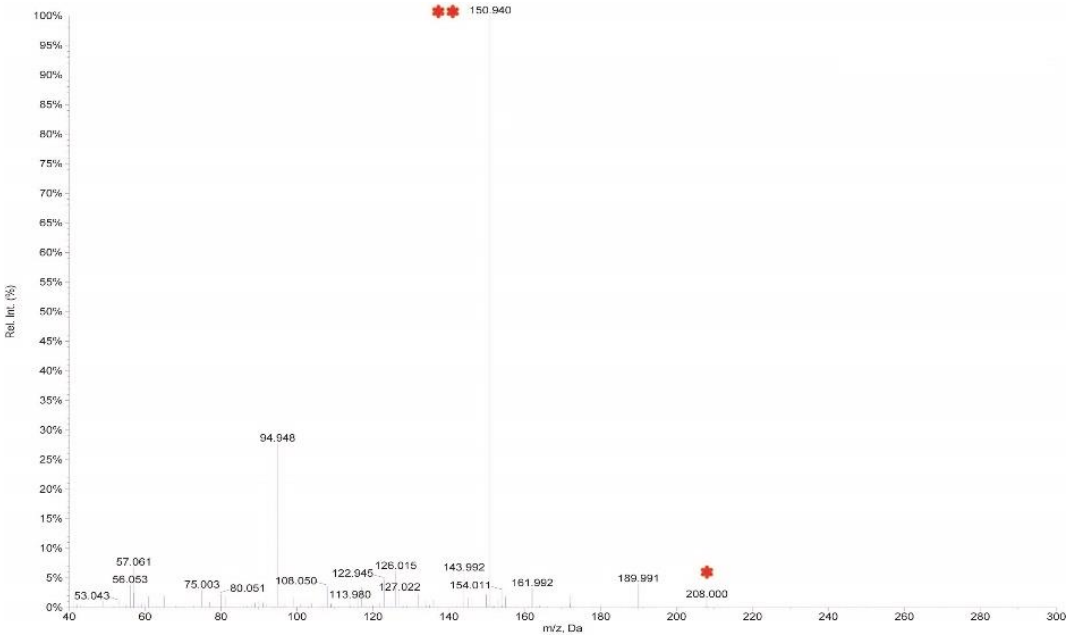
150.940
94.948
57.061
56.053
53.043
75.003
80.051
108.050
113.980
122.945
126.015
127.022
143.992
154.011
161.992
189.991
208.000
Rel. Int. (%)
m/z, Da

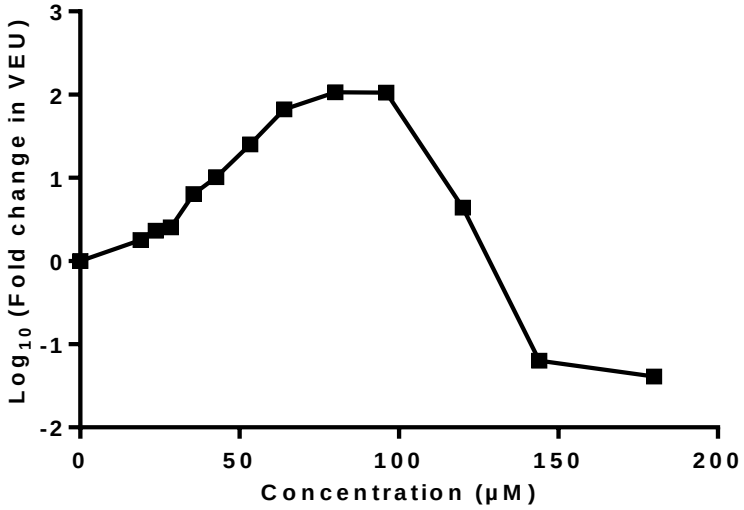
Log10 (Fold change in VEU)
Concentration (μM)

2.26

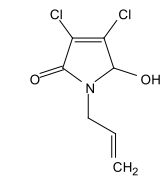
Cl
Cl
O
N
OH
CH2

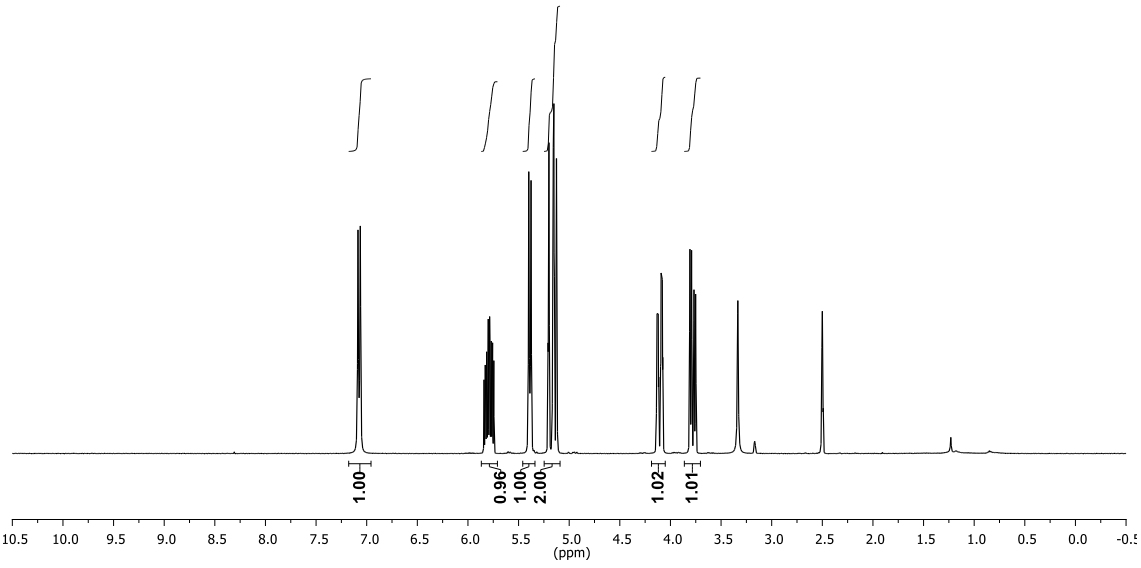
1.00
0.96
1.00
2.00
1.02
1.01
10.5 10.0 9.5 9.0 8.5 8.0 7.5 7.0 6.5 6.0 5.5 5.0 4.5 4.0 3.5 3.0 2.5 2.0 1.5 1.0 0.5 0.0
(ppm)

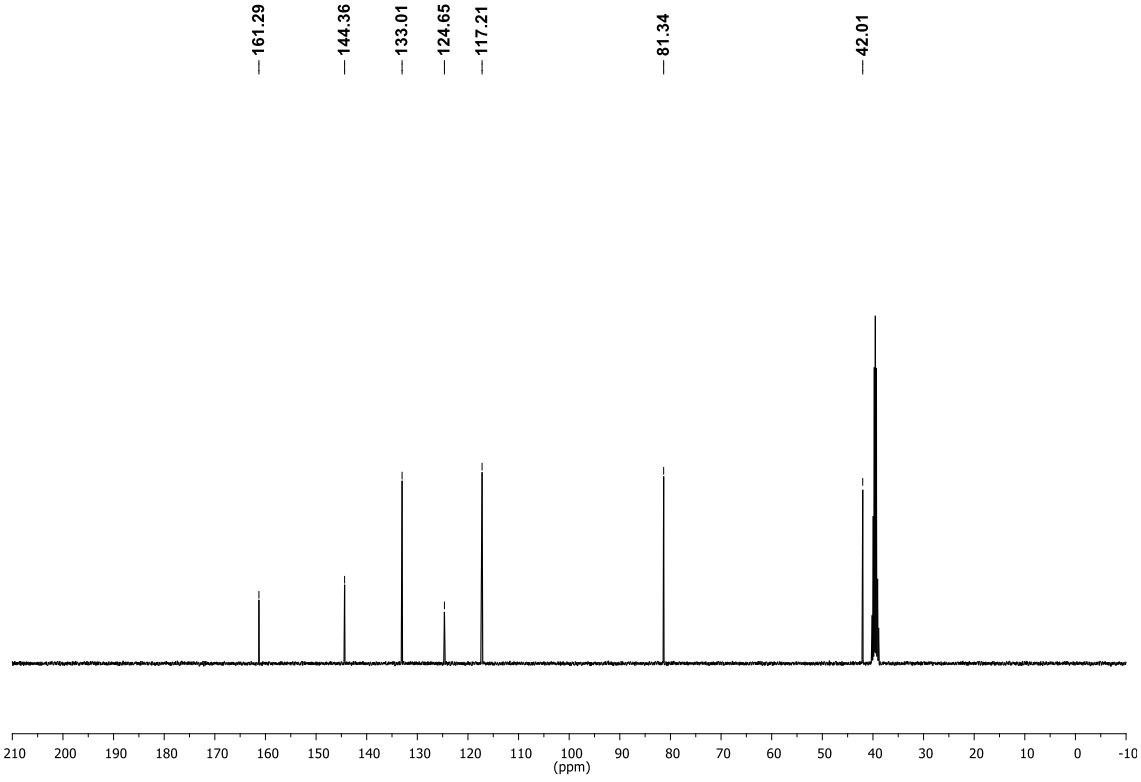
161.29
144.36
133.01
124.65
117.21
81.34
42.01
210 200 190 180 170 160 150 140 130 120 110 100 90 80 70 60 50 40 30 20 10 0
(ppm)

2.26

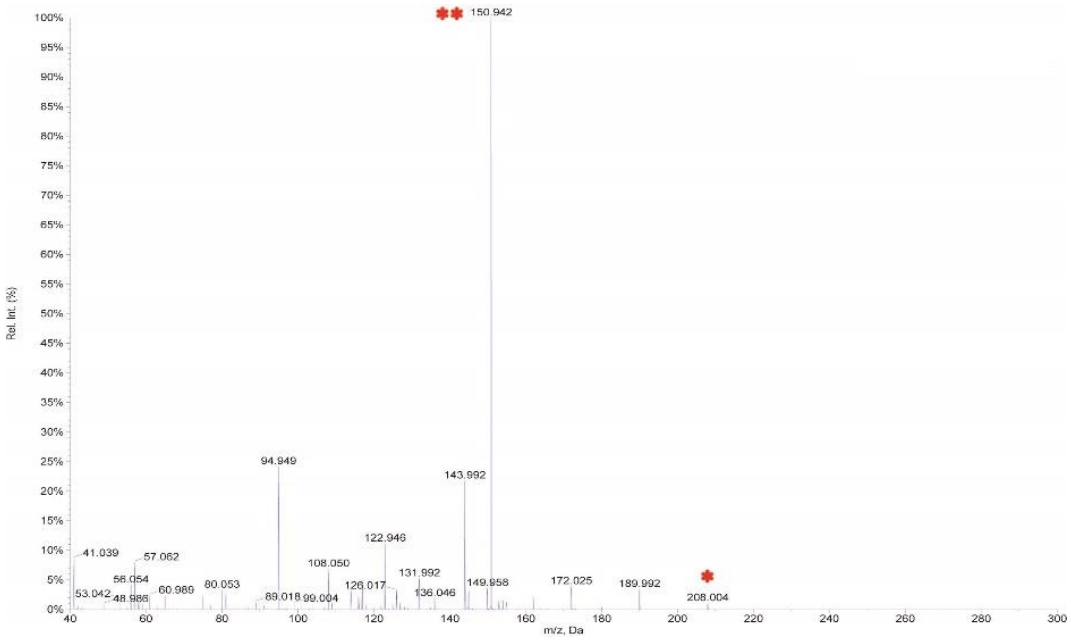
150.942
94.949
143.992
122.946
41.039
57.062
108.050
131.992
56.054
126.017
149.958
172.025
189.992
208.004
53.042
48.986
60.989
80.053
89.018
99.004
136.046
Rel. Int. (%)
m/z, Da

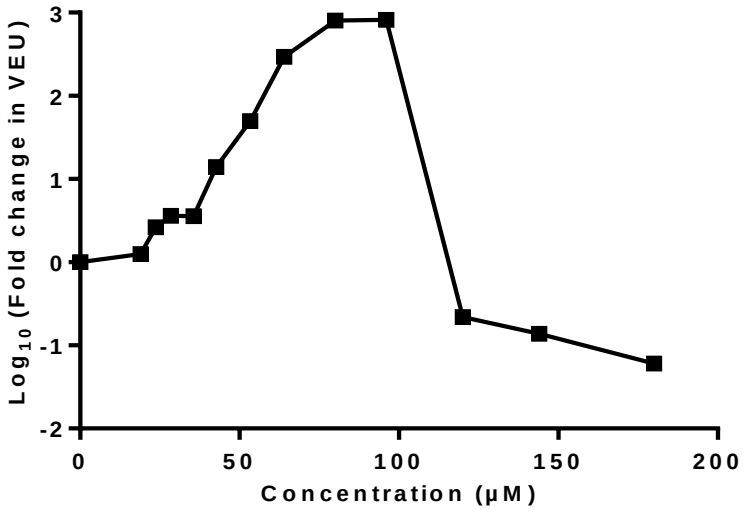
Log10 (Fold change in VEU)
Concentration (µM)

2.27

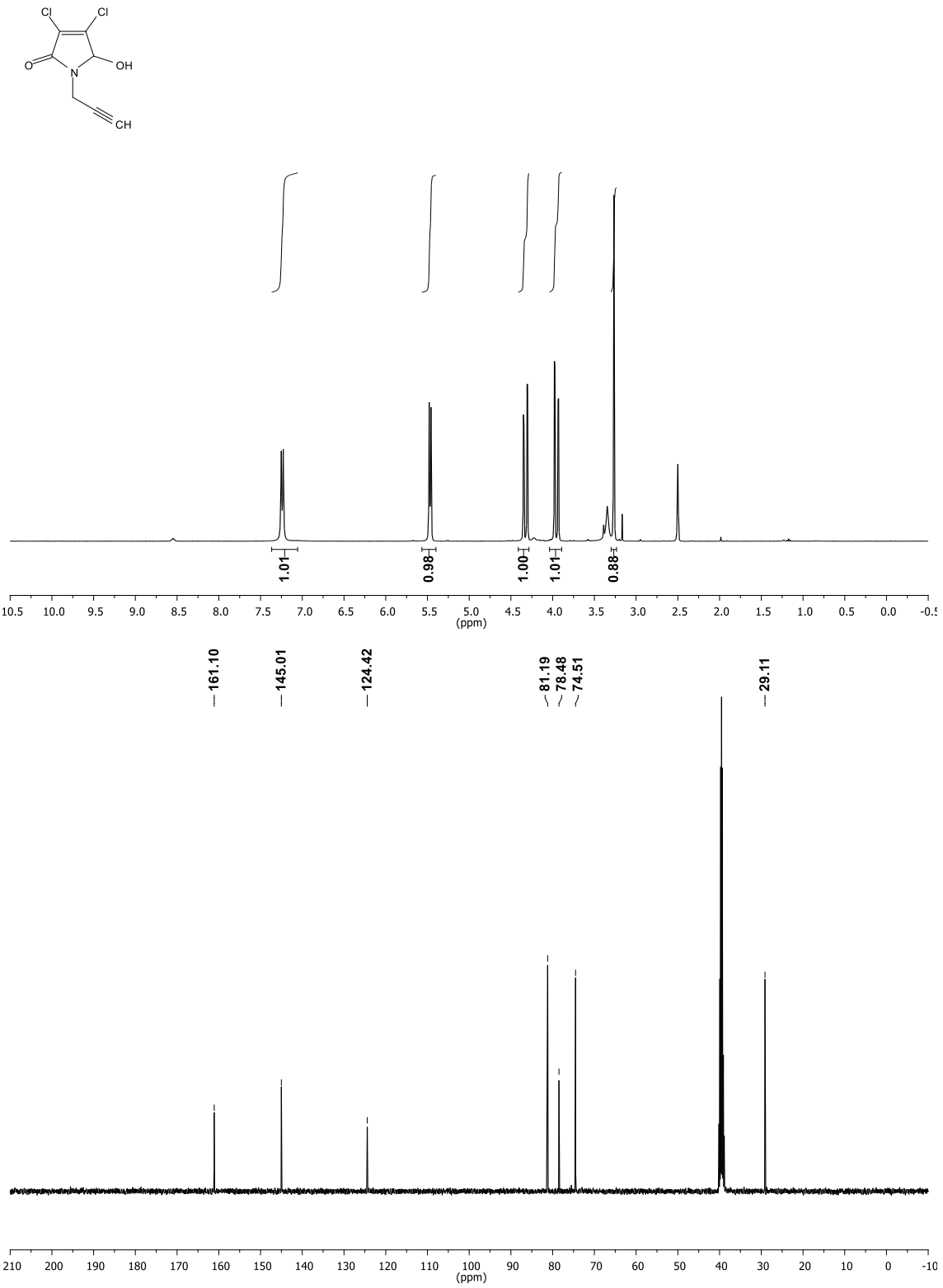
Cl
Cl
O
N
OH
CH
1.01
0.98
1.00
1.01
0.88
(ppm)
161.10
145.01
124.42
81.19
78.48
74.51
29.11
(ppm)

2.27

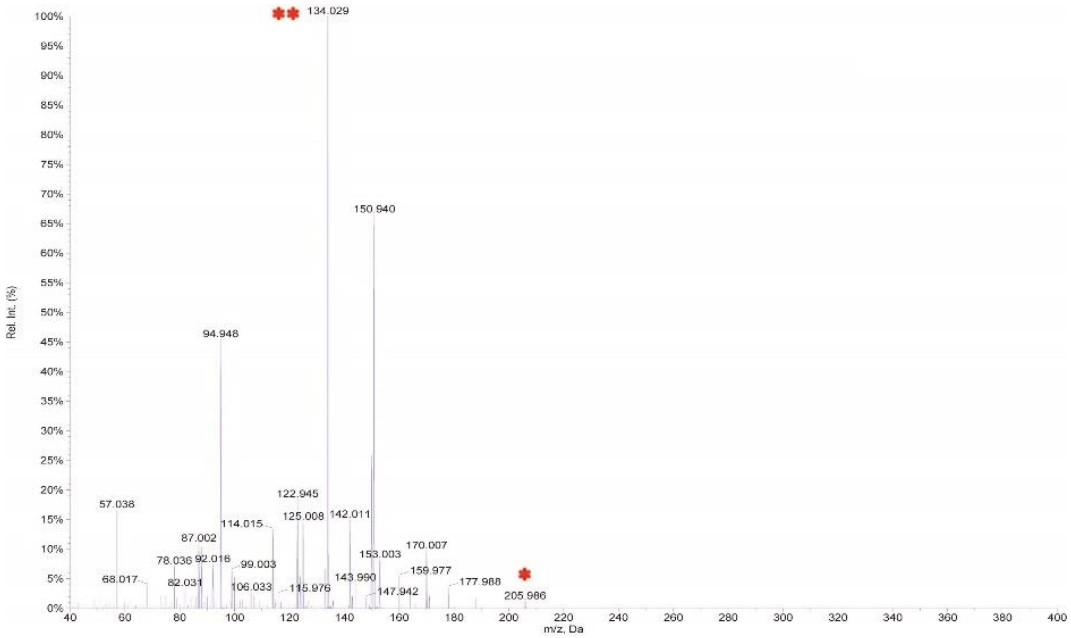
134.029
150.940
94.948
122.945
125.008
142.011
114.015
57.038
87.002
153.003
170.007
78.036
92.018
99.003
159.977
68.017
82.031
106.033
115.976
143.990
147.942
177.988
205.986
Rel. Int. (%)
m/z, Da

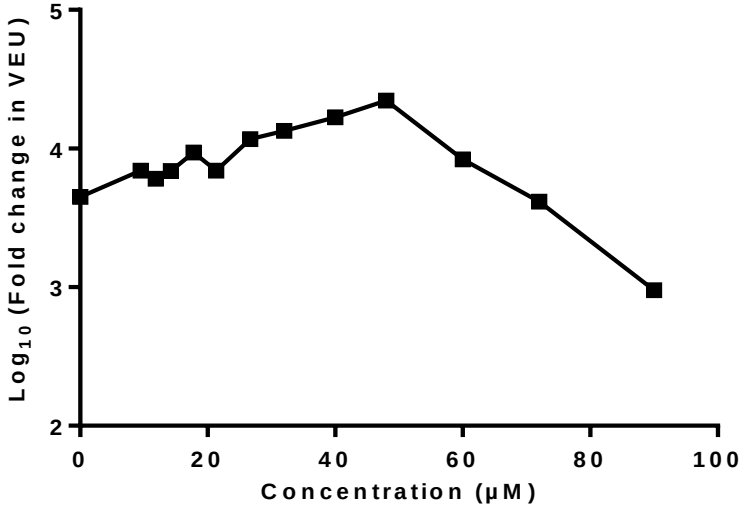
Log10 (Fold change in VEU)
Concentration (μM)

2.28

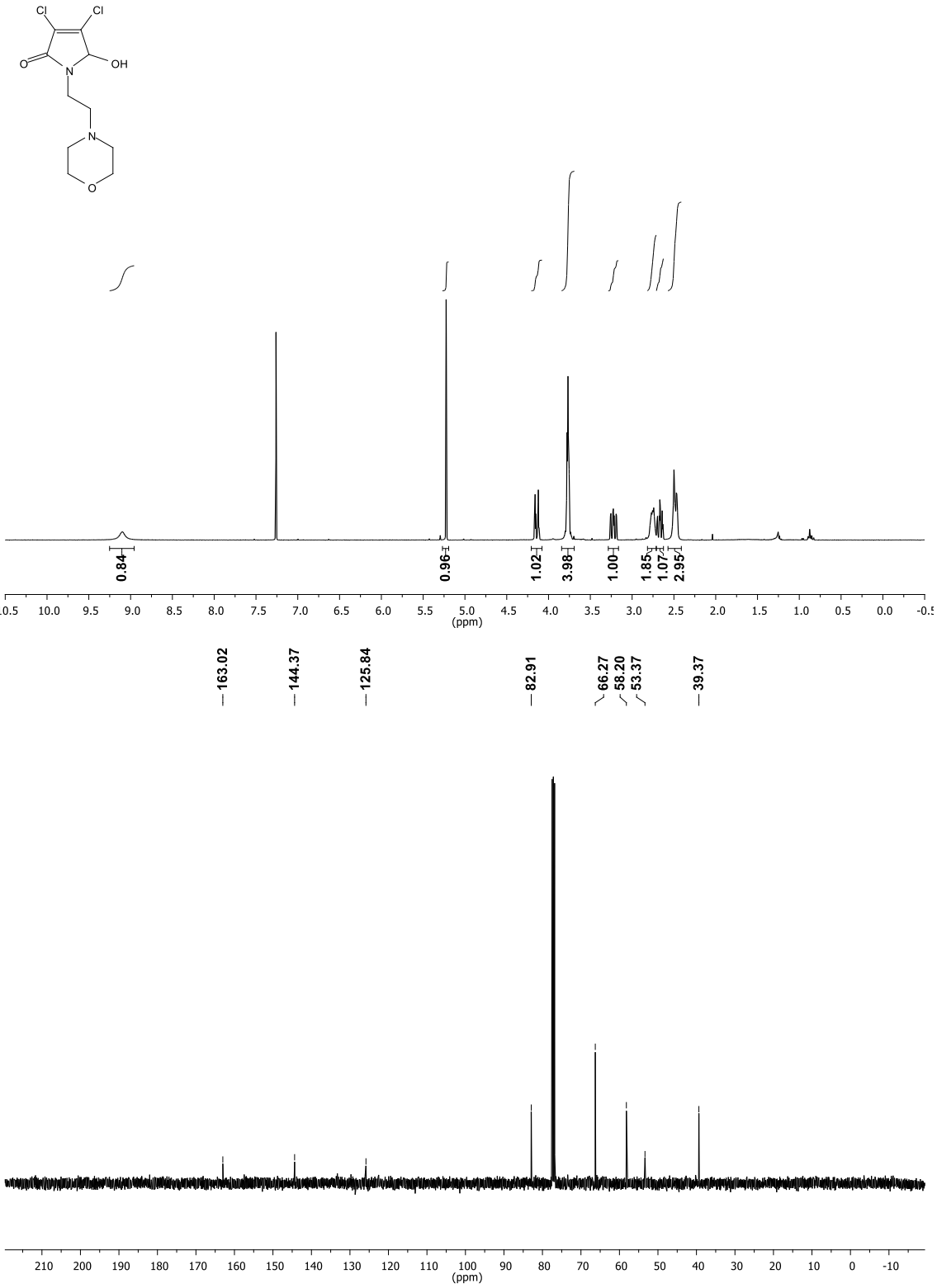
Cl
Cl
O
N
OH
N
O
0.84
0.96
1.02
3.98
1.00
1.85
1.07
2.95
(ppm)
163.02
144.37
125.84
82.91
66.27
58.20
53.37
39.37
(ppm)

2.28

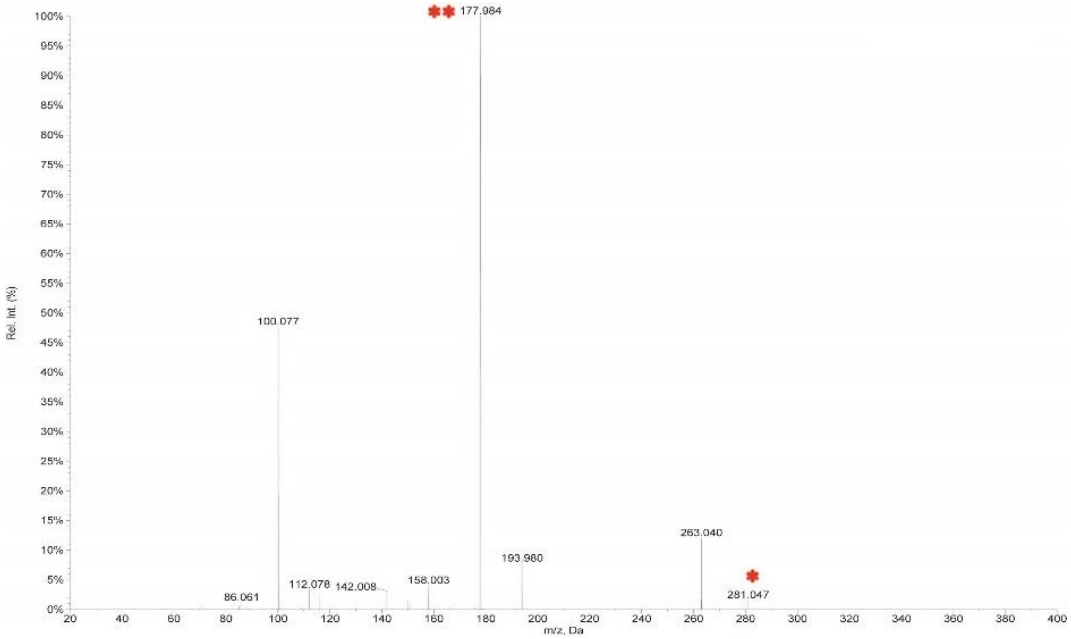
177.984
100.077
263.040
193.980
281.047
112.078
142.008
158.003
86.061
Rel. Int. (%)
m/z, Da

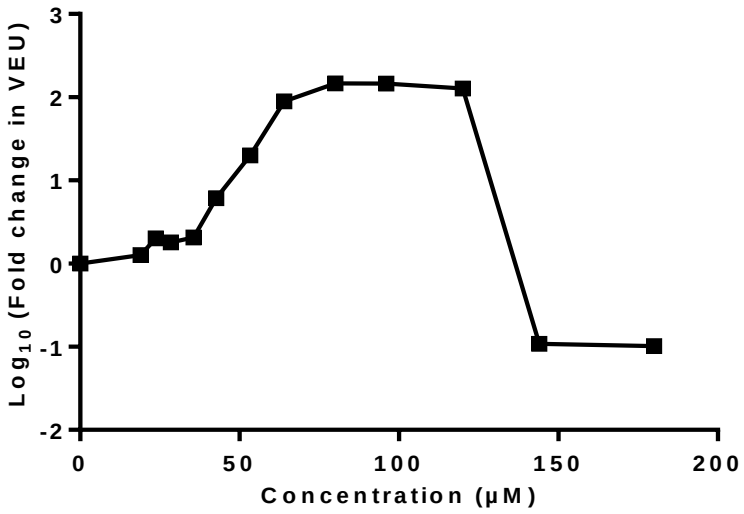
Log10 (Fold change in VEU)
Concentration (μM)

2.29

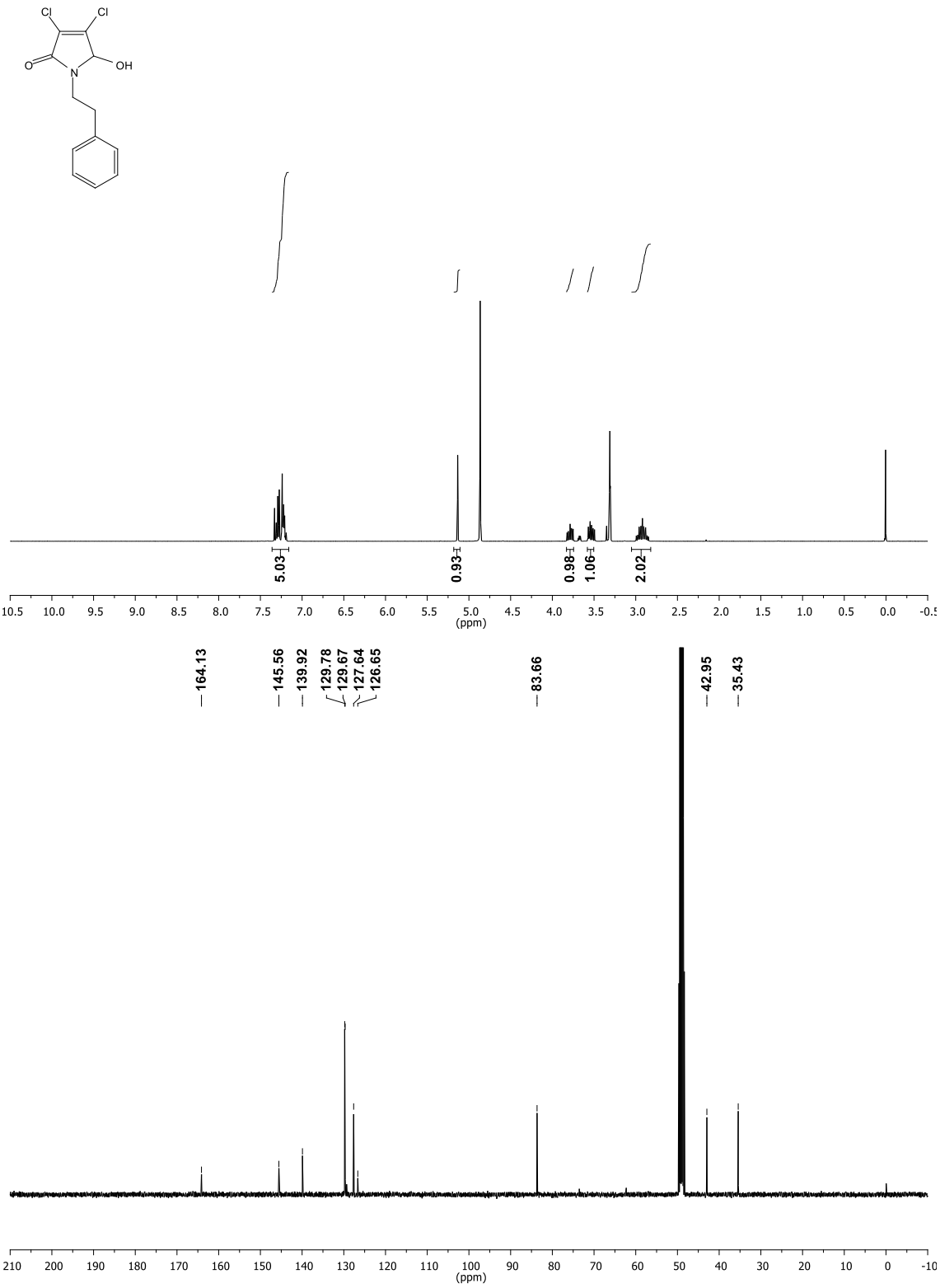
Cl
Cl
O
N
OH
5.03
0.93
0.98
1.06
2.02
(ppm)
164.13
145.56
139.92
129.78
129.67
127.64
126.65
83.66
42.95
35.43
(ppm)

2.29

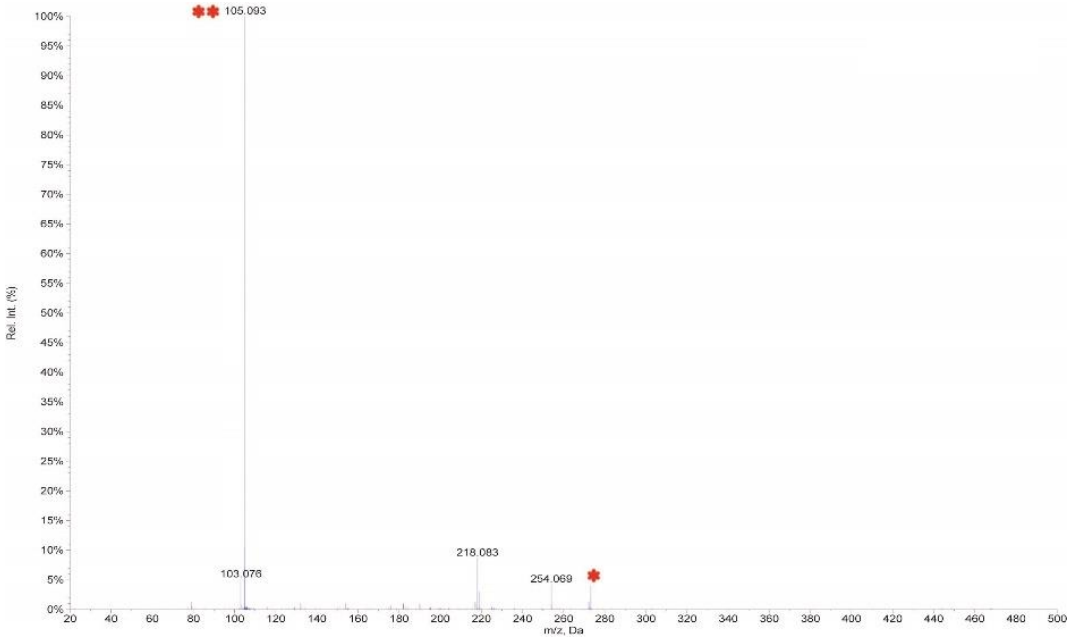
105.093
103.076
218.083
254.069
Rel. Int. (%)
m/z, Da

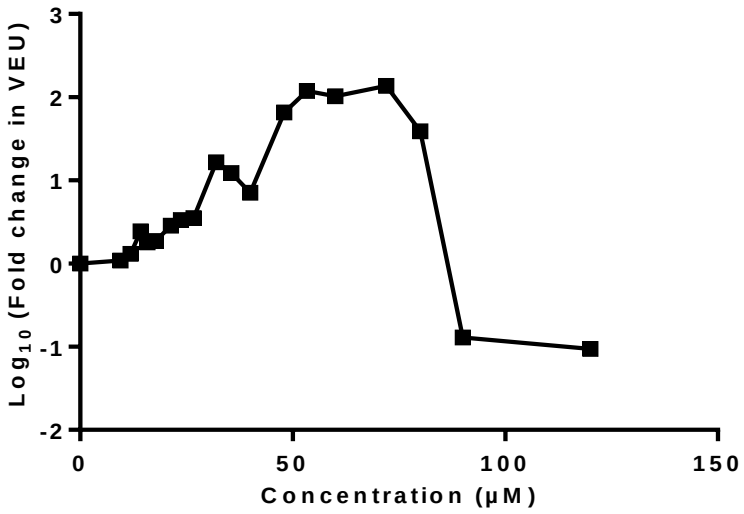
Log10 (Fold change in VEU)
Concentration (µM)

2.30

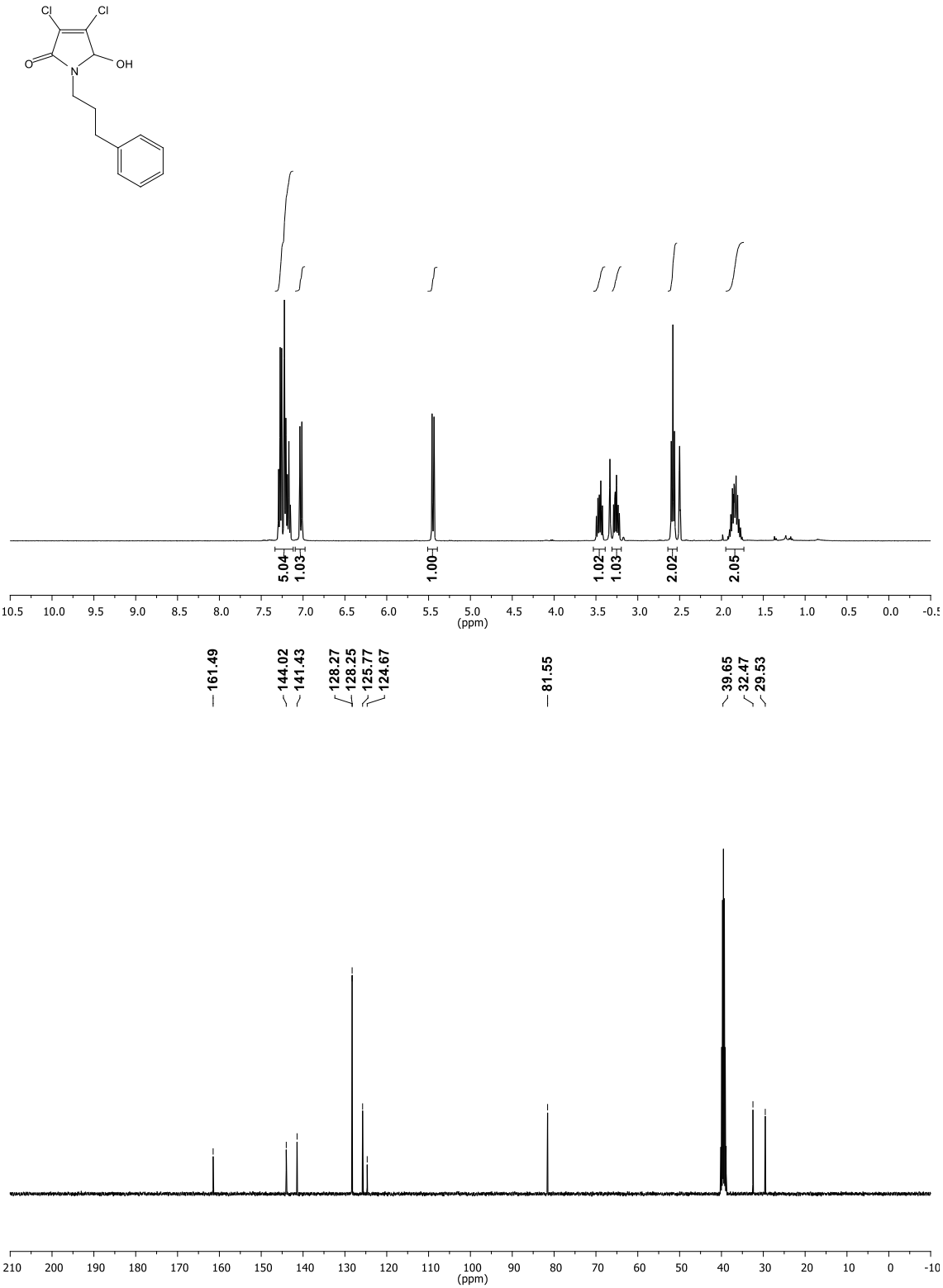
Cl
Cl
O
N
OH
5.04
1.03
1.00
1.02
1.03
2.02
2.05
(ppm)
161.49
144.02
141.43
128.27
128.25
125.77
124.67
81.55
39.65
32.47
29.53
(ppm)

2.30

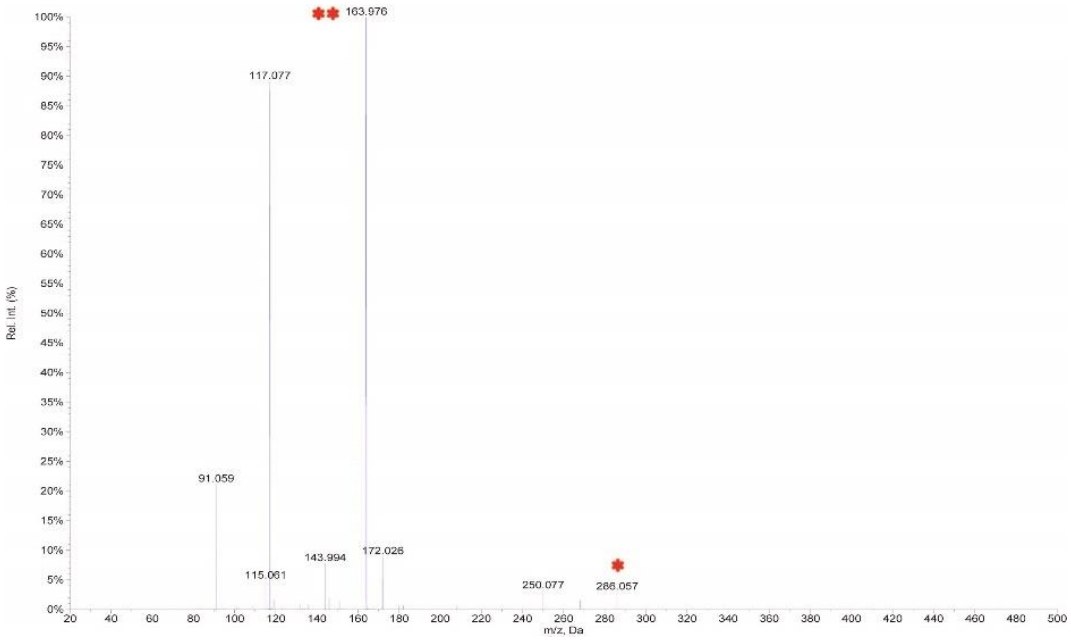
163.976
117.077
91.059
115.061
143.994
172.028
250.077
286.057
Rel. Int. (%)
m/z, Da

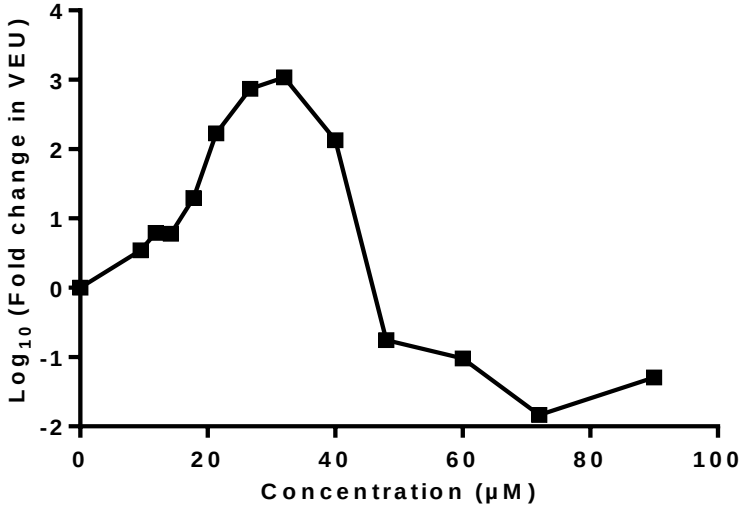
Log10 (Fold change in VEU)
Concentration (μM)

2.31

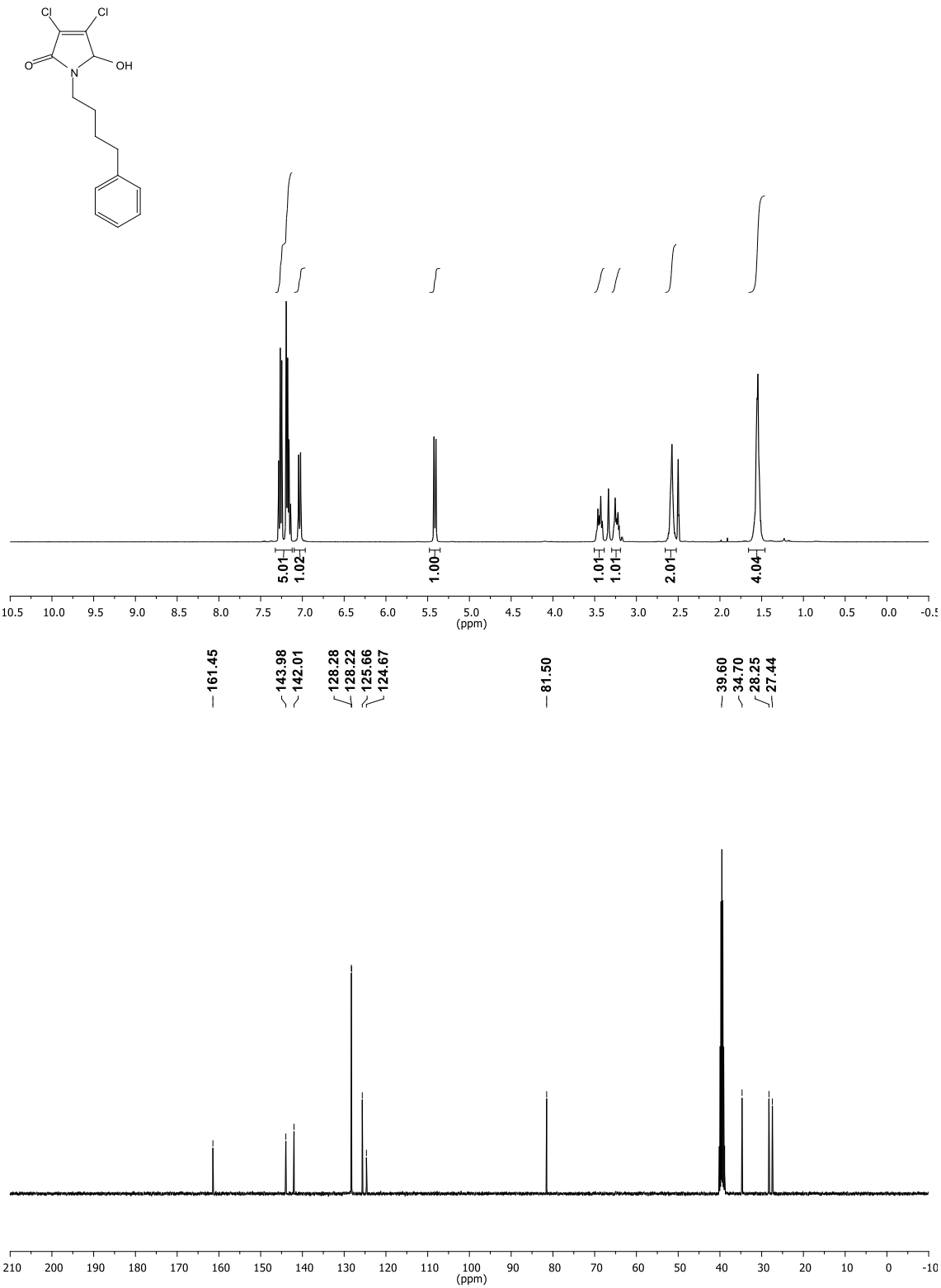
Cl
Cl
O
N
OH
5.01
1.02
1.00
1.01
1.01
2.01
4.04
(ppm)
161.45
143.98
142.01
128.28
128.22
125.66
124.67
81.50
39.60
34.70
28.25
27.44
(ppm)

2.31

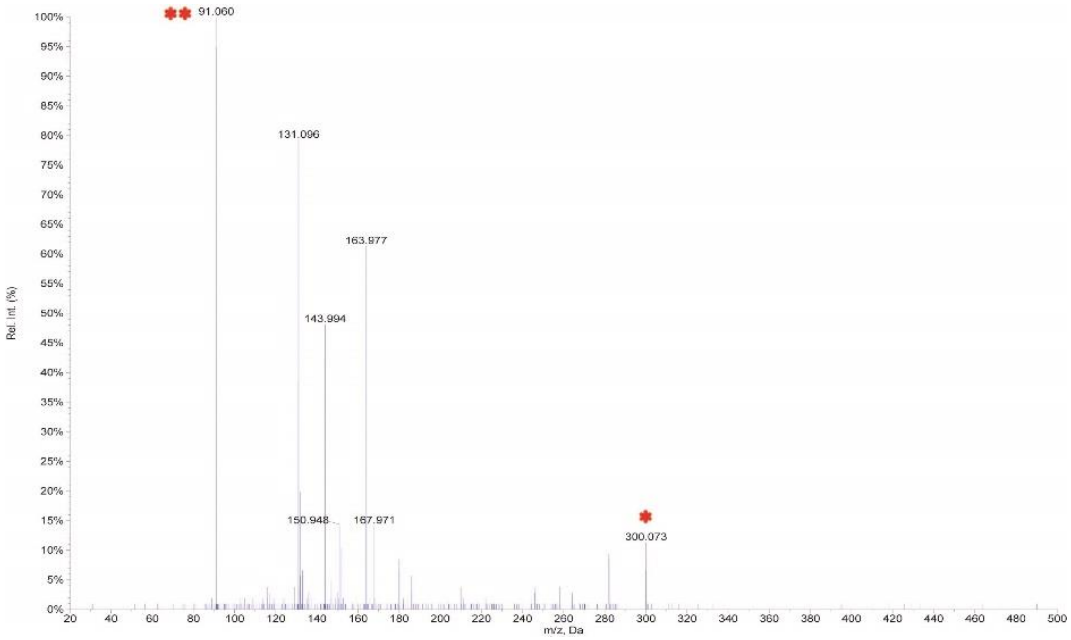
91.060
131.096
163.977
143.994
150.948
167.971
300.073
Rel. Int. (%)
m/z, Da

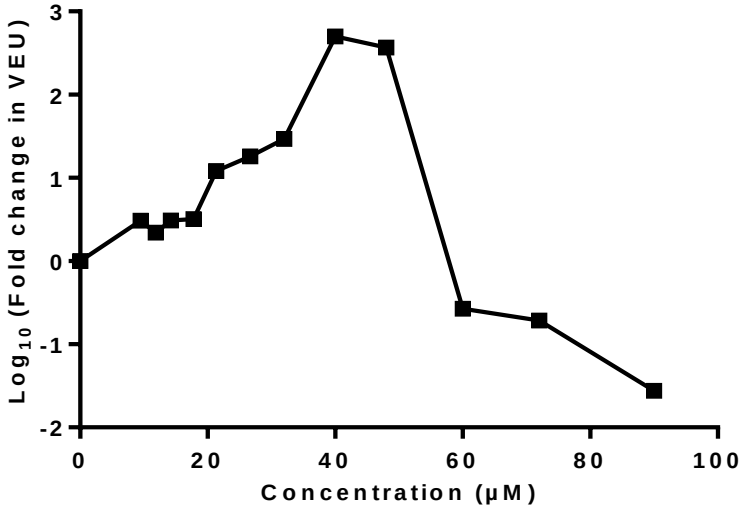
Log10 (Fold change in VEU)
Concentration (μM)

2.32

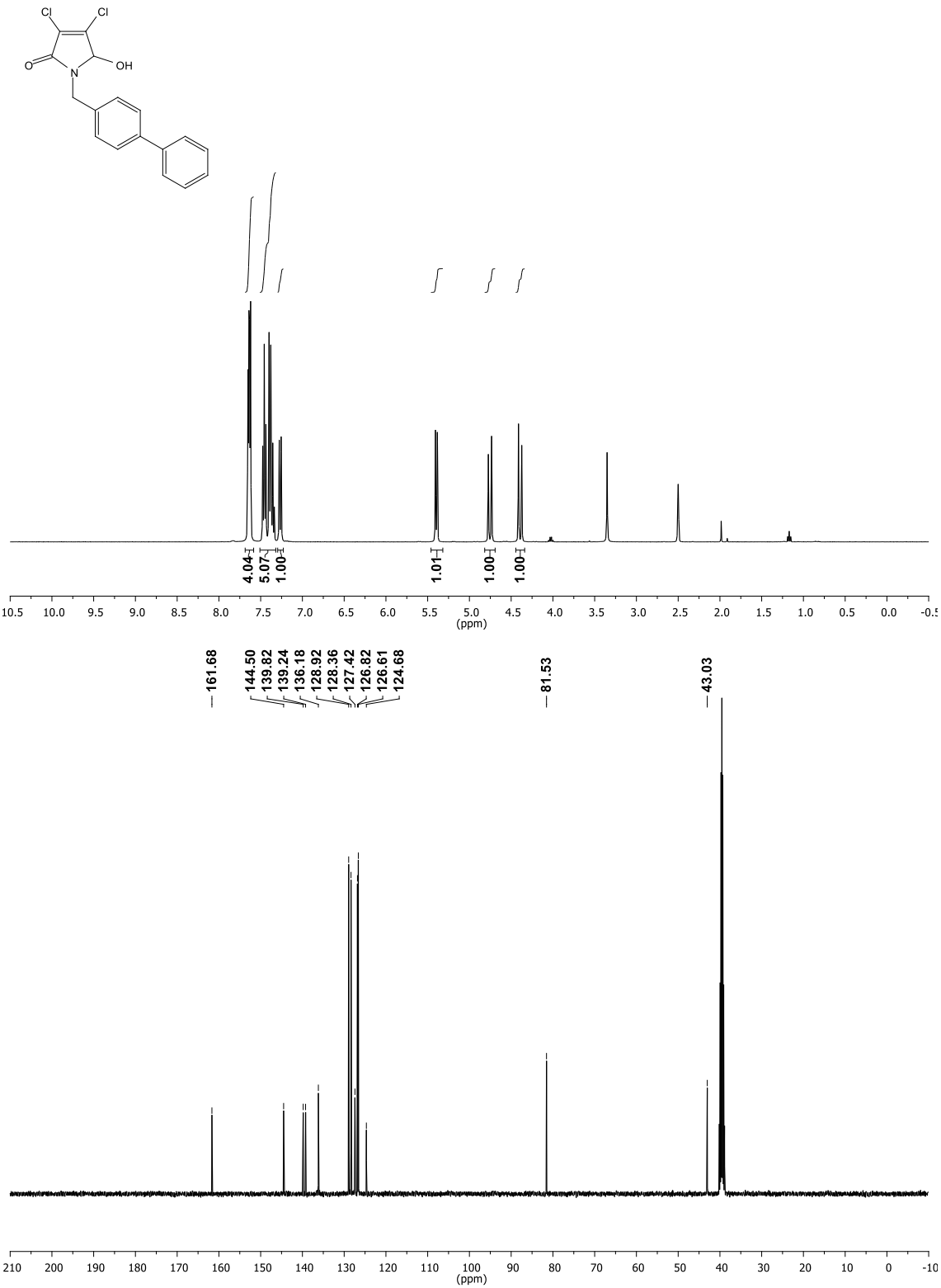
Cl
Cl
O
N
OH
4.04
5.07
1.00
1.01
1.00
1.00
(ppm)
161.68
144.50
139.82
139.24
136.18
128.92
128.36
127.42
126.82
126.61
124.68
81.53
43.03
(ppm)

2.32

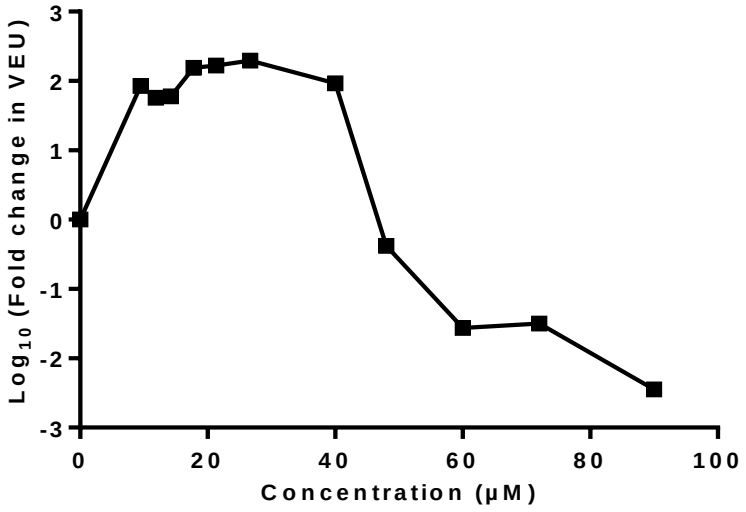
Log10 (Fold change in VEU)
3
2
1
0
-1
-2
-3
0
20
40
60
80
100
Concentration (µM)

2.33

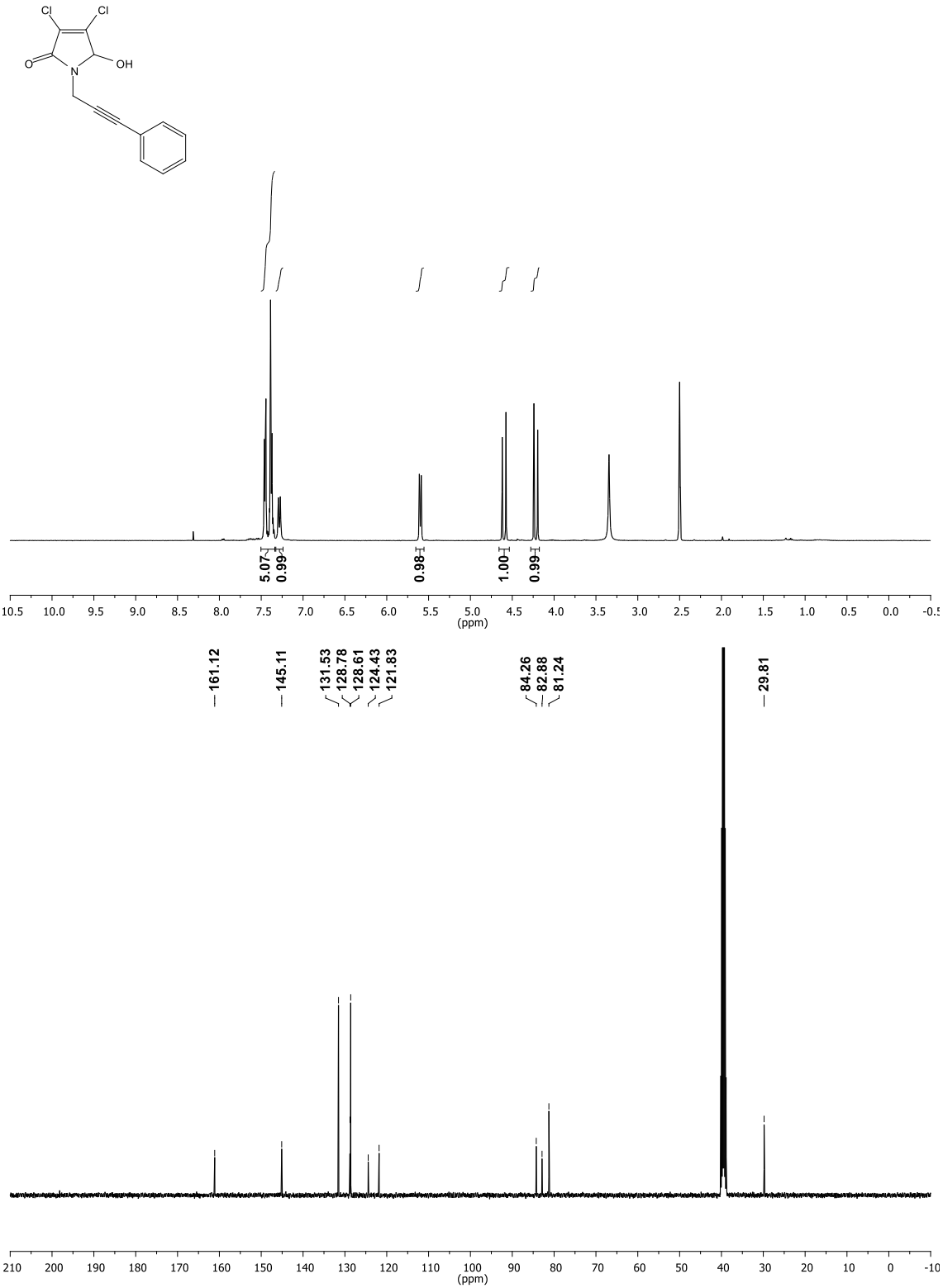
Cl
Cl
O
N
OH
5.07
0.99
0.98
1.00
0.99
(ppm)
161.12
145.11
131.53
128.78
128.61
124.43
121.83
84.26
82.88
81.24
29.81
(ppm)

2.33

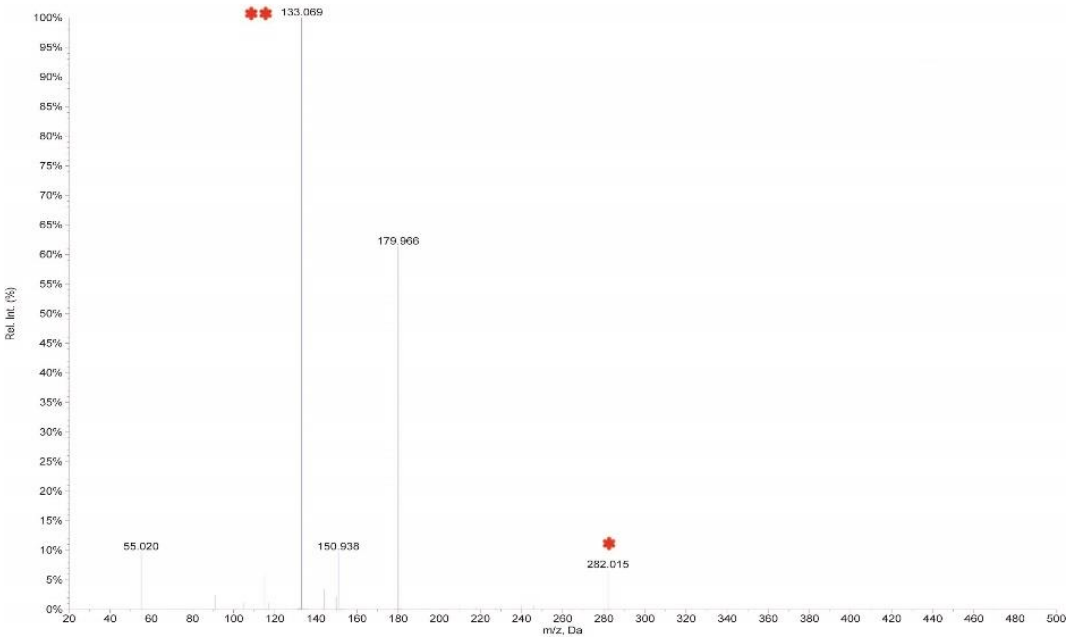
133.069
179.966
55.020
150.938
282.015
Rel. Int. (%)
m/z, Da

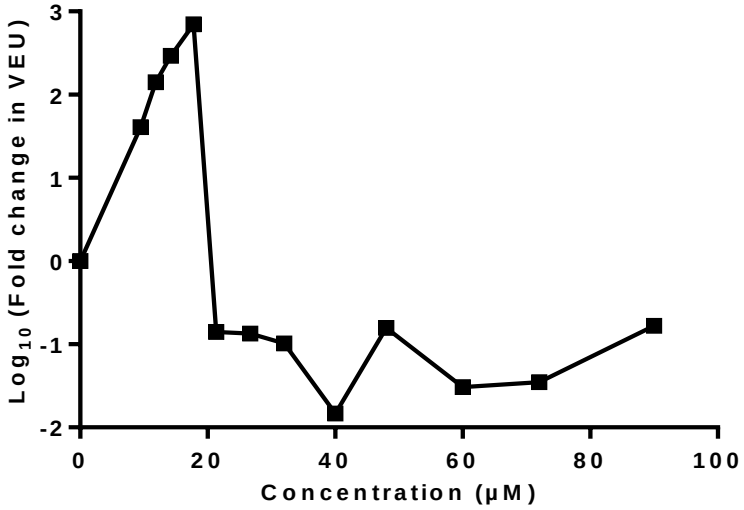
Log10 (Fold change in VEU)
Concentration (μM)

2.34

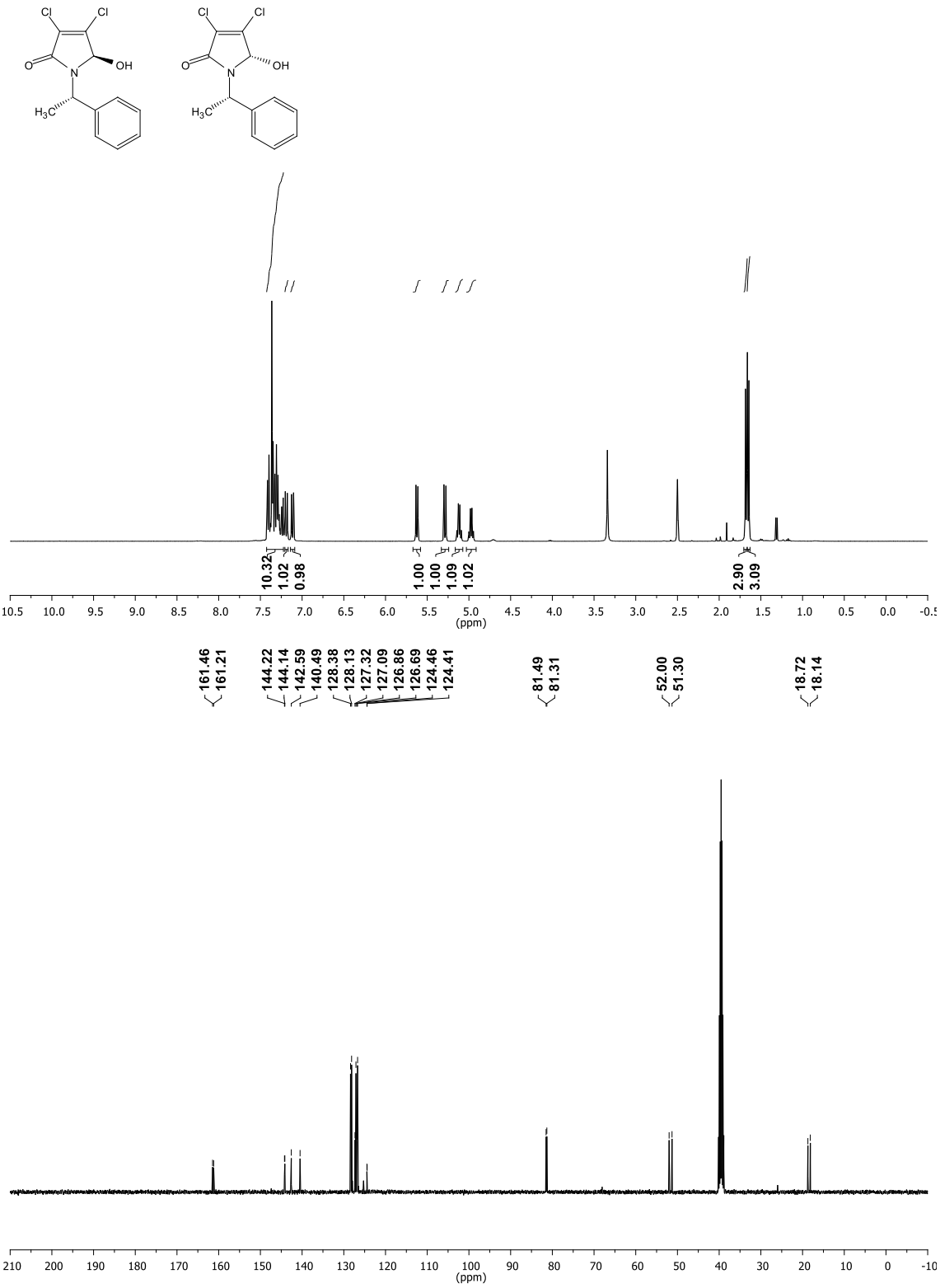
Cl
Cl
O
N
OH
H3C
10.32
1.02
0.98
1.00
1.00
1.09
1.02
2.90
3.09
(ppm)
161.46
161.21
144.22
144.14
142.59
140.49
128.38
128.13
127.32
127.09
126.86
126.69
124.46
124.41
81.49
81.31
52.00
51.30
18.72
18.14
(ppm)

2.34

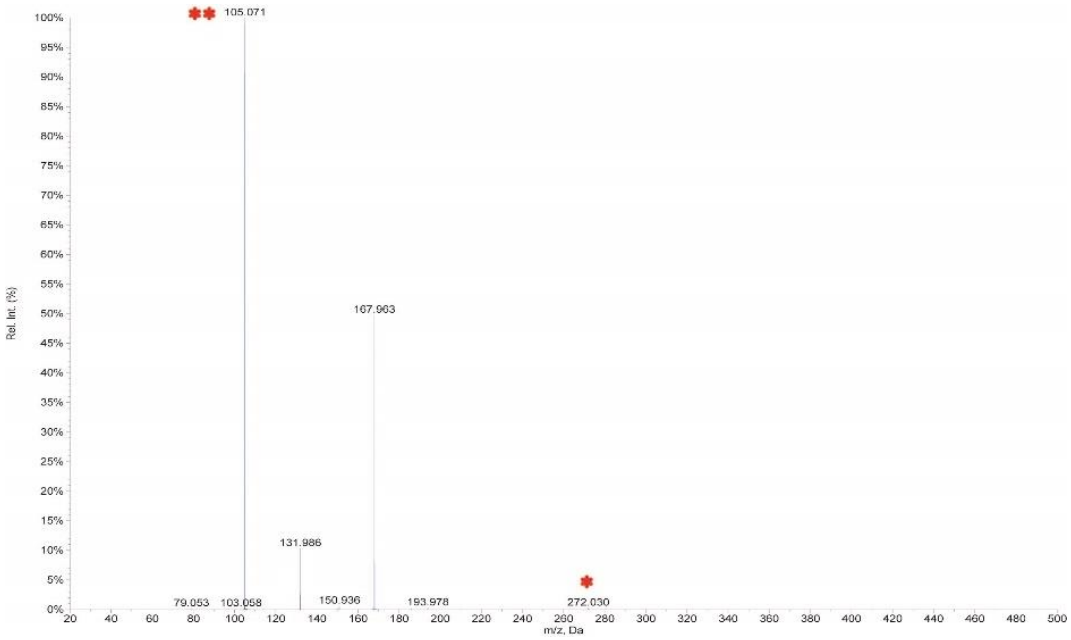
105.071
167.963
131.986
79.053
103.058
150.936
193.978
272.030
Rel. Int. (%)
m/z, Da

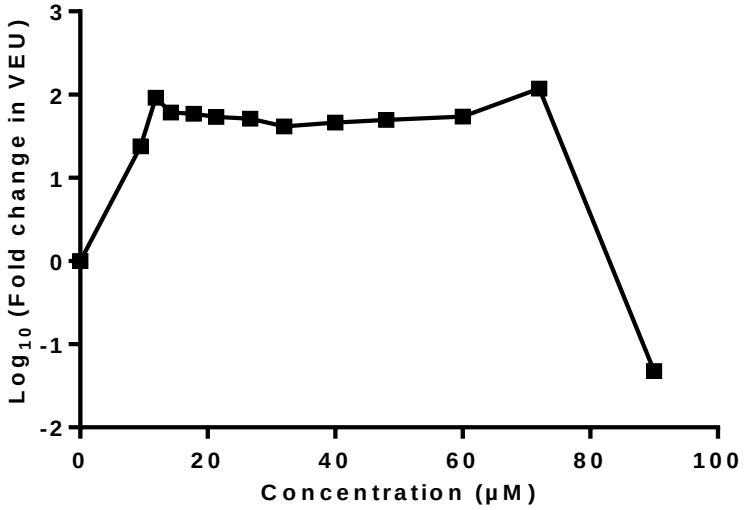
Log10 (Fold change in VEU)
Concentration (μM)

2.35

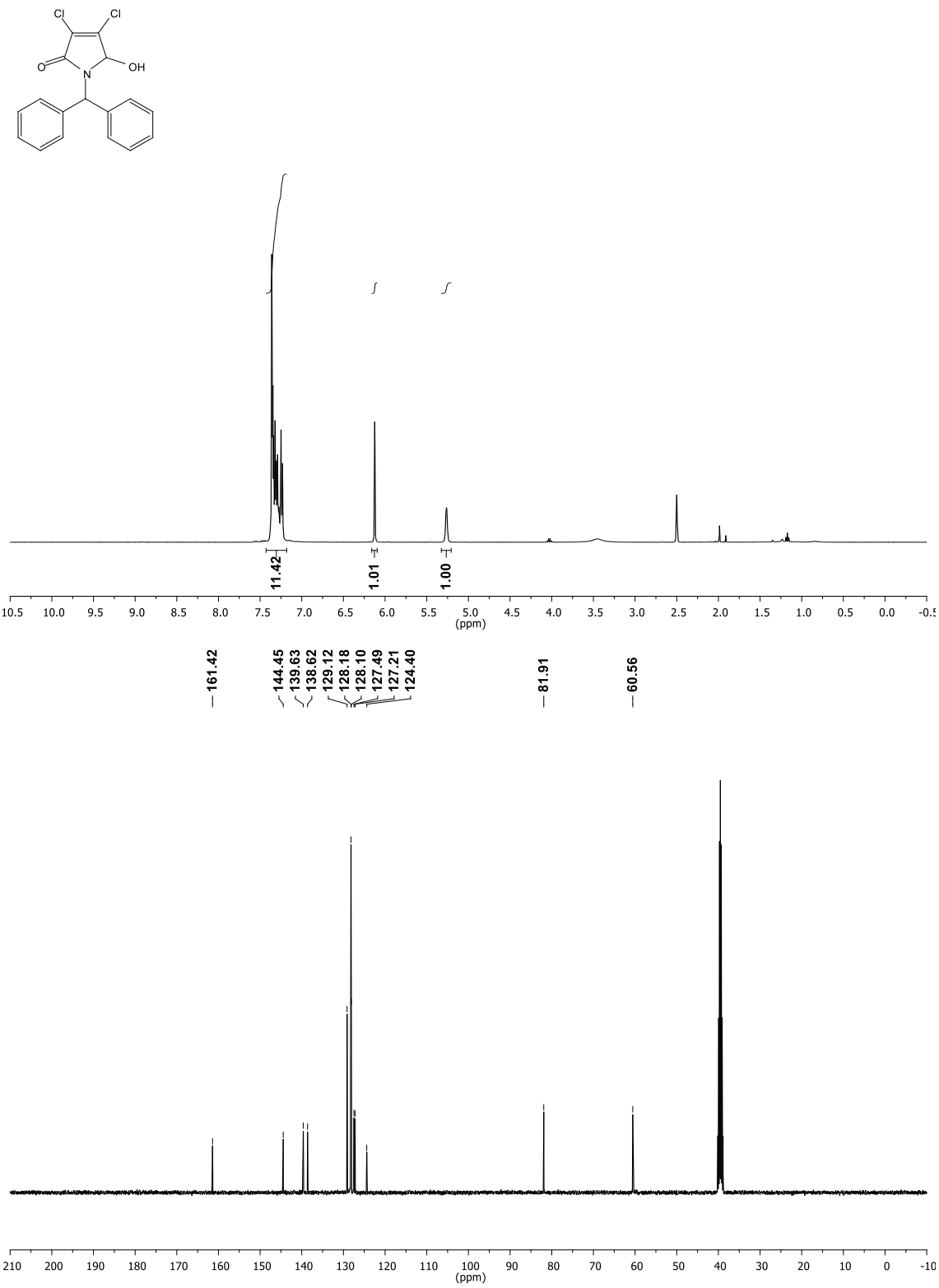
Cl
Cl
O
N
OH
11.42
1.01
1.00
(ppm)
161.42
144.45
139.63
138.62
129.12
128.18
128.10
127.49
127.21
124.40
81.91
60.56
(ppm)

2.35

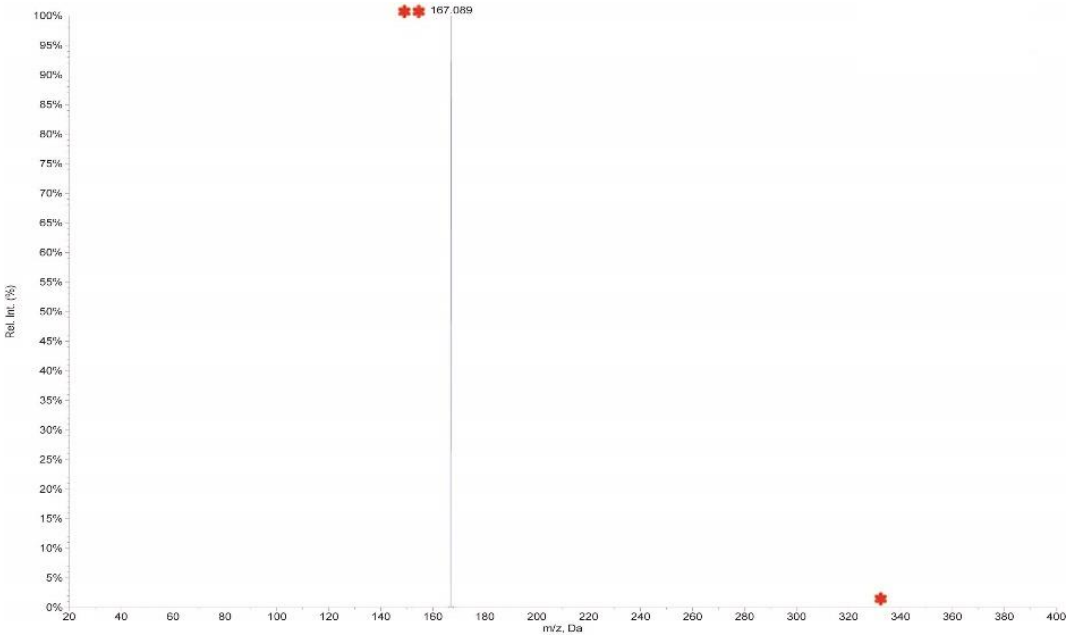
167.089
Rel. Int. (%)
m/z, Da

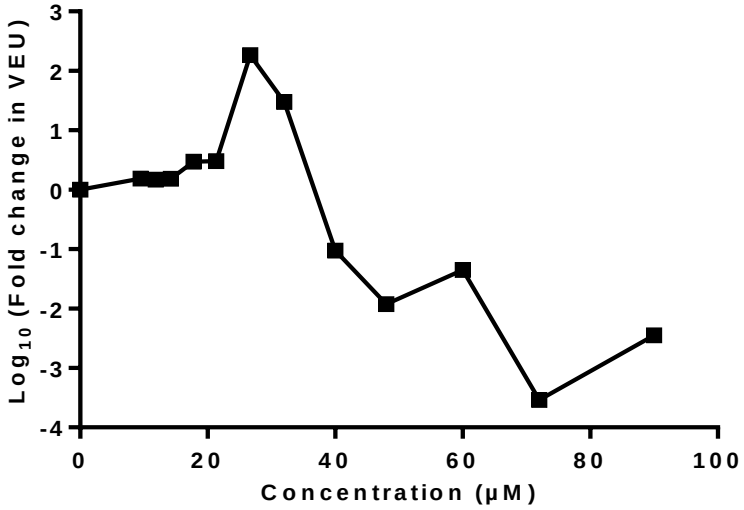
Log10 (Fold change in VEU)
Concentration (μM)

2.36

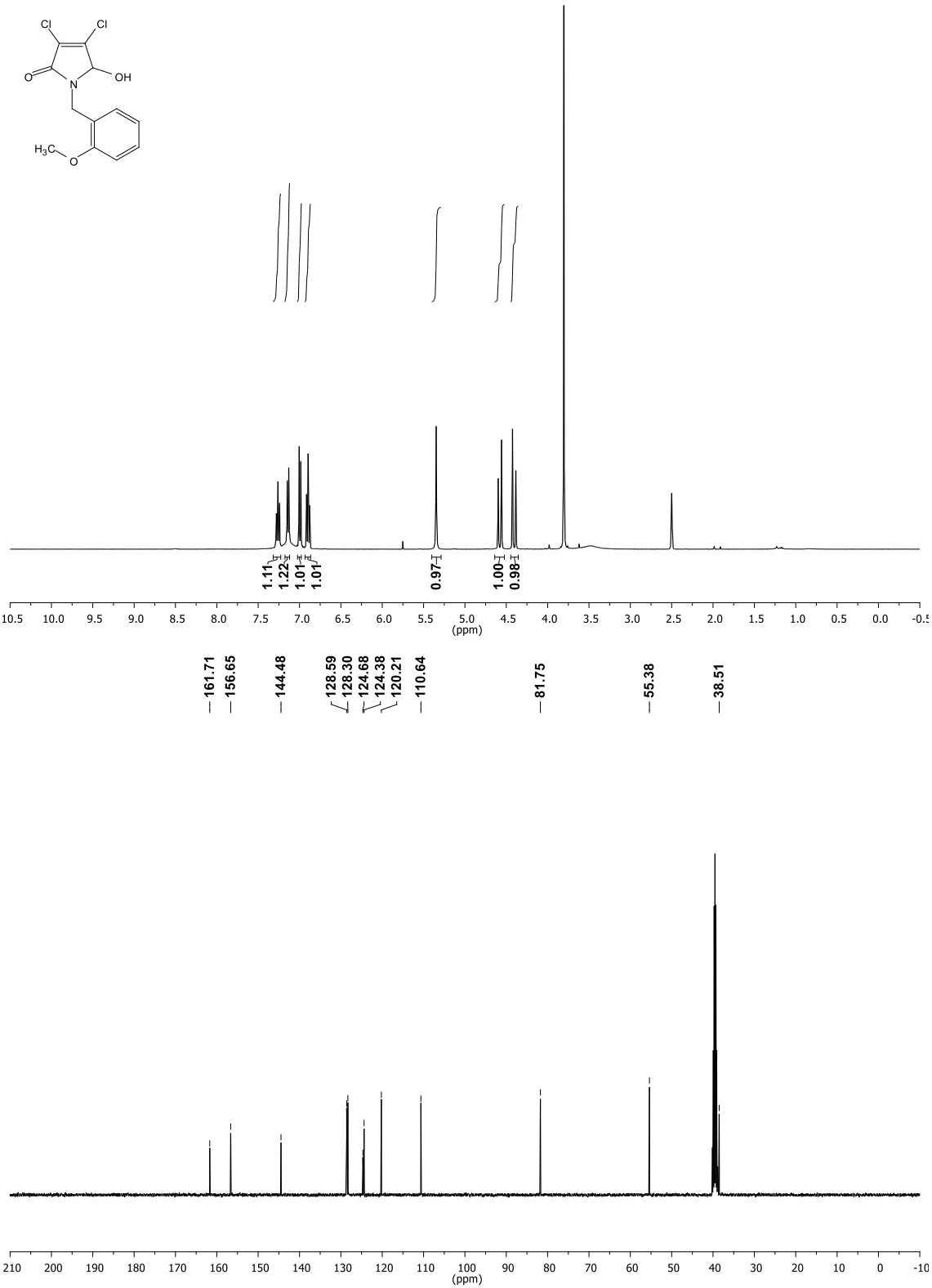
Cl
Cl
O
N
OH
H3C
O
1.11
1.22
1.01
1.01
0.97
1.00
0.98
(ppm)
161.71
156.65
144.48
128.59
128.30
124.68
124.38
120.21
110.64
81.75
55.38
38.51
(ppm)

2.36

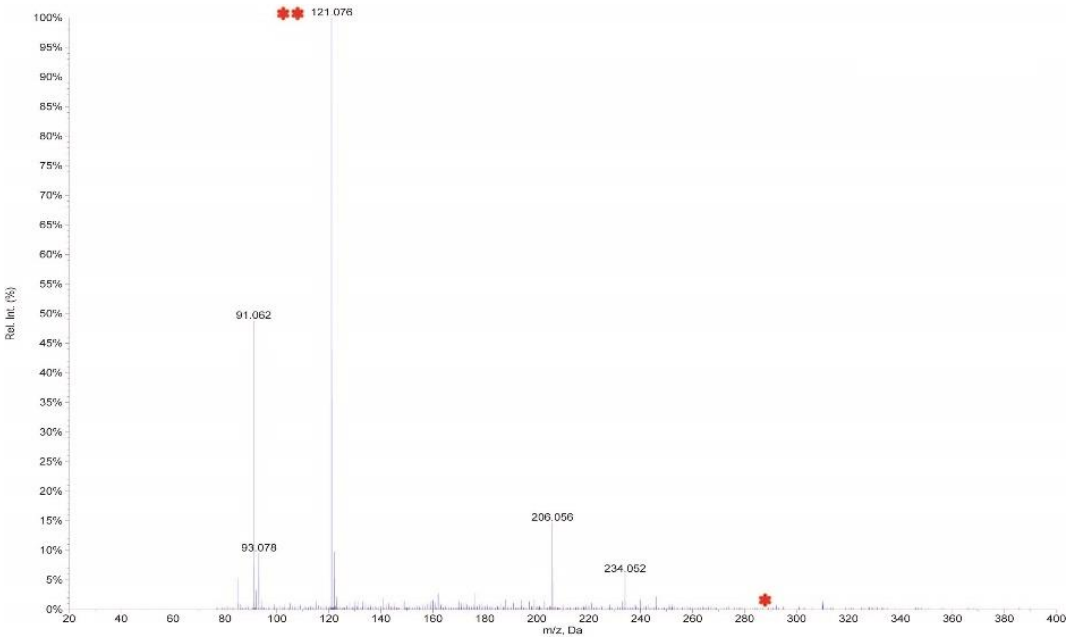
121.076
91.062
93.078
206.056
234.052
Rel. Int. (%)
m/z, Da

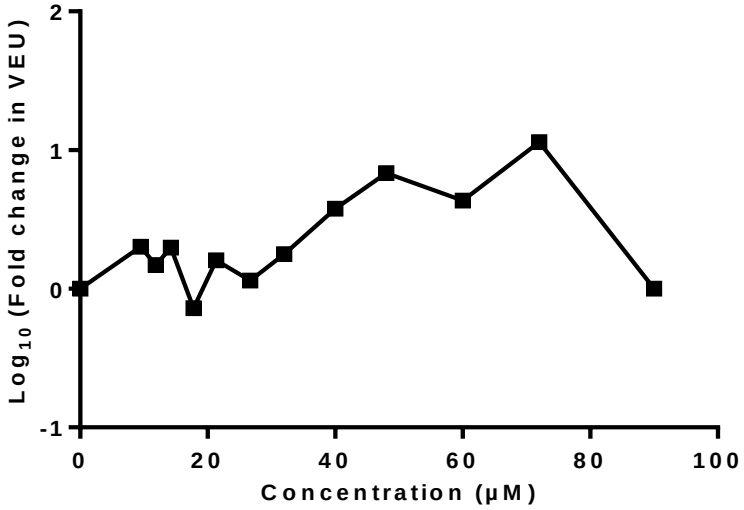
Log10 (Fold change in VEU)
Concentration (μM)

2.37

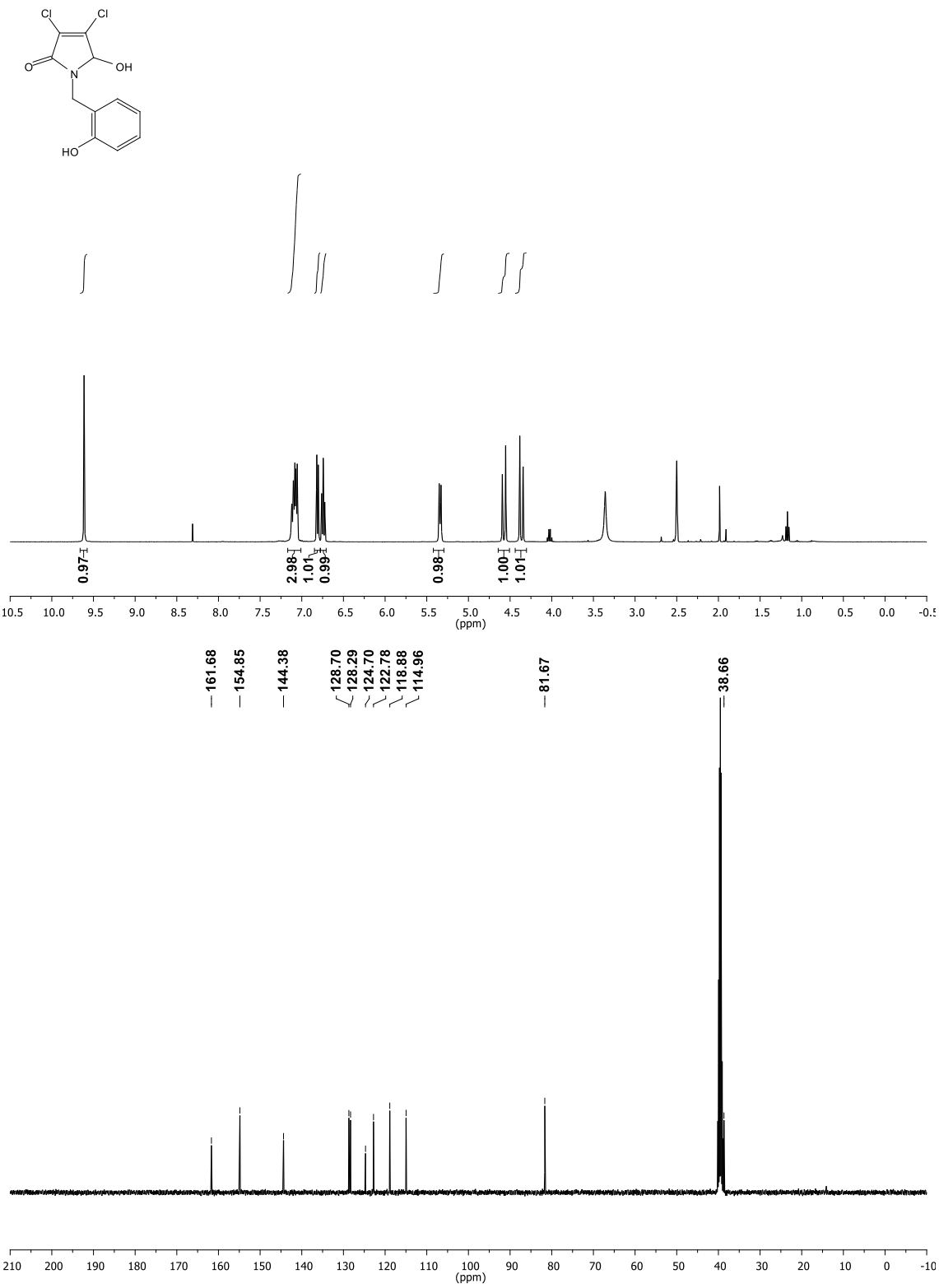
Cl
Cl
O
N
OH
HO
0.97
2.98
1.01
0.99
0.98
1.00
1.01
(ppm)
161.68
154.85
144.38
128.70
128.29
124.70
122.78
118.88
114.96
81.67
38.66
(ppm)

2.37

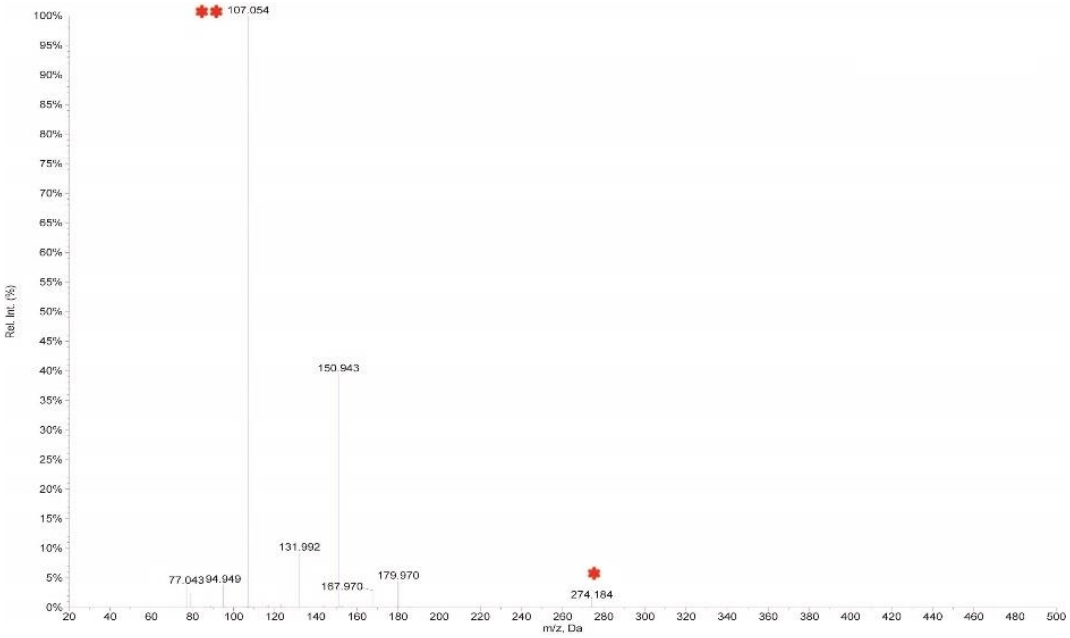
107.054
150.943
131.992
77.043
94.949
187.970
179.970
274.184
Rel. Int. (%)
m/z, Da

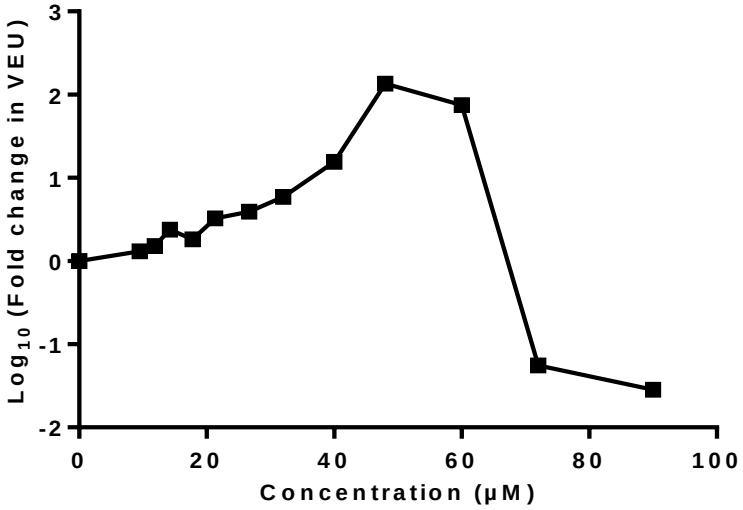
Log10 (Fold change in VEU)
Concentration (μM)

2.38

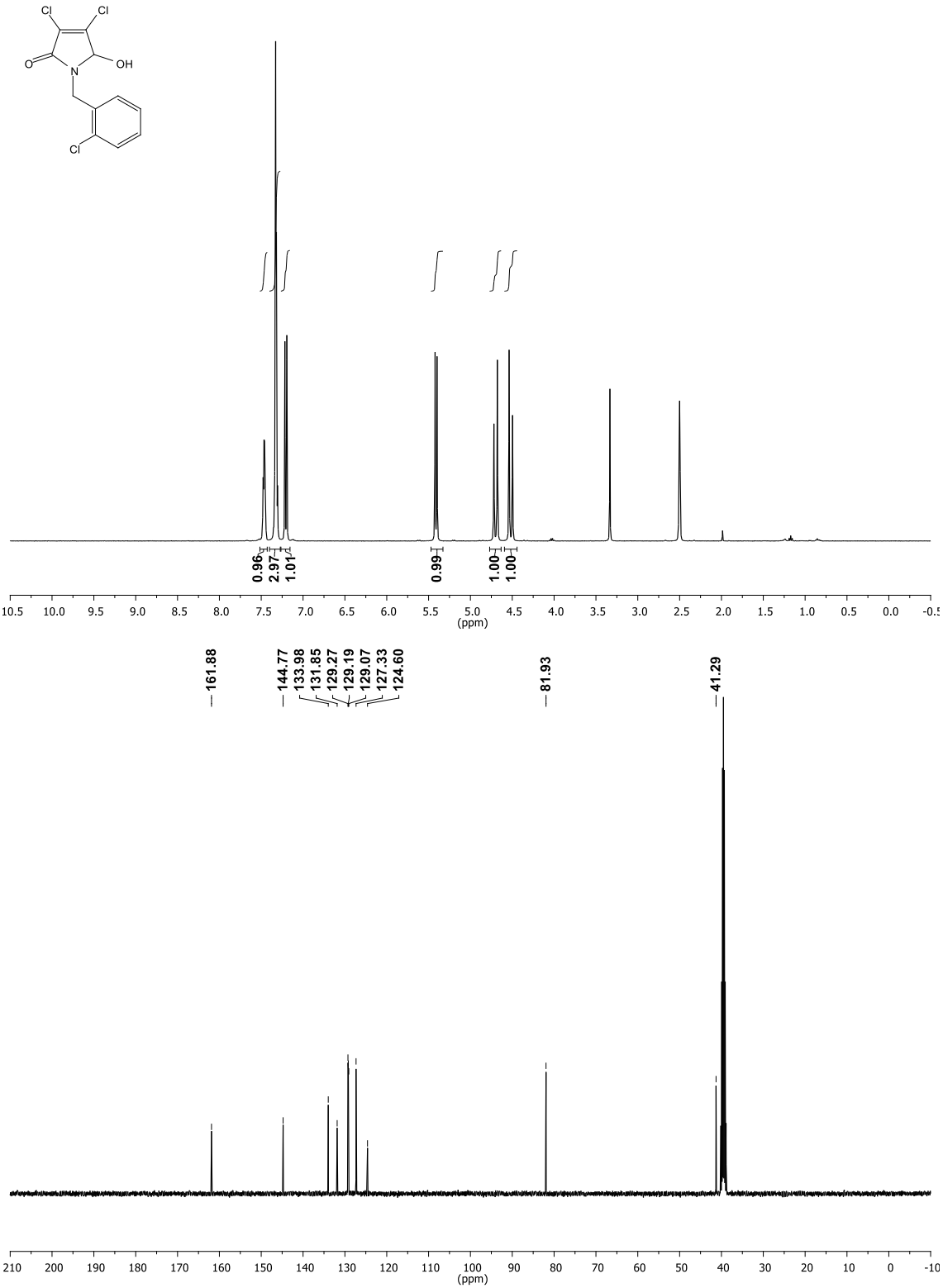
Cl
Cl
O
N
OH
Cl
0.96
2.97
1.01
0.99
1.00
1.00
(ppm)
161.88
144.77
133.98
131.85
129.27
129.19
129.07
127.33
124.60
81.93
41.29
(ppm)

2.38

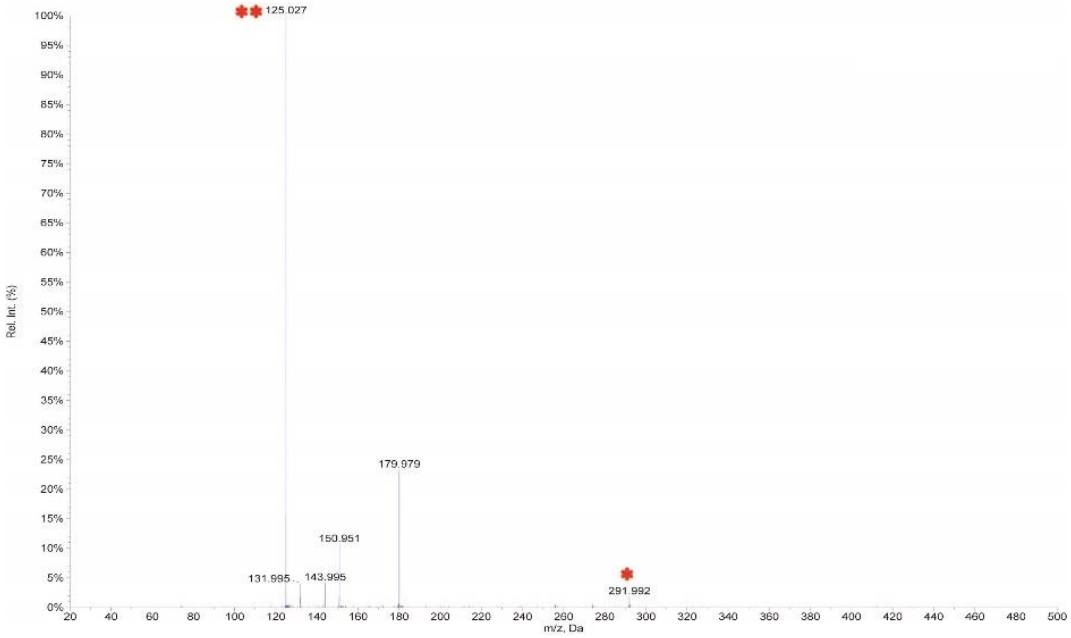
125.027
179.079
150.951
131.995
143.995
291.992
Rel. Int. (%)
m/z, Da

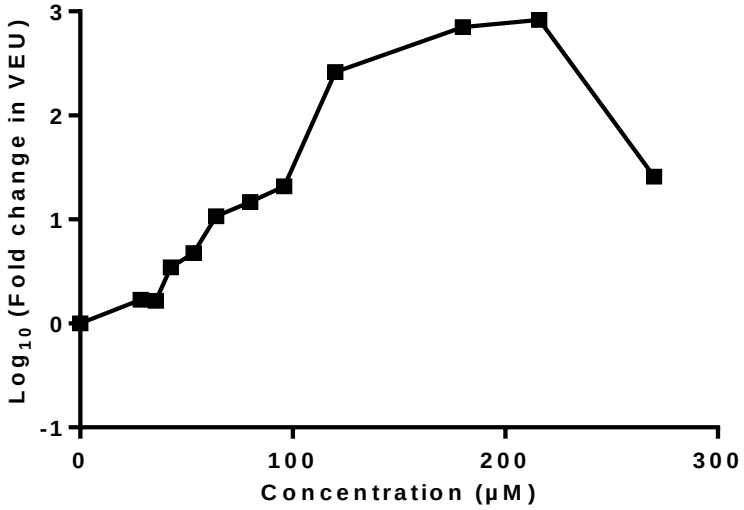
Log10 (Fold change in VEU)
Concentration (µM)

2.39

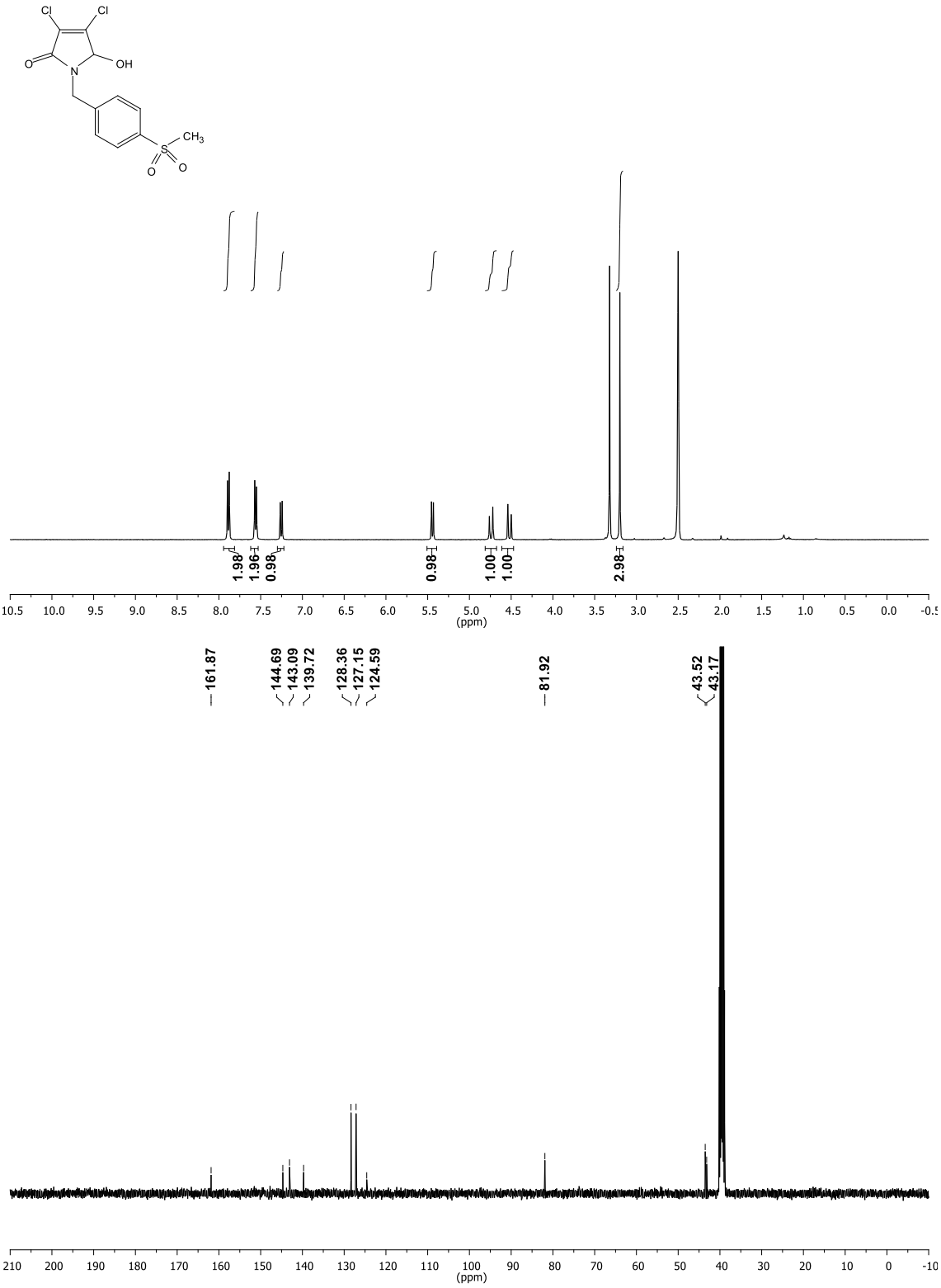
Cl
Cl
O
N
OH
CH3
S
O
O
1.98
1.96
0.98
0.98
1.00
1.00
2.98
(ppm)
161.87
144.69
143.09
139.72
128.36
127.15
124.59
81.92
43.52
43.17
(ppm)

2.39

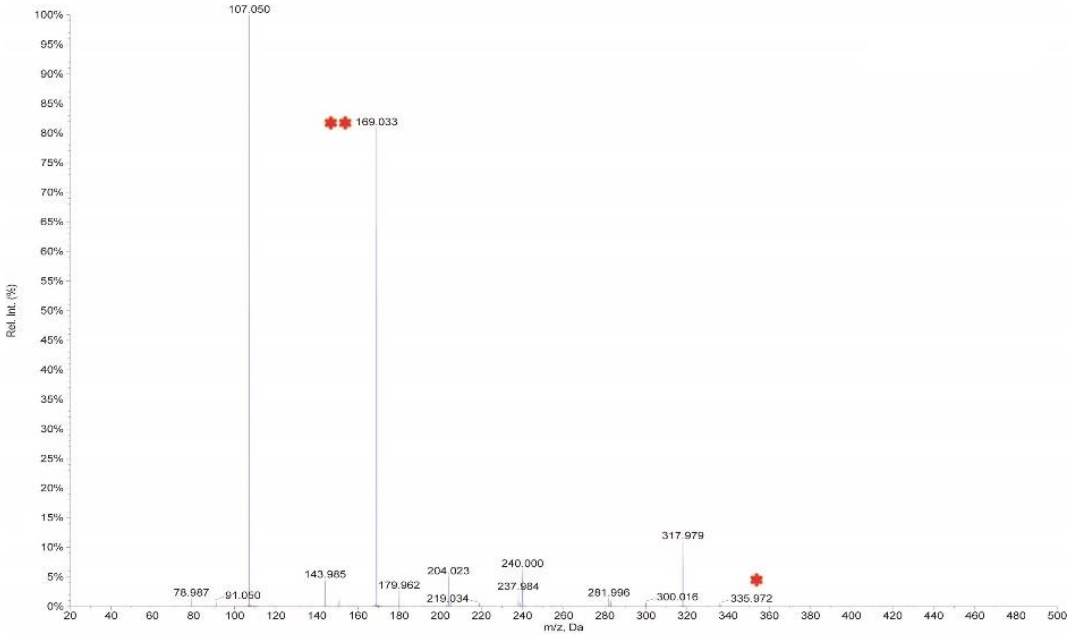
107.050
169.033
317.979
240.000
204.023
143.985
179.962
237.984
219.034
281.996
300.016
335.972
78.987
91.050
Rel. Int. (%)
m/z, Da

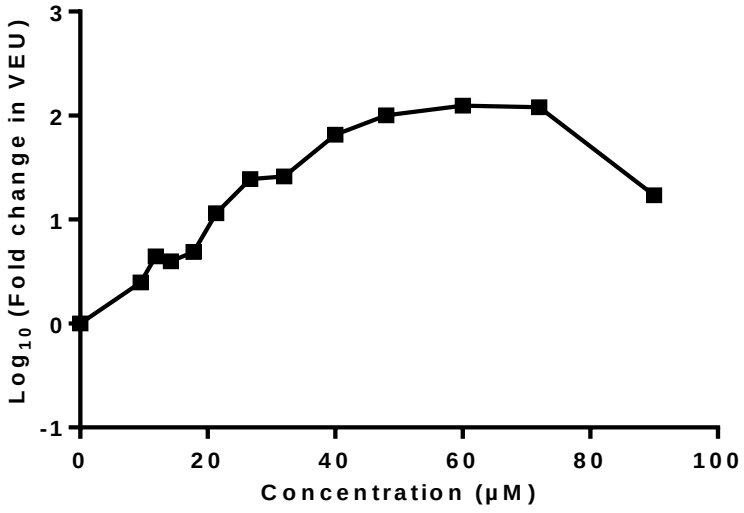
Log10 (Fold change in VEU)
Concentration (μM)

2.40

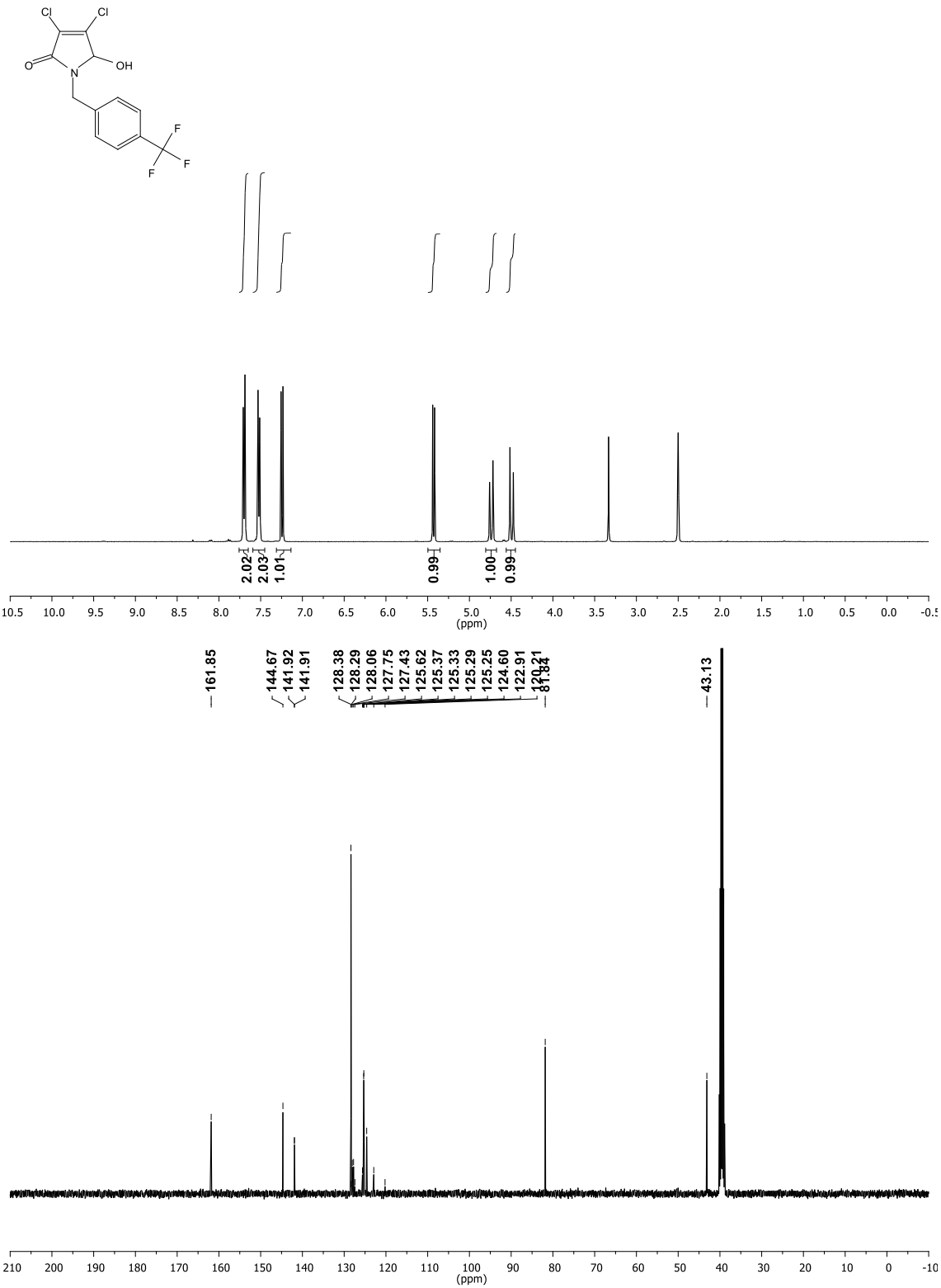
Cl
Cl
O
N
OH
F
F
F
2.02
2.03
1.01
0.99
1.00
0.99
(ppm)
161.85
144.67
141.92
141.91
128.38
128.29
128.06
127.75
127.43
125.62
125.37
125.33
125.29
125.25
124.60
122.91
120.21
81.84
43.13
(ppm)

2.40

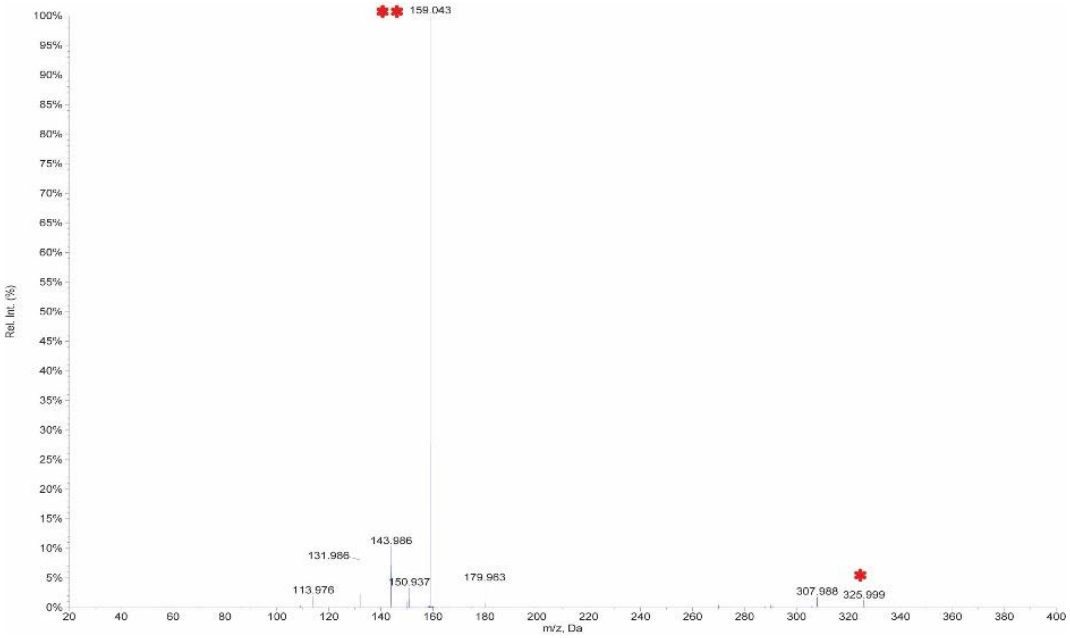
159.043
143.986
131.986
150.937
179.963
113.976
307.988
325.999
Rel. Int. (%)
m/z, Da

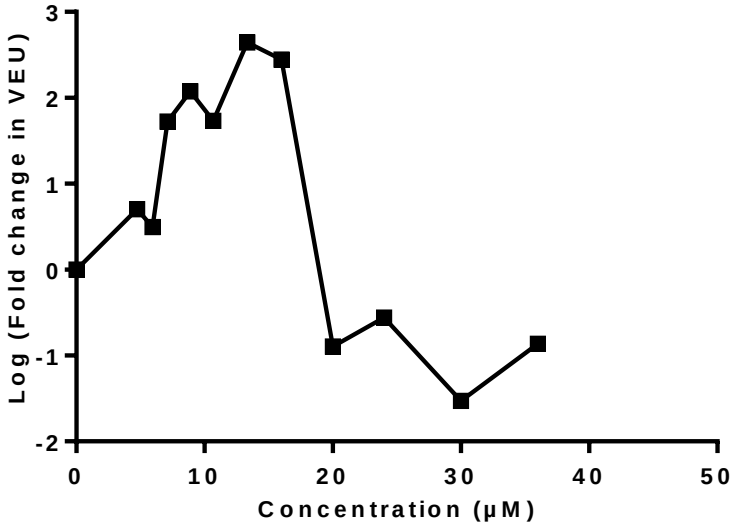
Log (Fold change in VEU)
Concentration (µM)

2.41

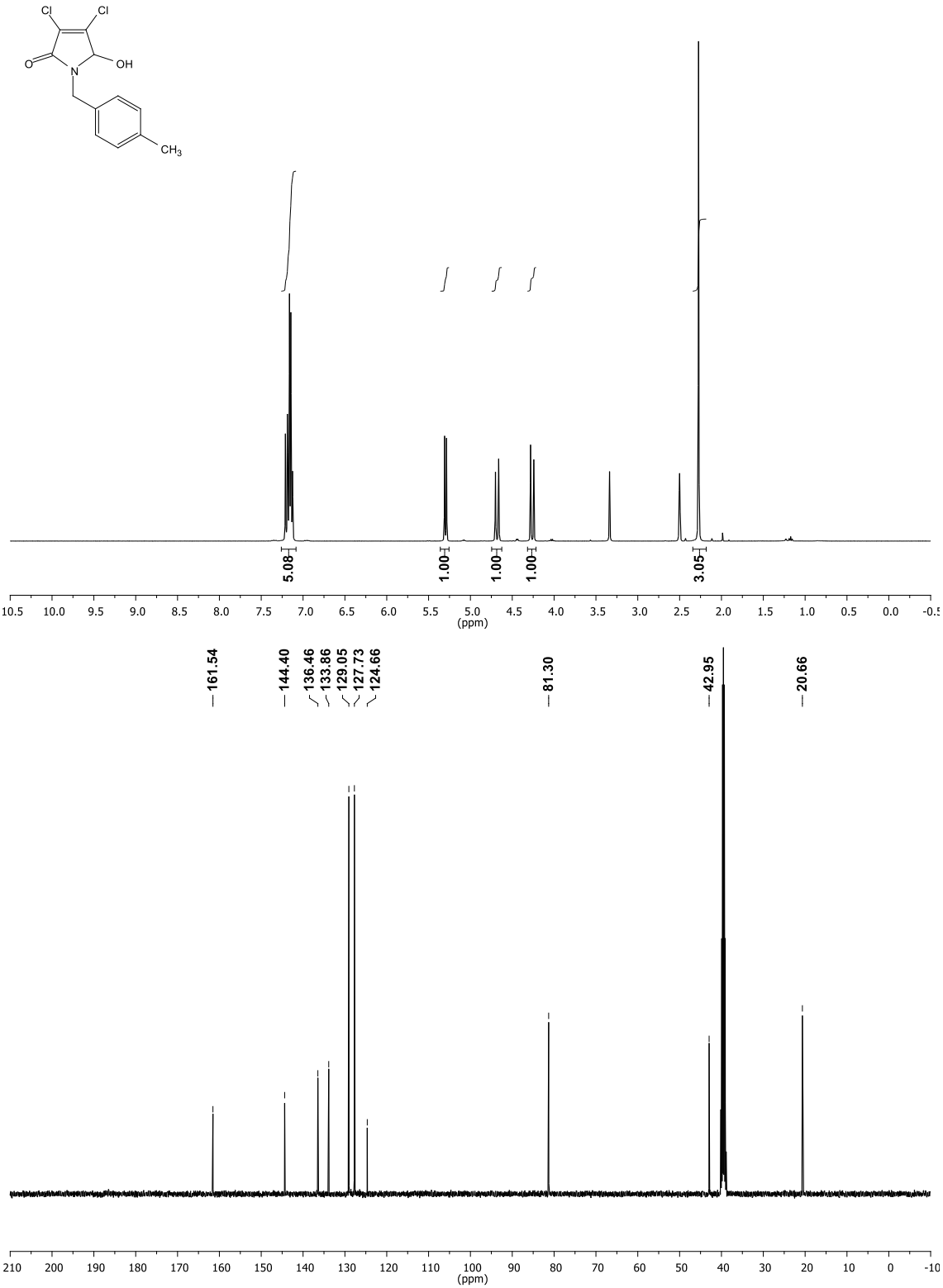
Cl
Cl
O
N
OH
CH3
5.08
1.00
1.00
1.00
3.05
(ppm)
161.54
144.40
136.46
133.86
129.05
127.73
124.66
81.30
42.95
20.66
(ppm)

2.41

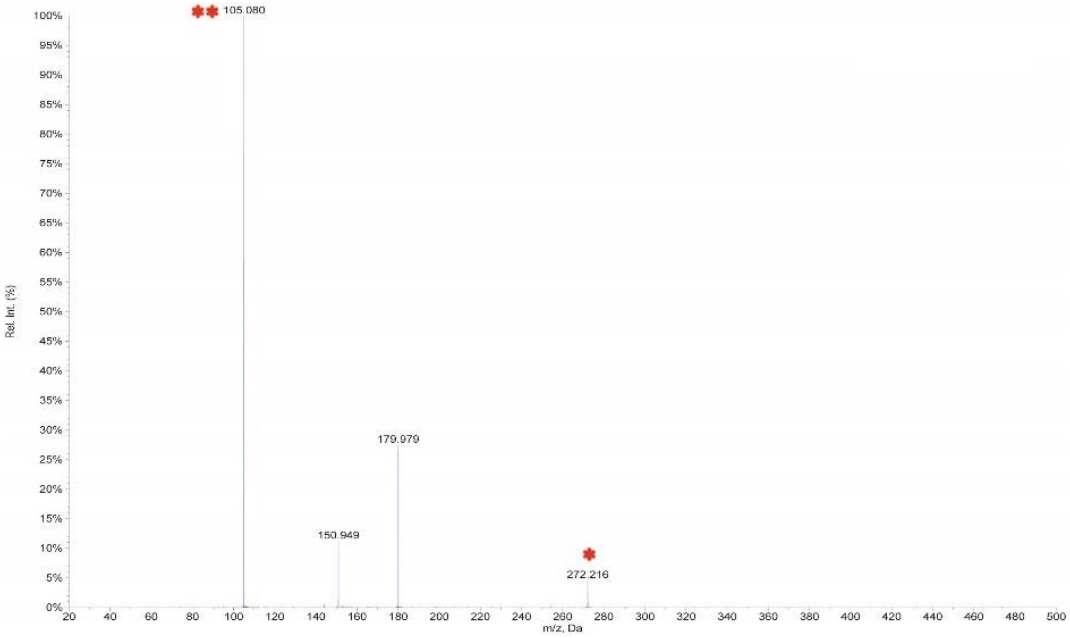
105.080
179.079
150.949
272.216
Rel. Int. (%)
m/z, Da

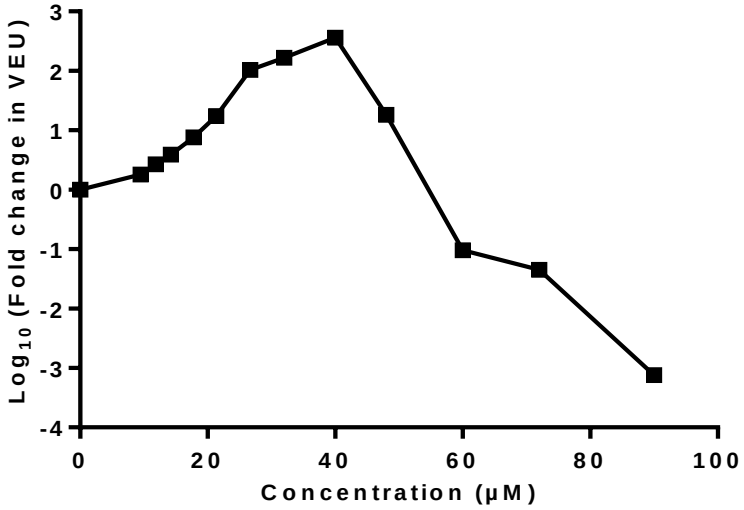
Log10 (Fold change in VEU)
Concentration (μM)

2.42

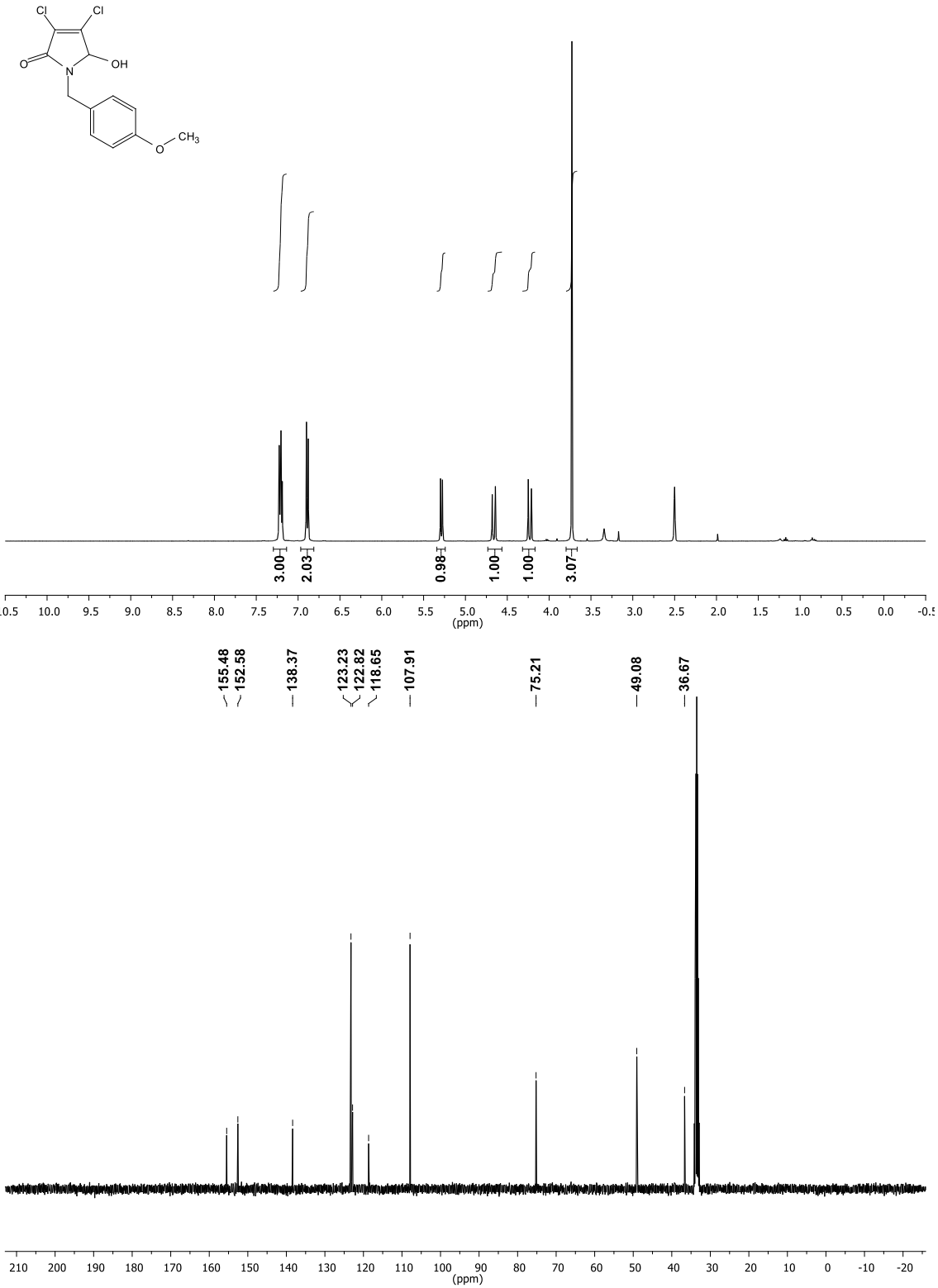
Cl
Cl
O
N
OH
O
CH3
3.00
2.03
0.98
1.00
1.00
3.07
(ppm)
155.48
152.58
138.37
123.23
122.82
118.65
107.91
75.21
49.08
36.67
(ppm)

2.42

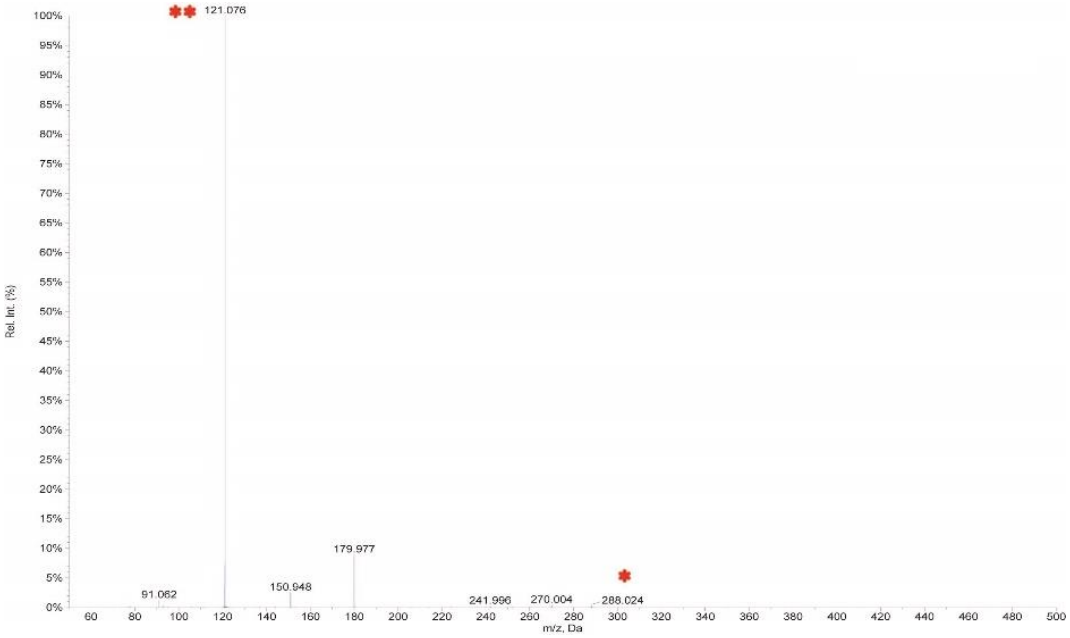
121.076
179.977
91.062
150.948
241.996
270.004
288.024
Rel. Int. (%)
m/z, Da

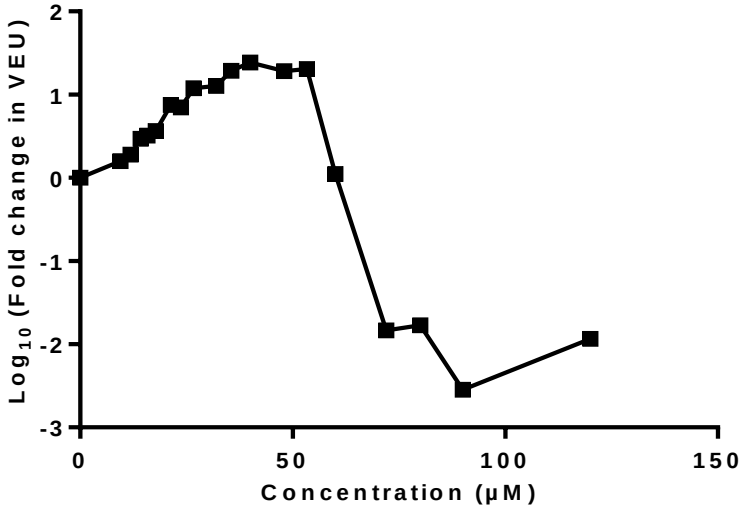
Log10 (Fold change in VEU)
Concentration (μM)

2.43

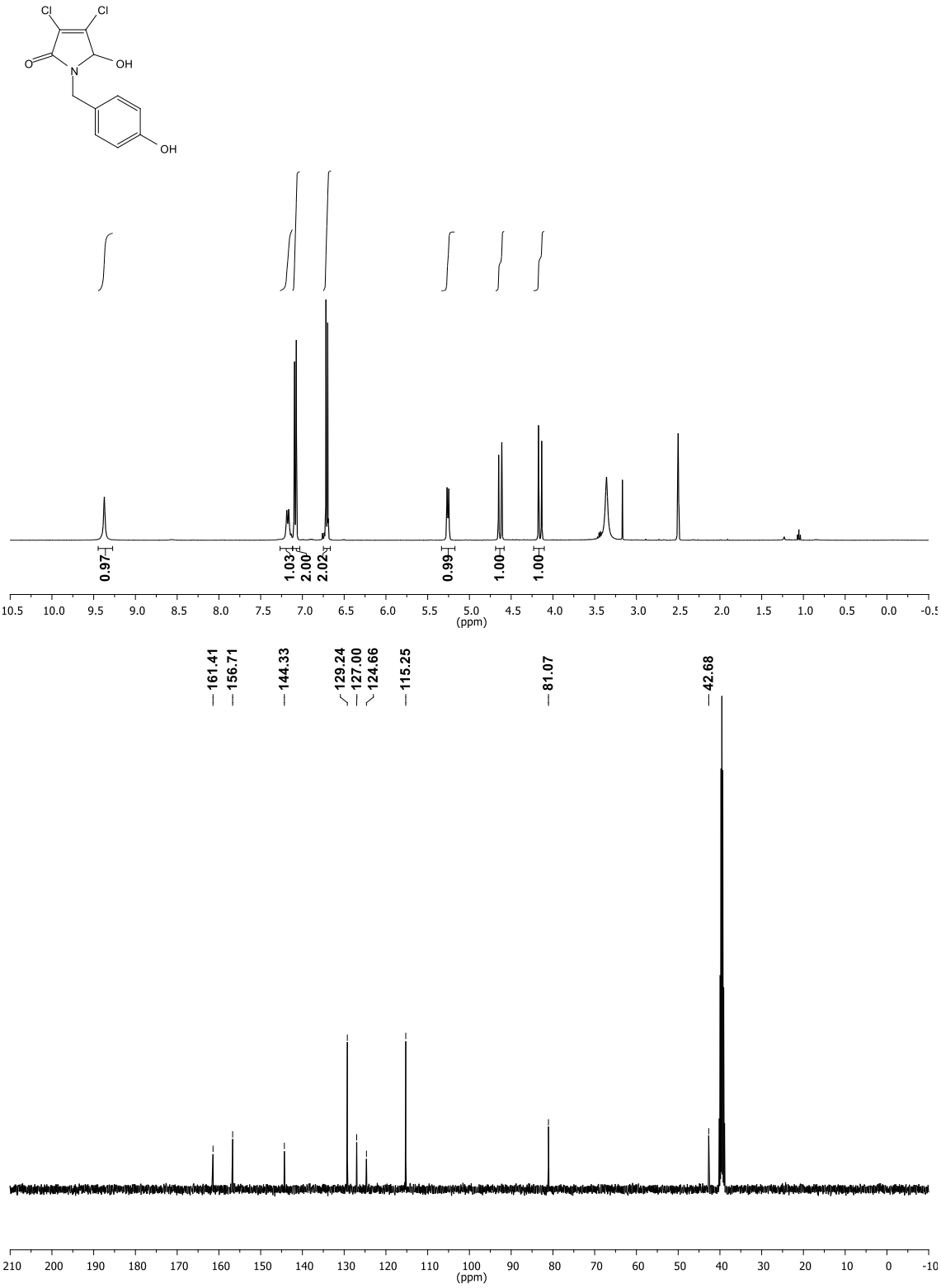
Cl
Cl
O
N
OH
OH
0.97
1.03
2.00
2.02
0.99
1.00
1.00
(ppm)
161.41
156.71
144.33
129.24
127.00
124.66
115.25
81.07
42.68
(ppm)

2.43

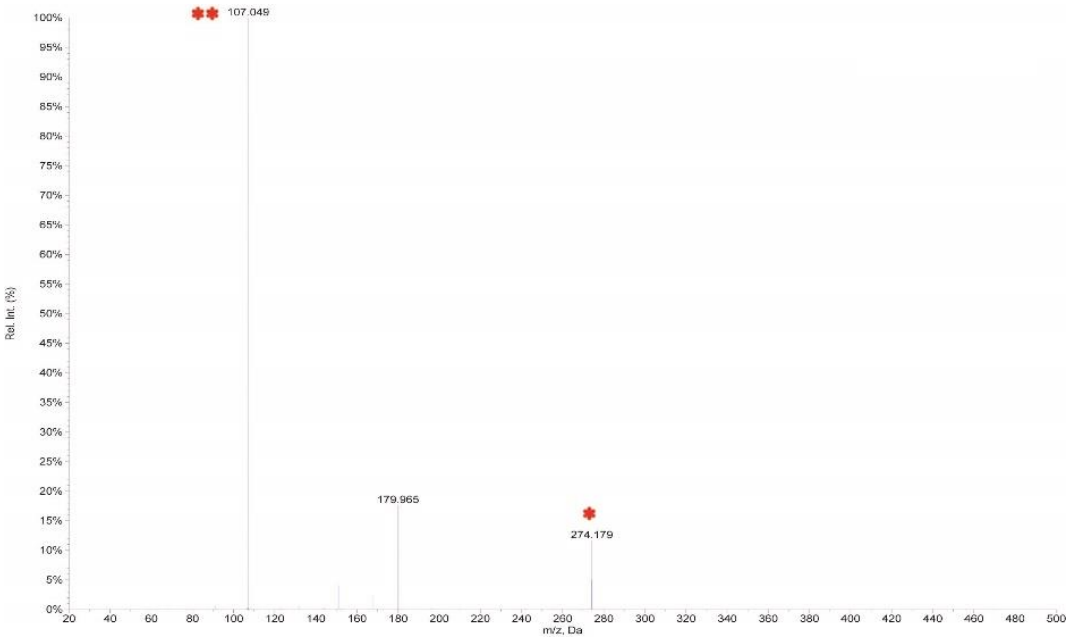
107.049
179.965
274.179
Rel. Int. (%)
m/z, Da

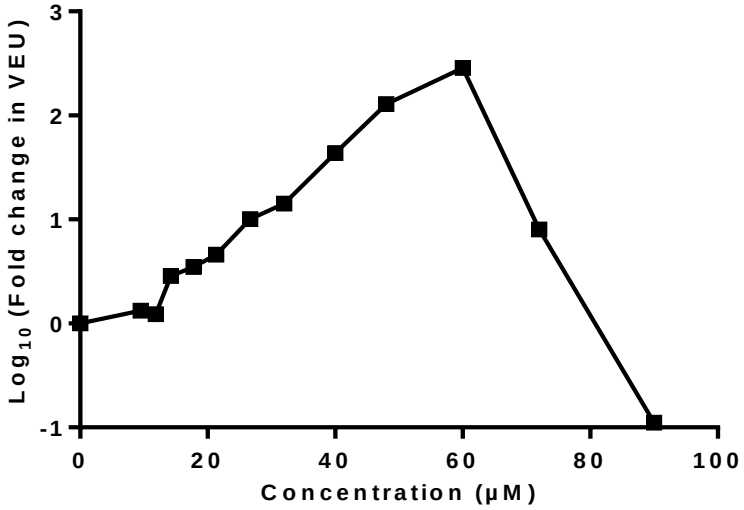
Log10 (Fold change in VEU)
Concentration (μM)

2.44

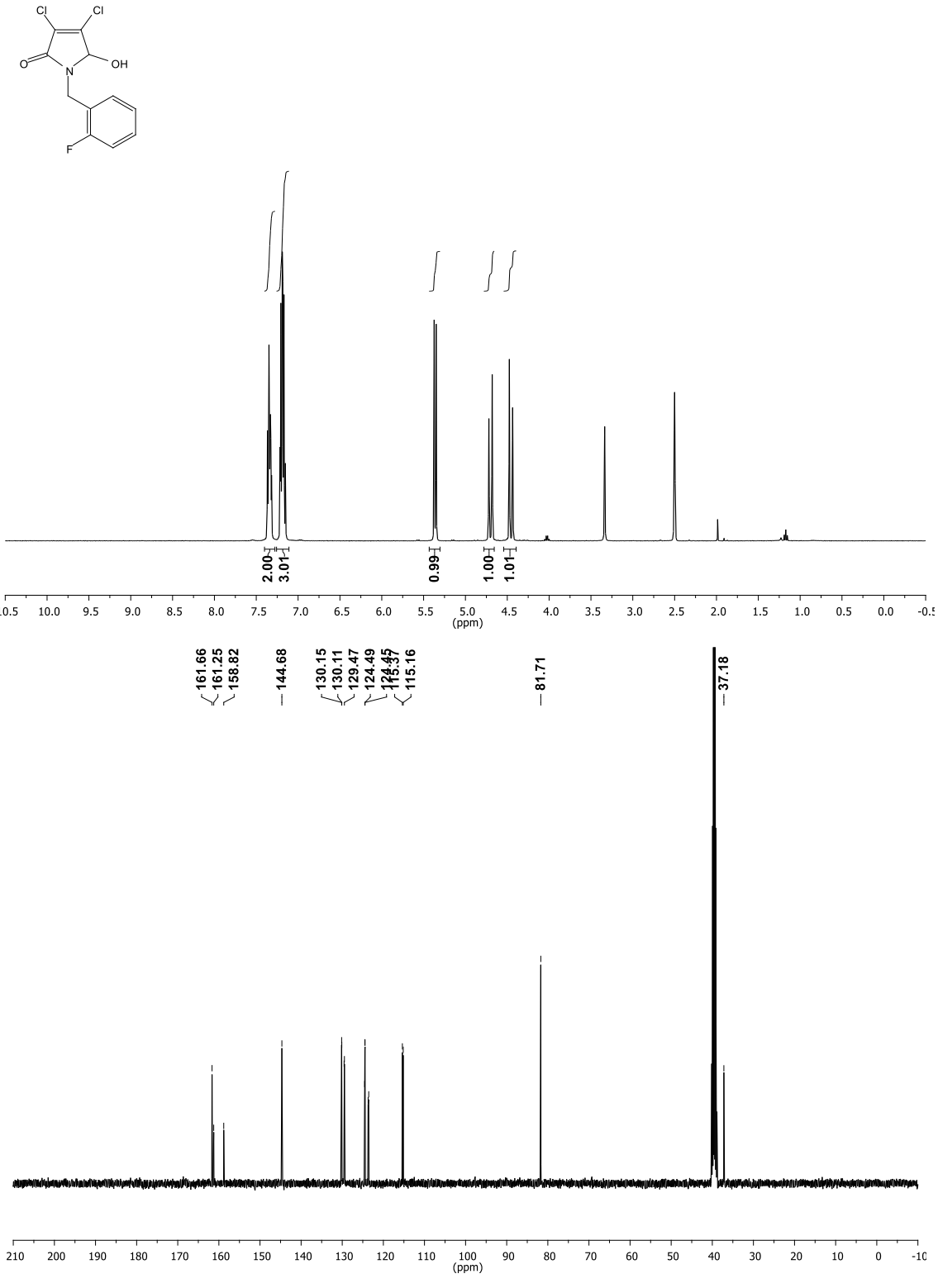
Cl
Cl
O
N
OH
F
2.00
3.01
0.99
1.00
1.01
(ppm)
161.66
161.25
158.82
144.68
130.15
130.11
129.47
124.49
124.45
115.37
115.16
81.71
37.18
(ppm)

2.44

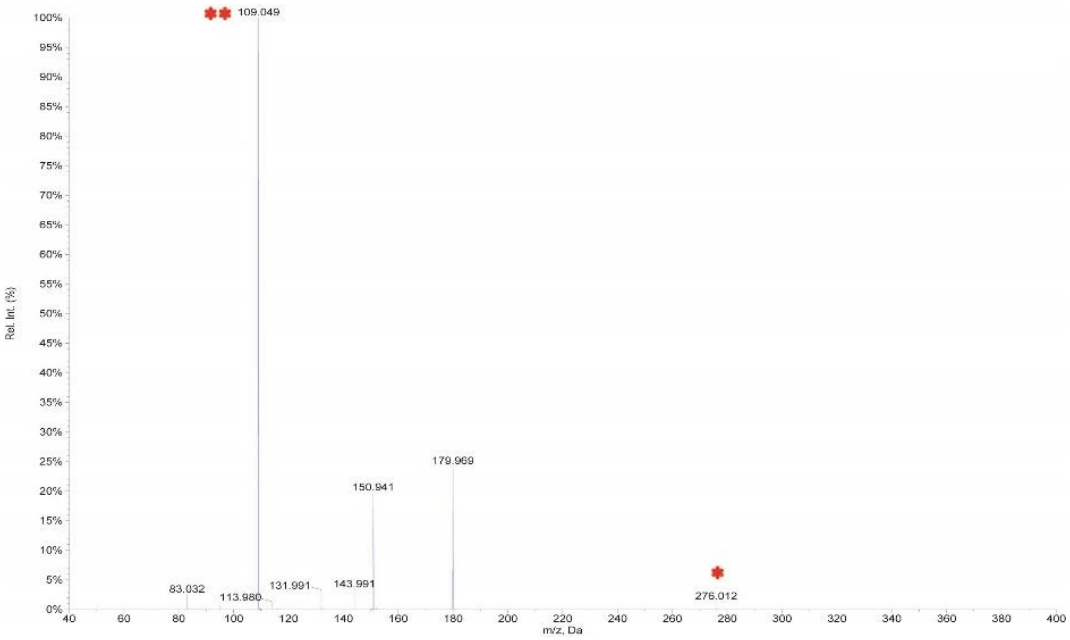
109.049
179.969
150.941
83.032
113.980
131.991
143.991
275.012
Rel. Int. (%)
m/z, Da

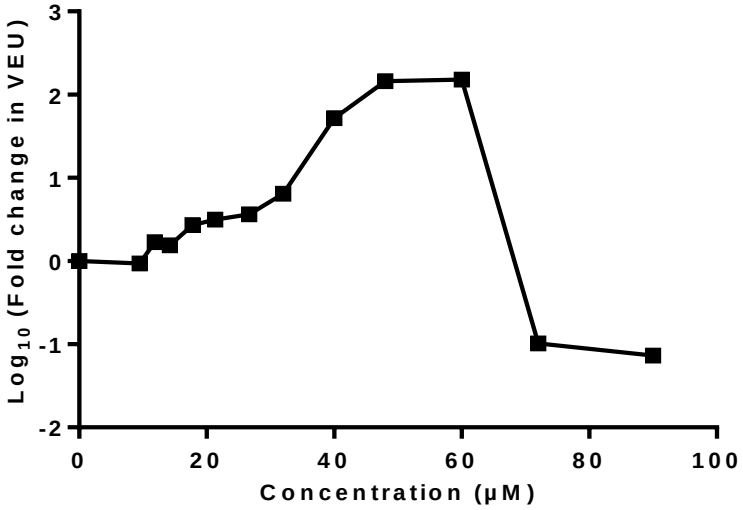
Log10 (Fold change in VEU)
Concentration (μM)

2.45

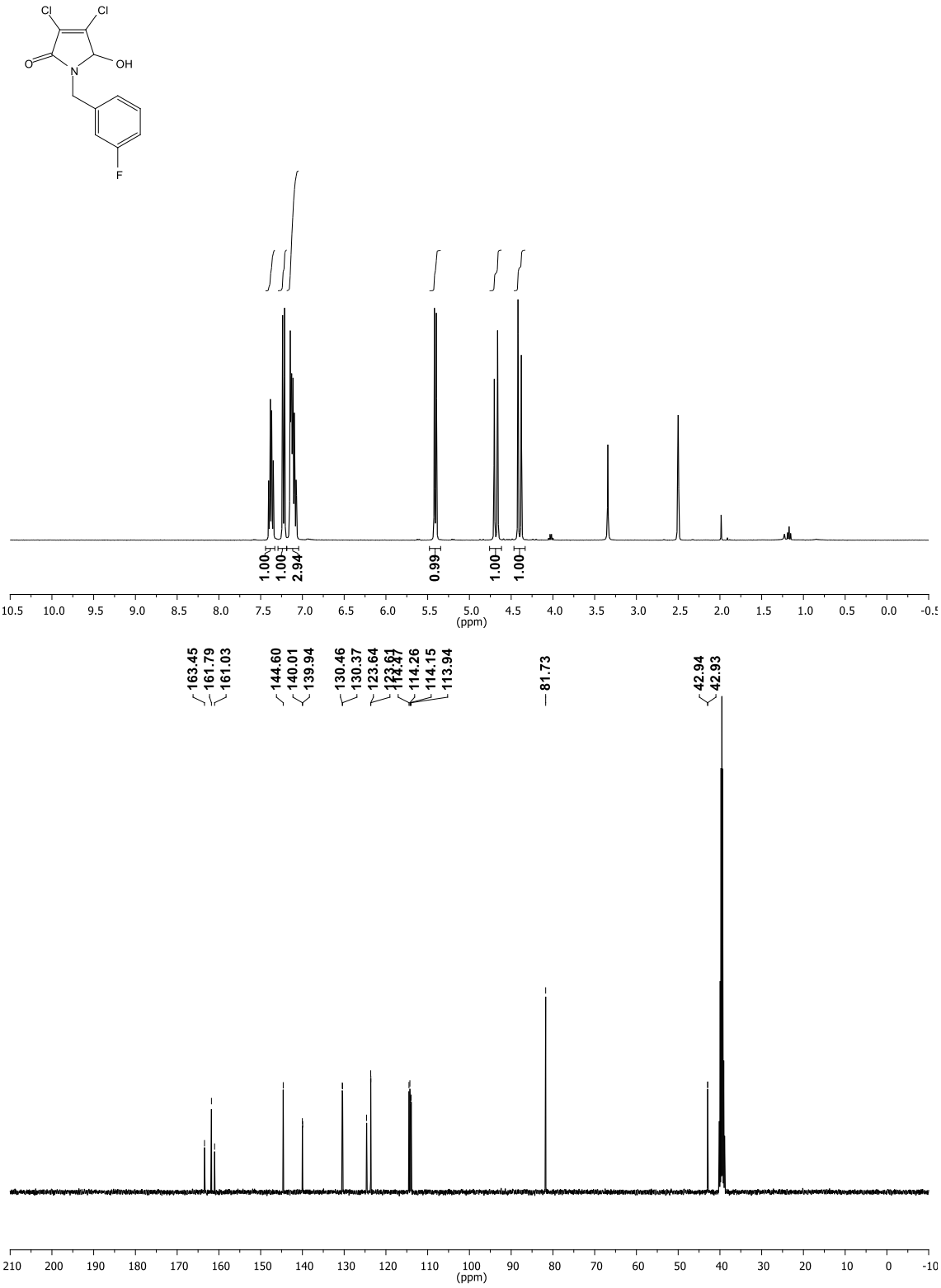
Cl
Cl
O
N
OH
F
1.00
1.00
2.94
0.99
1.00
1.00
(ppm)
163.45
161.79
161.03
144.60
140.01
139.94
130.46
130.37
123.64
114.26
114.15
113.94
81.73
42.94
42.93
(ppm)

2.45

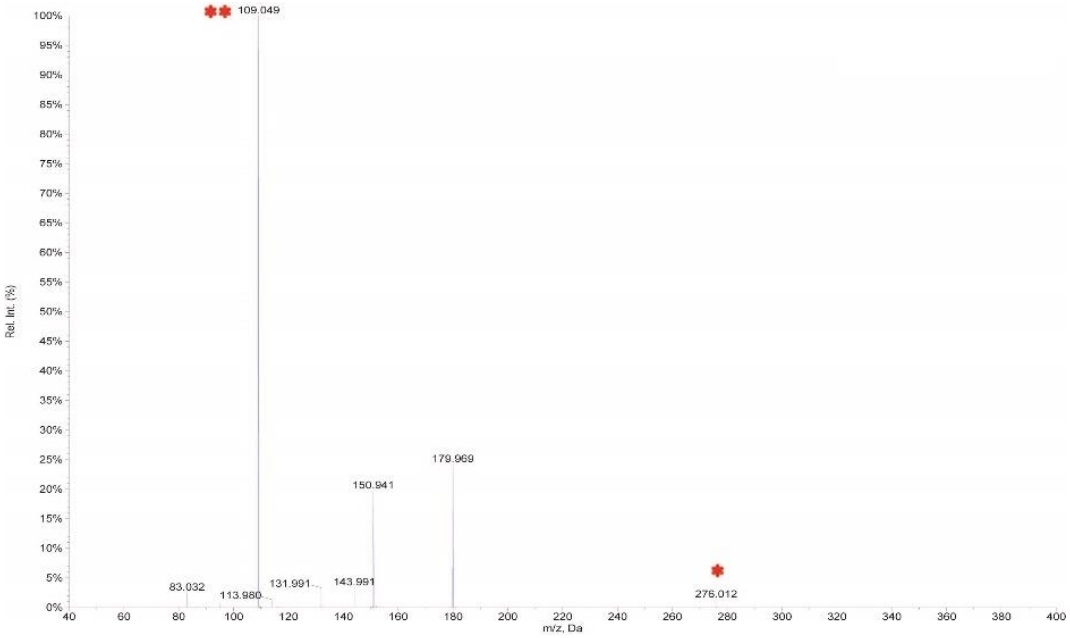
109.049
179.969
150.941
83.032
113.980
131.991
143.991
275.012
Rel. Int. (%)
m/z, Da

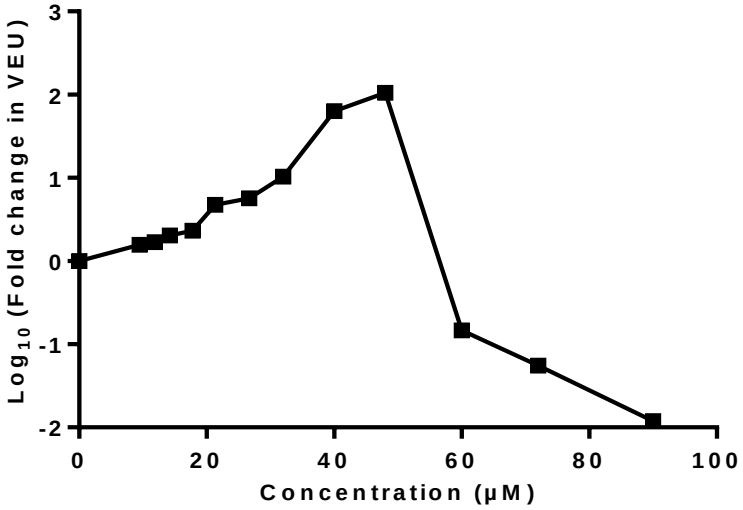
Log10 (Fold change in VEU)
Concentration (μM)

2.46

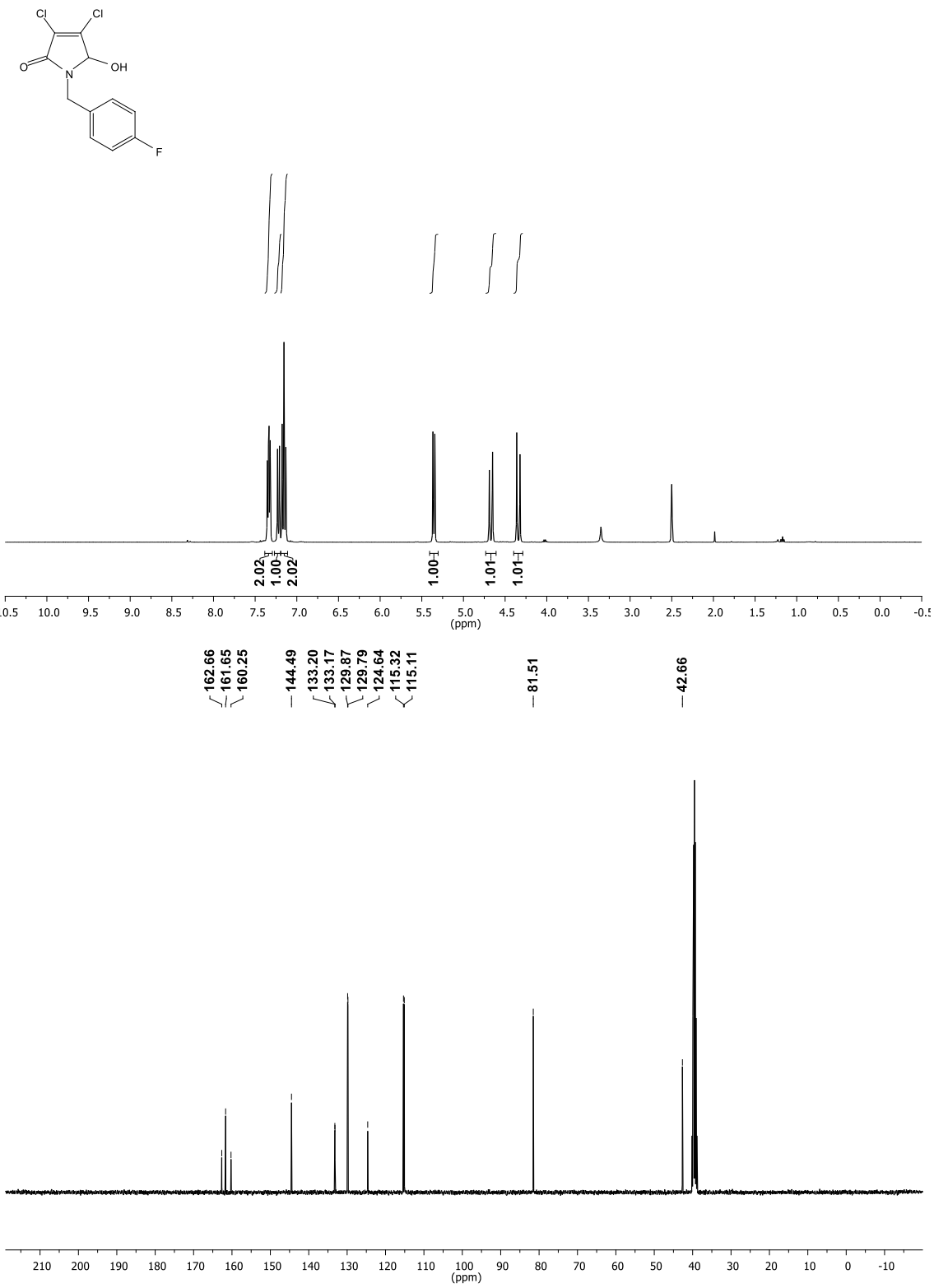
Cl
Cl
O
N
OH
F
2.02
1.00
2.02
1.00
1.01
1.01
(ppm)
162.66
161.65
160.25
144.49
133.20
133.17
129.87
129.79
124.64
115.32
115.11
81.51
42.66
(ppm)

2.46

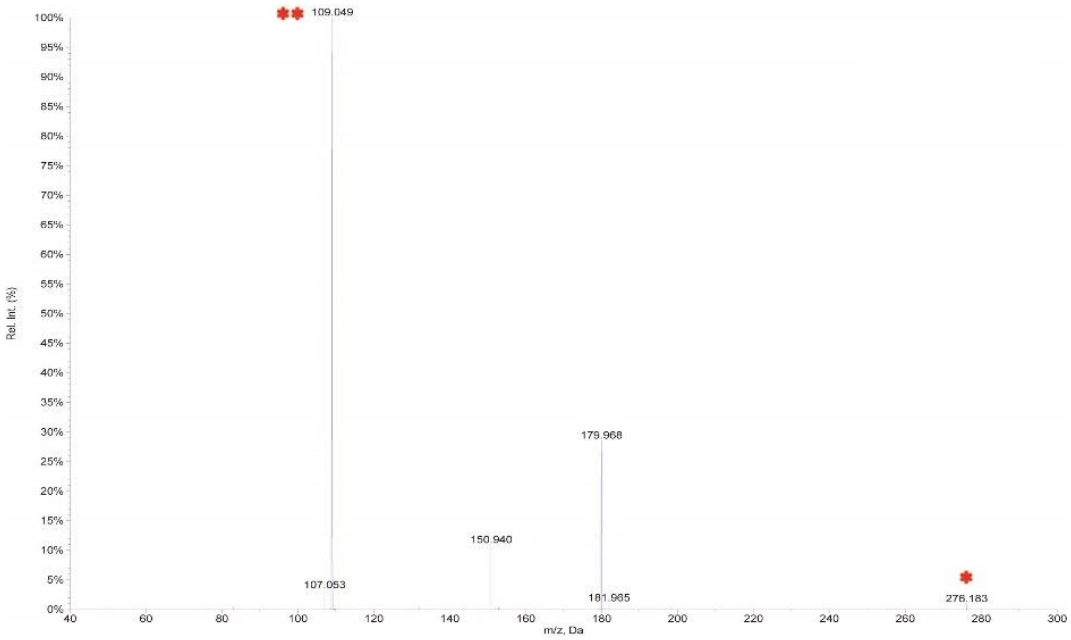
109.049
179.968
150.940
107.053
181.965
276.183
Rel. Int. (%)
m/z, Da

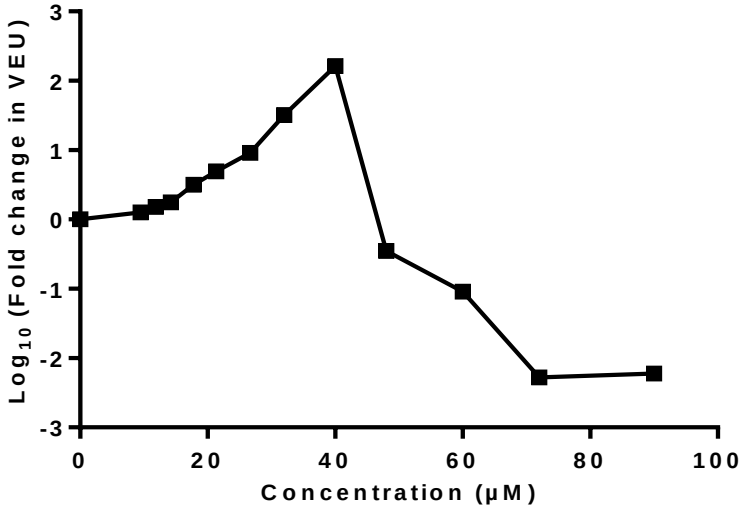
Log10 (Fold change in VEU)
Concentration (μM)

2.47

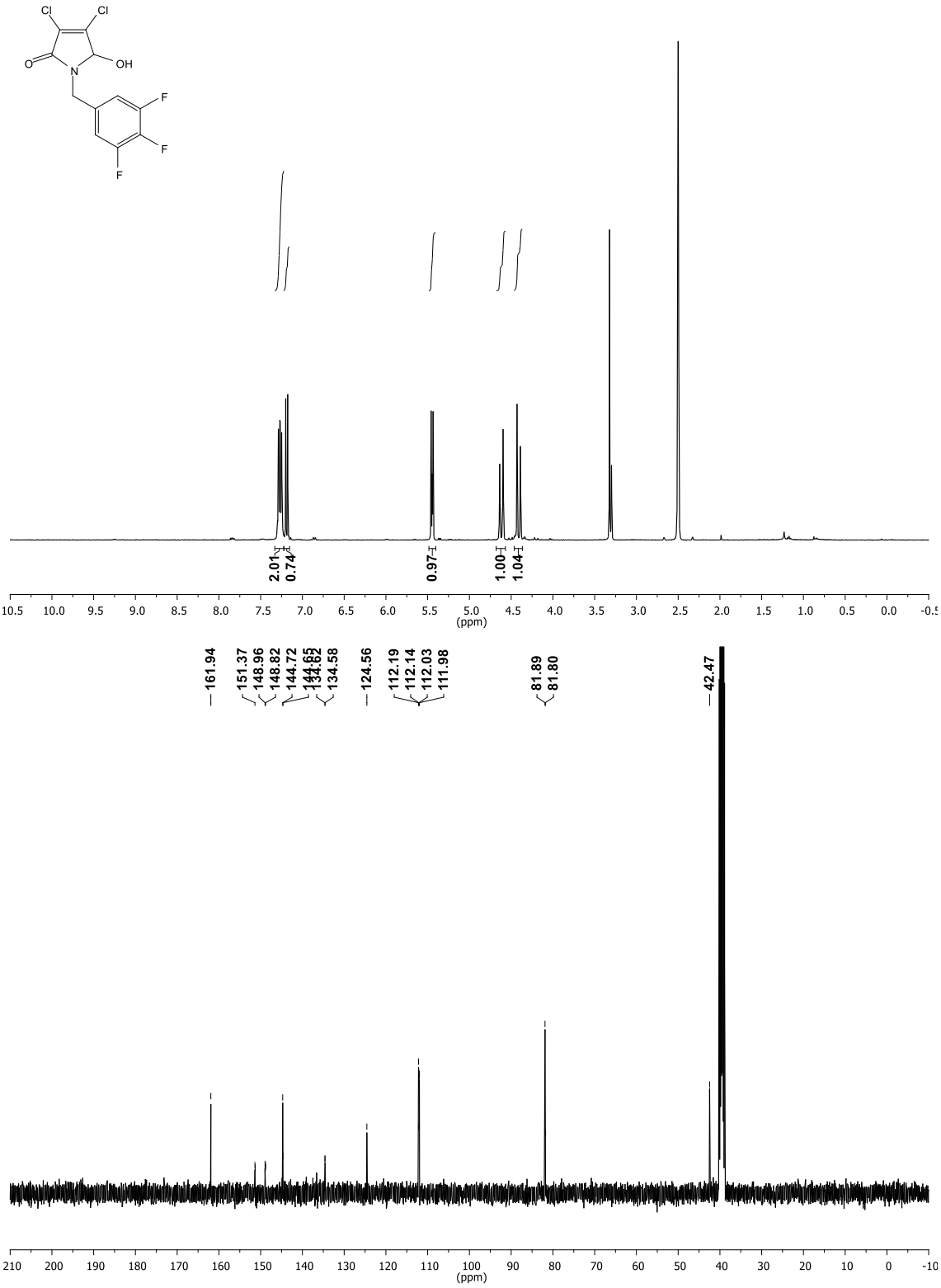
Cl
Cl
O
N
OH
F
F
F
2.01
0.74
0.97
1.00
1.04
(ppm)
161.94
151.37
148.96
148.82
144.72
134.58
124.56
112.19
112.14
112.03
111.98
81.89
81.80
42.47
(ppm)

2.47

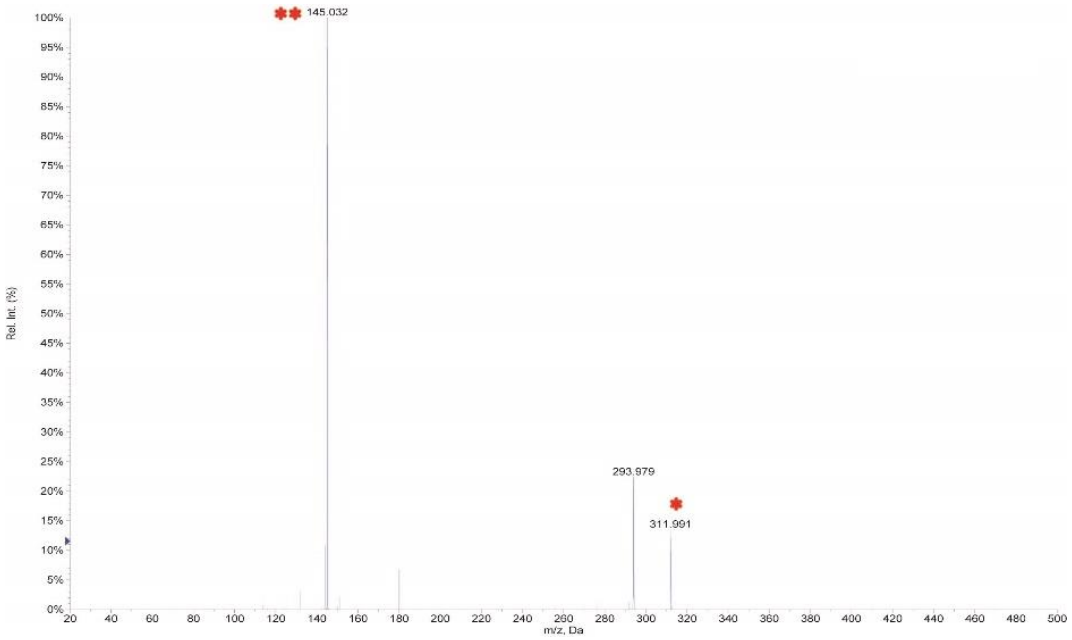
145.032
293.979
311.991
Rel. Int. (%)
m/z, Da

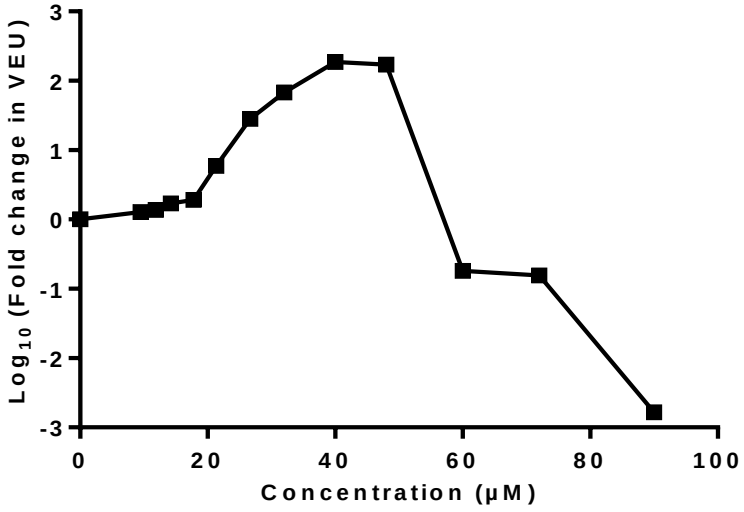
Log10 (Fold change in VEU)
Concentration (μM)

2.48

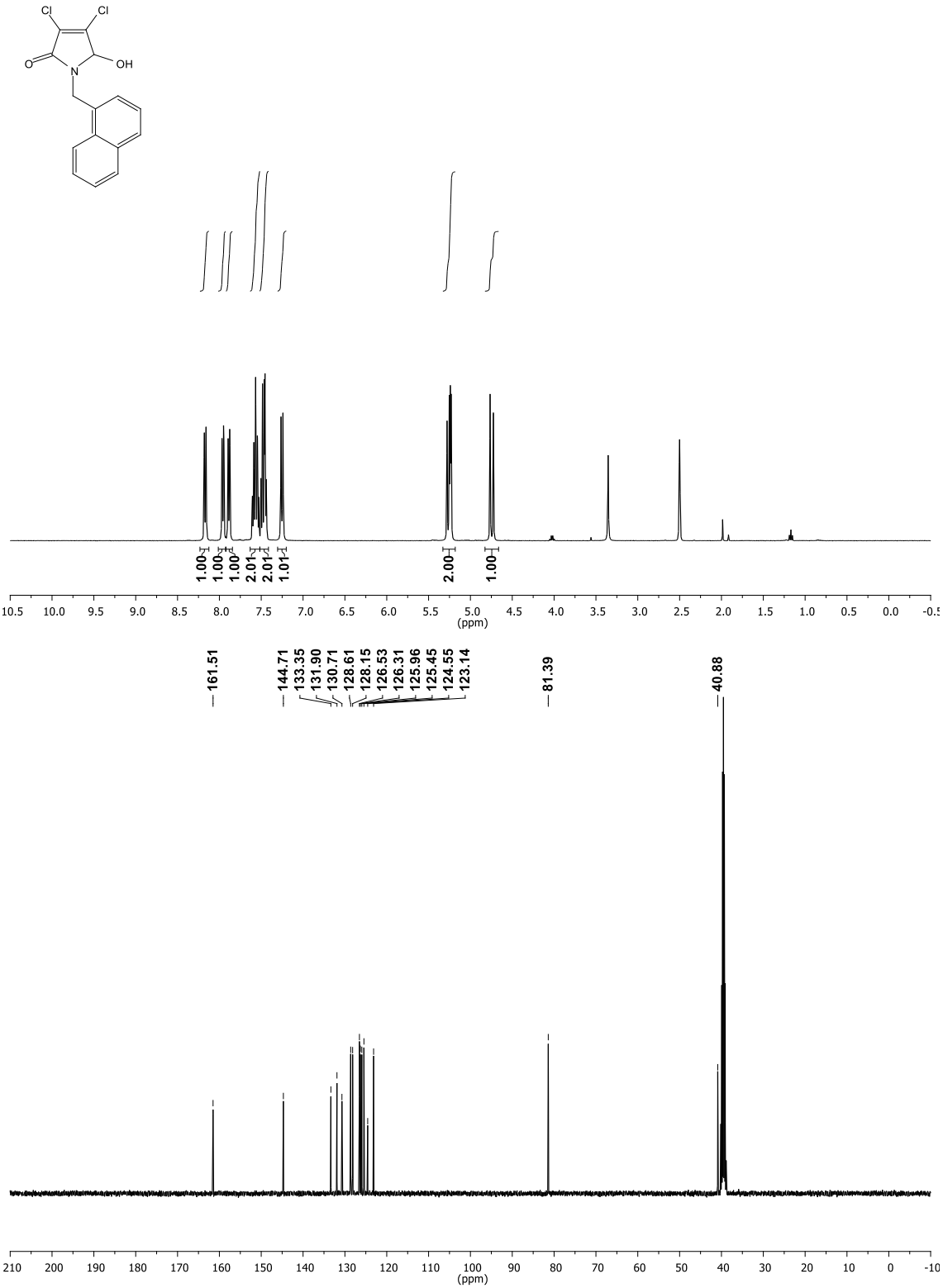
Cl
Cl
O
N
OH
1.00
1.00
1.00
2.01
2.01
1.01
2.00
1.00
(ppm)
161.51
144.71
133.35
131.90
130.71
128.61
128.15
126.53
126.31
125.96
125.45
124.55
123.14
81.39
40.88
(ppm)

2.48

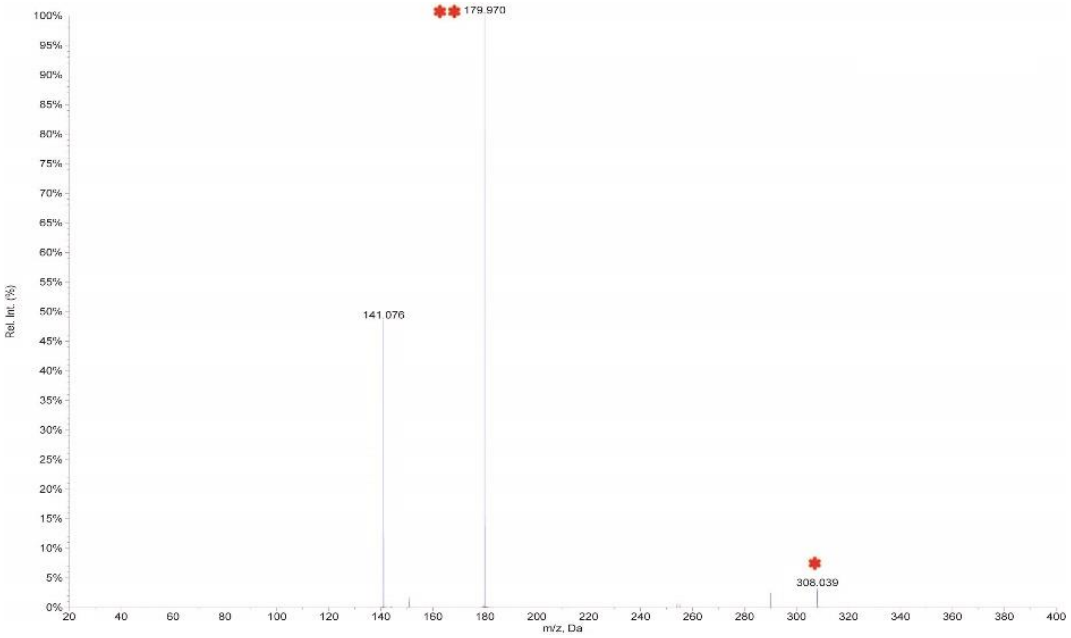
179.970
141.076
308.039
Rel. Int. (%)
m/z, Da

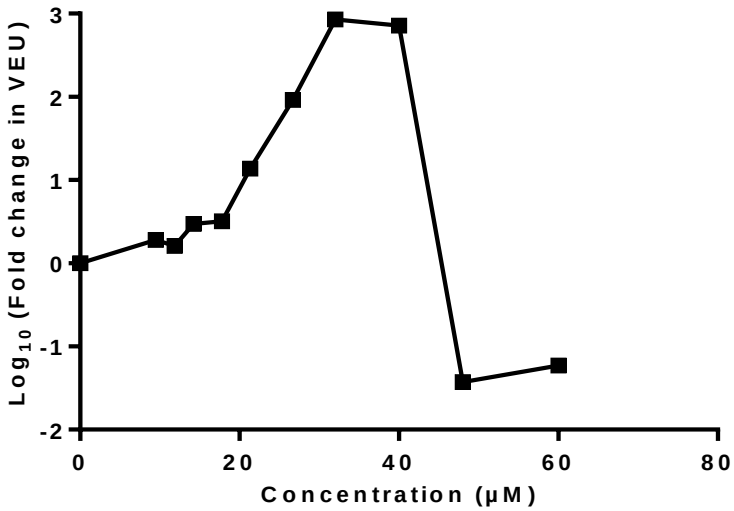
Log10 (Fold change in VEU)
Concentration (μM)

2.49

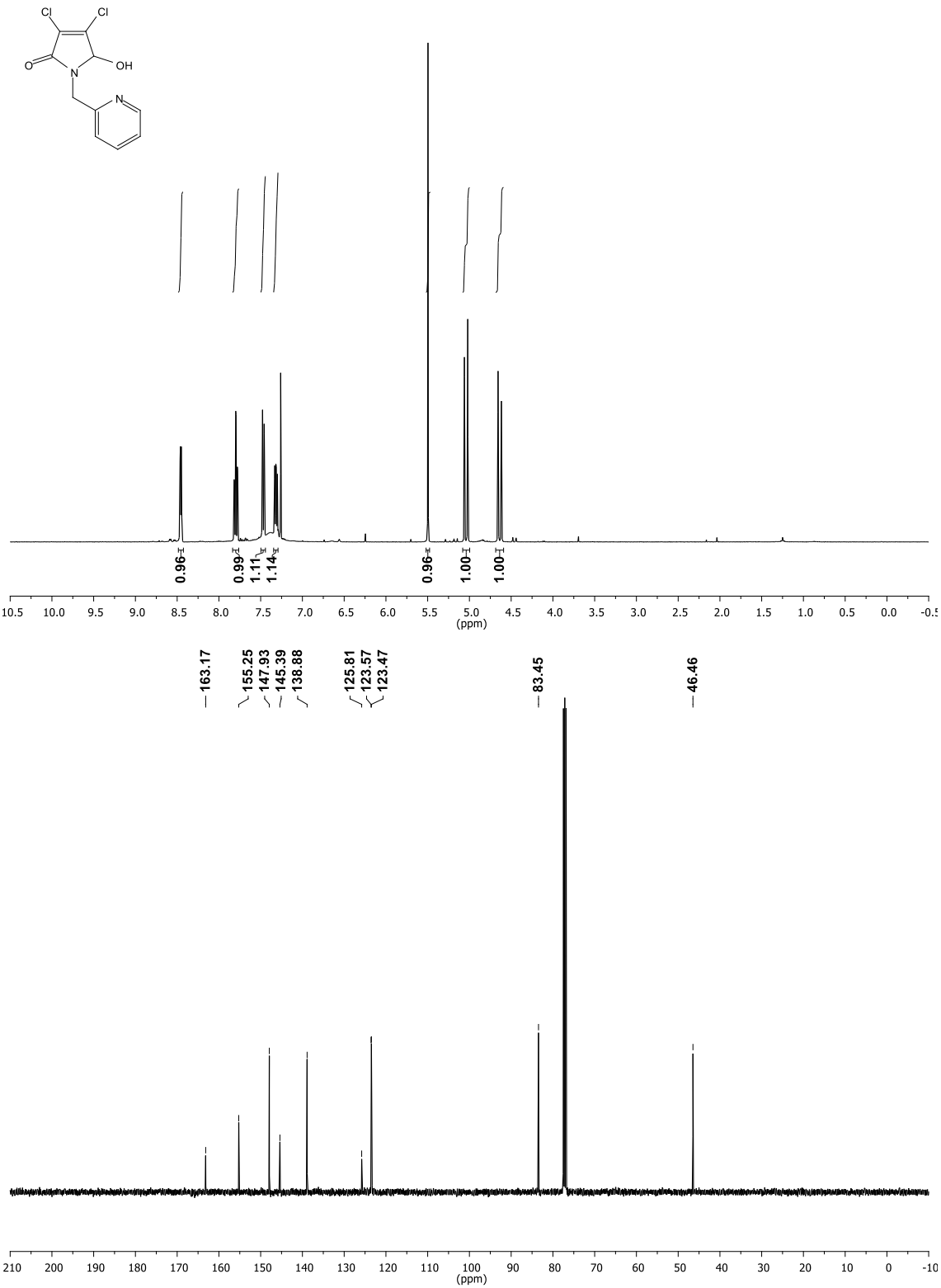
Cl
Cl
O
N
OH
N
0.96
0.99
1.11
1.14
0.96
1.00
1.00
(ppm)
163.17
155.25
147.93
145.39
138.88
125.81
123.57
123.47
83.45
46.46
(ppm)

2.49

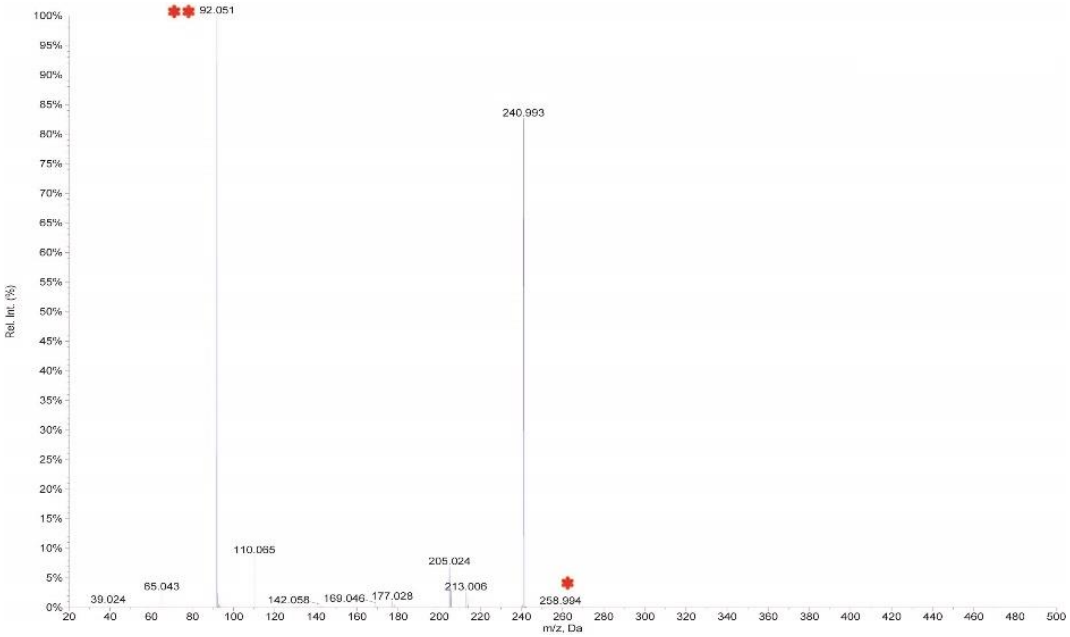
92.051
240.993
110.065
205.024
65.043
213.006
39.024
142.058
169.046
177.028
258.994
Rel. Int. (%)
m/z, Da

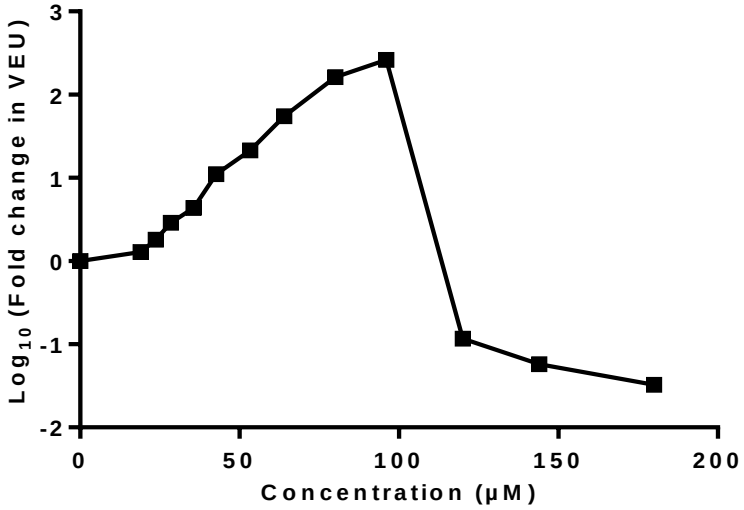
Log10 (Fold change in VEU)
Concentration (μM)

2.50

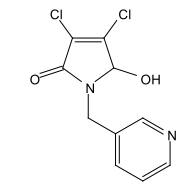
Cl
Cl
O
N
OH
N

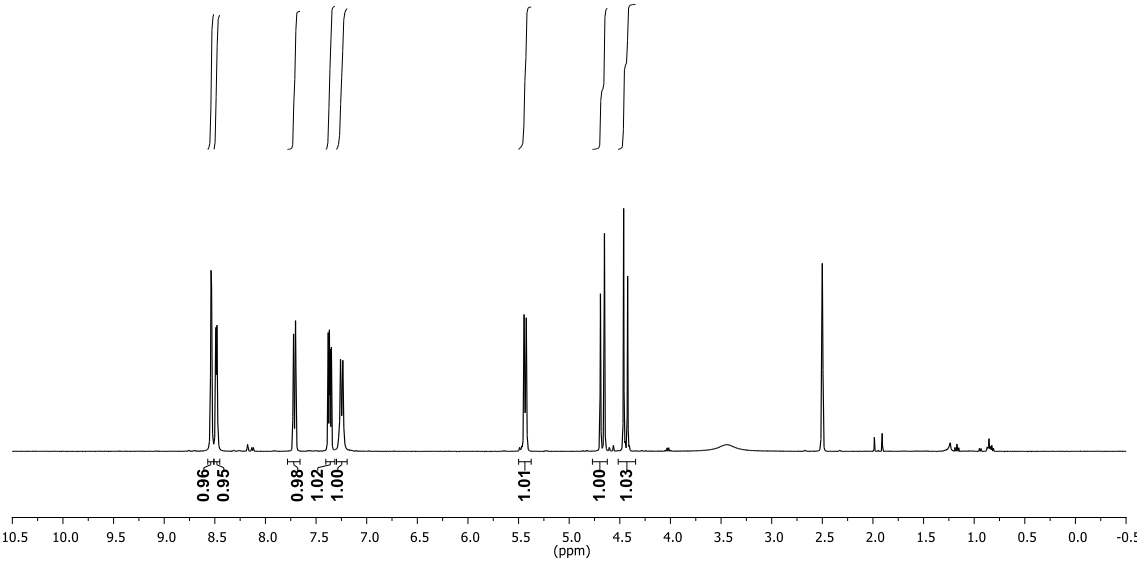
0.96
0.95
0.98
1.02
1.00
1.01
1.00
1.03
10.5 10.0 9.5 9.0 8.5 8.0 7.5 7.0 6.5 6.0 5.5 5.0 4.5 4.0 3.5 3.0 2.5 2.0 1.5 1.0 0.5 0.0
(ppm)

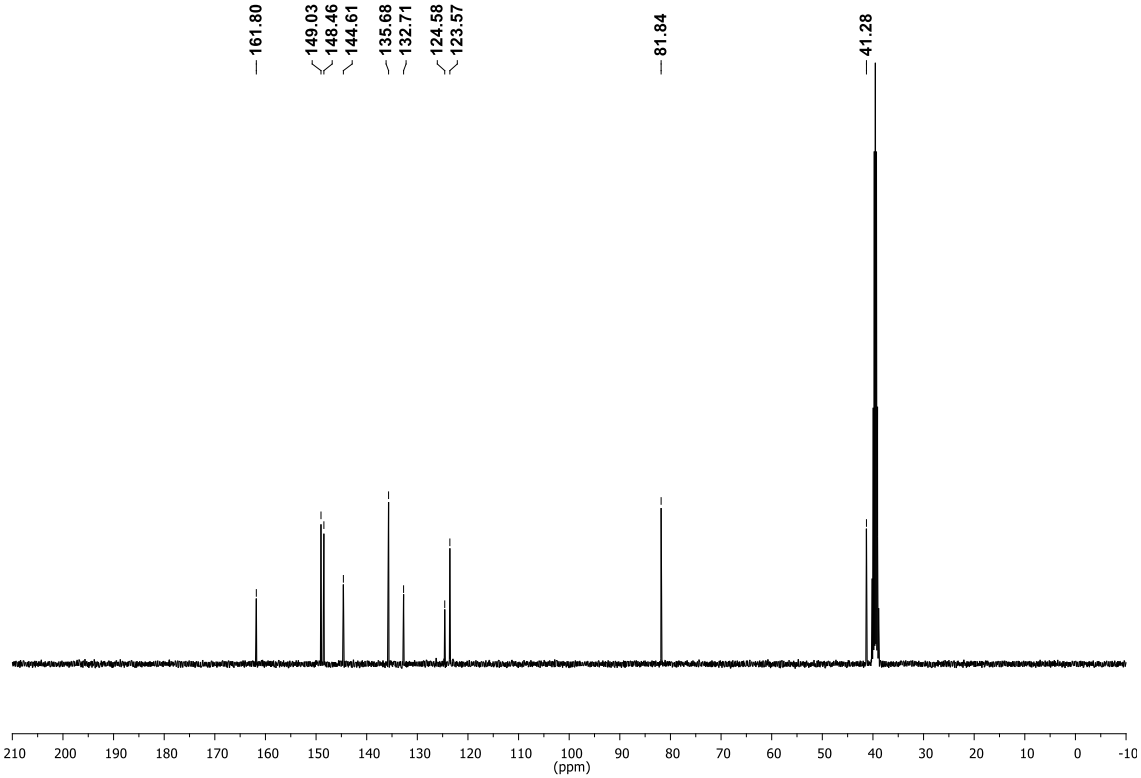
161.80
149.03
148.46
144.61
135.68
132.71
124.58
123.57
81.84
41.28
210 200 190 180 170 160 150 140 130 120 110 100 90 80 70 60 50 40 30 20 10 0
(ppm)

2.50

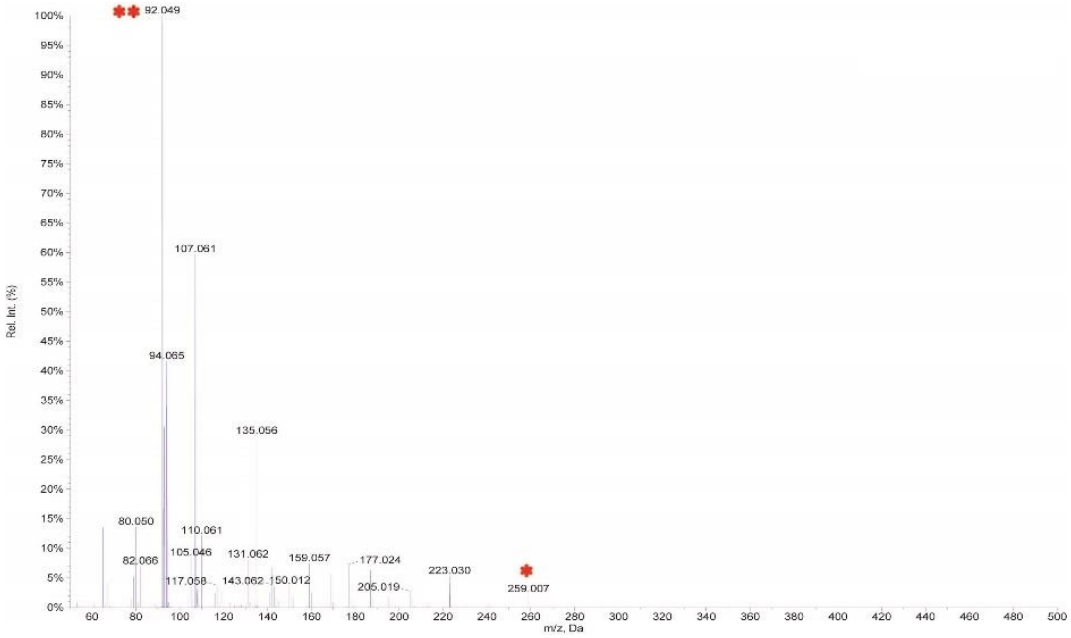
82.049
107.061
94.065
135.056
80.050
110.061
105.046
131.062
159.057
177.024
223.030
82.066
117.058
143.062
150.012
205.019
259.007
Rel. Int. (%)
m/z, Da

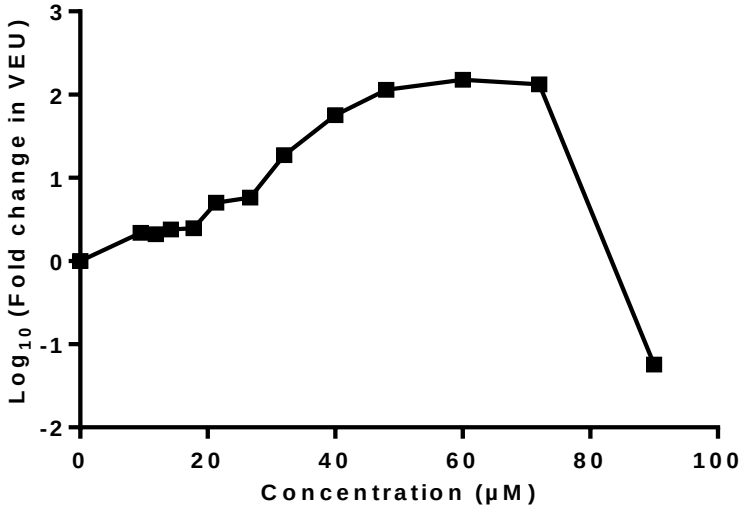
Log10 (Fold change in VEU)
Concentration (μM)

2.51

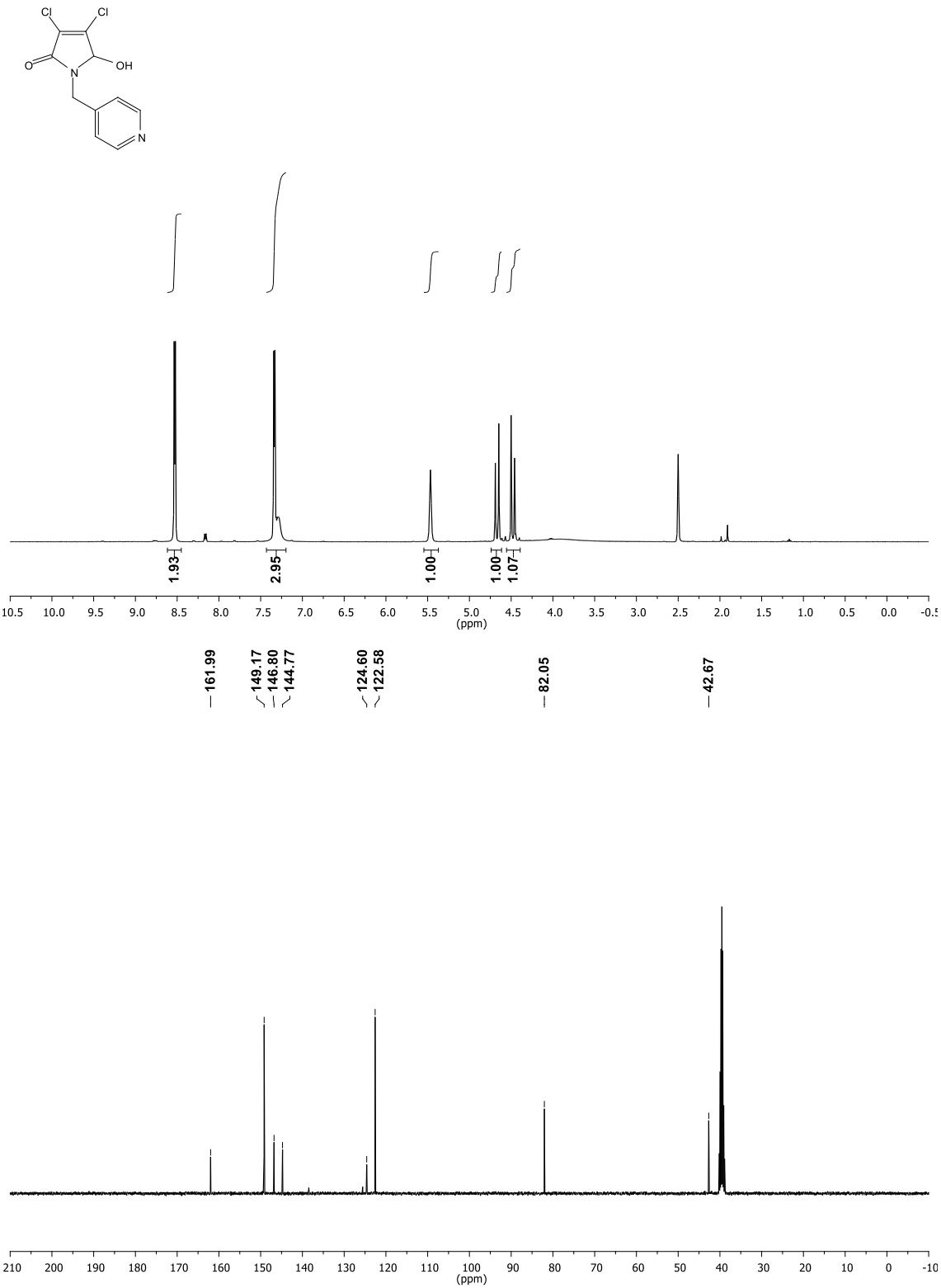
Cl
Cl
O
N
OH
N
1.93
2.95
1.00
1.00
1.07
(ppm)
161.99
149.17
146.80
144.77
124.60
122.58
82.05
42.67
(ppm)

2.51

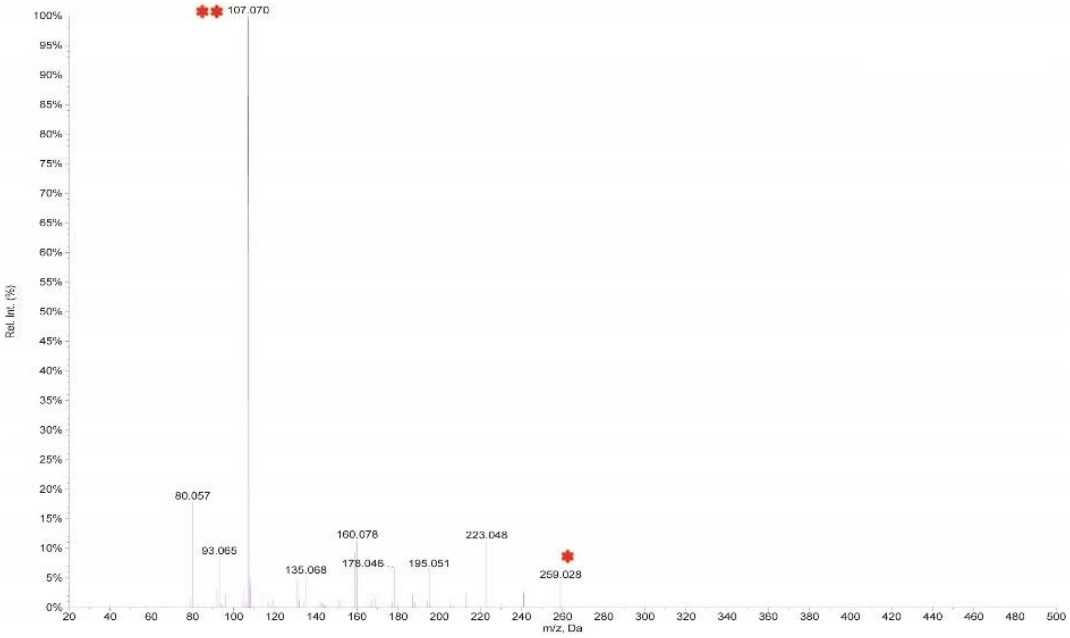
107.070
80.057
93.065
135.068
160.078
178.046
195.051
223.048
259.028
Rel. Int. (%)
m/z, Da

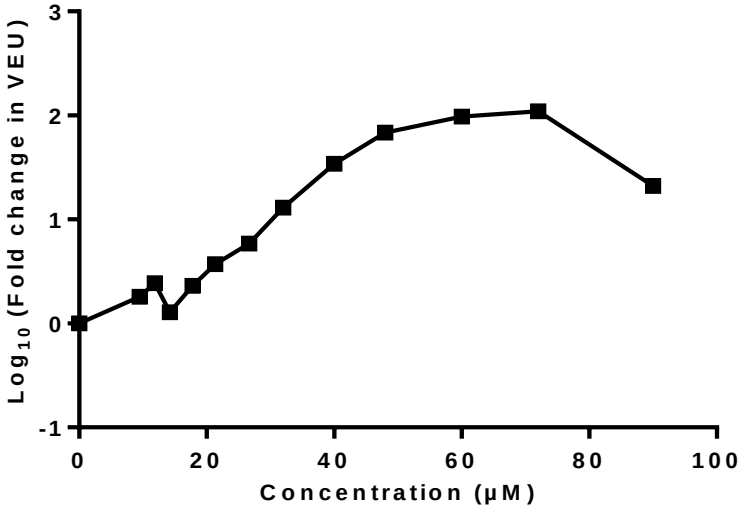
Log10 (Fold change in VEU)
Concentration (μM)

Chapter 3 spectra

3.14

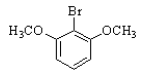
Br
H3CO
OCH3

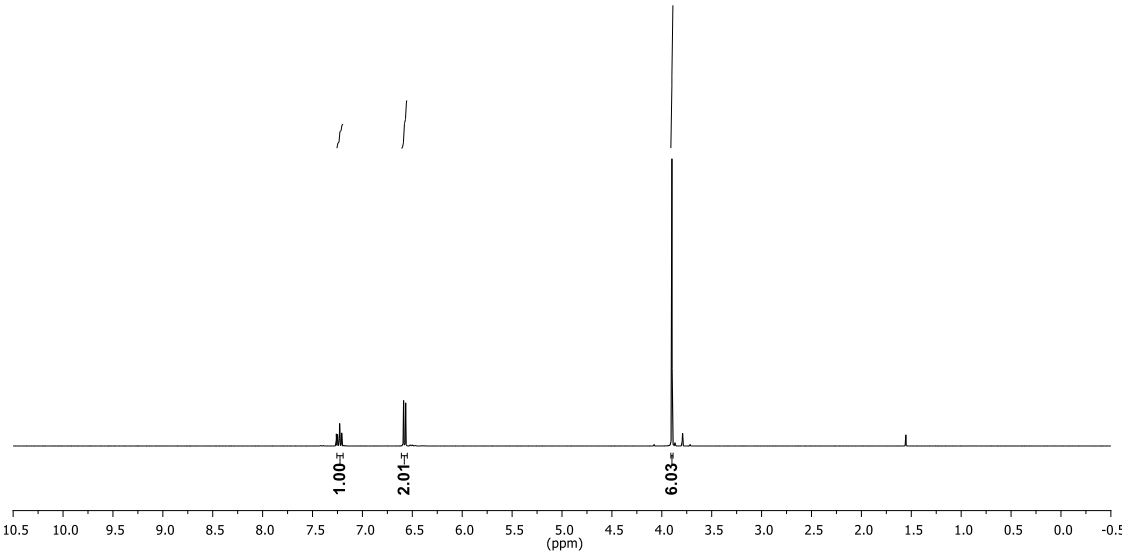
1.00
2.01
6.03
10.5 10.0 9.5 9.0 8.5 8.0 7.5 7.0 6.5 6.0 5.5 5.0 4.5 4.0 3.5 3.0 2.5 2.0 1.5 1.0 0.5 0.0 -0.5
(ppm)

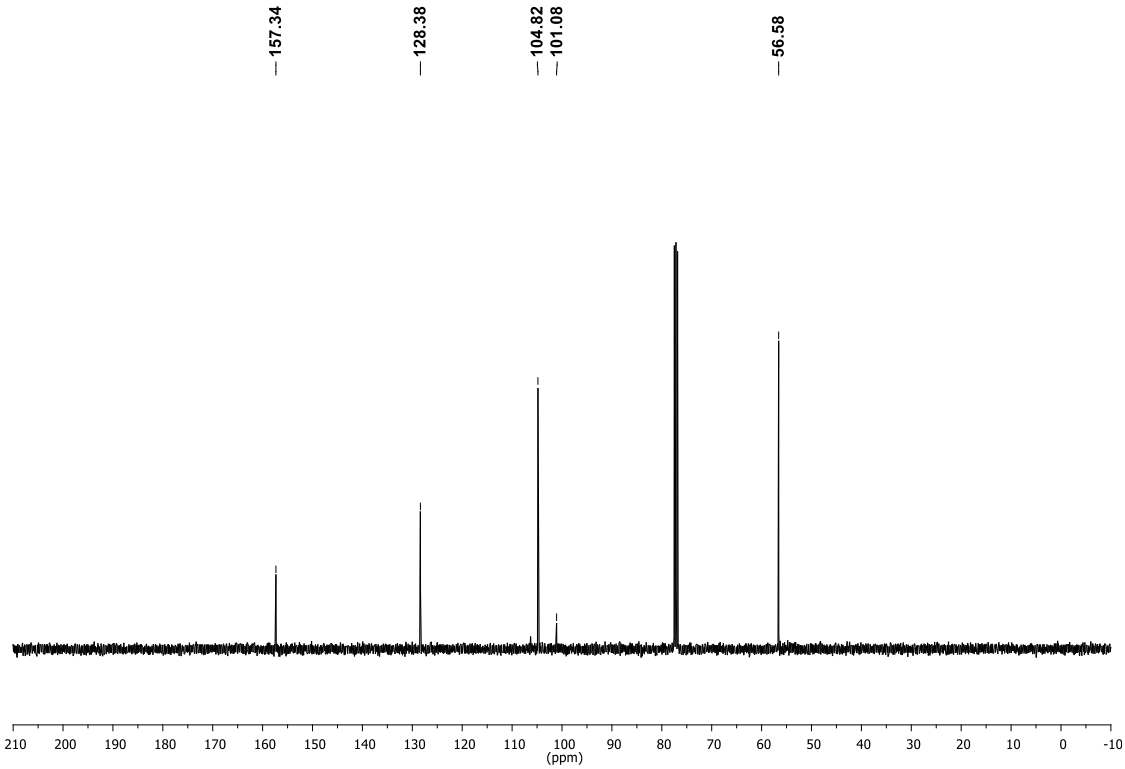
157.34
128.38
104.82
101.08
56.58
210 200 190 180 170 160 150 140 130 120 110 100 90 80 70 60 50 40 30 20 10 0 -10
(ppm)

3.15

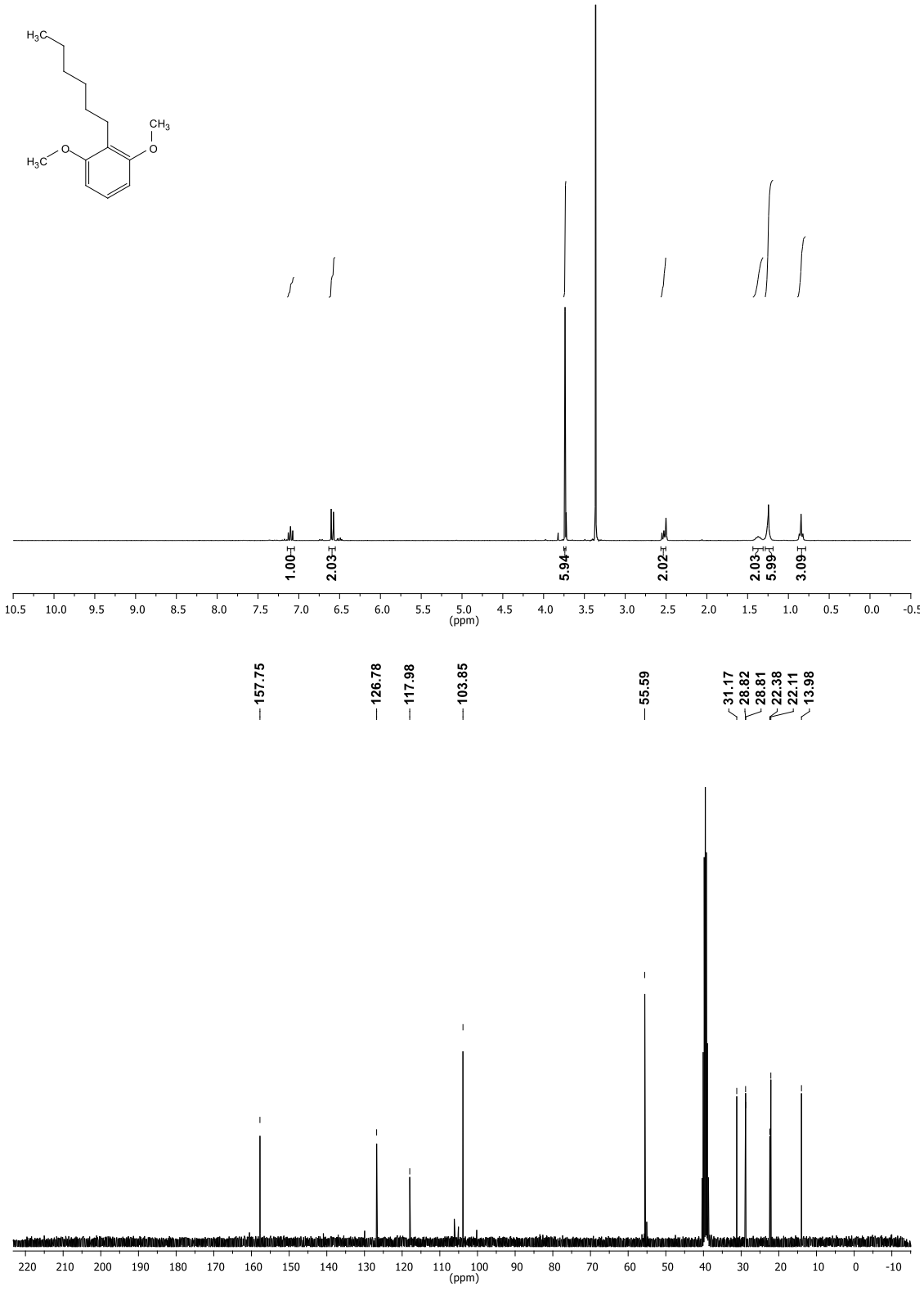
H3C
CH3
O
H3C
O
1.00
2.03
5.94
2.02
2.03
5.99
3.09
(ppm)
157.75
126.78
117.98
103.85
55.59
31.17
28.82
28.81
22.38
22.11
13.98
(ppm)

3.16

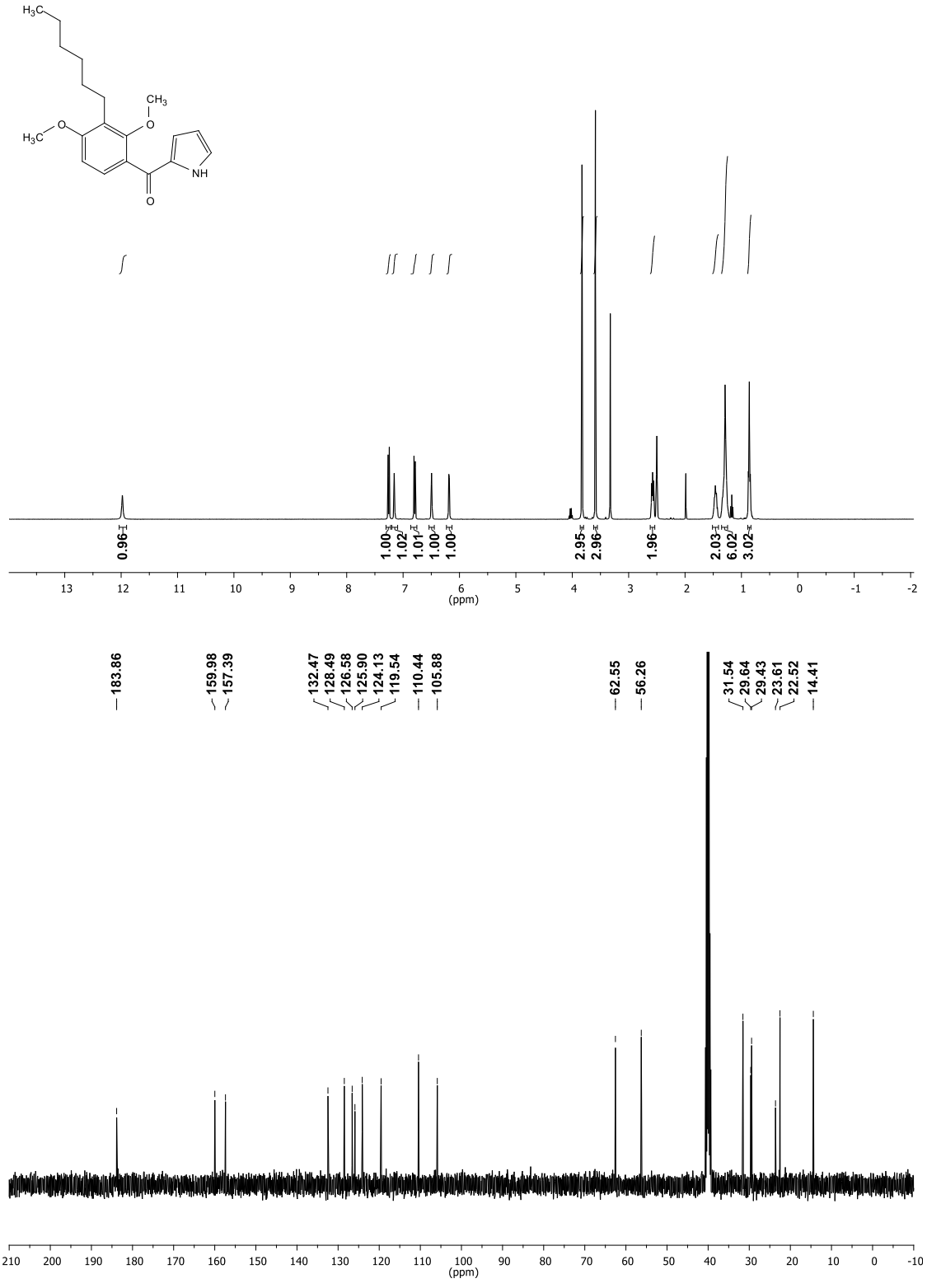
H3C
CH3
O
O
H3C
NH
O
0.96
1.00
1.02
1.01
1.00
1.00
2.95
2.96
1.96
2.03
6.02
3.02
(ppm)
183.86
159.98
157.39
132.47
128.49
126.58
125.90
124.13
119.54
110.44
105.88
62.55
56.26
31.54
29.64
29.43
23.61
22.52
14.41
(ppm)

3.17

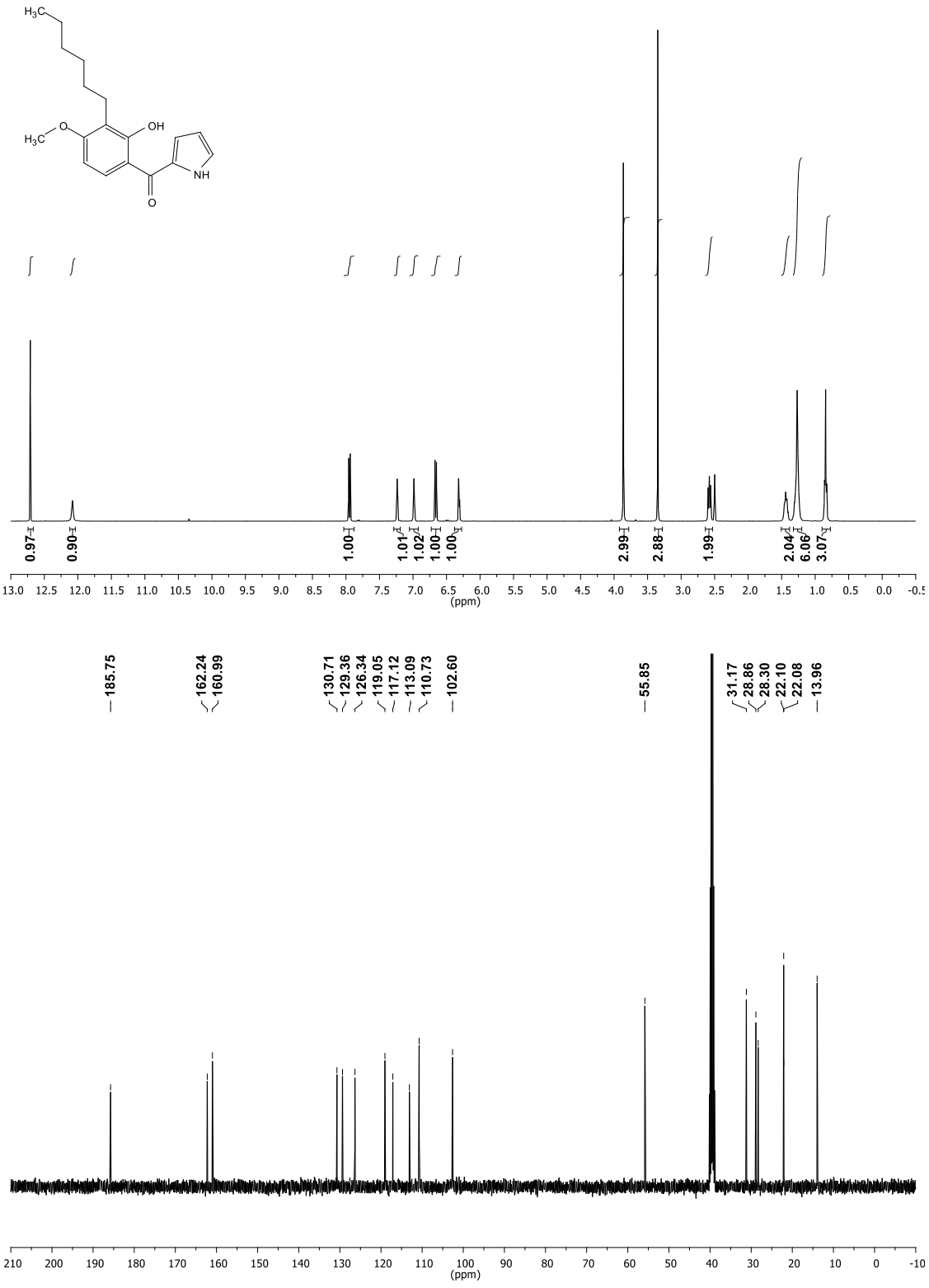
H3C
O
H3C
OH
NH
O
0.97
0.90
1.00
1.01
1.02
1.00
1.00
2.99
2.88
1.99
2.04
6.06
3.07
(ppm)
185.75
162.24
160.99
130.71
129.36
126.34
119.05
117.12
113.09
110.73
102.60
55.85
31.17
28.86
28.30
22.10
22.08
13.96
(ppm)

3.19

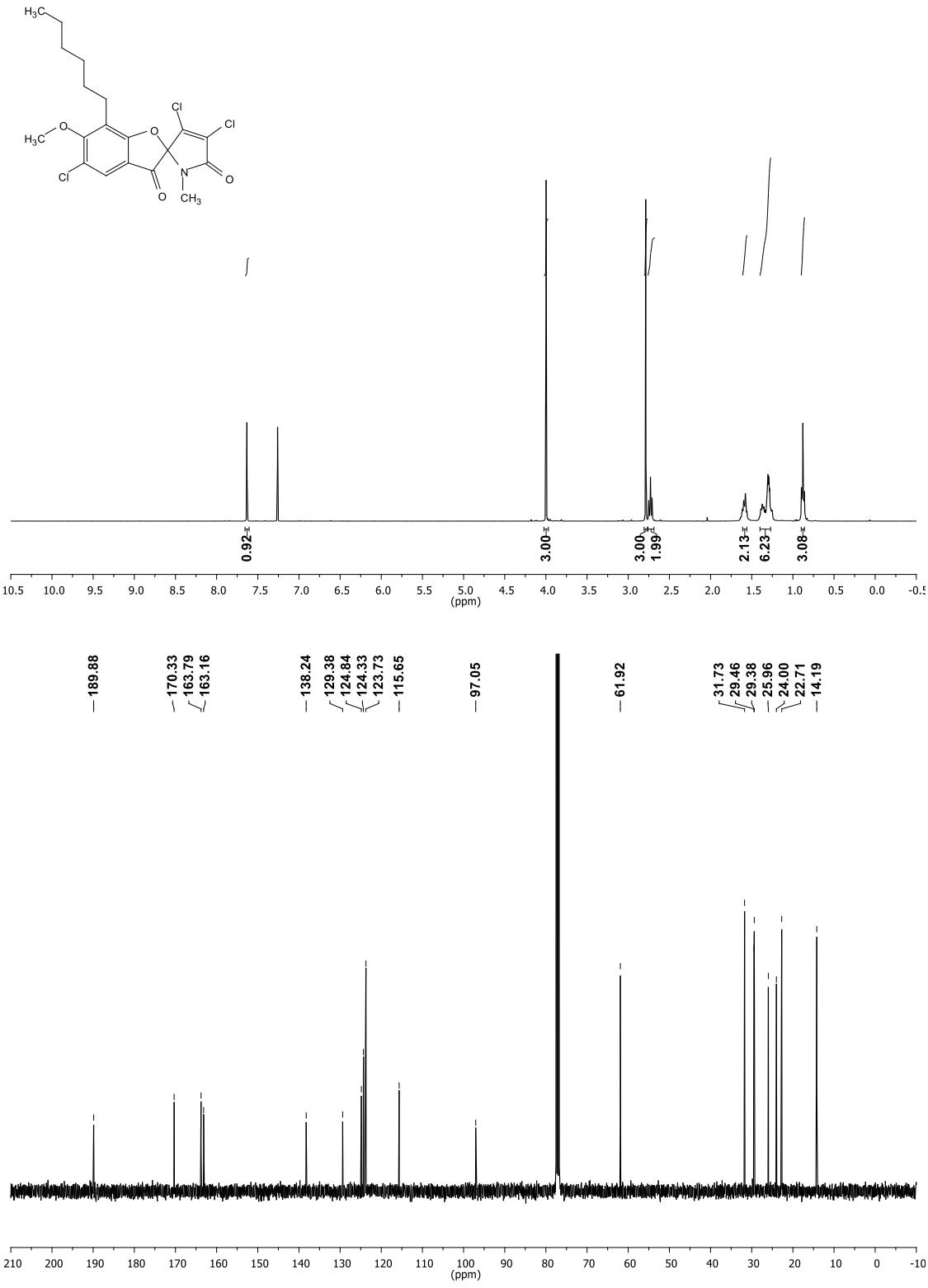
H3C
O
H3C
Cl
Cl
O
Cl
N
CH3
O
O
0.92
3.00
3.00
1.99
2.13
6.23
3.08
(ppm)
189.88
170.33
163.79
163.16
138.24
129.38
124.84
124.33
123.73
115.65
97.05
61.92
31.73
29.46
29.38
25.96
24.00
22.71
14.19
(ppm)

3.4

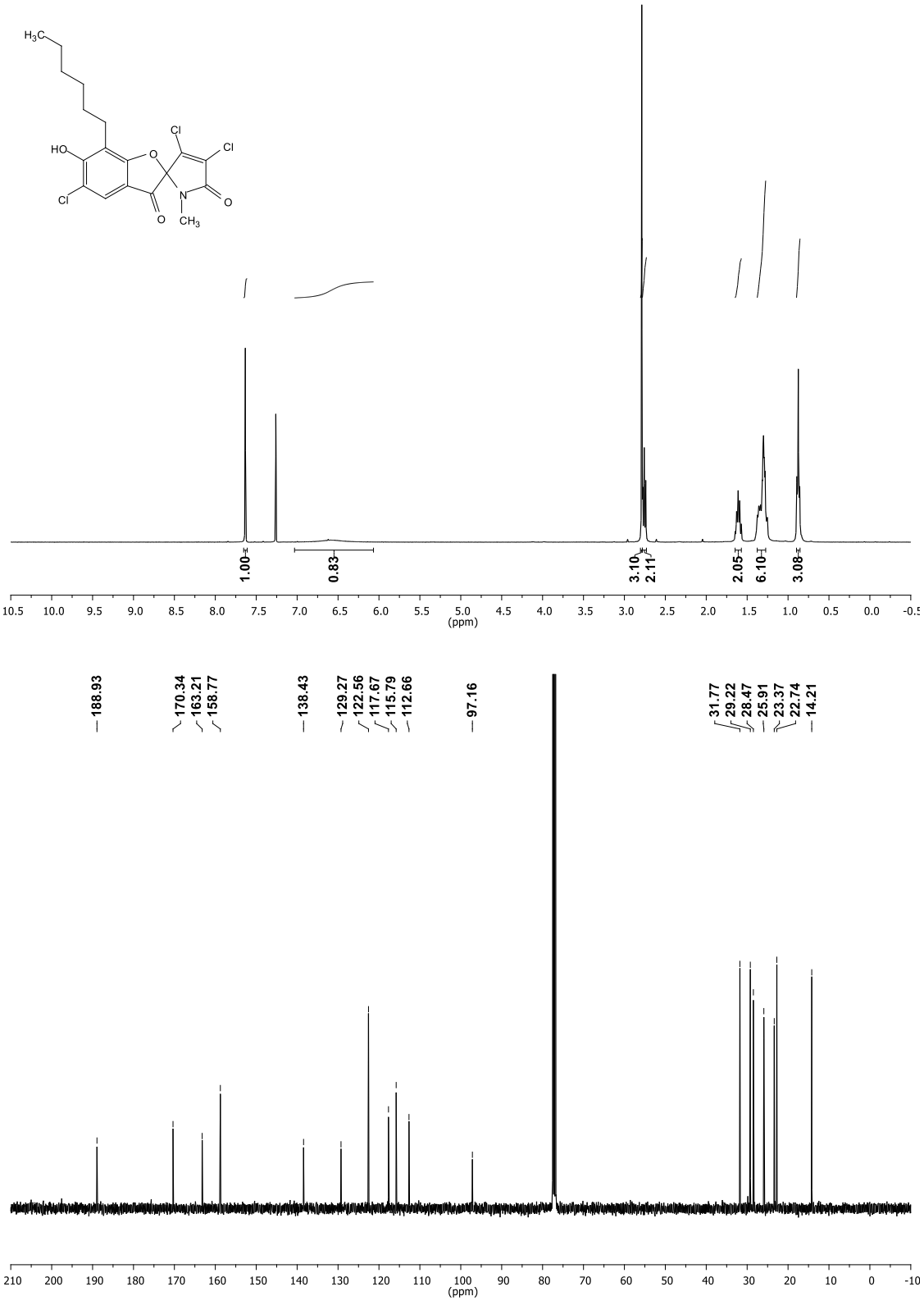
H3C
HO
Cl
Cl
Cl
O
O
N
O
O
CH3
1.00
0.83
3.10
2.11
2.05
6.10
3.08
(ppm)
188.93
170.34
163.21
158.77
138.43
129.27
122.56
117.67
115.79
112.66
97.16
31.77
29.22
28.47
25.91
23.37
22.74
14.21
(ppm)

3.20

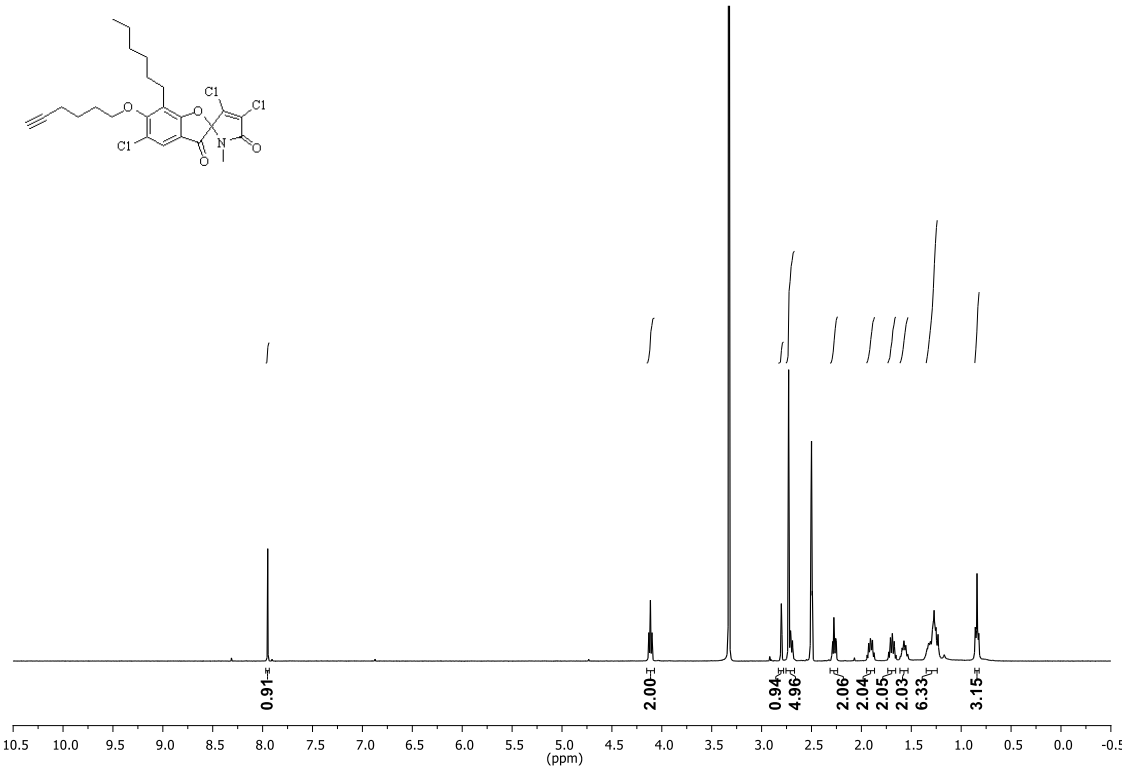
Cl
Cl
Cl
O
O
N
O
O
0.91
2.00
0.94
4.96
2.06
2.04
2.05
2.03
6.33
3.15
(ppm)

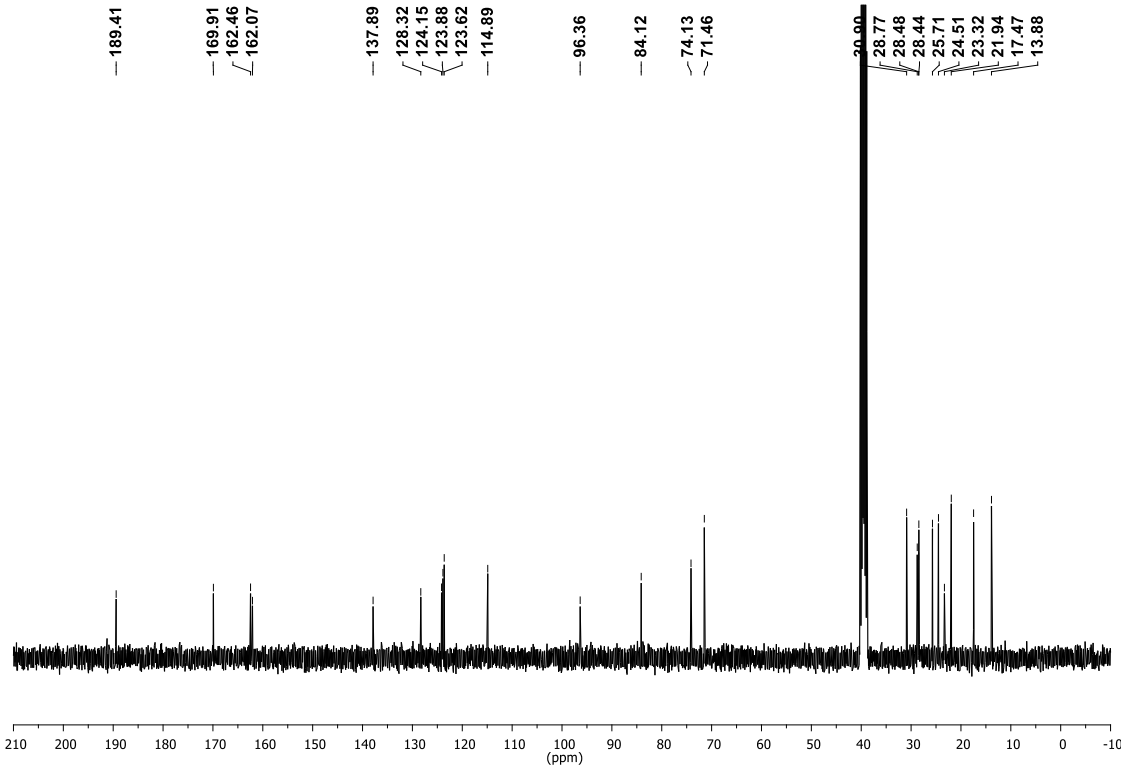
189.41
169.91
162.46
162.07
137.89
128.32
124.15
123.88
123.62
114.89
96.36
84.12
74.13
71.46
30.90
28.77
28.48
28.44
25.71
24.51
23.32
21.94
17.47
13.88
(ppm)

3.21

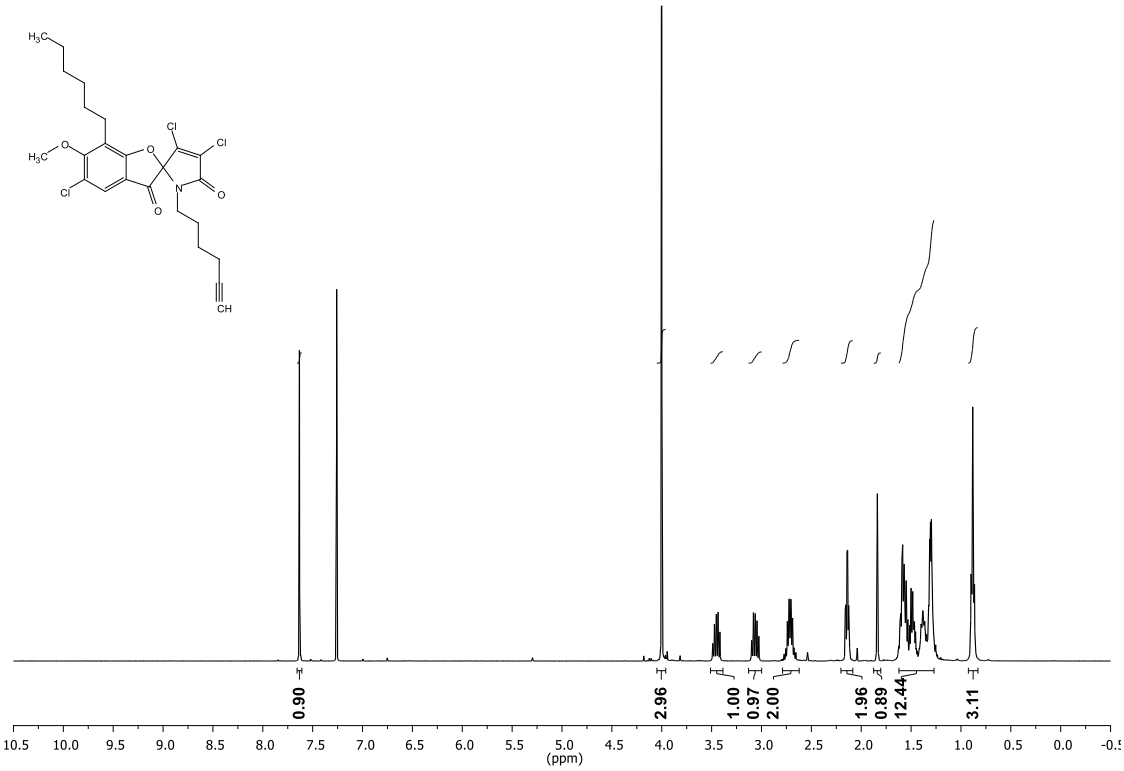
0.90
2.96
1.00
0.97
2.00
1.96
0.89
12.44
3.11
(ppm)

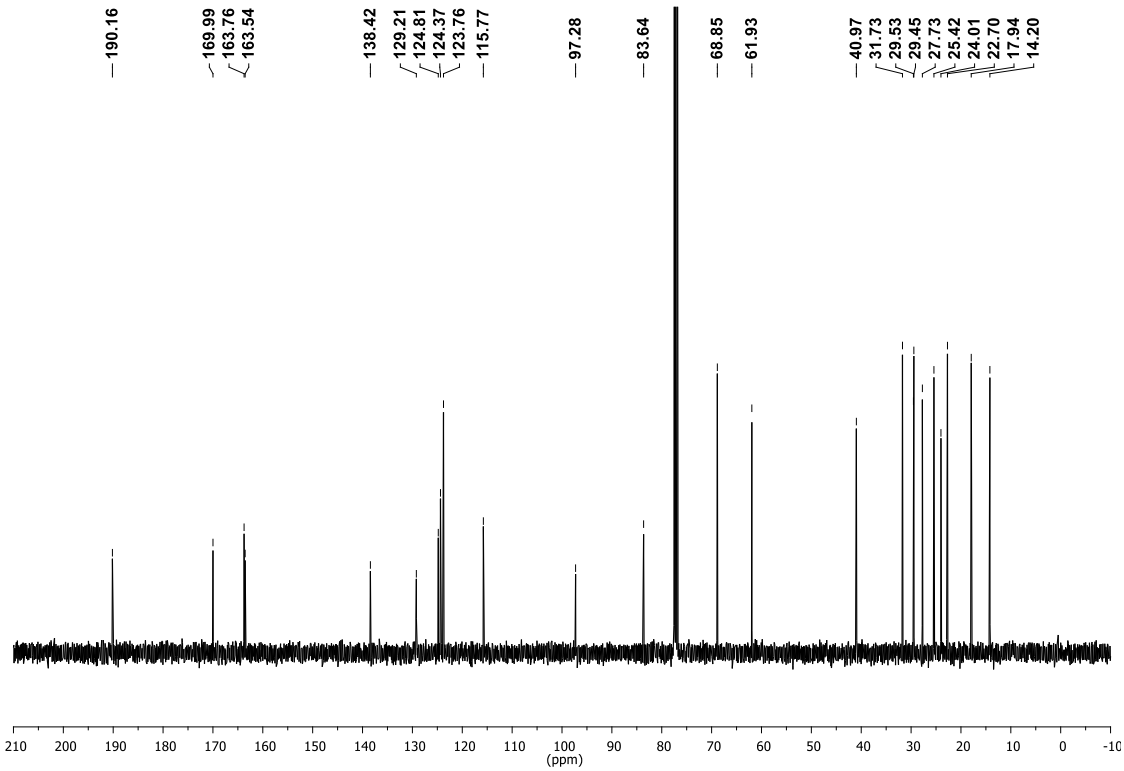
190.16
169.99
163.76
163.54
138.42
129.21
124.81
124.37
123.76
115.77
97.28
83.64
68.85
61.93
40.97
31.73
29.53
29.45
27.73
25.42
24.01
22.70
17.94
14.20
(ppm)

3.22

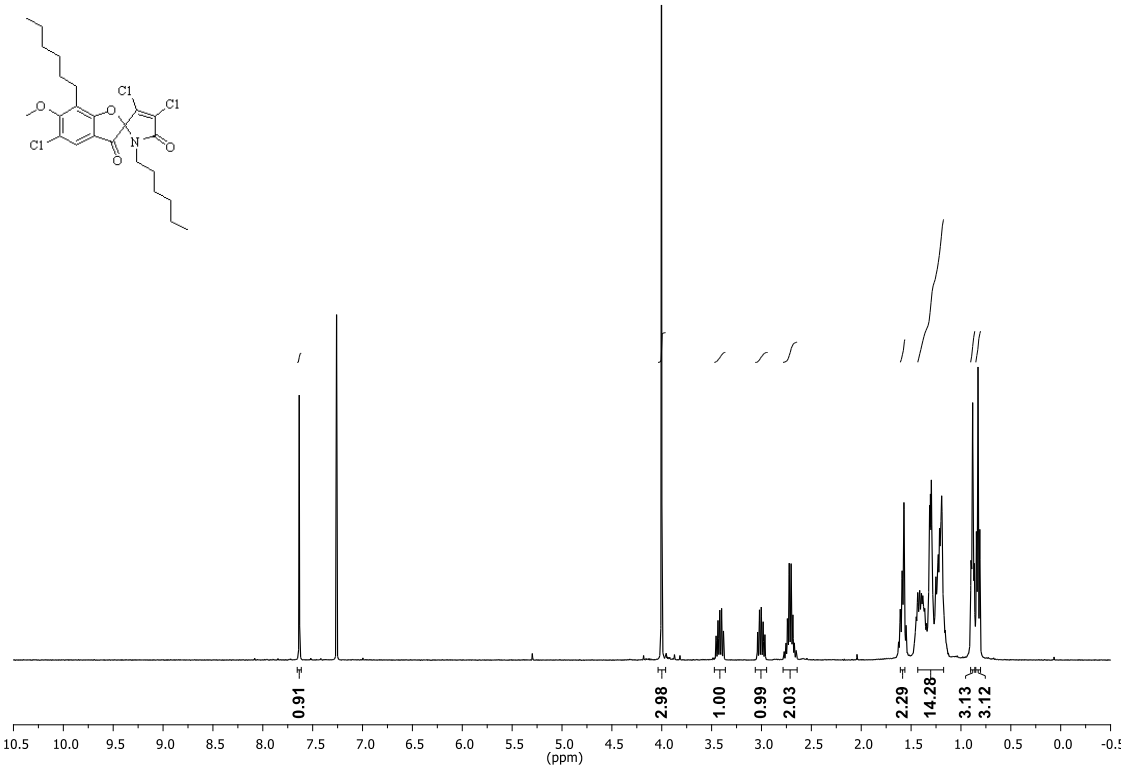
0.91
2.98
1.00
0.99
2.03
2.29
14.28
3.13
3.12
(ppm)

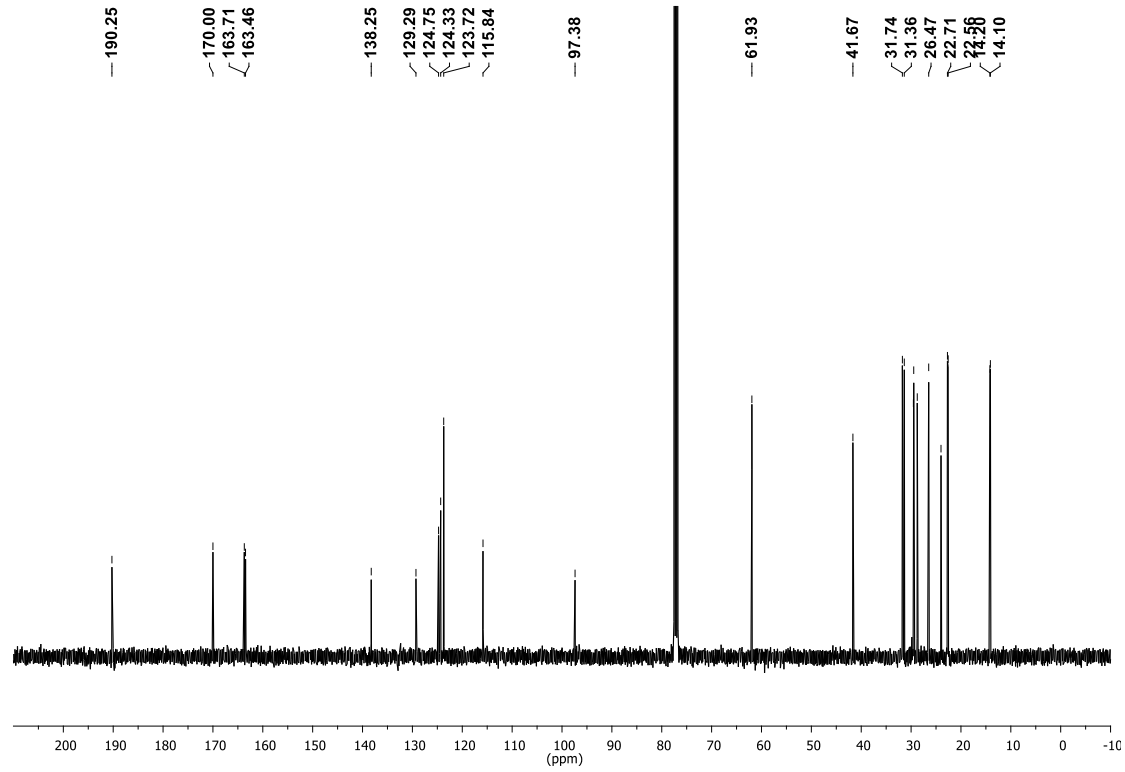
190.25
170.00
163.71
163.46
138.25
129.29
124.75
124.33
123.72
115.84
97.38
61.93
41.67
31.74
31.36
26.47
22.71
14.10
(ppm)

3.23

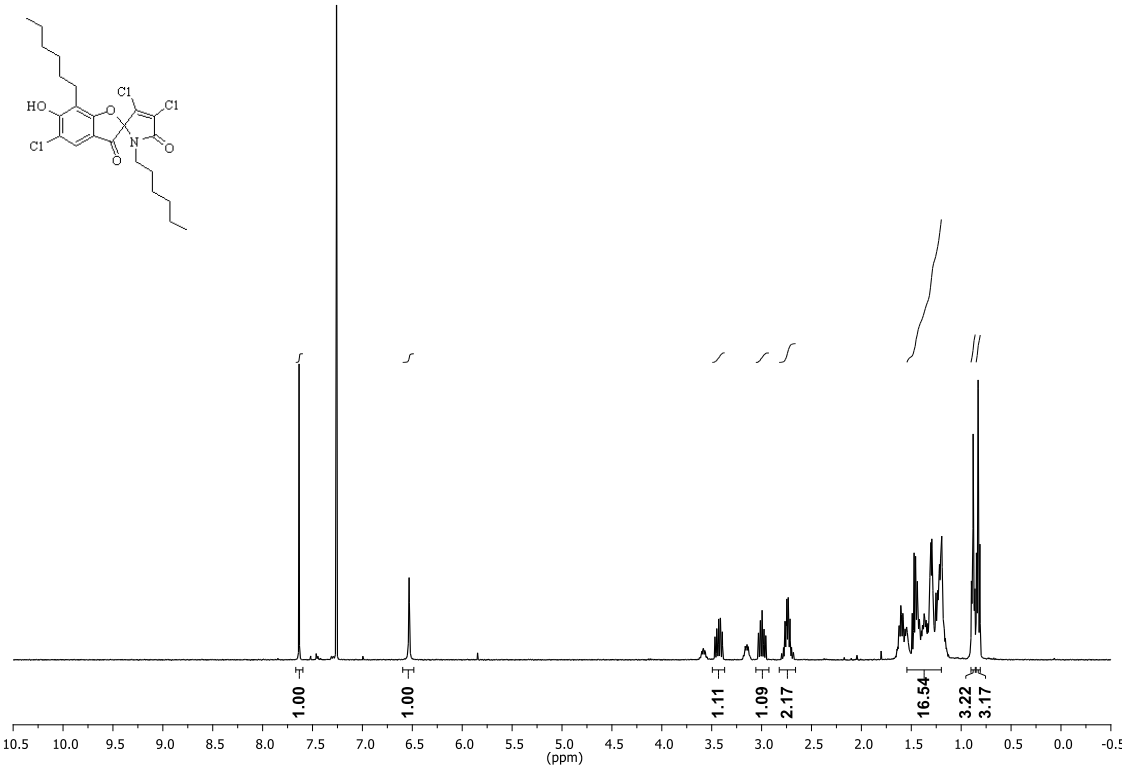
HO
Cl
Cl
Cl
O
N
O
O
1.00
1.00
1.11
1.09
2.17
16.54
3.22
3.17
(ppm)

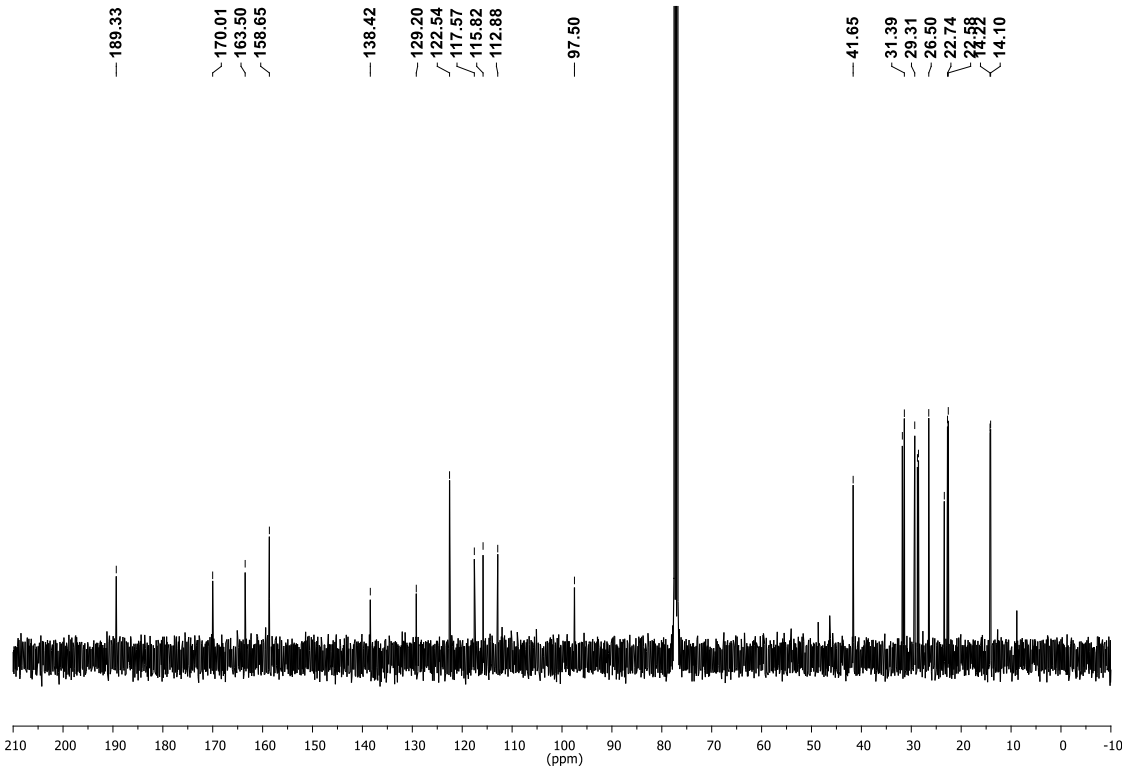
189.33
170.01
163.50
158.65
138.42
129.20
122.54
117.57
115.82
112.88
97.50
41.65
31.39
29.31
26.50
22.74
14.22
14.10
(ppm)

3.25

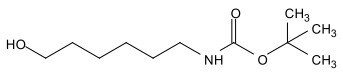
HO
NH
O
O
CH3
CH3
CH3

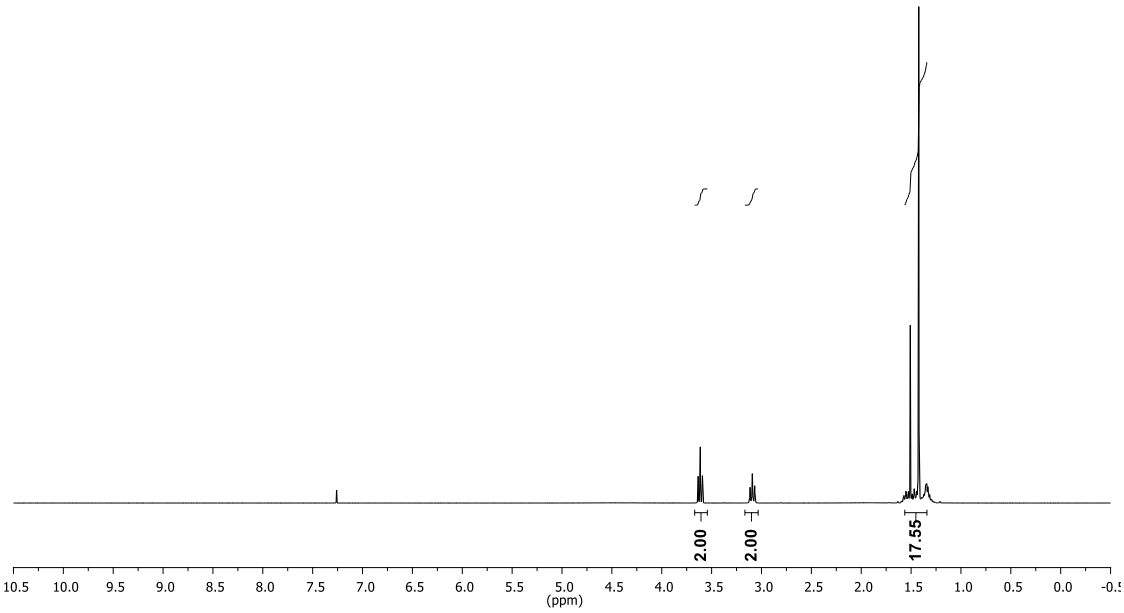
2.00
2.00
17.55
(ppm)

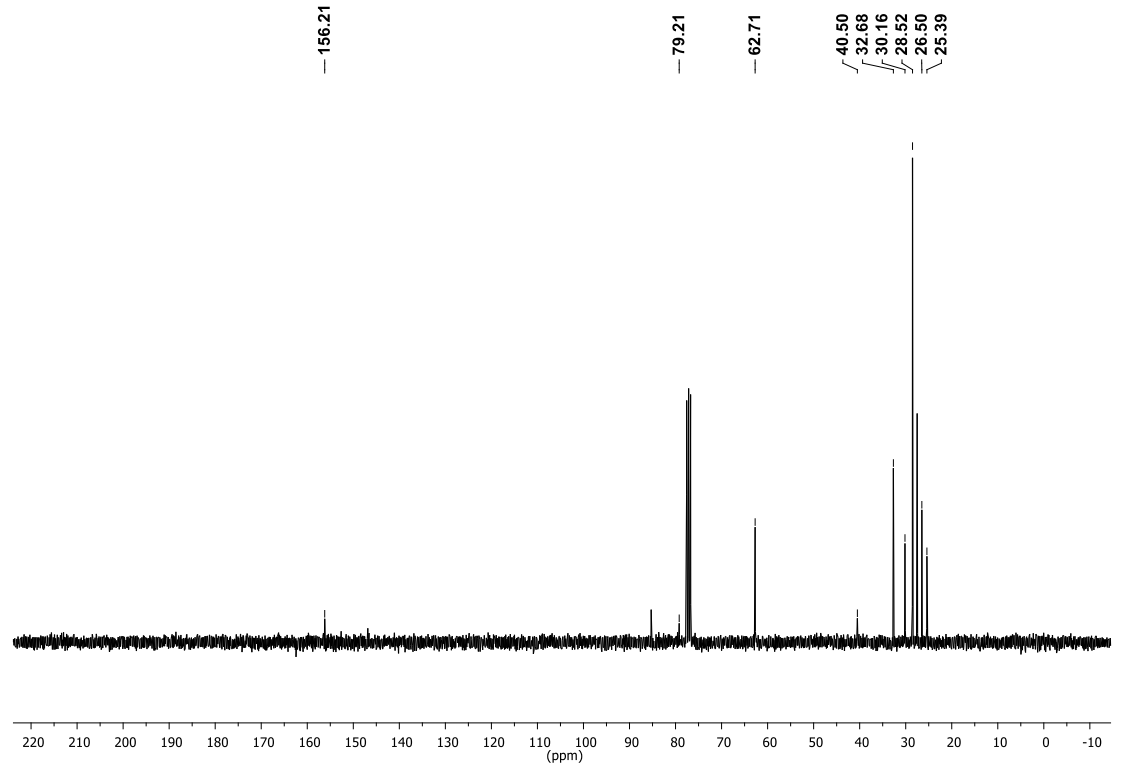
156.21
79.21
62.71
40.50
32.68
30.16
28.52
26.50
25.39
(ppm)

3.26

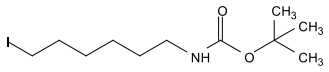
O
CH3
CH3
I
NH
O
CH3

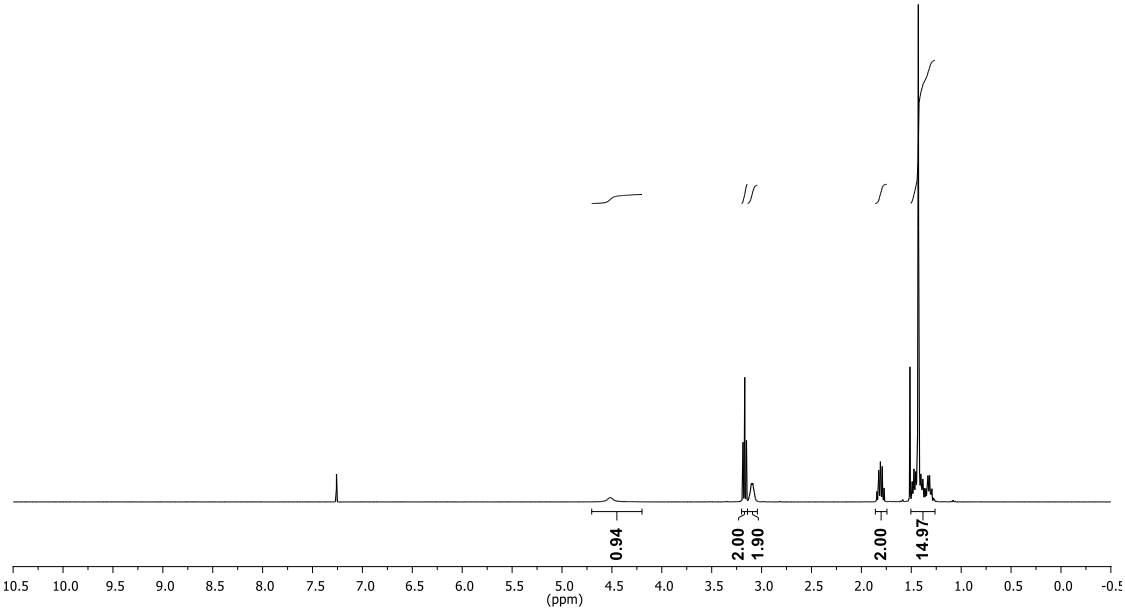
0.94
2.00
1.90
2.00
14.97
10.5 10.0 9.5 9.0 8.5 8.0 7.5 7.0 6.5 6.0 5.5 5.0 4.5 4.0 3.5 3.0 2.5 2.0 1.5 1.0 0.5 0.0
(ppm)

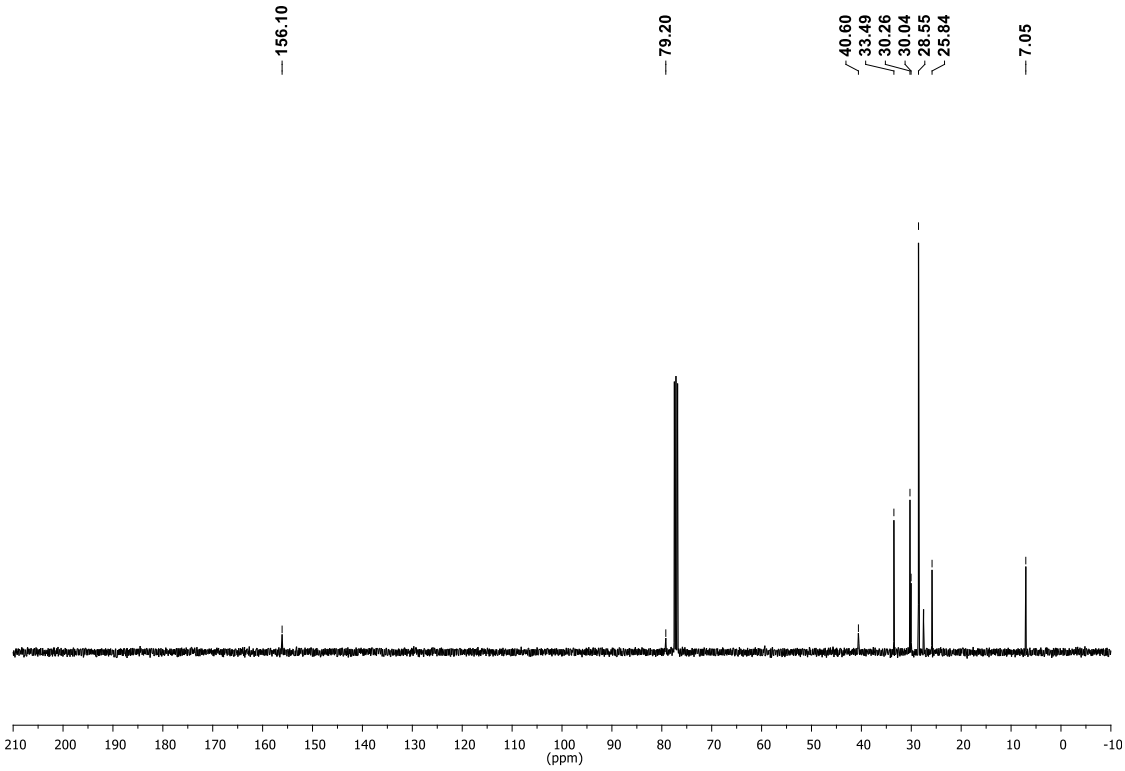
156.10
79.20
40.60
33.49
30.26
30.04
28.55
25.84
7.05
210 200 190 180 170 160 150 140 130 120 110 100 90 80 70 60 50 40 30 20 10 0
(ppm)

3.27

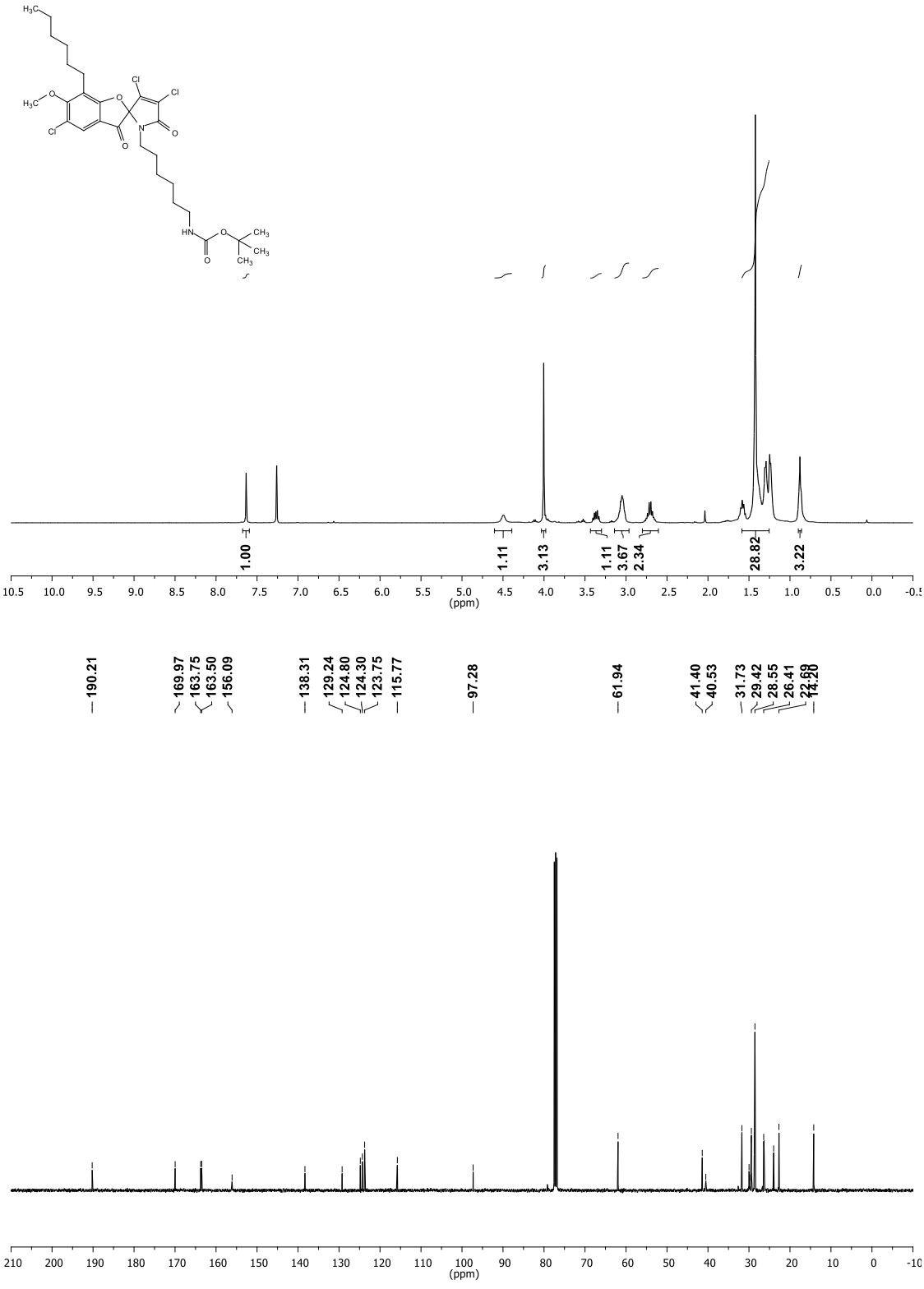
1.00
1.11
3.13
1.11
3.67
2.34
28.82
3.22
(ppm)
190.21
169.97
163.75
163.50
156.09
138.31
129.24
124.80
124.30
123.75
115.77
97.28
61.94
41.40
40.53
31.73
29.42
28.55
26.41
(ppm)

3.28

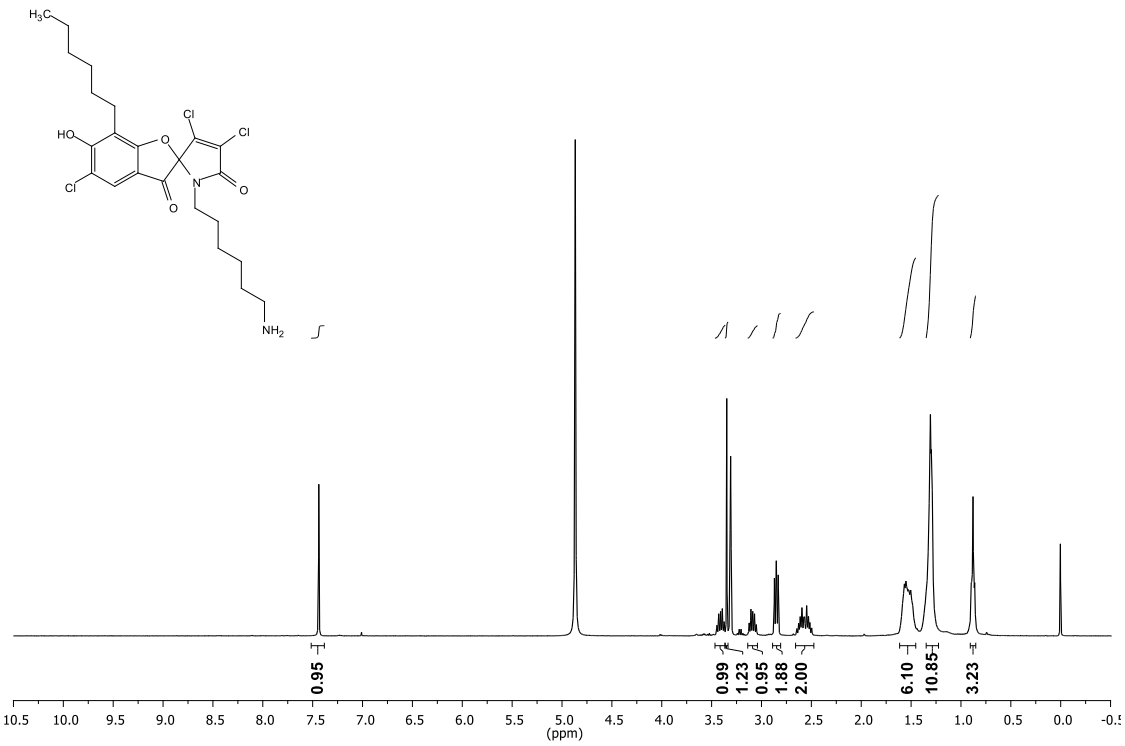
H3C
HO
O
Cl
Cl
Cl
N
O
O
O
NH2
0.95
0.99
1.23
0.95
1.88
2.00
6.10
10.85
3.23
(ppm)

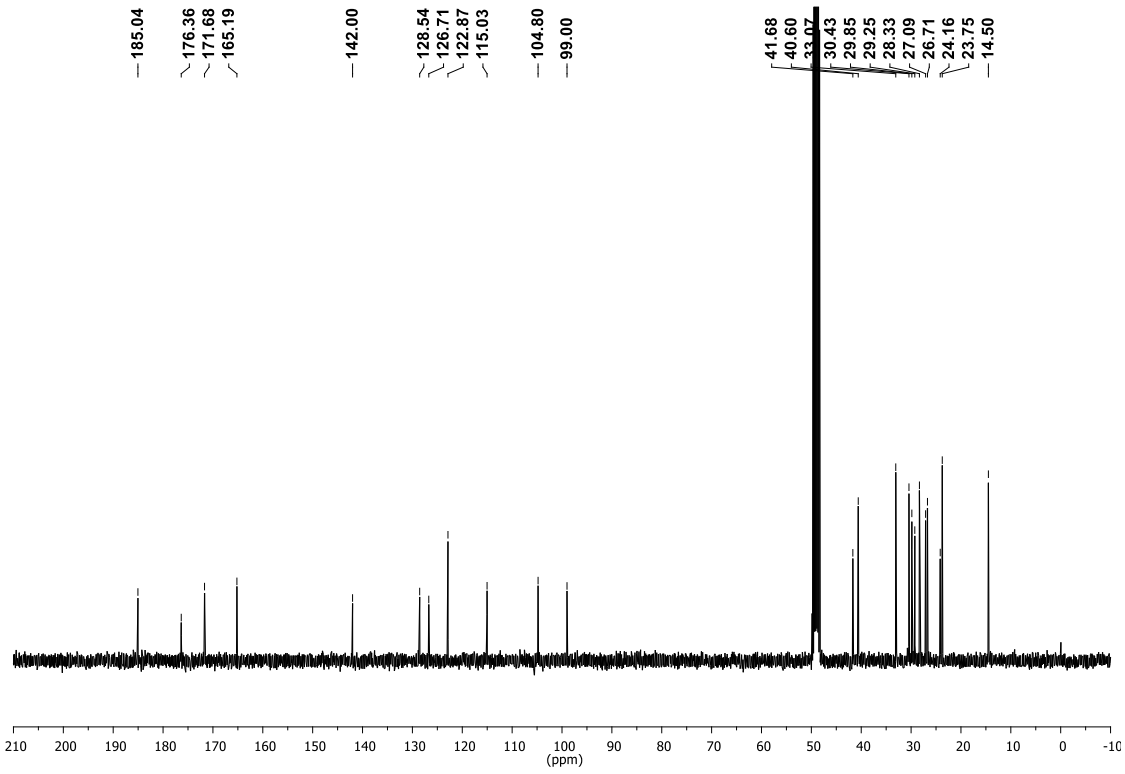
185.04
176.36
171.68
165.19
142.00
128.54
126.71
122.87
115.03
104.80
99.00
41.68
40.60
33.07
30.43
29.85
29.25
28.33
27.09
26.71
24.16
23.75
14.50
(ppm)

3.30

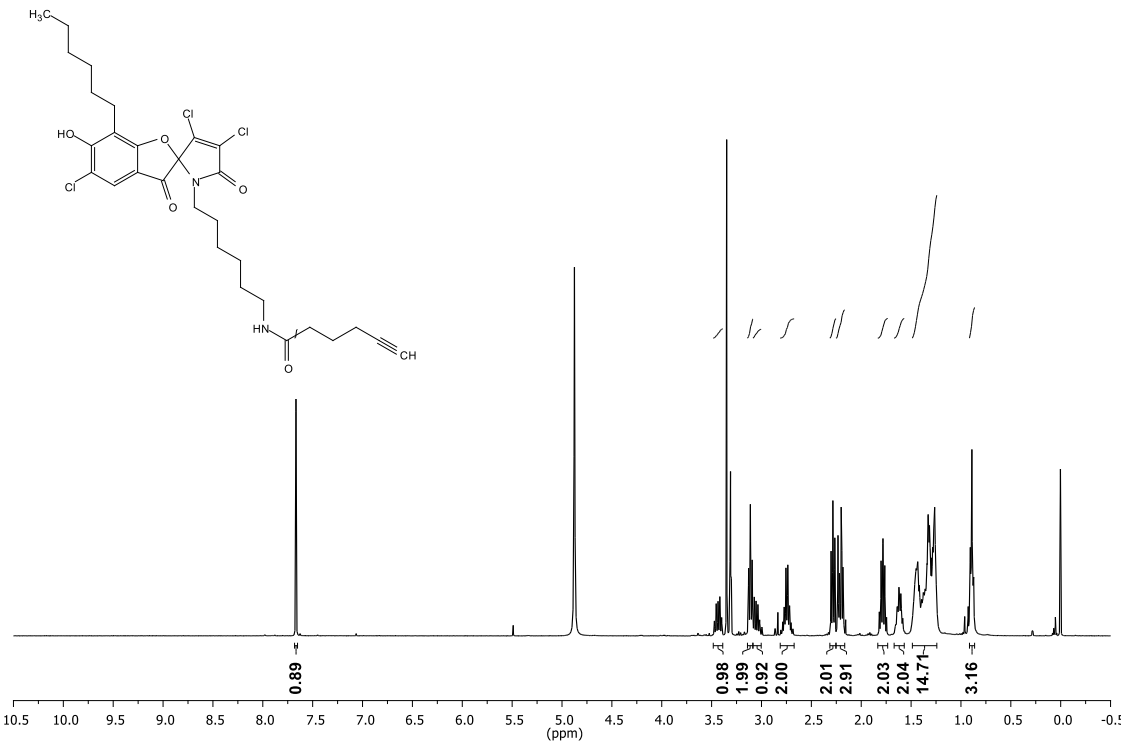
H3C
HO
Cl
Cl
Cl
O
O
O
N
O
HN
O
CH
0.89
0.98
1.99
0.92
2.00
2.01
2.91
2.03
2.04
14.71
3.16
(ppm)

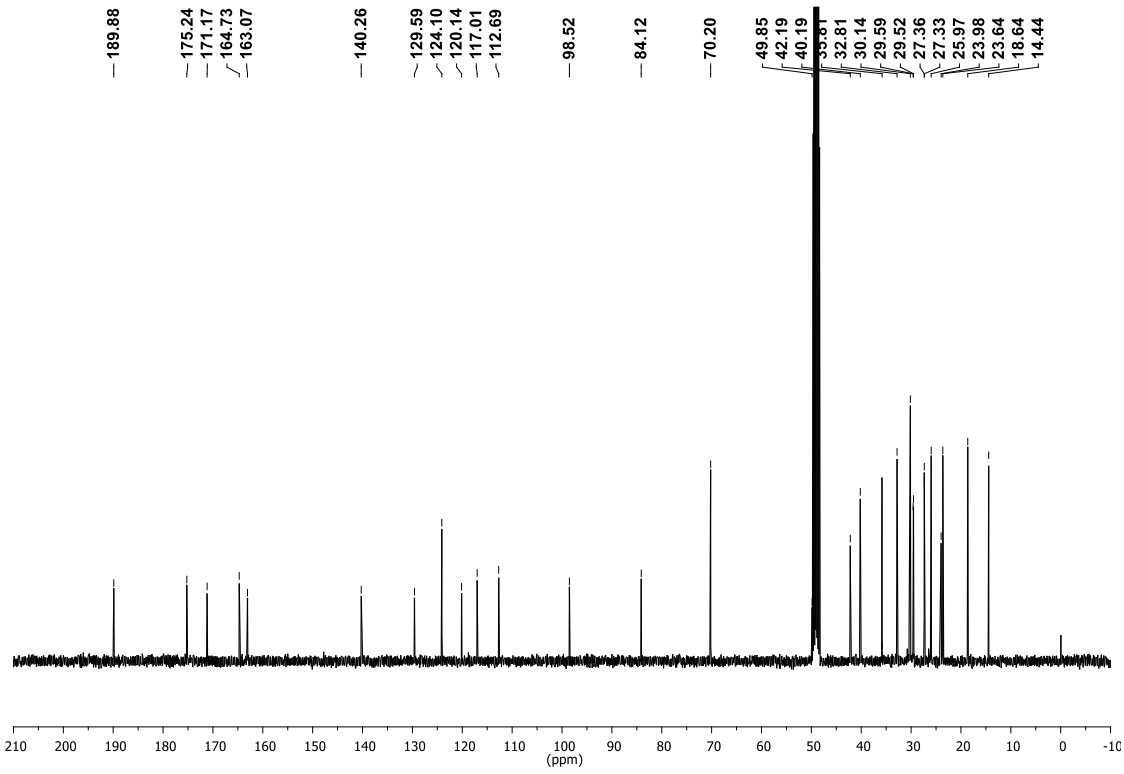
189.88
175.24
171.17
164.73
163.07
140.26
129.59
124.10
120.14
117.01
112.69
98.52
84.12
70.20
49.85
42.19
40.19
32.81
30.14
29.59
29.52
27.36
27.33
25.97
23.98
23.64
18.64
14.44
(ppm)

Chapter 4 spectra

4.2

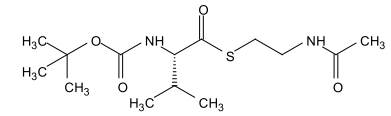

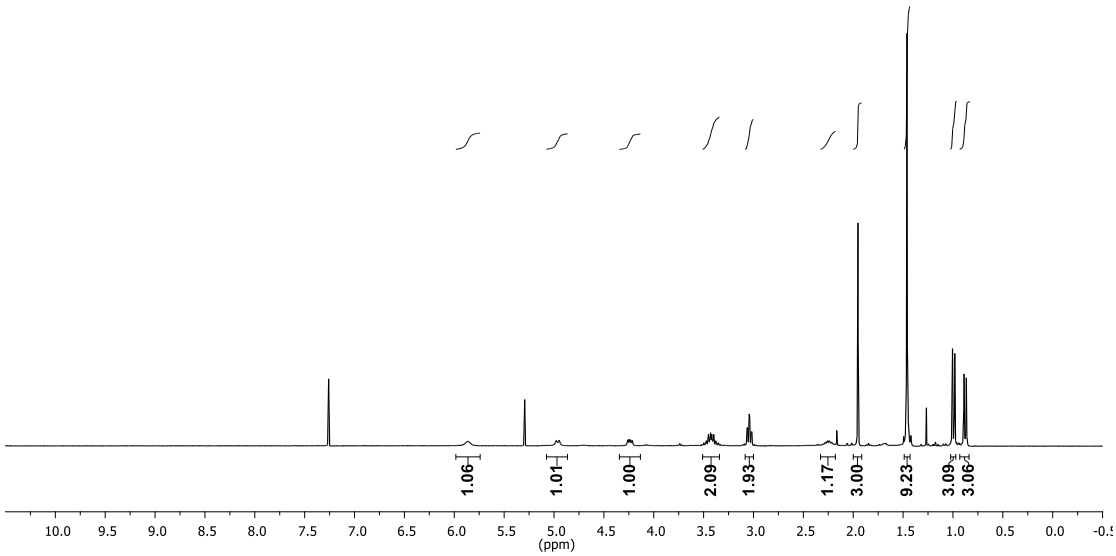
1.06
1.01
1.00
2.09
1.93
1.17
3.00
9.23
3.09
3.06
10.0
9.5
9.0
8.5
8.0
7.5
7.0
6.5
6.0
5.5
5.0
4.5
4.0
3.5
3.0
2.5
2.0
1.5
1.0
0.5
0.0
(ppm)

4.3

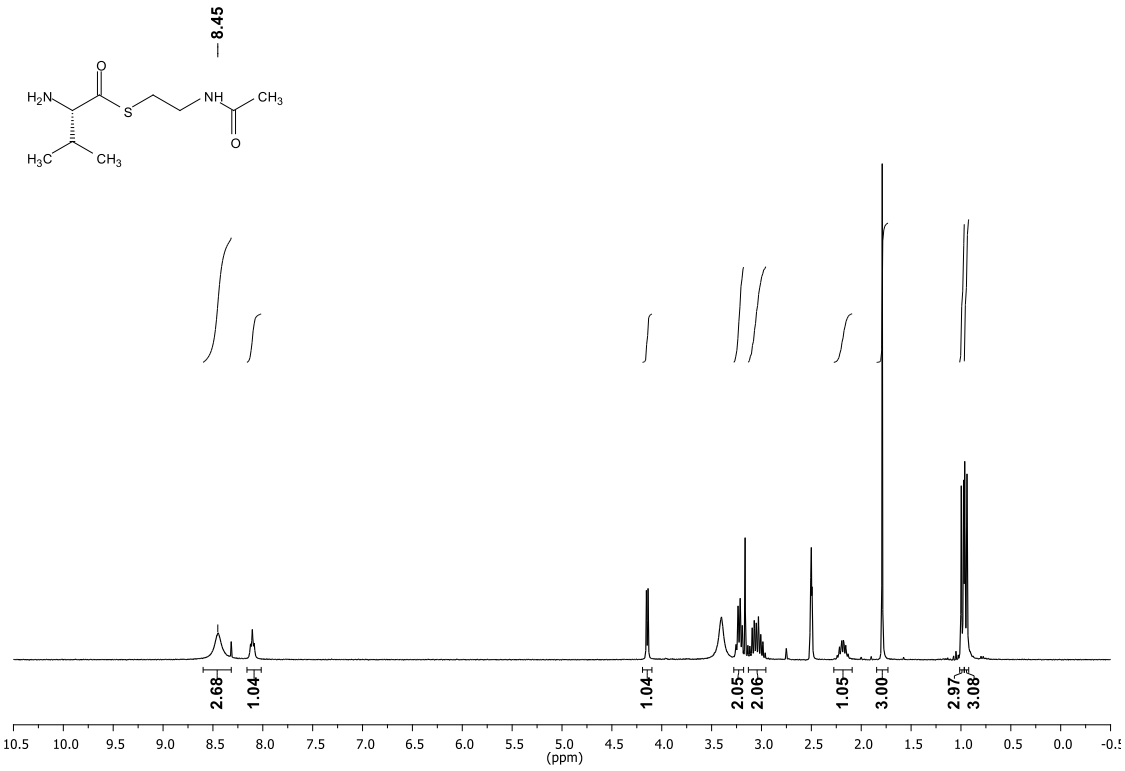
8.45
2.68
1.04
1.04
2.05
2.06
1.05
3.00
2.97
3.08
(ppm)

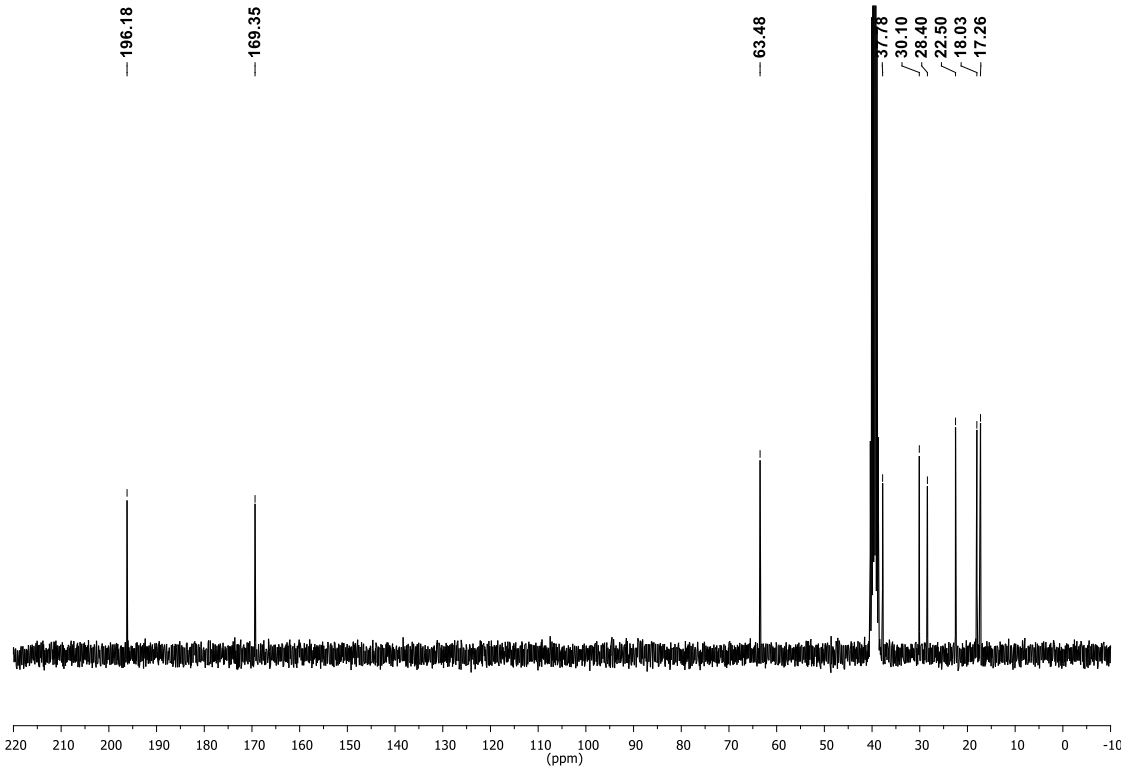
196.18
169.35
63.48
37.78
30.10
28.40
22.50
18.03
17.26
(ppm)

4.5

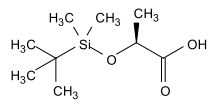
H3C
CH3
CH3
H3C
Si
O
OH
H3C
CH3
O

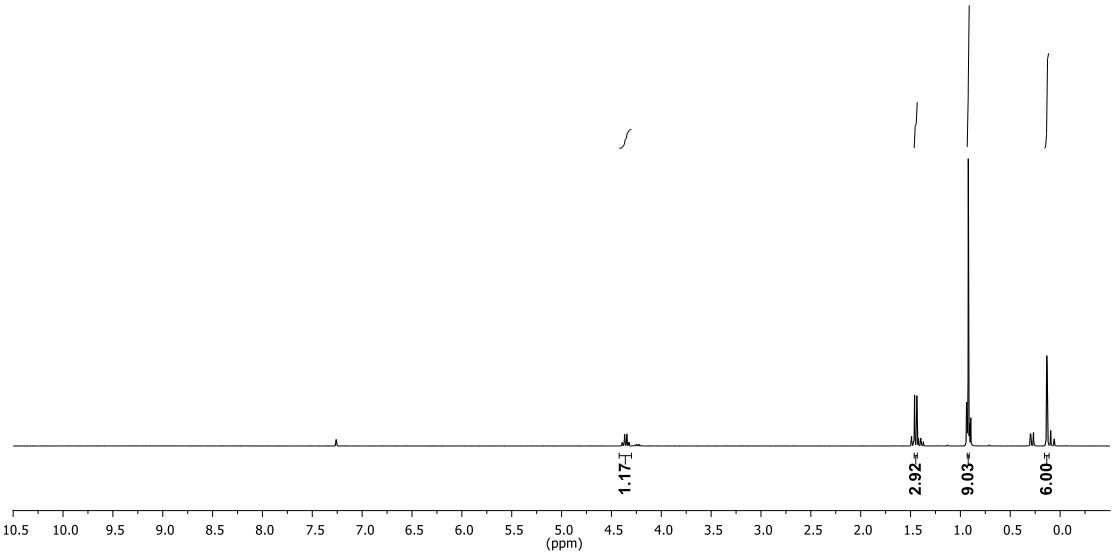
1.17
2.92
9.03
6.00
10.5
10.0
9.5
9.0
8.5
8.0
7.5
7.0
6.5
6.0
5.5
5.0
4.5
4.0
3.5
3.0
2.5
2.0
1.5
1.0
0.5
0.0
(ppm)

4.7

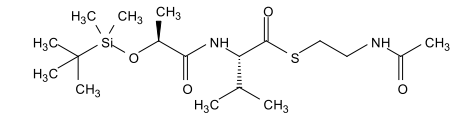

0.80
0.89
0.93
0.98
2.00
2.15
1.00
2.96
3.01
15.02
2.72
2.87
(ppm)

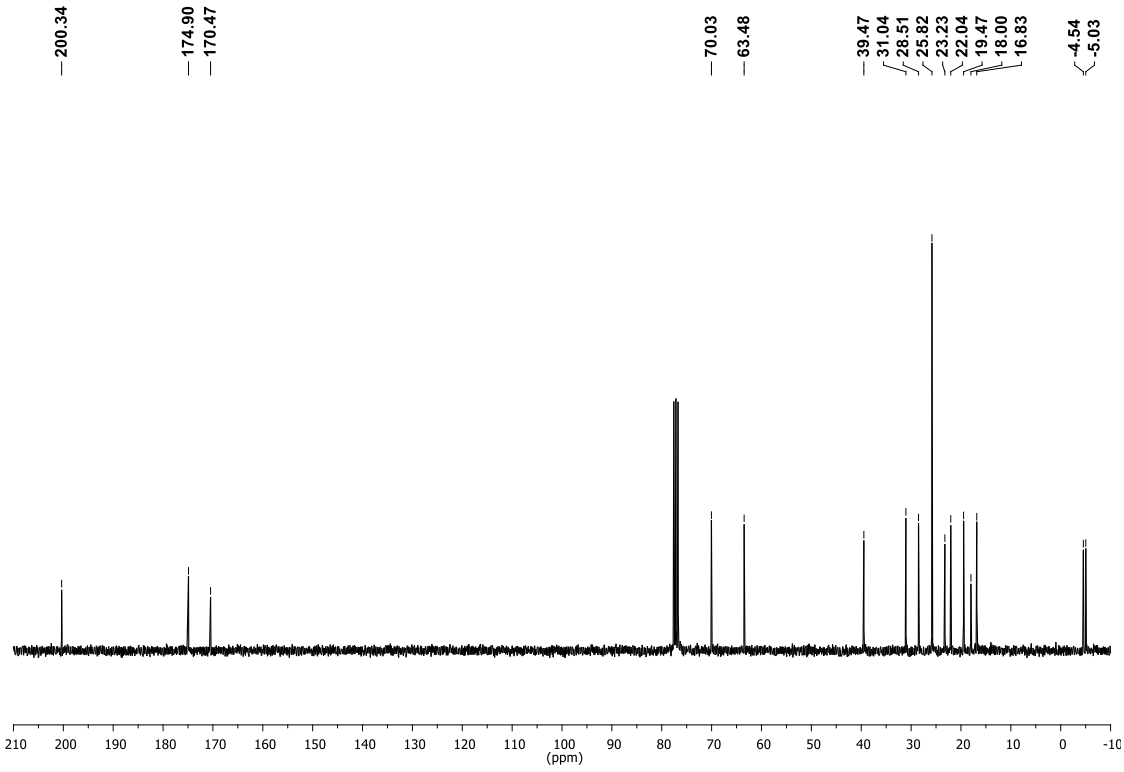
200.34
174.90
170.47
70.03
63.48
39.47
31.04
28.51
25.82
23.23
22.04
19.47
18.00
16.83
-4.54
-5.03
(ppm)

4.8

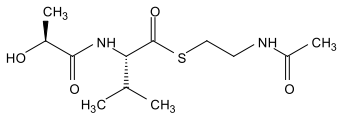
CH3
O
NH
HO
S
NH
CH3
O
O
H3C
CH3

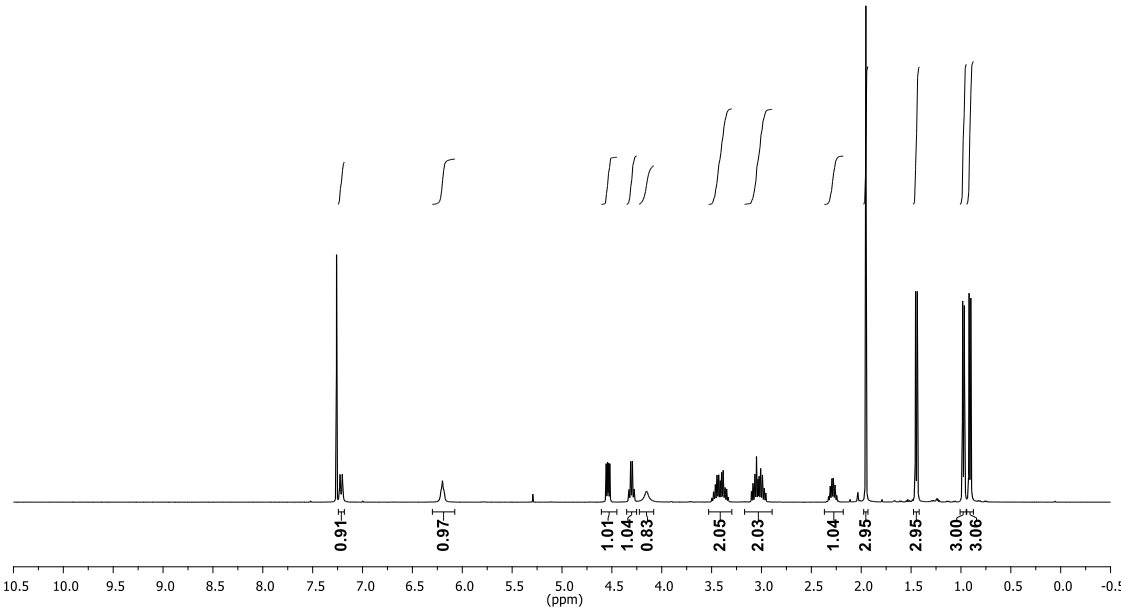
0.91
0.97
1.01
1.04
0.83
2.05
2.03
1.04
2.95
2.95
3.00
3.06
(ppm)

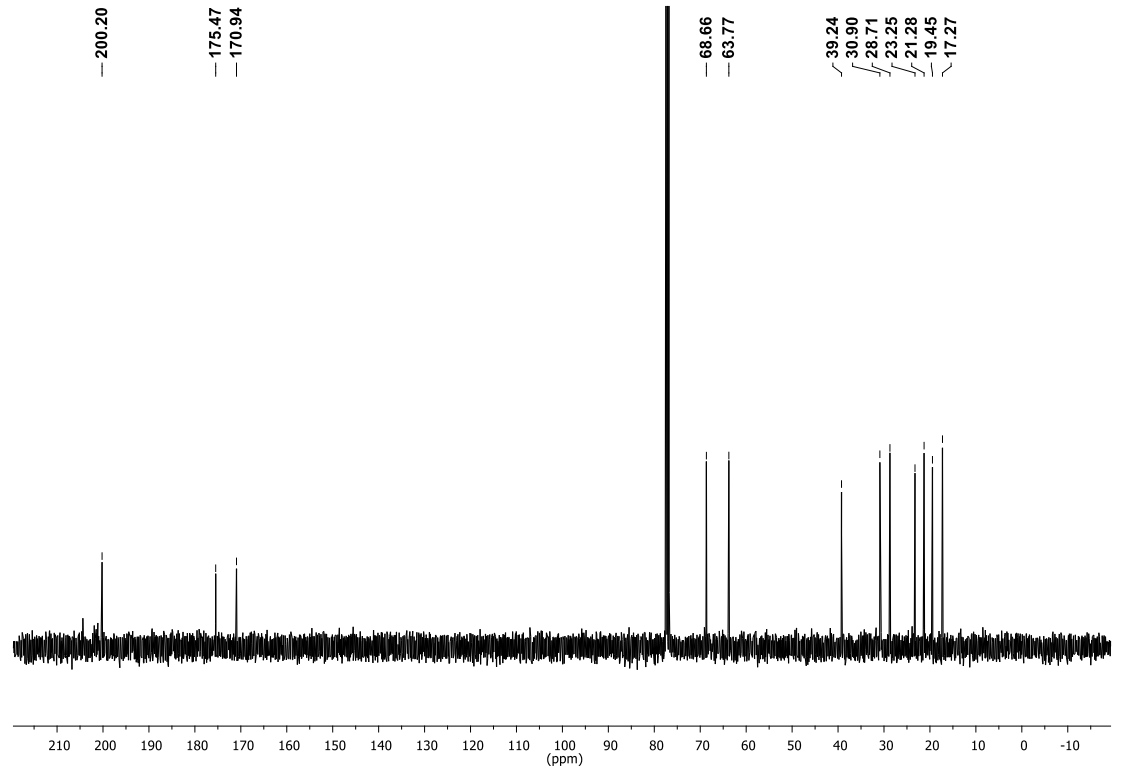
200.20
175.47
170.94
68.66
63.77
39.24
30.90
28.71
23.25
21.28
19.45
17.27
(ppm)

4.9

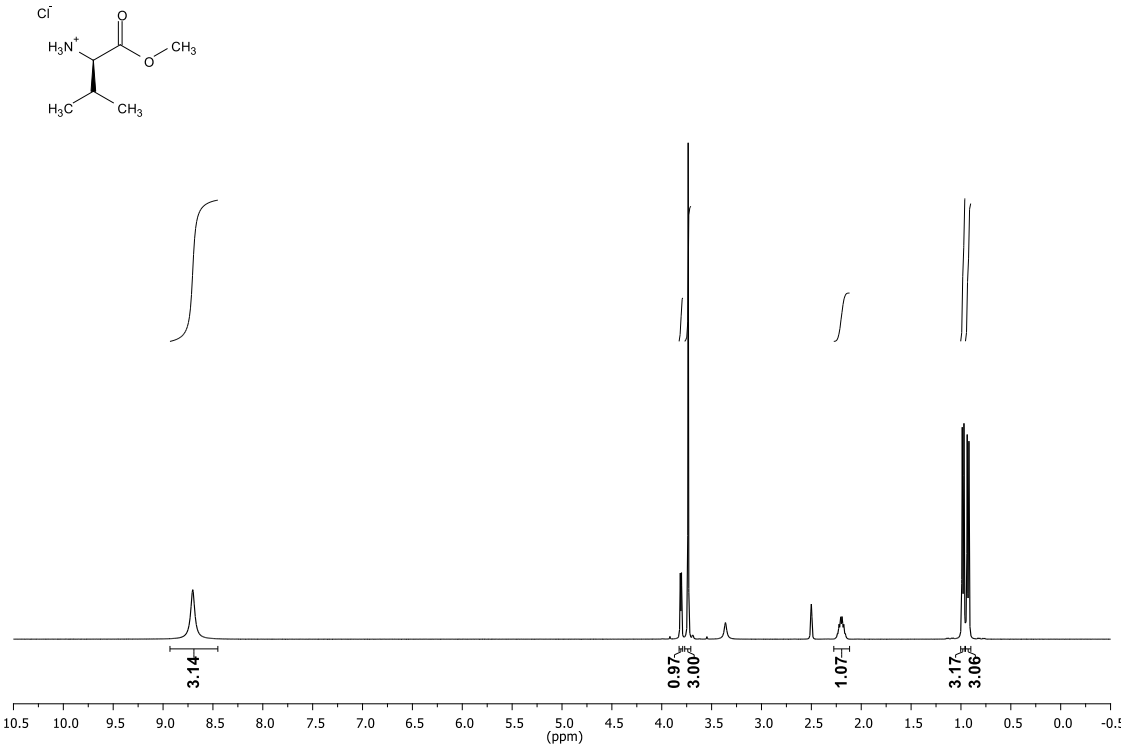
Cl-
O
H3N+
CH3
O
H3C
CH3
3.14
0.97
3.00
1.07
3.17
3.06
10.5 10.0 9.5 9.0 8.5 8.0 7.5 7.0 6.5 6.0 5.5 5.0 4.5 4.0 3.5 3.0 2.5 2.0 1.5 1.0 0.5 0.0
(ppm)

4.10

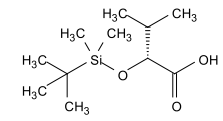
H3C
CH3
H3C
CH3
Si
H3C
H3C
CH3
O
OH
O

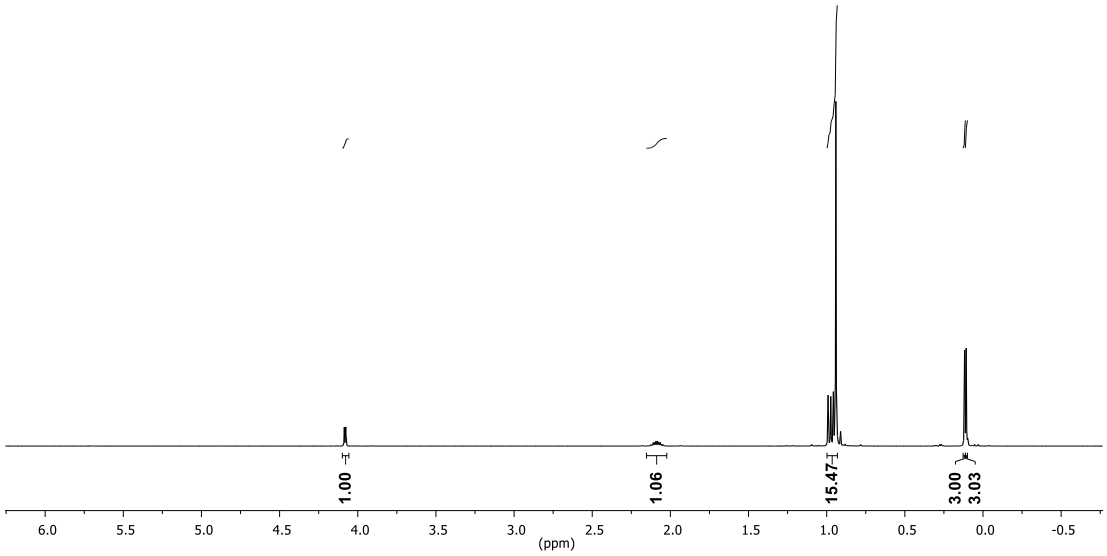
1.00
1.06
15.47
3.00
3.03
6.0
5.5
5.0
4.5
4.0
3.5
3.0
2.5
2.0
1.5
1.0
0.5
0.0
-0.5
(ppm)

4.12

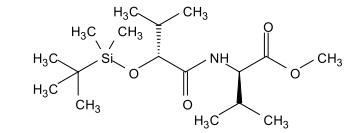

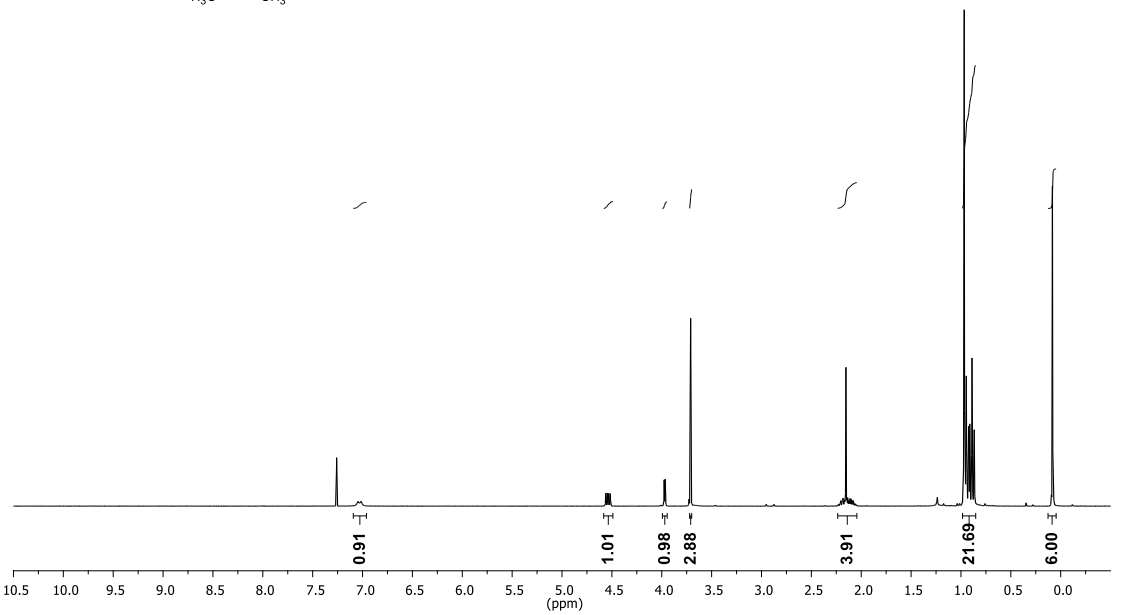
0.91
1.01
0.98
2.88
3.91
21.69
6.00
(ppm)

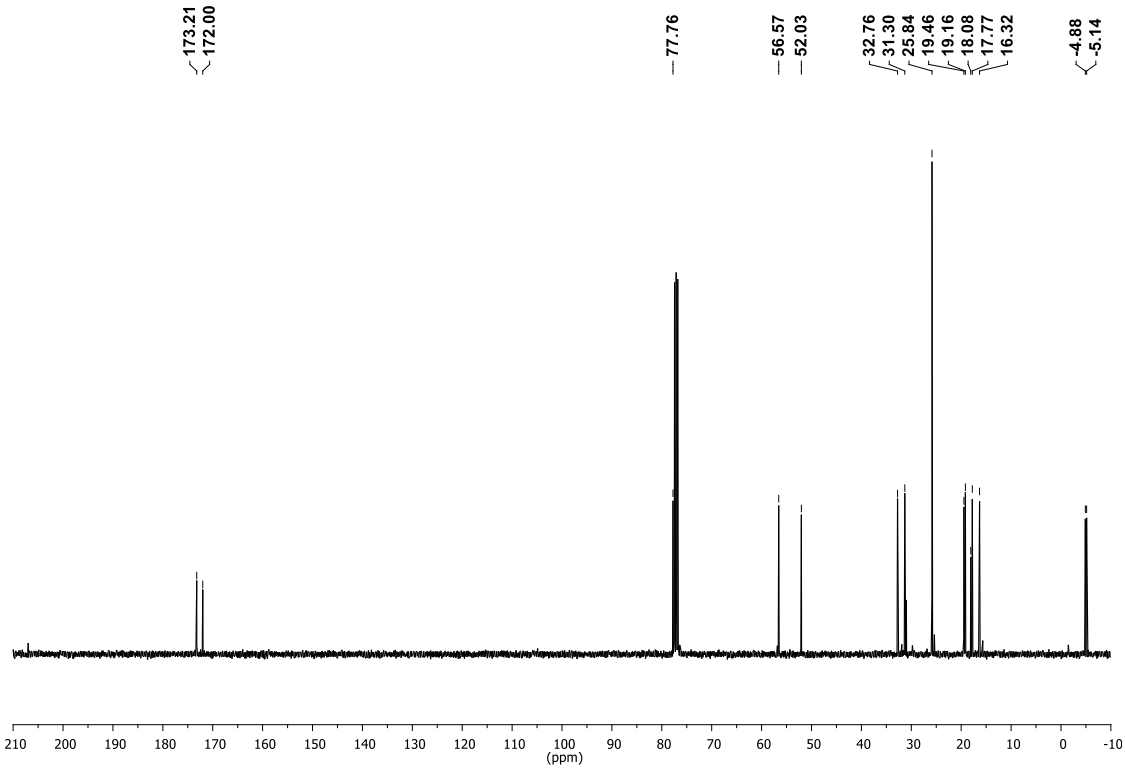
173.21
172.00
77.76
56.57
52.03
32.76
31.30
25.84
19.46
19.16
18.08
17.77
16.32
-4.88
-5.14
(ppm)

4.13

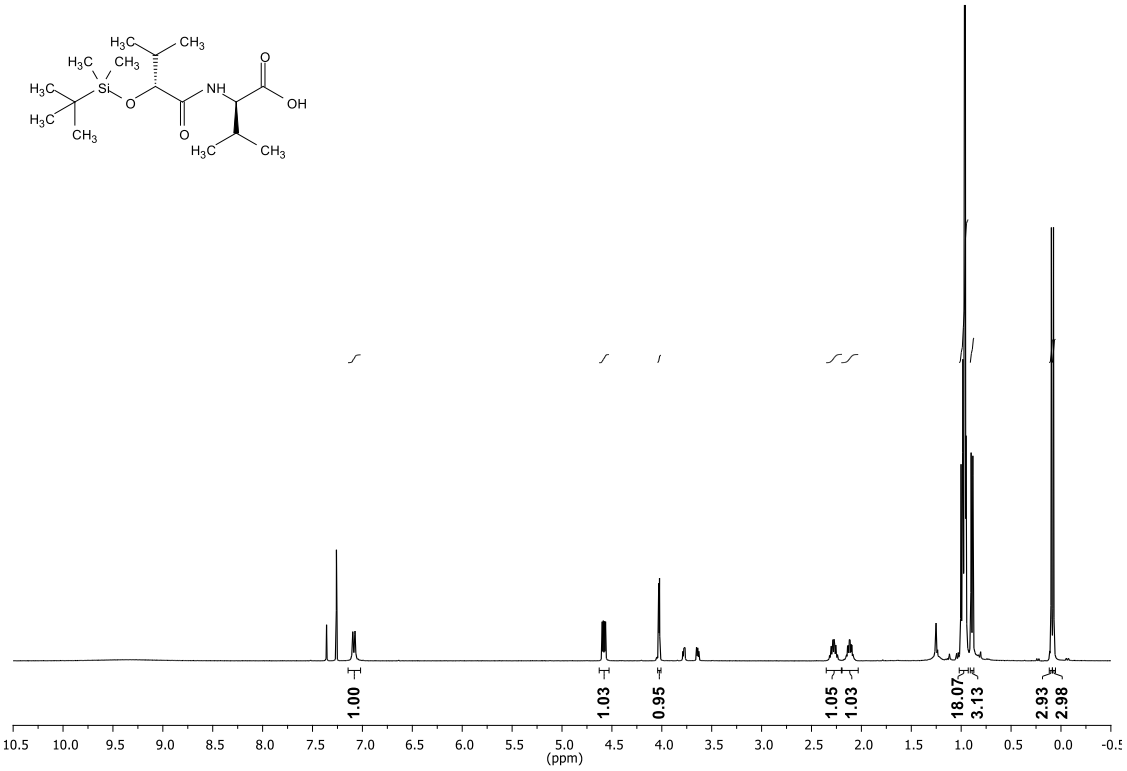
1.00
1.03
0.95
1.05
1.03
18.07
3.13
2.93
2.98
(ppm)

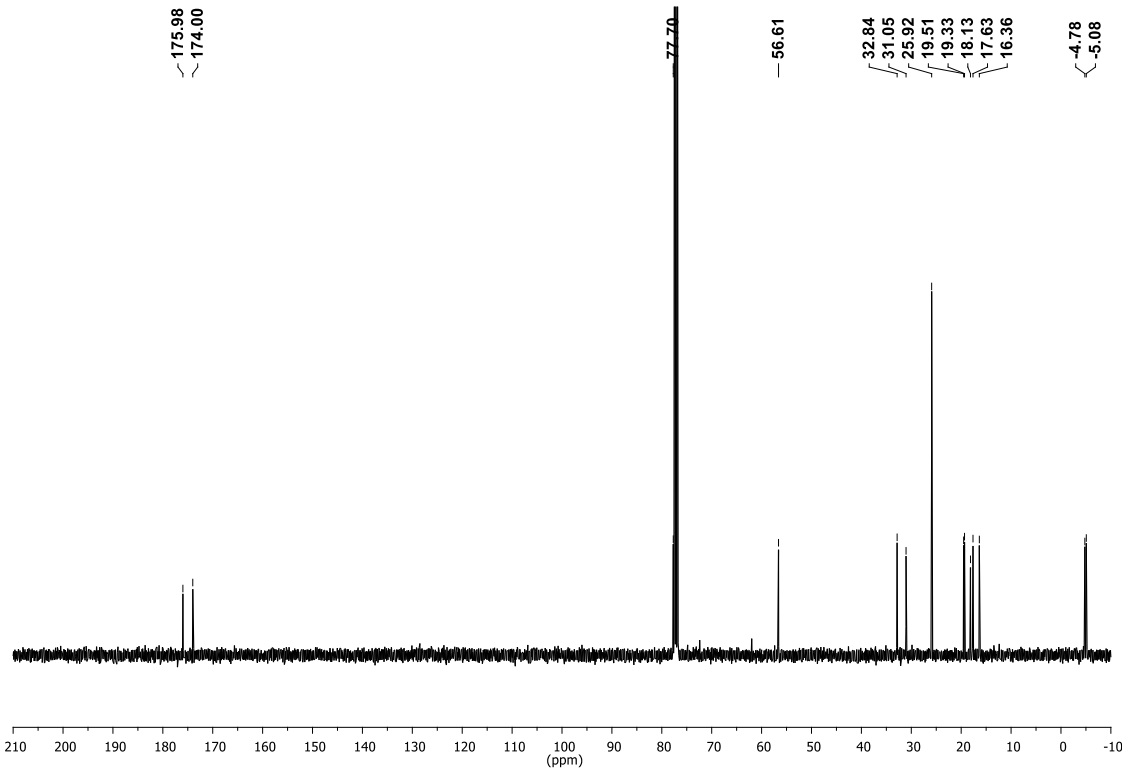
175.98
174.00
77.70
56.61
32.84
31.05
25.92
19.51
19.33
18.13
17.63
16.36
-4.78
-5.08
(ppm)

4.14A and **4.14B**

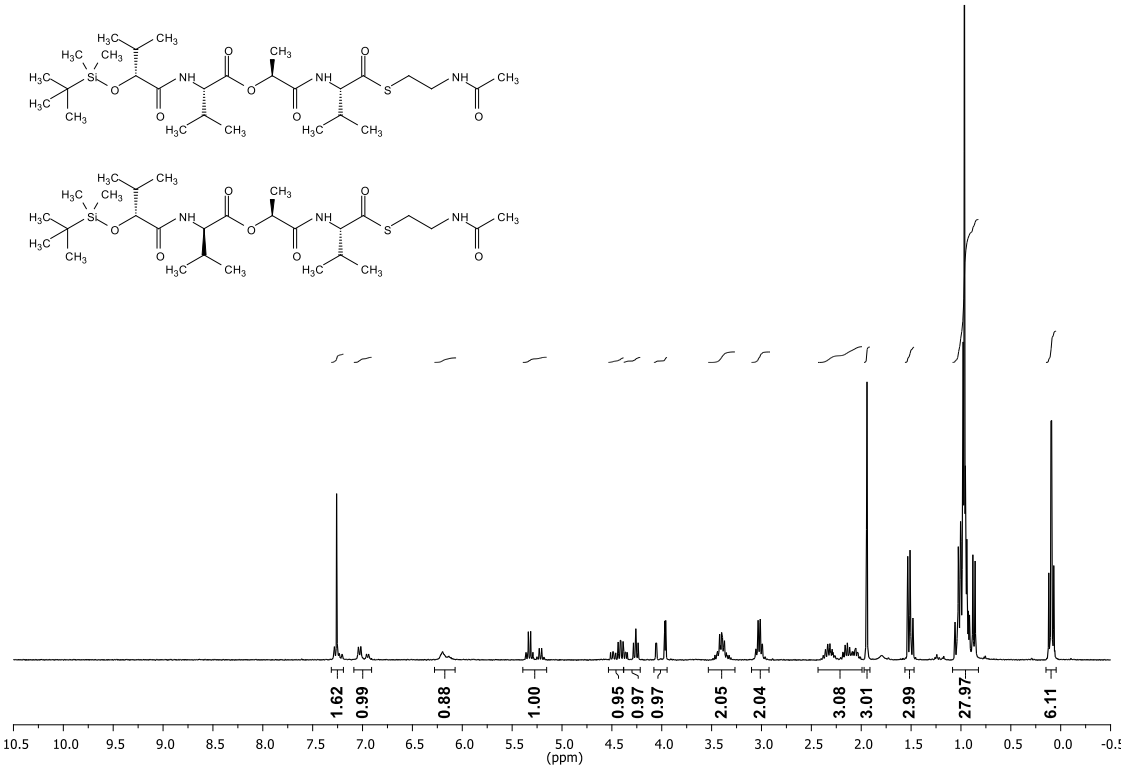

4.15A

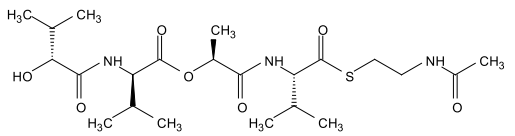

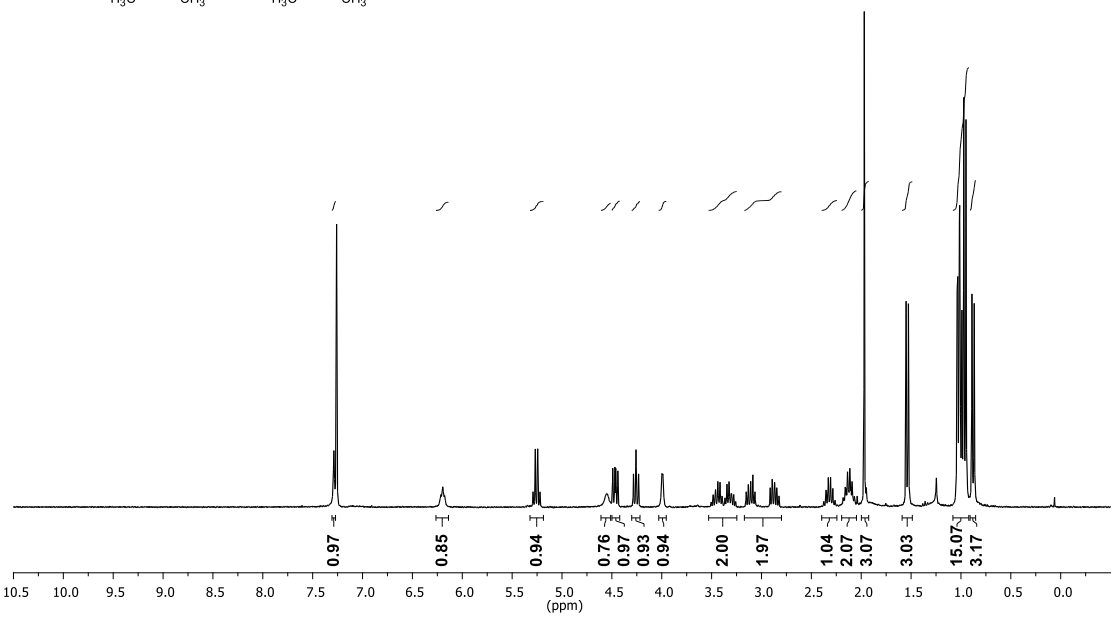
0.97
0.85
0.94
0.76
0.97
0.93
0.94
2.00
1.97
1.04
2.07
3.07
3.03
15.07
3.17
(ppm)

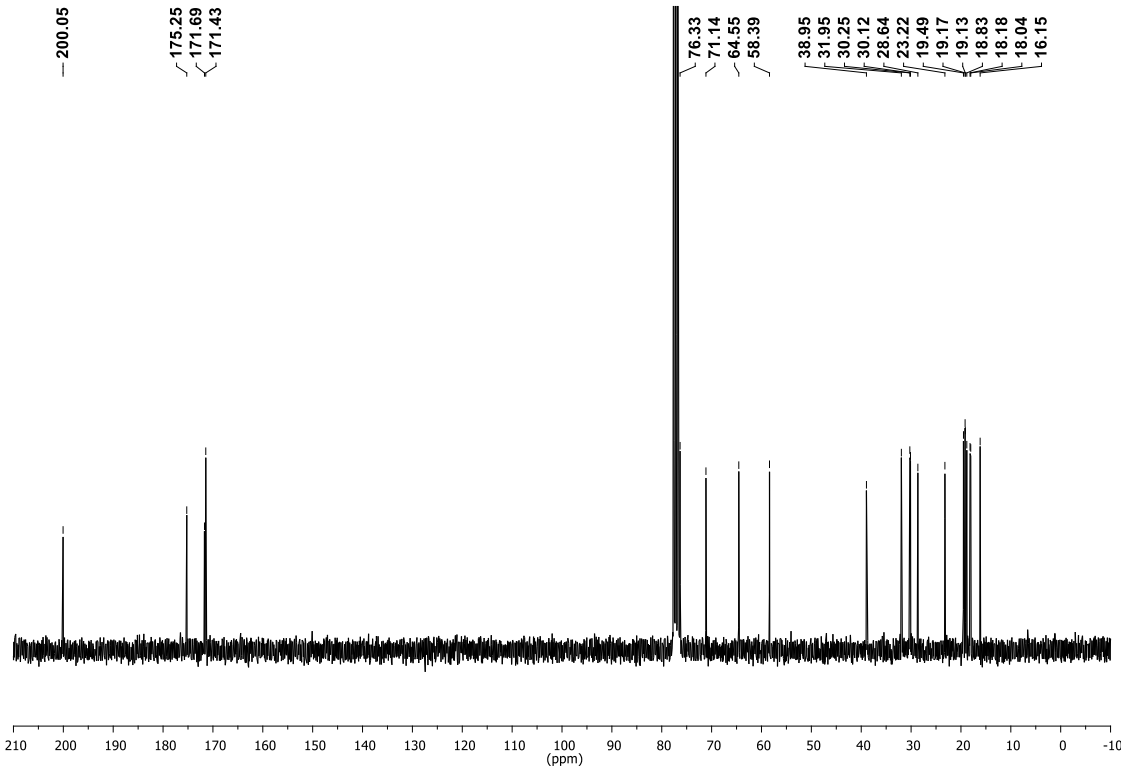
200.05
175.25
171.69
171.43
76.33
71.14
64.55
58.39
38.95
31.95
30.25
30.12
28.64
23.22
19.49
19.17
19.13
18.83
18.18
18.04
16.15
(ppm)

4.16

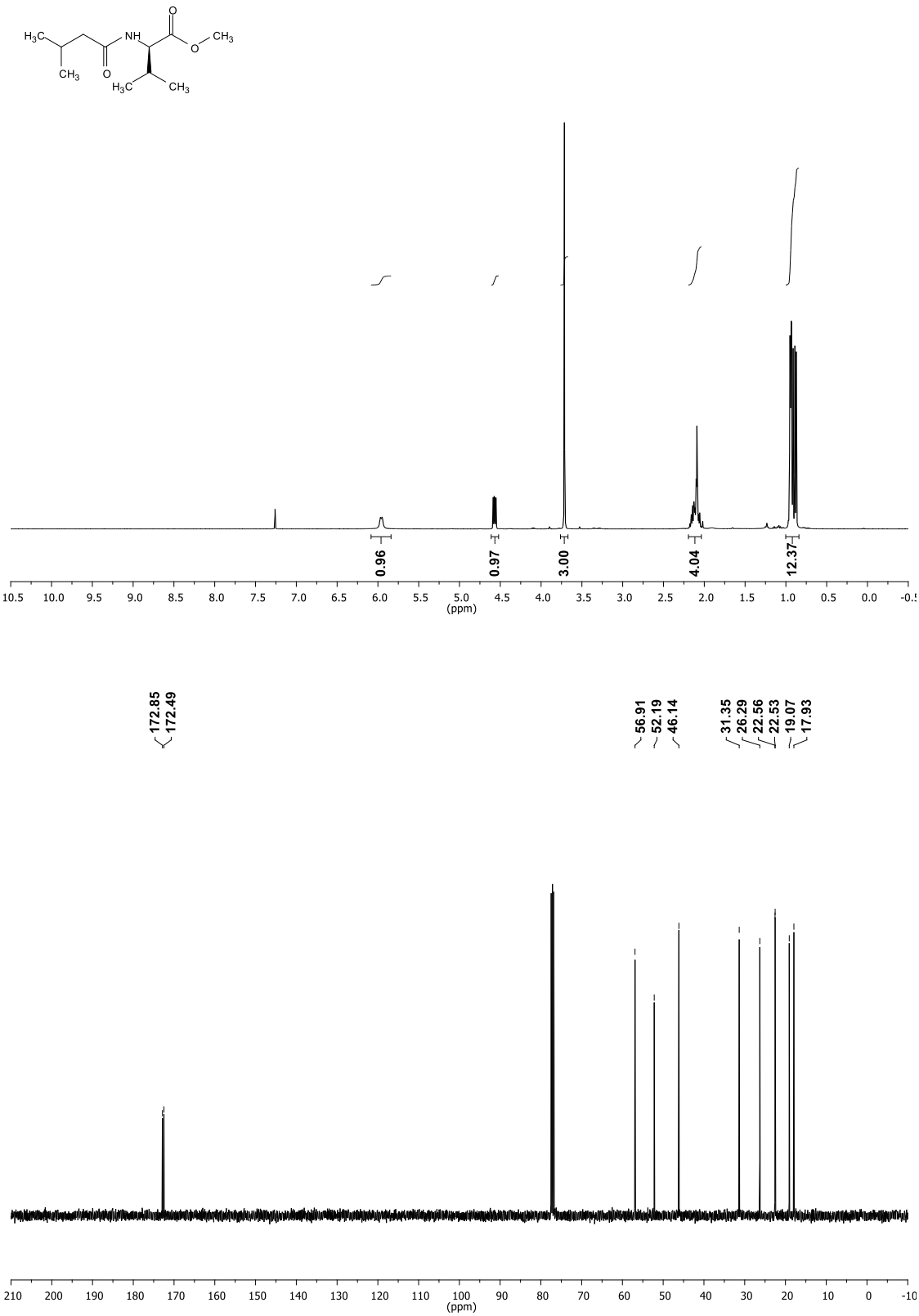
0.96
0.97
3.00
4.04
12.37
(ppm)
172.85
172.49
56.91
52.19
46.14
31.35
26.29
22.56
22.53
19.07
17.93
(ppm)

4.17

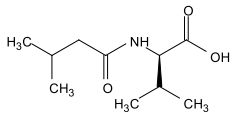
H3C
CH3
NH
O
O
OH
H3C
CH3

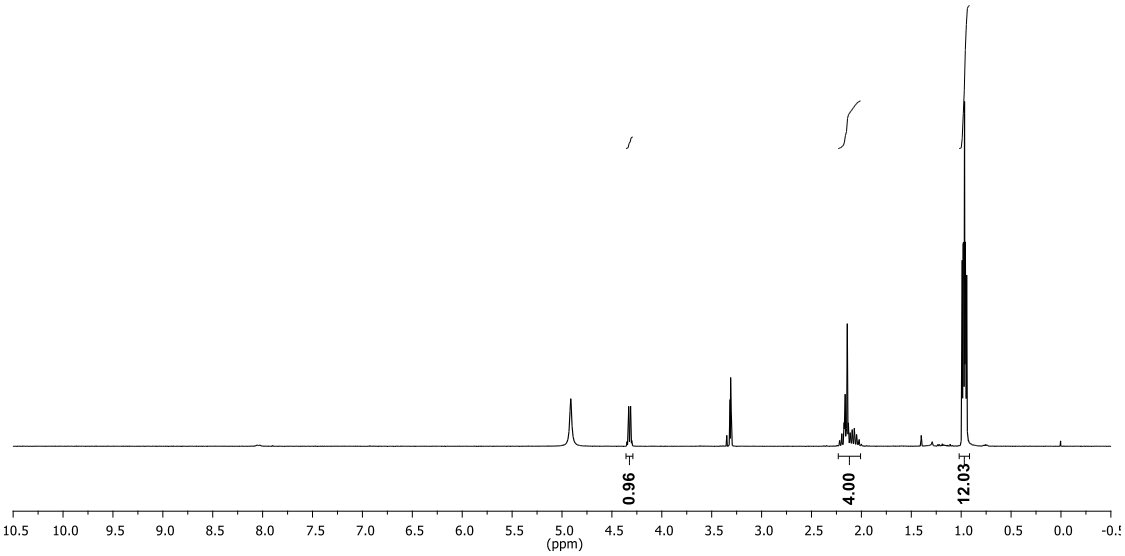
0.96
4.00
12.03
10.5 10.0 9.5 9.0 8.5 8.0 7.5 7.0 6.5 6.0 5.5 5.0 4.5 4.0 3.5 3.0 2.5 2.0 1.5 1.0 0.5 0.0
(ppm)

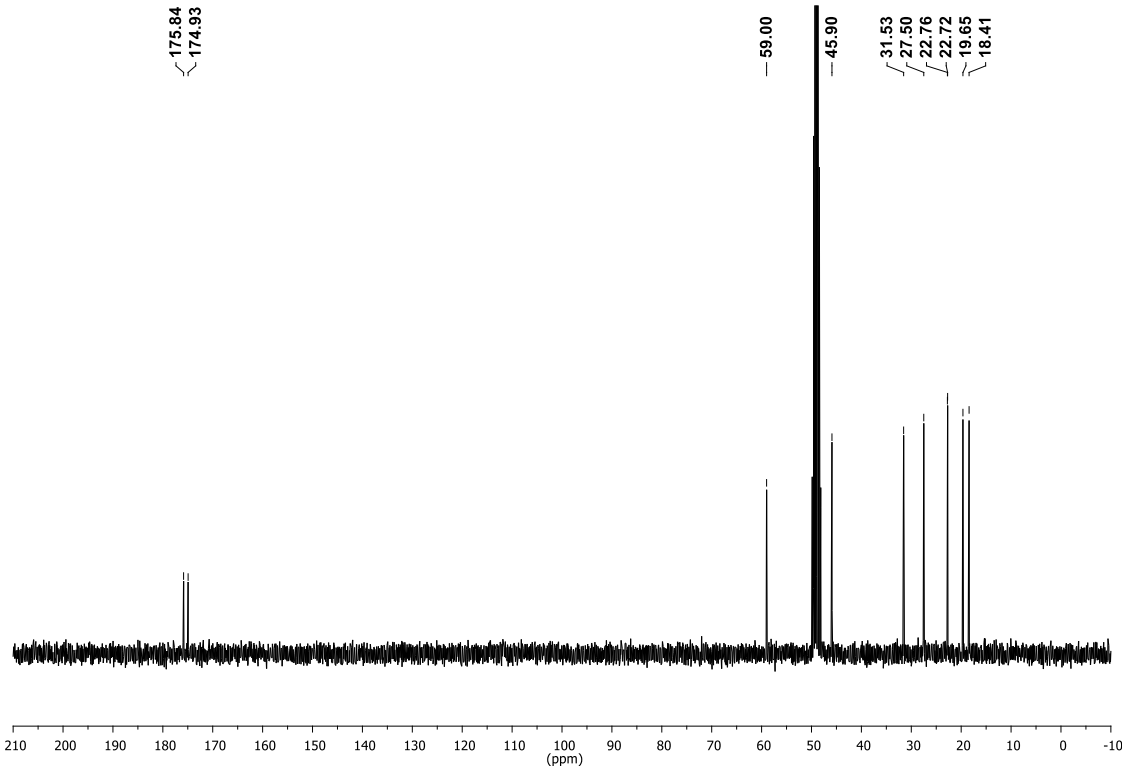
175.84
174.93
59.00
45.90
31.53
27.50
22.76
22.72
19.65
18.41
210 200 190 180 170 160 150 140 130 120 110 100 90 80 70 60 50 40 30 20 10 0
(ppm)

4.18A

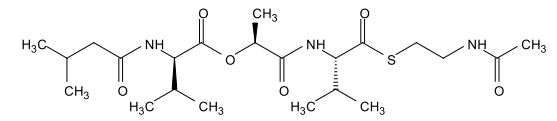

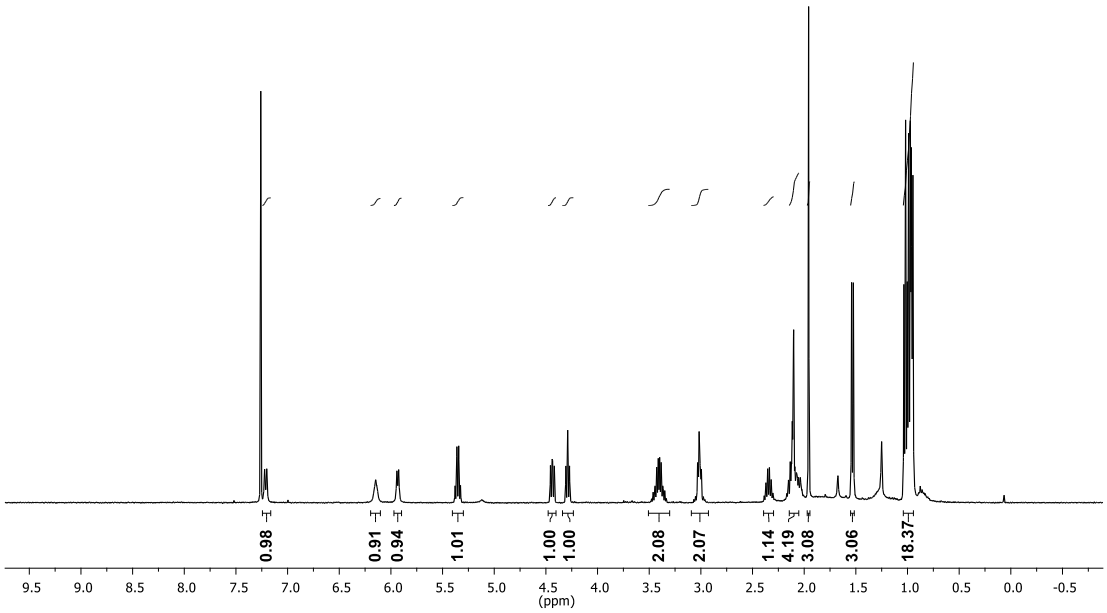
0.98
0.91
0.94
1.01
1.00
1.00
2.08
2.07
1.14
4.19
3.08
3.06
18.37
(ppm)

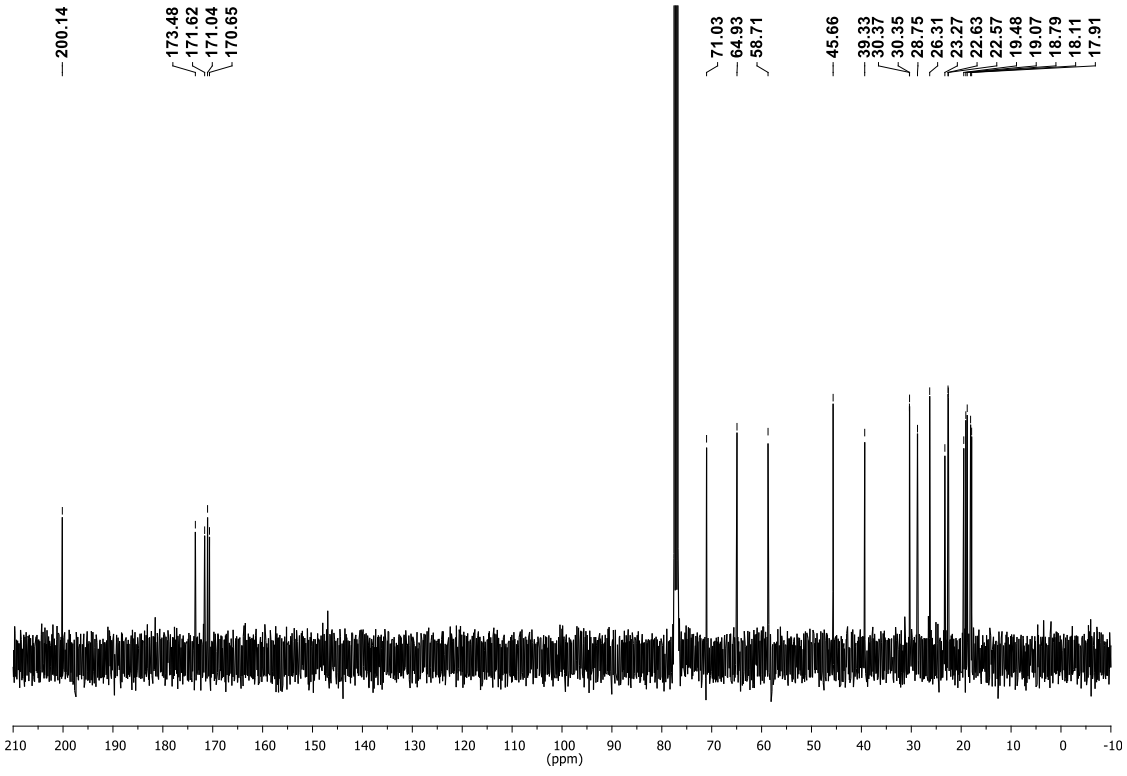
200.14
173.48
171.62
171.04
170.65
71.03
64.93
58.71
45.66
39.33
30.37
30.35
28.75
26.31
23.27
22.63
22.57
19.48
19.07
18.79
18.11
17.91
(ppm)

4.18B

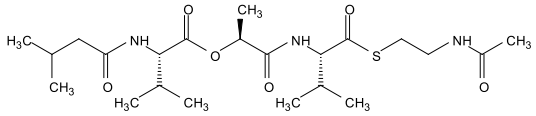

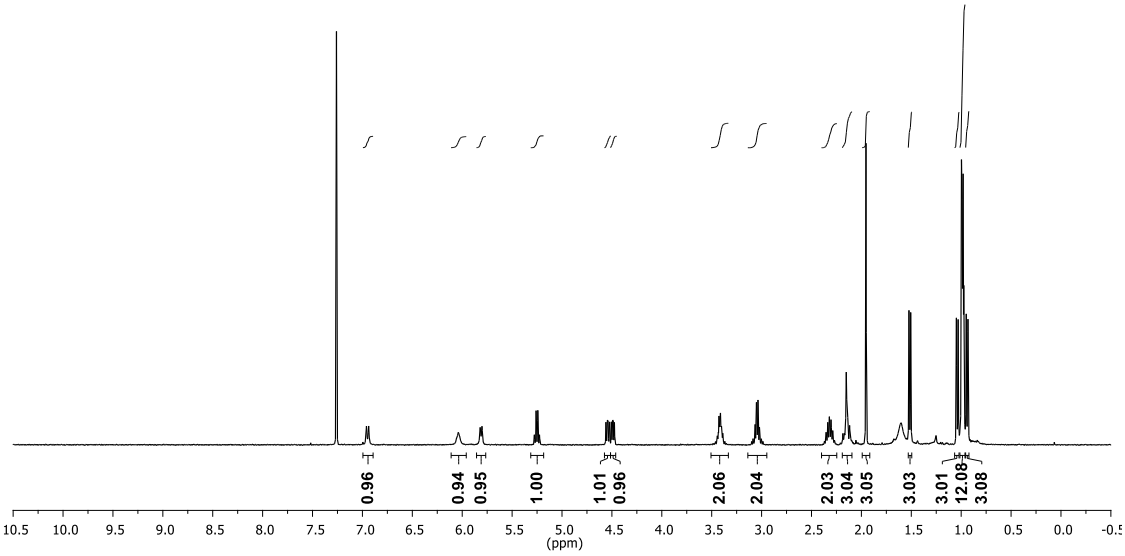
0.96
0.94
0.95
1.00
1.01
0.96
2.06
2.04
2.03
3.04
3.05
3.03
3.01
12.08
3.08
(ppm)

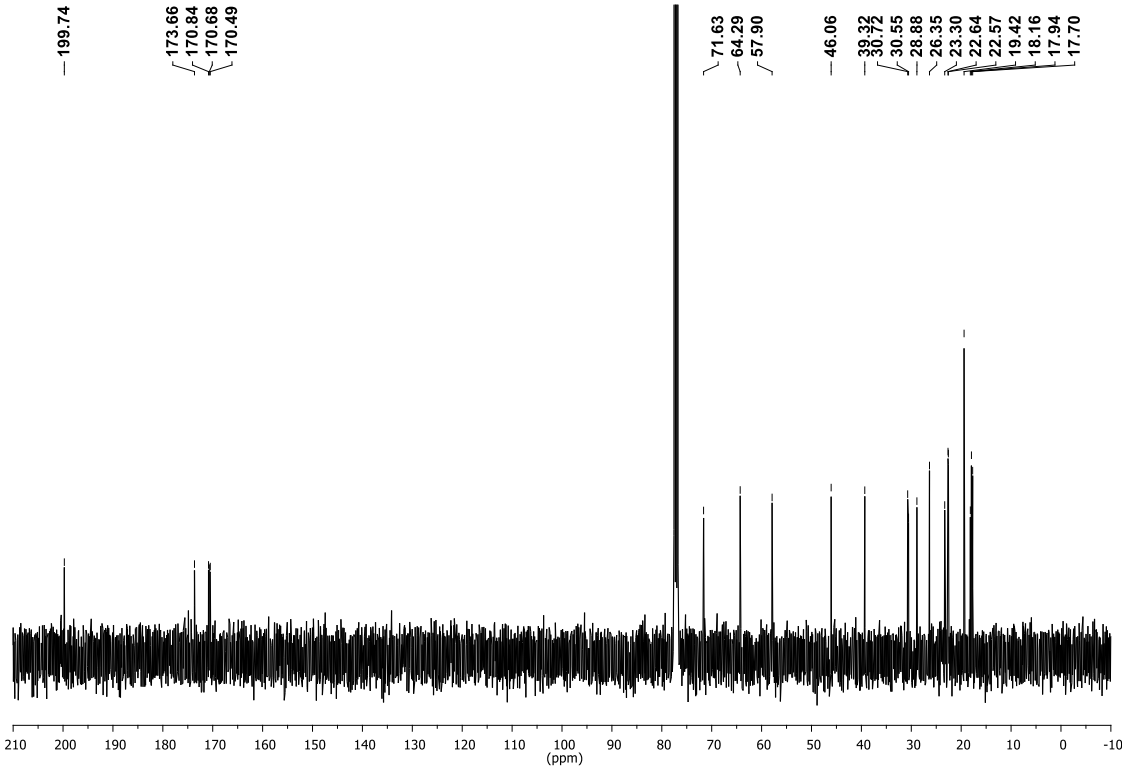
199.74
173.66
170.84
170.68
170.49
71.63
64.29
57.90
46.06
39.32
30.72
30.55
28.88
26.35
23.30
22.64
22.57
19.42
18.16
17.94
17.70
(ppm)